SURFACE INTERACTIONS OF HUMIC ACID - ANION DOPED TITANIA

BINARY SYSTEM

by

AYTAÇ PERİHAN AKAN

BS. in Environmental Engineering, Trakya University, 2008

Submitted to the Institute of Environmental Sciences in partial fulfillment of

the requirements for the degree of

Master of Science

in

Environmental Technology

Boğaziçi University

2014

SURFACE INTERACTIONS OF HUMIC ACID - ANION DOPED TITANIA
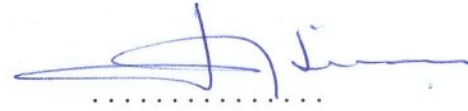
BINARY SYSTEM

APPROVED BY:

Prof. Dr. Miray Bekbölet
(Thesis Supervisor)

Prof. Dr. Ayşen Erdinçler

Prof. Dr. Hüseyin Selçuk

DATE OF APPROVAL . 23./01./20.14....

This work is dedicated to my family

Nazire & Kemal Akan

ACKNOWLEDGEMENTS

ABSTRACT

Humic acids are natural weak polyelectrolytes which play active role in binding mechanism of organic molecules that results in the transportation of contaminants in soils and aquifers. Humic acids constitute the major fraction of natural organic matter that should be removed during water treatment. Besides conventional treatment methods, application of advanced oxidation processes more specifically photocatalysis has gained much attention in recent decades. Titanium dioxide (TiO_2) is universally recognized as a standard photocatalyst. Since photocatalysis occurs through a surface oriented mechanism, the adsorptive properties of TiO_2 specimens deserve special attention. Moreover, nowadays visible light activated TiO_2 has been the subject of numerous investigations. The understanding of the surface interactions prevailing between the anion doped oxide surface and humic subfractions is important for the determination of the role of humic substances during photocatalysis. The aim of this study was to investigate surface interactions between different molecular size fractionations of humic acid and TiO_2 specimens, namely bare TiO_2 and anion doped TiO_2. In this study, two different commercial TiO_2 specimens (Degussa P-25 and Hombikat UV-100) were used.

Adsorption experiments were conducted with humic acid solutions having diverse molecular size fractions (0.45 μm filtered fraction, 100 kDa fraction and 30 kDa fraction). Moreover, bare TiO_2 and anion doped TiO_2 (N-doped TiO_2, S-doped TiO_2, C-doped TiO_2 and N-S co-doped TiO_2) specimens in the range of 0.1-1.0 mg mL^{-1} were used as adsorbents. Adsorption properties of humic acid and its molecular size fractions onto bare TiO_2 and anion doped TiO_2 specimens were evaluated and compared in terms of UV-vis spectroscopic parameters $i.e.$ color forming moieties ($Color_{436}$) and UV absorbing centers (UV_{365}, UV_{280} and UV_{254}) and fluorescence spectroscopy in emission and synchronous scan modes as well as dissolved organic carbon. Adsorption isotherms were evaluated in terms of the adsorption isotherm types (Types C, L and S). Adsorption isotherms were modeled to Freundlich and Langmuir adsorption isotherm models by evaluating the results of specified UV-vis parameters.

The effect of doping on two different TiO_2 specimens (Degussa P-25 and Hombikat UV-100) could be evaluated through the role of decreasing molecular size of humic acid. The most significant effect could be attributed to the surface properties of TiO_2 specimens present in aqueous solutions of humic acid. The results based on varying molecular size fractions of humic acid displayed remarkable differences with respect to the morphological character of TiO_2 specimens.

ÖZET

Hümik asitler toprakta ve sulu ortamdaki kirleticilerinin taşınımına sebep olan, organik moleküllerin bağlanma mekanizmasında aktif rol oynayan zayıf polielektrolitlerdir. Hümik asitler suyun arıtımı sırasında uzaklaştırılması gereken doğal organik maddelerin önemli fraksiyonlarını oluştururlar. Geleneksel arıtma yöntemlerine ilaveten, ileri oksidasyon yöntemlerinin uygulanması daha spesifik olarak fotokataliz son yıllarda çok dikkat kazanmıştır. Titanyum dioksit (TiO_2) evrensel olarak standart bir fotokatalist olarak tanımlanır. Fotokataliz yüzey odaklı bir mekanizma boyunca vuku bulduğundan dolayı, TiO_2 türlerinin adsorplama özellikleri özel ilgisini korur. Ayrıca, bugünlerde görünür ışıkta aktif olan TiO_2 sayısız araştırmanın konusu olmuştur. Anyon bağlı oksit yüzey ve hümik alt fonksiyonları arasında yaygın olan yüzey etkileşimlerinin anlaşılması, fotokataliz sırasında hümik maddelerin rolünün belirlenmesi için önemlidir. Bu çalışmanın amacı, yalın TiO_2 ve anyon bağlı TiO_2 gibi TiO_2 türleri ile hümik asitin farklı moleküler boyut fraksiyonları arasındaki yüzey etkileşimlerini araştırmaktır. Bu çalışmada, iki farklı ticari TiO_2 türü (Degussa P-25 ve Hombikat UV-100) kullanılmıştır.

Adsorpsiyon deneyleri, farklı moleküler boyut fraksiyonlarına sahip olan hümik asit çözeltileri (0.45 µm filtre edilmiş fraksiyon, 100 kDa fraksiyon ve 30 kDa fraksiyon) ile yürütüldü. Ayrıca adsorbanlar olarak 0.1-1.0 mg mL^{-1} aralığında yalın TiO_2 ve anyon bağlı TiO_2 türleri (N-bağlı TiO_2, S-bağlı TiO_2, C-bağlı TiO_2 ve N-S eş-bağlıTiO_2) kullanılmıştır. Hümik asit ve onun moleküler boyut fraksiyonlarının yalın TiO_2 ve anyon bağlı TiO_2 türleri üzerindeki adsorpsiyonu, UV-görünür bölge spektroskopik parametreleri; renk oluşturan gruplar ($Color_{436}$) ve UV absorplayan merkezler (UV_{365}, UV_{280} ve UV_{254}) ve emisyon ve eş zamanlı tarama modları içeren floresans spektoskopisi ve çözünmüş organik karbon bakımından değerlendirilmiş ve kıyaslanmıştır. Adsorpsiyon izotermleri, adsorpsiyon izoterm tiplerine göre değerlendirilmiştir (C, L ve S). Adsorpsiyon izotermlerinin, spesifik UV-görünür parametrelerinin sonuçları değerlendirilerek Freundlich ve Langmuir adsorpsiyon izoterm modellerine modellemeleri yapılır.

İki farklı TiO_2 türü (Degussa P-25 ve Hombikat UV-100) üzerindeki bağlanmanın etkisi, humik asitin azalan moleküler boyutunun rolü boyunca değerlendirilebilinir. En önemli etki, hümik asitin sulu çözeltilerinde mevcut olan TiO_2 türlerinin yüzey özelliklerine dayandırılabilinir. Hümik asitin değişen moleküler boyut fraksiyonlarına bağlı olan sonuçlar TiO_2 türlerinin şekilsel özelliklerine göre dikkate değer farklılıklar göstermiştir.

TABLE OF CONTENTS

LIST OF FIGURES

LIST OF TABLES

LIST OF SYMBOLS / ABBREVIATIONS

Symbol	Explanation	Units Used
AOPs	Advanced oxidation processes	
BOD	Biochemical oxygen demand	mg L^{-1}
C	Concentration	mg L^{-1}
C_e	Equilibrium concentration of adsorbate	mg L^{-1} (DOC) m^{-1} (UV-vis)
C_i	Initial concentration of adsorbate	mg L^{-1} (DOC) m^{-1} (UV-vis)
C_s	Amount of adsorbate adsorbed on adsorbent	mg L^{-1} (DOC) m^{-1} (UV-vis)
Color$_{436}$	Absorbance at 436 nm	
C-doped TiO$_2$	Carbon-doped TiO$_2$	
Da	Dalton	
DBPs	Disinfection by-products	
DOC	Dissolved organic carbon	
DOM	Dissolved organic matter	
DOMs	Dissolved organic matters	
DRS	UV-vis diffuse reflectance spectra	
FA	Fulvic acid	
FAs	Fulvic acids	
HA	Humic acid	
Has	Humic acids	
HAAs	Haloacetic acids	
HS	Humic substances	
E_{bg}	Bandgap energy	
E_c	Conduction band	
E_v	Valence band	

K_a	Langmuir Adsorption constant	mg L^{-1} (DOC)
		m^{-1} (UV-vis)
K_f	Freundlich adsorption capacity constant	
LDHs	Layered double hydroxides	
NOM	Natural organic matter	
NPOC	Non-purgeable organic carbon	
N-doped TiO$_2$	Nitrogen-doped TiO$_2$	
N-S co-doped TiO$_2$	Nitrogen-sulfur co-doped TiO$_2$	
OM	Organic matter	
OC	Organic carbon	
q_A	Adsorbed amount per unit weight of adsorbent	m^{-1}g^{-1}
q_{max}	Maximum adsorption	m^{-1}g^{-1}
SCOA	Specific color absorbance	m^{-1} mg^{-1} L
SCOA$_{436}$	Specific color absorbance at 436 nm	m^{-1} mg^{-1} L
SUVA	Specific UV absorbance	m^{-1} mg^{-1} L
SUVA$_{254}$	Specific UV absorbance at 254 nm	m^{-1} mg^{-1} L
SUVA$_{280}$	Specific UV absorbance at 280 nm	m^{-1} mg^{-1} L
SUVA$_{365}$	Specific UV absorbance at 365 nm	m^{-1} mg^{-1} L
S-doped TiO$_2$	Sulfur-doped TiO$_2$	
THM	Trihalomethane	
THMs	Trihalomethanes	
TOC	Total Organic Carbon	mg L^{-1}
TiO$_2$	Titanium dioxide	
UF	Ultrafiltration	
UV-vis	Ultraviolet-Visible	
UV$_{254}$	Absorbance at 254 nm	cm^{-1} or m^{-1}
UV$_{280}$	Absorbance at 280 nm	cm^{-1} or m^{-1}
UV$_{365}$	Absorbance at 365 nm	cm^{-1} or m^{-1}
XPS	X-ray diffraction	
XRD	X-ray photoelectron spectroscopy	
$\Delta\lambda$	Bandwidth	nm
1/n	Freundlich adsorption intensity parameter	

1. INTRODUCTION

Organic matter (OM) can result from both natural and anthropogenic sources. In order to determine OM in water, carbon content must be measured. Thus, organic and inorganic forms of organic materials can be separated. OM is present in dissolved and particulate forms in all natural waters (vanLoon and Duffy, 2010). Dissolved organic matter (DOM) in soils, surface and ground waters consists of chemically heterogeneous mixture of the acidic products resulting from particularly microbial degradation of plant and animals. DOMs such as humic and fulvic acid are abundantly present in acidic functional groups. DOMs considerably influence the surface charge of the mineral particles due to the fact that these substances tend to connect with the active zone of mobile particles like clay and metal oxides (Illés and Tombácz, 2006).

The most spread natural organic matter (NOM) existed in the water supplies is humic substances (HS), which are anionic hydrophobic macromolecules having surface functional groups containing carboxylic and phenolic groups (Moussavi et al., 2011). Humic acid (HA) that is widespread in the soil and in the water sources especially in the ground water results in some important problems such as developing color in the water source and occurring disinfection by products (DBPs) during chlorination process in the treatment systems. Because of these issues, the removal of HA from water sources has a very high importance (Suffet and MacCarthy, 1989).

Titanium dioxide (TiO_2), which is used as a standard photocatalyst, is preferred to cope with a great deal of environmental problems such as air clean, wastewater treatment owing to its advantageous features such as photochemical reactivity, high chemical stability, high UV absorption, commercial availability and inexpensiveness. The band gap energy of TiO_2 points out the wavelength of UV light < 400 nm. Due to the fact that sunlight comprises visible wavelengths, these do not correspond to TiO_2 band gap. This situation decreases the ability of TiO_2 as to the decomposition of toxic substances under natural illumination (Bangkedphol et al., 2010).

One of the solutions that have been found to increase the absorption wavelength range of TiO_2 to the visible region (400 nm $< \lambda <$ 700 nm) without the decrease of photocatalytic activity of TiO_2 is that to diminish the band gap energy of TiO_2 by doping with non-metallic elements such as carbon, nitrogen and sulfur.

Adsorption is the attachment of molecules or particles to a surface. The surface may be a part of any solid matter. Adsorption is a mass transfer process in that a component in the liquid phase is moved to the solid phase. Molecules that adsorb are largely organic, and include both natural and synthetic species. Particles include viruses, bacteria and others such as cysts and algae. The particle providing the bonding sites is called as the adsorbent; its scale is usually > 100 μm. The particle bonding to the site is the adsorbate; most are < 10 μm (Hendricks, 2006). In other words, the adsorbate is the substance that is being removed from the liquid phase at the interface. The adsorbent is the solid, liquid, or gas phase onto which the adsorbate accumulates (Tchobanoglous et al., 2003).

Adsorption of HA onto the bare TiO_2 and anion doped TiO_2 specimens is a very major step needed to explain its effects on photooxidation. The fundamental aim of this study is to evaluate the surface interactions existing between the anion doped oxide surface and humic acid subfractions. In this study, adsorption of HA and its molecular size fractions onto bare TiO_2 and anion doped TiO_2 as well as co-doped TiO_2 was investigated. HA was fractionated by ultrafiltration method to obtain diverse organic matter contents and also to decrease chemical heterogeneity of humic acids. The characterization of molecular size fractions of HA was determined by UV-vis spectroscopy and fluorescence spectroscopy in emission and synchronous scan modes. The data of batch adsorption experiments were assessed by Freundlich isotherm and Langmuir isotherm in order to provide comparing among experiment results and also to evaluate the adsorption model parameters.

2. THEORETICAL BACKGROUND

2.1. Natural Organic Matter

NOM existing in all surface, ground waters along with soil consists of a variety of constituents, from largely aliphatic to highly colored and aromatic as well as highly charged to uncharged, possessing also a variety of chemical compositions and molecular sizes (Matilainen and Sillanpää, 2010). NOM present in aquatic circle demonstrated differences in terms of its nature and quantity (Marshall et al., 1998).

NOM includes a mixture of well described weak organic acids and organic components which do not possess a defined chemical structure. Both NOM and mineral oxides have significant impacts on chemical speciation and transport of nutrients and pollutants in soils and sediments (Antelo et al., 2007). NOM comprises a variety of organic matters formed during decomposition of vegetation and animal tissues (Kumpulainen et al., 2008). NOM is a complex mixture of macro organic molecules, with a broad spectrum of sub-structures and molecular weight distribution with respect to its origin and genesis. NOM consists of both allochthonous (watershed or terrestrial) and autochthonous (algal or in situ) sources. In spite of the fact that allochthonous NOM usually consists of humic substances, autochthonous NOM extensively includes algal organic substances (Uyguner-Demirel and Bekbolet, 2011).

Complicated structure of NOM contains a great number of functional groups, such as carboxyl (-COOH) and phenolic (-OH) (Yan and Bai, 2005). The chemical properties of NOM are affected both by material source and biogeochemical processes involved in the carbon cycle in terrestrial and aquatic environments (Uyguner-Demirel and Bekbolet, 2011). The character of NOM can show alterations depending on source and time (season) due to the fact that climate and the hydrological regime as well as a number of other environmental factors affect the amount of NOM in water. Air and surface water temperature raising, increase in rainfall intensity as well as atmospheric CO_2 increase can be handled as factors resulting in the increase of the content of NOM in surface waters

(Matilainen and Sillanpää, 2010; Murray and Parsons, 2004). Some seasonal events having major impacts on water availability and quality, such as rainfall event, snowmelt, runoff, floods and droughts can influence the content of NOM. The alterations in quantity and quality of NOM have an important effect on the selection, design and operation of water treatment processes.

The water sources employed for drinking water objectives usually include NOM owing to interactions among the hydrological cycle, the biosphere and geosphere. NOM brings about corrosion and fouling of membrane and also determines the amount of the coagulant and disinfectant used in water treatment (Matilainen et al., 2010). Increasing of transportation and distribution of organic micropollutants, contributing of DBPs formation, decreasing of the efficiency of treatment processes and providing of an undesired biological growth substrate can be cited as factors that NOM influences drinkable water quality (Murray and Parsons, 2004). NOM exhibits temporal and spatial heterogeneity with significant effects on energy and carbon dynamics (Parilti et al., 2011).

Hydrophobic acids constituting approximately 50% of total organic carbon (TOC) in water make up the largest fraction of NOM, which consists of both hydrophobic and hydrophilic constituents. These hydrophobic acids can be classified as humic acid (HA), fulvic acid (FA) and humin considering as humic substances. Hydrophobic NOM is wealthy in respect to aromatic carbon, phenolic structures and conjugated double bonds, while hydrophilic NOM includes more aliphatic carbon and nitrogenous compounds, such as carbohydrates, sugars and amino acids. Hydrophobic NOM having high aromatic carbon content can be considered as the main DBPs. In addition to hydrophobic NOM, hydrophilic NOM play an important role in the formation of DBPs. DBPs found in the highest concentrations in drinking waters are trihalomethanes (THMs) and haloacetic acids (HAAs) (Matilainen and Sillanpää, 2010). One of the products including humic acids after chlorination process in water treatment plants has been described as trihalomathane (THM) (Wang et al., 2012). Some organic substances, such as THMs, HAAs and hypochlorite, used in water treatment as a biocide are needed to remove from water because of severe public health problems associated with central nervous system, bladder cancer, spontaneous abortions and birth defects (Al-Rasheed and Cardin, 2003; Kim and Walker, 2001; Matilainen and Sillanpää, 2010). Various regulations as to the forming of DBPs are

handled by many countries (Matilainen and Sillanpää, 2010). Maximum contaminant level of THMs was determined as 0.1 mg L^{-1}, 0.080 mg L^{-1} and 0.040 mg L^{-1} respectively in 1979, 2001 and 2002 by United States Environmental Protection Agency (USEPA) (Kim and Walker, 2001).

2.1.1. Humic Substances

Humic substances (HS) which are environmental decomposition products of plant, fungal and bacterial biopolymers, are important in the binding mechanism of toxic chemicals in soil and water, in contributing to plant growth as the source of nutrient, in the formation and maintenance of good soil structure (Leenheer et al., 2001). HS can be divided into three components: humic acid (HA), fulvic acid (FA) and humin according to their solubility features. HA forms one of the most significant parts of HS. HAs and FAs represent alkali-soluble humus fragments; HAs are generally extracted employing diluted alkali and precipitated with an acid, and so are separated from the soluble FAs. Humin represents the insoluble residue (Peña-Méndez et al., 2005).

Two general conceptual models have been discussed in literature for the formation of HS. The first one supposes that they are formed from the breakdown of plant materials and oxidation because of extracellular enzymes and abiotic processes. The second concept expresses a polymerization of simple compounds like quinones that are derived from degraded plant material. HS account for 40-80% of the dissolved organic matter in water. Moreover, HS may form more than 80% of the OM in soil (Antelo et al., 2007). Typical freshwater concentrations may be in the range of 1-25 mg L^{-1} states as dissolved organic carbon (DOC) (Suffet and MacCarthy, 1989; Leenheer, 1981; Thurman and Malcolm, 1981). HS are generated with complex sequence reactions. Several hypotheses have been put forward to clarify their synthesis in nature. One of hypotheses proposes that plant biopolymers are changed through decomposition to generate the central core of humic substances and labile macromolecules such as carbohydrates and proteins are degraded and lost during microbial attack, while refractory compounds or biopolymers such as lignin, paraffinic macromolecules, melanins and cutin are selectively converted to form a high molar mass precursor of humin. Further oxidation of these matters produces elevated oxygen content in the form of typical functional groups like carboxylic acids and the

molecules become small enough and hydrophilic enough to be soluble in alkali. Consequently, the molecules become even smaller and sufficiently oxygen-rich to dissolve in both acid and base. This pathway includes degradative theory as following:

| Plant material | → | Humin | → | Humic acid | → | Fulvic acid | → | Small molecule |
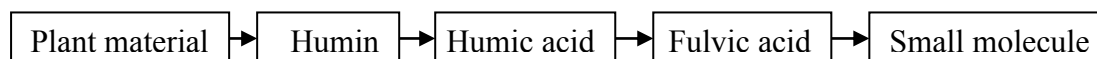
Another hypothesis associated with condensation polymerization proposes that plant biopolymers are initially decomposed to small molecules after which these molecules are repolymerized to generate humic substances. Eventually, fulvic acid would be precursor of humic acid and then of humic. This pathway is the reverse of degradative pathway as following:

| Plant material | → | Small molecule | → | Fulvic acid | → | Humic Acid | → | Humin |
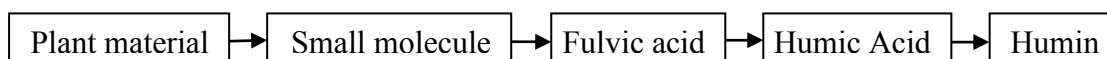
The humic material generated by the humification processes can be taken into account to be intermediate in the overall sequence of degradation and/or resynthesis reactions. However, contrary to many intermediates in chemical reactions fulfilled in the laboratory, humic material is a stable intermediate, particularly under conditions of restricted oxygen availability (vanLoon and Duffy, 2010).

2.1.1.1. Structure and Composition of Humic Substances. Aquatic humic substances exhibit a variety of structural properties such as polar, straw-colored and also they are organic acids stemming from soil and terrestrial and aquatic plants (Thurman and Malcolm, 1981). Humic substances generally include carbon, hydrogen, oxygen and nitrogen within ranges (%) as follows in accordance with various analyses regarding humic substances (Table 2.1).

Table 2.1. Elemental composition of humic substances (vanLoon and Duffy, 2010).

C	O	H	N	Inorganic elements (ash)
45-60	25-45	4-7	2-5	0.5-5

Since the carbon content is frequently closer to 60%, an approximate factor of 1.7 is employed as an estimate to transform mass values from organic carbon (OC) to OM. The carbon content among the three types of HS is known as FA< HA< Humin. The oxygen content of the same set of HS follows the reverse trend. The presence of oxygen and nitrogen in HS indicates that particular functional groups exist in humate molecules.

HS are found in various forms, including free HS, complexed HS and surface-bonded HS in aqueous and terrestrial systems. Free HS comprise soluble or insoluble forms of substances. Complexed HS are chemically connected to metals and other inorganic species such as phosphate or organic molecules. Surface-bonded HS are chemically tied to other solids such as clay minerals or iron and aluminum oxides (vanLoon and Duffy, 2010). HAs are sophisticated substances extracted from natural decomposition of products of plant and animal remainders and also they are substances which are structurally complex, polyelectrolytic, dark-colored, amorphous and high molecular weight organic acids that are existed in soils, sediments and natural waters (Hizal and Apak, 2006). HAs are considered to be complex aromatic macromolecules with amino acids, amino sugars, peptides, fatty acids, microbial cell walls, protoplasmic fractions, aliphatic compounds involved in linkages between the aromatic groups. They cannot be regarded as single chemical entities described by unique, chemically defined molecular structures (Burba et al., 1998; Zhao et al., 2008).

The hypothetical structure for HA as shown in Figure 2.1 consists of side aliphatic chains and a hydrophobic aromatic core that is highly substituted with functional groups such as free "and bound phenolic OH groups, quinone structures, nitrogen and oxygen as bridge units and COOH groups. The model properties both hydrophilic and hydrophobic sites, a highly polyelectrolytic character and several sites potentially available to bind with metal ions, mineral surfaces and organic compounds (Burba et al., 1998). The presence of chemical groups such as carboxylic, phenolic brings about humic acid to predominantly bear negative charges in aqueous solutions (Deng and Bai, 2003). The fundamental structure of HS consists of an aromatic ring of di- or tri-hydroxyl-phenol type bridged by -O-, $-CH_2-$, -NH-, -N=, -S-, and other groups including both free hydroxyl radicals and the double linkages of quinines (C=O) (Liao et al., 2001).
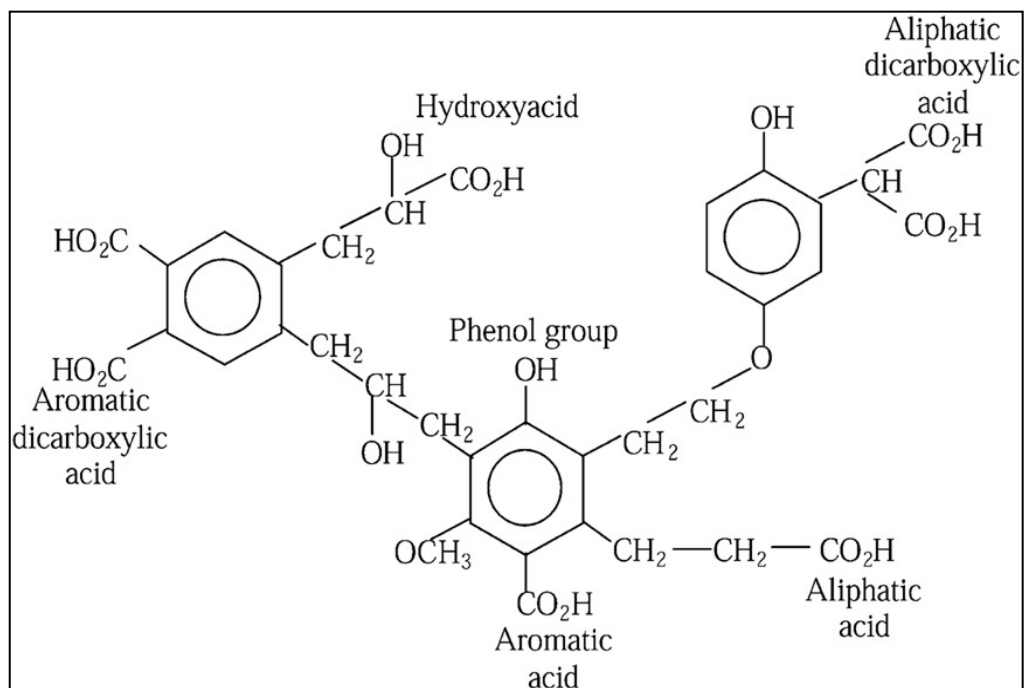
Figure 2.1. Hypothetical molecular structure of humic acid (Duan and Gregory, 2003).

The model structure of fulvic acid as presented in Figure 2.2. consists of both aromatic and aliphatic structures, both extensively substituted with oxygen-containing functional groups. On the other hand, the structures of fulvic acid are more aliphatic and less aromatic than humic acids. The reason for their high solubility in water at all pH values is mainly because of the presence of carboxylic acid, phenolic and ketonic groups in appreciable amounts (MacCarthy, 2001).
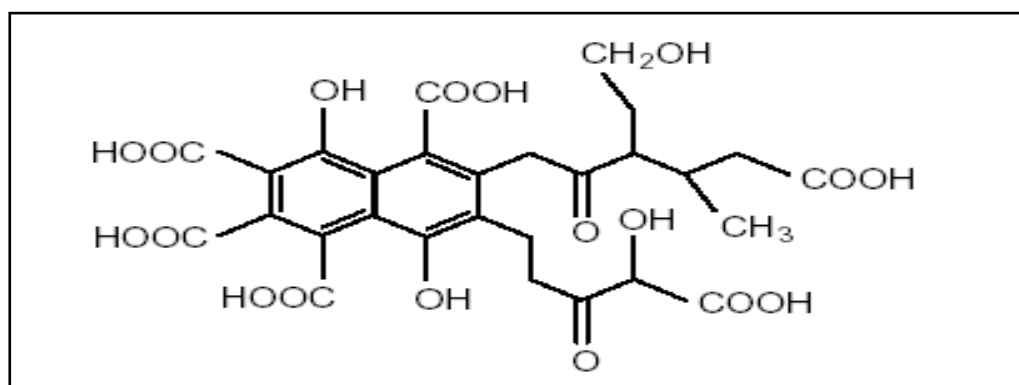
Figure 2.2. Structure of fulvic acid (Buffle, 1988).

Difference between humic acids and fulvic acids can be clarified by variations in molecular weight, the number of functional groups (carboxyl and phenolic OH) and the extent of polymerization. The chemical properties of HS are presented in Figure 2.3. in which it can be seen that carbon and oxygen contents, acidity and degree of polymerization all change systematically with increasing molecular weight. In general, fulvic acids have lower molecular weights than humic acids. It is also known that soil derived humic materials are larger than aquatic humic substances (Gaffney et al., l996).
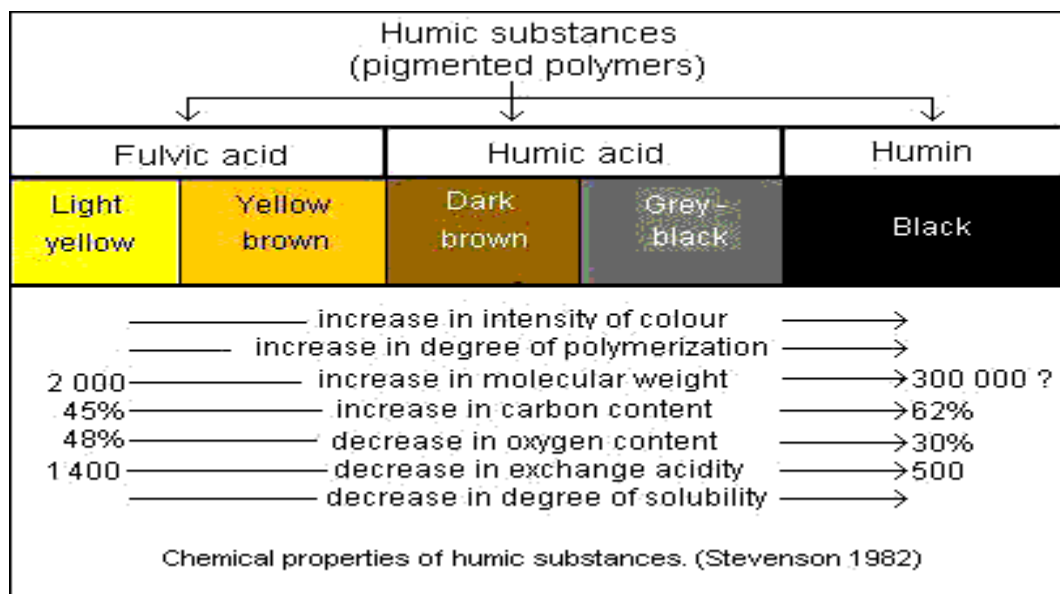
Figure 2.3. Chemical properties of humic substances (Stevenson, 1982).

The structure and composition of humic acids are apparently more complex than those of fulvic acids. The complex polymeric nature and interaction between component chains of humic material make structural analysis difficult; however, compositional information can be occurred from elemental and functional group analysis. The elemental analysis of humic and fulvic acids from a range of soils exhibit that the atomic H/C ratio is so low, and is lower for humic acid than fulvic acid, which is consistent with a higher aromatic content for humic acid. The atomic O/C ratio is also lower for humic acid than fulvic acid, reflecting the higher content of polar groups in fulvic acid. The greater water solubility of fulvic acids contrasted to humic acids can be attributed to the higher content of polar groups, especially carboxyl groups. Among the other functional groups existing in smaller quantities are ether, aldehyde and amine (Burba et al., 1998, Nifant'eva et al. 1999).

The solubility of humic acid exactly implements in powerful basic solution which humic acid is negatively charged and it raises with increasing pH and declines with increasing inert electrolyte concentration (Hizal and Apak, 2006). Contrary to FAs which are soluble pH < 2, HAs are usually precipitated in pH range of 2-3 (Kumpulainen et al., 2008). All of HS can be divided into components in accordance with their solubility in diverse media (Figure 2.4).

```
                    ┌──────────────────────────────┐
                    │   Organic compounds of soil   │
                    └──────────────────────────────┘
                          │                    │
              ┌────────────────┐        ┌──────────────┐
              │ Living organisms│◄───────│  Soil of OM  │
              └────────────────┘        └──────────────┘
                                              │
                                        Alkali precipitation
                          ┌──────────────────────────────┐   ┌──────────────────────────┐
                          │ Alkali-soluble humus fragments │   │ Insoluble residue HUMIN │
                          └──────────────────────────────┘   └──────────────────────────┘
                                  │
                            Acidic precipitation
              ┌──────────────────┐        ┌──────────────────┐
              │ Insoluble residue;│        │  Soluble part;   │
              │   HUMIC ACIDS     │        │  FULVIC ACIDS    │
              └──────────────────┘        └──────────────────┘
```
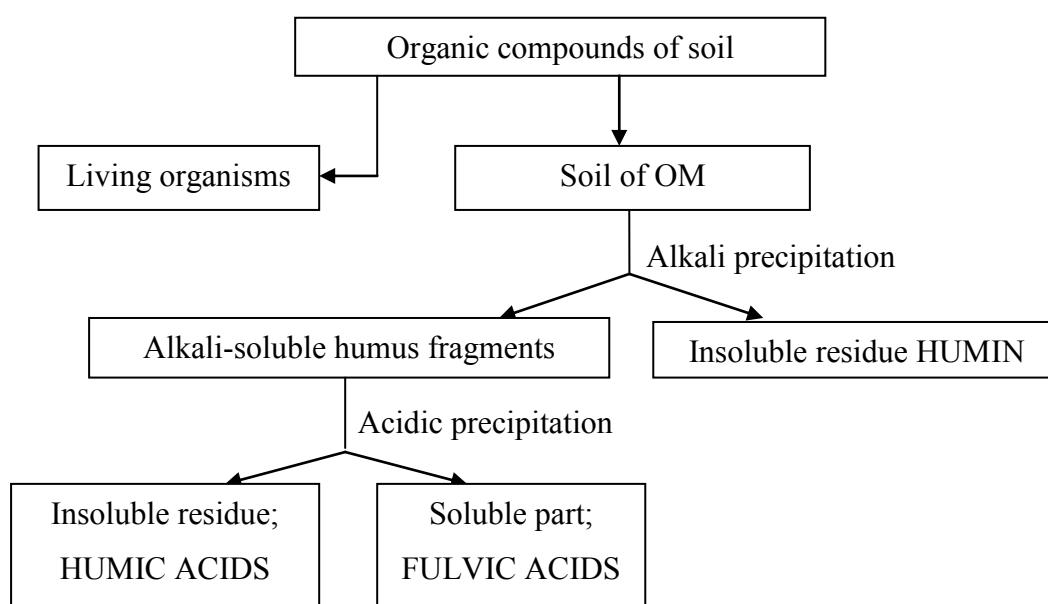
Figure 2.4.   Humic substances in dependence of their solubility (Peña-Méndez et al., 2005).

A better understanding of the macromolecule structure, molecular size distribution, and chemical heterogeneity in relation to molecular size is a prerequisite for the further development of geochemical models including humic and fulvic acids. The most valid discussion for HA fractionation is that many interactions and processes of HA in the environment can be more or less dependent on their molecular size. Among the fractionation methods available, ultrafiltration (UF) using different suitable membrane filters is a reasonably simple method to distinguish polydisperse mixtures of molecules (Burba et al., 1998; Nifant'eva et al., 1999). It is one of the few separation methods functioning without additional separation media and auxiliary reagents, thus avoiding blank substances as interferents. The simple and reliable scale-up of UF from the micro to the macro dimension in commercial UF units, which permits the rapid fractionation of

relatively large quantities of humic acid, is another relevant advantage of this separation method (Nifant'eva et al., 1999). HS can easily act by binding metal ions in water. In drinking water the presence of HS are not desirable situations due to their serious effects on membrane processes (Deng et al., 2003). When the mechanisms of binding of HS to oxide surfaces are considered, they demonstrate strong affinity and also HS are prone to be connected with particulate matter (Avena and Koopal, 1999). HAs play significant role in the arrangement of the transportation, transformation and bioactivity of metal ions (Wang et al., 2008). As a consequence of phenolate and carboxylate ligands, HA constitutes negatively charged complexes with heavy metal ions particularly Fe (III). Many heavy metal ions bind as inner-sphere complexes to the identical type of sites in HS namely the carboxylate and phenolate groups regardless of the type of metal and HA (Hizal and Apak, 2006).

2.1.1.2. Effects of Humic Substances on Treatment Processes and Environment. All over the world water includes NOM consisting of various organics such as HAs, hydrophilic acids, proteins, lipids, hydrocarbons and amino acids due to the interactions among the hydrological cycle and the biosphere and geosphere (Murray and Parsons, 2004). HS form 3-28 % of DOM in effluent waters of wastewater treatment plants. HS emerging with the decay of plant and animal remainders can result in many environmental and health problems such as contributing to bacterial growth in water distribution systems and reacting with chlorine in water treatment to constitute carcinogenic chlorinated organic compounds like THMs. The removal of these substances from wastewater treatment facilities is a very significant subject environmentally. In order to remove HAs from water and wastewater, there have been various methods such as chemical coagulation, membrane separation, ultrafiltration, biodegradation, ion exchange and adsorption, solvent extraction, precipitation and freeze-drying since HA cannot be sufficiently eliminated with conventional treatment procedures used in drinking water systems. HS forming from the end products of plant tissue decomposition are durable to biological oxidation. The best effective technique among these methods mentioned above can be considered as adsorption. Therefore, the adsorption of HS has been extensively explored to diminish their impacts on the adsorption of other components that are desired to remove from aquatic systems (Giasuddin et al., 2007; Moura et al., 2007; Anirudhan et al., 2008; Tang et al., 2012; Portjanskaja et al., 2006; Thurman and Malcolm, 1981).

Some treatment methods such as coagulation and flocculation that use aluminum sulfate or ferrous sulfate and lime in the case of excess chlorine are employed to remove NOM from raw water. The ratio of the removal of NOM with these processes is between 10 and 50 % (Wang et al., 2000). In the conventional treatment technique, the ratio of removal of DOC is 50-80 % by means of coagulation or flocculation processes removing NOM from water by adsorption onto flocs (Murray and Parsons, 2004). The conventional biological, physical and chemical treatment processes, such as coagulation with alum filtration and softening, which are not sufficient for decomposition of heavy metals and toxic organic contaminants, can remove 30 % of HS with high molecular weight (Tseng et al., 2012; Wang et al., 2001).

The problems resulting from humic acids in potable water can be listed as color and taste issues as well as biological instability. HAs send various pollutants including toxic heavy metals and synthetic organic chemicals such as pesticides into water treatment plants and distribution systems by binding them themselves (Lin and Zhan, 2012). Humic substances which are present in landfill leachate should be taken into account due to the high heavy metal and organic toxics (Portjanskaja et al., 2006). HA causes the formation of brown color in water and wastewater and also gives a high biochemical oxygen demand (BOD) load to the liquid waste (Gu et al., 1994). Biological treatment methods that are used to remove heavy metals and organic compounds are confined various physicochemical techniques such as ion-exchange, electron reduction having some problems like the formation of secondary contaminants and requiring a high capital cost. Advanced oxidation processes (AOPs) using highly oxidizing hydroxyl radical in order to decompose organic matters into CO_2 and H_2O are one of the most important methods to solve these problems (Rashed and El-Amin, 2007). AOPs including hydroxyl radical (OH^-) which is generated through chemical, photocatalytic and electro-chemical reactions are more effective techniques used in the removal of organic pollutants from wastewaters than direct chemical oxidation (Rajeswari and Kanmani, 2009). HS compete for adsorption sites with target matters in various treatment methods such as coagulation and activated carbon adsorption. Moreover, they make contribution to the fouling of membranes, constitute soluble groups with heavy metal ions and organic contaminants, and contribute to the formation of bio-film in water distribution pipelines (Liu et al., 2008). The removal of HS from water sources has a great importance due to the fact that they bring about a variety of

problems influencing negatively human health (Uyguner and Bekbolet, 2005a). Waters used in various industries such as laundry, paper and beverages and food industry are not suitable for processes in these industries due to dense color resulting from HS (Portjanskaja et al., 2006). Food processing factories, industrial wastewater streams include low amounts of DOC such as polysaccharides, proteins, amino sugars, nucleic acids, humic and cells. These dissolved matters result in a problem related to the direct reuse of the slightly polluted water without treatment, because of problems related to bacterial growth, odor generation and biofouling on the utility surface (Zhang et al., 2009b). Adverse effects of HS that are present in plants, animals, sediments, soils and waters are the formation of the yellowish-brown color in natural waters and the formation of a complex with metal ions as well as reaction with chlorine in order to generate THMs. Due to these negative effects, HS which are found in drinkable and industrial waters must be decreased (Zhao et al., 2008).

2.1.1.3. Application Areas of Humic Substances.   Agriculture, industry and environment as well as biomedicine are the most significant applications which are present in the use of HS.

Agriculture applications. HS affect considerably the quality and productivity of the soil. HS show a high base exchange capacity, which is important for soil fertility. Currently, humic materials are used as additives in fertilizers.

Industrial applications.   HS employ in the preparation of leather. Firstly, they were used as a leather dye, later on as an agent for tanning leather and, consequently, as an ingredient of a solution to finish leather. The woodworking industry is another area where HS have been used. In the ceramic industry, humic substances were used fundamentally as additives to increase the mechanical strength of unprocessed ceramics, to enhance the casting properties of ceramics. Moreover, HS have found application in the production of plastics, especially as dyes for coloring Nylon 6 or PVC plastics, hardeners of polyurethane foams or as plasticizer ingredients for PVC. HS found numerous applications in the paper industry too.

Environmental applications. Since HS form water-soluble complexes with many metals containing radionuclides, these organic colloids are very important as radionuclide transport agents through the environment. It is known that the existence of HS in natural waters can impact the uptake of radionuclides by natural solids and thus their migration to surface and ground waters. The fundamental task of HS in environmental chemistry is to remove toxic metals, anthropogenic organic chemicals and other pollutants from water. Ion-exchange materials based on calcium humate were found suitable for the removal of such heavy metals as iron, nickel, mercury, and cadmium as well as copper from water and also to remove radioactive elements from water discharges from nuclear power plants. Humus-based filters have been developed for sewage purification, with many applications.

Biomedicine applications. HS produced on a commercial scale are used in veterinary and human medicine. HS protected the organism against cell-wall disruption by the enzyme (Peña-Méndez et al., 2005).

2.2. Titanium Dioxide

TiO_2 is an important adsorbent with regard to the investigation of relationships between the surface charging and adsorption (Tan et al., 2007). In other words, one of the most ideal adsorbents that are used to explore the influence of the surface functional groups on adsorption is TiO_2 (Xu et al., 2012). TiO_2, also expressed as titanium oxide (IV) or titania (molecular weight 79.88), is not soluble in water, chloric acid, nitric acid and ethanol, but it is soluble in concentrated and heated sulfuric, hydrogen fluoride and alkaline media (Clemente et al., 2012).

TiO_2 is a wide band gap semiconductor that has been extensively investigated and applied to a wide spectrum of chemical disciplines. Aside from its excellent pigmentary properties, titanium dioxide, as a chemical has dielectric properties, high ultraviolet absorption and high stability and relative chemical and biological inertness, non-toxicity, high photocatalytic efficiency, relatively inexpensive and commercially available in various crystalline forms as well as strong oxidation activity which allow it to be used in special applications, such as electroceramics, glass, deodorization, sterilization, air purification, anti-fouling and mist removal as well as wastewater treatment (Balzani and

Scandola, 1991; Sayle et al., 1995; Zaleska, 2008a; Sato et al., 2005; Yu et al., 2006; Xekoukoulokatis et al., 2010).

TiO$_2$ powders are constituted by the precipitation of titanium hydroxide (Ti(OH)$_4$) from the hydrolysis of the titanium compounds and the following thermal decomposition of Ti(OH)$_4$ to TiO$_2$ (Kobayakawa et al., 2005). While the production capacity of TiO$_2$ was predicted as 4.6 million tons in 2002, the annual production of that was anticipated as 2000 metric tons in 2005 by USEPA. TiO$_2$ is acquired basically from ore containing ilmenite (FeTiO$_2$), natural rutile (TiO$_2$) and leucoxenelike ilmenite. TiO$_2$ particles are referred as primary, aggregates or agglomerates. Primary particles are individual crystals connected by planes. Aggregates are sintered primary particles bound by their crystal faces. Agglomerates are multiple primary particles and aggregated interconnected by van der Waal forces. The primary reserves of TiO$_2$ are found in Canada, Scandinavia, South Africa, The Mediterranean Sea and Australia (Xiao et al., 2011; Clemente et al., 2012).

Titanium dioxide is found in four crystalline phases: anatase (tetragonal), rutile (tetragonal), brookite (orthorhombic) and TiO$_2$ (B) in nature. Among these, anatase and rutile phases are remarkably preferred as photocatalysts. Rutile has a density of 4.2 mg L^{-1} while anatase has a density of 3.9 mg L^{-1}. This difference is explained by their different crystal structures. The rutile modification is more closely packed than the anatase crystal, where each metal center occupies the center of an octahedron of oxygen ligands, each of which is bound to three metals (Balzani and Scandola, 1991). Anatase form of TiO$_2$ considered as the most reactive phase of TiO$_2$ has a low quantum yield for oxidation steps (≤ 5 %) as a consequence of fast recombination of photogenerated charges. Furthermore, pure anatase can use < 10 % of the terrestrial solar spectrum due to its high band gap (3.2 eV), with rutile form of TiO$_2$ possessing a slightly smaller band gap (3.0 eV), but usually lower activity. Moreover, brookite phase of TiO$_2$ has a band gap of 3.4 eV at room temperature. These differences in band gap correspond to maximal wavelength absorptions ranging from 365 to 413 nm (Rockafellow et al., 2009). Titanium dioxide crystals are shown in Figure 2.5 in accordance with the order of their abundance, rutile, anatase and brookite.
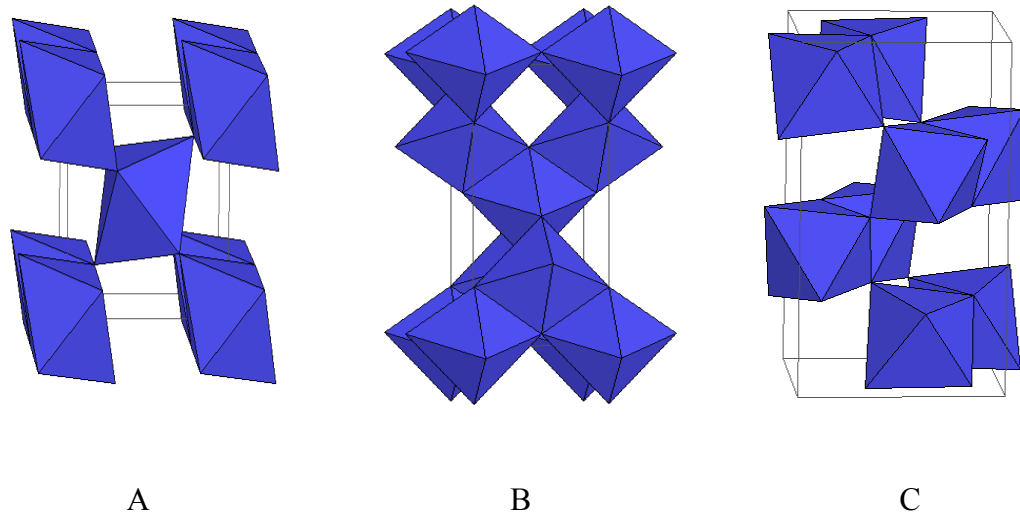
Figure 2.5. The crystal structures of A) rutile, B) anatase, C) brookite (Mansoori et al., 2008).

Anatase phase of TiO_2 is the most preferable material because of some properties, such as its non-toxic structure, large band gap, high stability, low cost and high photosensitivity (Sakthivel et al., 2004; Rajeswari and Kanmani, 2009). On the other hand, anatase phase of TiO_2 absorbs wavelengths in the near-UV region ($\lambda \leq 390$ nm), which is nearly 3 % of the solar spectrum. Therefore, solar energy cannot be sufficiently utilized for photocatalytic disinfection (Yu et al., 2005). As for rutile phase of TiO_2, it is devoid of oxygen at high temperature and low oxygen partial pressure (Sayle et al., 1995). When anatase and rutile phases of TiO_2 are compared, anatase structure generally demonstrates more superior photocatalytic activity than rutile form of TiO_2 demonstrating a narrower band-gap than the former because of its larger surface area (Zhang et al., 2009; Hanaor et al., 2012). Furthermore, anatase phase has a better combination of photoactivity and photostability, while rutile form is not active for the phodegradation of organic compounds (Clemente et al., 2012). Also, rutile phase has a smaller volume and lower energy than anatase phase of TiO_2 (Wang and Lewis, 2006). A semiconductor is divided into two energy regions: the region of lower energy is the valence band (E_v), where the electrons cannot move freely, and the higher region is the conduction band (E_c), where the electrons move freely through the crystal generating electrical conductivity similar to that of metals. These two regions are separated by a band- gap zone. Figure 2.6 exhibits a schematic

representation of a semiconductor particle. The absorption of photons with energy higher than the band-gap energy (E_{bg}) results in the movement of an electron from the E_v to the E_c.
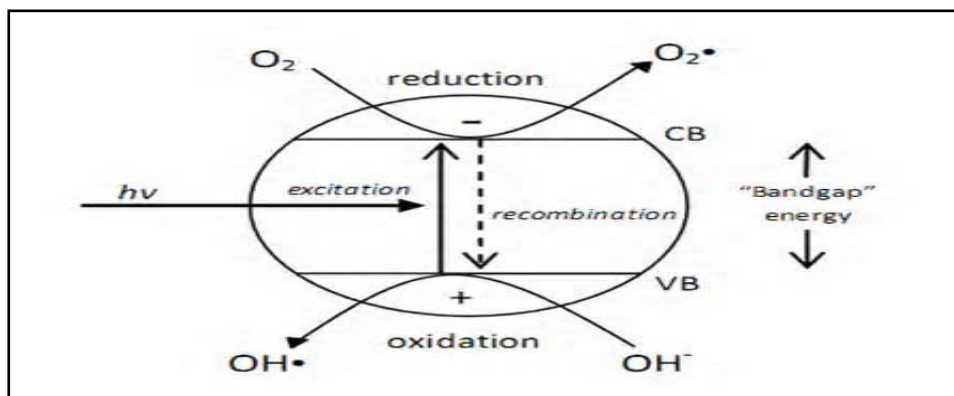
Figure 2.6. Schematic representation of a TiO_2 particle, where VB and CB are the valence band and conduction band, respectively (Clemente et al., 2012).

Valence band holes and conduction band electrons can be generated by irradiation of an aqueous TiO_2 suspension with photons of energy equal to or greater than E_{bg} of the semiconductor ($hv= E_{bg} = 3.2$ eV). Due to this wide E_{bg}, TiO_2 can be merely activated by ultraviolet irradiation of wavelengths below 385 nm, which is a small UV fraction of solar light, approximately 2-3 % (Yu et al., 2006; Ohno et al., 2004a; Xekoukoulokatis et al., 2010). Surface area, porosity and acid-basic properties of titanium dioxide determine its activity (Zaleska, 2008a). The photogenerated valence band holes and conduction band electrons can either recombine to release heat or make their distinct ways to the surface of TiO_2, where they can be trapped at surface sites at which interfacial electron transfer occurs from and to adsorbed species onto the catalyst surface and in the presence of oxygen results in the formation of hydroxyl radicals, $HO^{\cdot}$, and other reactive oxygen species (Xekoukoulokatis et al., 2010; Zaleska, 2008b).

In the presence of water, metal or metalloid oxides are generally enclosed with surface hydroxyl groups. A hydroxylated oxide particle can up to a certain degree be understood as a polymeric oxoacid or -base where surface coordination reactions occur at the oxide-water interface. The pH dependent charge of titanium dioxide stems from proton transfers at the amphoteric-hydrated-surface. Operationally there is a resemblance between H^+ and metal ions (Lewis acids) and OH^- and other bases (Lewis bases).

The OH group on a hydrous oxide surface has a complex-forming O- donor group like an OH$^-$ or an OH group attached to another element. Protons and metal ions compete with each other for the available coordinating sites on the surface. The extent of coordination is related to the exchange of H$^+$ by charged metal ions. Similarly, ligand exchange with coordinating anions leads to a release of OH$^-$ from surface. Because of this Lewis base character of the surface oxide ions of TiO$_2$, which acts as donor surface states, the chemisorption of water at the Ti^{IV} site is likely to be followed by the proton transfer to the - O- site. Two kinds of surface -OH groups are then produced (Boehm, 1971; van Veen, 1989; Süphandag and Bekbölet, 2000). The acidic one has a pK$_a$ value of 2.9, while the remainder behaves as weak acid with a pK$_a$ 12.7 (Boehm, 1971).

$$Ti^{IV} - OH + H^+_{aq} \longleftrightarrow Ti^{IV} - OH_2^+ \qquad Ka_1 \qquad\qquad (2.1)$$

$$Ti^{IV} - OH \longleftrightarrow Ti^{IV} - O^- + H^+_{aq} \qquad Ka_2 \qquad\qquad (2.2)$$

The pH value where the oxide surface bears no fixed charge is expressed as the point of zero charge (pzc) (Süphandag and Bekbölet, 2000).

$$pH_{pzc} = \tfrac{1}{2}\,(\,pK_{a1} + pK_{a2}) \qquad\qquad (2.3)$$

The point of zero charge (pH$_{pzc}$) at neutral pH value provides possibility for the investigation of the sorption efficiency of metal ions on TiO$_2$ over a wide range of pH and ionic strength (Xu et al., 2012). The measurements of surface charge density of titanium dioxide suspension, having the rutile crystal structure, as a function of pH place the point of zero charge (pzc) at pH 5.8 ± 0.1 (Yates and Healy, 1980).

Kind of TiO$_2$ can be cited as bare TiO$_2$ samples in the fundamental polymorphic phases, such as anatase, rutile and brookite as well as TiO$_2$- based samples, doped or loaded with transition or rare earth metal species or sensitized with metal and metal free TiO$_2$ specimens. The use of bare TiO$_2$ samples has some disadvantages including small amount of photons adsorbed in visible region with the consequent need to irradiate with UV light, high recombination rate for the photoproduced electron-hole pairs, difficulty to develop species that work as recombination centers, deactivation in the absence of water vapour observed in gas-solid systems when aromatic molecules must be abated and also

difficulty to support powdered TiO_2 on some materials. (Di Paola et al., 2012). The most outstanding obstacle as to TiO_2 photocatalyst is that it can only benefit from UV light in its photoactivation because of its wide band gap. However, solar light attaining the surface of the earth includes approximately 3 to 5 % UV light (Xekoukoulokatis et al., 2010; Rashed and El-Amin, 2007; Tryba et al., 2009). The ultraviolet region can be identified as zone in which is small from 5 % of the overall solar intensity (Anandan et al., 2008). Some solutions have been found to increase the absorption wavelength range of TiO_2 to the visible region (400 nm $< \lambda <$ 700 nm) without the decrease of photocatalytic activity of TiO_2. One of them is that red shift of the absorption edge of TiO_2 to wavelengths longer than 400 nm can be succeeded by doping TiO_2 with transition metal cations such as chromium, vanadium, iron and nickel into Ti sites in order to increase photocatalysis efficiency. Another solution is to decrease the band gap energy of TiO_2 by doping with non-metallic elements such as carbon, nitrogen and sulfur (Xekoukoulokatis et al., 2010; Tryba et al., 2009; Wang et al., 2009; Nakamura et al., 2004). In addition to these solutions, another solution developed by researchers is that mixed phase TiO_2, which includes anatase-rutile, anatase-brookite, brookite-rutile and anatase-TiO_2 (B). A well known example of mixed phase TiO_2 is the commercial Degussa P-25 material manufactured by Evonik Degussa Crop. (Germany), which consists of approximately 80 % anatase and 20 % rutile phases and also surface area of about 50 m^2/g and average particle size of 30 nm as well as a wide band gap of 3.0 – 3.2 eV corresponding to a wavelength range of 380 nm – 400 nm. (Li et al., 2012; Clemente et al., 2012; Adams and Impellitteri, 2009). This material has higher chemical stability and photocatalytic activity for oxidative degradation than its pure phase counterparts (Li et al., 2012; Clemente et al., 2012; Al-Rasheed and Cardin, 2003).

The benefits of surface modification are: (i) inhibiting recombination by increasing the charge separation and therefore the efficiency of the photocatalytic process; (ii) increasing the wavelength response range (*i.e.* the photocatalyst can be excited in the visible light region); and (iii) changing the selectivity or yield of a particular product (Linsebigler et al., 1995).

It is clear that cationic doping results in the localized d-states deep in the band-gap of TiO_2 generally acting as the recombination centers for photoexcited electrons and holes that cause lower photocatalytic activity (Wang et al., 2009). In recent years, the technique of metal ion-doped into TiO_2 has been widely studied. Noble metals, $e.g.$ Pt, are most commonly studied (Linsebigler et al., 1995; Sakthivel et al., 2004). Other metals, $e.g.$ Au, Pd, and Ru have been reported to be beneficial for photocatalytic reactions (Sakthivel et al., 2004). The transitional metal ions, $e.g.$ Fe (Hoffmann et al., 1995), have been used for increasing the photocatalytic activity. On the other hand, anionic doping causes the p-states near the valence band much like other deep donor levels in semiconductors in order to develop visible-light reactive photocatalysts (Wang et al., 2009; Zhang et al., 2009b).

Anion doped TiO_2 photocatalysts, such as N, S and C doped TiO_2, in anatase form have higher photoresponse, which provides the removal of environmental contaminants, from UV-light to visible light region than conventional TiO_2 (Dong et al., 2009; Ohno et al., 2004a; Li et al., 2005). Nonmetal-ion doped TiO_2 powders are developed in order to benefit from visible light representing approximately 42 % of energy of the solar spectrum. A most significant factor affecting the preparation of nonmetal-ion doped TiO_2 powders is the selection of ion donors such as thiourea and urea, which are potential donors of sulfur, nitrogen and carbon (Sun et al., 2006). Different precursors like titanium tetraisopropoxide, titanium tetraetoxide and titanium tetrabutoxide as well as titanium tetrachloride used in the synthesis of the photocatalysts influence the synthesis parameters (Pap et al., 2012). Anion doped TiO_2 photocatalysts give rise to some problems, such as producing electronic midgap states related to dopants, massive charge carrier recombination and instability of TiO_2 because of the introduction of lattice distortion and bond weakening (Nakamura et al., 2004). To alter the light absorption towards visible light and to enhance the lifetime of the photoproduced electron-hole pairs take place among objectives of the preparation of anion or cation doped TiO_2 powders (Di Paola et al., 2012). TiO_2 powders doped with either anions such as N, S and C or cations result in red-shift the absorption edge of TiO_2 to wavelengths longer than 400 nm and to lower energies. Thus, the overall photonic efficiencies of photoassisted surface redox reactions can be enhanced by developing these photocatalysts that bridge both the UV and the visible irradiation (Serpone, 2006). When the efficiencies of anion-doped TiO_2 and cation-doped TiO_2 are compared, both the absorbance and photocatalytic activity of S cation-doped TiO_2 in the visible region is

higher than those of N-, C- or S-anion doped TiO_2 (Ohno et al., 2004b). However, cationic impurities like transition metals possess some obstacles, such as thermal instability, higher probability to constitute charge carrier recombination centers and expensive synthesis protocols. Therefore, anionic impurities mentioned above are preferred because of their closer position to oxygen in the periodic table (Jagadale et al., 2008).

2.2.1. Anion Doped TiO_2 Specimens

Four diverse anion doped TiO_2 species, Nitrogen-doped TiO_2 (N-doped TiO_2), Carbon-doped TiO_2 (C-doped TiO_2), Sulfur-doped TiO_2 (S-doped TiO_2) and Nitrogen-Sulfur co-doped TiO_2 (N-S co-doped TiO_2), identified in the following section.

2.2.1.1. C-doped TiO_2. Khan and colleagues reported that carbon-doped TiO_2 (C-doped TiO_2) was obtained as a result of a chemical modification of TiO_2 by controlled combustion of titanium metal in a natural gas flame (Khan et al., 2002). Sakthivel and coworkers researched the preparation, photoelectrochemical and photocatalytic properties of C-doped TiO_2 under direct artificial and diffuse natural light. According to diffuse reflection spectra, the new absorption at 400 - 700 nm is stronger for $TiO_2 – C1a$ having a much more carbon content than $TiO_2 – C1b$. In other words, the capacity of absorption from UV-light region to visible-light region is associated with the amount of carbon (Sakthivel and Kisch, 2003a). Xiao and co-workers reported the synthesis of carbon-doped TiO_2 nanoparticles by sol-gel auto-combustion method and characterization by X-ray diffraction (XRD), X-ray photoelectron spectra (XPS), Brunauer-Emmett-Teller method (BET), and UV-vis diffuse reflectance spectroscopy (DRS). DRS demonstrated that C-doped TiO_2 showed clear absorption in the visible light region (Xiao et al., 2008).

A recent study was also carried out to explore the impact of calcination temperature on both photocatalytic activity and ˙OH radical's formation over carbon-doped TiO_2 samples under visible light irradiation and correlate the photocatalytic degradation of methylene blue with ˙OH radicals formed over carbon-doped TiO_2 samples. (Xiao and Ouyang, 2009). Park and co-workers reported the preparation details of C- doped TiO_2 using different synthetic methods and the state of impurity carbons in the TiO_2 lattice.

The carbon dopants had been described either as an anion that replaced oxygen substitutionally in the lattice or as a cation that occupied an interstitial lattice site. The formal oxidation state of carbon dopants ranges from -4 (as carbides with Ti-C bond) to +4 (as carbonates with C-O bond). Ti-C bond was constituted at conditions like flame pyrolysis of Ti metal sheet, annealing of TiC powders, and ion-assisted electron beam evaporation. On the other hand, C-O bond (carbonate) was often observed at conditions like sol-gel processes with carbon precursors and high temperature reactions of TiO_2 with carbon precursors. The existence of the former or the latter state reported to be strongly dependent on the preparation method and condition. Both carbon states might be even co-present related to the preparation condition. Although carbon is a ubiquitous impurity, the addition of external carbon precursors (*e.g.,* alkylammonium, urea, glucose) was essentially needed to make C- TiO_2 in all reported cases. However, park and coworkers prepared C-doped TiO_2 with a conventional sol-gel synthesis without using external carbon precursors (Park et al., 2009).

2.2.1.2. N-doped TiO_2. Nitrogen-doped TiO_2 can be cited as an example of a nonmetal doped of TiO_2. The photocatalytic activity and hydrophilicity of TiO_2 have been increasing by nitrogen doped into the substitutional sites of TiO_2 ($TiO_{2-x}N_x$) because of the fact that the band gap of TiO_2 can be narrowed by these elements doping. Therefore, the absorption edge of TiO_2 moves the visible-light region (Yu et al., 2006). In the present paper, the band structure of the $TiO_{2-x}N_x$ with small values of x (< 0.02) was experimentally investigated by comparing the quantum efficiency of decomposing gaseous 2-proponal under the same adsorbed photon number of vis or UV light. Regardless of the x value, the quantum yield values from irradiating with vis-light was lower than with UV-light, which suggests that the isolated narrow band formed above the valance band is responsible for the vis light response in the present N-doped TiO_2 (Irie et al., 2003). Nitrogen doped TiO_2 (N-doped TiO_2) can be handled as an influential way in the degradation of a variety of environmental contaminants due to its contribution to enhancement of photocatalytic activity of TiO_2. Thanks to hybridization of the N 2p states with O 2p states on the top of the valance band or the creation of a N-induced midgap level just above the O 2p valance band maximum, the decrease of the band gap leads to improve the photocatalytic activity of N-doped TiO_2. However, recent electronic structure calculations indicated that occupied N2p localized states appeared slightly above the valence band edge (Dong et al., 2009; Michalow et al.,

2009; Šojić et al., 2010). The photocatalytic activity demonstrates the increase with the decrease of doped N atoms in O site, while diminishing with the decrease of the other sites (Nosaka et al., 2005). Photocatalytic oxidation of organic substances on N-doped TiO_2 under visible light fundamentally increased by means of reactions with surface intermediates of water oxidation or oxygen reduction, not by direct reactions with holes trapped at the N-induced midgap level (Nakamura et al., 2004). The increase of the photocatalytic activity of TiO_2 in visible light region and the success in nitrogen doping presents major opportunities for many applications, such as oxidation of CO, ethanol, gaseous 2-propanal, acetaldehyde, NO_x and the decomposition of dyes like methylene blue (Cong et al., 2007a; Cong et al., 2007b).

There are two main theories exist explaining the mechanism of the response of N-doped TiO_2 in the visible light region: a mixing of 2p states in the doped nitrogen species with the O 2p states (Asahi et al., 2001) and the existence of an isolated N 2p narrow band lying above the O 2p valence band (Hoshimoto, et al., 2003). Hoshimoto and co-workers reported that the visible-light-induced hydrophilicity and photocatalytic degradation of gaseous 2-proponal on N-doped TiO_2. They found that lattice oxygen sites were substituted by nitrogen atoms and formed an isolated narrow band above the valance band and narrowed the band gap. The mechanism of the response of N-doped TiO_2 in the visible light region can be based on various factors, which influence the photocatalytic activity of TiO_2, such as oxygen vacancy, paramagnetic nitrogen species like NO, NO_2, NO_2^{2-}, NO^{2-} and also atomic nitrogen (Joung et al., 2006). The main mechanism of the visible light response in N-doped TiO_2 as well the other anion doped photocatalysts were attributed to the formation of color centers associated with the oxygen vacancies created during the doping. On the other hand, contrary opinions exist about whether substitutional or interstitial N-doping is more effective for the visible light activity of the samples (Kuznetsov and Serpone, 2006; Serpone, 2006).

Asahi and co-workers calculated electron densities of the substitutional N doping, interstitial N doping and mixed type states in an eight unit TiO_2 cell of anatase. They found that the substitutional N doped TiO_2 N 2p band overlapped with the O 2s state and thus concluded that the bands mixed. Hashimoto et al. the other hand believed that nitrogen doping formed a unique band above the valence band. He based this assertion on data

acquired from the mineralization of isopropyl alcohol. When isopropyl alcohol was exposed to dope titania under UV light, the quantum yield was higher than when exposed to visible light. Hashimoto concluded that this trend is plausible only if two distinct bands existed, as irradiation with UV light would cause excitation from both bands while visible light could only excite the higher lying band. He argued that this effect would not be seen if the N 2p band overlapped with the valence band of the TiO_2, forming a single, higher lying band. Pioneering work carried out on the modification of TiO_2 with N extended the use of adsorption region from UV to the visible area (Sato, 1986). Sato first prepared N-doped TiO_2 as a visible photocatalyst that has visible response ability. Later in 2001, Asahi and coworkers reported the synthesis of films and powders of N-doped TiO_2 (Asahi et al., 2001). Since then, nitrogen doping of TiO_2 received worldwide attention concerning the properties and application of these second generation photocatalysts (Di Paola et al., 2012). Asahi and co-workers reported that nitrogen doping causes the formation of a delocalized mixing between the O 2p and N 2p orbitals resulting in an increase in the valance band. They also reported that nitrogen atoms substituted the lattice oxygen sites and narrowed the band gap by mixing the N 2p and O 2p sites. Moreover, Asahi and co-workers found that N-doped TiO_2 alters the absorption edge of TiO_2 in $TiO_{2-x}N_x$ specimens to decrease energies and contributes to enhance photoactivity with a narrowing of the TiO_2 band gap (Asahi et al, 2001). Besides wet impregnation methods, N-doped TiO_2 samples have been obtained by a variety of techniques such as sputtering of TiO_2 in a N_2-Ar atmosphere, high-temperature exposure of TiO_2 to NH_3, hydrolysis of organic and inorganic titanium(IV) compounds such as titanium tetraisopropoxide, titanium butoxide, $Ti(SO_4)_2$, $TiOSO_4$, $TiCl_3$ and $TiCl_4$ with aqueous ammonia or ammonium salts. Sol-gel syntheses were usually followed by calcination of the resulting materials and the heating of TiO_2 powders with urea.

Nitrogen-doped TiO_2 photocatalysts have been applied to test the degradation of various compounds in aqueous medium *e.g.* dyes, organic compounds, volatile substances, pesticides, and organic groundwater pollutants under UV and visible light illumination (Liu et al., 2005; Wang et al., 2005; Zhang et al., 2011; Kobayakawa et al., 2005; Dong et al., 2009). In most of the studies, the photoactivity was tested by using model dye compounds that also absorb in the visible region. N-doped TiO_2 specimens have also been applied in air purification studies.

Wang and co-workers investigated the structures and the photocatalytic activity of N-doped TiO_2 under a variety of irradiation circumstances. They attained that the photocatalytic activity of the N-doped TiO_2 with anatase phases was higher than that of the commercial TiO_2 photocatalyst Degussa P-25 for phenol decomposition under visible light region but Degussa P-25 demonstrated a higher photocatalytic activity under solar region (Wang et al., 2005). Sathish and co-workers developed a simple and novel chemical preparation technique for N-doped TiO_2 and also the photocatalytic activity of N-doped TiO_2 in the degradation of methylene blue under both UV and visible irradiation was investigated. The results showed that N-doped TiO_2 has higher activity than Degussa P-25 TiO_2 photocatalyst in the visible region (Sathish et al., 2005).

Sakthivel and Kisch reported that the preparation of N-doped anatase powders, their photocatalytic characteristics, and their photochemical properties by the visible-light decomposition of aqueous 4-chlorophenol and gaseous acetaldehyde, benzene and carbon monoxide (Sakthivel and Kisch, 2003b). The studies related to the synthesis of the novel doped photocatalysts also covered the characterization of TiO_2 by various techniques such as X-ray diffraction (XRD), high-resolution transmission electron microscopy (HRTEM), transmission electron microscopy (TEM), UV-vis diffuse reflectance spectra (DRS), scanning electron microscopy (SEM), and X-ray photoelectron spectroscopy (XPS) as well as photoluminescence (PL) (Dong et al., 2009).

2.2.1.3. S-doped TiO_2. Sulfur anion-doping where a site of O^{2-} is substituted by an S anion and S cation-doping in which a site of Ti^{4+} is substituted by an S cation are two potential substitutional doping ways in order to dope TiO_2 photocatalyst with sulfur (Yang et al., 2007). The presence of anionic S^{2-} and cationic S^{4+}/S^{6+} species were experimentally identified on sulfur doped TiO_2, depending on the preparation circumstances and the sulfur precursor. This behavior can be qualitatively rationalized by the low solubility of S^{2-} ions in the titania lattice due to the relatively larger ionic radius of S^{2-} compared to that of O^{2-} and the contaminant increase of the Ti-S band formation energy. Recently, sulfuric acid and/or sulfate precursors, mainly ammonium sulfate $(NH_4)_2SO_4$, have been used as sulfur sources for the preparation of S doped TiO_2 (Han et al., 2011). For the preparation of S-doped TiO_2 can be used two diverse methods. One of them includes annealing titanium disulfide at 500 ^0C for 90 min. Another one is titanium tetraisopropoxide is mixed with thiourea in ethanol solution and followed by evaporation of ethanol under diminished

pressure and calcination at 500 ^{0}C (Sakthivel et al., 2004). When titanium dioxide dopes with sulfur, it cause to decrease its band gap and to change its optical response to e visible-light region (Yu et al., 2006). S-doped TiO_2 using titanium isopropoxide and thiourea was synthesized by Ohno and co-workers in. Ohno and co-workers reported that S atoms were incorporated as cations and were expected to be replaced by Ti ions. Furthermore, the prepared S cation-doped TiO_2 powder was reported to absorb visible light more strongly than N, C and the S anion-doped TiO_2 powders (Ohno et al, 2004a). Recently, Umebayashi and co-workers have succeeded in synthesizing TiO_2 doped with S anions (Umebayashi et al., 2002; Umebayashi et al., 2003).

Umebayashi and co-workers reported that TiO_2 doped with S was obtained by oxidation annealing of titanium disulfide (TiS_2). TiS_2 turned into anatase TiO_2 when annealed at 600 ^{0}C in accordance with X-ray diffraction measurements. The residual S atoms occupied O atom sites in TiO_2 to constitute Ti-S bands. The S doping resulted in the absorption edge of TiO_2 to be changed into the lower energy region. S-doped TiO_2 was used for visible light photocatalytic decomposition of methylene blue. They found that sulfur was doped as an anion and replaced the lattice oxygen in TiO_2 (Umebayashi et al., 2002). S-doped TiO_2 Degussa P-25 was prepared by ball-milling with thiourea and then annealing at 400 and 600 ^{0}C during 30 min or 2 h under vacuum atmospheres by Rengifo-Herrera and co-workers (Rengifo-Herrera et al., 2009).

Followed by characterization studies performed by XRD patterns, DRS, and XPS. The photocatalytic activity under visible light was examined by using a model compound, methylene blue. Rockafellow and co-workers reported an investigation of S- TiO_2 prepared in two ways - a conventional sol-gel preparation and a modification of existing TiO_2 by annealing with SB - and an evaluation of the chemical reactivity of these catalysts in the UV and visible ranges (Rockafellow et al., 2009). As chemical probes, three aromatic molecules with considerably different adsorption modes and modes of reactivity were employed. Hussain and colleagues reported the preparation of sulfur doped anatase TiO_2 nanoparticles (3 nm-12 nm) by the reaction of titanium tetra chloride, water and sulfuric acid with addition of 3M NaOH at room temperature. The electro-optical and photocatalytic properties of the synthesized sulfur doped TiO_2 nanoparticles were determined along with Degussa commercial TiO_2 particles (24 nm). The results showed that band gap of TiO_2 particles decreased from 3.31 to 3.25 eV and for that of commercial

TiO$_2$ to 3.2 eV when the particle sizes increased from 3 nm to 12 nm with increase in sulfur doping. The results of the photocatalytic activity under UV and sun radiation exhibited maximum phenol conversion at the particle size of 4 nm at 4.80 % S-doping (Hussain et al., 2009).

2.2.1.4. N-S co-doped TiO$_2$. Nitrogen-sulfur co-doped TiO$_2$ powders have a high photocatalytic activity under visible light region because of the consequences of the synergetic influences of strong absorption in the UV-vis light region, red shift in the adsorption edge, good crystallization, large surface area and two phase structures of undoped TiO$_2$ and N-S co-doped TiO$_2$ (Zhang et al., 2009a; Yu et al., 2006; Ksibi, et al., 2008; Xiao, et al, 2011). Zhang and co-workers prepared a facile one-step sol-gel method by employing tetrabutyltitanate and thiourea as precursors to synthesize N-S co-doped TiO$_2$ nanomaterials. The visible-light photocatalytic degradation of methylene blue reached the highest value. XRD, XPS and DRS measurements exhibited that the synergetic impact of N-S co-doped TiO$_2$ can cause the high visible-light photocatalytic activity of the doped TiO$_2$ (Zhang et al., 2009a).

The N-S co-doped TiO$_2$ was achieved by hydrolysis of titanium (disopropoxide) bis (2,4-pentadionate) in a mixed N-S-containing ligands solutions such as methyldibenzothiophene, urea, ammonia and thiourea. Komai and co-workers successfully immobilized N-S co-doped TiO$_2$ photocatalysts on the surface of plasma-nitrided pure Ti substrate by anodic oxidation in a sulfuric acid electrolyte and their photocatalytic activities were evaluated by using methylene blue aqueous solution under visible light illumination. It was reported that N-S codoping in the anodic TiO$_2$ narrows the band gap of pristine TiO$_2$ and improves the photocatalytic activity under visible light illumination (Komai et al., 2011).

Cinar and colleagues have been investigating the role of doping on TiO$_2$ (Gurkan et al., 2012; Hatipoglu et al., 2010; Yalcin et al., 2010). The research group reported the synthesis conditions and characterization of various doped TiO$_2$ specimens covering metal dopants as well as anion doped photocatalysts and explained the photocatalytic degradation mechanism by DFT calculations (Kasapbasi and Cinar, 2011; Sever et al., 2010; Yalcin Gurkan and Cinar, 2010a; Yalcin Gurkan and Cinar , 2010b; Yalcin et al., 2008a; Yalcin et al., 2008b; Yalcin et al., 2009a; Yalcin et al., 2009b; Yalcin et al., 2009c).

2.3. Adsorption

Adsorption is a process that occurs when a gas or liquid solute accumulates on the surface of a solid or a liquid (adsorbent), forming a molecular or atomic film (the adsorbate) (Weber, 1972). The process can occur at an interface between any two phases, such as, liquid-liquid, gas-liquid, gas-solid, or liquid-solid interfaces. The material being concentrated or adsorbed is the adsorbate, and the adsorbing phase is termed the adsorbent. Adsorption can be classified as physical adsorption, chemical adsorption, and exchange adsorption. In the physical adsorption which is relatively nonspecific there are weak forces of attraction or van der Waals forces between molecules and it is reversible. It is predominant at low temperature, and is characterized by a relatively low energy of adsorption while adsorbed molecule is free to move about over the adsorbent surface. In the chemical adsorption, adsorbed molecules form a layer on the surface. In chemical adsorption, there are much stronger forces between the molecules, so it is rarely reversible. Exchange adsorption refers to electrical attraction between the molecules because of opposite charge on the surface. Chemical adsorption is rarely reversible; hence, in order to remove the adsorbed materials, the adsorbent must be heated to higher temperatures. Electrical attraction between the adsorbate and the surface is classified as exchange adsorption.

Because of large surface areas per unit weight, most common industrial adsorbents are activated carbon, silica gel, and alumina. Adsorption is directly related with surface area of the absorbent, pore size distribution, as well as the properties of the adsorbate, such as water solubility, ionic charge, functional groups, pKa, polarity, functionality, molecular weight and size. Adsorbent particle size is also important because it fixes the time required for transport within the pore to available adsorption sites (Snoeyink and Summers, 1999; Deng and Bai, 2003; Soto et al., 2011). Large specific surface area and advancement of surface charge are also properties influencing adsorption capacity (Kumpulainen et al., 2008). In addition to these properties, acidity, hydrophobicity and molecular weight are factors affecting the adsorption of humic substances to sediment surfaces (Marshall et al., 1998). Diminishing pH and enhancing salt concentration can result in an increase in the adsorption of humic acid on positively charged minerals (Vermeer et al., 1998).

Major factors that affect the adsorption are pH and temperature. Generally, adsorption is increased at pH ranges where the species have no any charge. Many organics form negative ions at high pH, positive ions at low pH, and neutral species in intermediate pH ranges. Moreover, pH affects the charge on the surface, altering its ability to adsorb materials. Many organic pollutants in water are highly adsorbed by decreasing pH because of neutralization of negative charges at the carbon surface with increasing hydrogen concentration. When temperature is increased the adsorption extent decreases because adsorption reactions are exothermic. Since temperature effects on adsorption are important, measurements are usually carried out at a constant temperature effects on adsorption are important, measurements are usually carried out at a constant temperature so graphs of the data are called isotherm. The total amount of heat evolved in the adsorption of a definite quantity of solute on an adsorbent is termed the heat of adsorption, which is the change in the heat content of the system when adsorption occurs. Heats of gas-phase adsorption generally are several kcal per mole, but because water is desorbed from the surface when adsorption from aqueous solution occurs, heat effects for the latter process are somewhat smaller than those for gas-phase adsorption (Weber, 1972).

Adsorption is a more preferable method than alternative techniques to remove substances which cannot biologically decompose and to distinguish selected compounds from dilute solutions because of its relative simplicity of design, operation and scale up, high capacity and favorable rate, insensitivity to toxic substances, ease of regeneration and low cost (Soto et al., 2011; Rafatullah et al., 2010; Leenheer, 1981). Adsorption of molecules onto a surface can be clarified with a chemical reaction:

$$A + B \longleftrightarrow A \times B \tag{2.4}$$

Where A is the adsorbate , B is the adsorbent, and A.B is the adsorbed compound. Adsorbate is accumulated on the surface by a variety of types of chemical forces such as hydrogen bonds, dipole-dipole interactions, and van der Waals forces (Snoeyink and Summers, 1999). Adsorption of NOM has been observed during generation of surface complexes and ligand exchange reactions. Because of alterations of chemical and physical properties, different fractions of NOM demonstrate diverse adsorption properties (Kumpulainen et al., 2008).

The adsorption of molecules onto a surface is an essential prerequisite to any surface mediated chemical process. Hence, the mechanism of binding of humic acids to TiO_2 surface has to be handled to develop the understanding of photocatalytic degradation (Bekbolet et al., 2002). The adsorption of humic acid onto mineral surfaces can result in increased electrostatic and steric stabilization of particles thanks to adsorbed layer of greatly charged and macromolecular organic matter. Particles do not accumulate thanks to the negatively charged HA layer on the mineral surface due to electrostatic repulsion (Illés and Tombácz, 2006). The interaction mechanisms of NOM with nano-TiO_2 have been fundamentally made contribution to six categories including anion exchange, ligand exchange, hydrophobic interaction, entropic effect, hydrogen bonding and cation bridging. Interaction of nano-TiO_2 with HA cause two contrary impacts on the sorption of toxic matters. It might improve the available adsorption probability because of smaller aggregation sizes and better dispersion of nanoparticles in the presence of HA or it might diminish the available adsorption sites owing to competition and drawback by adsorbed HA fractions (Chen et al., 2012).

Activated carbon, ion exchange resins, adsorbent resins, metal oxides, hydroxides, carbonates, activated alumina, clays are important adsorbents used in water treatment (Snoeyink and Summers, 1999). Moreover, the adsorbents consist of agriculture waste (sugarcane bagasse pith), industrial waste products (fly ash and red mud) and natural organic products (algae) as well as natural inorganic matters. While some natural inorganic matters such as bentonite, gypsum, perlite, zeolite and kaolin are used to remove dyes from aquatic environments, natural substances, such as clays and siliceous materials are preferred for waste water treatment due to their high abundance availability and low cost (Awala and El Jamal, 2011).

2.3.1. Adsorption Equilibrium

Assessment of adsorption kinetics is an important criterion in evaluating the adsorption equilibrium condition. Therefore, adsorption kinetics should be determined experimentally to derive the equilibrium time at which no change in concentration of the substrate could be detected. If the reaction is reversible, it is at a critical time that the rate of the forward reaction (adsorption) equals the rate of the reverse reaction (desorption). When this condition is present, equilibrium has been attained and no further change in the

concentration of the reactants and products will occur. At this moment, both reactions continue on taking place simultaneously and there is a defined distribution of solute between the solid and the liquid phase.

In case of high molecular weight organic solutes such as humic acids, equilibrium may take place in longer time periods. The slow reaching of equilibrium during adsorption can be attributed to the fact that humic acids naturally have heterogeneous structure; particular humic acid sub-fractions might exhibit more capacity for adsorbing at the surface than others (Marshall et al., 1998). Adsorption equilibrium data are employed in the determination of adsorption capacity of a system and obtained adsorption equilibrium results are fitted to an isotherm model such as Freundlich, Langmuir and Redlich- Peterson isotherms which are extensively preferred in contrast to other isotherm models (Lin and Juang, 2009).

2.3.2. Adsorption Isotherm

The constant temperature equilibrium relationship between the quantity of adsorbate per unit of adsorbent q_A and its equilibrium solution concentration C_e is called the adsorption isotherm (Snoeyink and Summers, 1999). Adsorption isotherms relate the adsorbate or solute concentration in the bulk liquid to the concentration of the adsorbent on the solid phase at equilibrium. These isotherms are used in the design of adsorption beds and in determining the transport of solutes through them. Several equations or models are available that describe this function (Sontheimer, et al., 1988). Adsorption isotherms for solutes in dilute solution can be listed according to initial slope (Giles et al., 1960, 1974a, 1974b). It has been shown that different solutes show different behavior on the adsorbent (Weber, 1972). Hence, their adsorption isotherms can be termed according to their shapes resembling the letters, such as "L" type, "S" type, "C" type, "H" type (Giles et al., 1960). The type of the isotherm distinctly explains the prevailing adsorption mechanism. Adsorption isotherms of solutes (presented as adsorbed amount (Q) vs concentration in solution (C)), which are divided to four main classes are shown in Figure 2.7.
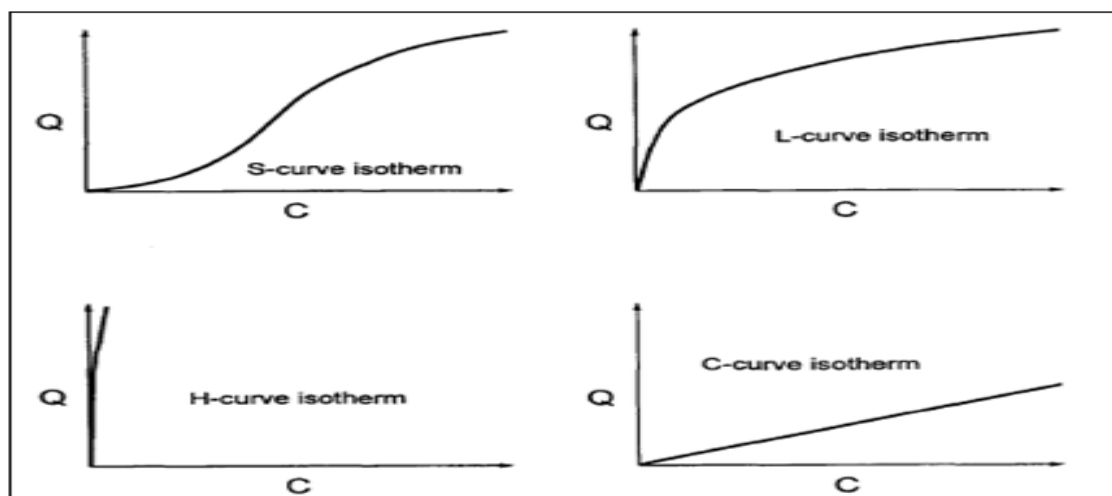
Figure 2.7. The four main classes of adsorption isotherm (Sposito, 1989).

The L-curve isotherm is the normal or Langmuir isotherm and it is generally indicative of molecules adsorbed flat on the surface, or sometimes, of vertically oriented adsorbed ions with particularly strong intermolecular attraction. In the L curve, the initial curvature exhibits that as more sites in the substrate are filled, it becomes increasingly difficult for a bombarding solute molecule to find a vacant site available. This expresses either that the adsorbed solute molecule is not vertically oriented or that there is no strong competition from the solvent. L-curve isotherm which typically concave to the concentration axis, is generally characterized by an initial slope that does not increase with the concentration of adsorptive in the solution. This type of isotherm is the resultant effect of a high relative affinity of the adsorbent particles for the adsorbate at low concentration. In addition, as the concentration of the adsorbate rises, the amount of the remaining adsorbing surface is decreased.

The S-curve isotherm indicates vertical orientation of adsorbed molecules at the surface. In the S-curve isotherm, the initial direction of curvature demonstrates that adsorption becomes easier as concentration increases. The S-curve isotherm generally occurs when three terms are carried out. These three conditions include that the solute molecule is monofunctional, it has moderate intermolecular attraction and it meets strong competition. The S-curve isotherm is characterized by initially small slope that proceeds with adsorptive concentration. This signifies that the affinity of the adsorbent for the adsorbate is less than that of the aqueous solution. It may also suppose the presence of

cooperative interactions such that increasing surface coverage increases the solute's affinity for the surface. The S-curve isotherm is the result of cooperative interactions among the adsorbed molecules. These interactions result in the adsorbate to become stabilized on a solid surface and, thus produce a developed affinity of the surface for the adsorbate as its concentration increases.

The C-curve isotherm is known as constant partition or linear curves. This is characterized by the fixed partition of solute between solution and substrate, right up to the maximum possible adsorption, in which an abrupt alteration to a horizontal plateau happens. The C-curve isotherm is obtained for the partition of a solute between two immiscible solvents. The circumstances supporting the C curve can be listed as a porous substrate with flexible molecules and regions of differing degrees of crystallinity and also higher affinity for the substrate than the solvent.

The H-curve isotherm is an extreme version of the L-curve isotherm and in the H-curve isotherm, the solute has high affinity that in dilute solutions it is completely adsorbed, or at least there is no measurable amount remaining in solution. The initial part of the isotherm is therefore vertical (Giles et al., 1960).

Equations preferred to explain the experimental isotherm data were developed by Freundlich, Langmuir, and Brunauer, Emmet, and Teller (BET isotherm) (Tchobanoglous et al., 2003).

2.3.2.1. Linear Model.   If the accumulation of solute on the adsorbent is directly proportional to the solution phase concentration, linear model can be employed.

$$C_s = K_d \cdot C_e \tag{2.5}$$

Where, K_d shows the distribution coefficient and also named as partition coefficient, C_e is the concentration of adsorbate remaining in the solution at equilibrium. Moreover, C_s stands for the mass of contaminant adsorbed per unit weight of the adsorbent.

2.3.2.2. Langmuir Isotherm. The Langmuir isotherm was developed several assumptions that the sorption for each molecule is independent of surface coverage and adsorbate and solvent molecules compete to adsorb on sites on the surface of the powder as well as adsorption is reversible (Weber, 1972; Tchobanoglous et al., 2003). Equilibrium is reached when the rate of adsorption of molecules onto the surface is the same as the rate of desorption of molecules from the surface (Tchobanoglous et al., 2003). The Langmuir relation assumes that maximum adsorption corresponds to a saturated monolayer of solute molecules on the adsorbent surface, that the energy of adsorption is constant, and that there is no transmigration of adsorbate in the plane of the surface. In other words, adsorption is limited to monolayer coverage. Therefore, the quantity adsorbed reaches the maximum quantity absorbable when all sites are occupied.

The Langmuir equation has the form,

$$q_A = \frac{q_m K_a C_e}{1 + K_a C_e} \qquad (2.6)$$

Where, q_A stands for the mass of the contaminant adsorbed per unit weight of the adsorbent. K_a represents an empirical constant, which is called the binding constant. C_e is the concentration of adsorbate in solution at equilibrium. q_m is the maximum quantity adsorbable when all the adsorption sites are occupied. The experimentally found values of q_m and K_a often are not constant over the concentration range of interest, possibly because of the heterogeneous nature of the adsorbent surface (a homogeneous surface was assumed in the model development), lateral interactions between adsorbed molecules (Weber, 1972).

2.3.2.3. Freundlich Isotherm. Freundlich isotherm is preferred more frequently than the Langmuir to explain adsorbate adsorbent equilibrium (Hendricks, 2006). Freundlich isotherm is a non-linear adsorption equilibrium model expressing the adsorption occurrences on heterogeneous surfaces including diverse adsorption sites with adsorption on each site following Langmuir isotherm. The equation does not imply any particular mechanism of adsorption, it is purely empirical, and has been found to be most suitable in the low concentration range (vanLoon and Duffy, 2010).

The Freundlich equation has the form

$$q_A = K_f \cdot C_e^{1/n} \qquad (2.7)$$

Where, C_e (with units of mass/volume, or moles/volume) is the concentration of adsorbate remaining in solution at equilibrium, q_A (with units of mass adsorbate/mass adsorbent, or mole adsorbate/mole adsorbent) expresses the mass of contaminant adsorbed per unit weight of the adsorbent. K_f and $1/n$ are system defined constants deduced from the experimental data. The terms $1/n$ is a constant for a given system; $1/n$ is unitless and it is a function of the strength of adsorption that the rate of the adsorption increase with solute concentration. K_f is also a constant in the Freundlich equation and it is related fundamentally to the capacity of the adsorbent for the adsorbate. The units of K_f are determined by the units of q_A and C_e (Snoeyink and Summers, 1999). Freundlich isotherm means the equilibrium on heterogeneous surfaces, while adsorption carries out on a homogeneous surface with no interaction between adsorbed molecules in the Langmuir isotherm (Lin and Juang, 2009; Wan Ngah et al., 2008). Logarithmic form of the Freundlich equation is expressed as;

$$\log q_A = \log K_f + \frac{1}{n} \log C_e \qquad (2.8)$$

The parameter K_f in Freundlich equation is associated with the capacity of the adsorbent for the adsorbate. For constant values of K_f and C_e, the smaller the value of $1/n$, the stronger is the adsorption bond. As $1/n$ becomes very small, the capacity tends to be independent of C_e and the isotherm plot approaches the horizontal level; the value of q_A then is essentially constant, and the isotherm is termed irreversible. If the value of $1/n$ is large, the adsorption bond is weak, and the value of q_A changes noticeably with small changes in C_e (Snoeyink and Summers, 1999).
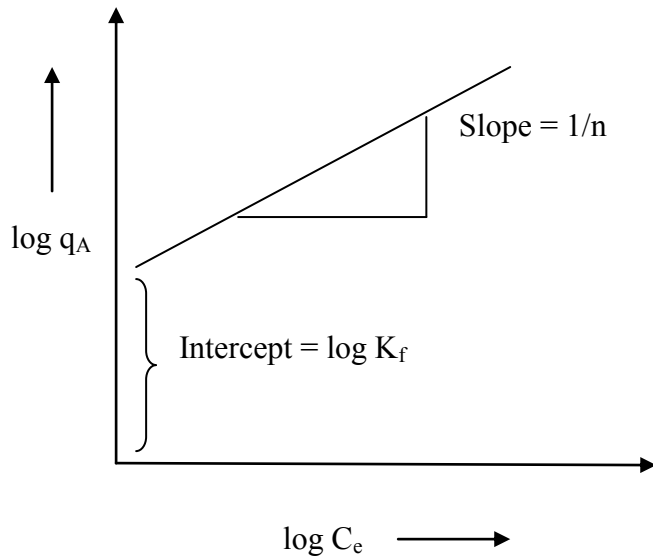
Figure 2.8. The straight line form of the Freundlich isotherm(Snoeyink and Summers, 1999).

The Freundlich isotherm is known to be effective solely within certain concentration restrictions that adsorbent approaches saturation. At the saturation point, q_A is independent of further increases in C_e, and the Freundlich equation no longer applies.

2.3.2.4. BET Isotherm. BET isotherm put forward by Brunauer, Emet and Teller (BET). The fundamental assumption for the Langmuir model is that adsorbates accumulate in a monolayer, whereas the BET model accommodates multilayer. Because most porous materials have large enough pores to allow more than one adsorbed layer, the Langmuir surface area results in overestimation and the BET surface area calculation is more reliable (Koh et al., 2009).

2.3.2.5. Sorption Efficiency. Percentage of the sorption which is also called as sorption efficiency is a parameter to be used to evaluate the experimental data.

$$\text{Sorption efficiency, \%} = \frac{C_s}{C_i} \qquad (2.9)$$

Where, C_i is the initial concentration of the adsorbate, and C_s is the concentration of the sorbed material.

2.3.3. Summary of the Previous Studies for the Assessment of Adsorptive Interactions of Humic Acids

Referring the literature findings related to the studies performed to investigate the adsorption characteristic of humic acids onto bare TiO_2 and modified TiO_2 specimens a brief summary is compiled and presented below:

Bekbolet et al. (1996) studied the effect of photocatalyzed oxidation on the degradation and decolorization of humic acid. Adsorptive behavior of humic acid was also studied for the photocatalytically oxidized humic acid. It was reported that with respect to a decrease in the content of organic matter and decolorization an increase in biodegradability was observed after the photocatalytic oxidation of humic acid. There was no major change in adsorptivity but when the irradiation time was increased the adsorption characteristic of humic acid showed an alteration.

Suphandag (1998) studied the adsorption capacity of natural organic matter on semi-conductor powders. The adsorption capacity of humic acid was investigated under different pH conditions (pH:5-12) onto three different crystal structures of TiO_2 powders that the range changed from 0.1 mg mL^{-1} to 1.0 mg mL^{-1}. The TiO_2 dose range was also extended to higher loading as 5 mg mL^{-1}. It was found that the adsorption capacity was higher at lower pH of humic acid solution (pH=5), irrespective of the crystal structures of TiO_2 powders used.

Bas (2001) examined humic acid and surface interactions for adsorption and desorption at three different pH levels. It was reported that the crystal structures of TiO_2 powders affect the adsorption and desorption behavior of humic acid. Higher adsorption efficiencies were observed for Degussa P-25 (mixed phase composed of 80 % anatase and 20 % rutile). Similarly, higher desorption efficiencies were observed for Millennium PC500 (pure anatase) within the studied TiO_2 range. Adsorption efficiencies of two commercial humic acids (Aldrich, aquatic origin and Roth, carbon based) were assessed at different pH conditions. It was concluded that Aldrich humic acid has higher adsorption efficiency because of the diversities in their structure and chemical composition than other carbon-based humic acid.

Bekbolet et al. (2002) explored the photocatalytic efficiencies of two commercial TiO$_2$ powders (Degussa P-25 and Hombikat UV-100) on the decolorization of humic acids, and adsorption properties of humic acids onto TiO$_2$ specimens. The photocatalytic degradation efficiencies and adsorption capacities for Degussa P-25 were found to be higher than for Hombikat UV-100. It was concluded that there was certain dependency between the adsorption characteristics and the photocatalytic decolorization rates but no dependency onto the surface area of TiO$_2$ powders.

Uyguner and Bekbolet (2004) studied the impact of the chromium ion concentration on the adsorption of humic acid onto TiO$_2$. It was concluded that both Color$_{436}$ and UV$_{254}$ was used as parameters in order to evaluate the adsorption effects of humic acid and chromium ions on the titanium dioxide surface. The presence of chromium ions was found to prevent the adsorption capacity of sole humic acid onto TiO$_2$ powder through complex formation with chromium ions leading to diverse surface interactions.

Suphandag (2006) investigated adsorption characteristic of a coal derived humic acid on the general semiconductor powder (Degussa P-25 TiO$_2$). It was concluded that the adsorption of humic acid onto TiO$_2$ is influenced by increase of negative surface charge, restricted size availability, and factors that control the size of humic acid molecules. Structural and conformational changes attained humic sub-fractions were discussed by humic macromolecular models.

Uyguner et al. (2007) investigated the ozonation, photocatalysis and sequential oxidation systems followed by adsorption and coagulation characteristic of humic acids. They used two types of activated carbons in adsorption experiments (PAC and GAC) and aluminum sulfate (Al$_2$(SO$_4$)$_3$.18H$_2$O), and ferric chloride (FeCl$_3$.6H$_2$O) in coagulation experiments. It was found that Color$_{436}$ removal efficiencies for untreated, photocatalytically oxidized, ozanated and sequentially oxidized humic acids increased for increasing PAC doses. Color$_{436}$ removal efficiencies for untreated photocatalytically oxidized, ozonated, and sequentially oxidized humic acids also increased for GAC. On the other hand, UV$_{254}$ removal efficiencies for untreated, photocatalytically oxidized, ozanated and sequentially oxidized humic acids decreased for increasing PAC and GAC doses. The

adsorption capacities at $Color_{436}$ were higher than for the UV absorbing centers after treatment.

Vreysen and Maes (2008) investigated the adsorption mechanism of humic acid and fulvic acid onto Mg/Al layered double hydroxides (LDHs) by means of adsorption isotherms at diverse ionic strengths and also the characterization of adsorbed humic substance size fractions by using gel permeation chromatography. The adsorption isotherms of HA and FA onto the nitrate, chloride and carbonate intercalated Mg/Al LDHs were fitted to the Langmuir isotherm model because of high correlation coefficient (R^2). Humic and fulvic acids having lower molecular weight mostly preferred in order to adsorb since these fractions include more carboxylic groups and also enter the mesoporous LDHs.

Ulker (2008) studied the impact of molecular size fractionation on the sorption characteristics of humic acid onto Fe-doped TiO_2, and TiO_2 modified with ascorbic acid samples in comparison with bare TiO_2 Degussa P-25. The adsorption profiles of the $Color_{436}$ and UV_{254} of humic acid and its molecular size fractions and Fe doped TiO_2 displayed major differences with regard to the circumstances of the humic acid and bare TiO_2 system. Moreover, ascorbic acid doped TiO_2 specimen displayed lower adsorption capacity due to the pH-dependent surface oriented organic (ascorbate) – organic (humic) repulsive interactions.

Degirmenci Ilhan (2010) studied the adsorption of humic acid and humic molecular size fractions (0.45 μm filtered fraction, 100 kDa fraction and 30 kDa fraction) in the presence and absence of zinc ions in connection with photocatalytic degradation experiments. The study showed that the complexity of the structure of humic acid molecule and the presence of zinc ions in the system can change the photocatalytic oxidation through complex formation, oxidation and adsorption processes. The reason of significant changes could be attributed to low concentrations of zinc with respect to humic acid concentration leading to complexation therefore to the reduced surface access due to the increased molecular size.

Recently, Sen-Kavurmaci (2013) studied the adsorption of humic acid onto TiO_2 Degussa P-25 both in the presence and absence of clay minerals as montmorillonite and kaolinite. Ionic strength effect was also discussed particularly with respect to the conformational and structural changes attained in humic structure. Calcium ions could also act as bridges in between humic sub-fractions and deprotonated TiO_2 surface sites as well as respective sites present on either montmorillonite or kaolinite. Scanning Electron Microscopic images were also presented to display the adsorptive interactions of humic acid and mixed oxide surfaces.

3. MATERIALS AND METHODS

3.1. Materials

3.1.1. Humic Acid

Commercial humic acid used in all experiments was obtained from Aldrich (Aldrich Co. Ltd., USA). Stock humic acid solution with a concentration of 1000 mg L^{-1} was prepared by adding 1 g humic acid into 1 L of ultra pure water and dissolved using the ultrasonic sonication waterbath in order to attain homogenous solution. Stock solution of humic acid was stored in amber glass bottles and was protected from sunlight to prevent decomposition. Ultra pure water was prepared by using Millipore Milli-Q system. While humic acid solution in 20 mg L^{-1} concentration prepared from stock solution by proper dilution was used for 0.45 μm filtration fraction, humic acid solution with 50 mg L^{-1} concentration was employed for both 100 kDa molecular size fraction and 30 kDa molecular size fraction.

3.1.2. Titanium Dioxide

Batch adsorption experiments were carried out by means of two different commercial titanium dioxide specimens, namely Degussa P-25 and Hombikat UV-100. Bare TiO_2 and anion doped TiO_2, such as nitrogen doped TiO_2, sulfur doped TiO_2, carbon doped TiO_2 and nitrogen-sulfur co-doped TiO_2, were used as adsorbents. N-doped, S-doped, C-doped and N-S co-doped TiO_2 specimens of Degussa P-25 and Hombikat UV-100 were prepared by Cinar and co-workers in the research laboratories of Yıldız Technical University, Department of Chemistry. Degussa P-25 and Hombikat UV-100 TiO_2 were used as precursors for anion doping processes which were based on an incipient wet impregnation method. Urea, glucose and thiourea were used for the generation of N-doped, C-doped and S-doped as well as N-S co-doped TiO_2 Degussa P-25 and Hombikat UV-100 specimens. In order to prepare anion doped TiO_2 specimens 8 g TiO_2 Degussa P25 was mixed with 10 mL of aqueous solutions of urea and stirred at room temperature for 1 h.

During this period, the photocatalyst changed color into a yellowish white depending upon the urea concentration. Doped photocatalysts containing 0.50 wt % N, C, S and N-S were prepared irrespective of TiO_2 types. Then, the prepared photocatalysts were washed with water and centrifugally separated three times, heat-treated at 378 K for 24 h to eliminate water, calcined at 623 K for 3 h, ground and sieved. In order to investigate the effects of calcination temperature and calcination period, the N-doped, C-doped, S-doped and N-S co-doped samples containing 0.50 wt % N, C, S and N-S which were determined to be the optimum concentration showing the highest activity was calcined at three different temperatures, 623, 723 and 823 K for three different times of calcinations, 1, 3 and 5 h.

Characterization of anion doped TiO_2 specimens were performed by X-Ray Diffraction patterns (XRD), Raman Spectroscopy and UV-visible diffuse reflectance spectra which were represented by Cinar and co-workers in their previous studies. Furthermore, Cinar and co-workers represented some qualifications of titanium dioxide powders supplied from Degussa P-25 and Hombikat UV-100 (Yalcin et al., 2010; Gurkan et al., 2012).

Table 3.1. Specifications of TiO_2 specimens (Yalcin et al., 2010; Gurkan et al., 2012).

Property	TiO_2 specimens	
Brand	Degussa P-25	Hombikat UV-100
Physical State	White Powder	White Powder
Composition, %	80 anatase and 20 rutile	100 anatase
Density, $g\ mL^{-1}$	3.8	3.9
BET surface area, $m^2\ g^{-1}$	~55	>250
Average primary particle size, nm	~30	<10
pH in aqueous solution	3-4	~6
Porosity	Non-porous	Porous

Table 3.2. Properties of undoped and anion doped TiO_2 (Yalcin et al., 2010; Gurkan et al., 2012).

TiO_2 specimens	E_{bg}, eV	λ, nm	pH_{zpc}	Crystallite size, nm
Bare Degussa P-25	3.01	411	6.25	22.3
Bare Hombikat UV-100	3.20	387	6.30	16.6
N-doped Degussa P-25	2.79	479	5.15	18.8
N-doped Hombikat UV-100	2.99	414	5.23	13.7
S-doped Degussa P-25	2.65	467	5.38	18.5
S-doped Hombikat UV-100	3.08	403	5.23	14.1
N-S co-doped Degussa P-25	2.68	463	5.61	16.9
N-S co-doped Hombikat UV-100	2.96	400	5.42	13.8

3.2. Methodology

3.2.1. Laboratory Equipments

General laboratory instruments, equipments and various types and sizes of glassware were used during the adsorption experiments.

3.2.2. Experimental Procedure

3.2.2.1. Batch Adsorption Experiments. Batch adsorption experiments were implemented using 100 mL Erlenmeyer Flask. Each flask was filled with 25 mL humic acid solution. Increased amounts of TiO_2 were added to each Erlenmeyer flask starting from 0.1 mg mL^{-1} to 1.0 mg mL^{-1}. Moreover, one extra flask was filled with only humic acid solution for comparative purposes. Each sample was sonicated before being placed to the shaker for homogeneous distribution of TiO_2 in the slurry. The samples were immersed in the water-bath at room temperature which is equipped with shaking device. The flasks were kept shaking for 24 hours.

Then samples were filtered by the 0.45 μm Millipore filter and clear solutions were subjected to analysis. In batch adsorption experiments, bare TiO_2 and anion doped TiO_2 namely nitrogen doped TiO_2, sulfur doped TiO_2, carbon doped TiO_2 and nitrogen-sulfur co-doped TiO_2 in the range of 0.1 - 1.0 mg mL^{-1} were used as adsorbents. Furthermore, batch adsorption experiments were carried out by means of two different commercial titanium dioxide specimens such as Degussa P-25 and Hombikat UV-100.

3.2.3. Molecular Size Fractionation with Ultrafiltration

Humic acid solutions were fractionated using a 50 mL Amicon Model 8010 ultrafiltration stirred cells into two different molecular size fractions (100 kDa and 30 kDa) in order to obtain diverse organic matter contents and then these solutions were exposed to batch adsorption experiments using bare and anion doped TiO_2 specimens as the adsorbent. The mechanism included an ultrafiltration cell with a magnetic stirrer, a nitrogen gas tube. A nitrogen gas tube equipped with a pressure control valve was connected to the stirred reactor to obtain the operating pressure inside the cell. The qualifications of the membranes were explained in Table 3.3.

Table 3.3. The specifications of the membranes used in ultrafiltration.

Membrane type	Nominal molecular weight cutoff (kDa)	Operating pressure (bar)
YM 100	100	0.7 - 1.0
YM 30	30	3.0 - 3.5

In the first step, humic acid solutions were filtered through 0.45 μm Millipore cellulose acetate filters. Then, filtration was repeated in a series mode using Millipore YM series cellulose membrane filters with 44.5 mm diameter and with nominal molecular weight cutoffs, 100 kDa and 30 kDa. The cell was run on a magnetic stirrer with 50 mL samples. Schematic diagram of ultrafiltration stirred cell unit was presented in Figure 3.1.
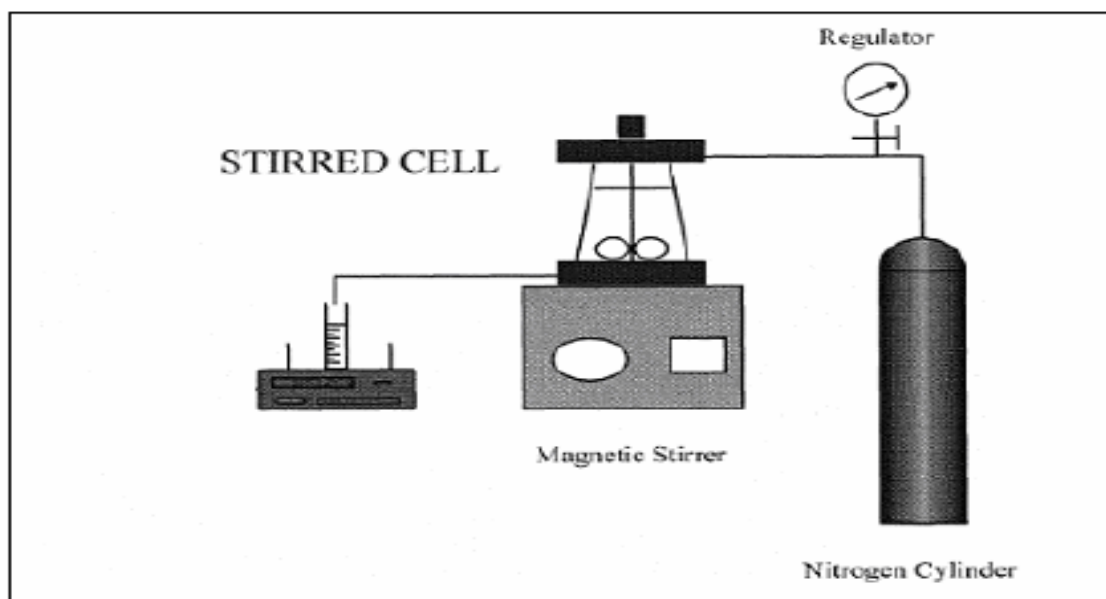
Figure 3.1. Schematic diagram of ultrafiltration stirred cell unit (Ulker, 2008).

At the beginning of each run, YM membranes were rinsed with deionized water for 15 minutes to remove ethanol and then the cell was run on a magnetic stirrer with 50 mL deionized water. At the end of ultrafiltration process, YM membrane was rinsed with 0.1 M NaOH solution for 30 minutes and kept in deionized water for 15 minutes before storage. YM membrane was stored in 10 % ethanol-water solution. Fractionated humic acid solutions were stored in dark glass bottles in refrigerator.

3.2.4. Analytical Methods

3.2.4.1. UV-vis Spectroscopic Measurements. UV-vis absorption spectra of humic acid solutions were recorded on a Perkin Elmer Lambda 35 UV-vis double beam spectrophotometer with Hellma quartz cuvettes of 1.0 cm optical path length. Humic acid solutions were characterized by UV-vis spectroscopy. UV-vis absorbance values of different molecular size fractions of humic acid were determined according to particular wavelengths that were at 436 nm, 365 nm, 280 nm and 254 nm. The absorbance values in these wavelengths were expressed for 436 nm as $Color_{436}$ representing color forming moieties at 436 nm, for 365 nm as UV_{365} representing organic matter content at 365 nm,

for 280 nm as UV_{280} that represented organic matter content at 280 nm, for 254 nm as UV_{254} that represented organic matter content at 254 nm.

3.2.4.2. Fluorescence Measurements. Fluorescence spectra in emission and synchronous scan modes were recorded on a Perkin Elmer LS 55 Luminescence Spectrometer equipped with a 150 W Xenon arc lamp and a red sensitive photomultiplier tube. Quartz cells with 1-cm path length were used in order to place the samples into the instrument. A scan speed of 400 nm min^{-1} with a slit width opening of 10 nm was used for all measurements. Synchronous scan spectra of humic acid solutions were recorded in the excitation wavelength range of 200-600 nm with the bandwidth of $\Delta\lambda = 18$ nm between the excitation and emission monochromators. The emission fluorescence spectra were recorded in the range of 360-600 nm and 380-600 nm at excitation wavelengths of 350 nm and 370 nm, respectively.

3.2.4.3. Non-Purgeable Organic Carbon (NPOC) Measurements. Non-Purgeable Organic Carbon (NPOC) measurements of HA solutions were implemented with a Shimadzu TOC Vwp Total Organic Carbon Analyzer. The calibration of the instrument was fulfilled with potassium hydrogen phthalate in the concentration range of 0 - 25 mg L^{-1}. NPOC was expressed simply as DOC, mg OrgC mL^{-1}.

4. RESULTS AND DISCUSSION

The objective of this study was to evaluate surface interactions between different molecular size fractionations of humic acid and TiO_2 specimens, namely bare TiO_2 and anion doped TiO_2. In other words, adsorption properties of molecular size fractions of humic acid onto commercially diverse type of TiO_2, namely, Degussa P-25 and Hombikat UV-100 would be elucidated. Spectroscopic properties and adsorption isotherm modeling of different molecular size fractions of humic acid onto bare TiO_2 and anion doped TiO_2 specimens constituted the main subjects of the discussion part.

Adsorption experiments were conducted with humic acid solution in different molecular size fractions, such as 0.45 μm filtration fraction of 20 mg L^{-1} humic acid solution and 100 kDa and 30 kDa fractions of 50 mg L^{-1} humic acid solution. Dosage of bare TiO_2 and anion doped TiO_2 specimens were chosen in the range of 0.1-1.0 mg mL^{-1}.

The properties of humic acid and its molecular size fractions were determined by means of UV-vis spectroscopy and fluorescence spectroscopy used in emission and synchronous scan modes. Moreover, NPOC content of organic matter was a major parameter used in the characterization of humic acid and its molecular size fractions.

4.1. Characterization of Humic Acid and Its Molecular Size Fractions

Humic acid and its molecular size fractions were characterized with spectroscopic analyses including UV-vis spectroscopy and fluorescence spectroscopy. The aim of application of UV-vis and fluorescence spectroscopy is to better evaluate the origin and sources of organic matter (Knapik et al., 2011). Furthermore, fluorescence spectroscopy has preferred in many studies because of the fact that it provides the determination of the source and composition of DOM in marine, wastewater, surface water, ground water and terrestrial environments (Lapworth et al., 2008). Furthermore, both of the spectroscopic methods were successfully used for the characterization of humic properties under non-oxidative as well as oxidative conditions (Uyguner-Demirel and Bekbolet, 2011).

4.1.1. UV-vis Spectroscopic Properties of Humic Acid and Its Molecular Size Fractions

UV-vis absorption is generally considered as conventional and versatile in the characterization of dissolved organic substances in natural water. The UV-vis spectrum of humic acid is generally broad, does not demonstrate any peak properties and monotonously diminish with increasing wavelength (Uyguner and Bekbolet, 2005b).
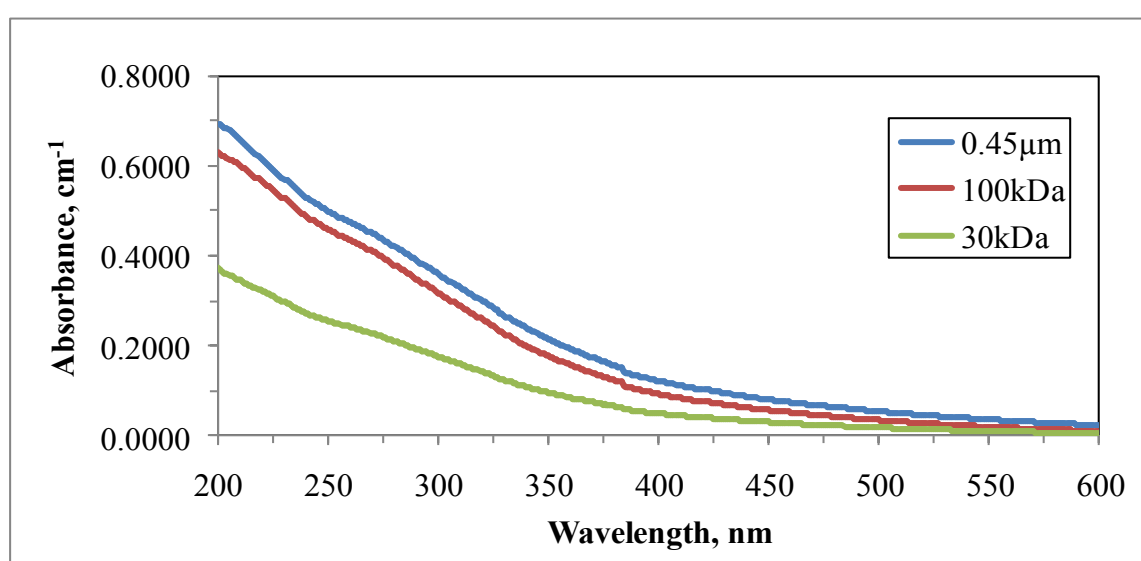
Figure 4.1. UV-vis absorbance spectra of 0.45 μm filtered fraction, 100 kDa fraction and 30 kDa fraction of humic acid.

UV-vis absorbance values of various molecular size fractions of humic acid were analyzed between 200-600 nm wavelength regions. UV-vis absorbance values of humic acid with diverse molecular size fraction decreased with increasing wavelength and they leveled off after 400 nm. UV-vis absorbance values recorded at wavelengths longer than 400nm express the presence of conjugated systems and chromophoric groups displaying color, it could be seen that the humic acid molecular size fractions displayed lower color properties. Furthermore, humic acid with higher molecular size fraction exhibited higher UV-vis absorbance values than others. Moreover, 0.45 μm filtered fraction of humic acid had the highest UV-vis absorbance value whereas 30 kDa fraction of humic acid had the lowest value as expected. 100 kDa fraction and 0.45 μm filtered fraction of humic acid

showed UV-vis absorbance values that were very close to each other (Figure 4.1). Through ultrafiltration process, UV-vis absorbance values of humic acid exhibited a decreasing trend owing to decreasing molecular size (Uyguner and Bekbolet, 2005a). A decreasing trend was observed among UV-vis absorbance values of distinct molecular size fractions of humic acid as 0.45 μm filtered fraction > 100 kDa > 30 kDa. Previous studies presented by Ulker (2008) and Aykac (2011) demonstrated the similar consequences including a decreasing trend with decreasing molecular size fraction.

UV-vis absorbance at 254 nm (UV_{254}) is interchangeably measured with TOC in order to represent NOM content in natural waters (Uyguner and Bekbolet, 2005b). Therefore, UV_{254} accepted as a surrogate parameter of organic carbon content was measured as 0.4889 cm^{-1} for 0.45 μm filtered fraction, 0.4490 cm^{-1} for 100 kDa fraction and 0.2501 cm^{-1} for 30 kDa fraction of humic acid.
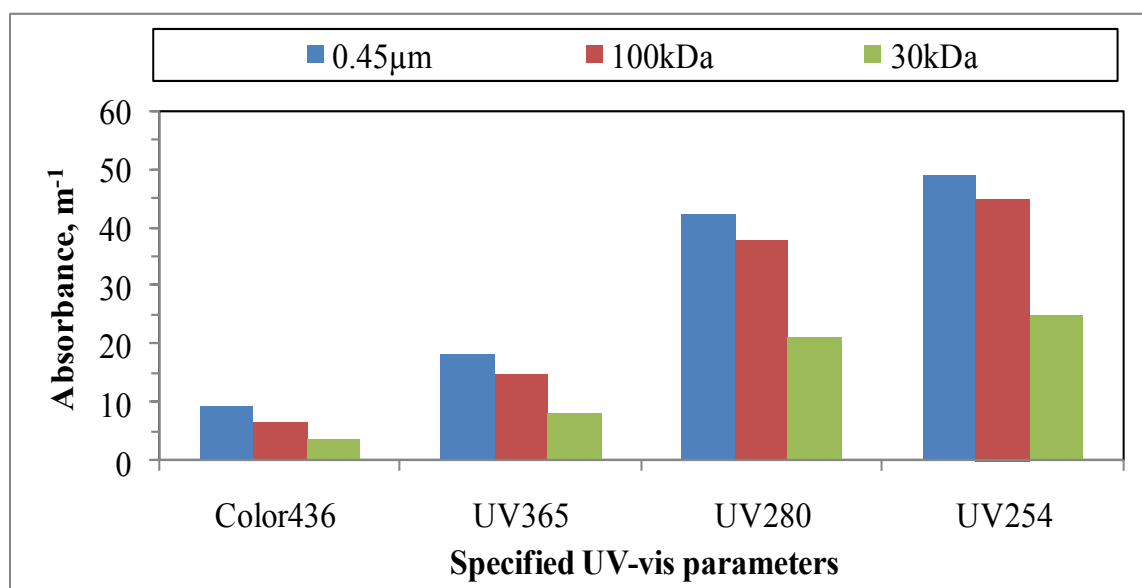
Figure 4.2. Comparative presentation of the specified UV-vis parameters of 0.45 μm filtered fraction, 100 kDa fraction and 30 kDa fraction of humic acid.

As seen from Figure 4.2, UV-vis parameters recorded for all molecular size fractions *i.e.* 0.45 μm, 100 kDa and 30 kDa of humic acid displayed decreasing trend. UV-vis absorbance value of 0.45 μm filtered fraction of humic acid was approximately half of that of 30 kDa fraction of humic acid in all of the specified UV-vis parameters, namely

Color$_{436}$, UV$_{365}$, UV$_{280}$ and UV$_{254}$. It should also be mentioned that the organic carbon contents of the molecular size fractions of humic acid also displayed a decreasing trend as expected.

4.1.2. Fluorescence Spectroscopic Properties of Humic Acid and Its Molecular Size Fractions

The emission scan fluorescence spectra of different molecular size fractions of humic acid were shown in Figure 4.3 and Figure 4.4. The emission scan fluorescence spectra were recorded in the range of 360-600 nm and 380-600 nm at the excitation wavelengths of 350 nm and 370 nm, respectively.
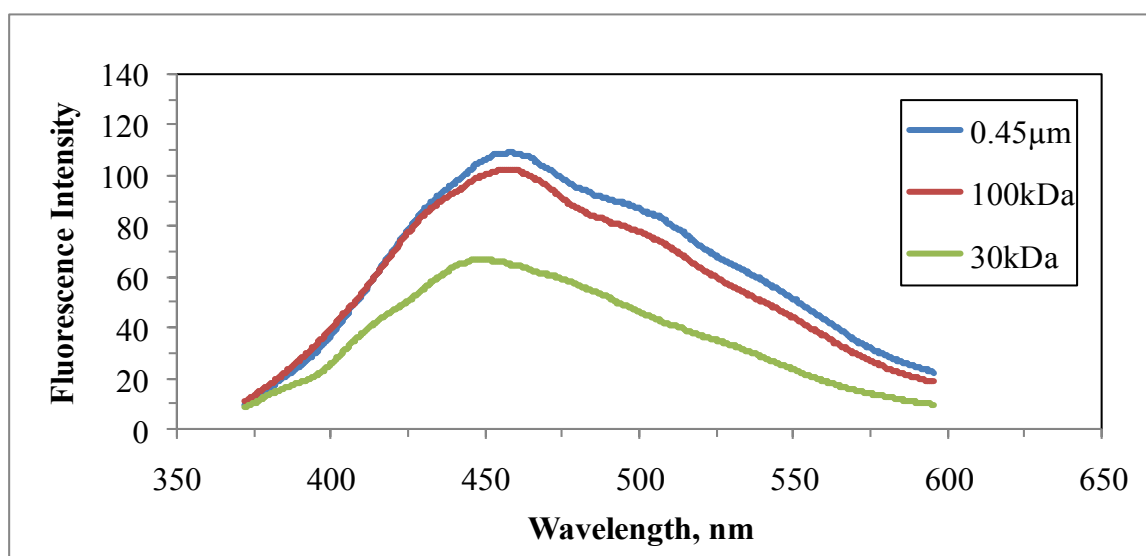
Figure 4.3.   Emission scan fluorescence spectra of 0.45 µm filtered fraction, 100 kDa fraction and 30 kDa fraction of humic acid at 350 nm excitation wavelength .

Generally, the fluorescence intensities diminish with increasing molecular size fraction of humic acid. Moreover, smaller molecules stated as electron-donating groups such as hydroxyl can increase fluorescence by providing the transition possibility between the singlet and ground states (Uyguner et al., 2007). Figure 4.3 displayed that emission fluorescence intensity decreased as a result of decreasing molecular size fractions of humic acid. In other words, 30 kDa fraction of humic acid possessed the lowest fluorescence

intensity, while 0.45 µm filtered fraction of humic acid had the highest value in the emission scan fluorescence spectra. Fluorescence intensity attained a prominent peak at approximately 450 nm emission wavelength for all of the molecular size fractions of humic acid. It could be easily seen from Figure 4.3 that the fluorescence emission trends of 0.45 µm filtered fraction and 100 kDa fraction of humic acid crossed over in the region of 400 - 425 nm emission wavelengths.
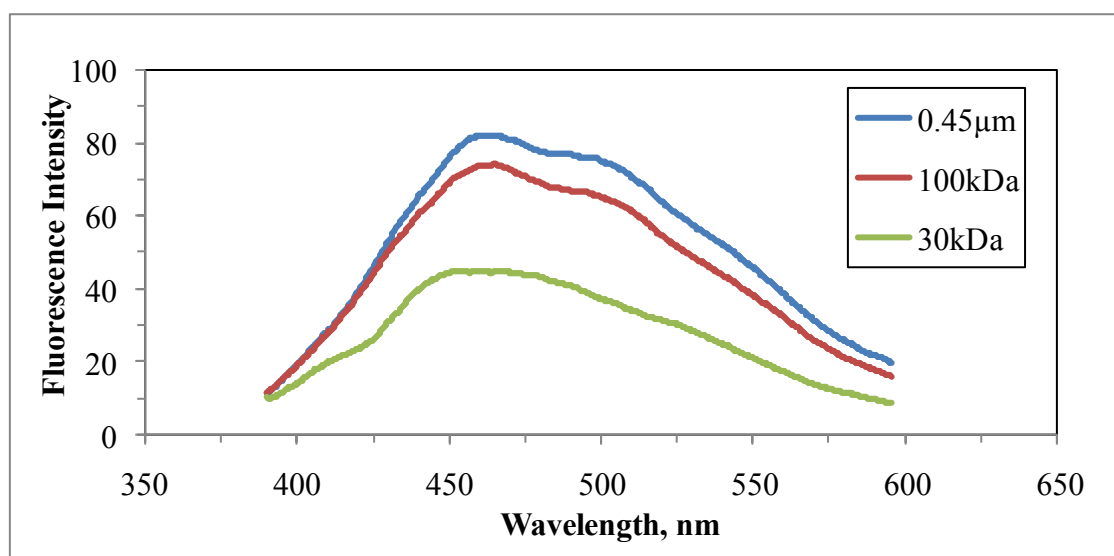
Figure 4.4. Emission scan fluorescence spectra of 0.45 µm filtered fraction, 100 kDa fraction and 30 kDa fraction of humic acid at 370 nm excitation wavelength.

It was obvious from Figure 4.4 that consequences obtained by emission scan fluorescence spectra at the excitation wavelength of 370 nm were similar to results at the excitation wavelength of 350 nm presented in Figure 4.3. When Figure 4.3 and Figure 4.4 were compared in terms of fluorescence intensity of various molecular size fractions of humic acid, it could be easily said that emission scan fluorescence spectra at the excitation wavelength of 350 nm gave higher values than at that of 370 nm.

Synchronous scan excitation spectra are attained with the measurement of the fluorescence intensity while simultaneously scanning over both the excitation and emission wavelengths and sustaining a fixed value for $\Delta\lambda = \lambda_{em} - \lambda_{ex}$. Synchronous scan fluorescence can demonstrate better sensibility and developed peak resolution in contrast

to the conventional emission fluorescence method and possibly permit separation of the fluorescence spectra of samples in a variety of sources. Some studies as to the characterization of NOMs exhibited that synchronous scan fluorescence has several advantages over conventional fluorescence excitation and emission spectroscopy (Chen et al., 2012). Synchronous scan fluorescence spectra scanned for different molecular size fractions of humic acid were presented in Figure 4.5.
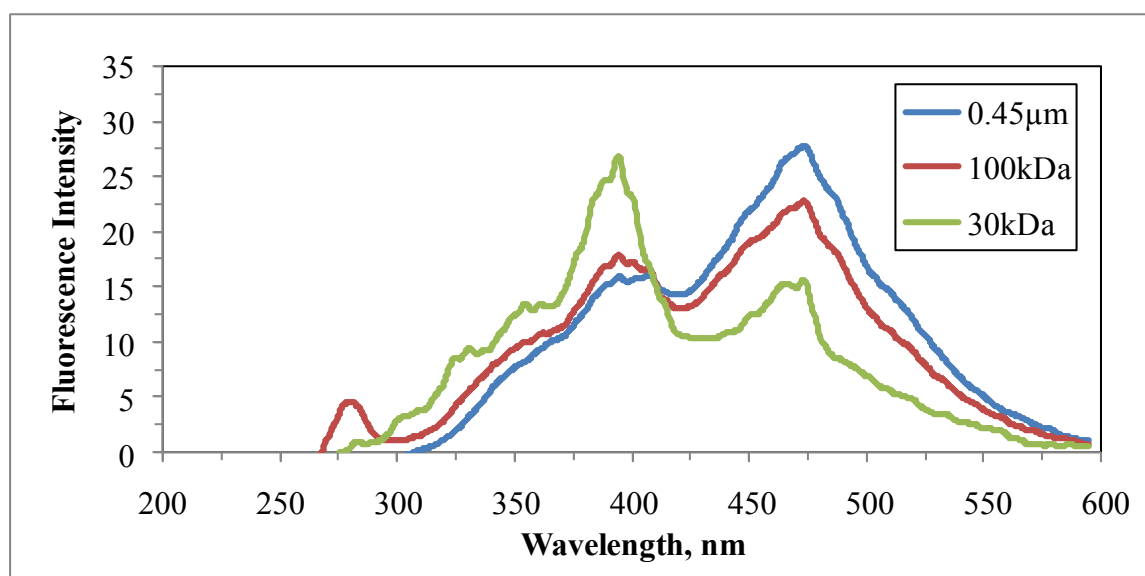
Figure 4.5. Synchronous scan fluorescence spectra of 0.45 μm filtered fraction, 100 kDa fraction and 30 kDa fraction of humic acid.

The synchronous scan fluorescence spectra have been widely employed to characterize humic substances and also it has a more structured property (Uyguner et al., 2007). Synchronous scan fluorescence spectra were measured in the range of 200-600 nm excitation wavelength, with Δλ=18 nm, frequently applied in the studies as to humic substances or natural organic matters (Senesi et al., 1989, Peuravuori and Pihlija, 1997 and Knapik et al., 2011). The synchronous scan fluorescence spectra of all of the molecular size fractions of humic acid mentioned before displayed two notable fluorescence peaks at almost 390 and 475 nm emission wavelengths. One of the most remarkable outcomes that were obtained from Figure 4.5 and also consistent with studies implemented by (Ulker, 2008) and (Aykac, 2011) was that the fluorescence intensity of 0.45 μm filtered fraction,

100 kDa fraction and 30 kDa fraction of humic acid measured by employing synchronous scan mode decreased with decreasing molecular size filtration.

4.1.3. Specific Parameters of Humic Acid

UV-vis spectral parameters, namely $Color_{436}$, UV_{365}, UV_{280} and UV_{254}, fluorescence spectral parameters like FI_{emis} and FI_{sync}, non-purgeable organic carbon (NPOC) and derived parameters, such as $SCoA_{436}$, $SUVA_{365}$, $SUVA_{280}$, $SUVA_{254}$, $SFI_{emis\ 350}$, $SFI_{emis370}$, SFI_{sync}, could be described as specific parameters for different molecular size fractions of humic acid. UV-vis absorbance at 254 nm is frequently used a measurement representing DOC in waters including aquatic humics (Edzwald et al., 1985; Edzwald, 1993). The UV-vis absorptivity 280 nm represents total aromaticity since $\pi - \pi^*$ electron transition is present in this region for phenolic arenes, benzoic acids, aniline derivatives, polyenes and polycyclic aromatic hydrocarbons with two or more rings (Uyguner and Bekbolet, 2005b). $Color_{436}$ states the color forming moieties that are the chromophoric groups including conjugated double bond systems (delocalized electrons) and heteroatoms with lone pair of electrons like O, N and S (Bekbolet et al., 2002).

Specific UV absorbance (SUVA) is identified as the UV absorbance of a water sample at a given wavelength normalized for dissolved organic carbon (DOC) concentration (Weishaar et al., 2003). Specific UV absorbance ($SUVA_{254}$ m^{-1} mg^{-1} L) was defined as UV_{254} absorbance value divided by the NPOC. Moreover, specific UV absorbance ($SUVA_{254}$ m^{-1} mg^{-1} L and $SUVA_{280}$ m^{-1} mg^{-1} L) were used to represent NPOC normalized aromatic moieties (UV_{254}, UV_{280}), while $SUVA_{365}$ was calculated in a similar fashion as the ratio of the UV_{365} absorbing species to NPOC. Specific color absorbance ($SCoA_{436}$, m^{-1} mg^{-1} L) was defined as $Color_{436}$ absorbance value divided by the NPOC to indicate organic carbon normalized color forming moieties. Furthermore, SFI_{emis} was described as the ratio of the FI_{emis} values to NPOC (Uyguner and Bekbolet, 2005b).

The method mentioned in the materials and methods section was used for the determination of non-purgeable organic carbon (NPOC) contents of the prepared humic acid solutions. Through ultrafiltration process, NPOC values of humic acid solutions exhibited a decreasing trend due to decreasing molecular size as 5.98 mg OrgC L^{-1} for 0.45

µm filtered fraction, 4.93 mg OrgC L^{-1} for 100 kDa fraction and 2.74 mg OrgC L^{-1}. All specific parameters of three diverse molecular size fractions of humic acid including UV-vis absorbance spectral parameters, such as $Color_{436}$, UV_{365}, UV_{280}, UV_{254}, fluorescence spectral parameters like $FI_{emis\ 350}$, $FI_{emis\ 370}$, FI_{sync} and non-purgeable organic carbon (NPOC) as well as derived parameters, such as $SCoA_{436}$, $SUVA_{365}$, $SUVA_{280}$, $SUVA_{254}$, $SFI_{emis\ 350}$, $SFI_{emis\ 370}$, SFI_{syn} were presented in Table 4.1.

Table 4.1. Specific and specified parameters of 0.45 µm filtered fraction, 100 kDa fraction and 30 kDa fraction of humic acid.

Humic Acid	0.45 µm	100 kDa	30 kDa
UV-vis spectral parameters			
$Color_{436}$, m^{-1}	9.11	6.61	3.53
UV_{365}, m^{-1}	18.35	14.90	7.97
UV_{280}, m^{-1}	42.16	38.03	21.11
UV_{254}, m^{-1}	48.89	44.90	25.01
Fluorescence spectral parameters			
$FL_{emis\ 350}$, cm^{-1}	106.26	100.38	66.74
$FL_{emis\ 370}$, cm^{-1}	76.02	69.22	44.38
FI_{sync}, cm^{-1}	27.54	22.43	14.62
Non-purgable organic carbon			
NPOC, mg L^{-1}	5.981	4.926	2.739
Derived parameters : $SCoA_{436}$, $SUVA_{365}$, $SUVA_{280}$, $SUVA_{254}$ (m^{-1} mg^{-1} L) $SFI_{emis\ 350}$, $SFI_{emis\ 370}$, SFI_{syn} (cm^{-1} mg^{-1} L)			
$SCoA_{436}$	1.52	1.34	1.29
$SUVA_{365}$	3.06	3.02	2.91
$SUVA_{280}$	7.05	7.72	7.70
$SUVA_{254}$	8.18	9.11	9.13
$SFI_{emis\ 350}$	17.77	20.38	24.37
$SFI_{emis370}$	12.71	14.05	16.20
SFI_{syn}	4.60	4.55	5.33

The relative order of 0.45 µm filtered fraction, 100 kDa fraction and 30 kDa fraction of humic acid for its all specific parameters, containing $Color_{436}$, UV_{365}, UV_{280}, UV_{254}, $SCoA_{436}$, $SUVA_{365}$, $SUVA_{280}$ and $FI_{emis\ 350}$, $FI_{emis\ 370}$, FI_{sync} was 0.45 µm filtration fraction > 100 kDa fraction > 30 kDa fraction. However, for only $SUVA_{254}$, this order was altered as 0.45 µm filtration fraction > 30 kDa fraction > 100 kDa fraction as seen from Table 4.1.

If $SUVA_{254}$ is bigger than 4, it points out that organic matter composes hydrophobic and particularly aromatic material. In addition to this, $SUVA_{254}$ value is smaller than 3 when organic matter consists of hydrophilic materials (Uyguner and Bekbolet, 2005b). According to Table 4.1, $SUVA_{254}$ values recorded for different molecular size fractions of humic acid were in the range of 8.18 - 9.13 m^{-1} mg^{-1} L. These values showed that humic acid employed in this study had hydrophobic structure and also high molar mass.

High SUVA value points out that the organic matter consisted of hydrophobic, high molar mass (HMM) organic material, while low SUVA value means that the organic matter in water is composed largely of hydrophilic, low molar mass (LMM) (Matilainen and Sillanpää, 2010; Matilainen et al., 2010).

While the relative order of 0.45 µm filtration fraction, 100 kDa fraction and 30 kDa fraction of humic acid for $SFI_{emis\ 350}$ and $SFI_{emis\ 370}$ was 30 kDa fraction > 100 kDa fraction > 0.45 µm filtration fraction, for SFI_{syn} this order changed as 30 kDa fraction > 0.45 µm filtration fraction > 100 kDa fraction.

4.2. Adsorption Studies of Humic Acid and Its Molecular Size Fractions onto Bare TiO$_2$ and Anion Doped TiO$_2$

In this study, batch adsorption experiments were implemented to determine the influence of molecular size fractionation on the sorption capacity of humic acid onto bare TiO$_2$ and anion doped TiO$_2$ specimens, such as nitrogen doped TiO$_2$, sulfur doped TiO$_2$, carbon doped TiO$_2$ and nitrogen-sulfur co-doped TiO$_2$. In batch adsorption experiments, humic acid solutions having diverse molecular size fractions, such as 0.45 μm filtration fraction, 100 kDa fraction and 30 kDa fraction were employed. While humic acid solution in 20 mg L^{-1} concentration was used for 0.45 μm filtration fraction, humic acid solution with 50 mg L^{-1} concentration was practiced for both 100 kDa molecular size fraction and 30 kDa molecular size fraction.

Bare TiO$_2$ and anion doped TiO$_2$ specimens in the range of 0.1-1.0 mg mL^{-1} mentioned above were used as adsorbents. Furthermore, batch adsorption experiments were carried out by means of two different commercial titanium dioxide specimens such as Degussa P-25 and Hombikat UV-100. After batch adsorption experiments, the humic acid samples prepared according to the method, which was outlined in materials and methods section, were analyzed by UV-vis spectroscopy and fluorescence spectroscopy. Adsorption isotherms were fitted to Freundlich and Langmuir adsorption isotherm models by evaluating the results of specified UV-vis parameters like Color$_{436}$, UV$_{365}$, UV$_{280}$ and UV$_{254}$. Batch adsorption experiments were implemented to according to the methods presented in the materials and methods section. The evaluation of the experiment results was carried out according to the methodology outlined in section 2.3. Adsorption isotherms of specified UV-vis parameters, namely Color$_{436}$ and UV$_{254}$, presented in the following sections for the different molecular size fractions of humic acid and also adsorption isotherm models of UV$_{365}$ and UV$_{280}$ parameters presented in Appendix A and Appendix B for Freundlich and Langmuir adsorption isotherm models, respectively. Emission scan fluorescence spectra of diverse molecular size fractions namely 0.45 μm, 100 kDa and 30 kDa filtered fraction of humic acid following adsorption onto bare TiO$_2$ and anion doped TiO$_2$ specimens at excitation wavelength of 370 nm were presented in Appendix C.

In order to apply Freundlich adsorption isotherm model, q_A versus C_e graphs were plotted for the diverse molecular size fractions of humic acid whereas $1/q_A$ versus $1/C_e$ graphs were plotted for Langmuir adsorption isotherm models. By the logarithmic linearization of equation (2.7) presented in section 2.3, two parameters of the Freundlich equation, K_f and $1/n$ could be estimated from the intercept and the slope of the straight line, respectively. Moreover, two parameters of Langmuir equation outlined in section 2.3, q_m and K_a could be found from the intercept and the slope of the straight line obtained from the linearization of equation (2.6).

4.3. Spectroscopic Properties of 0.45 μm Filtered Fraction of Humic Acid Following Adsorption onto TiO₂ Specimens

Batch adsorption experiments were implemented by using 0.45 μm filtered fraction of humic acid as the adsorbate and bare and doped TiO_2 Degussa P-25 and TiO_2 Hombikat UV-100 specimens as the adsorbent in the loading range of $0.1 - 1.0$ mg mL^{-1}. UV-vis and fluorescence spectroscopic properties of humic acid were evaluated by presenting respective figures where "Initial" term was used to indicate the 0.45 μm filtered fraction of humic acid and "0.1-1.0" represented dose range of TiO_2 (mgmL^{-1}).

4.3.1. Spectroscopic Properties of 0.45 μm Filtered Fraction of Humic Acid Following Adsorption ontoTiO₂ Degussa P-25 Specimens.

Batch adsorption experiments were conducted by using 0.45 μm filtered fraction of humic acid and TiO_2 Degussa P-25 specimens *i.e.* bare TiO_2, C-doped TiO_2, N-doped TiO_2, S-doped TiO_2 and N-S co-doped TiO_2.

4.3.1.1. Spectroscopic Properties of 0.45 μm Filtered Fraction of Humic Acid Following Adsorption onto Bare TiO₂ Degussa P-25 Specimen. UV-vis absorbance spectra of 0.45 μm filtered fraction of humic acid following adsorption onto bare TiO_2 Degussa P-25 were presented in Figure 4.6. UV-vis absorbance spectra of humic acids exhibited generally a logarithmic declining trend with increasing wavelength. UV-vis absorbance spectral features displayed a decreasing trend with respect to increasing dose of TiO_2 (Figure 4.6). Previous studies performed by both Degirmenci Ilhan (2010) and Aykac (2011) also reported that UV-vis spectra of humic acid solutions monotonously decreased with respect to increasing dose of TiO_2.

Emission scan fluorescence spectral features attained through adsorption of 0.45 μm filtered fraction of humic acid samples onto bare TiO_2 Degussa P-25 were presented in Figure 4.7.
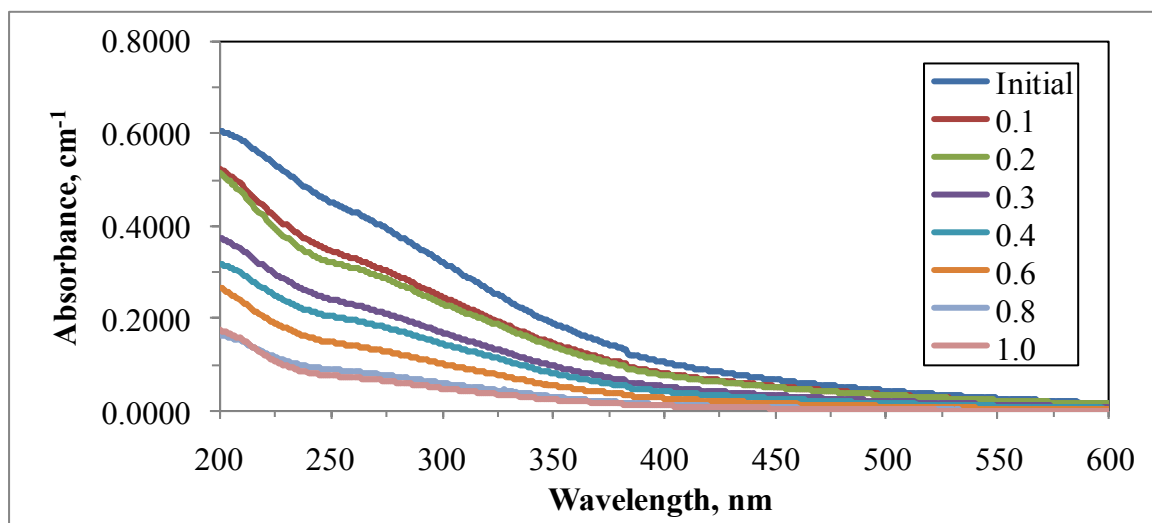
Figure 4.6.   UV-vis absorbance spectra of 0.45 μm filtered fraction of humic acid following adsorption onto bare TiO_2 Degussa P-25.
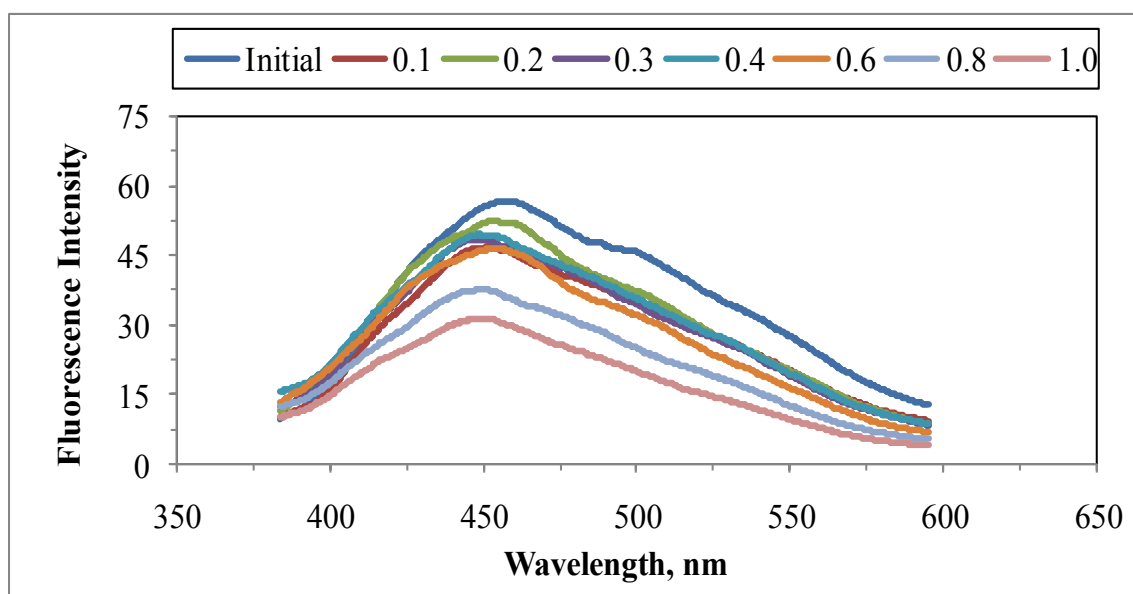
Figure 4.7. Emission scan fluorescence spectra of 0.45 μm filtered fraction of humic acid following adsorption onto bare TiO_2 Degussa P-25 at 350 nm emission wavelength.

Emission scan fluorescence spectrum of initial 0.45 μm filtered fraction of humic acid exhibited a broad peak around 450 nm emission wavelength and a minor shoulder around 500 nm emission wavelength. The results were found to be in good agreement with the results reported by both Degirmenci Ilhan, (2010) and Aykac, (2011).

A continuously decreasing trend was observed in fluorescence intensity with the addition of increased dose of TiO_2. Following adsorption onto 0.1 mg mL^{-1} and 0.3 mg mL^{-1} as well as 0.4 mg mL^{-1} bare TiO_2 Degussa P-25, emission scan fluorescence spectra of 0.45 μm filtered fraction of humic acid displayed an overlapping trend onto each other (Figure 4.7).

Synchronous scan fluorescence spectra scanned for 0.45 μm filtration fraction of humic acid following adsorption onto bare TiO_2 Degussa P-25 were presented in Figure 4.8.

Figure 4.8. Synchronous scan fluorescence spectra of 0.45 μm filtered fraction of humic acid following adsorption onto bare TiO_2 Degussa P-25.

Synchronous scan fluorescence spectra for 0.45 μm filtered fraction of humic acid showed two sharp peaks around emission wavelengths of 325 nm and 400 nm, while the fluorescence spectra displayed two moderate peaks around 275 nm and 475 nm emission wavelengths. The highest fluorescence intensity for 0.45 μm filtered fraction of humic acid following adsorption onto 0.4 mg mL^{-1} bare TiO_2 Hombikat UV-100 was observed at 400 nm emission wavelength because of the fact that the functional groups of humic acids displayed diverse binding properties to TiO_2 surface after adsorption (Figure 4.8).

4.3.1.2. Spectroscopic Properties of 0.45 μm Filtered Fraction of Humic Acid Following Adsorption onto C-doped TiO$_2$ Degussa P-25 Specimen. Adsorption characteristics of humic acid were evaluated through UV-vis and fluorescence spectroscopic properties. UV-vis absorbance spectra of 0.45 μm filtration fraction of humic acid following adsorption onto C-doped TiO$_2$ Degussa P-25 were presented in Figure 4.9.
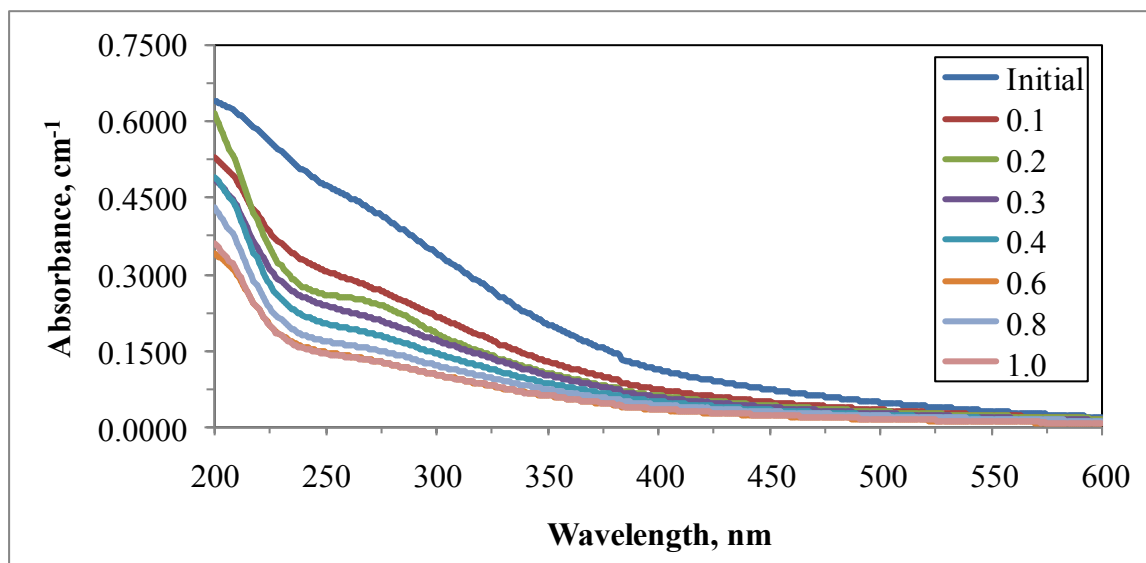
Figure 4.9. UV-vis absorbance spectra of 0.45 μm filtration fraction of humic acid following adsorption onto C-doped TiO$_2$ Degussa P-25.

UV-vis absorbance spectra of humic acids exhibited a decreasing trend with increasing wavelength with respect to increasing dose of TiO$_2$ loading. UV-vis absorbance spectra demonstrated a similar overlapping trend on each other for 0.45 μm filtration fraction of humic acid adsorption onto 0.6 mg mL^{-1} and 1.0 mg mL^{-1} doses of C-doped TiO$_2$ Degussa P-25 (Figure 4.9).

Emission scan and synchronous scan fluorescence spectral features were presented in Figure 4.10 and Figure 4.11, respectively. Emission scan fluorescence spectra of 0.45 μm filtration fraction of humic acid following adsorption onto C-doped TiO$_2$ Degussa P-25 in minimum dose (0.1 mg mL^{-1} TiO$_2$) had the highest intensity (Figure 4.10).Synchronous scan fluorescence spectra for 0.45 μm filtration fraction of humic acid showed one sharp

peak around emission wavelength of 400 nm, while the fluorescence spectra displayed two moderate peaks around 325 nm and 475 nm emission wavelengths (Figure 4.11).

Figure 4.10. Emission scan fluorescence spectra of 0.45 µm filtration fraction of humic acid following adsorption onto C-doped TiO_2 Degussa P-25 at 350 nm excitation wavelength.
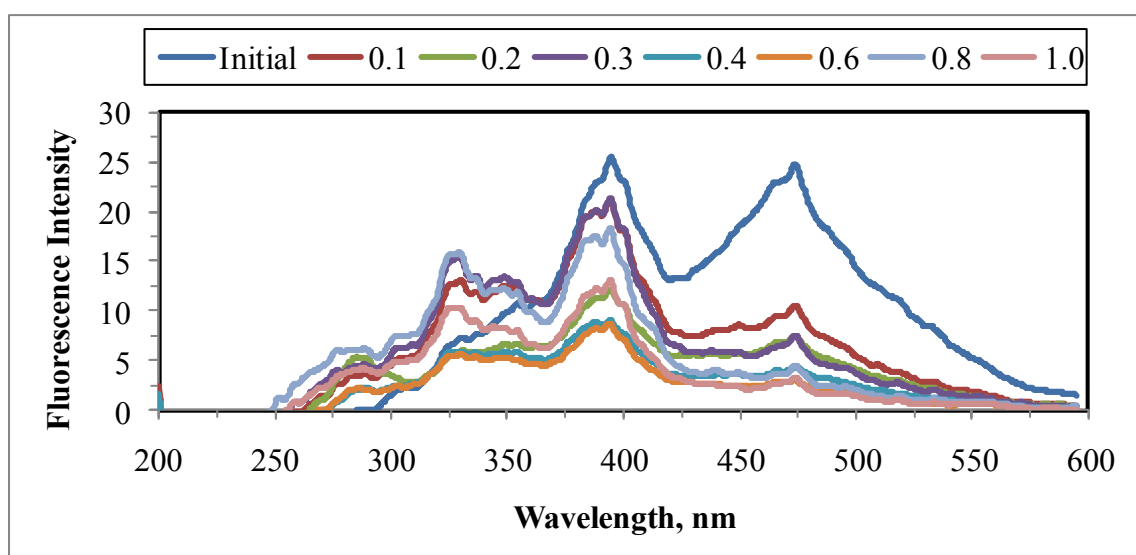
Figure 4.11. Synchronous scan fluorescence spectra of 0.45 µm filtered fraction of humic acid following adsorption onto C-doped TiO_2 Degussa P-25.

4.3.1.3. Spectroscopic Properties of 0.45 μm Filtered Fraction of Humic Acid Following Adsorption onto N-doped TiO₂ Degussa P-25 Specimen. UV-vis absorbance spectra of 0.45 μm filtration fraction of humic acid following adsorption onto N-doped TiO₂ Degussa P-25 were presented in Figure 4.12.
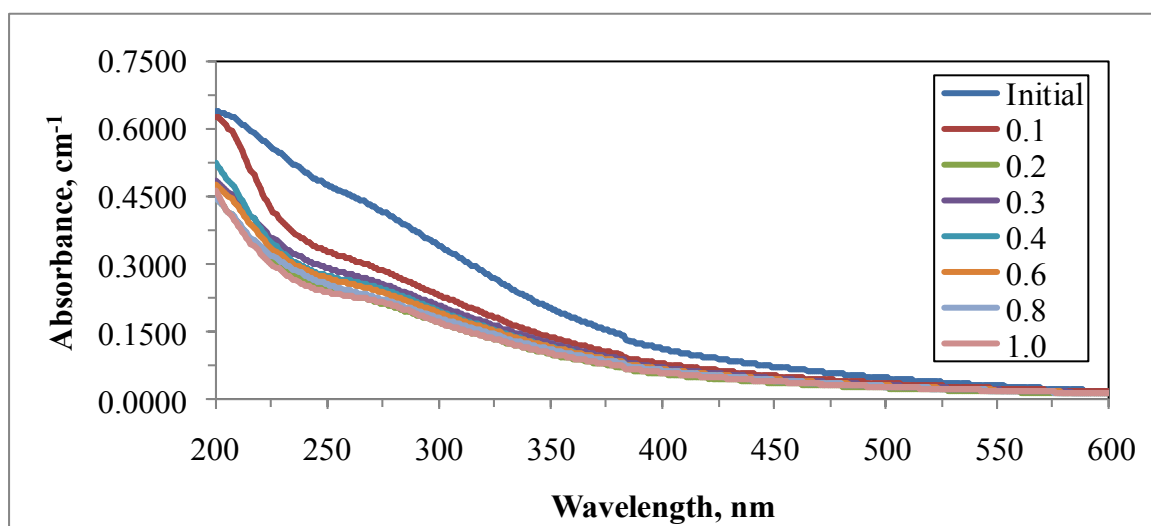
Figure 4.12.   UV-vis absorbance spectra of 0.45 μm filtration fraction of humic acid following adsorption onto N-doped TiO₂ Degussa P-25.

It could be easily seen from Figure 4.12 that after UV-vis absorbance trend of 0.45 μm filtration fraction of humic acid following adsorption onto 0.1 mg mL⁻¹ N-doped TiO₂, UV-vis absorbance spectra demonstrated a similar overlapping trend onto each other for 0.45 μm filtration fraction of humic acid following adsorption onto N-doped TiO₂ in the range of 0.2 – 1.0 mg mL⁻¹.

Emission scan fluorescence spectra and synchronous scan fluorescence spectra for 0.45 μm filtration fraction of humic acid following adsorption onto N-doped TiO₂ Degussa P-25were presented in Figure 4.13 and Figure 4.14. The emission scan fluorescence spectra of 0.45 μm filtration fraction of humic acid following adsorption onto 0.8 mg mL⁻¹ dose of N-doped TiO₂ Degussa P-25 demonstrated a characteristic peak around 400 nm emission wavelength. Synchronous scan fluorescence spectra for 0.45 μm filtration fraction of humic acid showed one sharp peak around emission wavelength of 400 nm,

while the fluorescence spectra displayed two moderate peaks around 325 nm and 475 nm emission wavelengths (Figure 4.14).

Figure 4.13. Emission scan fluorescence spectra of 0.45 µm filtration fraction of humic acid following adsorption onto N-doped TiO$_2$ Degussa P-25 at 350 nm excitation wavelength.
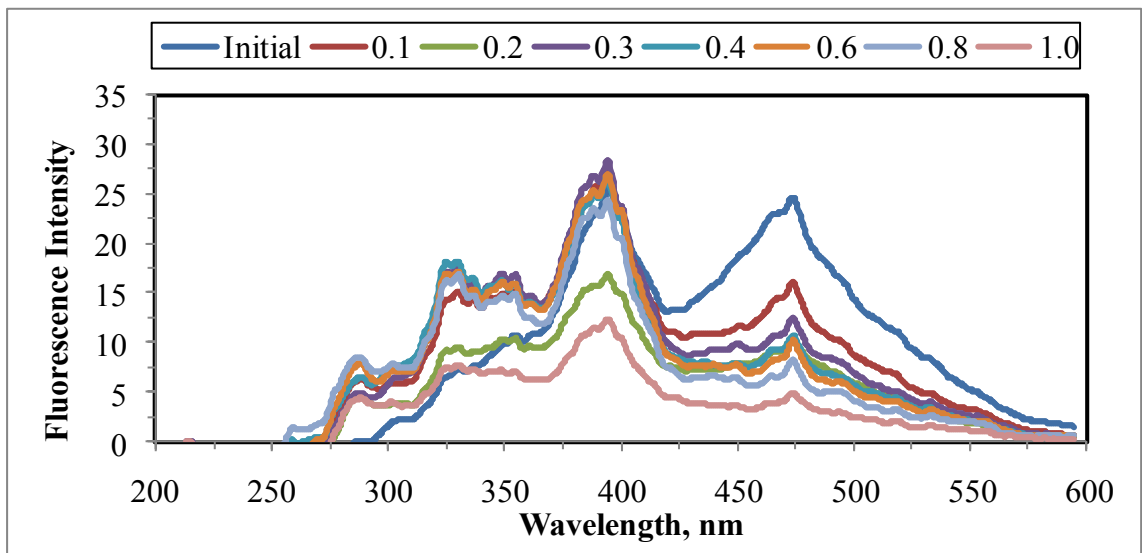
Figure 4.14. Synchronous scan fluorescence spectra of 0.45 µm filtration fraction of humic acid following adsorption onto N-doped TiO$_2$ Degussa P-25.

4.3.1.4. Spectroscopic Properties of 0.45 μm Filtered Fraction of Humic Acid Following Adsorption onto S-doped TiO_2 Degussa P-25 Specimen. Adsorption characteristics of humic acid were evaluated through UV-vis and fluorescence spectroscopic properties. UV-vis absorbance spectra of 0.45 μm filtration fraction of humic acid following adsorption onto S-doped TiO_2 Degussa P-25 were presented in Figure 4.15.
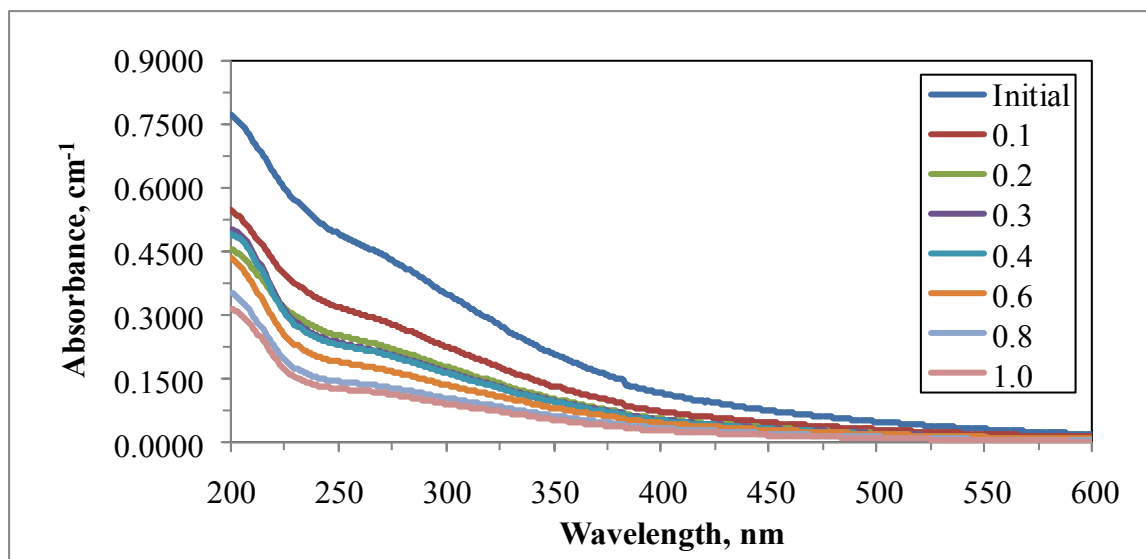
Figure 4.15. UV-vis absorbance spectra of 0.45 μm filtration fraction of humic acid following adsorption onto S-doped TiO_2 Degussa P-25.

UV-vis absorbance spectra of humic acids exhibited a decreasing trend with increasing wavelength with respect to increasing dose of TiO_2 loading. UV-vis absorbance spectra demonstrated a similar overlapping trend on each other for 0.45 μm filtration fraction of humic acid following adsorption onto 0.2 mg mL^{-1} and 0.3 mg mL^{-1} as well as 0.4 mg mL^{-1} doses of S-doped TiO_2 Degussa P-25 (Figure 4.15).

Emission scan fluorescence spectra and synchronous scan fluorescence spectra for 0.45 μm filtration fraction of humic acid following adsorption onto S-doped TiO_2 Degussa P-25were presented in Figure 4.16 and Figure 4.17, respectively. Emission scan fluorescence spectra demonstrated a similar overlapping trend on each other for 0.45 μm filtration fraction of humic acid following adsorption onto0.6 mg mL^{-1}, 0.8 mg mL^{-1} and 1.0 mg mL^{-1} doses of S-doped TiO_2 Degussa P-25 (Figure 4.16).
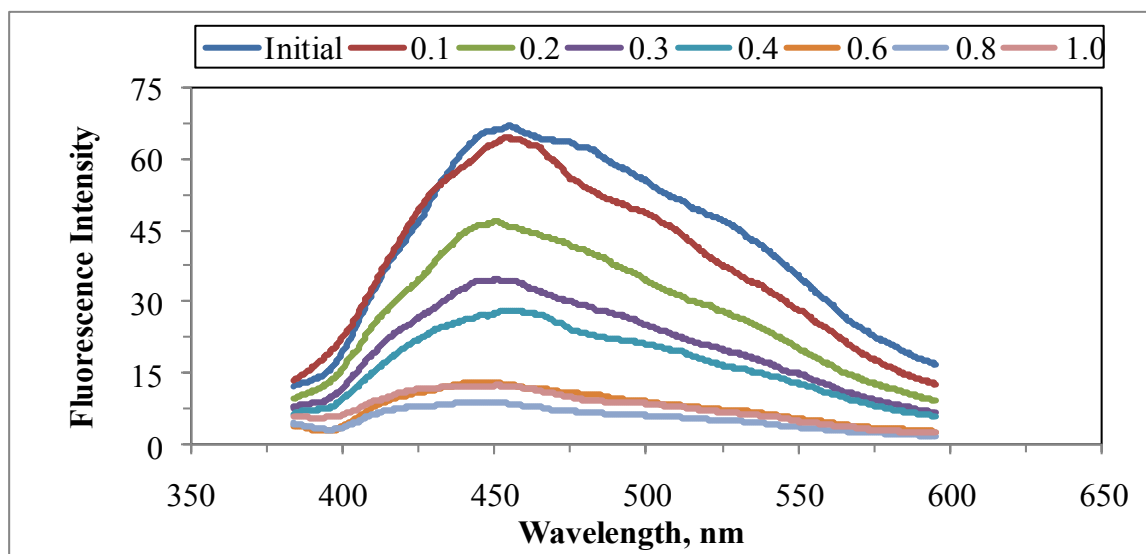
Figure 4.16. Emission scan fluorescence spectra of 0.45 µm filtration fraction of humic acid following adsorption onto S-doped TiO_2 Degussa P-25 at 350 nm excitation wavelength.

Synchronous scan fluorescence spectra for 0.45 µm filtration fraction of humic acid showed two sharp peaks around emission wavelengths of 325 nm and 400 nm, while the displayed one moderate peak around 475 nm emission wavelength (Figure 4.17).
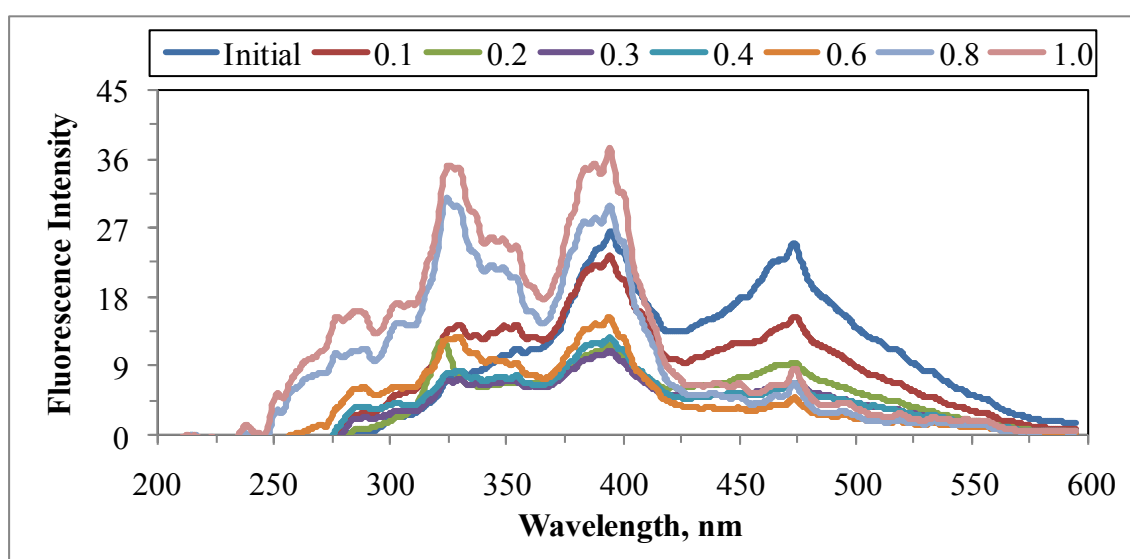
Figure 4.17. Synchronous scan fluorescence spectra of 0.45 µm filtration fraction of humic acid following adsorption onto S-doped TiO_2 Degussa P-25.

4.3.1.5. Spectroscopic Properties of 0.45 μm Filtered Fraction of Humic Acid Following Adsorption onto N-S co-doped TiO_2 Degussa P-25 Specimen. UV-vis absorbance spectra of 0.45 μm filtration fraction of humic acid following adsorption onto N-S co-doped TiO_2 Degussa P-25 were presented in Figure 4.18.
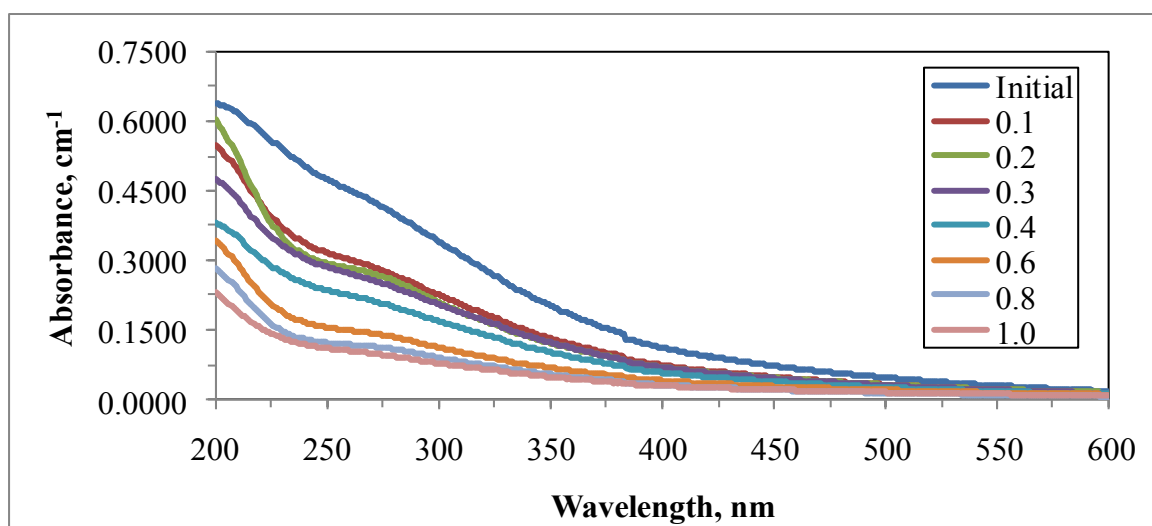
Figure 4.18.   UV-vis absorbance spectra of 0.45 μm filtration fraction of humic acid following adsorption onto N-S co-doped TiO_2 Degussa P-25.

UV-vis absorbance spectra of humic acids exhibited a decreasing trend with increasing wavelength with respect to increasing dose of TiO_2 as expected. UV-vis absorbance spectra followed an overlapping trend onto each other for 0.45 μm filtration fraction of humic acid following adsorption onto 0.1 mg mL^{-1}, 0.2 mg mL^{-1} and 0.3 mg mL^{-1} loadings of N-S co-doped TiO_2 Degussa P-25 (Figure 4.18).

Emission scan fluorescence spectra and synchronous scan fluorescence spectra of 0.45 μm filtration fraction of humic acid following adsorption onto N-S co-doped TiO_2 Degussa P-25 were presented in Figure 4.19 and Figure 4.20. The emission scan fluorescence spectra of 0.45 μm filtration fraction of humic acid following adsorption onto 0.6 mg mL^{-1}, 0.8 mg mL^{-1} and 1.0 mg mL^{-1} doses of N-S co-doped TiO_2 Degussa P-25 showed an overlapping trend onto each other (Figure 4.19). Synchronous scan fluorescence spectra for 0.45 μm filtration fraction of humic acid showed two sharp peaks around emission wavelengths of 325 nm and 400 nm, while the fluorescence spectra displayed two moderate peaks around 275 nm and 475 nm emission wavelengths (Figure 4.20).

Figure 4.19. Emission scan fluorescence spectra of 0.45 μm filtration fraction of humic acid following adsorption onto N-S co-doped TiO_2 Degussa P-25 at 350 nm excitation wavelength.
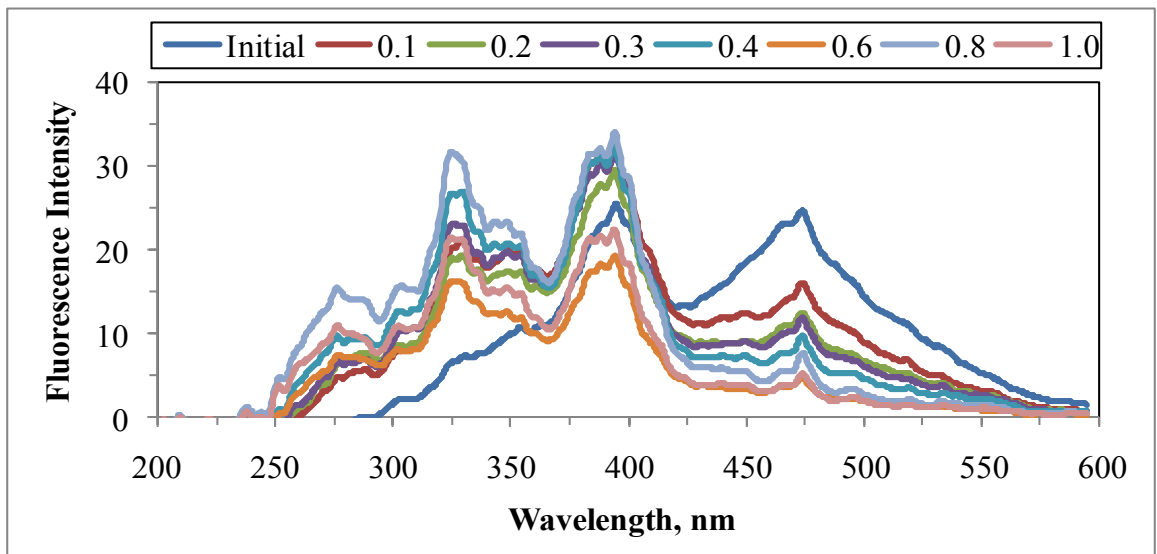
Figure 4.20. Synchronous scan fluorescence spectra of 0.45 μm filtration fraction of humic acid following adsorption onto N-S co-doped TiO_2 Degussa P-25.

4.3.2. Spectroscopic Properties of 0.45 µm Filtered Fraction of Humic Acid Following Adsorption onto TiO₂ Hombikat UV-100 Specimens

Batch adsorption experiments were conducted by using 0.45 µm filtered fraction of humic acid and TiO₂ Hombikat UV-100 specimens *i.e.* bare TiO_2, C-doped TiO_2, N-doped TiO_2, S-doped TiO_2 and N-S co-doped TiO_2.

4.3.2.1. Spectroscopic Properties of 0.45 µm Filtered Fraction of Humic Acid Following Adsorption onto Bare TiO₂ Hombikat UV-100 Specimen. UV-vis absorbance spectra of 0.45 µm filtration fraction of humic acid following adsorption onto bare TiO_2 Hombikat UV-100 were presented in Figure 4.21.
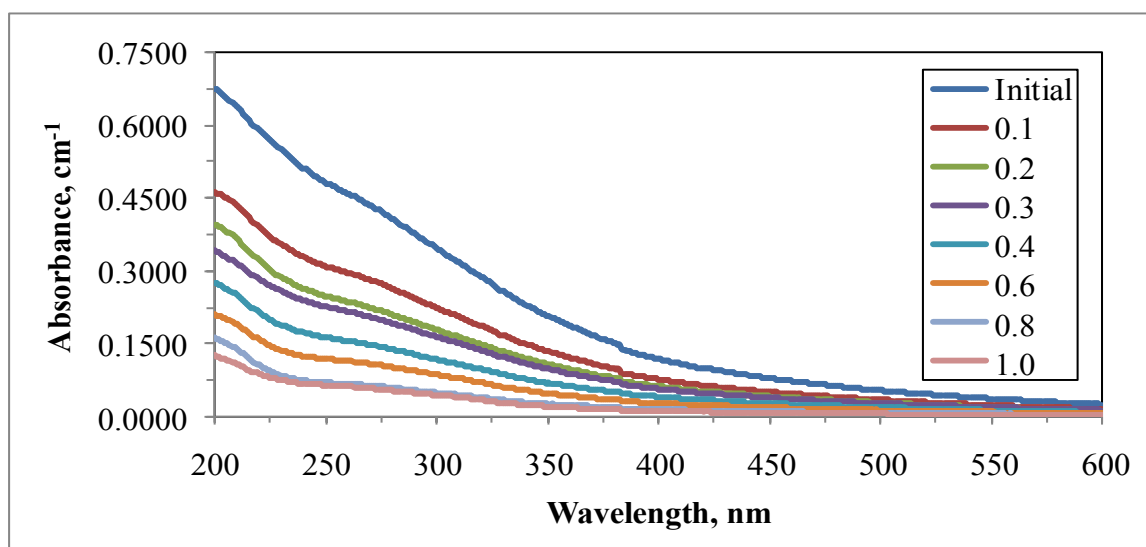
Figure 4.21.   UV-vis absorbance spectra of 0.45 µm filtration fraction of humic acid following adsorption onto bare TiO₂ Hombikat UV-100.

UV-vis absorbance spectra of humic acids exhibited generally a decreasing trend with increasing wavelength with respect to increasing dose of TiO_2 as expected. UV-vis absorbance values for all of the humic acid solutions approached to zero and also leveled off after 400 nm wavelength. UV- vis absorbance spectra exhibited a similar overlapping trend on each other for 0.45 µm filtration fraction of humic acid following adsorption onto 0.2 mg mL^{-1} and 0.3 mg mL^{-1} TiO_2 as well as 0.8 mg mL^{-1} and 1.0 mg mL^{-1} TiO_2 doses.

Emission scan fluorescence spectra and synchronous scan fluorescence spectra of 0.45 μm filtration fraction of humic acid following adsorption onto bare TiO₂ Hombikat UV-100 were presented in Figure 4.22 and Figure 4.23, respectively.
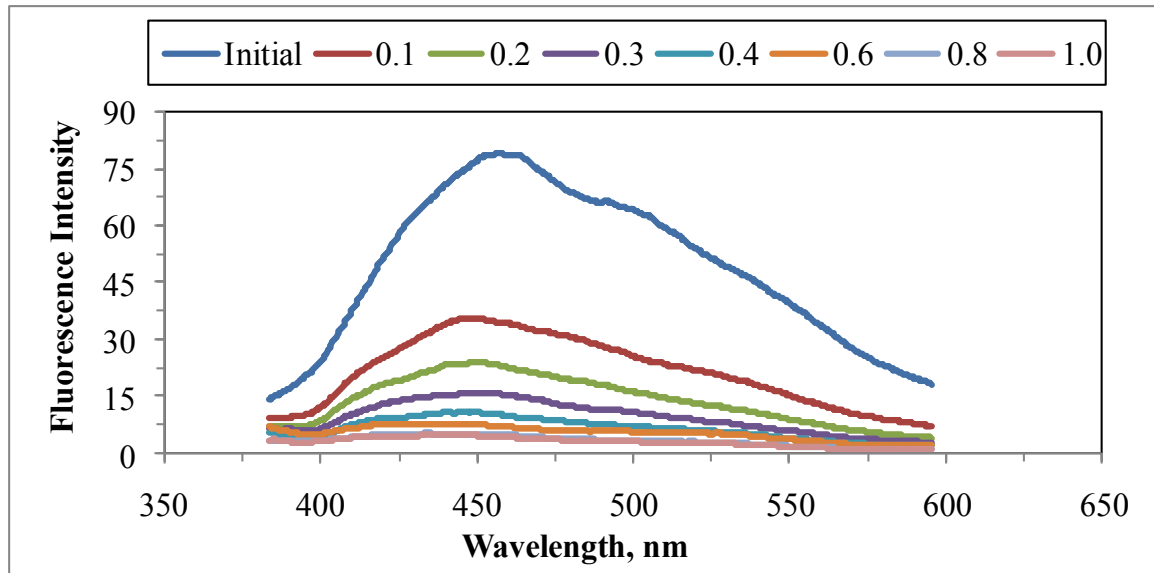
Figure 4.22. Emission scan fluorescence spectra of 0.45 μm filtration fraction of humic acid following adsorption onto bare TiO₂ Hombikat UV-100 at 350 nm excitation wavelength.
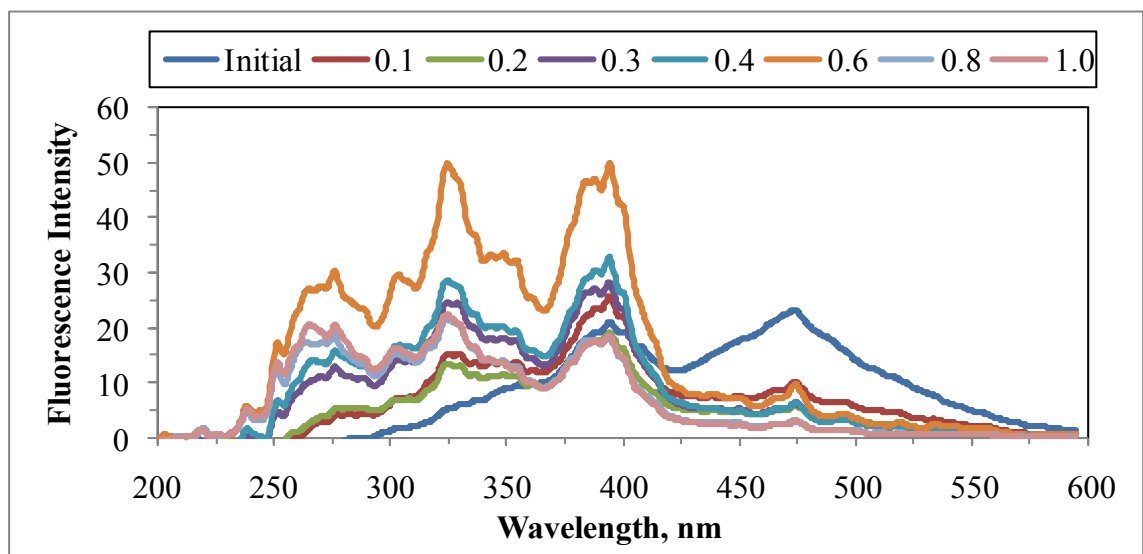
Figure 4.23. Synchronous scan fluorescence spectra of 0.45 μm filtration fraction of humic acid following adsorption onto bare TiO₂ Hombikat UV-100.

Emission scan fluorescence spectra displayed a similar overlapping trend on each other for 0.45 μm filtration fraction of humic acid following adsorption onto 0.6 mg mL^{-1}, 0.8 mg mL^{-1} and 1.0 mg mL^{-1} bare TiO$_2$ Hombikat UV-100. A characteristic decreasing was observed with the addition of increased dose of TiO$_2$ in fluorescence intensity. A broader peak around 450 nm emission wavelength and minor shoulder around 500 nm emission wavelength for initial humic acid that had relatively higher fluorescence intensity than fluorescence intensities of increased doses of TiO$_2$ were observed (Figure 4.22).

Synchronous scan fluorescence spectra for 0.45 μm filtration fraction of humic acid showed two sharp peaks around emission wavelengths of 325 nm and 400 nm, while the fluorescence spectra displayed two moderate peaks around 275 nm and 475 nm emission wavelengths. The highest fluorescence intensity for 0.45 μm filtration fraction of humic acid following adsorption onto 0.6 mg mL^{-1} bare TiO$_2$ Hombikat UV-100 was observed at 325 nm and 400 nm emission wavelengths. The lowest fluorescence intensity for 0.45 μm filtration fraction of humic acid following adsorption onto 1.0 mg mL^{-1} TiO$_2$ dose was observed at 475 nm emission wavelength (Figure 4.23).

UV-vis spectral features of 0.45 μm filtration fraction of humic acid recorded following adsorption onto two different bare TiO$_2$ specimens (Degussa P-25 and Hombikat UV-100) were compared (Figure 4.6 and Figure 4.21). It could be clearly deduced that the effect of pure anatase form (Hombikat UV-100) was more pronounced with respect to the presence of mixed crystal phases (Degussa P-25) in the UV region. However, no distinct difference could be visualized in the visible region.

Similar effect could also be indicated for the emission scan fluorescence spectral features (Figure 4.7 and Figure 4.22). Moreover, synchronous scan fluorescence spectral features displayed close similarities both in terms of shape and fluorescence intensity measures (Figure 4.8 and Figure 4.23).

4.3.2.2. Spectroscopic Properties of 0.45 μm Filtered Fraction of Humic Acid Following Adsorption onto C-doped TiO_2 Hombikat UV-100 Specimen. UV-vis absorbance spectra of 0.45 μm filtration fraction of humic acid following adsorption onto C-doped TiO_2 Hombikat UV-100 were presented in Figure 4.24.
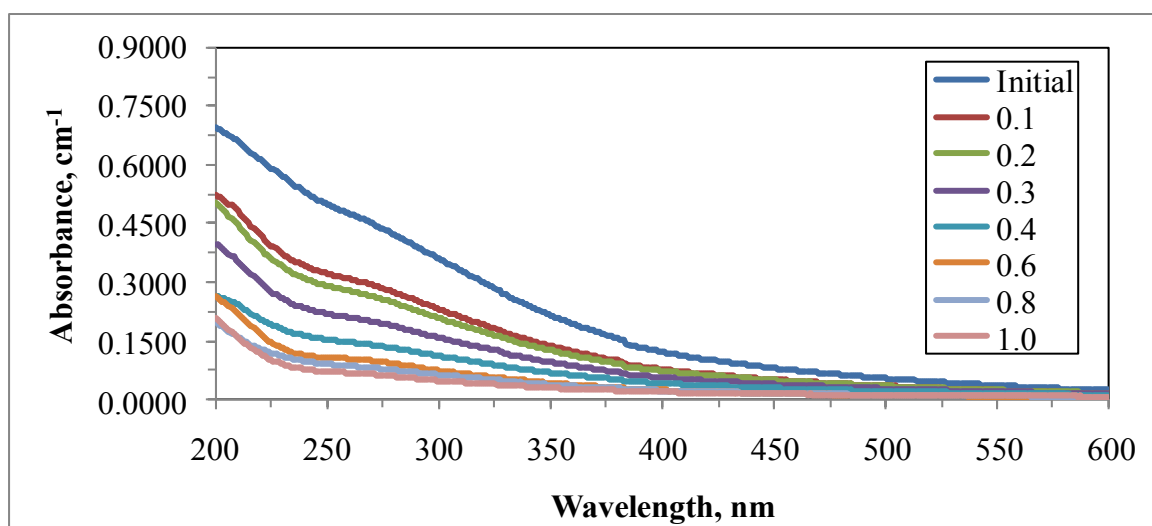
Figure 4.24. UV-vis absorbance spectra of 0.45 μm filtration fraction of humic acid following adsorption onto C-doped TiO_2 Hombikat UV-100.

UV-vis absorbance spectra of humic acids exhibited a decreasing trend with increasing wavelength and also with increasing TiO_2 loading. Furthermore, after 275 nm wavelength, UV-vis absorbance spectra exhibited an overlapping trend onto each other for 0.45 μm filtration fraction of humic acid following adsorption onto 0.6 mg mL^{-1}, 0.8 mg mL^{-1} and 1.0 mg mL^{-1} loadings of C-doped TiO_2 Hombikat UV-100 (Figure 4.24).

Emission scan fluorescence spectra and synchronous scan fluorescence spectra of 0.45 μm filtration fraction of humic acid following adsorption onto C-doped TiO_2 Hombikat UV-100 were presented in Figure 4.25 and Figure 4.26, respectively. The emission scan fluorescence spectra of 0.45 μm filtration fraction of humic acid following adsorption onto C-doped TiO_2 Hombikat UV-100 in doses, 0.6 mg mL^{-1} 0.8 mg mL^{-1} and 1.0 mg mL^{-1} had the lowest fluorescence intensity. Particularly after adsorption onto 0.6 mg mL^{-1} TiO_2, the decrease of emission scan fluorescence intensity was easily noticed. Synchronous scan fluorescence spectra showed one sharp peak around emission

wavelength of 400 nm, while the fluorescence spectra displayed three moderate peaks around 275 nm, 325 nm and 475 nm emission wavelengths (Figure 4.26).

Figure 4.25. Emission scan fluorescence spectra of 0.45 µm filtration fraction of humic acid following adsorption onto C-doped TiO_2 Hombikat UV-100 at 350 nm excitation wavelength.

Figure 4.26. Synchronous scan fluorescence spectra of 0.45 µm filtration fraction of humic acid following adsorption onto C-doped TiO_2 Hombikat UV-100.

4.3.2.3. Spectroscopic Properties of 0.45 μm Filtered Fraction of Humic Acid Following Adsorption onto N-doped TiO₂ Hombikat UV-100 Specimen. UV-vis absorbance spectra of 0.45 μm filtration fraction of humic acid following adsorption onto N-doped TiO₂ Hombikat UV-100 were presented in Figure 4.27.
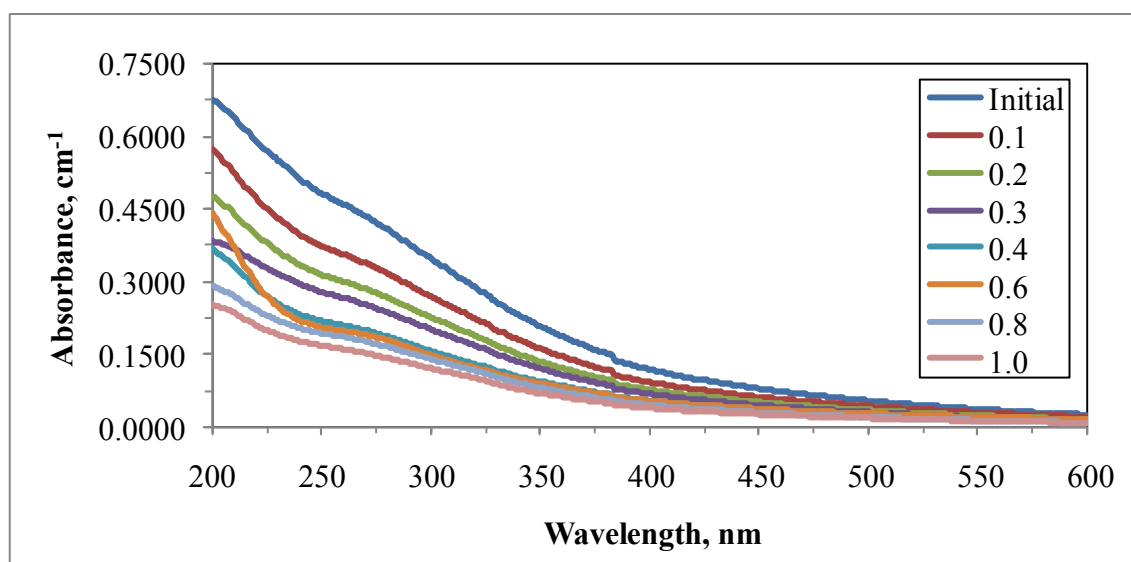
Figure 4.27. UV-vis absorbance spectra of 0.45 μm filtration fraction of humic acid following adsorption onto N-doped TiO₂ Hombikat UV-100.

UV-vis absorbance spectra of humic acid solutions exhibited a declining trend with increasing wavelength and also with increasing TiO₂ loadings. UV-vis absorbance spectra exhibited a similar overlapping trend onto each other for 0.45 μm filtration fraction of humic acid following adsorption onto 0.4 mg mL⁻¹ and 0.6 mg mL⁻¹ loadings of N-doped TiO₂ Hombikat UV-100 after 275 nm wavelength (Figure 4.27).

Emission scan fluorescence spectra and synchronous scan fluorescence spectra of 0.45 μm filtration fraction of humic acid following adsorption onto N-doped TiO₂ Hombikat UV-100 were presented in Figure 4.28 and Figure 4.29, respectively. The lowest fluorescence intensity was observed for 0.45 μm filtration fraction of humic acid following adsorption onto higher dosages of N-doped TiO₂ Hombikat UV-100, such as, 0.6 mg mL⁻¹, 0.8 mg mL⁻¹ and 1.0 mg mL⁻¹, which displayed a similar overlapping trend onto each other (Figure 4.28).
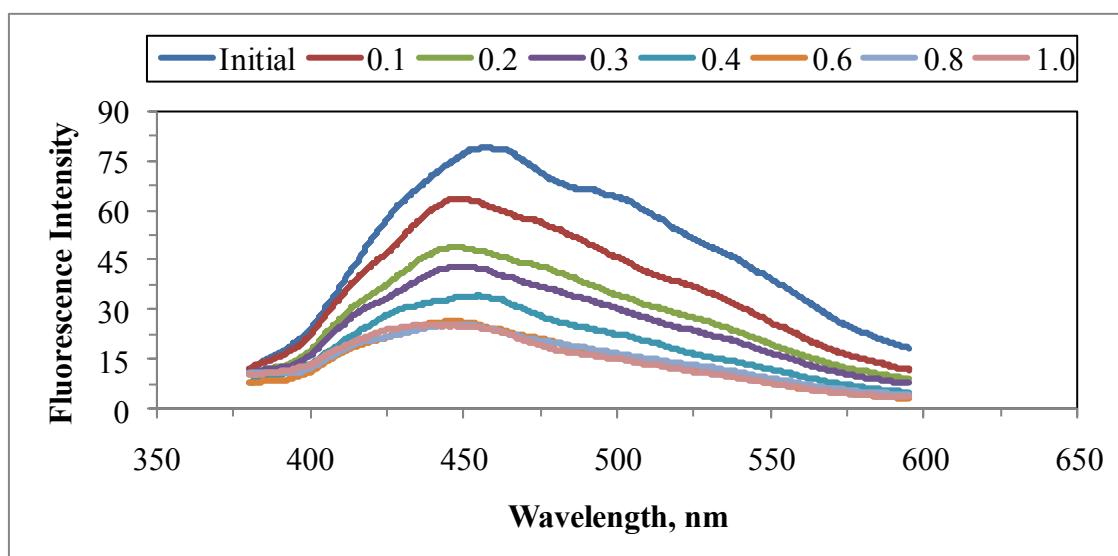
Figure 4.28. Emission scan fluorescence spectra of 0.45 μm filtration fraction of humic acid following adsorption onto N-doped TiO_2 Hombikat UV-100 at 350 nm excitation wavelength.

Synchronous scan fluorescence spectra showed two sharp peaks around emission wavelengths of 325 nm and 400 nm, while the fluorescence spectra displayed two moderate peaks around 275 nm and 475 nm emission wavelengths (Figure 4.29).

Figure 4.29. Synchronous scan fluorescence spectra of 0.45 μm filtration fraction of humic acid following adsorption onto N-doped TiO_2 Hombikat UV-100.

4.3.2.4. Spectroscopic Properties of 0.45 μm Filtered Fraction of Humic Acid Following Adsorption onto S-Doped TiO$_2$ Hombikat UV-100 Specimen. UV-vis absorbance spectra of 0.45 μm filtration fraction of humic acid following adsorption onto S-doped TiO$_2$ Hombikat UV-100 were presented in Figure 4.30.
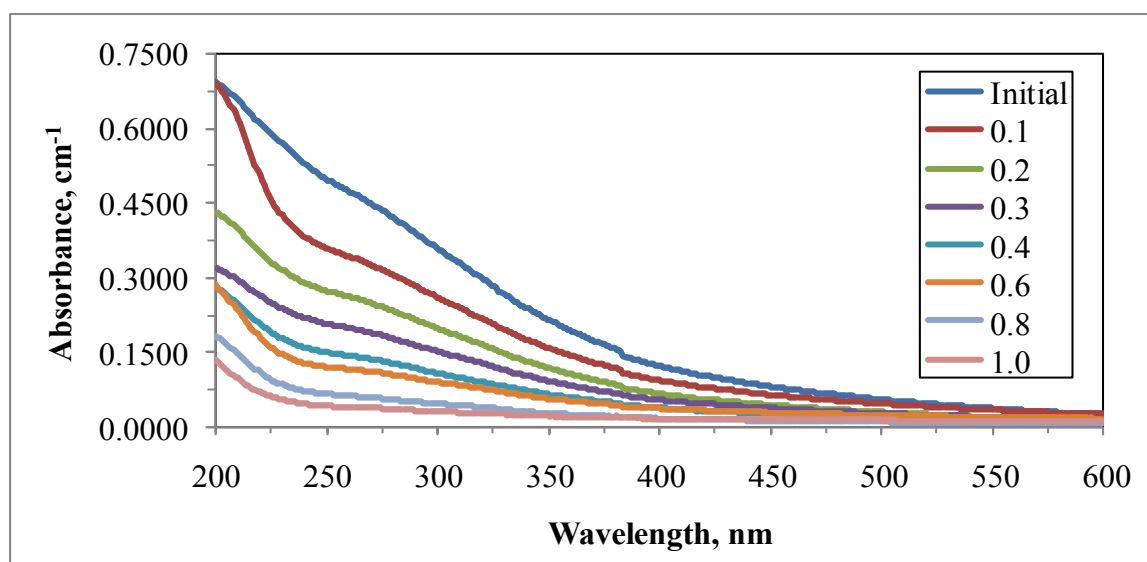
Figure 4.30. UV-vis absorbance spectra of 0.45 μm filtration fraction of humic acid following adsorption onto S-doped TiO$_2$ Hombikat UV-100.

UV-vis absorbance spectra of humic acid solutions exhibited a decreasing trend with increasing wavelength with respect to increasing dose of TiO$_2$ as expected. The UV-vis absorbance trends of 0.45 μm filtration fraction of humic acid following adsorption onto 0.8 mg mL^{-1} and 1.0 mg mL^{-1}as well as 0.4mg mL^{-1}and 0.6mg mL^{-1}loadings of S-doped TiO$_2$ Hombikat UV-100 were very close to each other after 300 nm wavelength (Figure 4.30).

Emission scan fluorescence spectra and synchronous scan fluorescence spectra of 0.45 μm filtration fraction of humic acid following adsorption onto S-doped TiO$_2$ Hombikat UV-100 were presented in Figure 4.31 and Figure 4.32, respectively. The emission fluorescence spectra of 0.45 μm filtration fraction of humic acid following adsorption onto 0.6 mg mL^{-1}, 0.8 mg mL^{-1} and 1.0 mg mL^{-1} doses of S-doped TiO$_2$ Hombikat UV-100 had the lowest fluorescence intensity (Figure 4.31).
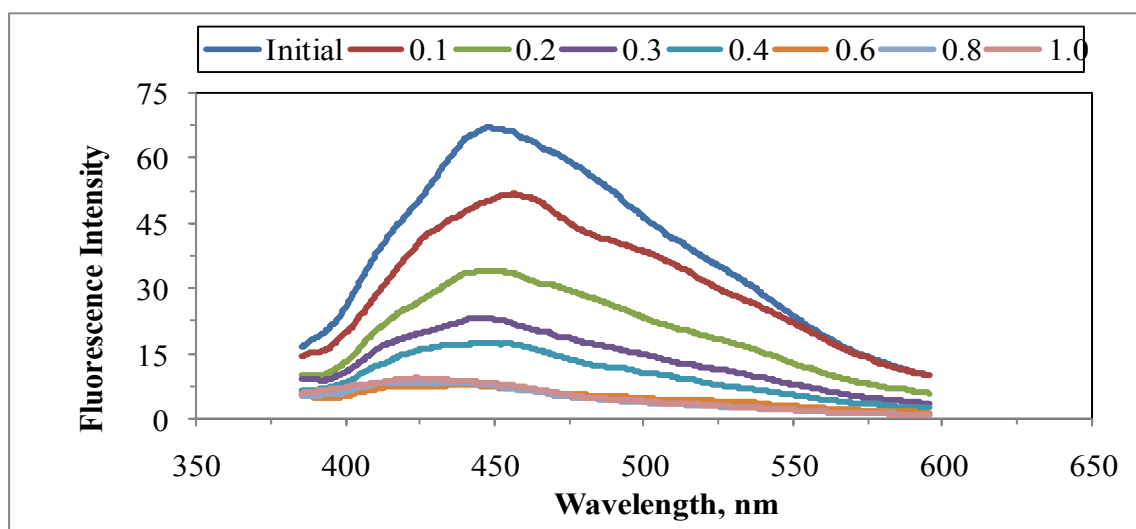
Figure 4.31. Emission scan fluorescence spectra of 0.45 µm filtration fraction of humic acid following adsorption onto S-doped TiO_2 Hombikat UV-100 at 350 nm excitation wavelength.

Synchronous scan fluorescence spectra showed one sharp peak around emission wavelength of 400 nm, while the fluorescence spectra displayed two moderate peaks around 325 nm and 475 nm emission wavelengths (Figure 4.32).

Figure 4.32. Synchronous scan fluorescence spectra of 0.45 µm filtration fraction of humic acid following adsorption onto S-doped TiO_2 Hombikat UV-100.

4.3.2.5. Spectroscopic Properties of 0.45 μm Filtered Fraction of Humic Acid Following Adsorption onto N-S co-doped TiO$_2$ Hombikat UV-100 Specimen. UV-vis absorbance spectra of 0.45 μm filtration fraction of humic acid following adsorption onto N-S co-doped TiO$_2$ Hombikat UV-100 were presented in Figure 4.33.
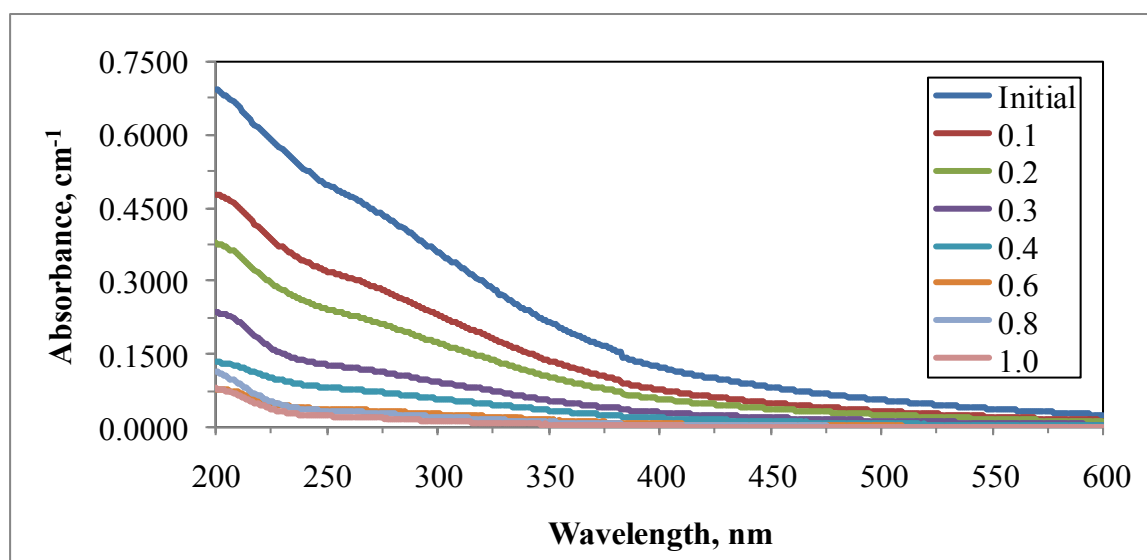
Figure 4.33. UV-vis absorbance spectra of 0.45 μm filtered fraction of humic acid following adsorption onto N-S co-doped TiO$_2$ Hombikat UV-100.

UV-vis absorbance spectra of humic acid solutions exhibited the major decreases with increasing wavelength and also with increasing TiO$_2$ loading. UV-vis absorbance spectra followed an overlapping trend for 0.45 μm filtration fraction of humic acid following adsorption onto 0.6 mg mL^{-1}, 0.8 mg mL^{-1} and 1.0 mg mL^{-1} loadings of N-doped TiO$_2$ Hombikat UV-100 (Figure 4.33).

Emission scan fluorescence spectra and synchronous scan fluorescence spectra of 0.45 μm filtration fraction of humic acid following adsorption onto N-S co-doped TiO$_2$ Hombikat UV-100 were presented in Figure 4.34 and Figure 4.35, respectively. The emission scan fluorescence spectra of 0.45 μm filtration fraction of humic acid following adsorption onto 0.6 mg mL^{-1}, 0.8 mg mL^{-1} and 1.0 mg mL^{-1} doses of N-S co-doped TiO$_2$ Hombikat UV-100, which displayed a similar overlapping trend onto each other, had the lower fluorescence intensity (Figure 4.34).
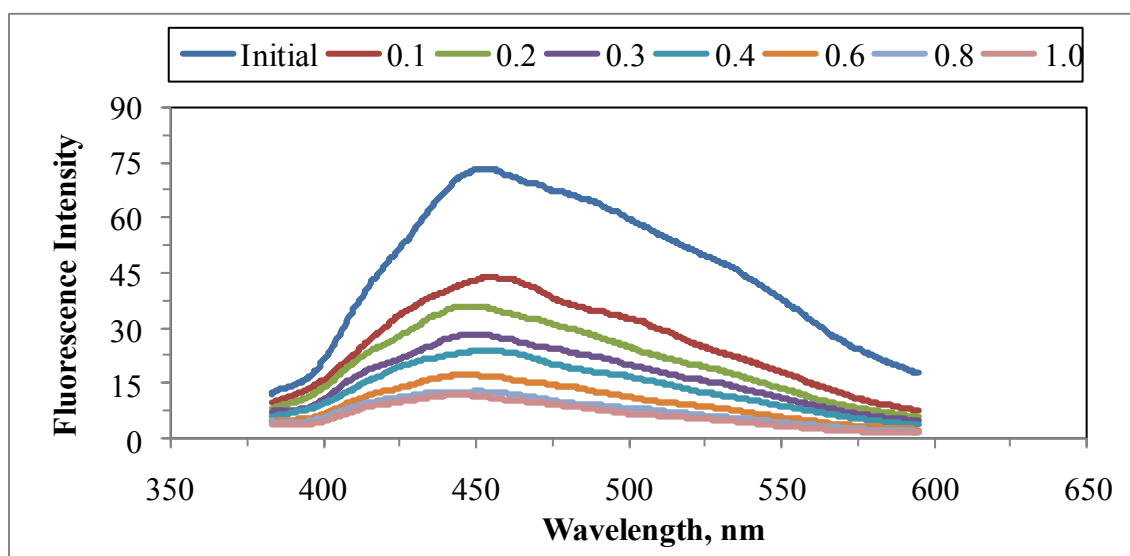
Figure 4.34. Emission scan fluorescence spectra of 0.45 μm filtration fraction of humic acid following adsorption onto N-S co-doped TiO_2 Hombikat UV-100 at 350 nm excitation wavelength.

Synchronous scan fluorescence spectra displayed two sharp peaks around 325 nm and 400 nm emission wavelengths, while the fluorescence spectra displayed two moderate peaks around 275 nm and 475 nm emission wavelengths (Figure 4.35).
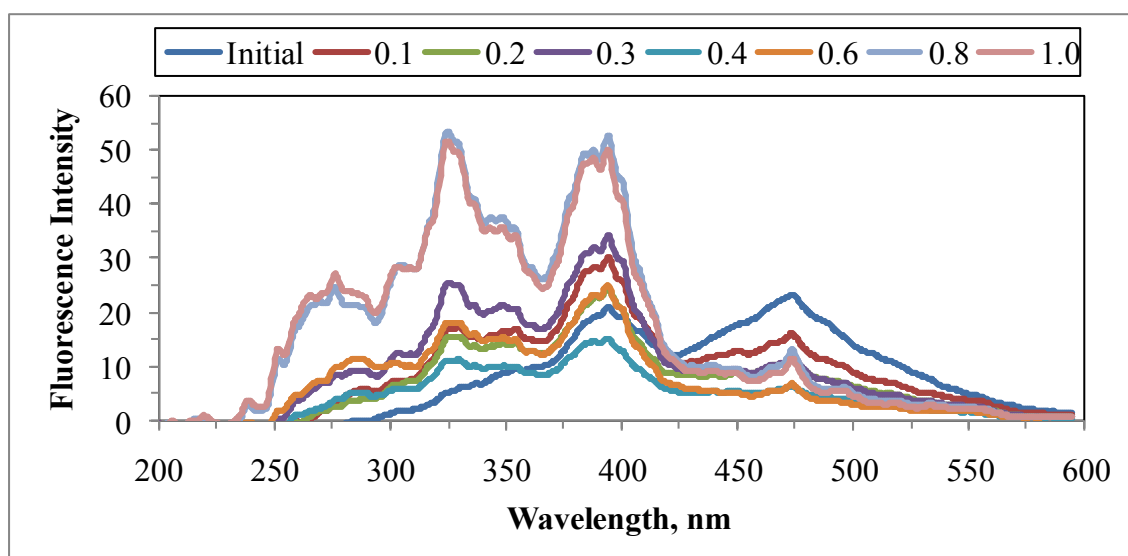
Figure 4.35. Synchronous scan fluorescence spectra of 0.45 μm filtration fraction of humic acid following adsorption onto N-S co-doped TiO_2 Hombikat UV-100.

4.4. Spectroscopic Properties of 100 kDa Fraction of Humic Acid Following Adsorption onto TiO$_2$ Specimens

Batch adsorption experiments were implemented by using 100 kDa fraction of humic acid as the adsorbate and bare and also doped TiO$_2$ Degussa P-25 and TiO$_2$ Hombikat UV-100 specimens as the adsorbent in the loading range of 0.1 – 1.0 mg mL^{-1}. Adsorption data were evaluated by presenting respective figures where 'Initial' term was used to indicate the 100 kDa fraction of humic acid and '0.1-1.0' represented dose range of TiO$_2$ (mgmL^{-1}).

4.4.1. Spectroscopic Properties of 100 kDa Fraction of Humic Acid Following Adsorption onto TiO$_2$ Degussa P-25 Specimens

Batch adsorption experiments were conducted by using 100 kDa fraction of humic acid and TiO$_2$ Degussa P-25 specimens *i.e.* bare TiO$_2$, C-doped TiO$_2$, N-doped TiO$_2$, S-doped TiO$_2$ and N-S co-doped TiO$_2$.

4.4.1.1. Spectroscopic Properties of 100 kDa Fraction of Humic Acid Following Adsorption onto Bare TiO$_2$ Degussa P-25 Specimen. UV-vis absorbance spectra of 100 kDa fraction of humic acid following adsorption onto bare TiO$_2$ Degussa P-25 were displayed in Figure 4.36.

UV-vis absorbance spectra displayed a decreasing trend for 100 kDa fraction of humic acid following adsorption onto bare TiO$_2$ Degussa P-25. Moreover, UV-vis absorbance spectra of humic acids exhibited the major decreases with increasing wavelength and also with increasing TiO$_2$ loading. UV-vis absorbance spectra demonstrated a similar overlapping trend on each other for 100 kDa fraction of humic acid adsorption onto 0.2 mg mL^{-1}, 0.3 mg mL^{-1} and 0.4 mg mL^{-1} TiO$_2$ doses (Figure 4.36).

Emission scan fluorescence spectral features attained through adsorption of 100 kDa fraction of humic acid samples onto bare TiO$_2$ Degussa P-25 was presented in Figure 4.37.

Figure 4.36. UV-vis absorbance spectra of 100 kDa fraction of humic acid following adsorption onto bare TiO$_2$ Degussa P-25.

Figure 4.37. Emission scan fluorescence spectra of 100 kDa fraction of humic acid following adsorption onto bare TiO$_2$ Degussa P-25 at 350 nm excitation wavelength.

The emission scan fluorescence spectra of 100 kDa fraction of humic acid following adsorption onto 0.4 mg mL^{-1} dose of bare TiO$_2$ Degussa P-25 had the highest fluorescence intensity contrary to maximum dosage of TiO$_2$ (1.0 mg mL^{-1}), having the lowest fluorescence intensity (Figure 4.37).

Moreover, emission scan fluorescence spectra of 100 kDa fraction of humic acid adsorption onto bare TiO_2 Degussa P-25 attained maximum fluorescence intensity around 450 nm emission wavelength. (Figure 4.37). Synchronous scan fluorescence spectra scanned for 100 kDa fraction of humic acid following adsorption onto bare TiO_2 Degussa P-25 were presented in Figure 4.38.
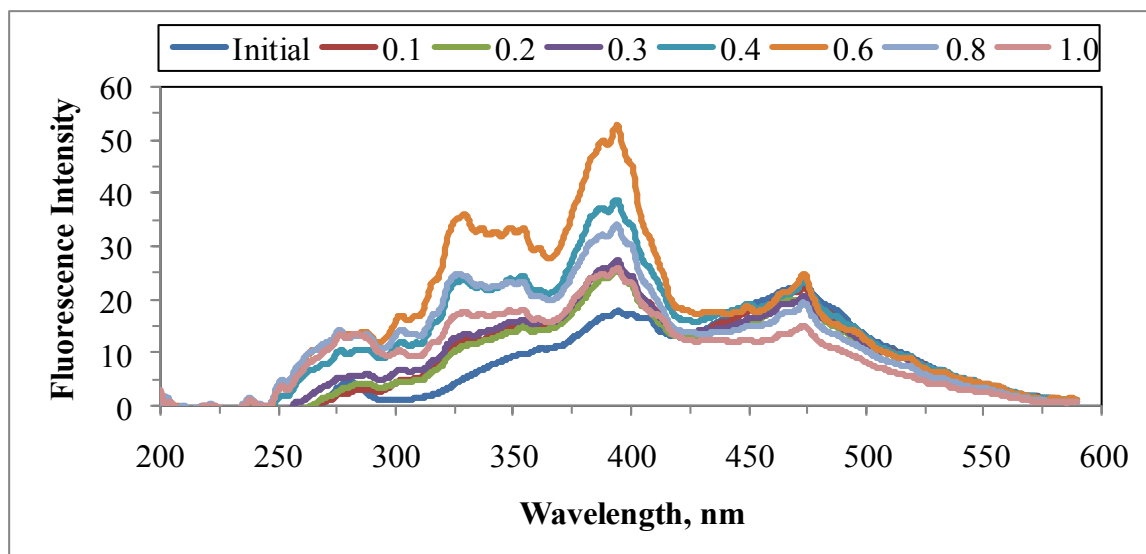
Figure 4.38. Synchronous scan fluorescence spectra of 100 kDa fraction of humic acid following adsorption onto bare TiO_2 Degussa P-25.

Synchronous scan fluorescence spectra for 100 kDa fraction of humic acid showed a sharp peak around emission wavelength of 400 nm, while the fluorescence spectra displayed two moderate peaks around 325 nm and 475 nm emission wavelengths. The lowest fluorescence intensity was observed for 100 kDa fraction of humic acid following adsorption onto 0.8 mg mL^{-1} dose of TiO_2 along with initial concentration of humic acid at 475 nm emission wavelength. The highest fluorescence intensity for 100 kDa fraction of humic acid was observed at 400 nm emission wavelength (Figure 4.38). Comparative evaluation of the spectroscopic features of 100 kDa fraction of humic acid with 0.45 μm filtration fraction of humic acid revealed the most significant difference in emission scan fluorescence spectral features (Figure 4.7 and Figure 4.37). The reason could be attributed to the role of the fluorophoric groups present on the different molecular size fractions of humic acid.

4.4.1.2. Spectroscopic Properties of 100 kDa Fraction of Humic Acid Following Adsorption onto C-doped TiO$_2$ Degussa P-25 Specimen. UV-vis absorbance spectra of 100 kDa fraction of humic acid following adsorption onto C-doped TiO$_2$ Degussa P-25 were displayed in Figure 4.39.
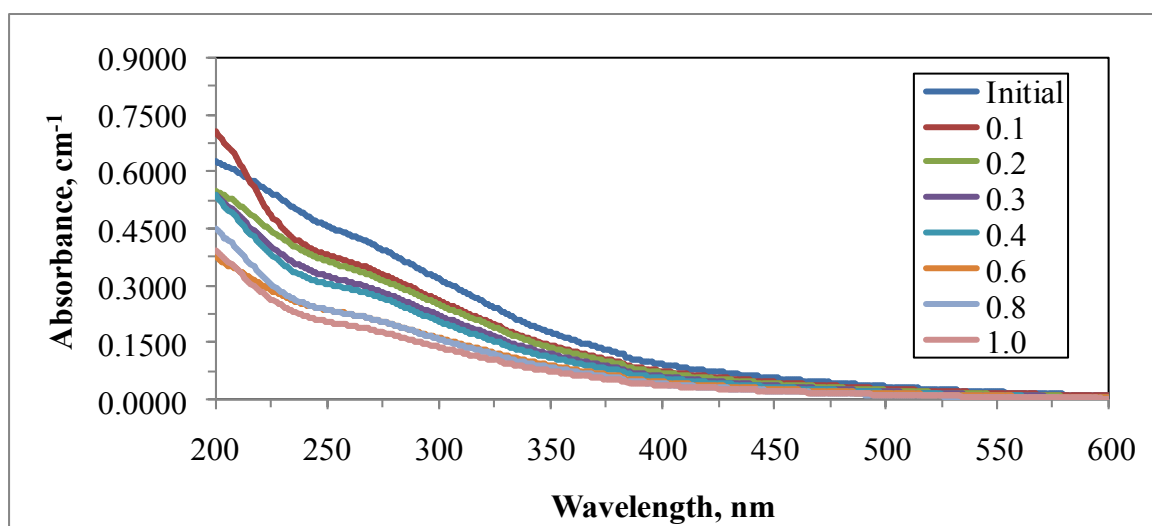
Figure 4.39. UV-vis absorbance spectra of 100 kDa fraction of humic acid following adsorption onto C-doped TiO$_2$ Degussa P-25.

UV-vis absorbance spectra of humic acid solutions exhibited a declining trend with increasing wavelength. Moreover, UV-vis absorbance spectra demonstrated a similar overlapping trend onto each other for 100 kDa fraction of humic acid following adsorption onto 0.6 mg mL^{-1} and 1.0 mg mL^{-1} as well as 0.3 mg mL^{-1} and 0.4 mg mL^{-1} doses of C-doped TiO$_2$ Degussa P-25. 100 kDa fraction of humic acid following adsorption onto higher dosages of C-doped TiO$_2$ Degussa P-25, such as 0.6 mg mL^{-1} and 1.0 mg mL^{-1} showed the lower absorbances (Figure 4.39).

Emission scan fluorescence spectra and synchronous scan fluorescence spectra of 100 kDa fraction of humic acid following adsorption onto C-doped TiO$_2$ Degussa P-25 were presented in Figure 4.40 and Figure 4.41, respectively. The emission scan fluorescence spectra displayed a similar overlapping trend onto each other for 100 kDa fraction of humic acid following adsorption onto 0.6 mg mL^{-1} and 1.0 mg mL^{-1} loadings of C-doped TiO$_2$ Degussa P-25 (Figure 4.40).

Figure 4.40. Emission scan fluorescence spectra of 100 kDa fraction of humic acid following adsorption onto C-doped TiO_2 Degussa P-25 at 350 nm excitation wavelength.

Synchronous scan fluorescence spectra showed two sharp peaks around emission wavelengths of 400 nm and 475 nm. Moreover, 100 kDa fraction of humic acid following adsorption onto 0.3 mg mL^{-1} dose of TiO_2 had the highest fluorescence intensity around 400 nm emission wavelength (Figure 4.41).

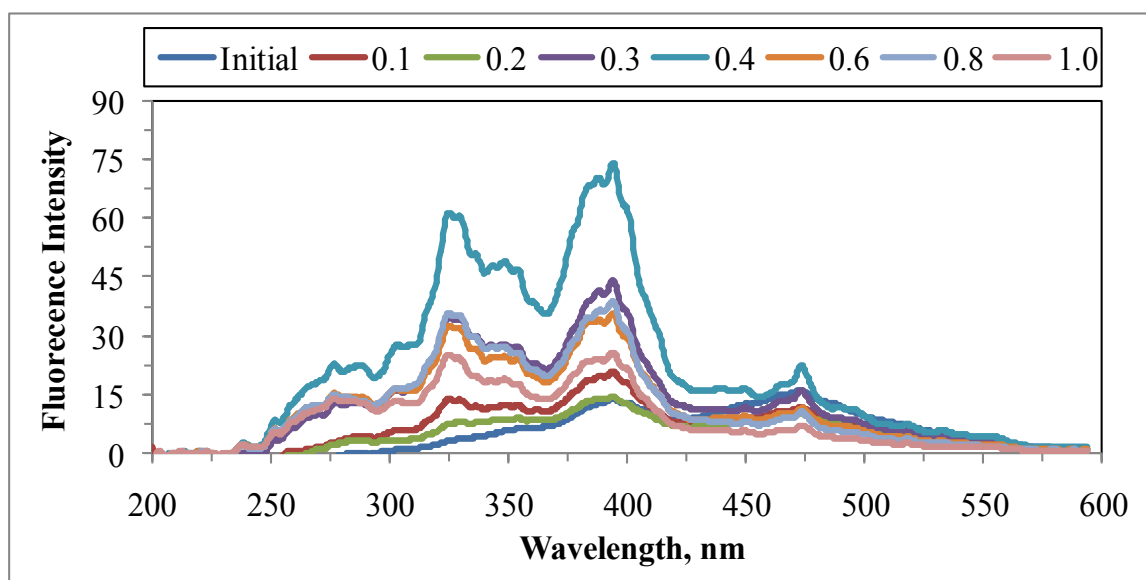

Figure 4.41. Synchronous scan fluorescence spectra of 100 kDa fraction of humic acid following adsorption onto C-doped TiO_2 Degussa P-25.

4.4.1.3. Spectroscopic Properties of 100 kDa Fraction of Humic Acid Following Adsorption onto N-doped TiO_2 Degussa P-25 Specimen. UV-vis absorbance spectra of 100 kDa fraction of humic acid following adsorption onto N-doped TiO_2 Degussa P-25 were displayed in Figure 4.42.

Figure 4.42. UV-vis absorbance spectra of 100 kDa fraction of humic acid following adsorption onto N-doped TiO_2 Degussa P-25.

UV-vis absorbance spectra demonstrated a similar overlapping trend onto each other for 100 kDa fraction of humic acid following adsorption onto 0.6 mg mL^{-1}, 0.8 mg mL^{-1} and 0.4 mg mL^{-1} as well as 1.0 mg mL^{-1} loadings of N-doped TiO_2 Degussa P-25.UV-vis absorbance spectra of humic acid solutions demonstrated a decreasing trend with increasing wavelength (Figure 4.42).

Emission scan fluorescence spectra and synchronous scan fluorescence spectra of 100 kDa fraction of humic acid following adsorption onto N-doped TiO_2 Degussa P-25 were presented in Figure 4.43 and Figure 4.44, respectively. The emission scan fluorescence spectra showed an overlapping trend on each other for 100 kDa fraction of humic acid following adsorption onto 0.6 mg mL^{-1}, 0.8 mg mL^{-1} and 1.0 mg mL^{-1} doses of N-doped TiO_2 Degussa P-25 (Figure 4.43). Synchronous scan fluorescence spectra showed two sharp peaks around emission wavelengths of 400 nm and 475 nm, while the fluorescence spectra displayed a small peak around 300 nm emission wavelength (Figure 4.44).
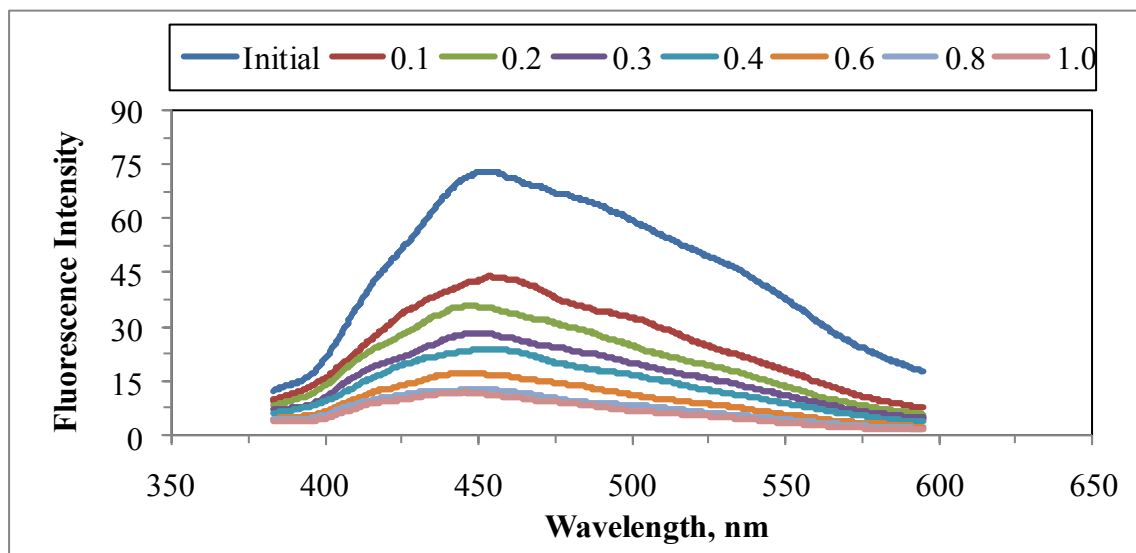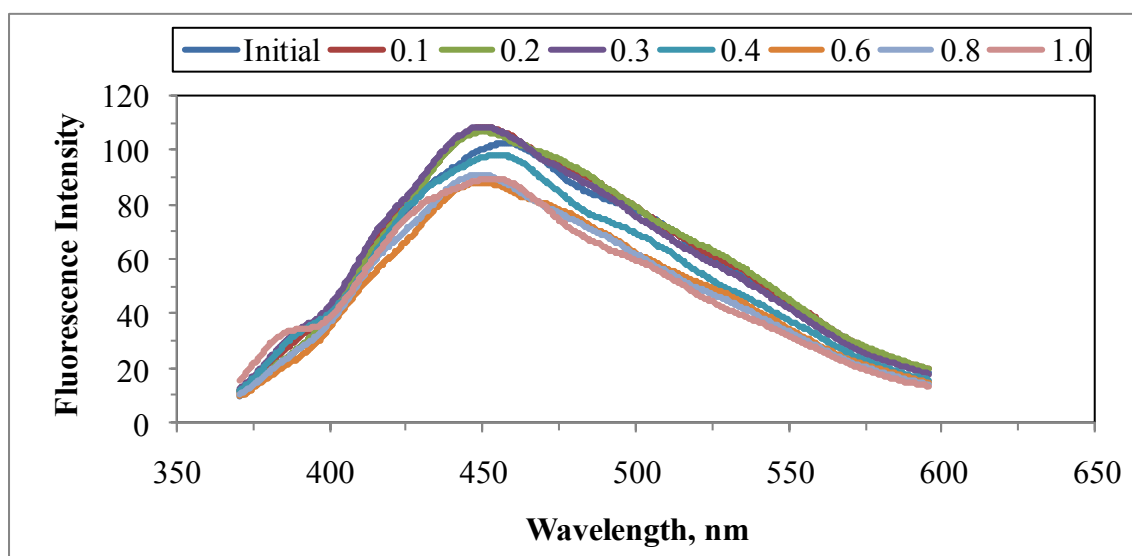
Figure 4.43. Emission scan fluorescence spectra of 100 kDa fraction of humic acid following adsorption onto N-doped TiO_2 Degussa P-25 at 350 nm excitation wavelength.

The highest fluorescence intensity was observed for 100 kDa fraction of humic acid following adsorption onto 0.1 mg mL^{-1} and 0.2 mg mL^{-1} loadings of N-doped TiO_2 Degussa P-25 around 400 nm emission wavelength (Figure 4.44).

Figure 4.44. Synchronous scan fluorescence spectra of 100 kDa fraction of humic acid following adsorption onto N-doped TiO_2 Degussa P-25.

4.4.1.4. Spectroscopic Properties of 100 kDa Fraction of Humic Acid Following Adsorption onto S-doped TiO₂ Degussa P-25 Specimen. UV-vis absorbance spectra of 100 kDa fraction of humic acid following adsorption onto S-doped TiO₂ Degussa P-25 were presented in Figure 4.45.
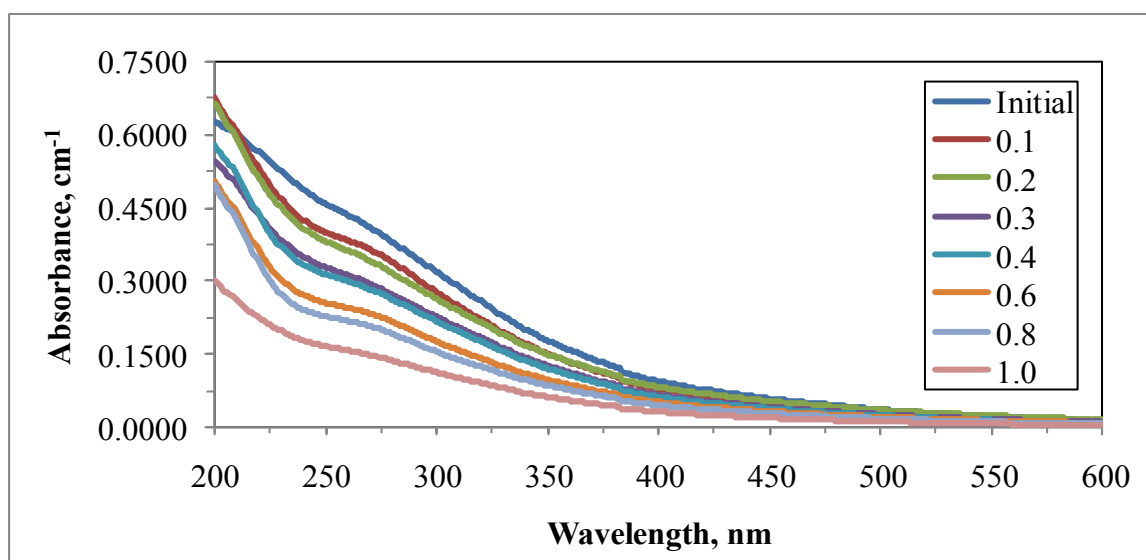
Figure 4.45. UV-vis absorbance spectra of 100 kDa fraction of humic acid following adsorption onto S-doped TiO$_2$ Degussa P-25.

UV-vis absorbance spectra of humic acids exhibited a declining trend with increasing wavelength with respect to increasing dose of TiO$_2$ as expected. UV-vis absorbance spectra demonstrated a similar overlapping trend onto each other for 100 kDa fraction of humic acid following adsorption onto 0.3 mg mL^{-1} and 0.4 mg mL^{-1} doses of S-doped TiO$_2$ Degussa P-25 (Figure 4.45).

Emission scan fluorescence spectra and synchronous scan fluorescence spectra of 100 kDa fraction of humic acid following adsorption onto S-doped TiO$_2$ Degussa P-25 were presented in Figure 4.46 and Figure 4.47, respectively. The emission scan fluorescence spectra showed a similar overlapping trend onto each other for 100 kDa fraction of humic acid following adsorption onto 0.2 mg mL^{-1} and 0.3 mg mL^{-1} doses of TiO$_2$ (Figure 4.46).

Figure 4.46. Emission scan fluorescence spectra of 100 kDa fraction of humic acid following adsorption onto S-doped TiO$_2$ Degussa P-25 at 350 nm excitation wavelength.

Synchronous scan fluorescence spectra showed one sharp peak around emission wavelength of 400 nm, while the fluorescence spectra displayed two moderate peaks around 325 nm and 475 nm emission wavelengths (Figure 4.47).
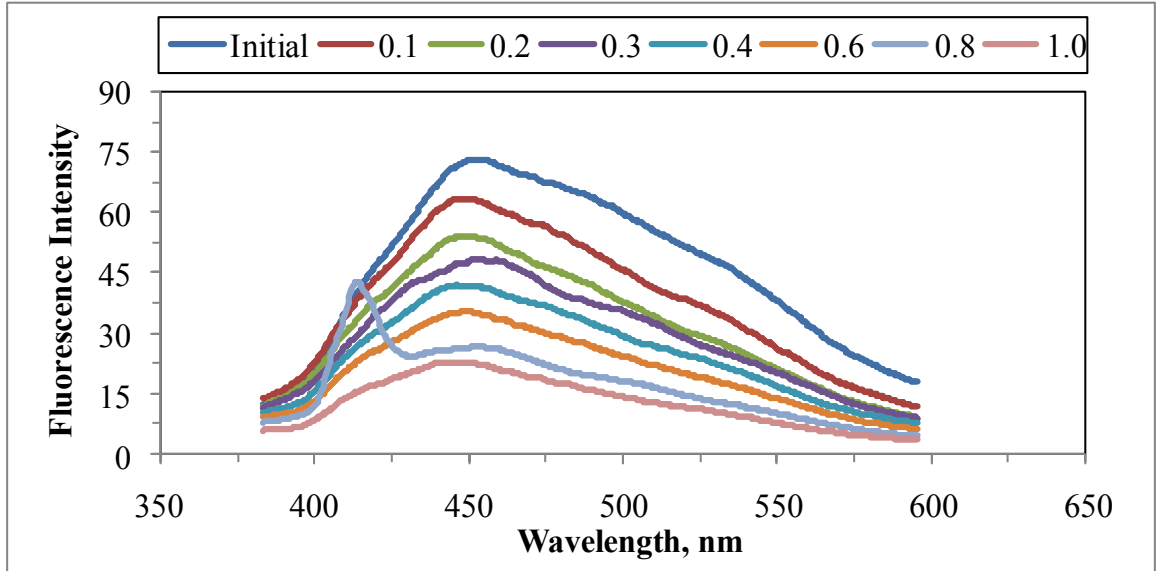

Figure 4.47. Synchronous scan fluorescence spectra of 100 kDa fraction of humic acid following adsorption onto S-doped TiO$_2$ Degussa P-25.

4.4.1.5. Spectroscopic Properties of 100 kDa Fraction of Humic Acid Following Adsorption onto N-S co-doped TiO_2 Degussa P-25 Specimen. UV-vis absorbance spectra of 100 kDa fraction of humic acid following adsorption onto N-S co-doped TiO_2 Degussa P-25 were displayed in Figure 4.48.

Figure 4.48. UV-vis absorbance spectra of 100 kDa fraction of humic acid following adsorption onto N-S co-doped TiO_2 Degussa P-25.

UV-vis absorbance spectra of humic acid solutions exhibited a decreasing trend with increasing wavelength with respect to increasing dose of N-S co-doped TiO_2 Degussa P-25 as expected. The UV-vis absorbance trends exhibited an overlapping trend onto each other for 100 kDa fraction of humic acid following adsorption onto 0.2 mg mL^{-1}, 0.3 mg mL^{-1} and 0.4 mg mL^{-1} loadings of N-S co-doped TiO_2Degussa P-25 (Figure 4.48).

Emission scan fluorescence spectra and synchronous scan fluorescence spectra of 100 kDa fraction of humic acid following adsorption onto N-S co-doped TiO_2Degussa P-25 were presented in Figure 4.49 and Figure 4.50, respectively. The emission scan fluorescence spectra showed an overlapping trend on each other for 100 kDa fraction of humic acid following adsorption onto 0.1 mg mL^{-1}and 0.2 mg mL^{-1} doses of N-S co-doped TiO_2 Degussa P-25.Furthermore, 0.1 mg mL^{-1} dose of N-S co-doped TiO_2 Degussa P-25 showed one minor shoulder around 400 nm emission wavelength (Figure 4.49).

Figure 4.49. Emission scan fluorescence spectra of 100 kDa fraction of humic acid following adsorption onto N-S co-doped TiO_2 Degussa P-25 at 350 nm excitation wavelength.

Synchronous scan fluorescence spectra showed three sharp peaks around emission wavelengths of 325 nm, 400 nm and 475 nm, while the fluorescence spectra displayed one moderate peak around 275 nm emission wavelength (Figure 4.50).

Figure 4.50. Synchronous scan fluorescence spectra of 100 kDa fraction of humic acid following adsorption onto N-S co-doped TiO_2 Degussa P-25.

4.4.2. Spectroscopic Properties of 100 kDa Fraction of Humic Acid Following Adsorption onto TiO$_2$ Hombikat UV-100 Specimens

Batch adsorption experiments were carried out by using 100 kDa fraction of humic acid and TiO$_2$ Hombikat UV-100 specimens *i.e.* bare TiO$_2$, C-doped TiO$_2$, N-doped TiO$_2$, S-doped TiO$_2$ and N-S co-doped TiO$_2$.

4.4.2.1. Spectroscopic Properties of 100 kDa Fraction of Humic Acid Following Adsorption onto Bare TiO$_2$ Hombikat UV-100 Specimen. UV-vis absorbance spectra of 100 kDa fraction of humic acid following adsorption onto bare TiO$_2$ Hombikat UV-100 were presented in Figure 4.51.

Figure 4.51. UV-vis absorbance spectra of 100 kDa fraction of humic acid following adsorption onto bare TiO$_2$ Hombikat UV-100.

UV-vis absorbance spectra of humic acids exhibited a decreasing trend with increasing wavelength with respect to dose of TiO$_2$ loading. UV-vis absorbance spectra exhibited a similar overlapping trend onto each other for 100 kDa fraction of humic acid adsorption onto 0.1 mg mL^{-1} and 0.2 mg mL^{-1} doses of TiO$_2$ as well as 0.3 mg mL^{-1}, 0.4 mg mL^{-1} and 0.6 mg mL^{-1} loadings of TiO$_2$ (Figure 4.51).

Emission scan fluorescence spectra and synchronous scan fluorescence spectra of 100 kDa fraction of humic acid following adsorption onto bare TiO_2 Hombikat UV-100 were presented in Figure 4.52 and Figure 4.53, respectively.

Figure 4.52.   Emission scan fluorescence spectra of 100 kDa fraction of humic acid following adsorption onto bare TiO_2 Hombikat UV-100 at 350 nm excitation wavelength.

The emission scan fluorescence spectra displayed a similar overlapping trend on each other for 100 kDa fraction of humic acid following adsorption onto 0.3 mg mL^{-1} and 0.4 mg mL^{-1} as well as 0.8 mg mL^{-1} and 1.0 mg mL^{-1} doses of bare TiO_2 Hombikat UV-100. Moreover, the emission scan fluorescence spectra of 100 kDa fraction of humic acid following adsorption onto bare TiO_2 Hombikat UV-100 exhibited a characteristic decreasing with the addition of increased dose of TiO_2. In addition to these observations, a broader peak around 450 nm and minor shoulder around 500 nm wavelength for initial humic acid were observed (Figure 4.52).

Synchronous scan fluorescence spectra for 100 kDa fraction of humic acid following adsorption onto bare TiO_2 Hombikat UV-100 showed two sharp peaks around emission wavelengths of 325 nm and 400 nm, while the fluorescence spectra displayed two moderate peaks around 275 nm and 475 nm emission wavelengths (Figure 4.53).
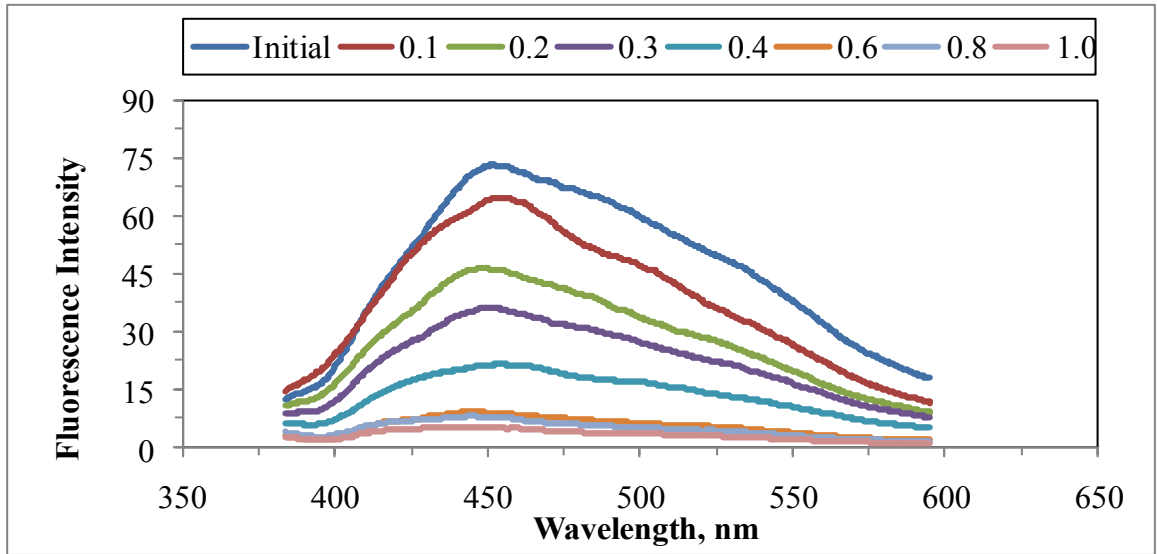
Figure 4.53. Synchronous scan fluorescence spectra of 100 kDa fraction of humic acid following adsorption onto bare TiO_2 Hombikat UV-100.

The highest fluorescence intensity was observed for 100 kDa fraction of humic acid following adsorption onto 0.8 mg mL^{-1} dose of bare TiO_2 Hombikat UV-100 at 325 nm and 400 nm emission wavelengths. The lowest fluorescence intensity was observed for 100 kDa fraction of humic acid following adsorption onto 1.0 mg mL^{-1} TiO_2 at 475 nm emission wavelength (Figure 4.53).

Comparison of two different TiO_2 specimens as Degussa P-25 and Hombikat UV-100 revealed the significance of the UV-vis spectral features (Figure 4.36 and Figure 4.51). Emission scan fluorescence spectral features reflected the role of the different fluorophores active on adsorption (Figure 4.37 and Figure 4.52). The synchronous scan fluorescence spectral features were also significantly different both in terms of fluorescence intensities and in spectral shapes (Figure 4.38 and Figure 4.53).

4.4.2.2. Spectroscopic Properties of 100 kDa Fraction of Humic Acid Following Adsorption onto C-doped TiO$_2$ Hombikat UV-100 Specimen. UV-vis absorbance spectra of 100 kDa fraction of humic acid following adsorption onto C-doped TiO$_2$ Hombikat UV-100 were presented in Figure 4.54.

Figure 4.54. UV-vis absorbance spectra of 100 kDa fraction of humic acid following adsorption onto C-doped TiO$_2$ Hombikat UV-100.

UV-vis absorbance spectra of humic acids exhibited a decreasing trend with increasing wavelength with respect to increasing dose of TiO$_2$. The UV-vis absorbance trends demonstrated a similar overlapping trend onto each other for 100 kDa fraction of humic acid following adsorption onto 0.1 mg mL^{-1} and 0.2 mg mL^{-1} as well as 0.6 mg mL^{-1} and 0.8 mg mL^{-1} loadings of C-doped TiO$_2$ Hombikat UV-100 (Figure 4.54).

Emission scan fluorescence spectra and synchronous scan fluorescence spectra of 100 kDa fraction of humic acid following adsorption onto C-doped TiO$_2$ Hombikat UV-100 were presented in Figure 4.55 and Figure 4.56, respectively. Maximum fluorescence intensity for 100 kDa fraction of humic acid following adsorption onto C-doped TiO$_2$ Hombikat UV-100 was observed around 450 nm emission wavelength (Figure 4.55).

Figure 4.55. Emission scan fluorescence spectra of 100 kDa fraction of humic acid following adsorption onto C-doped TiO_2 Hombikat UV-100 at 350 nm excitation wavelength.

Synchronous scan fluorescence spectra showed two sharp peaks around emission wavelengths of 325 nm and 400 nm, while the fluorescence spectra displayed two moderate peaks around 275 nm and 475 nm emission wavelengths (Figure 4.56).

Figure 4.56. Synchronous scan fluorescence spectra of 100 kDa fraction of humic acid following adsorption onto C-doped TiO_2 Hombikat UV-100.

4.4.2.3. Spectroscopic Properties of 100 kDa Fraction of Humic Acid Following Adsorption onto N-doped TiO$_2$ Hombikat UV-100 Specimen. UV-vis absorbance spectra of 100 kDa fraction of humic acid following adsorption onto N-doped TiO$_2$ Hombikat UV-100 were displayed in Figure 4.57.

Figure 4.57. UV-vis absorbance spectra of 100 kDa fraction of humic acid following adsorption onto N-doped TiO$_2$ Hombikat UV-100.

UV-vis absorbance spectra of humic acid solutions exhibited a decreasing trend with increasing wavelength and with increasing TiO$_2$ loading. UV-vis absorbance spectra followed an overlapping trend onto each other for 100 kDa fraction of humic acid following adsorption onto 0.6 mg mL^{-1} and 0.8 mg mL^{-1} as well as 0.1 mg mL^{-1} and 0.2 mg mL^{-1} loadings of N-doped TiO$_2$ Hombikat UV-100 (Figure 4.57).

Emission scan fluorescence spectra and synchronous scan fluorescence spectra of 100 kDa fraction of humic acid following adsorption onto N-doped TiO$_2$ Hombikat UV-100 were presented in Figure 4.58 and Figure 4.59, respectively. The emission scan fluorescence spectra displayed a similar overlapping trend on each other for 100 kDa fraction of humic acid following adsorption onto 0.6 mg mL^{-1} and 0.8 mg mL^{-1} dosages of N-doped TiO$_2$ Hombikat UV-100 (Figure 4.58).

Figure 4.58. Emission scan fluorescence spectra of 100 kDa fraction of humic acid following adsorption onto N-doped TiO_2 Hombikat UV-100 at 350 nm excitation wavelength.

Synchronous scan fluorescence spectra displayed one sharp peak around emission wavelength of 400 nm, while the fluorescence spectra displayed two moderate peaks around 325 nm and 475 nm emission wavelengths (Figure 4.59).
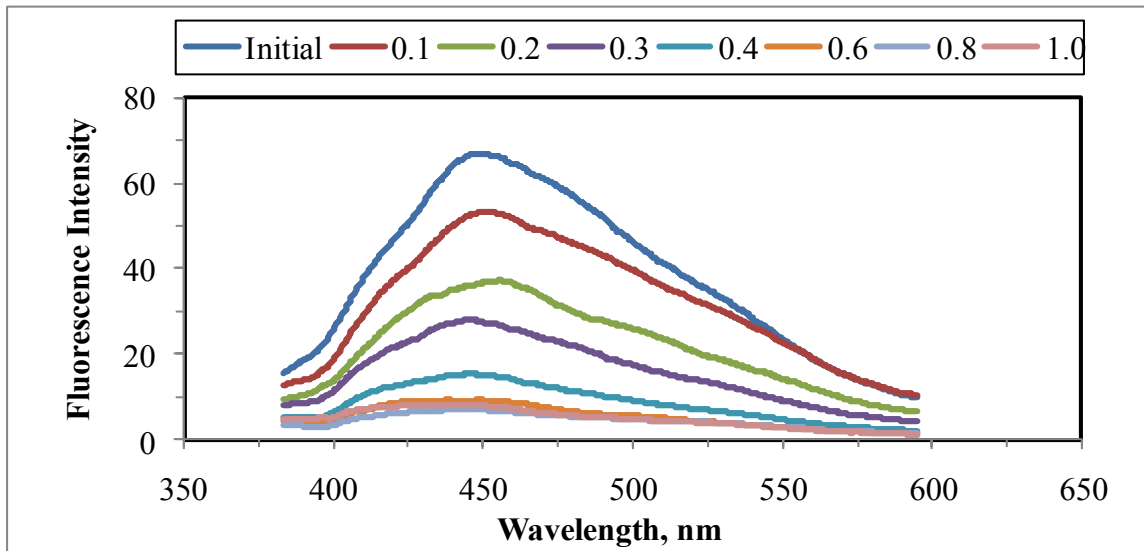

Figure 4.59. Synchronous scan fluorescence spectra of 100 kDa fraction of humic acid following adsorption onto N-doped TiO_2 Hombikat UV-100.

4.4.2.4. Spectroscopic Properties of 100 kDa Fraction of Humic Acid Following Adsorption onto S-doped TiO$_2$ Hombikat UV-100 Specimen. UV-vis absorbance spectra of 100 kDa fraction of humic acid following adsorption onto S-doped TiO$_2$ Hombikat UV-100 were displayed in Figure 4.60.
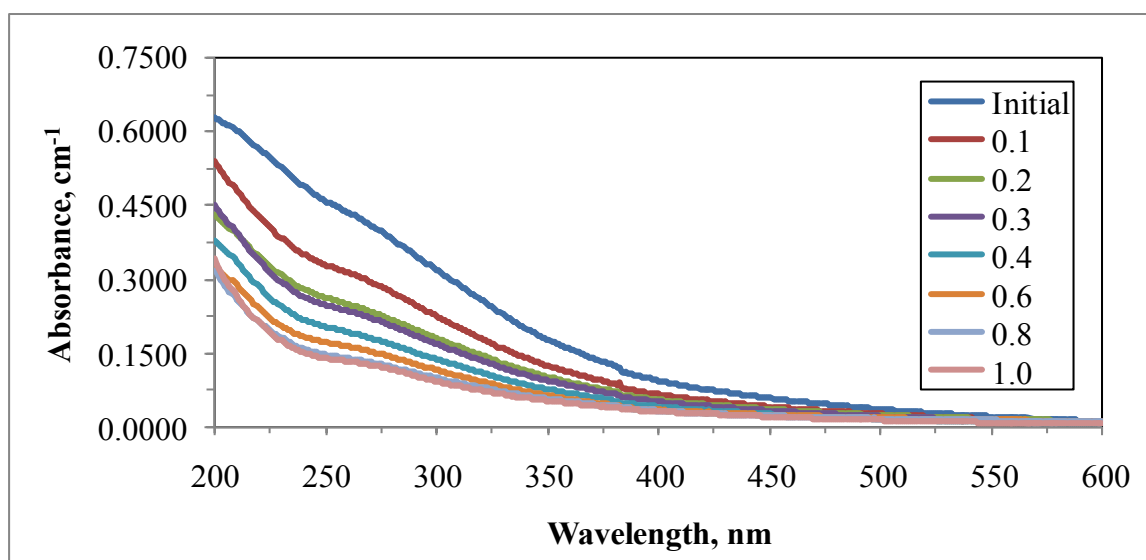
Figure 4.60. UV-vis absorbance spectra of 100 kDa fraction of humic acid following adsorption onto S-doped TiO$_2$ Hombikat UV-100.

UV-vis absorbance spectra of humic acid solutions exhibited a decreasing trend with increasing wavelength with respect to increasing dose of TiO$_2$. The UV-vis absorbance trends of 100 kDa fraction of humic acid following adsorption onto 0.2 mg mL^{-1} and 0.3 mg mL^{-1}as well as 0.8 mg mL^{-1}and 1.0 mg mL^{-1} loadings of S-doped TiO$_2$ Hombikat UV-100 were very close to each other (Figure 4.60).

Emission scan fluorescence spectra and synchronous scan fluorescence spectra of 100 kDa fraction of humic acid following adsorption onto S-doped TiO$_2$ Hombikat UV-100 were presented in Figure 4.61 and Figure 4.62, respectively. The emission fluorescence spectra of 100 kDa fraction of humic acid following adsorption onto 1.0 mg mL^{-1} dose of S-doped TiO$_2$ Hombikat UV-100 had the lowest fluorescence intensity. Moreover, maximum fluorescence intensity for all of the humic acid solutions attained around 450 nm emission wavelength (Figure 4.61).
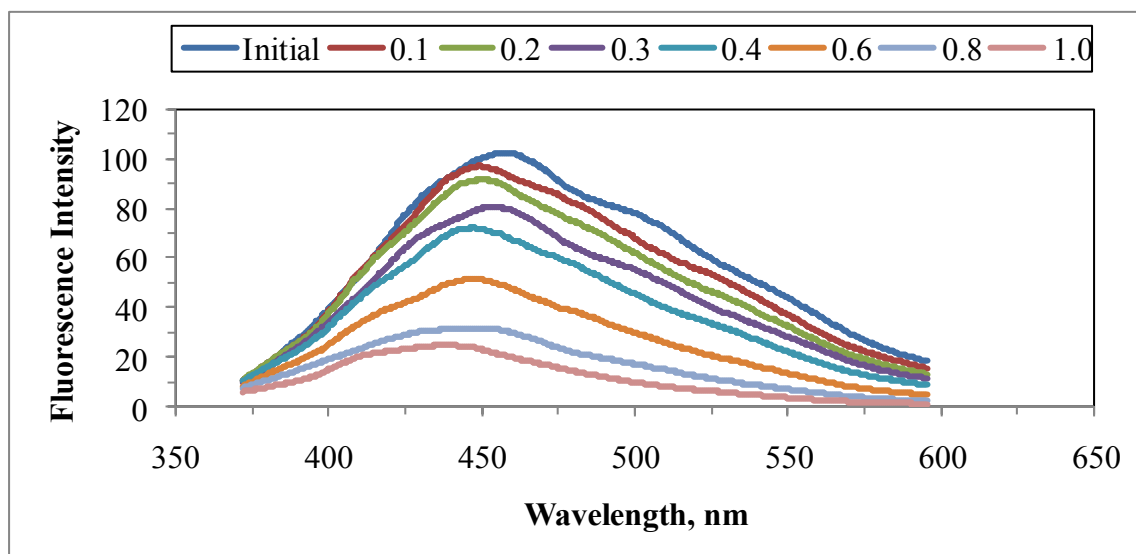
Figure 4.61. Emission scan fluorescence spectra of 100 kDa fraction of humic acid following adsorption onto S-doped TiO$_2$ Hombikat UV-100 at 350 nm excitation wavelength.

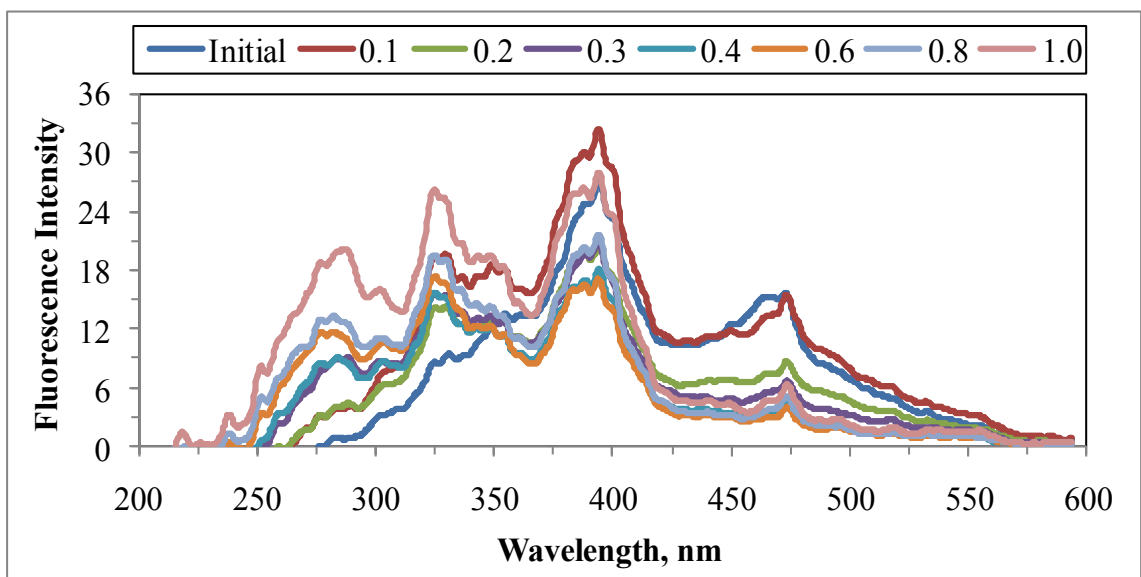Synchronous scan fluorescence spectra showed two sharp peaks around emission wavelengths of 400 nm and 475 nm, while the fluorescence spectra displayed two moderate peaks around 275 nm and 325 nm emission wavelengths (Figure 4.62).
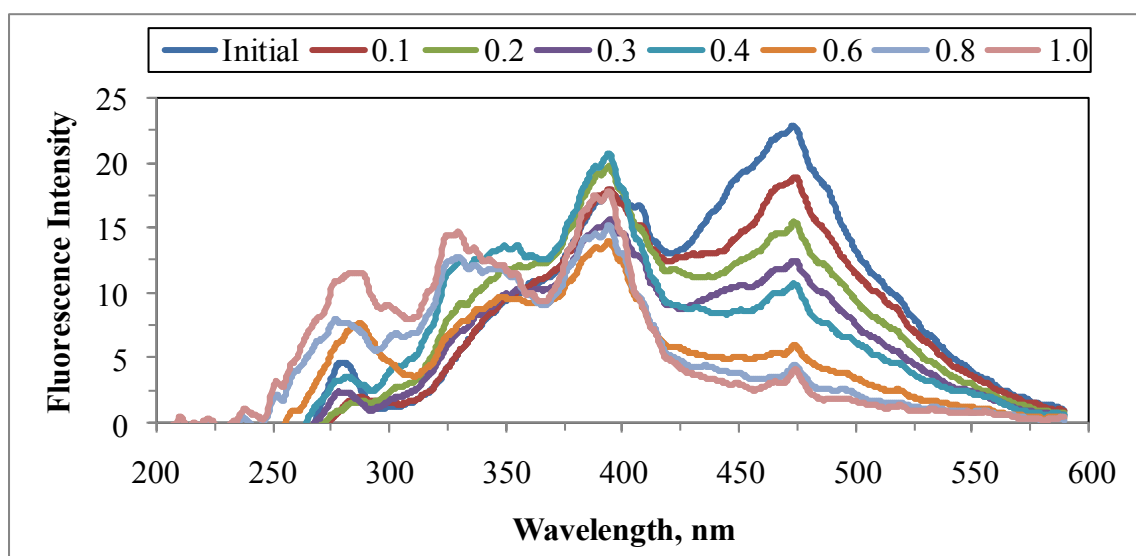
Figure 4.62. Synchronous scan fluorescence spectra of 100 kDa fraction of humic acid following adsorption onto S-doped TiO$_2$ Hombikat UV-100.

4.4.2.5. Spectroscopic Properties of 100 kDa Fraction of Humic Acid Following Adsorption onto N-S co-doped TiO$_2$ Hombikat UV-100 Specimen. UV-vis absorbance spectra of 100 kDa fraction of humic acid following adsorption onto N-S co-doped TiO$_2$ Hombikat UV-100 were displayed in Figure 4.63.
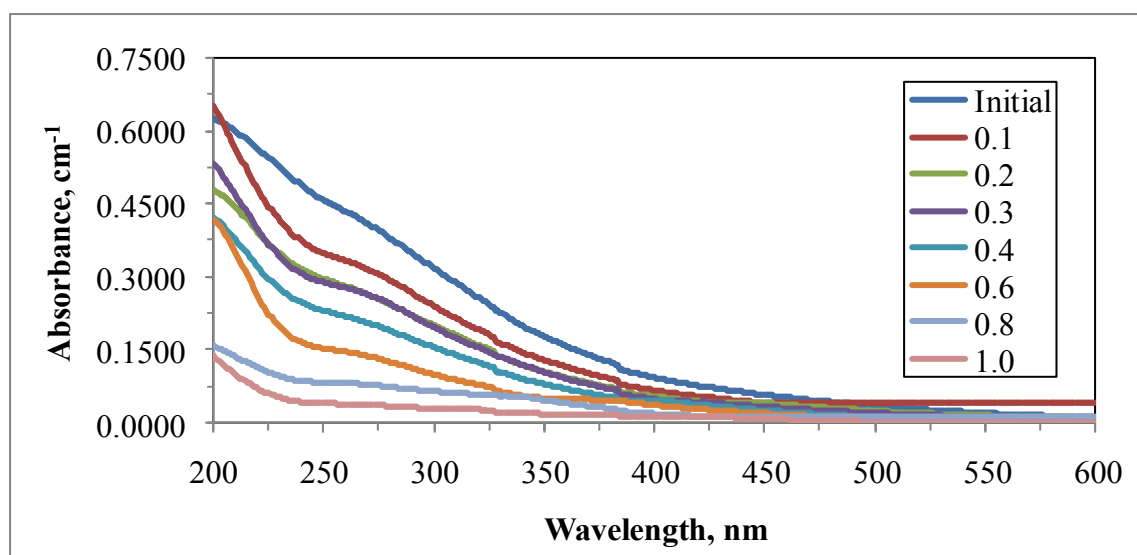
Figure 4.63. UV-vis absorbance spectra of 100 kDa fraction of humic acid following adsorption onto N-S co-doped TiO$_2$ Hombikat UV-100.

UV-vis absorbance spectra of humic acid solutions exhibited a decreasing trend with increasing wavelength with respect to increasing dose of TiO$_2$ as expected. The UV-vis absorbance trends exhibited an overlapping trend onto each other for 100 kDa fraction of humic acid adsorption 0.3 mg mL^{-1} and 0.4 mg mL^{-1} doses of N-S co-doped TiO$_2$ Hombikat UV-100 (Figure 4.63).

Emission scan fluorescence spectra and synchronous scan fluorescence spectra of 100 kDa fraction of humic acid following adsorption onto N-S co-doped TiO$_2$ Hombikat UV-100 were presented in Figure 4.64 and Figure 4.65, respectively. The emission scan fluorescence spectra of 100 kDa fraction of humic acid following adsorption onto 0.8 mg mL^{-1} and 1.0 mg mL^{-1} doses of N- S co-doped TiO$_2$ Hombikat UV-100, which displayed a similar overlapping trend on each other, exhibited lower fluorescence intensities (Figure 4.64).
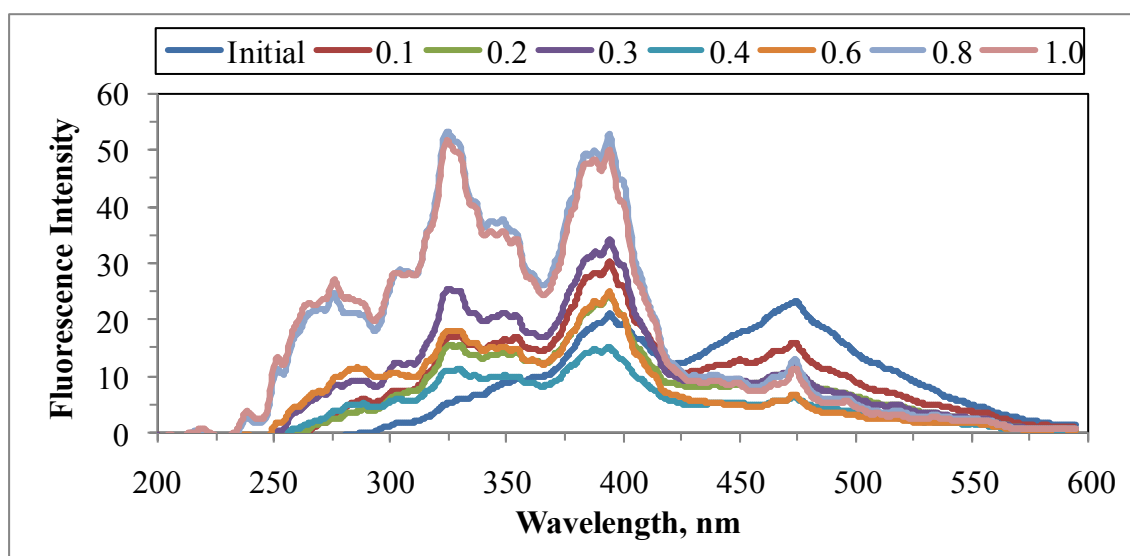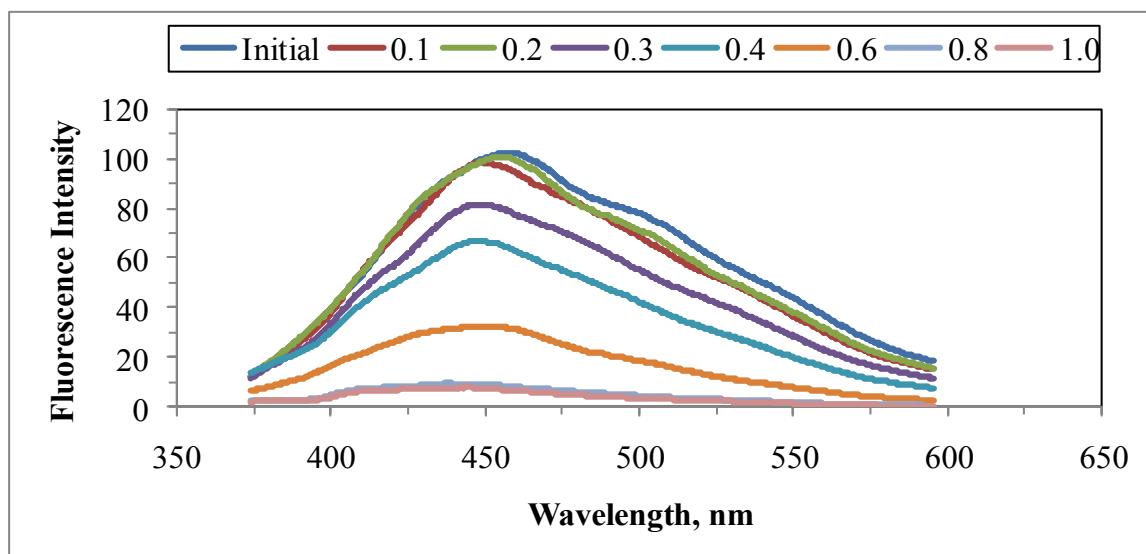
Figure 4.64. Emission scan fluorescence spectra of 100 kDa fraction of humic acid following adsorption onto N-S co-doped TiO_2 Hombikat UV-100 at 350 nm excitation wavelength.

Synchronous scan fluorescence spectra displayed one sharp peak around 400 nm emission wavelength, while the fluorescence spectra displayed two moderate peaks around 325 nm and 475 nm emission wavelengths (Figure 4.65).
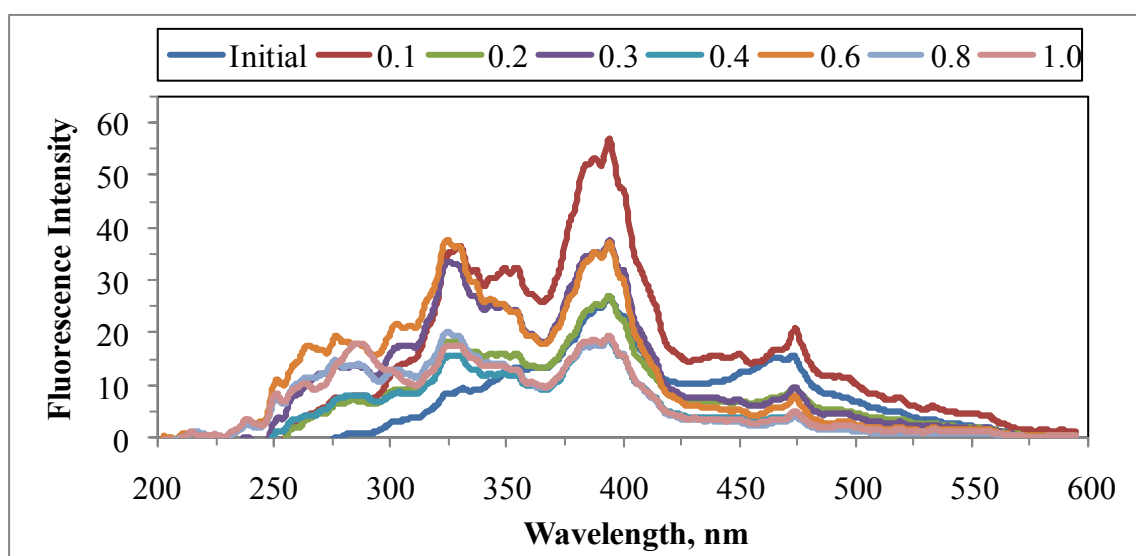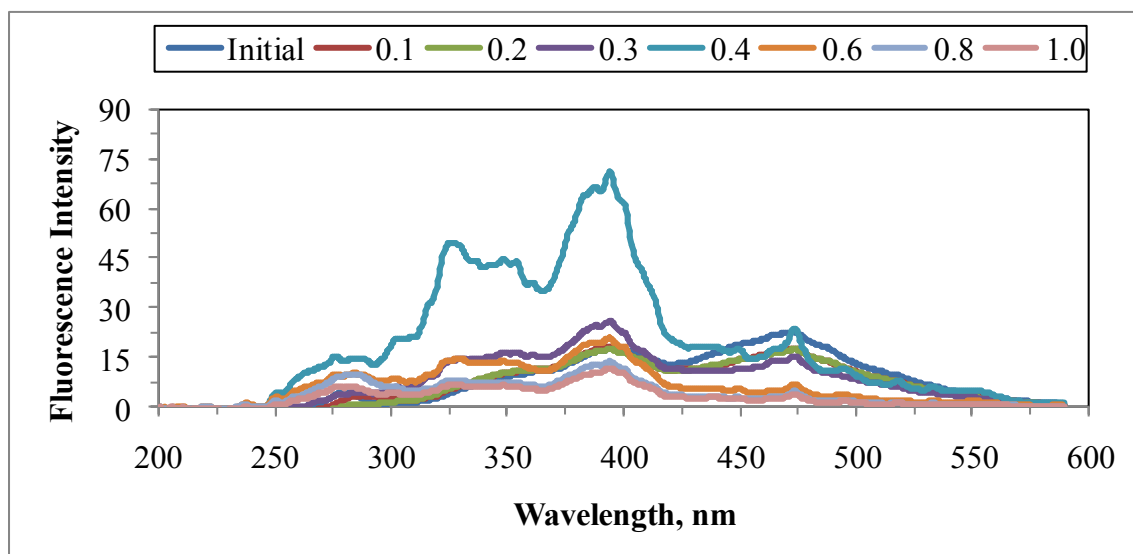

Figure 4.65. Synchronous scan fluorescence spectra of 100 kDa fraction of humic acid following adsorption onto N-S co-doped TiO_2 Hombikat UV-100.

4.5. Spectroscopic Properties of 30 kDa Fraction of Humic Acid Following Adsorption onto TiO₂ Specimens

Batch adsorption experiments were implemented by using 30 kDa fraction of humic acid as the adsorbate and TiO₂ Degussa P-25 and TiO₂ Hombikat UV-100 specimens as the adsorbent in the loading range of $0.1 - 1.0$ mg mL^{-1}. Adsorption data were evaluated by presenting respective figures where "Initial" term was used to indicate the 30 kDa fraction of humic acid and "0.1-1.0" represented dose range of TiO₂ (mg mL^{-1}).

4.5.1. Spectroscopic Properties of 30 kDa Fraction of Humic Acid Following Adsorption onto TiO₂ Degussa P-25 Specimens

Batch adsorption experiments were conducted by using 30 kDa fraction of humic acid and TiO₂ Degussa P-25 specimens *i.e.* bare TiO₂, C-doped TiO₂, N-doped TiO₂, S-doped TiO₂ and N-S co-doped TiO₂.

4.5.1.1. Spectroscopic Properties of 30 kDa Fraction of Humic Acid Following Adsorption onto Bare TiO₂ Degussa P-25 Specimen. UV-vis absorbance spectra of 30 kDa fraction of humic acid following adsorption onto bare TiO₂ Degussa P-25 were displayed in Figure 4.66.

UV-vis absorbance spectra displayed a decreasing trend with increasing wavelength for 30 kDa fraction of humic acid following adsorption onto bare TiO₂ Degussa P-25. Furthermore, UV-vis absorbance spectra showed an overlapping trend onto each other for 30 kDa fraction of humic acid following adsorption onto 0.6 mg mL^{-1} and 0.8 mg mL^{-1} doses of TiO₂ (Figure 4.66).

Emission scan fluorescence spectra and synchronous scan fluorescence spectra of 30 kDa fraction of humic acid following adsorption onto bare TiO₂ Degussa P-25 were presented in Figure 4.67 and Figure 4.68, respectively. The emission scan fluorescence spectra exhibited a similar overlapping trend onto each other for 30 kDa fraction of humic acid following adsorption onto 0.6 mg mL^{-1} and 0.8 mg mL^{-1} doses of bare TiO₂ Degussa P-25 (Figure 4.67).

Furthermore, emission scan fluorescence spectra of 30 kDa fraction of humic acid following adsorption onto bare TiO$_2$ Degussa P-25 attained maximum fluorescence intensity around 450 nm emission wavelength (Figure 4.67).
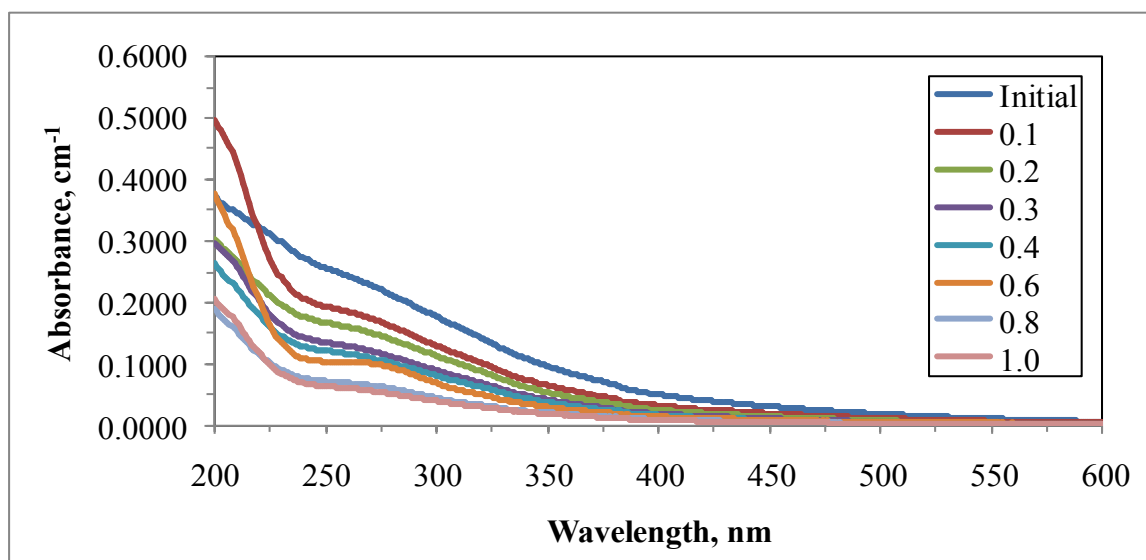
Figure 4.66.   UV-vis absorbance spectra of 30 kDa fraction of humic acid following adsorption onto bare TiO$_2$ Degussa P-25.
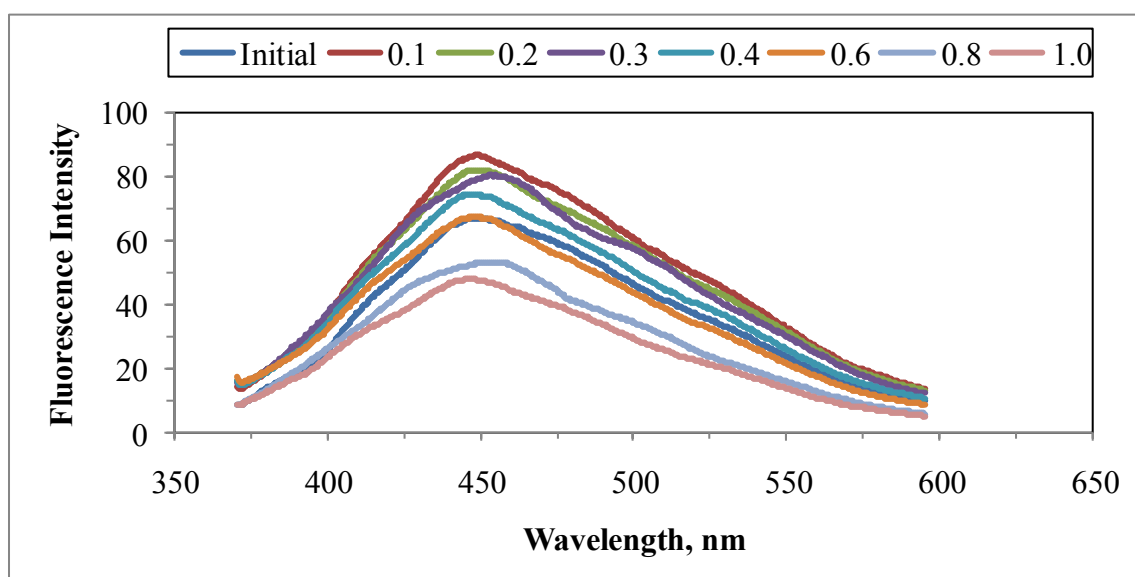
Figure 4.67.   Emission scan fluorescence spectra of 30 kDa fraction of humic acid following adsorption onto bare TiO$_2$ Degussa P-25 at 350 nm excitation wavelength.
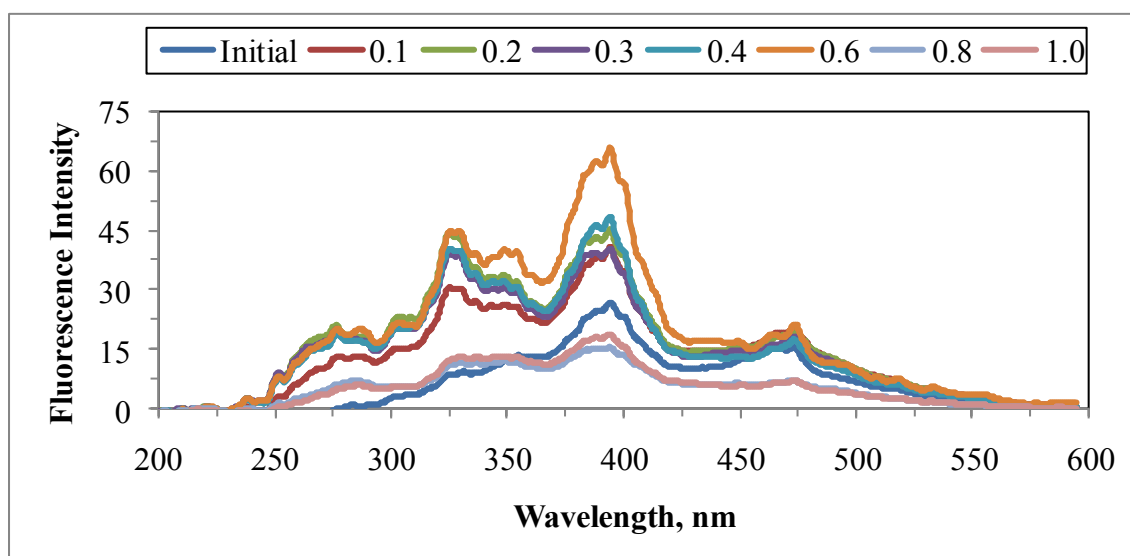
Figure 4.68. Synchronous scan fluorescence spectra of 30 kDa fraction of humic acid following adsorption onto bare TiO$_2$ Degussa P-25.

Synchronous scan fluorescence spectra for 30 kDa fraction of humic acid showed a sharp peak around emission wavelength of 400 nm, while the fluorescence spectra displayed two moderate peaks around 325 nm and 475 nm emission wavelengths. The highest fluorescence intensity was observed for 30 kDa fraction of humic acid following adsorption onto 0.6 mg mL^{-1}dose of TiO$_2$ at 400 nm emission wavelength. The lowest fluorescence intensity was observed for 30 kDa fraction of humic acid following adsorption onto higher dosages TiO$_2$, such as 0.8 mg mL^{-1} and 1.0 mg mL^{-1} TiO$_2$, which had a similar overlapping trend on each other, at 475 nm wavelength (Figure 4.68).

The lower molecular size fraction of humic acid (30 kDa) displayed similar UV-vis spectral features as expected (Figure 4.6, Figure 4.36 and Figure 4.66). Similar trends could also be visualized in both the emission scan (Figure 4.7, Figure 4.37 and Figure 4.67) and synchronous scan (Figure 4.8, Figure 4.38 and Figure 4.68) fluorescence spectral features. It should also be indicated that decreasing size resulted in decreasing amounts of chromophores and fluorophores in accordance with decreasing DOC.

4.5.1.2. Spectroscopic Properties of 30 kDa Fraction of Humic Acid Following Adsorption onto C-doped TiO2 Degussa P-25 Specimen. UV-vis absorbance spectra of 30 kDa fraction of humic acid following adsorption onto C-doped TiO_2 Degussa P-25 were displayed in Figure 4.69.
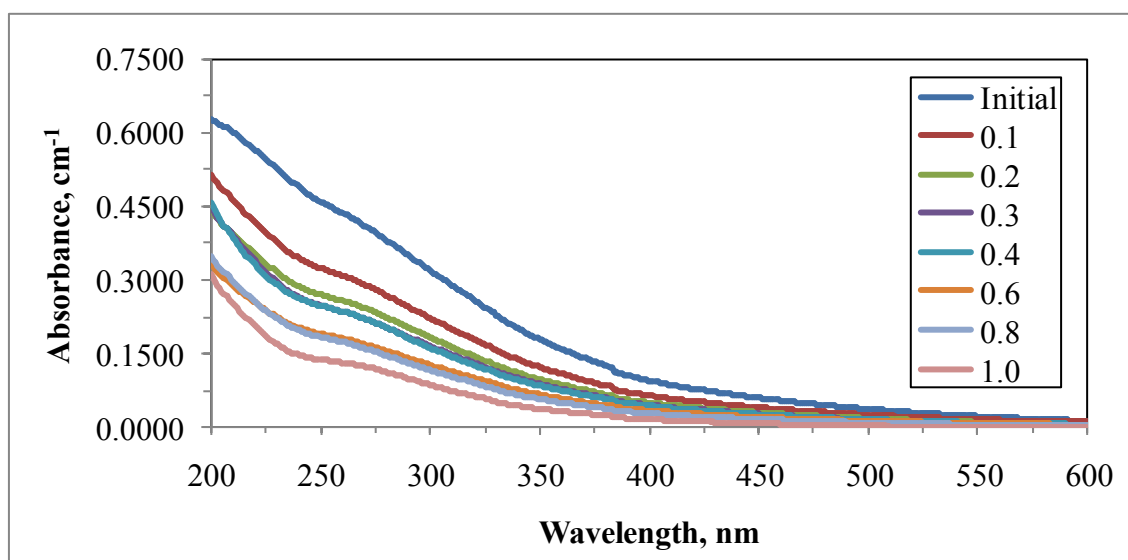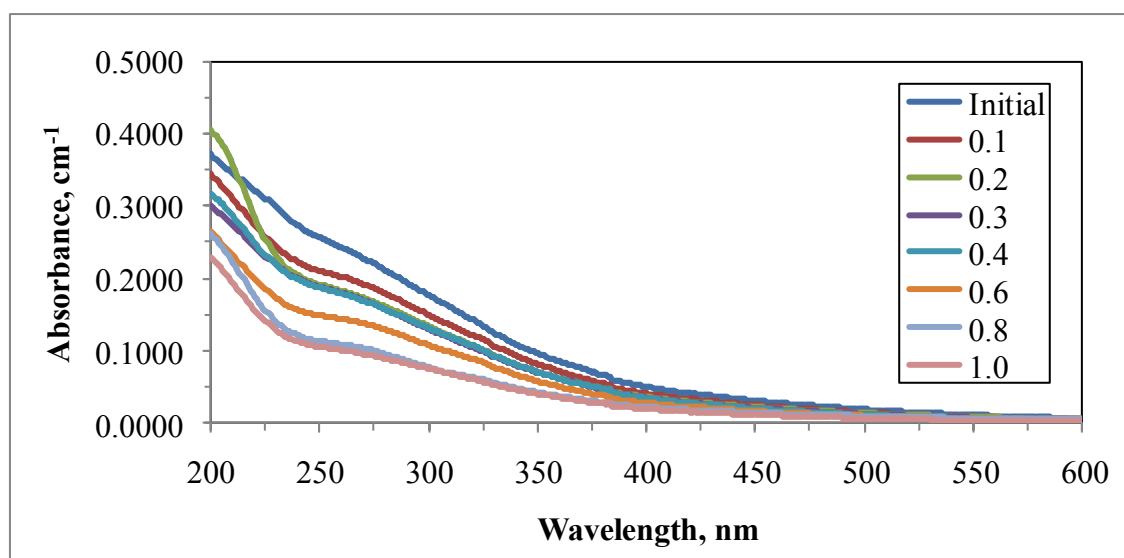

Figure 4.69. UV-vis absorbance spectra of 30 kDa fraction of humic acid following adsorption onto C-doped TiO_2 Degussa P-25.

UV-vis absorbance spectra of humic acid solutions exhibited a decreasing trend with increasing wavelength with respect to increasing dose of TiO_2 as expected. UV-vis absorbance spectra demonstrated a similar overlapping trend onto each other for 30 kDa fraction of humic acid adsorption onto 0.8 mg mL^{-1} and 1.0 mg mL^{-1} doses of C-doped TiO_2 as well as onto 0.2 mg mL^{-1}, 0.3 mg mL^{-1} and 0.4 mg mL^{-1} doses of C-doped TiO_2.

Emission scan fluorescence spectra and synchronous scan fluorescence spectra of 30 kDa fraction of humic acid following adsorption onto C-doped TiO_2 Degussa P-25 were presented in Figure 4.70 and Figure 4.71, respectively. The emission scan fluorescence spectra displayed a similar overlapping trend on each other for 30 kDa fraction of humic acid adsorption onto maximum loadings of C-doped TiO_2 Degussa P-25, such as 0.8 mg mL^{-1} and 1.0 mg mL^{-1}. Moreover, fluorescence intensity attained the maximum values around 450 nm emission wavelength (Figure 4.70).
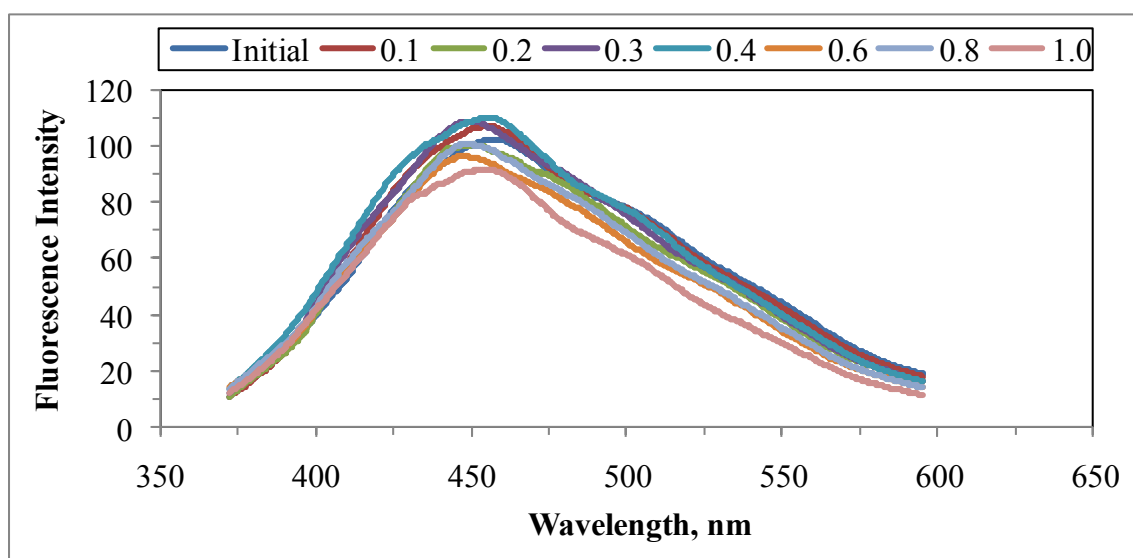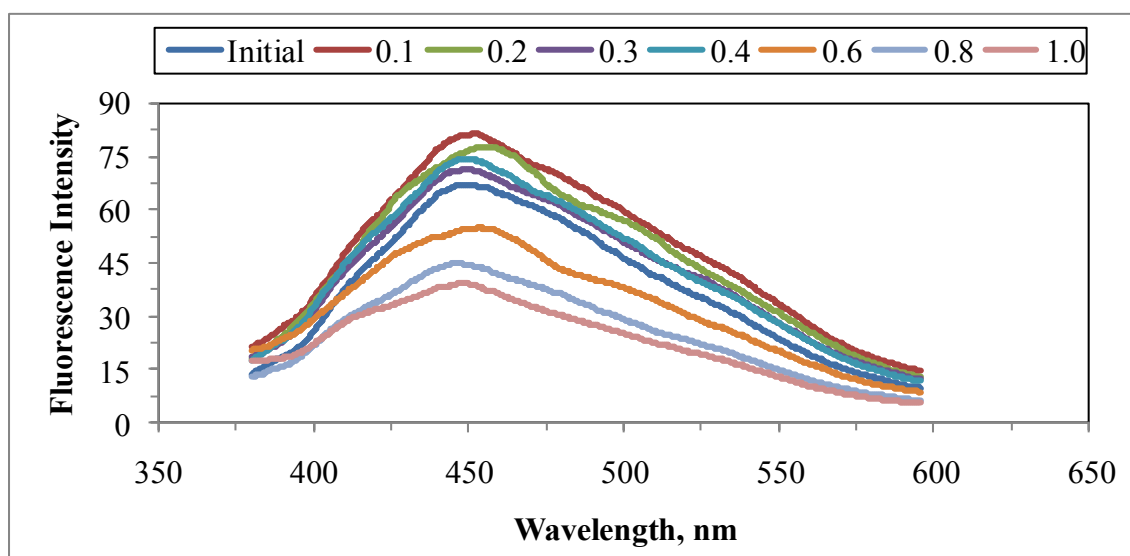
Figure 4.70. Emission scan fluorescence spectra of 30 kDa fraction of humic acid following adsorption onto C-doped TiO$_2$ Degussa P-25 at 350 nm excitation wavelength.

Synchronous scan fluorescence spectra showed two sharp peaks around emission wavelengths of 325 nm and 400 nm, while the fluorescence spectra displayed two moderate peaks around 275 nm and 475 nm emission wavelengths (Figure 4.71).
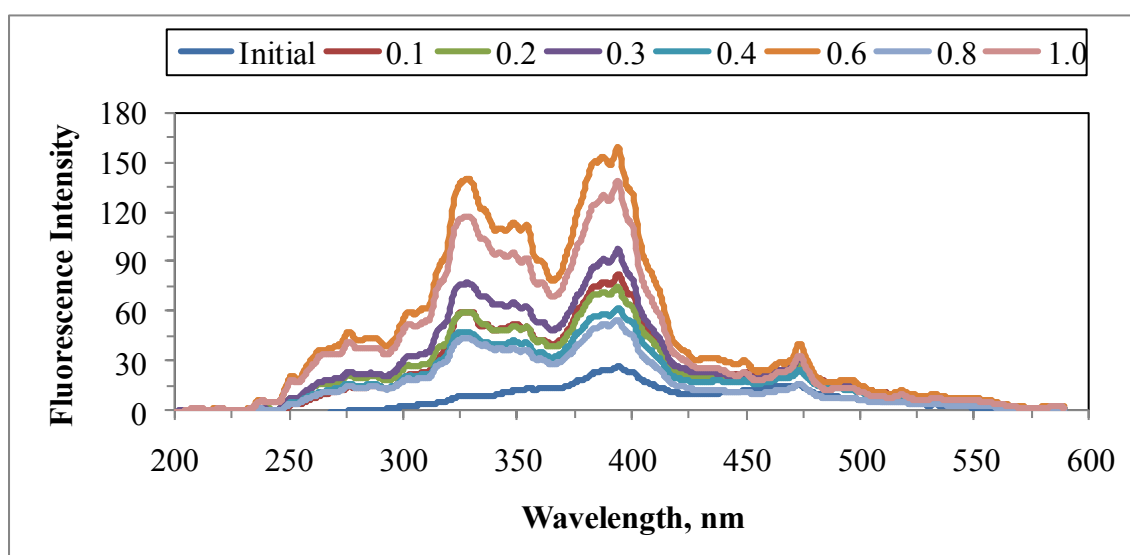
Figure 4.71. Synchronous scan fluorescence spectra of 30 kDa fraction of humic acid following adsorption onto C-doped TiO$_2$ Degussa P-25.

4.5.1.3. Spectroscopic Properties of 30 kDa Fraction of Humic Acid Following Adsorption onto N-doped TiO$_2$ Degussa P-25 Specimen. UV-vis absorbance spectra of 30 kDa fraction of humic acid following adsorption onto N-doped TiO$_2$ Degussa P-25 were displayed in Figure 4.72.
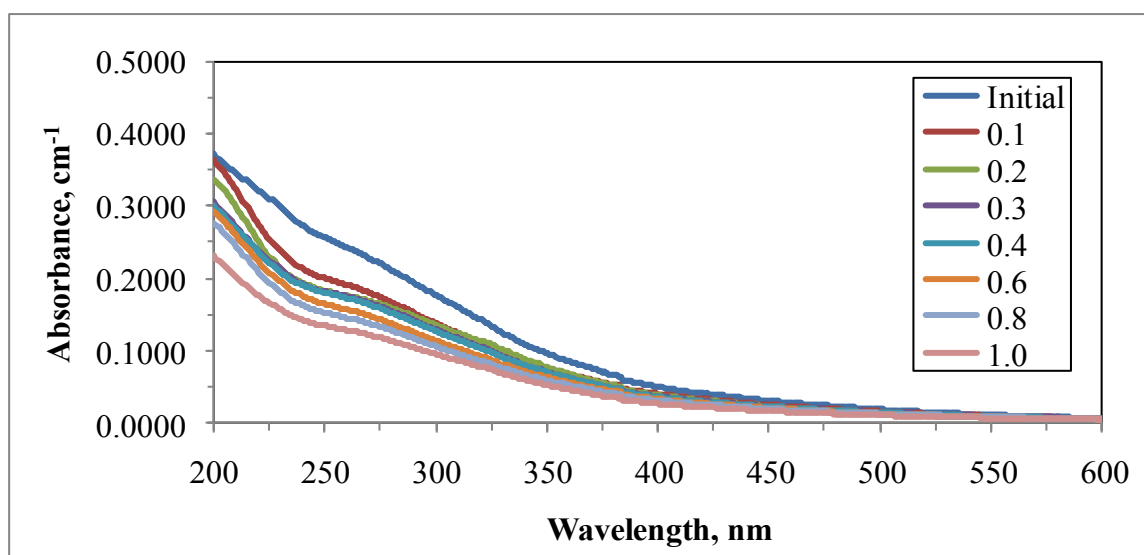
Figure 4.72.   UV-vis absorbance spectra of 30 kDa fraction of humic acid following adsorption onto N-doped TiO$_2$ Degussa P-25.

UV-vis absorbance spectra of humic acid solutions displayed a declining trend with increasing wavelength. UV-vis absorbance spectra demonstrated a similar overlapping trend onto each other 30 kDa fraction of humic acid following adsorption onto N-doped TiO$_2$ Degussa P-25 in the range of 0.1-0.8 mg mL^{-1}. Moreover, UV-vis absorbance spectra values for all of the humic acid solutions approached to zero at wavelengths longer than 450 nm.

Emission scan fluorescence spectra and synchronous scan fluorescence spectra of 30 kDa fraction of humic acid following adsorption onto N-doped TiO$_2$ Degussa P-25 were presented in Figure 4.73 and Figure 4.74, respectively. The emission scan fluorescence spectra displayed an overlapping trend onto each other for 30 kDa fraction of humic acid following adsorption onto 0.3 mg mL^{-1} and 0.4 mg mL^{-1} doses of N-doped TiO$_2$ Degussa P-25 (Figure 4.73).
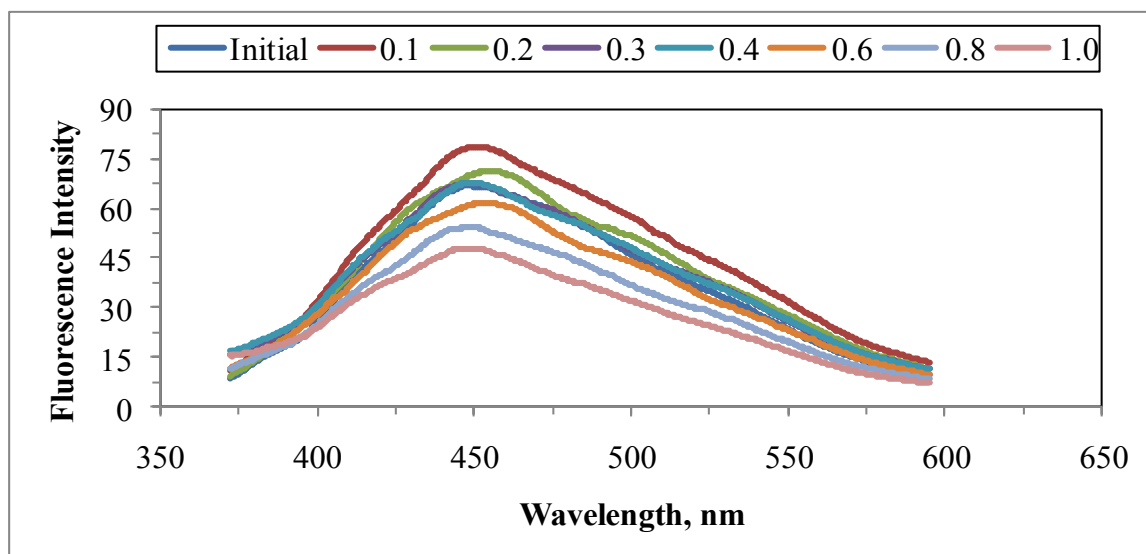
Figure 4.73. Emission scan fluorescence spectra of 30 kDa fraction of humic acid following adsorption onto N-doped TiO_2 Degussa P-25 at 350 nm excitation wavelength.

Synchronous scan fluorescence spectra showed two sharp peaks around emission wavelengths of 325 nm and 400 nm, while the fluorescence spectra displayed two moderate peaks around 275 nm and 475 nm emission wavelengths (Figure 4.74).
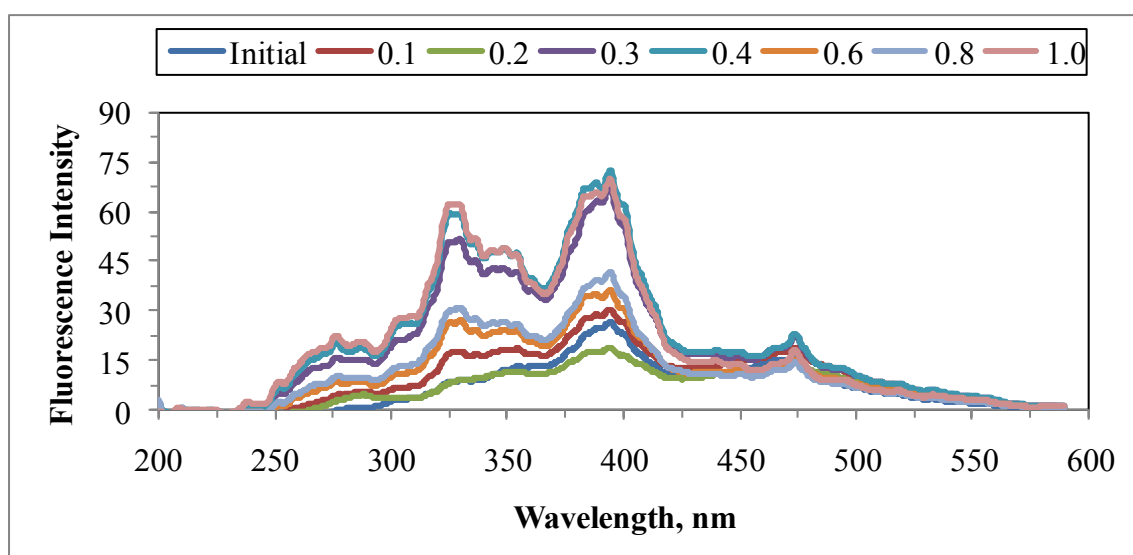
Figure 4.74. Synchronous scan fluorescence spectra of 30 kDa fraction of humic acid following adsorption onto N-doped TiO_2 Degussa P-25.

4.5.1.4. Spectroscopic Properties of 30 kDa Fraction of Humic Acid Following Adsorption onto S-doped TiO$_2$ Degussa P-25 Specimen. UV-vis absorbance spectra of 30 kDa fraction of humic acid following adsorption onto S-doped TiO$_2$ Degussa P-25 were displayed in Figure 4.75.
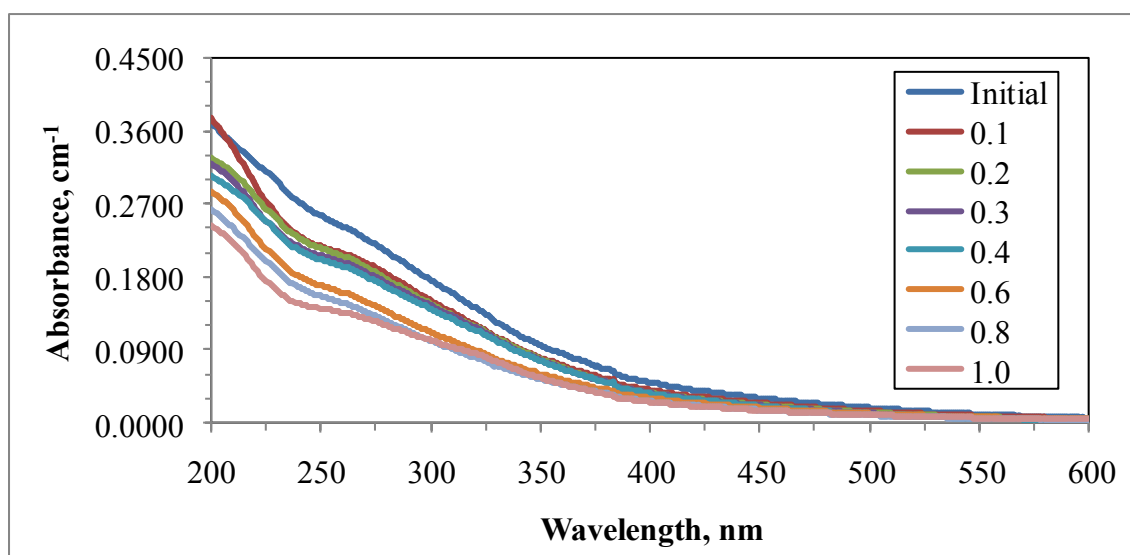
Figure 4.75.   UV-vis absorbance spectra of 30 kDa fraction of humic acid following adsorption onto S-doped TiO$_2$ Degussa P-25.

UV-vis absorbance spectra of humic acids displayed a declining trend with increasing wavelength and also with increasing TiO$_2$ loadings. UV-vis absorbance spectra demonstrated a similar overlapping trend on each other for 30 kDa fraction of humic acid following adsorption onto S-doped TiO$_2$ Degussa P-25 in the range of 0.1 - 0.4 mg mL^{-1}.

Emission scan fluorescence spectra and synchronous scan fluorescence spectra of 30 kDa fraction of humic acid following adsorption onto S-doped TiO$_2$ Degussa P-25 were presented in Figure 4.76 and Figure 4.77, respectively. The emission scan fluorescence spectra showed a similar overlapping trend onto each other for 30 kDa fraction of humic acid adsorption onto S-doped TiO$_2$ Degussa P-25 in the range of 0.3 - 0.6 mg mL^{-1} (Figure 4.76).
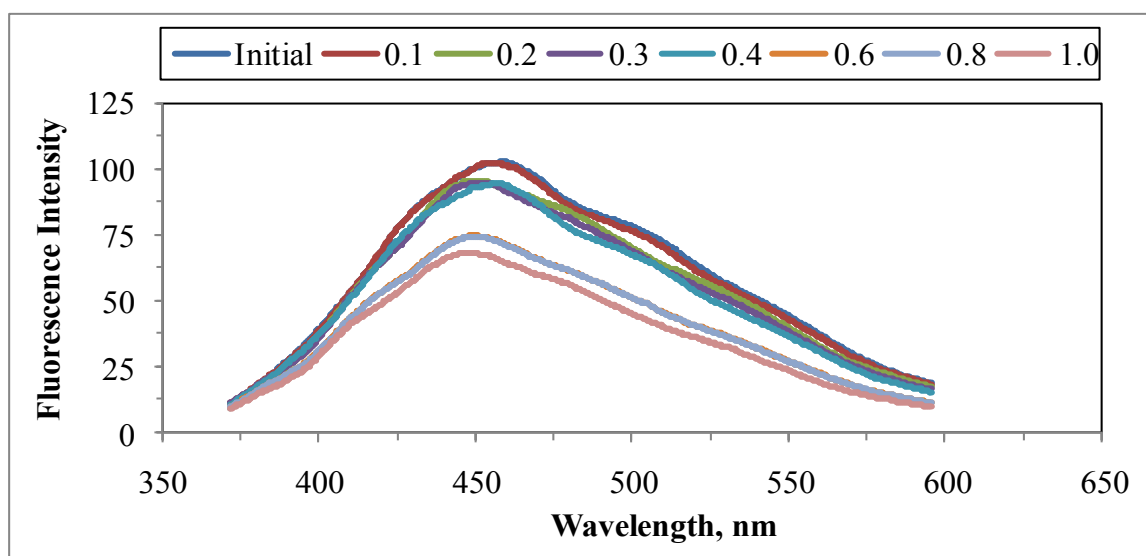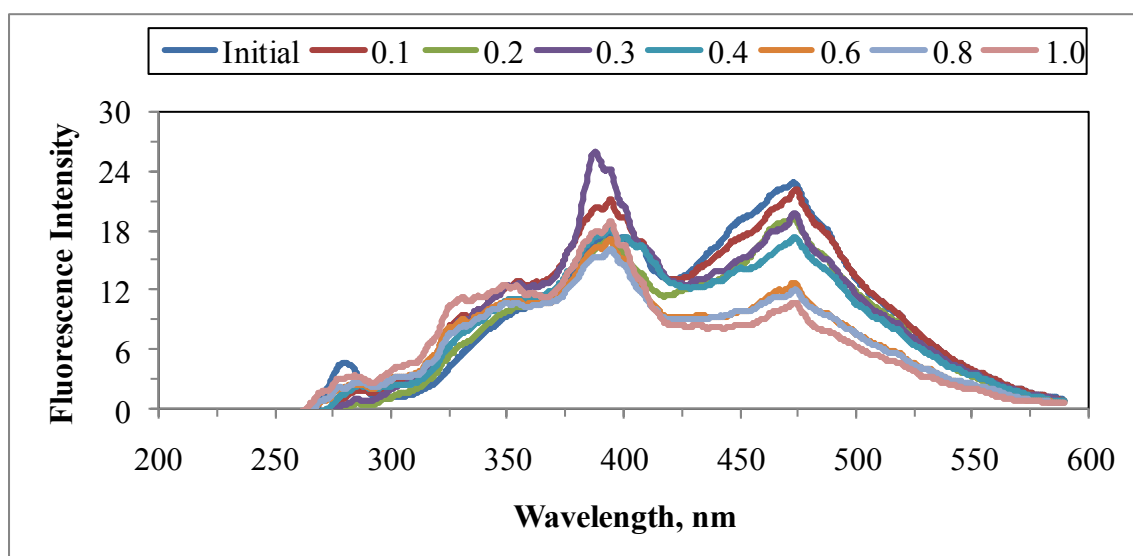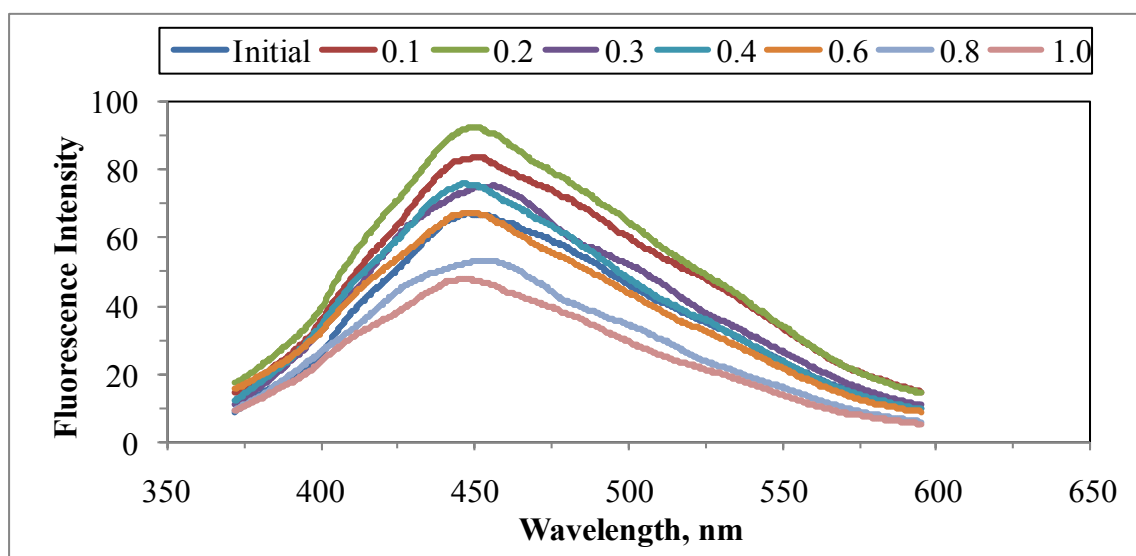
Figure 4.76.   Emission scan fluorescence spectra of 30 kDa fraction of humic acid following adsorption onto S-doped TiO_2 Degussa P-25 at 350 nm excitation wavelength.

Synchronous scan fluorescence spectra showed two sharp peaks around emission wavelengths of 325 nm and 400 nm, while the fluorescence spectra displayed two moderate peaks around 275 nm and 475 nm emission wavelengths (Figure 4.77).
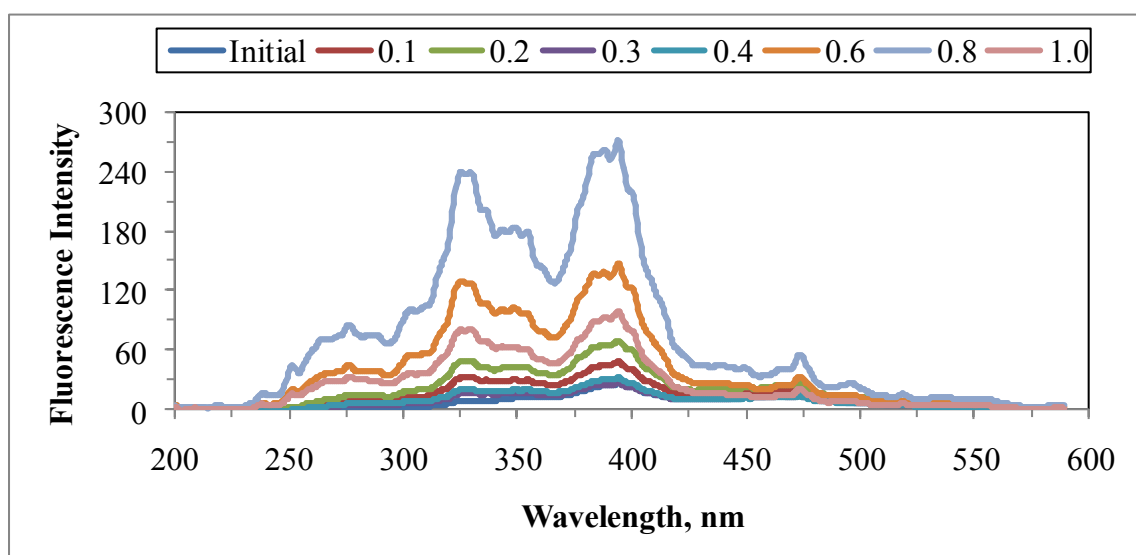
Figure 4.77.   Synchronous scan fluorescence spectra of 30 kDa fraction of humic acid following adsorption onto S-doped TiO_2 Degussa P-25.

4.5.1.5. Spectroscopic Properties of 30 kDa Fraction of Humic Acid Following Adsorption onto N-S co-doped TiO$_2$ Degussa P-25 Specimen. UV-vis absorbance spectra of 30 kDa fraction of humic acid following adsorption onto N-S co-doped TiO$_2$ Degussa P-25 were displayed in Figure 4.78.
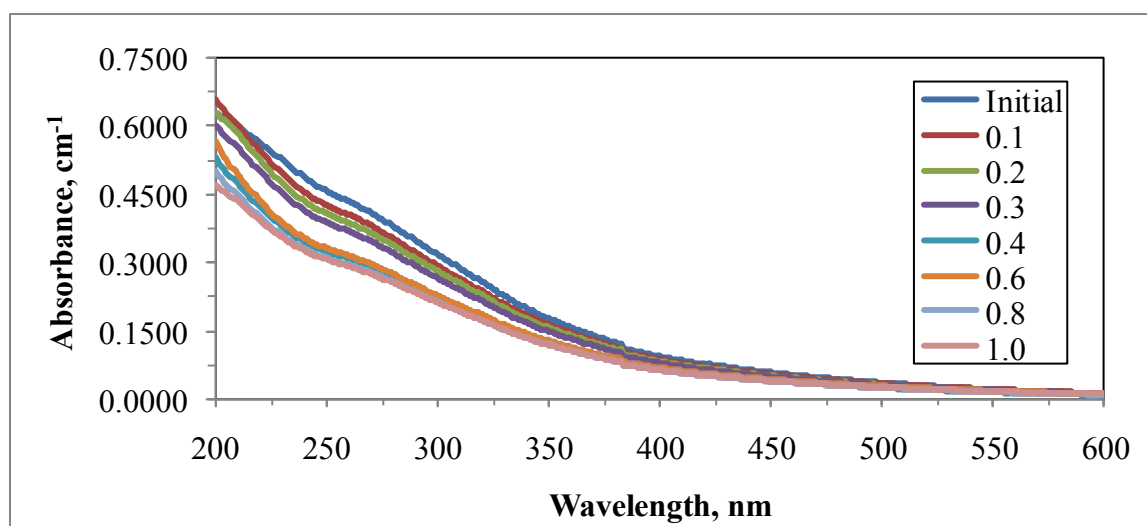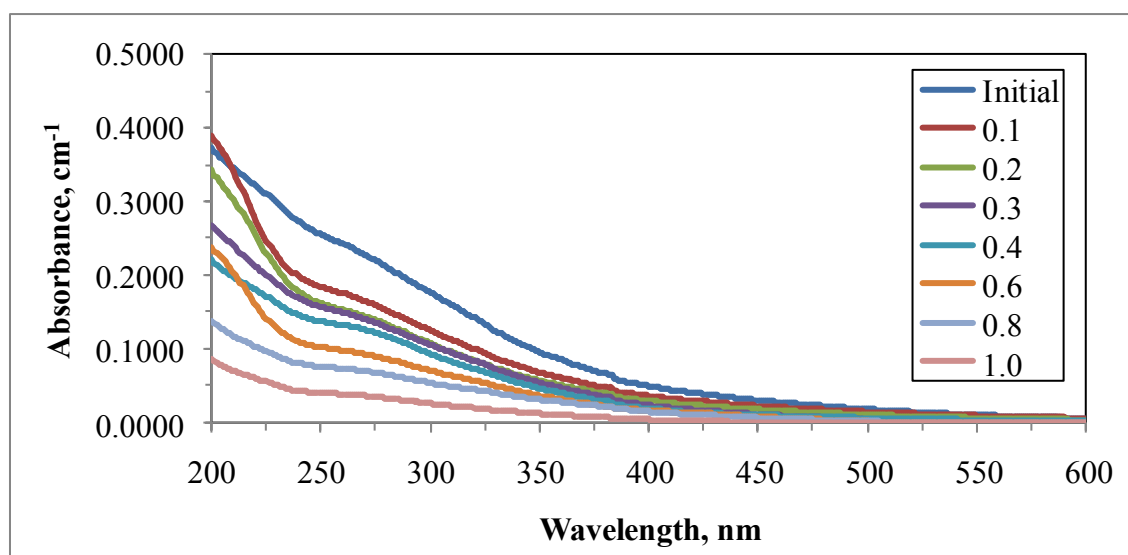

Figure 4.78.   UV-vis absorbance spectra of 30 kDa fraction of humic acid following adsorption onto N-S co-doped TiO$_2$ Degussa P-25.

UV-vis absorbance spectra of humic acids demonstrated a decreasing trend with increasing wavelength. UV-vis absorbance spectra for all of the humic acid solutions approached to zero and leveled off at wavelengths longer than 350 nm. UV-vis absorbance spectra exhibited an overlapping trend onto each other for 30 kDa fraction of humic acid following adsorption onto 0.2 mg mL^{-1} and 0.3 mg mL^{-1} doses of N-S co-doped TiO$_2$ Degussa P-25 (Figure 4.78).

Emission scan fluorescence spectra and synchronous scan fluorescence spectra of 30 kDa fraction of humic acid following adsorption onto N-S co-doped TiO$_2$ Degussa P-25 were presented in Figure 4.79 and Figure 4.80, respectively. The significant decreases were observed in fluorescence intensity with respect to increasing dose of TiO$_2$ loadings. The synchronous scan fluorescence spectra for 30 kDa fraction of humic acid exhibited two sharp peaks around emission wavelengths of 325 nm and 400 nm, while the fluorescence

spectra displayed two moderate peaks around 275 nm and 475 nm emission wavelengths (Figure 4.80).
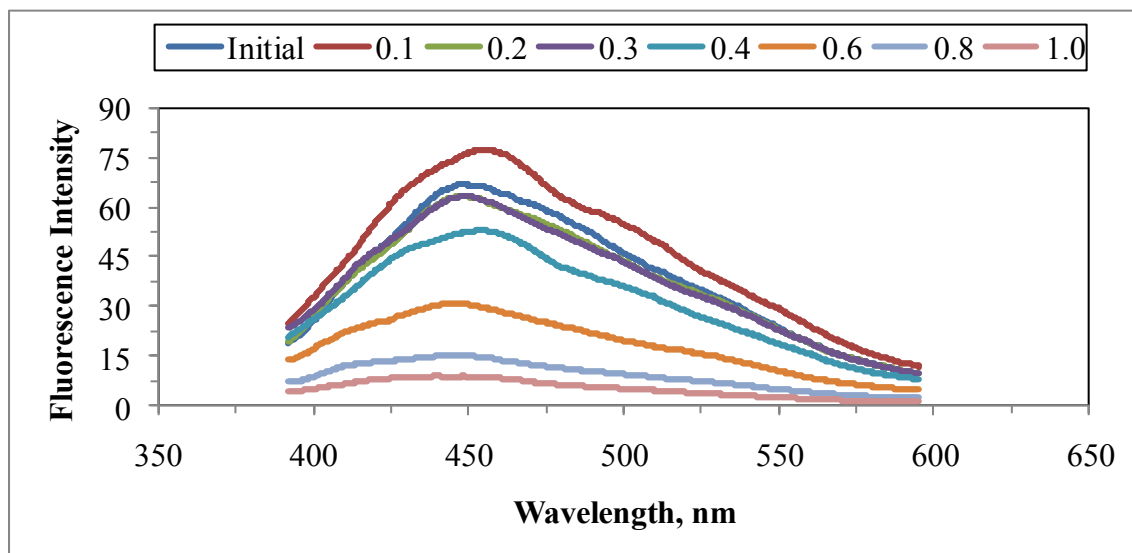
Figure 4.79. Emission scan fluorescence spectra of 30 kDa fraction of humic acid following adsorption onto N-S co-doped TiO_2 Degussa P-25 at 350 nm excitation wavelength.
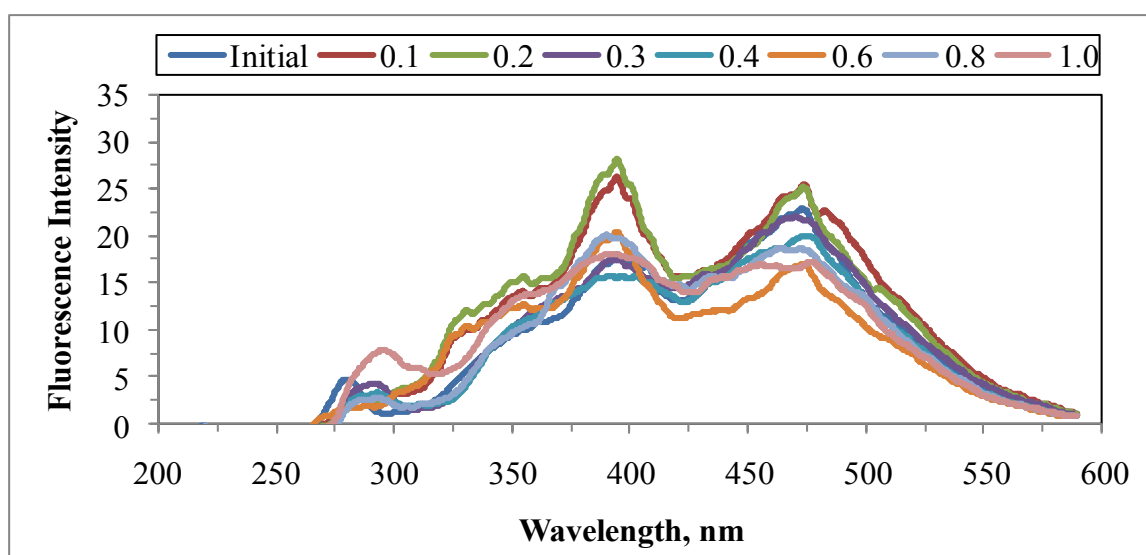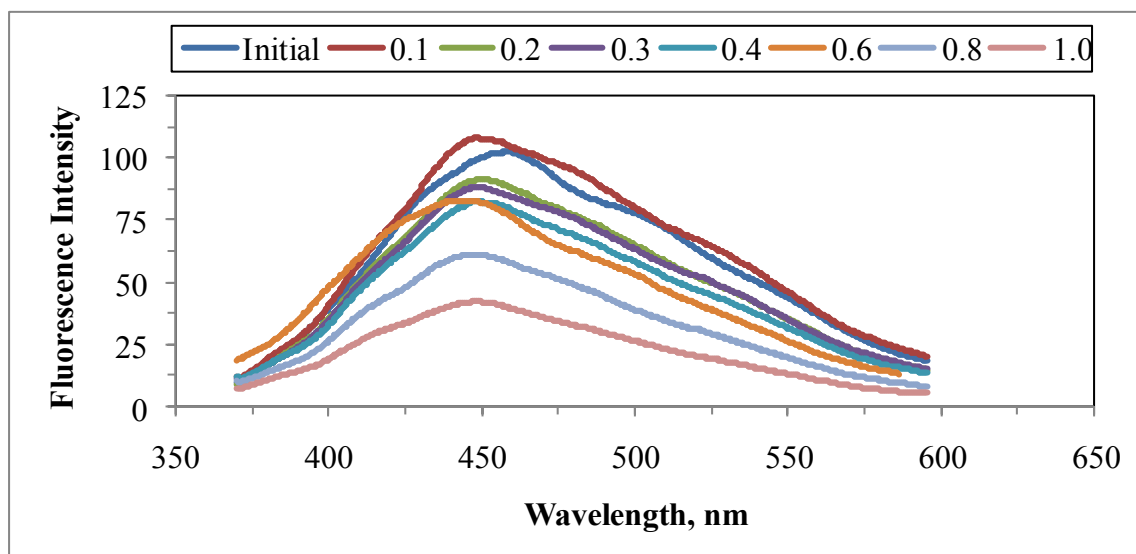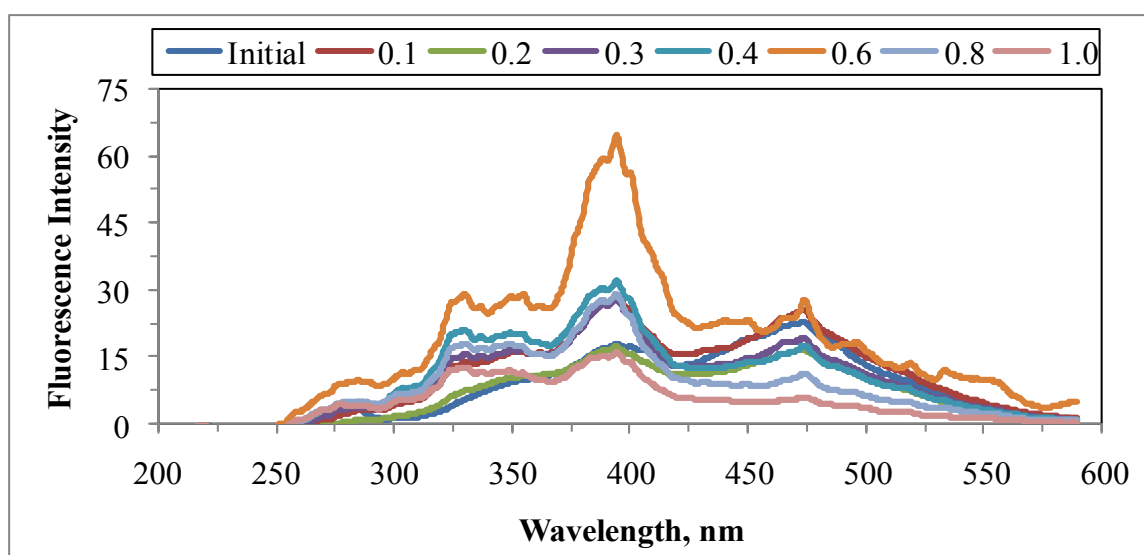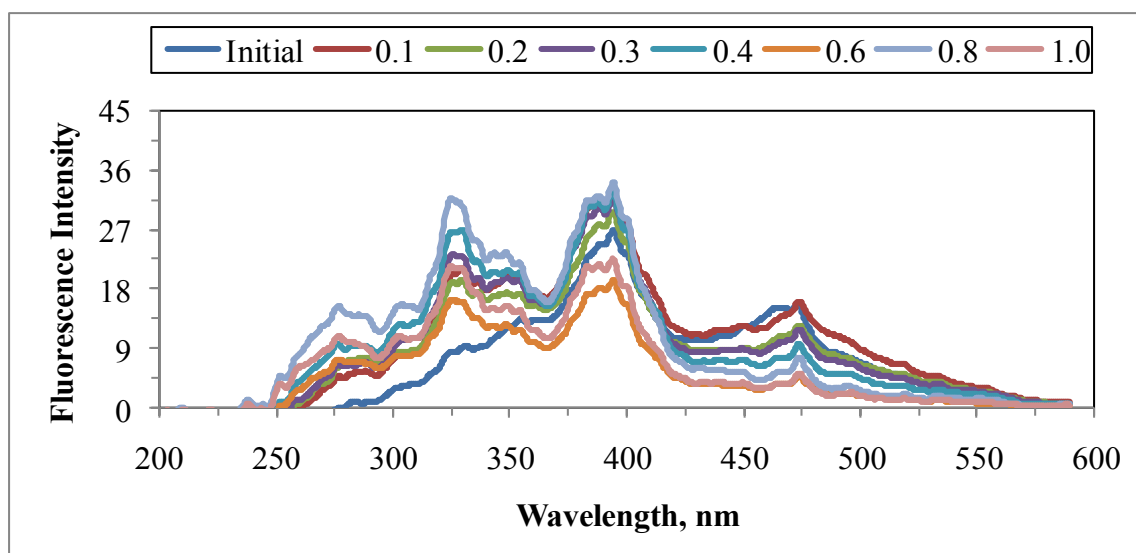

Figure 4.80. Synchronous scan fluorescence spectra of 30 kDa fraction of humic acid following adsorption onto N-S co-doped TiO_2 Degussa P-25.

4.5.2. Spectroscopic Properties of 30 kDa Fraction of Humic Acid Following Adsorption onto TiO₂ Hombikat UV-100 Specimens

Batch adsorption experiments were conducted by using 30 kDa fraction of humic acid and TiO$_2$ Hombikat UV-100 specimens *i.e.* bare TiO$_2$, C-doped TiO$_2$, N-doped TiO$_2$, S-doped TiO$_2$ and N-S co-doped TiO$_2$.

4.5.2.1. <u>Spectroscopic Properties of 30 kDa Fraction of Humic Acid Following Adsorption onto Bare TiO$_2$ Hombikat UV-100 Specimen.</u> UV-vis absorbance spectra of 30 kDa fraction of humic acid following adsorption onto bare TiO$_2$ Hombikat UV-100 were displayed in Figure 4.81.

UV-vis absorbance spectra of humic acids exhibited generally a decreasing trend with increasing wavelength. UV-vis absorbance values for all of the humic acid solutions approached to zero and also leveled off after 300 nm wavelength (Figure 4.81).

Emission scan fluorescence spectra and synchronous scan fluorescence spectra of 30 kDa fraction of humic acid following adsorption onto bare TiO$_2$ Hombikat UV-100 were presented in Figure 4.82 and Figure 4.83, respectively.
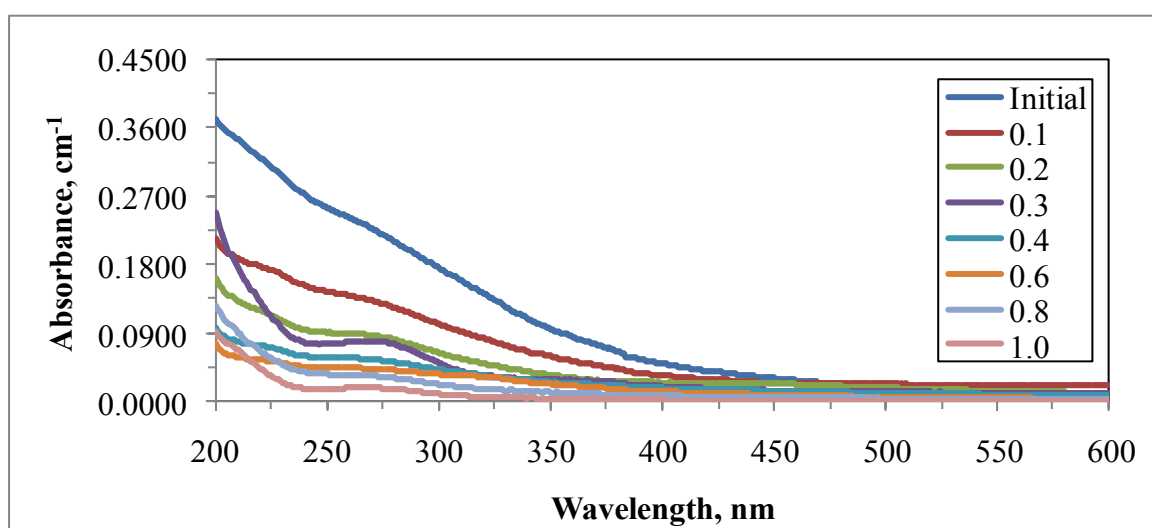
Figure 4.81. UV-vis absorbance spectra of 30 kDa fraction of humic acid following adsorption onto bare TiO$_2$ Hombikat UV-100.
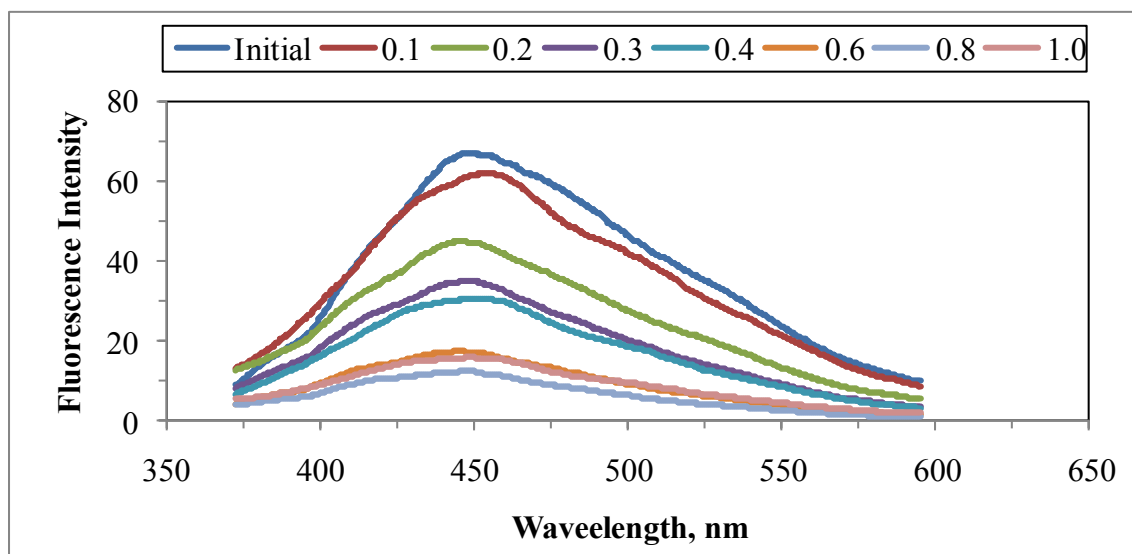
Figure 4.82. Emission scan fluorescence spectra of 30 kDa fraction of humic acid following adsorption onto bare TiO_2 Hombikat UV-100 at 350 nm excitation wavelength.

The fluorescence intensity attained the maximum fluorescence intensity value at emission wavelength of 450 nm (Figure 4.82).Synchronous scan fluorescence spectra showed one sharp peak at emission wavelength of 400 nm, while these spectra shown three moderate peaks around 275 nm, 325 nm and 475 nm emission wavelengths (Figure 4.83).
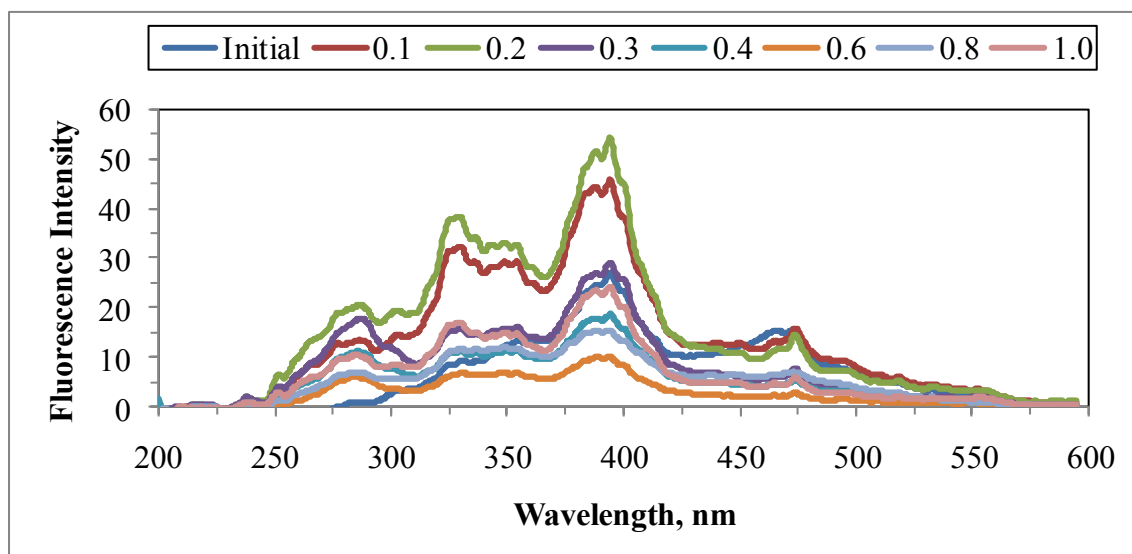
Figure 4.83. Synchronous scan fluorescence spectra of 30 kDa fraction of humic acid following adsorption onto bare TiO_2 Hombikat UV-100.

4.5.2.2. Spectroscopic Properties of 30 kDa Fraction of Humic Acid Following Adsorption onto C-doped TiO$_2$ Hombikat UV-100 Specimen. UV-vis absorbance spectra of 30 kDa fraction of humic acid following adsorption onto C-doped TiO$_2$ Hombikat UV-100 were displayed in Figure 4.84.
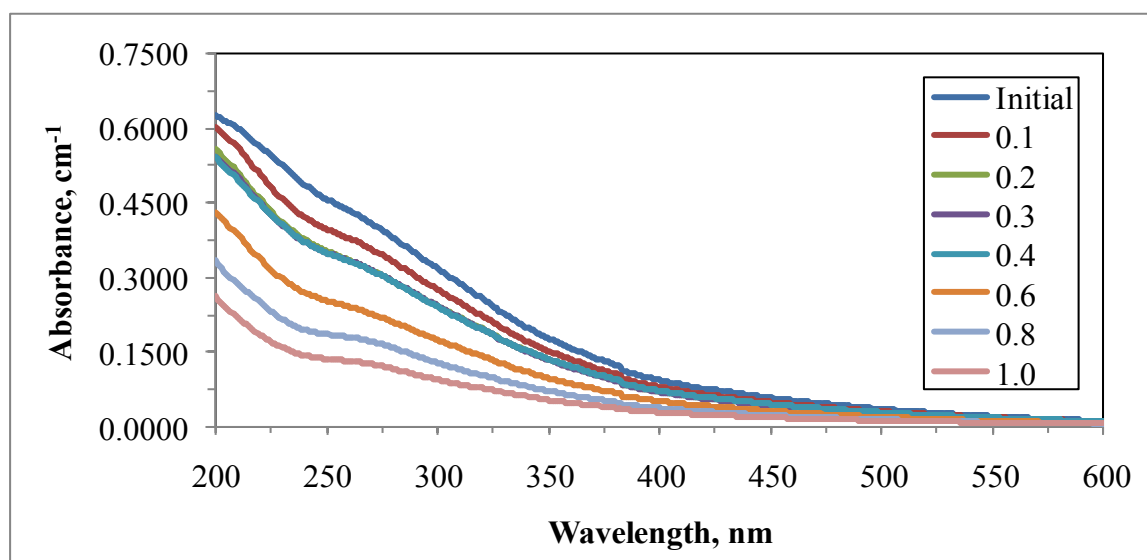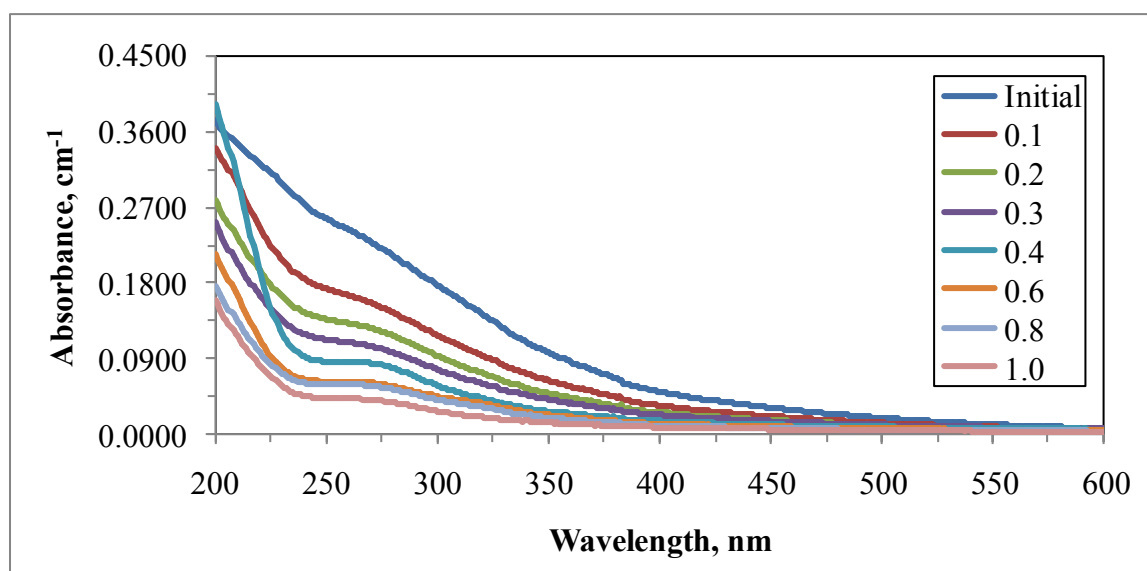

Figure 4.84. UV-vis absorbance spectra of 30 kDa fraction of humic acid following adsorption onto C-doped TiO$_2$ Hombikat UV-100.

UV-vis absorbance spectra of humic acids exhibited a decreasing trend with increasing wavelength with respect to increasing dose of TiO$_2$ as expected. UV-vis absorbance spectra values for all of the humic acid solutions approached to zero and also leveled off after 400 nm wavelength (Figure 4.84).

Emission scan fluorescence spectra and synchronous scan fluorescence spectra of 30 kDa fraction of humic acid following adsorption onto C-doped TiO$_2$ Hombikat UV-100 were presented in Figure 4.85 and Figure 4.86, respectively. The maximum fluorescence intensity for 30 kDa fraction of humic acid following adsorption onto C-doped TiO$_2$ Hombikat UV-100 was observed around 450 nm emission wavelength (Figure 4.85). Synchronous scan fluorescence spectra showed two sharp peaks around emission wavelengths of 325 nm and 400 nm, while the fluorescence spectra displayed two moderate peaks around 275 nm and 475 nm emission wavelengths (Figure 4.86).
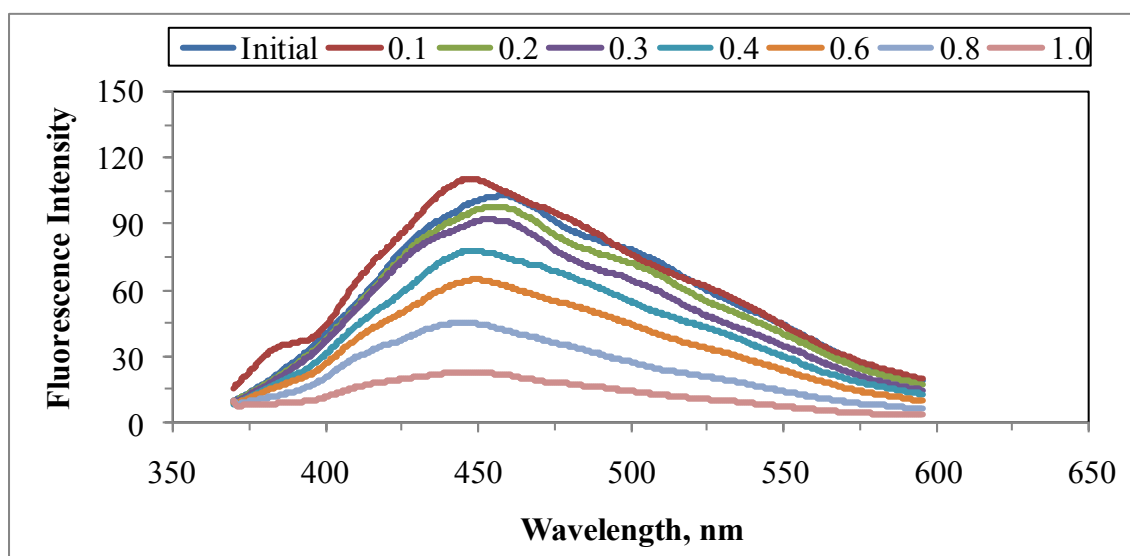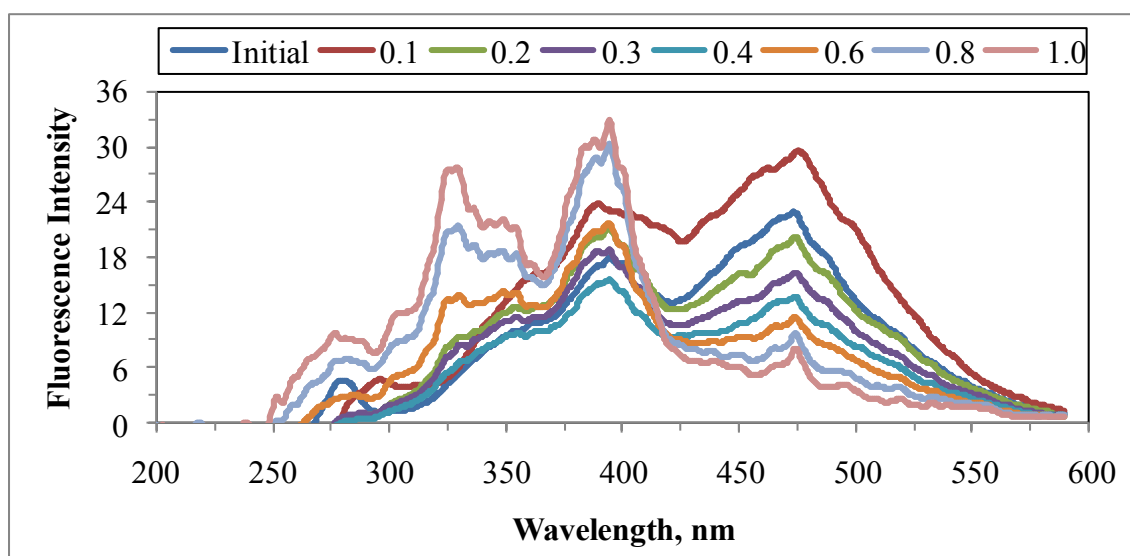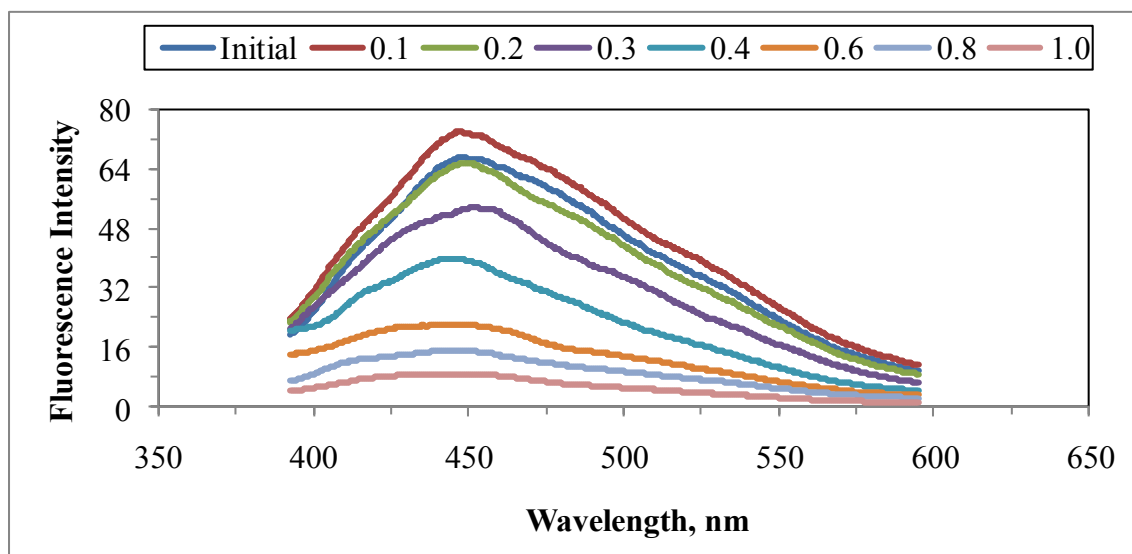
Figure 4.85. Emission scan fluorescence spectra of 30 kDa fraction of humic acid following adsorption onto C-doped TiO$_2$ Hombikat UV-100 at 350 nm excitation wavelength.

The highest fluorescence intensity was observed for 30 kDa fraction of humic acid adsorption onto C-doped TiO$_2$ Hombikat UV-100 around emission wavelength of 400 nm (Figure 4.86).
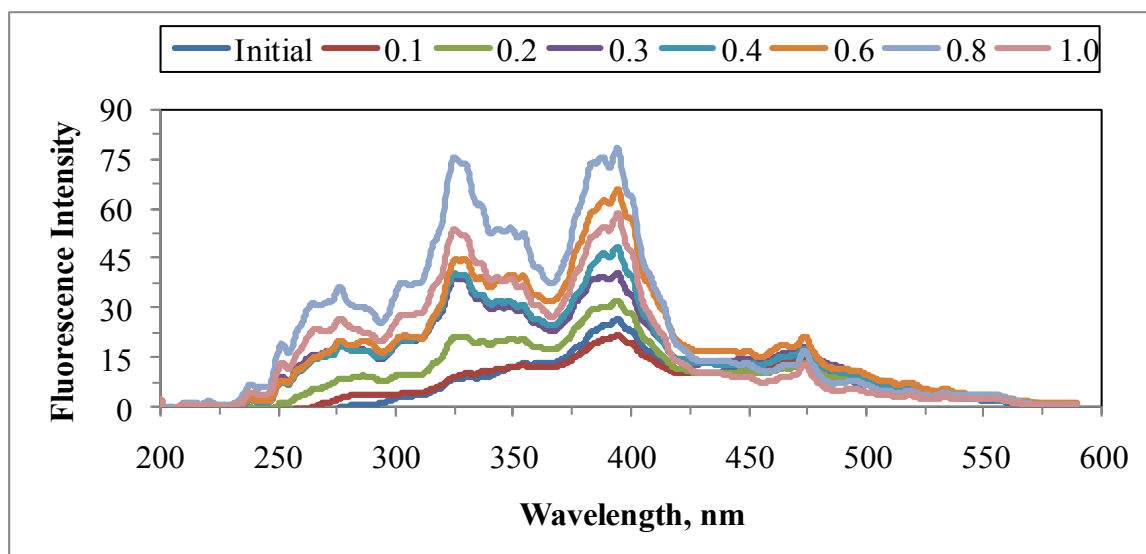
Figure 4.86. Synchronous scan fluorescence spectra of 30 kDa fraction of humic acid following adsorption onto C-doped TiO$_2$ Hombikat UV-100.

4.5.2.3. Spectroscopic Properties of 30 kDa Fraction of Humic Acid Following Adsorption onto N-doped TiO_2 Hombikat UV-100 Specimen. UV-vis absorbance spectra of 30 kDa fraction of humic acid following adsorption onto N-doped TiO_2 Hombikat UV-100 were displayed in Figure 4.87.
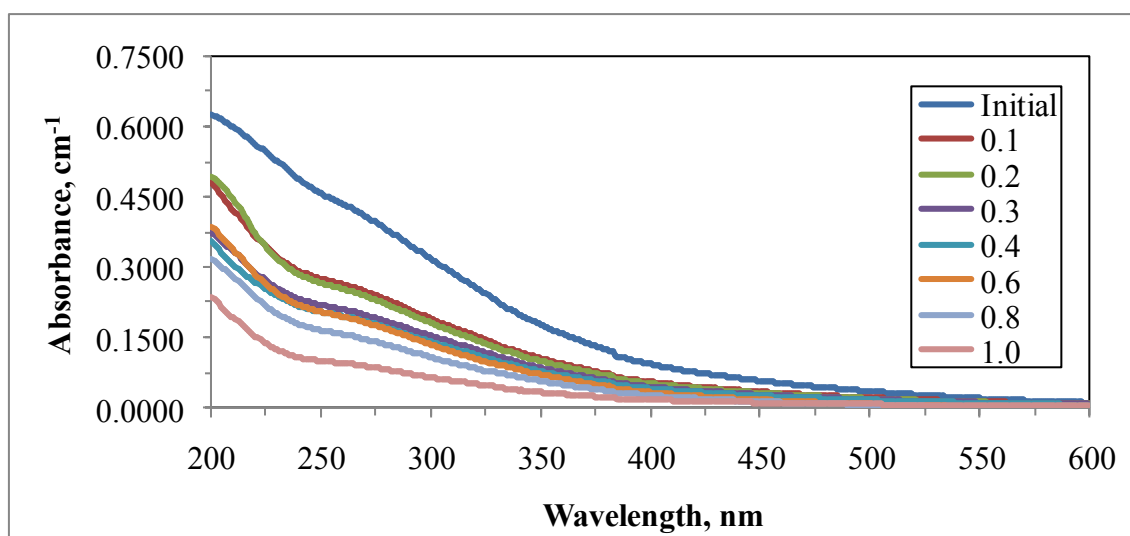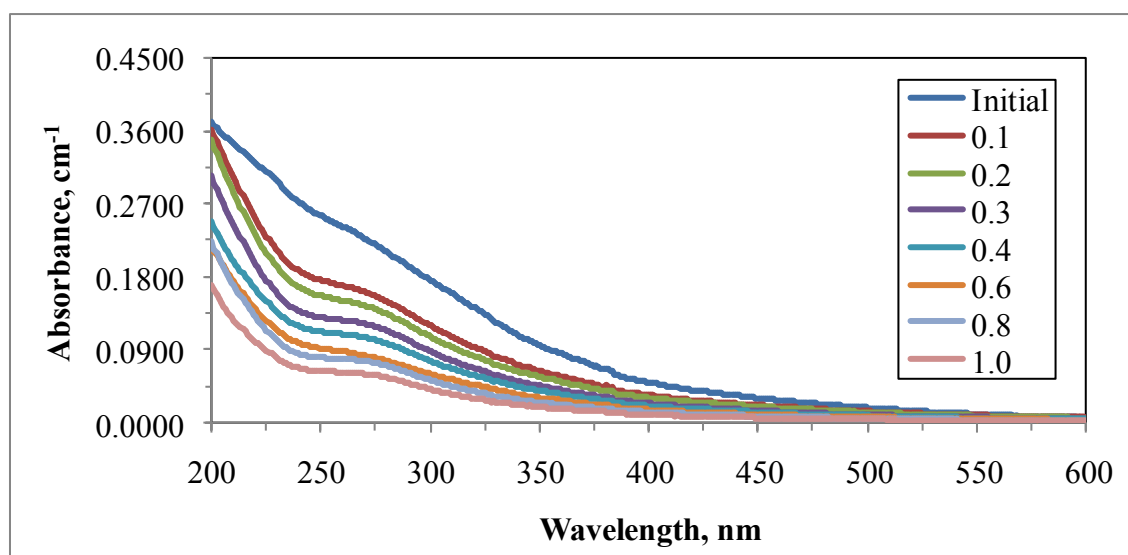

Figure 4.87. UV-vis absorbance spectra of 30 kDa fraction of humic acid following adsorption onto N-doped TiO_2 Hombikat UV-100.

UV-vis absorbance spectra of humic acids exhibited generally a decreasing trend with increasing wavelength with respect to increasing dose of TiO_2 as expected. Furthermore, UV-vis absorbance spectra showed an overlapping trend onto each other for 30 kDa fraction of humic acid following adsorption onto 0.6 mg mL^{-1} and 0.8 mg mL^{-1} loadings of N-doped TiO_2 Hombikat UV-100 (Figure 4.87).

Emission scan fluorescence spectra and synchronous scan fluorescence spectra of 30 kDa fraction of humic acid following adsorption onto N-doped TiO_2 Hombikat UV-100 were presented in Figure 4.88 and Figure 4.89, respectively. The emission scan fluorescence spectra displayed a similar overlapping trend onto each other for 30 kDa fraction of humic acid following adsorption onto 0.6 mg mL^{-1} and 0.8 mg mL^{-1} doses of N-doped TiO_2 Hombikat UV-100 (Figure 4.88).
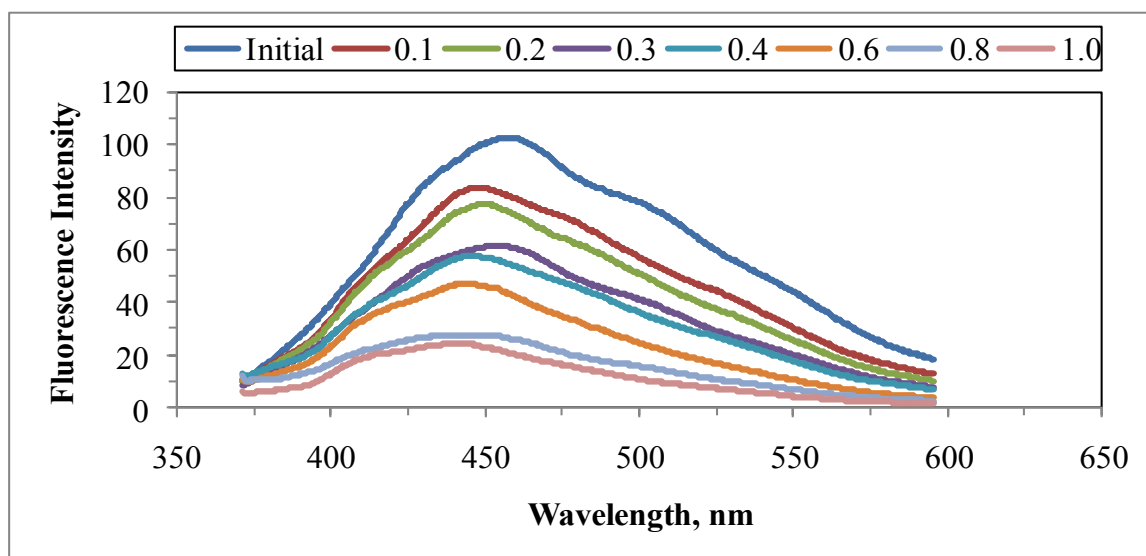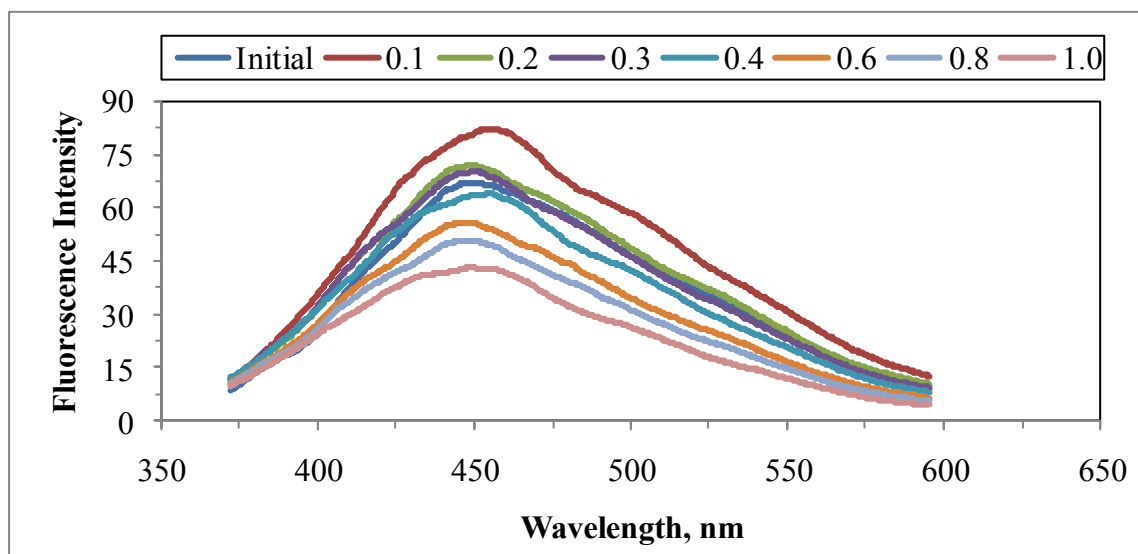
Figure 4.88. Emission scan fluorescence spectra of 30 kDa fraction of humic acid following adsorption onto N-doped TiO_2 Hombikat UV-100 at 350 nm excitation wavelength.

Synchronous scan fluorescence spectra displayed one sharp peak around emission wavelength of 400 nm, while the fluorescence spectra displayed three moderate peaks around 275 nm, 325 nm and 475 nm emission wavelengths (Figure 4.89).
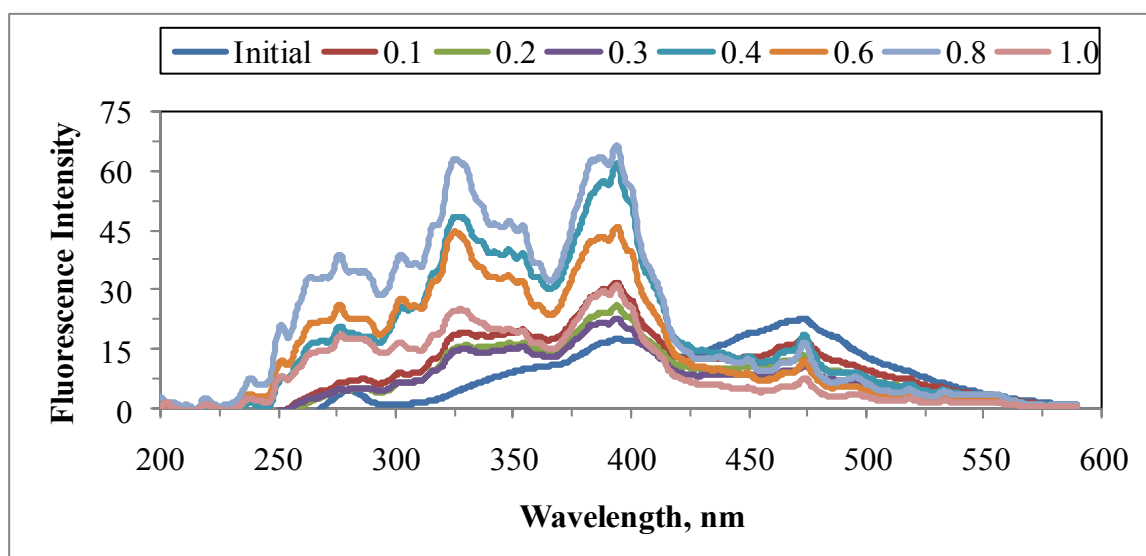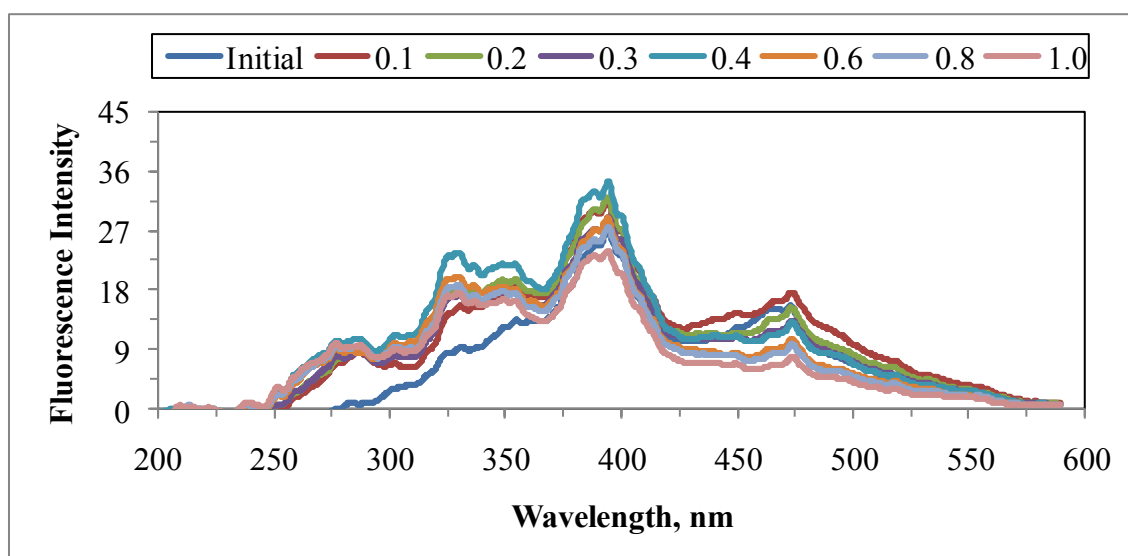

Figure 4.89. Synchronous scan fluorescence spectra of 30 kDa fraction of humic acid following adsorption onto N-doped TiO_2 Hombikat UV-100.

4.5.2.4. Spectroscopic Properties of 30 kDa Fraction of Humic Acid Following Adsorption onto S-doped TiO_2 Hombikat UV-100 Specimen. UV-vis absorbance spectra of 30 kDa fraction of humic acid following adsorption onto S-doped TiO_2 Hombikat UV-100 were displayed in Figure 4.90.
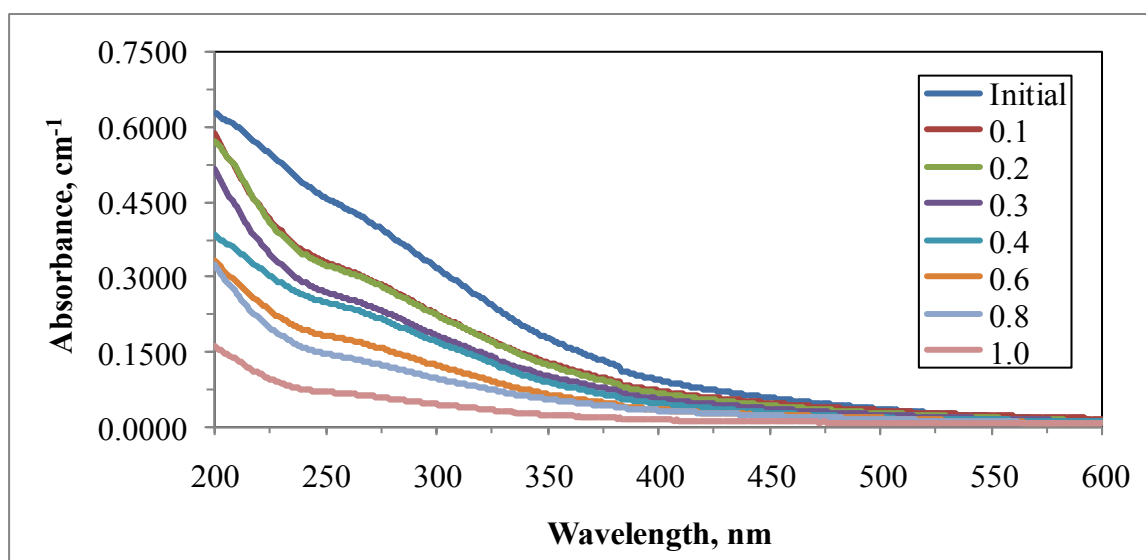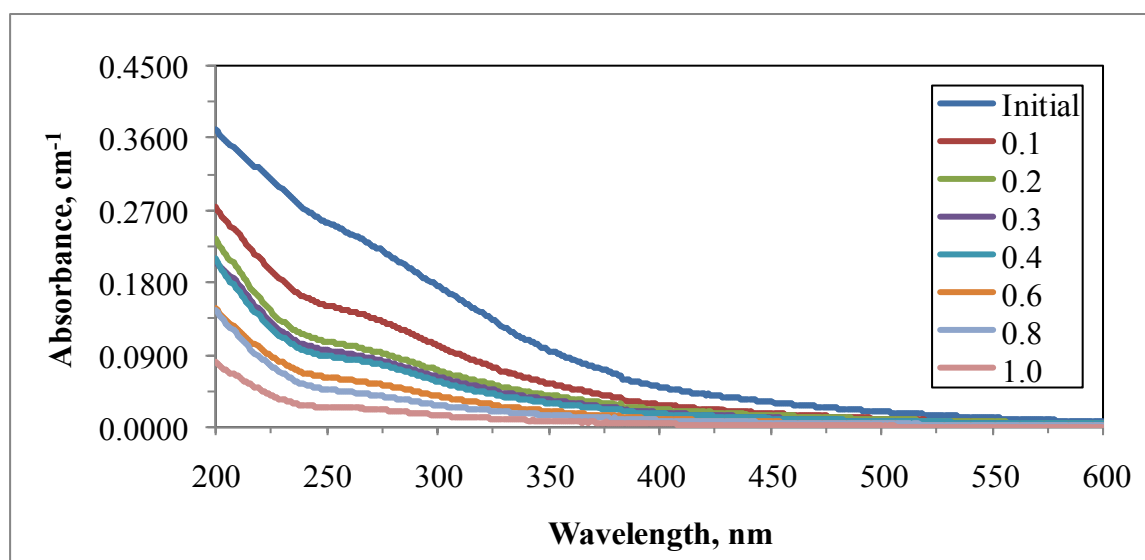

Figure 4.90. UV-vis absorbance spectra of 30 kDa fraction of humic acid following adsorption onto S-doped TiO_2 Hombikat UV-100.

UV-vis absorbance spectra of 30 kDa fraction of humic acid adsorption onto S-doped TiO_2 Hombikat UV-100 exhibited a logarithmic decaying trend with increasing wavelength with respect to increasing dose of TiO_2 as expected. Moreover, UV-vis absorbance spectra exhibited an overlapping trend onto each other for 30 kDa fraction of humic acid following adsorption onto 0.2 mg mL^{-1}, 0.3 mg mL^{-1} and 0.4 mg mL^{-1} loadings of S-doped TiO_2 Hombikat UV-100 (Figure 4.90).

Emission scan fluorescence spectra and synchronous scan fluorescence spectra of 30 kDa fraction of humic acid following adsorption onto S-doped TiO_2 Hombikat UV-100 were presented in Figure 4.91 and Figure 4.92, respectively. The emission fluorescence spectra of 30 kDa fraction of humic acid following adsorption onto 0.6 mg mL^{-1}, 0.8 mg mL^{-1} and 1.0 mg mL^{-1} doses of S-doped TiO_2 Hombikat UV-100, which exhibited a similar overlapping trend onto each other, had the lower fluorescence intensity values (Figure 4.91).
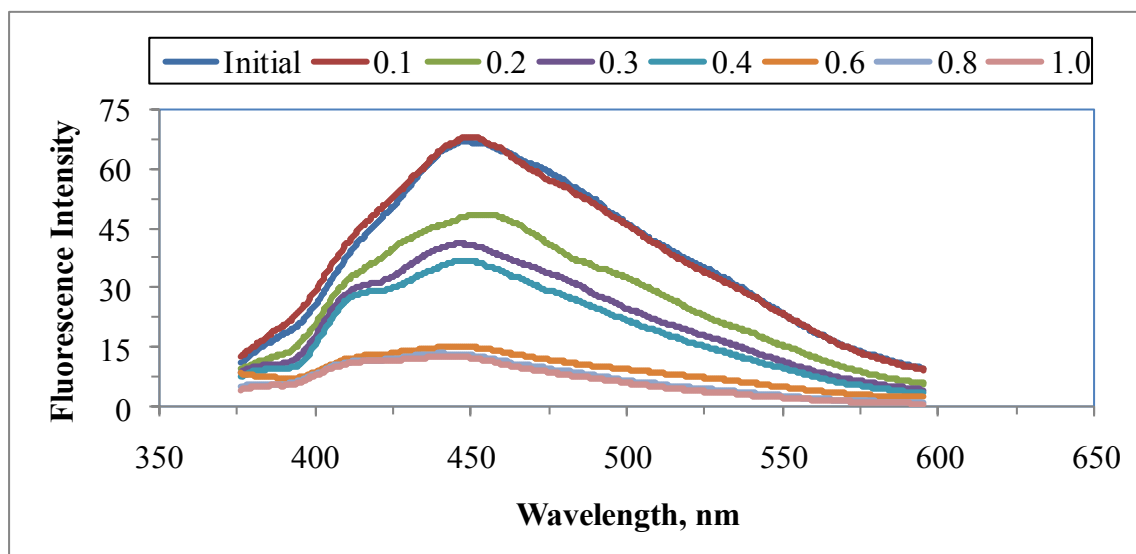
Figure 4.91. Emission scan fluorescence spectra of 30 kDa fraction of humic acid following adsorption onto S-doped TiO_2 Hombikat UV-100 at 350 nm excitation wavelength.

Synchronous scan fluorescence spectra showed one sharp peak around emission wavelengths of 400 nm, while the fluorescence spectra displayed two moderate peaks around 325 nm and 475 nm emission wavelengths (Figure 4.92).
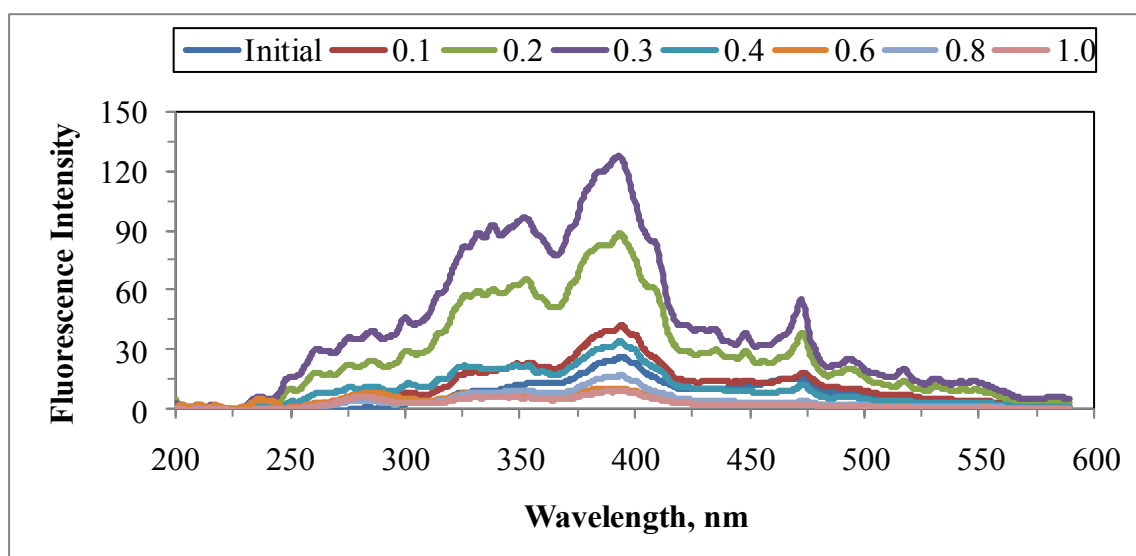
Figure 4.92. Synchronous scan fluorescence spectra of 30 kDa fraction of humic acid following adsorption onto S-doped TiO_2 Hombikat UV-100.

4.5.2.5. Spectroscopic Properties of 30 kDa Fraction of Humic Acid Following Adsorption onto N-S co-doped TiO_2 Hombikat UV-100 Specimen. UV-vis absorbance spectra of 30 kDa fraction of humic acid following adsorption onto N-S co-doped TiO_2 Hombikat UV-100 were displayed in Figure 4.93.
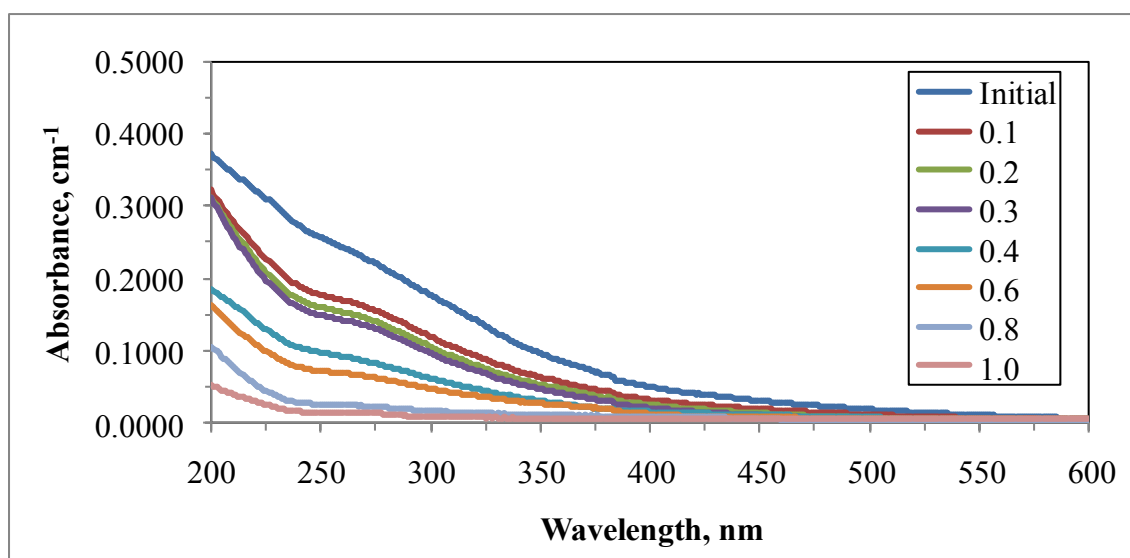
Figure 4.93. UV-vis absorbance spectra of 30 kDa fraction of humic acid following adsorption onto N-S co-doped TiO_2 Hombikat UV-100.

UV-vis absorbance spectra of humic acid solutions exhibited a logarithmic decreasing trend with increasing wavelength and also with increasing TiO_2 loadings. UV-vis absorbance spectra displayed an overlapping trend onto each other for 30 kDa fraction of humic acid following adsorption onto 0.2 mg mL^{-1} and 0.3 mg mL^{-1} doses of N-S co-doped TiO_2 Hombikat UV-100 (Figure 4.93).

Emission scan fluorescence spectra and synchronous scan fluorescence spectra of 30 kDa fraction of humic acid following adsorption onto N-S co-doped TiO_2 Hombikat UV-100 were presented in Figure 4.94 and Figure 4.95, respectively. Emission fluorescence spectra of 30 kDa fraction of humic acid following adsorption onto high dosages of N- S co-doped TiO_2 Hombikat UV-100, such as 0.6 mg mL^{-1}, 0.8 mg mL^{-1} and 1.0 mg mL^{-1}, which displayed a similar overlapping trend on each other, had the lowest fluorescence intensity values measured (Figure 4.94).
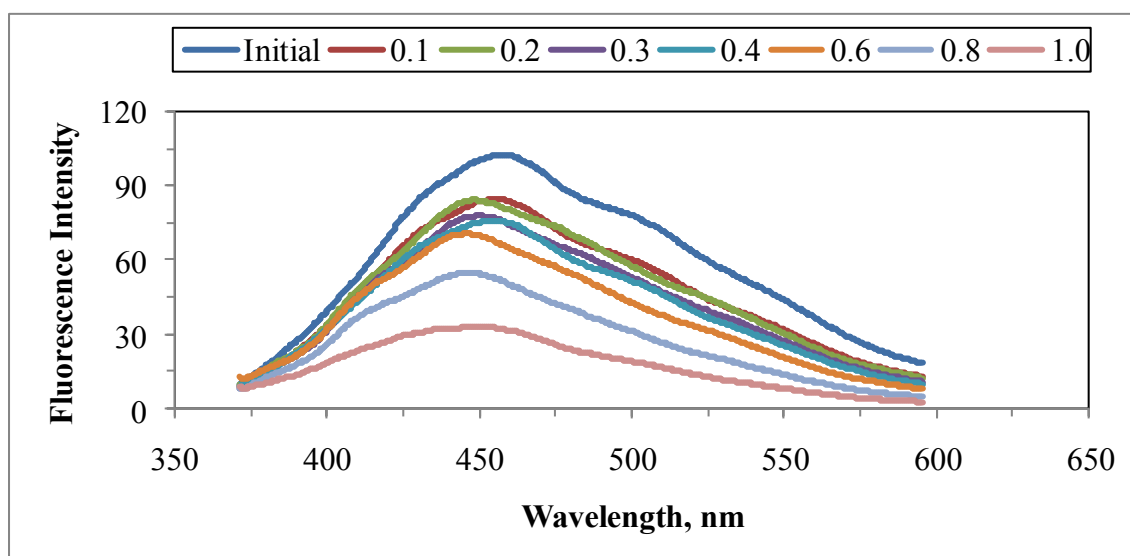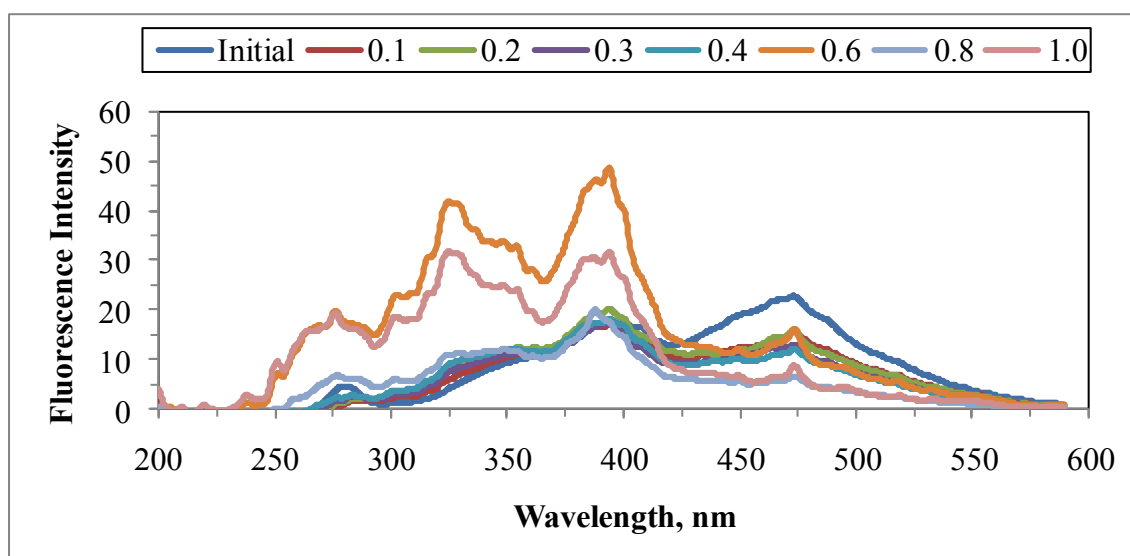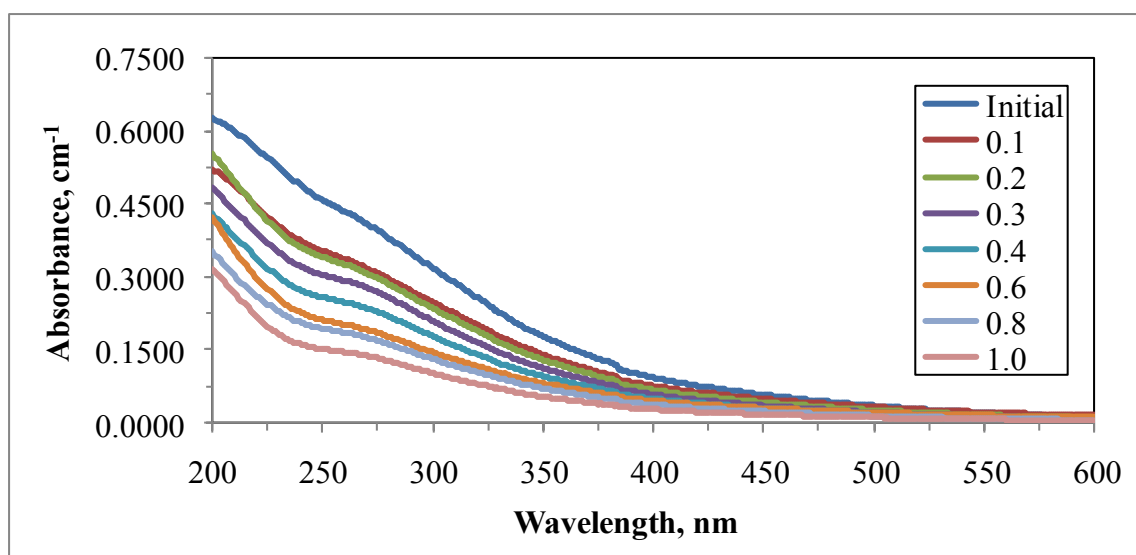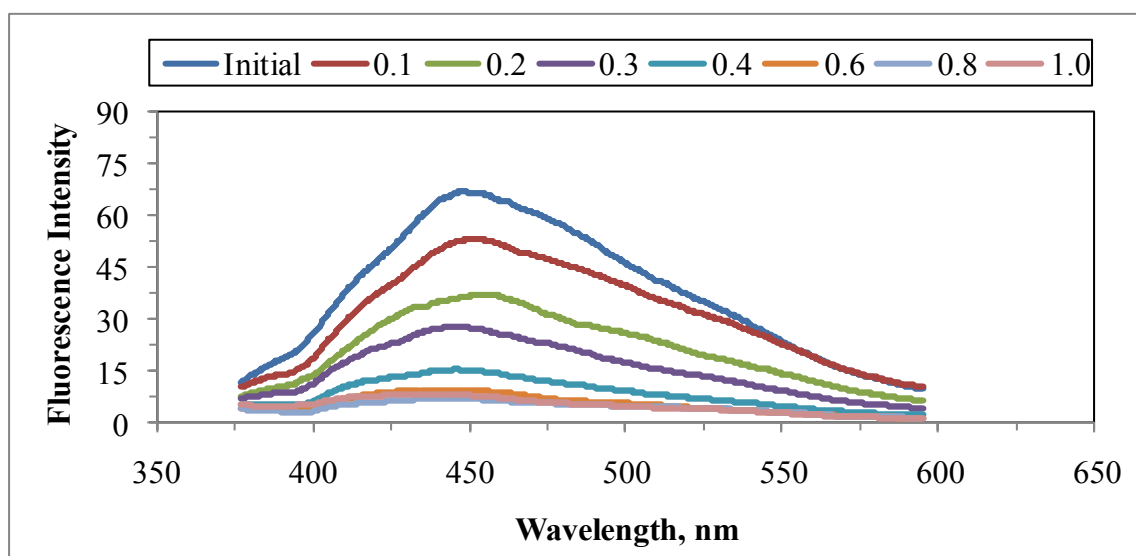
Figure 4.94. Emission scan fluorescence spectra of 30 kDa fraction of humic acid following adsorption onto N-S co-doped TiO$_2$ Hombikat UV-100 at 350 nm excitation wavelength.

Synchronous scan fluorescence spectra displayed one sharp peak around 400 nm emission wavelength, while the fluorescence spectra displayed three moderate peaks around 275 nm, 325 nm and 475 nm emission wavelengths (Figure 4.95).
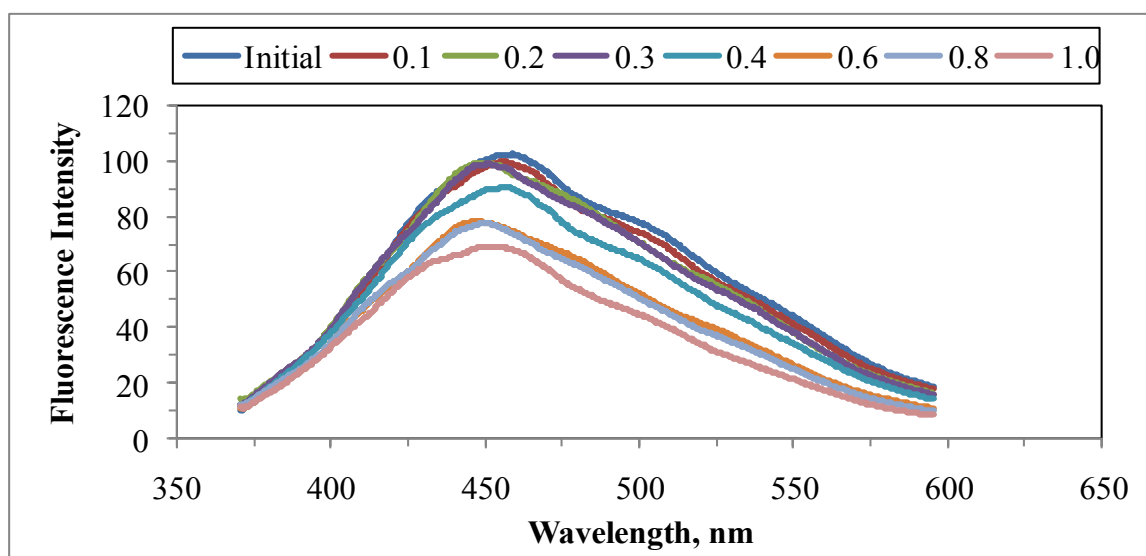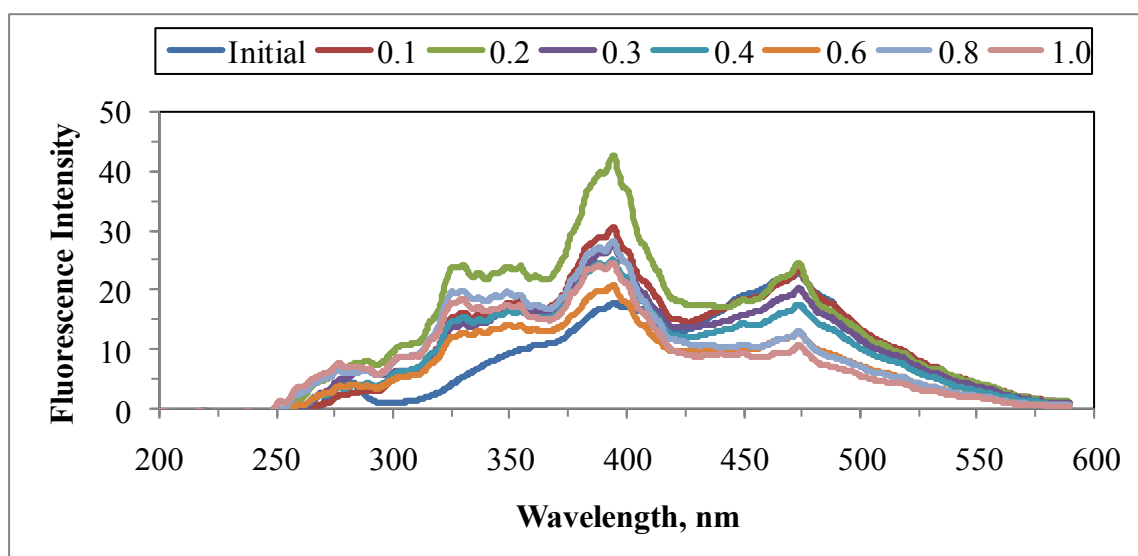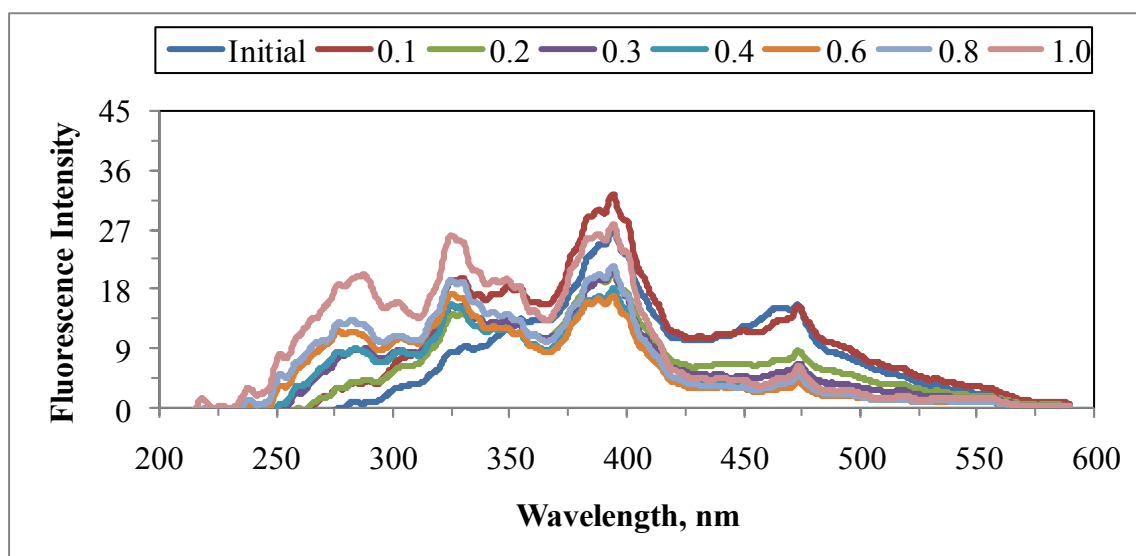

Figure 4.95. Synchronous scan fluorescence spectra of 30 kDa fraction of humic acid following adsorption onto N-S co-doped TiO$_2$ Hombikat UV-100.

The effect of doping on two TiO_2 specimens (Degussa P-25 and Hombikat UV-100) could be evaluated through the role of decreasing molecular size of humic acid. The most significant effect could be attributed to the surface properties of TiO_2 specimens present in aqueous solutions of humic acid.

The morphological properties of C-doped, N-doped, S-doped, and N-S co-doped TiO_2 specimens were determined by instrumental methods in dry forms (Yalcin et al., 2010; Gurkan et al., 2012). Upon introduction of the TiO_2 specimens to aqueous humic solutions surface hydration took place and pH dependent surface charge development occurred equation (2.1), equation (2.2) and equation (2.3). It should also be indicated that depending on the pH_{zpc} condition, positively and negatively charged surface sites developed and played significant roles on the adsorptive properties of the deprotonated humic functional groups. Point of zero charge values determined for anion doped Degussa P-25 and Hombikat UV-100 TiO_2 specimens were listed in Table 4.2.

Table 4.2. Point of zero charge values determined for anion doped Degussa P-25 and Hombikat UV-100 TiO_2 specimens.

TiO_2 specimens	Degussa P-25	Hombikat UV-100
C-doped	4.00	5.38
N-doped	6.23	5.23
S- doped	4.90	5.23
N-S co-doped	5.95	5.42

The chromophoric as well as fluorophoric groups of humic acid could be expressed by the UV-vis and fluorescence spectral features. The observed close similarities in the UV-vis spectroscopic features indicated the possible use of these UV-vis parameters in presentation of the adsorption isotherms and adsorption isotherm modeling. Fluorescence spectral features attained either upon emission scan mode or synchronous scan mode displayed an inconsistent trend both with respect to type of the dopant as well as the molecular size of humic acid. These results indicated that fluorescence intensities should be regarded as non-specific in terms of quantification of humic acid.

4.6. Adsorption Isotherm Modeling of 0.45 μm Filtered Fraction of Humic Acid onto TiO$_2$ Specimens

The data obtained for the adsorption of 0.45 μm filtered fraction of humic acid onto TiO$_2$ specimens were fitted to both Freundlich and Langmuir isotherm models. Freundlich isotherm model was explained with equation (2.7) as outlined in the theoretical background section and Langmuir isotherm model was expressed with equation (2.6).

4.6.1. Adsorption Isotherm Modeling of 0.45 μm Filtered Fraction of Humic Acid onto TiO$_2$ Degussa P-25 Specimens

The experimental data related to 0.45 μm filtered fraction of humic acid following adsorption onto TiO$_2$ Degussa P-25 specimens were fitted to both Freundlich and Langmuir isotherm models.

4.6.1.1. Adsorption Isotherm Modeling of 0.45 μm Filtered Fraction of Humic Acid onto Bare TiO$_2$ Degussa P-25 Specimen. UV-vis spectroscopic parameters (Color$_{436}$, UV$_{365}$, UV$_{280}$, and UV$_{254}$) and DOC were fitted to Freundlich (2.7) and Langmuir (2.6) adsorption isotherm models.

Freundlich adsorption model. Freundlich adsorption isotherms were presented in Figure 4.96 for Color$_{436}$, UV$_{254}$ and DOC parameters. Freundlich isotherms for UV$_{365}$ and UV$_{280}$ were presented in Appendix A.

C$_e$ values altered between 0.53 – 5.87 m^{-1} for Color$_{436}$ in concern with the loading of bare TiO$_2$ Degussa P-25 in the solution. The calculated values of q$_A$ were in the range of 278 – 640 m^{-1}g^{-1} for the corresponding to C$_e$ values. ΔC$_e$ and Δq$_A$ values for 0.45 μm filtration fraction of humic acid were calculated as 5.34 m^{-1} and 362 m^{-1} g^{-1} for Color$_{436}$. C$_e$ values altered between 7.23 - 33.85 m^{-1} for UV$_{254}$. The values of q$_A$ were calculated as between 1480 - 4152 m^{-1}g^{-1} for the corresponding to the C$_e$ values. ΔC$_e$ and Δq$_A$ values for UV$_{254}$ were found as 26.62 m^{-1} and 2672 m^{-1} g^{-1}; respectively (Figure 4.96).

Figure 4.96. Freundlich adsorption isotherm of Color$_{436}$, UV$_{254}$ and DOC parameters of 0.45 μm filtration fraction of humic acid following adsorption onto bare TiO$_2$ Degussa P-25.

Adsorption isotherms relatively exhibited similar trend for both of the UV-vis parameters as expressed by $Color_{436}$ and UV_{254} as well as UV_{365} and UV_{280} parameters (Appendix A). The trends exhibited by the respective adsorption isotherms could be illustrated as C-curve type isotherm. This kind of adsorption isotherm is characterized by an initial slope remaining independent of adsorptive concentration revealing a constant partitioning of humic acid between TiO_2 surface and the aqueous solution (Uyguner and Bekbolet, 2004).

C_e values altered between 1.27 - 3.30 mg L^{-1} for DOC. The values of q_A corresponding to the C_e values were calculated as between 159 - 780 mg L^{-1} g^{-1}. ΔC_e and Δq_A values for DOC were calculated as 2.03 mg L^{-1} and 621 mg L^{-1} g^{-1}, respectively (Figure 4.96).

Freundlich Isotherm model coefficients; adsorption capacity, K_f, and adsorption intensity, 1/n, for 0.45 μm filtration fraction of humic acid following adsorption onto bare TiO_2 Degussa P-25 were listed in Table 4.3 ($R^2 \geq 0.94$).

UV-vis parameters of 0.45 μm filtration fraction of humic acid as expressed by $Color_{436}$ and UV_{254} displayed similar trends contrary to the DOC adsorption profile (Figure 4.96). DOC adsorption isotherm displayed an increasing trend with respect to the decreasing dose of TiO_2 Degussa P-25. Considering the initial DOC of 0.45 μm filtration fraction of humic acid (5.25 mg L^{-1}), 37 % DOC was removed for 0.1 mg mL^{-1} dose of bare TiO_2 Degussa P-25 and 76 % DOC was removed for 1.0 mg mL^{-1} dose of bare TiO_2 Degussa P-25 upon adsorption under equilibrium conditions.

Increasing humic acid concentration to 50 mgL^{-1} and considering the initial DOC of 0.45μm filtration fraction of 50 mgL^{-1}humic acid (14.5 mg L^{-1}), 30 % DOC was removed for 0.1 mg mL^{-1} dose of bare TiO_2 Degussa P-25 and 75% DOC was removed for 1.0 mg mL^{-1} dose of bare TiO_2 Degussa P-25 upon adsorption under equilibrium conditions (Ulker, 2088). These results pointed out to a non-specific effect of initial humic acid concentration on the adsorption.

Table 4.3. Freundlich isotherm model parameters for 0.45 µm filtration fraction of humic acid following adsorption onto bare TiO_2 Degussa P-25.

Humic acid, 0.45 µm filtration fraction		
UV-vis parameter	K_f	$1/n$
$Color_{436}$	349.2	0.307
UV_{365}	443.1	0.442
UV_{280}	451.6	0.572
UV_{254}	455.5	0.589
Dissolved Organic Carbon	K_f	$1/n$
DOC	108.2	1.49

Comparison of the UV-vis parameters indicated that adsorption capacity constant of $Color_{436}$ was the lowest value. Moreover, adsorption capacity constants of UV_{280} and UV_{254} were nearly equal to each other. Adsorption capacity constants were found to be in the order of $Color_{436} < UV_{365} < UV_{280} < UV_{254}$. Also, adsorption intensity of $Color_{436}$ was the lowest value. Furthermore, adsorption intensity of UV_{280} and UV_{254} were very much close to each other and found to be lower than 1.0 representing strong adsorption bond; the capacity tended to be independent of C_e and the isotherm plot approaches the horizontal level. An increasing order of adsorption intensity could be given as $Color_{436} < UV_{365} < UV_{280} < UV_{254}$. Adsorption intensity of DOC was found to be >1 due to the binding mechanism of humic acid that could be affected by mixed crystalline nature of Degussa P-25, which was one of commercially diverse type of TiO_2, in such a way that adsorption constants increased as well as photocatalytic activity rates (Bekbolet et al., 2002).

Langmuir adsorption model. Langmuir adsorption isotherms for 0.45 µm filtration fraction of humic acid were presented in Figure 4.97 for $Color_{436}$, UV_{254} and DOC parameters. Langmuir isotherms for UV_{365} and UV_{280} were presented in Appendix B.

Two parameters of Langmuir equation outlined in section 2.3, q_m and K_a, were listed in Table 4.4 for 0.45 µm filtration fraction of humic acid following adsorption onto bare TiO_2 Degussa P-25 ($R^2 \geq 0.90$).

Figure 4.97. Langmuir adsorption isotherm of Color$_{436}$, UV$_{254}$ and DOC parameters of 0.45 μm filtration fraction of humic acid following adsorption onto bare TiO$_2$ Degussa P-25.

Table 4.4. Langmuir adsorption isotherm model parameters for 0.45 μm filtration fraction of humic acid following adsorption onto bare TiO_2 Degussa P-25.

Humic acid, 0.45 μm filtration fraction		
UV-vis parameter	q_m m^{-1}g^{-1}	K_a m^{-1}
Color$_{436}$	500	2.00
UV$_{365}$	1429	0.350
UV$_{280}$	3333	0.100
UV$_{254}$	5000	0.0590
Dissolved Organic Carbon	q_m mg L^{-1}g^{-1}	K_a mg L^{-1}
DOC	1000	0.111

The order of all UV-vis spectroscopic parameters for q_m value was $UV_{254} > UV_{280} > UV_{365} > Color_{436}$ and this order was reverse for K_a value, namely $UV_{254} < UV_{280} < UV_{365} < Color_{436}$. The model parameters as q_m and K_a values for DOC were calculated as 1000 mg L^{-1} g^{-1} and 0.111 mg L^{-1}, respectively. When this study was compared with other studies implemented by Degirmenci Ilhan (2010) and Aykac (2011) by means of model parameters of Freundlich and Langmuir adsorption isotherms (K_f and 1/n as well as q_m), the results in this study had higher values indicating higher adsorption capacity as well as higher adsorption intensity. The reason could be attributed to the initial properties of 0.45 μm filtration fraction of humic acid.

Moreover, with respect to higher initial humic acid concentration as 50 mg L^{-1} representing 14.5 mg L^{-1} DOC, Freundlich adsorption isotherm model parameters were found to be as K_F = 39.12 and 1/n as 1.17 (Ulker, 2008). A plausible reason could be attributed to the polydisperse character of humic acid rather than initial concentration effect.

It should be indicated that adsorption of 0.45 μm filtered fraction of humic acid onto bare TiO_2 Degussa P-25 could well be characterized both by Freundlich and Langmuir adsorption isotherm models. Moreover, it should also be kept in mind that humic acid should be visualized as macromolecules expressing different conformational as well as structural features leading to diverse oxide surface interactions.

4.6.1.2. Adsorption Isotherm Modeling of 0.45 μm Filtered Fraction of Humic Acid onto C-doped TiO_2 Degussa P-25 Specimen. UV-vis spectroscopic parameters ($Color_{436}$, UV_{365}, UV_{280}, and UV_{254}) and DOC were fitted to Freundlich (2.7) and Langmuir (2.6) adsorption isotherm models.

Freundlich adsorption model. Freundlich adsorption isotherms were presented in Figure 4.98 for $Color_{436}$, UV_{254} and DOC parameters. Freundlich isotherms for UV_{365} and UV_{280} were presented in Appendix A.

C_e values altered between 2.55 – 5.43 m^{-1} for $Color_{436}$. The calculated values of q_A were in the range of 228 - 1124 $m^{-1}g^{-1}$ for the corresponding to the C_e values. ΔC_e and Δq_A values were calculated as 2.88 m^{-1} and 896 $m^{-1} g^{-1}$ for $Color_{436}$. C_e values altered between 14.05 – 29.96 m^{-1} for UV_{254}. The calculated values of q_A were in the range of 1300 - 6636 $m^{-1}g^{-1}$ for the corresponding to the C_e values. ΔC_e and Δq_A values for UV_{254} were calculated as 15.91 m^{-1} and 5336 $m^{-1} g^{-1}$, respectively (Figure 4.98).

Adsorption isotherms relatively exhibited similar trend for both of the UV-vis parameters as expressed by $Color_{436}$ and UV_{254} parameters. The trends exhibited by the respective adsorption isotherms could be considered as S-curve type isotherm. S curve is identified as adsorption in which individual solute molecule connected with the solid interacts with each other (Uyguner and Bekbolet, 2004). The role of C-doping could be visualized in adsorption isotherm profiles of UV-vis parameters (Figure 4.96 and Figure 4.98).

C_e values altered between 2.14 – 4.49 mg L^{-1} for DOC. The calculated values of q_A were in the range of 266 - 1716 mg $L^{-1} g^{-1}$ for the corresponding to the C_e values. ΔC_e and Δq_A values for DOC were calculated as 2.35 mg L^{-1} and 1450 mg $L^{-1} g^{-1}$, respectively (Figure 4.98). The effect of C-doping did not significantly alter the DOC adsorption isotherm trend of 0.45 μm filtration fraction of humic acid onto TiO_2 Degussa P-25.

Freundlich Isotherm model coefficients; adsorption capacity, K_f, and adsorption intensity, 1/n, for 0.45 μm filtration fraction of humic acid following adsorption onto C-doped TiO_2 Degussa P-25 were listed in Table 4.5 ($R^2 \geq 0.95$).

Figure 4.98. Freundlich adsorption isotherm of Color$_{436}$, UV$_{254}$ and DOC parameters of 0.45 μm filtration fraction of humic acid following adsorption onto C-doped TiO$_2$ Degussa P-25.

Table 4.5. Freundlich isotherm model parameters for 0.45 µm filtration fraction of humic acid following adsorption onto C-doped TiO_2 Degussa P-25.

Humic acid, 0.45 µm filtration fraction		
UV-vis parameter	K_f	$1/n$
$Color_{436}$	24.06	2.22
UV_{365}	10.41	2.26
UV_{280}	4.953	2.13
UV_{254}	4.093	2.15
Dissolved Organic Carbon	K_f	$1/n$
DOC	49.15	2.46

Comparison of the UV-vis parameters indicated that adsorption capacity constant of $Color_{436}$ was the highest value. Moreover, adsorption capacity constants of UV_{280} and UV_{254} were nearly equal to each other and also they had the lowest values. A decreasing order of adsorption capacity, K_f, could be given as $UV_{254} < UV_{280} < UV_{365} < Color_{436}$. Also, adsorption intensity of UV_{280} was the lowest value. Furthermore, adsorption intensity of UV_{280} and UV_{254} were relatively closed to each other. The order of adsorption intensity, $1/n$, could be given as $UV_{280} = UV_{254} < Color_{436} < UV_{365}$. Adsorption intensity of DOC was found to be > 1. Adsorption intensity values were found to be > 1 representing strong adsorption bond. Freundlich isotherm model parameters displayed significantly lower values for C-doping TiO_2 Degussa P-25 (Table 4.3 and Table 4.5). Although lower Freundlich K_f values were attained, adsorption intensity values, $1/n > 2$ reflected the effect of surface modification of TiO_2.

Langmuir adsorption model.   Langmuir adsorption isotherms for 0.45 µm filtration fraction of humic acid following adsorption onto C-doped TiO_2 Degussa P-25 were presented in Figure 4.99 for $Color_{436}$, UV_{254} and DOC parameters. Langmuir adsorption isotherm models for UV_{365} and UV_{280} were presented in Appendix B. Two parameters of Langmuir equation outlined in section 2.3, q_m and K_a, were listed in Table 4.6 for 0.45 µm filtration fraction of humic acid following adsorption onto C- doped TiO_2 Degussa P-25 ($R^2 \geq 0.94$).

Figure 4.99. Langmuir adsorption isotherm of $Color_{436}$, UV_{254} and DOC parameters of 0.45 μm filtration fraction of humic acid following adsorption onto C-doped TiO_2 Degussa P-25.

Table 4.6. Langmuir isotherm model parameters for 0.45 μm filtration fraction of humic acid following adsorption onto C-doped TiO_2 Degussa P-25.

Humic acid, 0.45 μm filtration fraction		
UV-vis parameter	q_m m^{-1}g^{-1}	K_a m^{-1}
Color$_{436}$	406	0.135
UV$_{365}$	820	0.0700
UV$_{280}$	2062	0.0280
UV$_{254}$	2364	0.0250
Dissolved Organic Carbon	q_m mg L^{-1}g^{-1}	K_a mg L^{-1}
DOC	380	0.210

It could be easily seen from Table 4.6 that q_m values of UV$_{280}$ and UV$_{254}$ spectroscopic parameters were almost equal to each other and K_a values of the same UV-vis specific parameters were nearly equal to each other, too. The order of all UV-vis spectroscopic parameters in terms of q_m value was UV$_{254}$ > UV$_{280}$ > UV$_{365}$ > Color$_{436}$ and this order was reverse for K_a value, namely, Color$_{436}$ > UV$_{365}$ > UV$_{280}$ > UV$_{254}$. The model parameters as q_m and K_a values for DOC were found to be 380 mg L^{-1}g^{-1} and 0.210 mg L^{-1}; respectively.

It should be indicated that adsorption of 0.45 μm filtered fraction of humic acid onto C-doped TiO_2 Degussa P-25 could well be characterized both by Freundlich and Langmuir adsorption isotherm models. Langmuir isotherm model parameters of 0.45 μm filtration fraction of humic acid recorded following adsorption onto two different TiO_2 specimens were compared (Table 4.4 and Table 4.6).

Comparison of Table 4.4 and Table 4.6 could display the role of C-doping on adsorption of 0.45 μm filtration fraction of humic acid onto TiO_2 Degussa P-25. Although a consistent trend could be expressed within the UV-vis parameters and DOC, q_m was significantly higher for bare TiO_2 Degussa P-25 in comparison to slightly different K_a values as K_a = 0.111 mg L^{-1} for bare TiO_2 Degussa P-25 and K_a = 0.210 mg L^{-1} for C-doped TiO_2 Degussa P-25.

4.6.1.3. Adsorption Isotherm Modeling of 0.45 µm Filtered Fraction of Humic Acid onto N-doped TiO_2 Degussa P-25 Specimen. UV-vis spectroscopic parameters ($Color_{436}$, UV_{365}, UV_{280}, and UV_{254}) and DOC were fitted to Freundlich (2.7) and Langmuir (2.6) adsorption isotherm models.

Freundlich adsorption model. Freundlich adsorption isotherms were presented in Figure 4.100 for $Color_{436}$, UV_{254} and DOC parameters. Freundlich isotherms for UV_{365} and UV_{280} were presented in Appendix A.

C_e values altered between 4.47 – 5.88 m^{-1} for $Color_{436}$ according to the loading of N-doped TiO_2 Degussa P-25 in the solution. The values of q_A were found in the range of 151 - 944 $m^{-1} g^{-1}$ for the corresponding to the C_e values. ΔC_e and Δq_A values for $Color_{436}$ were calculated as 1.14 m^{-1} and 793 $m^{-1} g^{-1}$, respectively. C_e values altered between 23.37 – 32.12 m^{-1} for UV_{254}. The calculated values of q_A were in the range of 927 - 5772 $m^{-1} g^{-1}$ for the corresponding to the C_e values. ΔC_e and Δq_A values for UV_{254} were calculated as 8.75 m^{-1} and 4845 $m^{-1} g^{-1}$, respectively (Figure 4.100).

Freundlich adsorption isotherms of 0.45 µm filtration fraction of humic acid following adsorption onto 0.4 mg mL^{-1} N-doped TiO_2 Degussa P-25 demonstrated a notable difference in $Color_{436}$ and UV_{254} specific parameters. The trend exhibited by respective adsorption isotherms could be considered as L-curve type isotherm.

N-doping of TiO_2 Degussa P-25 significantly altered the adsorption isotherm trend of 0.45 µm filtration fraction of humic acid in comparison to both bare and C-doped TiO_2 Degussa P-25 (Figure 4.96, Figure 4.98 and Figure 4.100).

C_e values altered between 5.65 – 6.50 mg L^{-1} for DOC. The values of q_A corresponding to the C_e values were calculated as between 125 - 912 mg $L^{-1} g^{-1}$. ΔC_e and Δq_A values for DOC were calculated as 0.85 mg L^{-1} and 787 mg $L^{-1} g^{-1}$; respectively (Figure 4.100). Freundlich isotherm model coefficients; adsorption capacity, K_f, and adsorption intensity, 1/n, for 0.45 µm filtration fraction of humic acid following adsorption onto N-doped TiO_2 Degussa P-25 were listed in Table 4.7 ($R^2 \geq 0.93$).

Figure 4.100. Freundlich adsorption isotherm of Color$_{436}$, UV$_{254}$ and DOC parameters of 0.45 μm filtration fraction of humic acid following adsorption onto N-doped TiO$_2$ Degussa P-25.

Table 4.7. Freundlich isotherm model parameters for 0.45 μm filtration fraction of humic acid following adsorption onto N-doped TiO_2 Degussa P-25.

Humic acid, 0.45 μm filtration fraction		
UV-vis parameter	K_f	1/n
$Color_{436}$	4.18×10^{-3}	6.95
UV_{365}	1.83×10^{-4}	6.55
UV_{280}	1.52×10^{-6}	6.59
UV_{254}	5.99×10^{-6}	5.93
Dissolved Organic Carbon	K_f	1/n
DOC	3.24×10^{-3}	12.6

Comparison of UV-vis parameters indicated that the adsorption capacity constant of $Color_{436}$ was the highest value. Moreover, adsorption capacity constants of UV_{254} had the lowest value. A declining order of adsorption capacity constant, K_f could be given as $UV_{254} < UV_{280} < UV_{365} < Color_{436}$. Also, adsorption intensity of UV_{254} was the lowest value. Furthermore, adsorption intensity of UV_{280} and UV_{365} were relatively close to each other. The order of adsorption intensity, 1/n could be given as $UV_{254} < UV_{365} < UV_{280} < Color_{436}$. Adsorption intensity of DOC was found to be >1. Adsorption intensity, 1/n values were found to be >1 representing strong adsorption bond.

With reference to the differences observed in adsorption isotherm profiles of bare TiO_2 and C-doped TiO_2 Degussa P-25 specimens, the Freundlich isotherm model parameters were significantly different as expected (Table 4.3, Table 4.5 and Table 4.7).

Langmuir adsorption model.   Langmuir adsorption isotherms for 0.45 μm filtration fraction of humic acid following adsorption onto N-doped TiO_2 Degussa P-25 were presented in Figure 4.101 for $Color_{436}$, UV_{254} and DOC parameters. Langmuir isotherms for UV_{365} and UV_{280} were presented in Appendix B.

Two parameters of Langmuir equation outlined in section 2.3, q_m and K_a, were listed in Table 4.8 for 0.45 μm filtration fraction of humic acid following adsorption onto N-doped TiO_2 Degussa P-25 ($R^2 \geq 0.91$).

Figure 4.101. Langmuir adsorption isotherm of Color$_{436}$, UV$_{254}$ and DOC parameters of 0.45 μm filtration fraction of humic acid following adsorption onto N-doped TiO$_2$ Degussa P-25.

Table 4.8. Langmuir isotherm model parameters for 0.45 μm filtration fraction of humic acid following adsorption onto N-doped TiO_2 Degussa P-25.

Humic acid, 0.45 μm filtration fraction		
UV-vis parameter	q_m $m^{-1}g^{-1}$	K_a
$Color_{436}$	57	0.165
UV_{365}	135	0.0810
UV_{280}	311	0.0350
UV_{254}	414	0.0300
Dissolved Organic Carbon	q_m mg $L^{-1}g^{-1}$	K_a mg L^{-1}
DOC	23	0.146

It could be easily seen from Table 4.8 the order of all of the UV-vis spectroscopic parameters in terms of q_m value was $UV_{254} > UV_{280} > UV_{365} > Color_{436}$ and this order was reverse for K_a value, namely, $Color_{436} > UV_{365} > UV_{280} > UV_{254}$. The model parameters as q_m and K_a values for DOC were found to be 23 mg $L^{-1}g^{-1}$ and 0.146 mg L^{-1}, respectively.

It should be indicated that adsorption of 0.45 μm filtered fraction of humic acid onto N-doped TiO_2 Degussa P-25 could well be characterized both by Freundlich and Langmuir adsorption isotherm models.

Langmuir isotherm model parameters of 0.45 μm filtration fraction of humic acid recorded following adsorption onto three different TiO_2 specimens were compared (Table 4.4, Table 4.6 and Table 4.8).

Langmuir isotherm model parameter, q_m was found to be significantly lower than the values calculated from the data attained in case of bare TiO_2 and C-doped TiO_2 Degussa P-25 (Table 4.4, Table 4.6 and Table 4.8) for both UV-vis parameters and DOC. Langmuir isotherm model parameter, K_a was found to be slightly different for diverse TiO_2 Degussa P-25 specimens, namely $K_a = 0.111$ mg L^{-1} for bare TiO_2 Degussa P-25 and $K_a = 0.210$ mg L^{-1} for C-doped TiO_2 Degussa P-25 as well as $K_a = 0.146$ mg L^{-1} for N-doped TiO_2 Degussa P-25 in terms of DOC. Comparison of C-doping and N-doping with bare TiO_2 Degussa P-25 could be regarded as non-discriminating between the effects of dopants.

4.6.1.4. Adsorption Isotherm Modeling of 0.45 μm Filtered Fraction of Humic Acid onto S-doped TiO_2 Degussa P-25 Specimen. UV-vis spectroscopic parameters ($Color_{436}$, UV_{365}, UV_{280}, and UV_{254}) and DOC were fitted to Freundlich (2.7) and Langmuir (2.6) adsorption isotherm models.

Freundlich adsorption model. Freundlich adsorption isotherms were presented in Figure 4.102 for $Color_{436}$, UV_{254} and DOC parameters. Freundlich isotherms for UV_{365} and UV_{280} were presented in Appendix A.

C_e values altered between 2.05 – 5.39 m^{-1} for $Color_{436}$ according to the loading of S-doped TiO_2 Degussa P-25 in the solution. The values of q_A were found in the range of 262 - 1288 $m^{-1} g^{-1}$ for the corresponding to the C_e values. ΔC_e and Δq_A values for 0.45 μm filtration fraction of humic acid were found as 3.34 m^{-1} and 1026 $m^{-1} g^{-1}$ for $Color_{436}$. C_e values altered between 12.62 – 31.37 m^{-1} for UV_{254}. The values of q_A were calculated as between 1431 - 6808 $m^{-1} g^{-1}$ for the corresponding to the C_e values. ΔC_e and Δq_A values for UV_{254} were calculated as 18.75 m^{-1} and 5377 $m^{-1} g^{-1}$, respectively (Figure 4.102).

Adsorption isotherms relatively exhibited similar trend for both of the UV-vis parameters as expressed by $Color_{436}$ and UV_{254} parameters. The trends exhibited by the respective adsorption isotherms could be considered as S-curve type isotherm.

S-doping of TiO_2 Degussa P-25 affected the adsorption isotherm profiles of UV-vis spectral parameters as well as DOC in comparison to the bare TiO_2 Degussa P-25 (Figure 4.96 and Figure 4.102).

C_e values altered between 2.24 - 4.08 mg L^{-1} for DOC. The values of q_A corresponding to the C_e values were calculated in the range of 148 – 740 mg $L^{-1} g^{-1}$. ΔC_e and Δq_A values for DOC were calculated as 1.84 mg L^{-1} and 592 mg $L^{-1} g^{-1}$; respectively (Figure 4.102).

Freundlich isotherm model coefficients; adsorption capacity, K_f, and adsorption intensity, 1/n, for 0.45 μm filtration fraction of humic acid following adsorption onto S-doped TiO_2 Degussa P-25 were listed in Table 4.9 ($R^2 \geq 0.86$).

Figure 4.102. Freundlich adsorption isotherm of Color$_{436}$, UV$_{254}$ and DOC parameters of 0.45 μm filtration fraction of humic acid following adsorption onto S-doped TiO$_2$ Degussa P-25.

Table 4.9. Freundlich isotherm model parameters for 0.45 μm filtration fraction of humic acid following adsorption onto S-doped TiO_2 Degussa P-25.

Humic acid, 0.45 μm filtration fraction		
UV-vis parameter	K_f	$1/n$
$Color_{436}$	67.64	1.665
UV_{365}	32.46	1.740
UV_{280}	18.10	1.706
UV_{254}	18.93	1.660
Dissolved Organic Carbon	K_f	$1/n$
DOC	45.79	1.781

Comparison of UV-vis parameters indicated that the adsorption capacity constant of $Color_{436}$ was the highest value. Moreover, adsorption capacity constants of UV_{280} and UV_{254} were nearly equal to each other and also they had the lowest values. The order was $Color_{436} > UV_{365} > UV_{254} > UV_{280}$ for adsorption capacity constant. Also, adsorption intensity of UV_{254} was the lowest value. Moreover, adsorption intensity of $Color_{436}$ and UV_{254} were relatively close to each other. The order of adsorption intensity values could be given as $UV_{365} > UV_{280} > Color_{436} > UV_{280}$. Adsorption intensity of DOC was found to be >1 representing strong adsorption bond.

Freundlich isotherm model parameters attained for S-doped of TiO_2 Degussa P-25 could be more resembled to C-doped TiO_2 rather than N-doped TiO_2 Degussa P-25. K_f values could be displayed as following an order of bare TiO_2 > C-doped TiO_2 > S-doped TiO_2 >>> N-doped TiO_2 Degussa P-25. The order of $1/n$ values could be given as N-doped TiO_2 > C-doped TiO_2 > S-doped TiO_2 > bare TiO_2 Degussa P-25.

Langmuir adsorption model. Langmuir adsorption isotherms for 0.45 μm filtration fraction of humic acid following adsorption onto S-doped TiO_2 Degussa P-25 were presented in Figure 4.103 for $Color_{436}$, UV_{254} and DOC parameters. Langmuir isotherms for UV_{365} and UV_{280} were presented in Appendix B. Two parameters of Langmuir equation outlined in section 2.3, q_m and K_a, were listed in Table 4.10 for 0.45 μm filtration fraction of humic acid following adsorption onto S- doped TiO_2 Degussa P-25 ($R^2 \geq 0.89$).
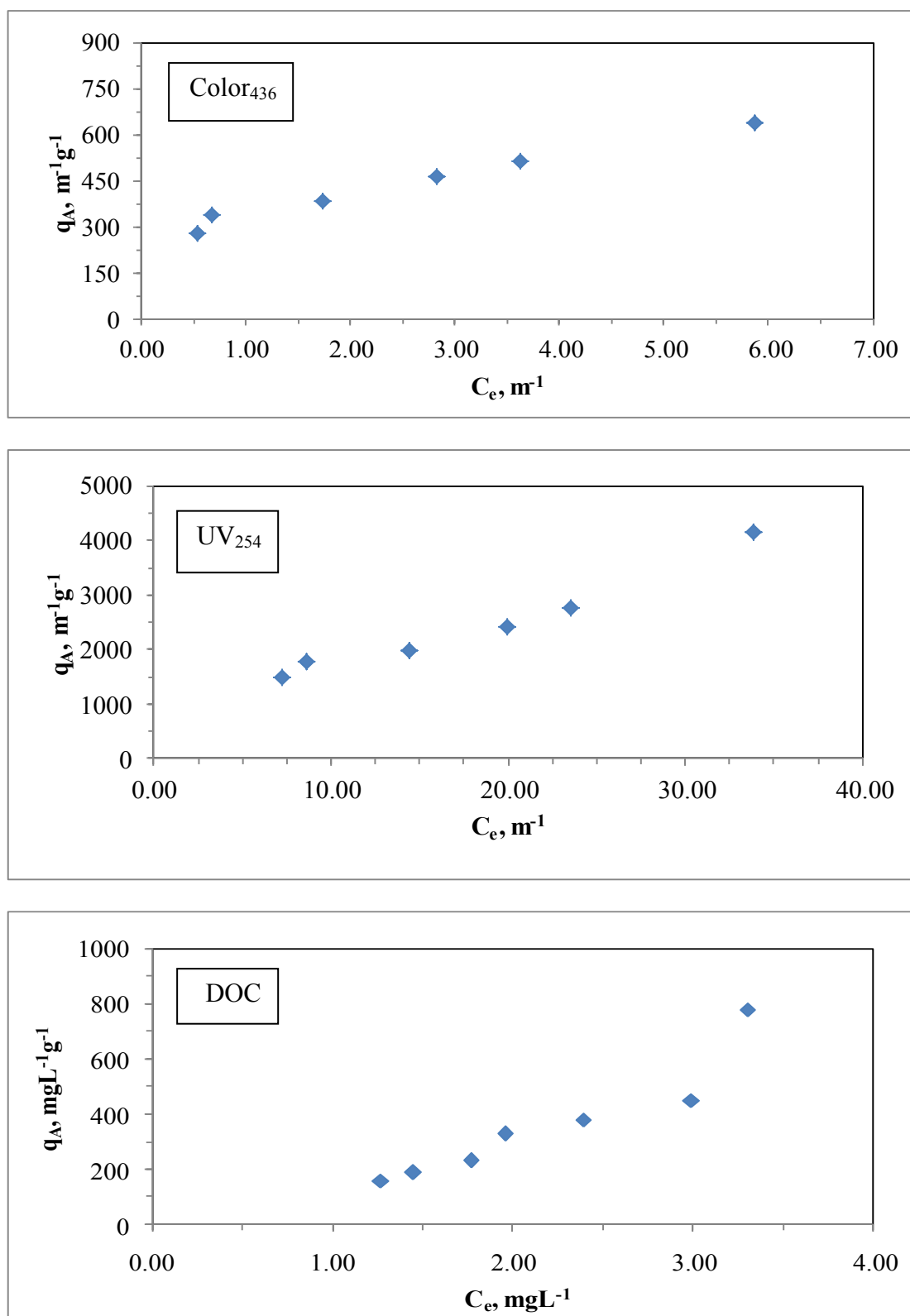
Figure 4.103. Langmuir adsorption isotherm of Color$_{436}$, UV$_{254}$ and DOC parameters of 0.45 μm filtration fraction of humic acid following adsorption onto S-doped TiO$_2$ Degussa P-25.

Table 4.10. Langmuir isotherm model parameters for 0.45 μm filtration fraction of humic acid following adsorption onto S-doped TiO_2 Degussa P-25.

Humic acid, 0.45 μm filtration fraction		
UV-vis parameter	q_m m^{-1}g^{-1}	K_a
Color$_{436}$	1111	0.0890
UV$_{365}$	2000	0.0430
UV$_{280}$	5000	0.0170
UV$_{254}$	5000	0.0180
Dissolved Organic Carbon	q_m mg L^{-1}g^{-1}	K_a mg L^{-1}
DOC	250	0.174

It could be easily seen from Table 4.10 the order of all of the UV-vis spectroscopic parameters in terms of q_m value was UV$_{254}$ = UV$_{280}$ > UV$_{365}$ > Color$_{436}$ and this order was reverse for K_a value, namely, Color$_{436}$ > UV$_{365}$ > UV$_{254}$ > UV$_{280}$. The model parameters as q_m and K_a values for DOC were found to be 250 mg L^{-1}g^{-1} and 0.174 mg L^{-1}, respectively. It should be indicated that adsorption of 0.45 μm filtered fraction of humic acid onto S-doped TiO_2 Degussa P-25 could well be characterized both by Freundlich and Langmuir adsorption isotherm models.

Langmuir isotherm model parameters of 0.45 μm filtration fraction of humic acid recorded following adsorption onto four different TiO_2 specimens were compared (Table 4.4, Table 4.6 and Table 4.8 as well as Table 4.10). An inconsistent trend could be visualized for the UV-vis parameters (Table 4.4, Table 4.6 and Table 4.8 as well as Table 4.10) upon comparison of the Langmuir isotherm model parameters, q_m and K_a. Langmuir isotherm model parameters of DOC could be presented in a decreasing order of; for q_m: bare TiO_2 > C-doped TiO_2 > S-doped TiO_2 > N-doped TiO_2 for K_a: S-doped TiO_2 > C-doped TiO_2 > N-doped TiO_2 > bare TiO_2. K_a was found to be slightly different for diverse TiO_2 Hombikat UV-100 specimens, namely K_a = 0.167 mg L^{-1} for C-doped TiO_2 and K_a = 0.172 mg L^{-1} for N-doped TiO_2 and also K_a = 0.111 mg L^{-1} for S-doped TiO_2 in terms of DOC. Comparison of C-doping and N-doping with S-doping TiO_2 Hombikat UV-100 could be regarded as non-discriminating between the effects of dopants.

4.6.1.5. Adsorption Isotherm Modeling of 0.45 μm Filtered Fraction of Humic Acid onto N-S co-doped TiO_2 Degussa P-25 Specimen. UV-vis spectroscopic parameters ($Color_{436}$, UV_{365}, UV_{280}, and UV_{254}) and DOC were fitted to Freundlich (2.7) and Langmuir (2.6) adsorption isotherm models.

Freundlich adsorption model. Freundlich adsorption isotherms were presented in Figure 4.104 for $Color_{436}$, UV_{254} and DOC parameters. Freundlich isotherms for UV_{365} and UV_{280} were presented in Appendix A.

C_e values altered between 2.38 – 5.51 m^{-1} for $Color_{436}$ according to the loading of N-S co – doped TiO_2 Degussa P-25 in the solution. The values of q_A were found in the range of 234 - 1092 $m^{-1} g^{-1}$ for the corresponding to the C_e values. ΔC_e and Δq_A values for 0.45 μm filtration fraction of humic acid were found as 3.13 m^{-1} and 858 $m^{-1} g^{-1}$ for $Color_{436}$. C_e values altered between 10.88 – 31.06 m^{-1} for UV_{254}. The calculated values of q_A were in the range of 1427 - 6196 $m^{-1} g^{-1}$ for the corresponding to the C_e values. ΔC_e and Δq_A values for UV_{254} were calculated as 20.18 m^{-1} and 4769 $m^{-1} g^{-1}$, respectively (Figure 4.104).

Adsorption isotherms relatively exhibited similar trend for both of the UV-vis parameters as expressed by $Color_{436}$ and UV_{254} parameters. The trends exhibited by the respective adsorption isotherms could be considered as S-curve type isotherm. N-S co-doping of TiO_2 Degussa P-25 did not significantly alter the adsorption profiles of UV-vis spectral parameters in comparison to S-doping and N-doping of TiO_2 Degussa P-25.

C_e values altered between 1.94 – 3.55 $mg L^{-1}$ for DOC. The values of q_A corresponding to the C_e values were calculated as between 274 – 2092 $mg L^{-1} g^{-1}$. ΔC_e and Δq_A values for DOC were calculated as 1.61 $mg L^{-1}$ and 1818 $mg L^{-1} g^{-1}$, respectively (Figure 4.104). Freundlich isotherm model coefficients; adsorption capacity, K_f, and adsorption intensity, $1/n$, for 0.45 μm filtration fraction of humic acid following adsorption onto N-S co-doped TiO_2 Degussa P-25 were listed in Table 4.11. ($R^2 \geq 0.73$). DOC adsorption isotherm profile could be visualized as composed of two regions displaying a rather smooth linear profile followed by a steep increase.
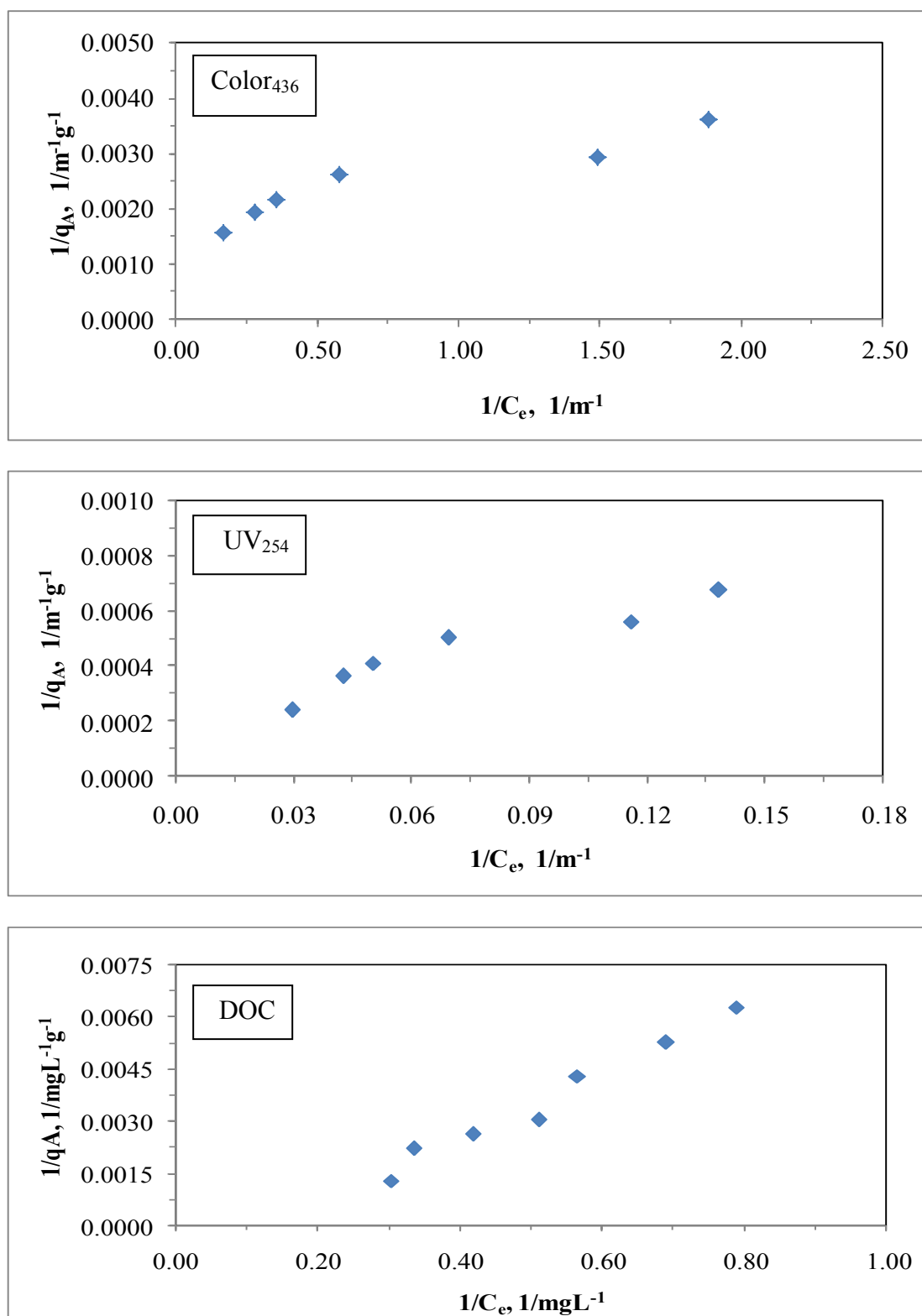
Figure 4.104. Freundlich adsorption isotherm of Color$_{436}$, UV$_{254}$ and DOC parameters of 0.45 μm filtration fraction of humic acid following adsorption onto N-S co-doped TiO$_2$ Degussa P-25.

Table 4.11. Freundlich isotherm model parameters for 0.45 μm filtration fraction of humic acid following adsorption onto N-S co-doped TiO_2 Degussa P-25.

Humic acid, 0.45 μm filtration fraction		
UV-vis parameter	K_f	$1/n$
$Color_{436}$	75.22	1.34
UV_{365}	114.2	1.04
UV_{280}	144.5	0.945
UV_{254}	150.0	0.945
Dissolved Organic Carbon	K_f	$1/n$
DOC	60.16	2.31

Comparison of UV-vis parameters point out that the adsorption capacity constant of $Color_{436}$ was the lowest value. Moreover, adsorption capacity constants of UV_{280} and UV_{254} were almost equal to each other and also they had the highest values. The order of adsorption capacity constant could be given as $Color_{436} < UV_{365} < UV_{280} < UV_{254}$. Also, adsorption intensity values of UV_{254} and UV_{280} were equal to each other and they had the lowest values. The order of adsorption intensity could be given as $Color_{436} > UV_{365} > UV_{280} = UV_{254}$. Adsorption intensity of DOC was found to be >1 representing strong adsorption bond.

Freundlich isotherm model parameters of DOC for 0.45 μm filtration fraction of humic acid could be expressed by a decreasing order for K_f: bare TiO_2 > N-S co-doped TiO_2 > C-doped TiO_2 > S-doped TiO_2 > N-doped TiO_2 for $1/n$: N-doped TiO_2 > C-doped TiO_2 > N-S co-doped TiO_2 > S-doped TiO_2 > bare TiO_2 Degussa P-25.

Langmuir adsorption model. Langmuir adsorption isotherms for 0.45 μm filtration fraction of humic acid following adsorption onto N-S co-doped TiO_2 Degussa P-25 were presented in Figure 4.105 for $Color_{436}$, UV_{254} and DOC parameters. Langmuir isotherms for UV_{365} and UV_{280} were presented in Appendix B. Two parameters of Langmuir equation outlined in section 2.3, q_m and K_a, were listed in Table 4.12 for 0.45 μm filtration fraction of humic acid following adsorption onto N-S co-doped TiO_2 Degussa P-25 ($R^2 \geq 0.81$).
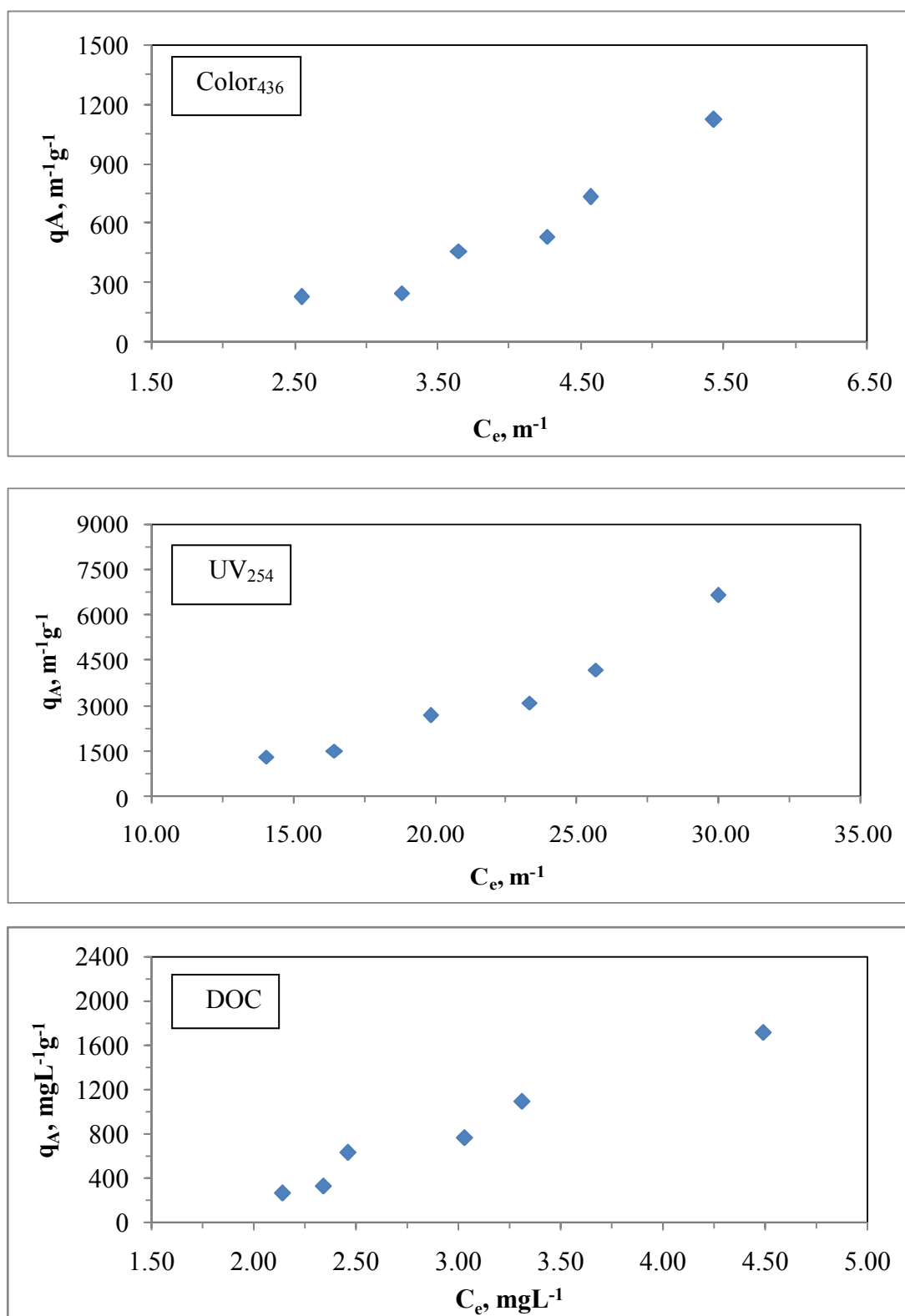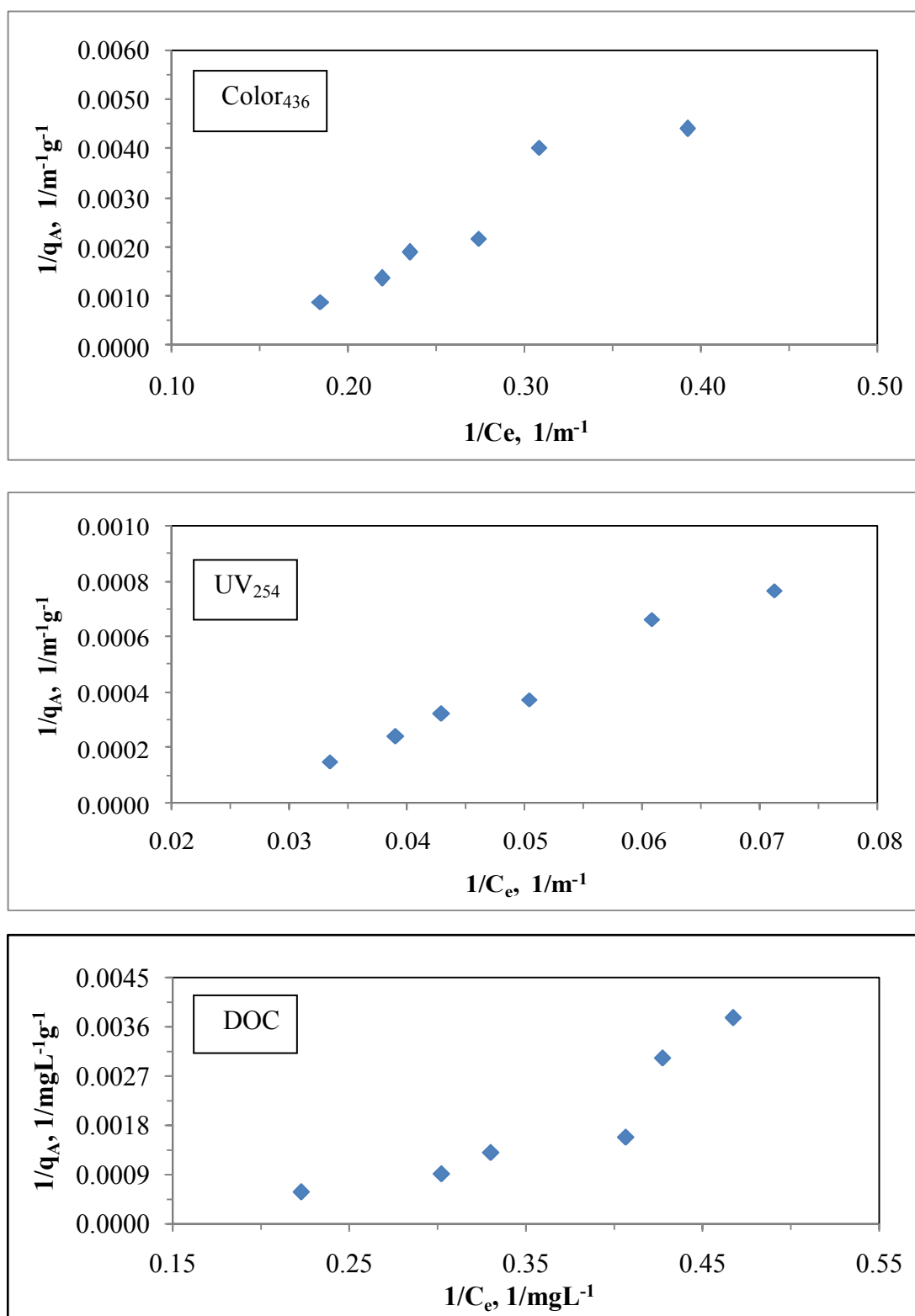
Figure 4.105. Langmuir adsorption isotherm of Color$_{436}$, UV$_{254}$ and DOC parameters of 0.45 μm filtration fraction of humic acid following adsorption onto N-S co-doped TiO$_2$ Degussa P-25.

Table 4.12. Langmuir isotherm model parameters for 0.45 µm filtration fraction of humic acid following adsorption onto N-S co-doped TiO_2 Degussa P-25.

Humic acid, 0.45 µm filtration fraction		
UV-vis parameter	q_m m^{-1}g^{-1}	K_a
Color$_{436}$	33333	0.00400
UV$_{365}$	10000	0.0130
UV$_{280}$	12500	0.0130
UV$_{254}$	14286	0.0120
Dissolved Organic Carbon	q_m mg L^{-1}g^{-1}	K_a mg L^{-1}
DOC	500	0.200

It could be easily seen from Table 4.12 the order of all of UV-vis spectroscopic parameters in terms of q_m value was Color$_{436}$ > UV$_{254}$ > UV$_{280}$ > UV$_{365}$ and also this order was Color$_{436}$ < UV$_{254}$ ≤ UV$_{365}$ = UV$_{280}$ for K_a value. The model parameters as q_m and K_a values for DOC were found to be 500 mg L^{-1}g^{-1} and 0.200 mg L^{-1}, respectively.

It should be indicated that adsorption of 0.45 µm filtered fraction of humic acid onto N-S co-doped TiO_2 Degussa P-25 could well be characterized both by Freundlich and Langmuir adsorption isotherm models.

Langmuir isotherm model parameters calculated for UV-vis parameters displayed a different trend with respect to the both N-doped TiO_2 and S-doped TiO_2. This difference was more significant in terms of K_a with respect to q_m (Table 4.8, Table 4.10 and Table 4.12). K_a was found to be slightly different for diverse TiO_2 Degussa P-25 specimens, namely K_a = 0.167 mg L^{-1} for C-doped TiO_2 and K_a = 0.172 mg L^{-1} for N-doped TiO_2 and also K_a = 0.111 mg L^{-1} for S-doped TiO_2 as well as K_a = 0.0330 mg L^{-1} for N-S co-doped TiO_2 in terms of DOC. Comparison of C-doping and N-doping with N-S co-doping TiO_2 Degussa P-25 could be regarded as discriminating between the effects of dopants. Langmuir isotherm model parameters of DOC could be expressed in a decreasing order of; q_m: bare TiO_2 > N-S co-doped TiO_2 > C-doped TiO_2 > S-doped TiO_2 > N-doped TiO_2, K_a: C-doped TiO_2 > N-S co-doped TiO_2 > S-doped TiO_2 > N-doped TiO_2 > bare TiO_2.

4.6.2. Adsorption Isotherm Modeling of 0.45 μm Filtered Fraction of Humic Acid ontoTiO$_2$ Hombikat UV-100 Specimens

The experimental data related to 0.45 μm filtered fraction of humic acid following adsorption onto TiO$_2$ Hombikat UV-100 specimens were fitted to both Freundlich and Langmuir isotherm models.

4.6.2.1. Adsorption Isotherm Modeling of 0.45 μm Filtered Fraction of Humic Acid onto Bare TiO$_2$ Hombikat UV-100 Specimen. UV-vis spectroscopic parameters (Color$_{436}$, UV$_{365}$, UV$_{280}$, and UV$_{254}$) and DOC were fitted to Freundlich (2.7) and Langmuir (2.6) adsorption isotherm models.

Freundlich adsorption model. Freundlich adsorption isotherms were presented in Figure 4.106 for Color$_{436}$, UV$_{254}$ and DOC parameters. Freundlich isotherms for UV$_{365}$ and UV$_{280}$ were presented in Appendix A. C$_e$ values changed between 0.78 – 5.63 m^{-1} for Color$_{436}$ in concern with the loading of bare TiO$_2$ Hombikat UV-100 in the solution. The values of q$_A$ were found in the range of 321-1268 m^{-1}g^{-1} for the corresponding to the C$_e$ values. ΔC$_e$ and Δq$_A$ values for 0.45 μm filtration fraction of humic acid were found as 4.85 m^{-1} and 947 m^{-1} g^{-1}, for Color$_{436}$. C$_e$ values altered between 6.32 – 30.46 m^{-1} for UV$_{254}$. The values of q$_A$ were calculated as between 1640 - 6744 m^{-1} g^{-1} for the corresponding to the C$_e$ values. ΔC$_e$ and Δq$_A$ values for UV$_{254}$ were calculated as 24.14 m^{-1} and 5104 m^{-1} g^{-1}; respectively. C$_e$ values altered between 1.84 – 4.18 mg L^{-1} for DOC. The values of q$_A$ corresponding to the C$_e$ values were calculated as between 141– 472 mg L^{-1} g^{-1}. ΔC$_e$ and Δq$_A$ values for DOC were calculated as 2.34 mg L^{-1} and 331 mg L^{-1} g^{-1} (Figure 4.106).

Adsorption isotherms relatively exhibited similar trends for both of the UV-vis parameters as expressed by Color$_{436}$ and UV$_{254}$ parameters. These trends exhibited by the respective adsorption isotherms could be considered as S-curve type isotherm. This kind of adsorption isotherm is because of cooperative interactions among the adsorbed molecules (Uyguner and Bekbolet, 2004). Freundlich isotherm model coefficients; adsorption capacity, K$_f$, and adsorption intensity, 1/n, for 0.45 μm filtration fraction of humic acid following adsorption onto bare TiO$_2$ Hombikat UV-100 were listed in Table 4.13. (R^2≥0.88).

Figure 4.106. Freundlich adsorption isotherm of $Color_{436}$, UV_{254} and DOC parameters of 0.45 μm filtered fraction of humic acid following adsorption onto bare TiO_2 Hombikat UV-100.

Table 4.13. Freundlich isotherm model parameters for 0.45 μm filtration fraction of humic acid following adsorption onto bare TiO_2 Hombikat UV-100.

Humic acid, 0.45 μm filtration fraction		
UV-vis parameter	K_f	1/n
$Color_{436}$	343.5	0.573
UV_{365}	459.3	0.580
UV_{280}	416.7	0.731
UV_{254}	419.9	0.744
Dissolved Organic Carbon	K_f	1/n
DOC	65.75	1.31

Comparison of UV-vis parameters that the adsorption capacity constant of $Color_{436}$ was the lowest value. Moreover, adsorption capacity constants of UV_{280} and UV_{254} were nearly equal to each other. The order was $Color_{436} < UV_{280} < UV_{254} < UV_{365}$ for adsorption capacity constant. Also, adsorption intensity of $Color_{436}$ was the lowest value. Furthermore, adsorption intensity of UV_{280} and UV_{254} were relatively closed to each other. An increasing order of adsorption intensity, 1/n could be given as $Color_{436} < UV_{365} < UV_{280} < UV_{254}$. Adsorption intensity of DOC was found to be >1 representing strong adsorption bond.

Freundlich isotherm model parameters of 0.45 μm filtration fraction of humic acid recorded following adsorption onto two different bare TiO_2 specimens were compared (Table 4.3 and Table 4.13). Freundlich isotherm model parameters displayed significantly lower values for bare TiO_2 Hombikat UV-100.

Langmuir adsorption model. Langmuir adsorption isotherms for 0.45 μm filtration fraction of humic acid following adsorption onto bare TiO_2 Hombikat UV-100 were presented in Figure 4.107 for $Color_{436}$, UV_{254} and DOC parameters. Langmuir isotherms for UV_{365} and UV_{280} were presented in Appendix B. Two parameters of Langmuir equation outlined in section 2.3, q_m and K_a, were listed in Table 4.14 for 0.45 μm filtration fraction of humic acid following adsorption onto bare TiO_2 Hombikat UV-100 ($R^2 \geq 0.90$).
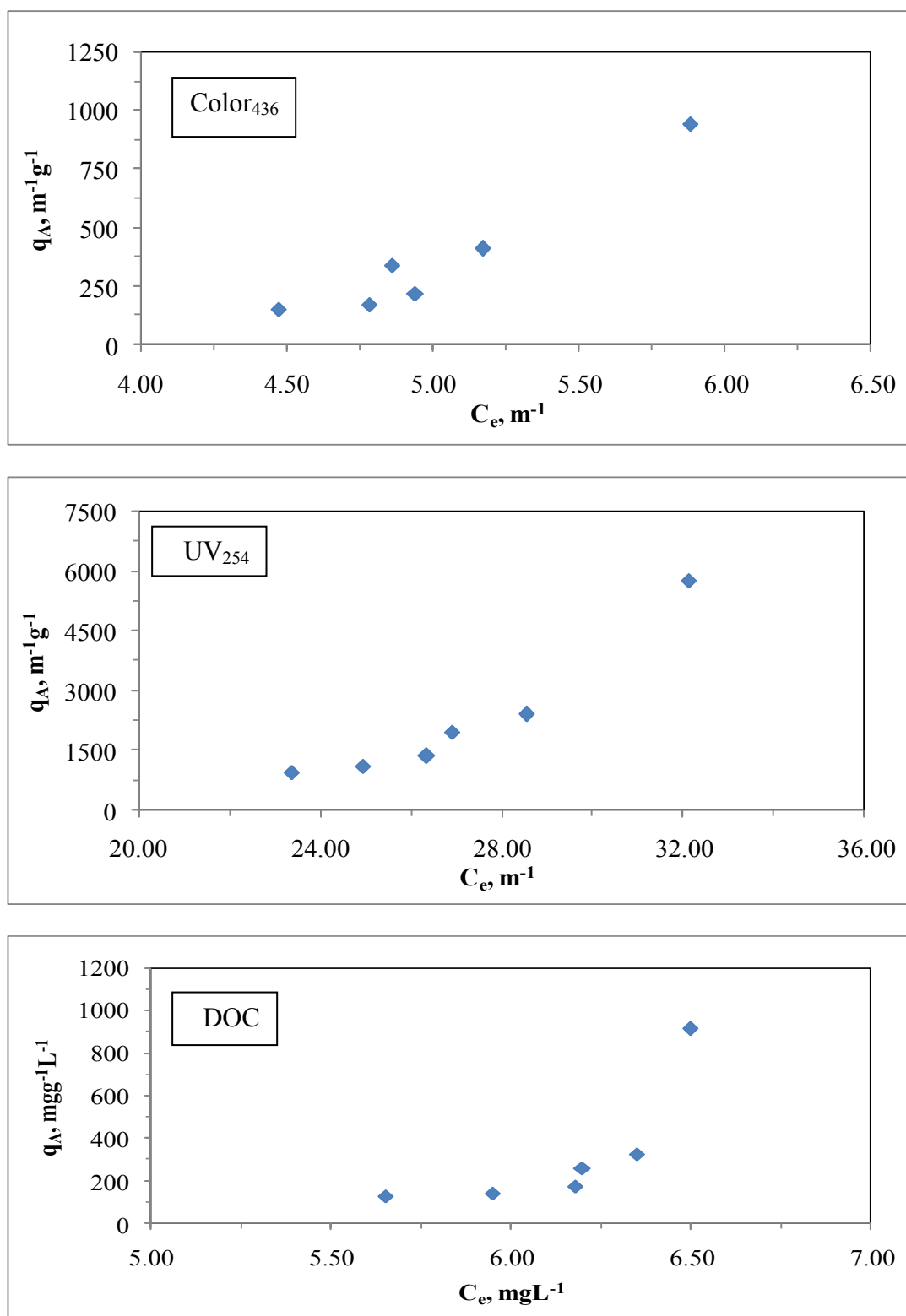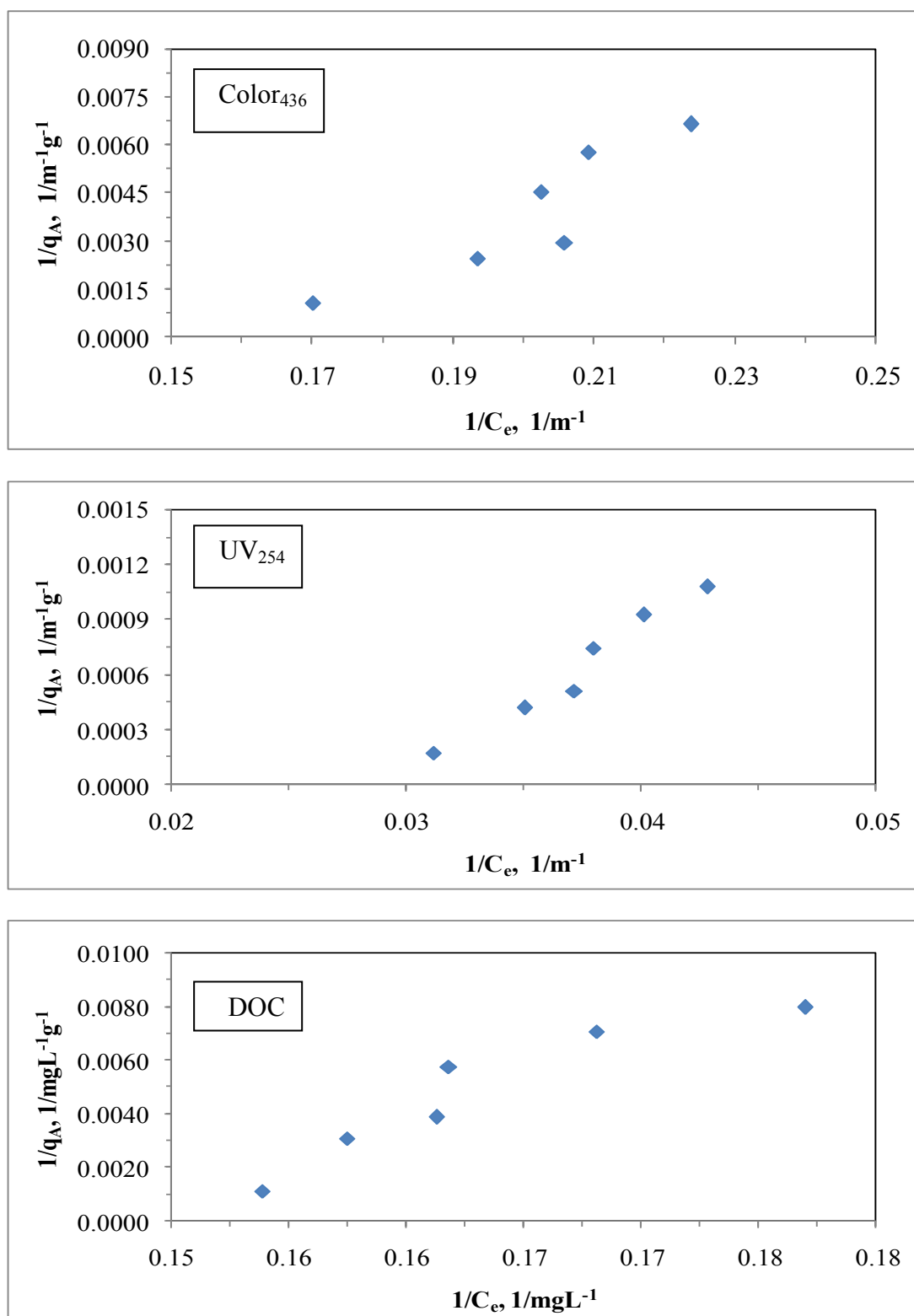
Figure 4.107. Langmuir adsorption isotherm of Color$_{436}$, UV$_{254}$ and DOC parameters of 0.45 μm filtration fraction of humic acid following adsorption onto bare TiO$_2$ Hombikat UV-100.

Table 4.14. Langmuir isotherm model parameters for 0.45 μm filtration fraction of humic acid following adsorption onto bare TiO_2 Hombikat UV-100.

Humic acid, 0.45 μm filtration fraction		
UV-vis parameter	q_m $m^{-1}g^{-1}$	K_a
$Color_{436}$	1000	0.500
UV_{365}	2000	0.250
UV_{280}	7194	0.0480
UV_{254}	8772	0.0380
Dissolved Organic Carbon	q_m mg $L^{-1}g^{-1}$	K_a mg L^{-1}
DOC	926	0.0750

It could be easily seen from Table 4.14 that the order of all of UV-vis spectroscopic parameters in terms of q_m value was $UV_{254} > UV_{280} > UV_{365} > Color_{436}$ and this order was reverse for K_a value, namely $Color_{436} > UV_{365} > UV_{280} > UV_{254}$. The model parameters as q_m and K_a values for DOC were found to be 926 mg $L^{-1}g^{-1}$ and 0.0750 mg L^{-1}, respectively.

It should be indicated that adsorption of 0.45 μm filtered fraction of humic acid onto bare TiO_2 Hombikat UV-100 could well be characterized both by Freundlich and Langmuir adsorption isotherm models.

Langmuir isotherm model parameters of 0.45 μm filtration fraction of humic acid recorded following adsorption onto two different TiO_2 specimens (Degussa P-25 and Hombikat UV-100) were compared (Table 4.4 and Table 4.14). Langmuir isotherm model parameter, q_m was found to be significantly higher than the values calculated from the data attained in case of bare TiO_2 Degussa P-25 (Table 4.4 and Table 4.14) for UV-vis parameters in comparison to DOC. Langmuir isotherm model parameter, K_a was found to be significantly different for two diverse bare TiO_2 specimens, namely $K_a = 0.111$ mg L^{-1} for bare TiO_2 Degussa P-25 and $K_a = 0.0750$ mg L^{-1} for bare TiO_2 Hombikat UV-100 in terms of DOC. Comparison of bare TiO_2 Degussa P-25 and bare TiO_2 Hombikat UV-100 could be regarded as discriminating between the effects of dopants.

4.6.2.2. Adsorption Isotherm Modeling of 0.45 µm Filtered Fraction of Humic Acid onto C-doped TiO_2 Hombikat UV-100 Specimen. UV-vis spectroscopic parameters ($Color_{436}$, UV_{365}, UV_{280}, and UV_{254}) and DOC were fitted to Freundlich (2.7) and Langmuir (2.6) adsorption isotherm models.

Freundlich adsorption model. Freundlich adsorption isotherms were presented in Figure 4.108 for $Color_{436}$, UV_{254} and DOC parameters. Freundlich isotherms for UV_{365} and UV_{280} were presented in Appendix A.

C_e values altered between 1.63 – 5.80 m^{-1} for $Color_{436}$ according to the loading of C-doped TiO_2 Hombikat UV-100 in the solution. The values of q_A were found in the range of 299 - 1324 $m^{-1} g^{-1}$ for the corresponding to the C_e values. ΔC_e and Δq_A values for 0.45 µm filtration fraction of humic acid were found as 4.17 m^{-1} and 1025 $m^{-1} g^{-1}$ for $Color_{436}$. C_e values altered between 7.09 – 31.60 m^{-1} for UV_{254}. The values of q_A were calculated as between 1672 - 6916 $m^{-1} g^{-1}$ for the corresponding to the C_e values. ΔC_e and Δq_A values for UV_{254} were calculated as 24.51 m^{-1} and 5244 $m^{-1}g^{-1}$, respectively (Figure 4.108).

Adsorption isotherms relatively exhibited similar trends for both of the UV-vis parameters as expressed by $Color_{436}$ and UV_{254} parameters. These trends exhibited by the respective adsorption isotherms could be considered as S-curve type isotherm. The effect of C-doping did not significantly alter the DOC adsorption isotherm trend of 0.45 µm filtration fraction of humic acid onto TiO_2 Hombikat UV-100. C-doping of TiO_2 Hombikat UV-100 affected the adsorption isotherm profiles of UV-vis spectral parameters as well as DOC in comparison to the C-doped TiO_2 Degussa P-25 (Figure 4.98 and Figure 4.108).

C_e values altered between 0.93 - 3.34 mg L^{-1} for DOC. The values of q_A corresponding to the C_e values were calculated as between 143 - 464 mg $L^{-1} g^{-1}$. ΔC_e and Δq_A values for DOC were calculated as 2.41 mg L^{-1} and 321 mg $L^{-1} g^{-1}$ (Figure 4.108).

Freundlich isotherm model coefficients; adsorption capacity, K_f, and adsorption intensity, 1/n, for 0.45 µm filtration fraction of humic acid following adsorption onto C-doped TiO_2 Hombikat UV-100 were listed in Table 4.15 ($R^2 \geq 0.86$).
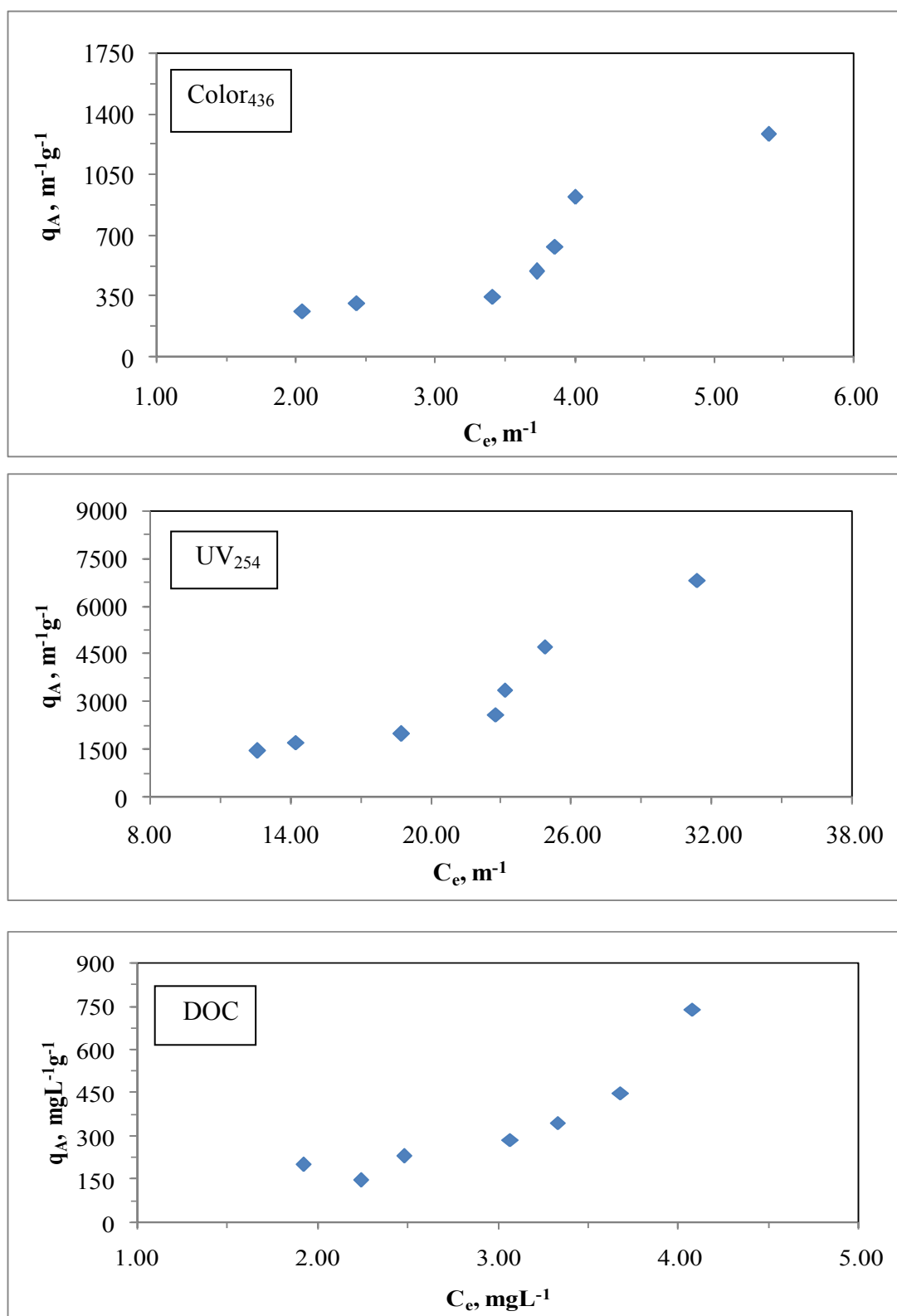
Figure 4.108. Freundlich adsorption isotherm of Color$_{436}$, UV$_{254}$ and DOC parameters of 0.45 μm filtration fraction of humic acid following adsorption onto C-doped TiO$_2$ Hombikat UV-100.

Table 4.15. Freundlich isotherm model parameters for 0.45 µm filtration fraction of humic acid following adsorption onto C-doped TiO_2 Hombikat UV-100.

Humic acid, 0.45 µm filtration fraction		
UV-vis parameter	K_f	$1/n$
Color$_{436}$	228	0.801
UV$_{365}$	317	0.751
UV$_{280}$	379	0.757
UV$_{254}$	376	0.776
Dissolved Organic Carbon	K_f	$1/n$
DOC	163	0.746

Comparison of UV-vis parameters signified that the adsorption capacity constant of Color$_{436}$ was the lowest value. Moreover, adsorption capacity constants of UV$_{280}$ and UV$_{254}$ were nearly equal to each other and also they had the highest values. The order of adsorption capacity constant, K_f could be given as Color$_{436}$ < UV$_{365}$ < UV$_{280}$ ≤ UV$_{254}$. Also, adsorption intensity of UV$_{365}$ was the lowest value. Furthermore, adsorption intensity of UV$_{280}$ and UV$_{365}$ were relatively closed to each other. The order of adsorption intensity, $1/n$ could be given as Color$_{436}$ > UV$_{254}$ > UV$_{280}$ ≥ UV$_{365}$.

Freundlich isotherm model parameter, K_f displayed significantly higher values for C-doping TiO_2 Hombikat UV-100 (Table 4.5 and Table 4.15). Although lower Freundlich K_f values were attained, adsorption intensity values, $1/n > 2$ reflected the effect of surface modification of TiO_2 for C-doped TiO_2 Degussa P-25.

Langmuir adsorption model. Langmuir adsorption isotherms for 0.45 µm filtration fraction of humic acid following adsorption onto C-doped TiO_2 Hombikat UV-100 were presented in Figure 4.109 for Color$_{436}$, UV$_{254}$ and DOC parameters. Langmuir isotherms for UV$_{365}$ and UV$_{280}$ were presented in Appendix B.

Two parameters of Langmuir equation outlined in section 2.3, q_m and K_a, were listed in Table 4.16 for 0.45 µm filtration fraction of humic acid following adsorption onto C-doped TiO_2 Hombikat UV-100 ($R^2 \geq 0.93$).
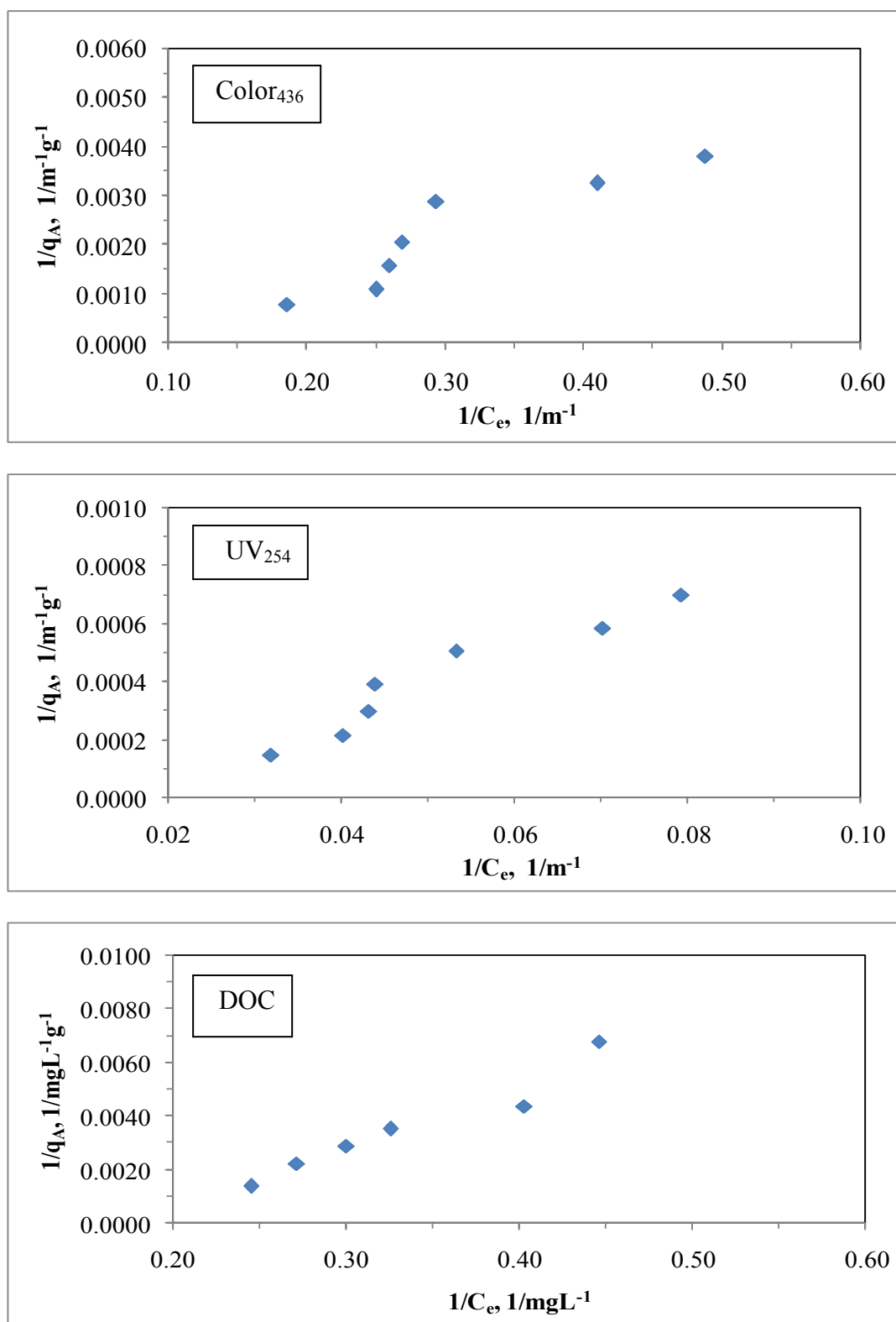

158

Figure 4.109. Langmuir adsorption isotherm of Color₄₃₆, UV₂₅₄ and DOC parameters of 0.45 μm filtration fraction of humic acid following adsorption onto C-doped TiO₂ Hombikat UV-100.

Table 4.16. Langmuir isotherm model parameters for 0.45 μm filtration fraction of humic acid following adsorption onto C-doped TiO$_2$ Hombikat UV-100.

Humic acid, 0.45 μm filtration fraction		
UV-vis parameter	q$_m$ m^{-1}g^{-1}	K$_a$
Color$_{436}$	2500	0.100
UV$_{365}$	4525	0.0630
UV$_{280}$	10526	0.0270
UV$_{254}$	14286	0.0230
Dissolved Organic Carbon	q$_m$ mg L^{-1}g^{-1}	K$_a$ mg L^{-1}
DOC	1111	0.167

The order of all of the UV-vis spectroscopic parameters in terms of q$_m$ value was UV$_{254}$ > UV$_{280}$ > UV$_{365}$ > Color$_{436}$ and this order was reverse for K$_a$ value, namely, Color$_{436}$ > UV$_{365}$ > UV$_{280}$ > UV$_{254}$. It could be easily seen from Table 4.16 that q$_m$ value had the highest value in UV$_{254}$ spectroscopic parameter. The model parameters as q$_m$ and K$_a$ values for DOC were found to be 1111 mg L^{-1}g^{-1} and 0.167 mg L^{-1}, respectively.

It should be indicated that adsorption of 0.45 μm filtered fraction of humic acid onto C-doped TiO$_2$ Hombikat UV-100 could well be characterized both by Freundlich and Langmuir adsorption isotherm models.

Langmuir isotherm model parameters of 0.45 μm filtration fraction of humic acid recorded following adsorption onto two different C-doped TiO$_2$ specimens (Degussa P-25 and Hombikat UV-100) were compared (Table 4.6 and Table 4.16). Langmuir isotherm model parameter, q$_m$ was found to be significantly higher than the values calculated from the data attained in case of C-doped TiO$_2$ Degussa P-25 (Table 4.6 and Table 4.16) for both UV-vis parameters and DOC. Langmuir isotherm model parameter, K$_a$ was found to be slightly different for diverse C-doped TiO$_2$ Degussa P-25 specimens, namely K$_a$ = 0.210 mg L^{-1} for C-doped TiO$_2$ Degussa P-25 and K$_a$ = 0.167 mg L^{-1} for C-doped TiO$_2$Hombikat UV-100 in terms of DOC. Comparison of C-doping TiO$_2$ Degussa P-25 and Hombikat UV-100 could be regarded as non-discriminating between the effects of dopants.

4.6.2.3. Adsorption Isotherm Modeling of 0.45 μm Filtered Fraction of Humic Acid onto N-doped TiO_2 Hombikat UV-100 Specimen. UV-vis spectroscopic parameters ($Color_{436}$, UV_{365}, UV_{280}, and UV_{254}) and DOC were fitted to Freundlich (2.7) and Langmuir (2.6) adsorption isotherm models.

Freundlich adsorption model. Freundlich adsorption isotherms were presented in Figure 4.110 for $Color_{436}$, UV_{254} and DOC parameters. Freundlich isotherms for UV_{365} and UV_{280} were presented in Appendix A.

C_e values altered between 2.87 – 6.87 m^{-1} for $Color_{436}$ according to the loading of N-doped TiO_2 Hombikat UV-100 in the solution. The values of q_A were found in the range of 237 - 772 $m^{-1} g^{-1}$ for the corresponding to the C_e values. ΔC_e and Δq_A values for 0.45 μm filtration fraction of humic acid were found as 4.00 m^{-1} and 535 $m^{-1} g^{-1}$ for $Color_{436}$. C_e values altered between 16.50 – 36.65 m^{-1} for UV_{254}. The values of q_A were calculated as between 1233 - 4268 $m^{-1} g^{-1}$ for the corresponding to the C_e values. ΔC_e and Δq_A values for UV_{254} were calculated as 20.15 m^{-1} and 3035 $m^{-1} g^{-1}$, respectively (Figure 4.110).

Adsorption isotherms relatively exhibited similar trend for both of the UV-vis parameters as expressed by $Color_{436}$ and UV_{254} parameters. The trends exhibited by the respective adsorption isotherms could be considered as C-curve type isotherm.

N-doping of TiO_2 Hombikat UV-100 significantly altered the adsorption isotherm trend of 0.45 μm filtration fraction of humic acid in comparison to both bare and C-doped TiO_2 Hombikat UV-100 (Figure 4.106, Figure 4.108 and Figure 4.110)

C_e values altered between 2.19 – 4.01 mg L^{-1} for DOC. The values of q_A corresponding to the C_e values were in the range of 127- 540 mg $L^{-1} g^{-1}$. ΔC_e and Δq_A values for DOC were calculated as 1.82 mg L^{-1} and 413 mg $L^{-1} g^{-1}$, respectively (Figure 4.110).

Freundlich isotherm model coefficients; adsorption capacity, K_f, and adsorption intensity, 1/n, for 0.45 μm filtration fraction of humic acid following adsorption onto N-doped TiO_2 Hombikat UV-100 were listed in Table 4.17 ($R^2 \geq 0.91$).
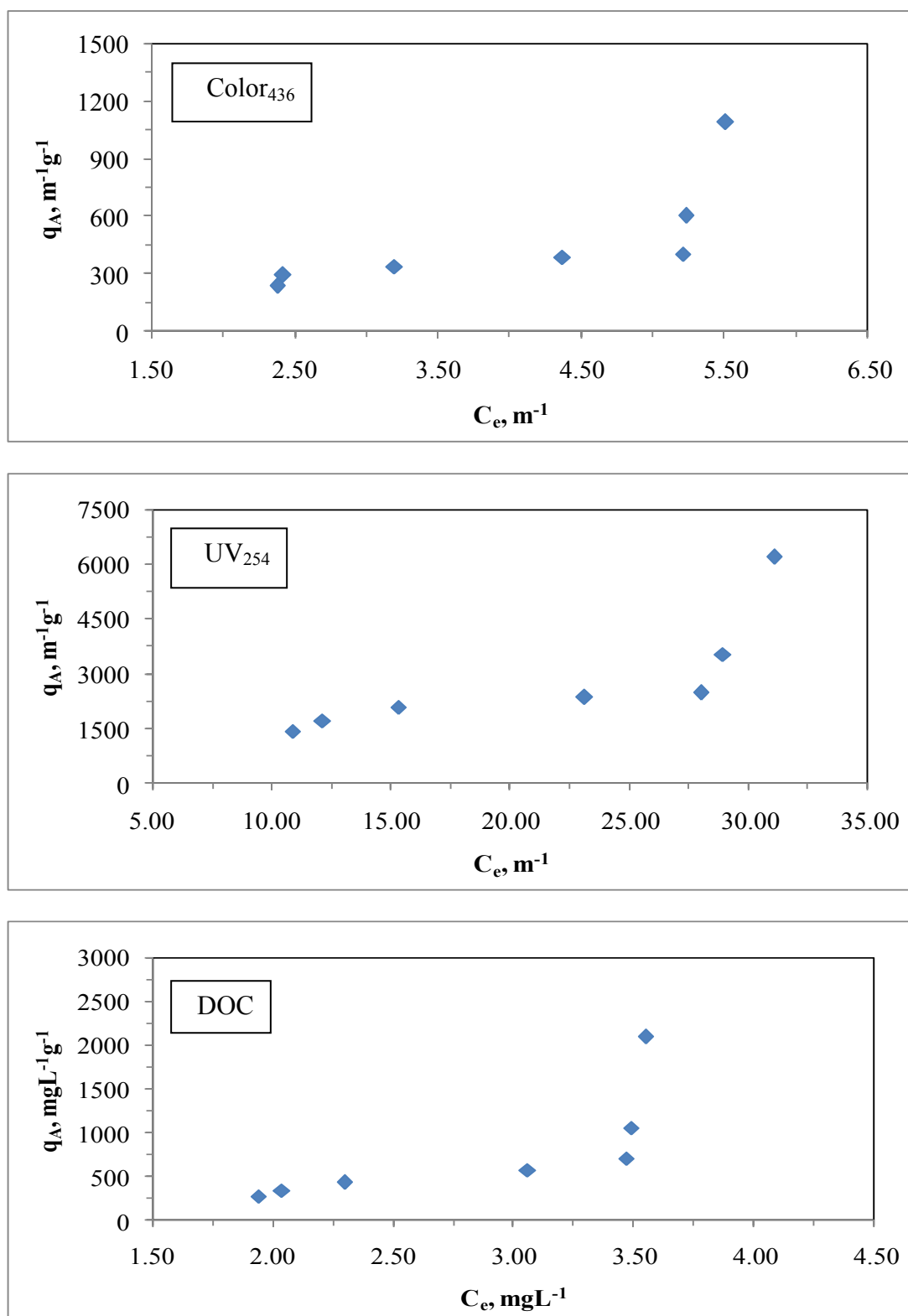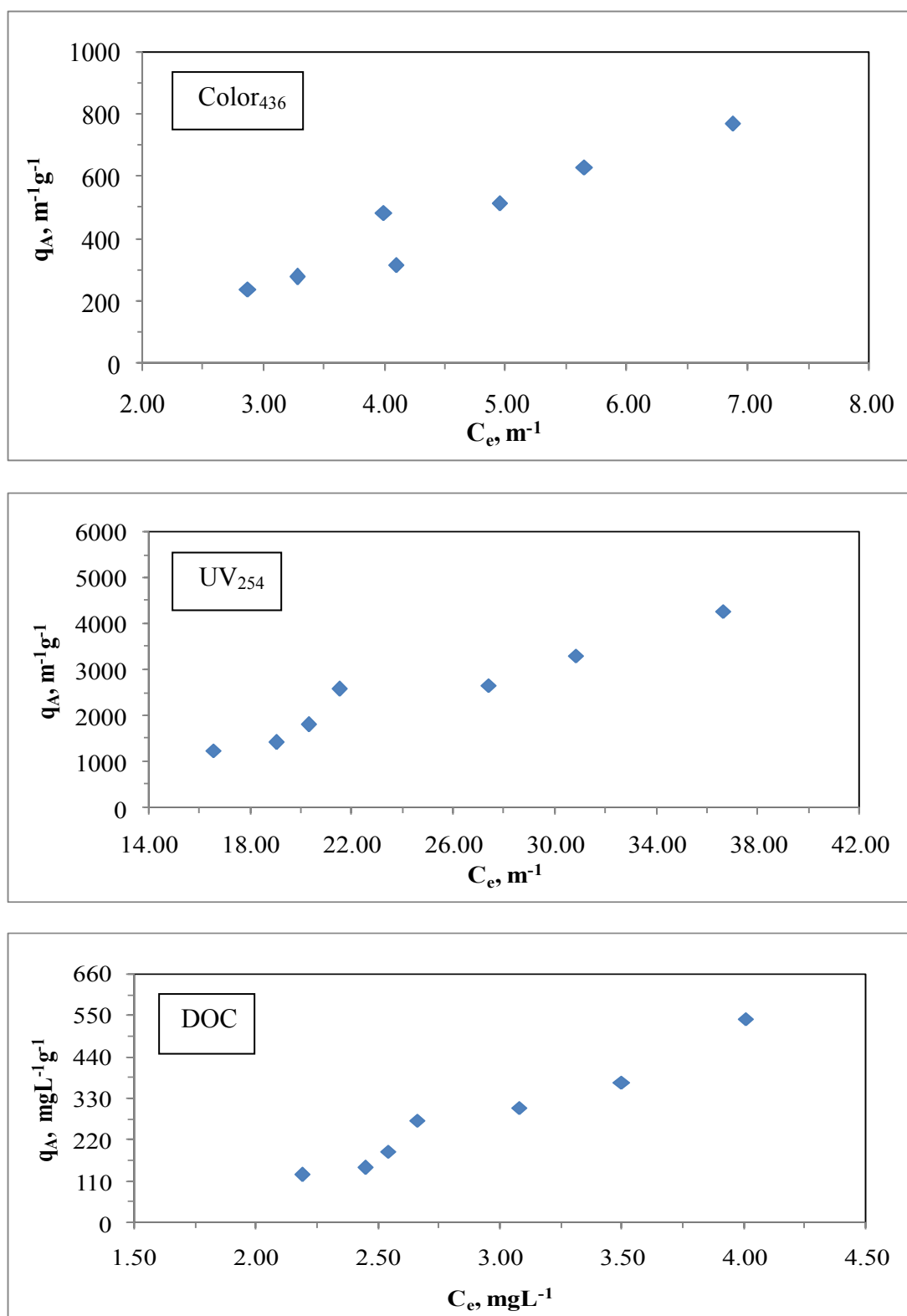
Figure 4.110. Freundlich adsorption isotherm of Color$_{436}$, UV$_{254}$ and DOC parameters of 0.45 μm filtration fraction of humic acid following adsorption onto N-doped TiO$_2$ Hombikat UV-100.

Table 4.17. Freundlich isotherm model parameters for 0.45 μm filtration fraction of humic acid following adsorption onto N-doped TiO_2 Hombikat UV-100.

Humic acid, 0.45 μm filtration fraction		
UV-vis parameter	K_f	$1/n$
$Color_{436}$	55.35	1.38
UV_{365}	42.75	1.38
UV_{280}	19.44	1.52
UV_{254}	18.92	1.51
Dissolved Organic Carbon	K_f	$1/n$
DOC	20.80	2.36

Comparison of UV-vis parameters indicated that the adsorption capacity constant of $Color_{436}$ was the highest value. Moreover, adsorption capacity constants of UV_{280} and UV_{254} were nearly equal to each other and also they had the lowest values. A decreasing order of adsorption capacity constant, K_f could be given as $Color_{436} > UV_{365} > UV_{280} \geq UV_{254}$. Adsorption intensity, $1/n$ values were found to be > 1 representing strong adsorption bond. The binding mechanism of humic acid could be affected by mixed crystalline nature of TiO_2, in such a way that adsorption constants increased as mentioned before. A decreasing order of adsorption intensity values, $1/n$ could be given as $UV_{280} \geq UV_{254} > Color_{436} = UV_{365}$. Freundlich isotherm model parameters of 0.45 μm filtration fraction of humic acid recorded following adsorption onto two different N-doped TiO_2 specimens (Degussa P-25 and Hombikat UV-100) were compared (Table 4.7 and Table 4.17). Freundlich isotherm model parameter, K_f displayed significantly higher values for N-doped TiO_2 Hombikat UV-100.

Langmuir adsorption model. Langmuir adsorption isotherms for 0.45 μm filtration fraction of humic acid following adsorption onto N-doped TiO_2 Hombikat UV-100 were presented in Figure 4.111 for $Color_{436}$, UV_{254} and DOC parameters. Langmuir isotherms for UV_{365} and UV_{280} were presented in Appendix B. Two parameters of Langmuir equation outlined in section 2.3, q_m and K_a, were listed in Table 4.18 for 0.45 μm filtration fraction of humic acid following adsorption onto N- doped TiO_2 Hombikat UV-100 ($R^2 \geq 0.91$).
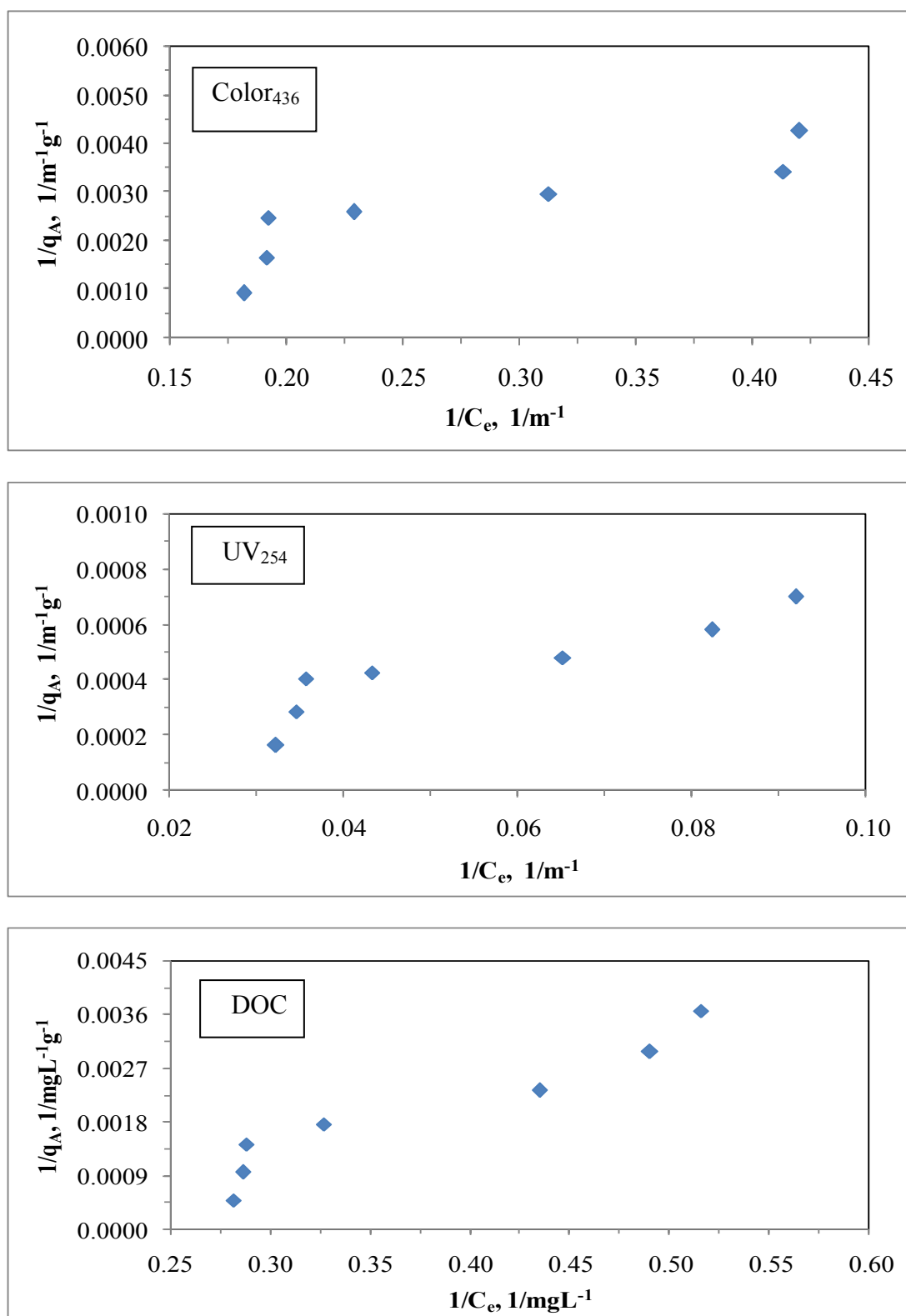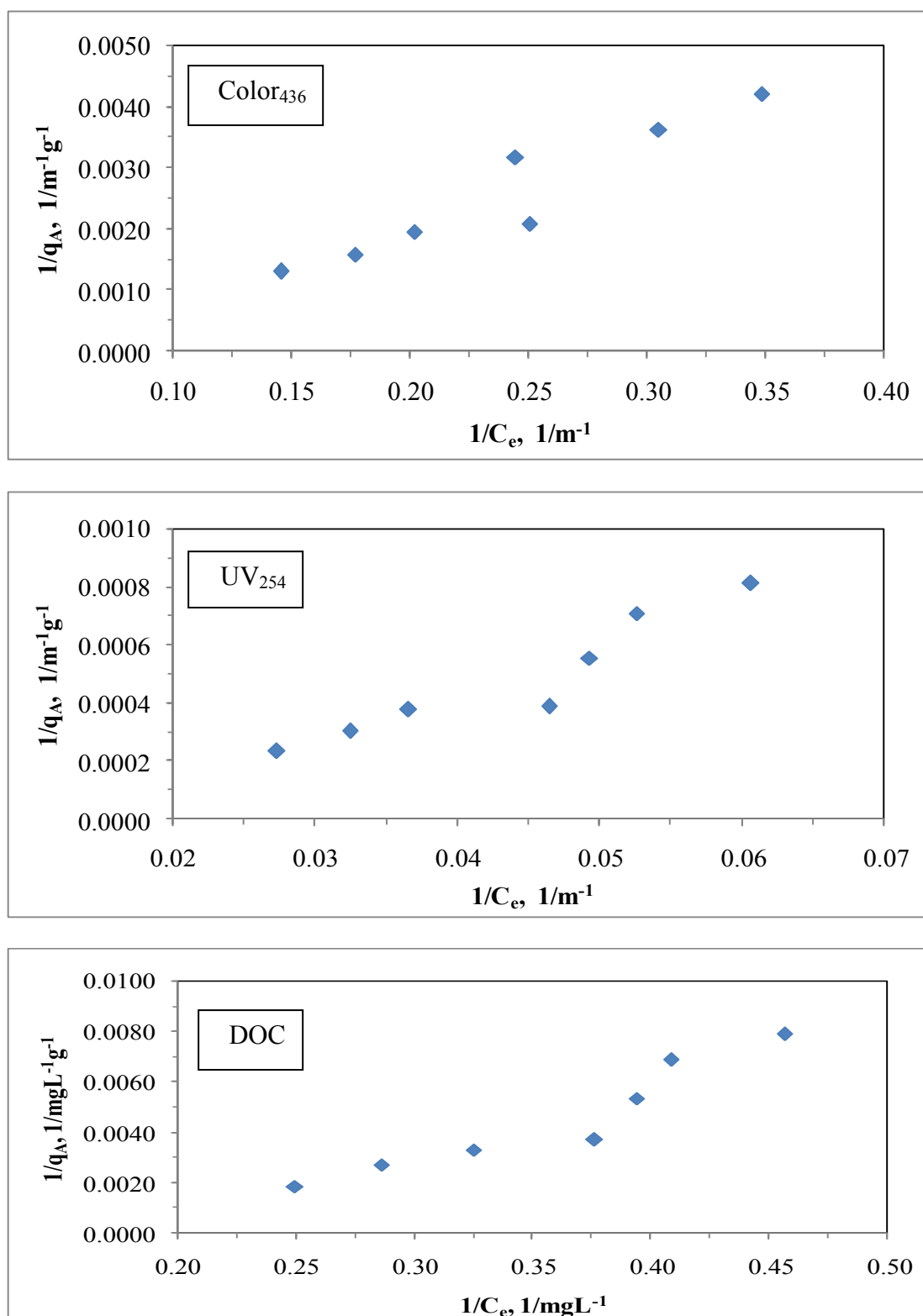
Figure 4.111. Langmuir adsorption isotherm of Color$_{436}$, UV$_{254}$ and DOC parameters of 0.45 μm filtration fraction of humic acid following adsorption onto N-doped TiO$_2$ Hombikat UV-100.

Table 4.18. Langmuir isotherm model parameters for 0.45 μm filtration fraction of humic acid following adsorption onto N-doped TiO_2 Hombikat UV-100.

Humic acid, 0.45 μm filtration fraction		
UV-vis parameter	q_m $m^{-1}g^{-1}$	K_a
$Color_{436}$	3333	0.0180
UV_{365}	3333	0.0170
UV_{280}	2000	0.0340
UV_{254}	1000	0.0710
Dissolved Organic Carbon	q_m mg $L^{-1}g^{-1}$	K_a mg L^{-1}
DOC	200	0.172

It could be easily seen from Table 4.18 that the order of all of the UV-vis spectroscopic parameters in terms of q_m value was $Color_{436} = UV_{365} > UV_{280} > UV_{254}$ and this order was $UV_{254} > UV_{280} > Color_{436} \geq UV_{365}$ for K_a. The model parameters as q_m and K_a values for DOC were found to be 200 mg $L^{-1}g^{-1}$ and 0.172 mg L^{-1}, respectively.

It should be indicated that adsorption of 0.45 μm filtered fraction of humic acid onto N-doped TiO_2 Hombikat UV-100 could well be characterized both by Freundlich and Langmuir adsorption isotherm models.

Langmuir isotherm model parameters of 0.45 μm filtration fraction of humic acid recorded following adsorption onto three different TiO_2 specimens were compared (Table 4.14, Table 4.16 and Table 4.18). Langmuir isotherm model parameter, q_m was found to be significantly lower than the values calculated from the data attained in case of bare TiO_2 and C-doped TiO_2 Hombikat UV-100 (Table 4.14, Table 4.16 and Table 4.18) for both UV-vis parameters and DOC. Langmuir isotherm model parameter, K_a was found to be slightly different for diverse TiO_2 Hombikat UV-100 specimens, namely K_a = 0.0750 mg L^{-1} for bare TiO_2 Hombikat UV-100 and K_a = 0.167 mg L^{-1} for C-doped TiO_2 Hombikat UV-100 as well as K_a = 0.172 mg L^{-1} for N-doped TiO_2 Hombikat UV-100 in terms of DOC. Comparison of C-doping and N-doping TiO_2 Hombikat UV-100 could be regarded as non-discriminating between the effects of dopants.

4.6.2.4. Adsorption Isotherm Modeling of 0.45 μm Filtered Fraction of Humic Acid onto S-doped TiO_2 Hombikat UV-100 Specimen. UV-vis spectroscopic parameters ($Color_{436}$, UV_{365}, UV_{280}, and UV_{254}) and DOC were fitted to Freundlich (2.7) and Langmuir (2.6) adsorption isotherm models.

Freundlich adsorption model. Freundlich adsorption isotherms were presented in Figure 4.112 for $Color_{436}$ and UV_{254} parameters. Freundlich isotherms for UV_{365} and UV_{280} were presented in Appendix A.

C_e values altered between 1.48 – 7.13 m^{-1} for $Color_{436}$ according to the loading of S-doped TiO_2 Hombikat UV-100 in the solution. The values of q_A were found in the range of 305 - 792 $m^{-1} g^{-1}$ for the corresponding to the C_e values. ΔC_e and Δq_A values for 0.45 μm filtration fraction of humic acid were found as 5.65 m^{-1} and 487 $m^{-1} g^{-1}$ for $Color_{436}$. C_e values altered between 4.05 – 35.27 m^{-1} for UV_{254}. The calculated values of q_A were in the range of 1794 - 5448 $m^{-1} g^{-1}$ for the corresponding to the C_e values. ΔC_e and Δq_A values for UV_{254} were calculated as 31.22 m^{-1} and 3654 $m^{-1} g^{-1}$, respectively (Figure 4.112).

Adsorption isotherms relatively exhibited similar trend both of the UV-vis parameters as expressed by $Color_{436}$ and UV_{254} parameters. However, Freundlich adsorption isotherms of 0.45 μm filtration fraction of humic acid following adsorption onto 0.8 mg mL^{-1} dose of S-doped TiO_2 Hombikat UV-100 demonstrated a notable difference for both of the UV-vis parameters as expressed by $Color_{436}$ and UV_{254} specific parameters. The trends exhibited by the respective adsorption isotherms could be considered as L-curve type isotherm.

C_e values altered between 1.06 - 3.09 mg L^{-1} for DOC. The values of q_A corresponding to the C_e values were in the range of 138 - 564 mg $L^{-1} g^{-1}$. ΔC_e and Δq_A values for DOC were calculated as 2.03 mg L^{-1} and 426 mg $L^{-1} g^{-1}$, respectively (Figure 4.112).

Freundlich isotherm model coefficients; adsorption capacity, K_f, and adsorption intensity, 1/n, for 0.45 μm filtration fraction of humic acid following adsorption onto S-doped TiO_2 Hombikat UV-100 were listed in Table 4.19 ($R^2 \geq 0.90$).
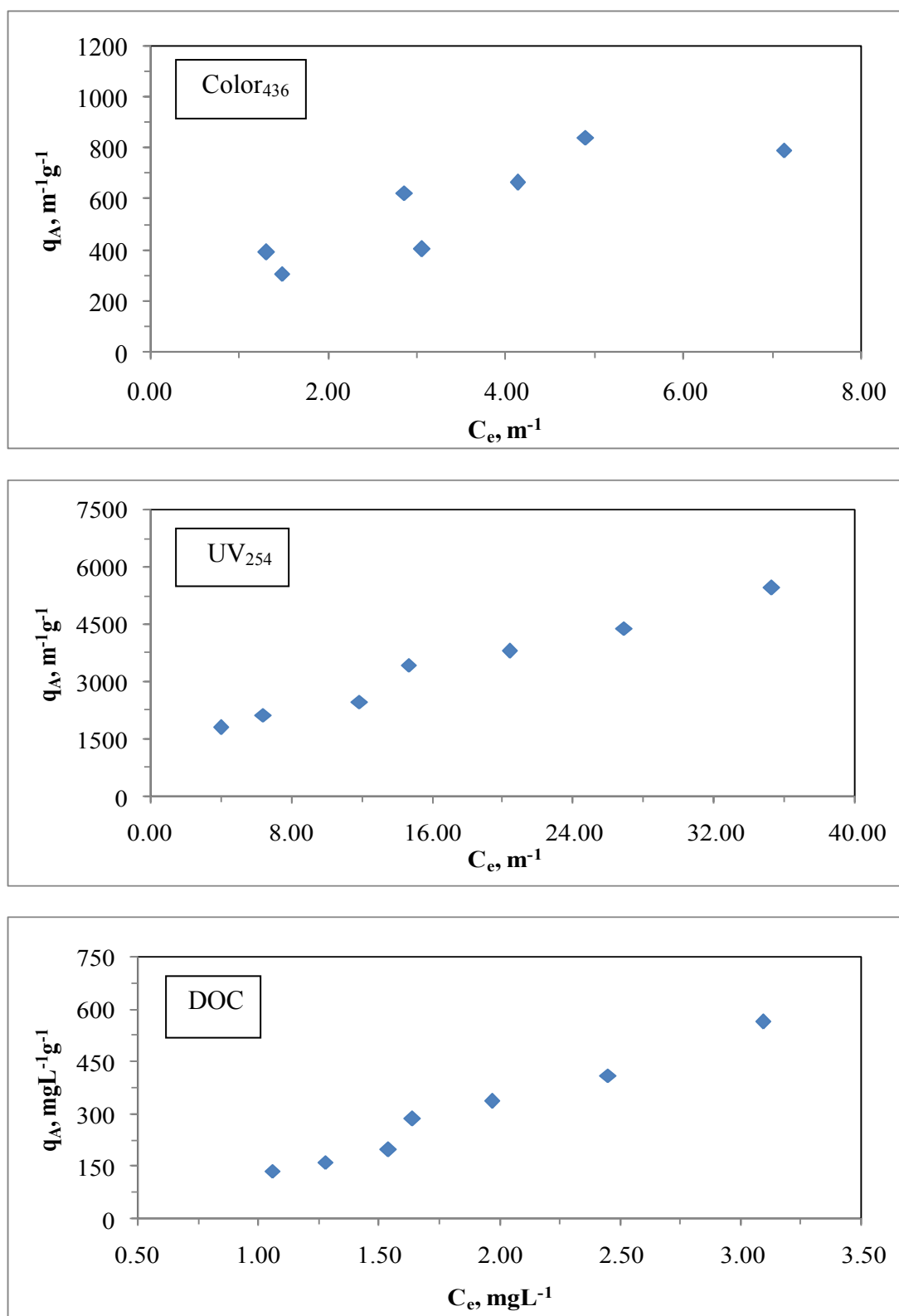
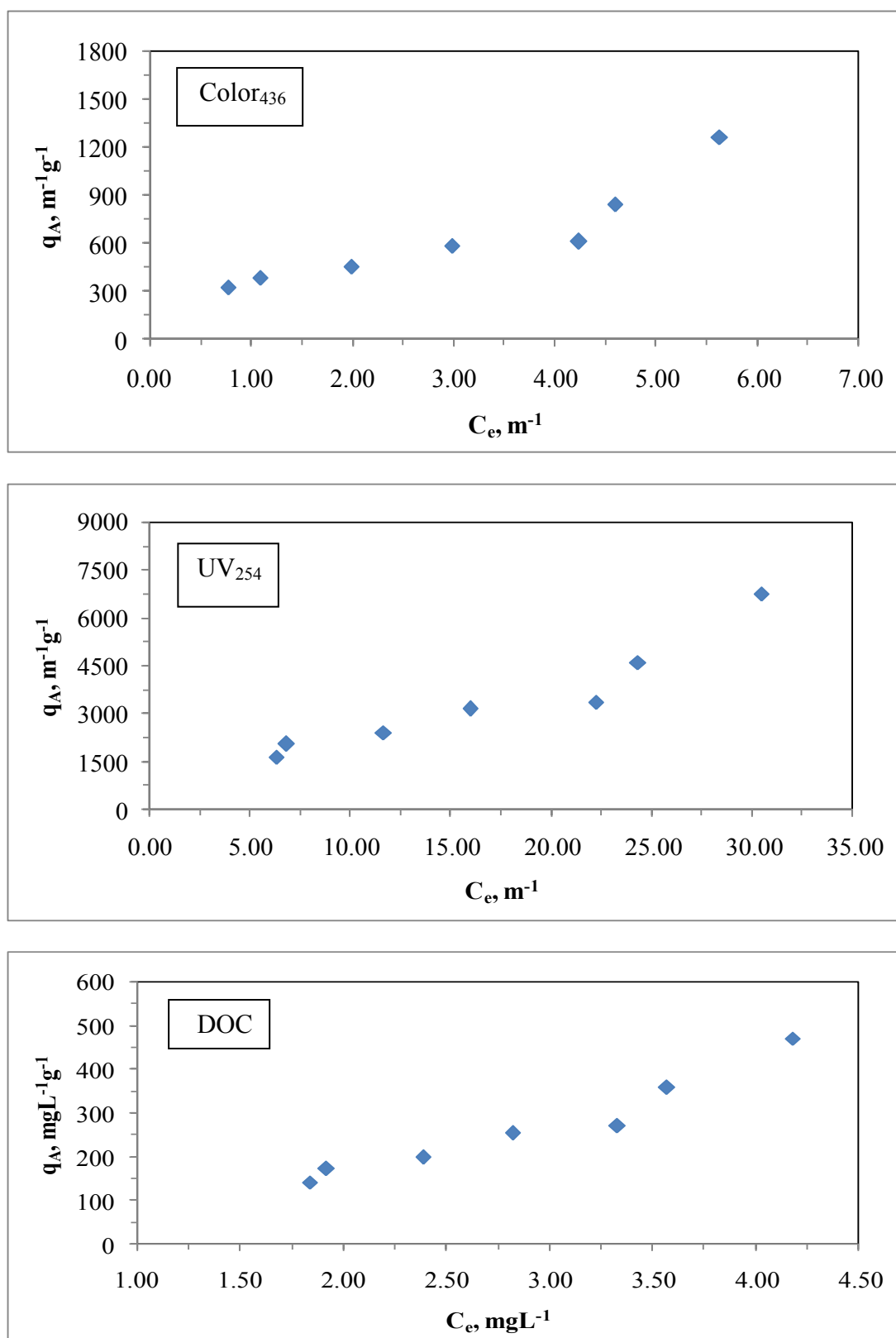Figure 4.112. Freundlich adsorption isotherm of Color$_{436}$, UV$_{254}$ and DOC parameters of 0.45 μm filtration fraction of humic acid following adsorption onto S-doped TiO$_2$ Hombikat UV-100.

Table 4.19. Freundlich isotherm model parameters for 0.45 μm filtration fraction of humic acid following adsorption onto S-doped TiO_2 Hombikat UV-100.

Humic acid, 0.45 μm filtration fraction		
UV-vis parameter	K_f	1/n
$Color_{436}$	289	0.559
UV_{365}	471	0.527
UV_{280}	770	0.504
UV_{254}	818	0.513
Dissolved Organic Carbon	K_f	1/n
DOC	124	1.37

Comparison of UV-vis parameters indicated that adsorption capacity constant of $Color_{436}$ was the lowest value. Moreover, adsorption capacity constant of UV_{254} was the highest value. An increasing order of adsorption capacity constant could be given as $Color_{436} < UV_{365} < UV_{280} < UV_{254}$. According to Table 4.19, adsorption intensity of UV_{280} was the lowest value. Furthermore, adsorption intensity of $Color_{436}$ had the highest value. The order was $Color_{436} > UV_{365} > UV_{254} > UV_{280}$ for adsorption intensity.

Freundlich isotherm model parameters attained for S-doped of TiO_2 Hombikat UV-100 could be more resembled to C-doped TiO_2 rather than N-doped TiO_2 Hombikat UV-100. K_f values in terms of DOC could be displayed as following an order of C-doped TiO_2 > S-doped TiO_2 > bare TiO_2 > N-doped TiO_2 Hombikat UV-100. The order of 1/n values could be given as N-doped TiO_2 > S-doped TiO_2 > bare TiO_2 > C-doped TiO_2 Hombikat UV-100.

Langmuir adsorption model. Langmuir adsorption isotherms for 0.45 μm filtration fraction of humic acid following adsorption onto S-doped TiO_2 Hombikat UV-100 were presented in Figure 4.113 for $Color_{436}$, UV_{254} and DOC parameters. Langmuir isotherms for UV_{365} and UV_{280} were presented in Appendix B. Two parameters of Langmuir equation outlined in section 2.3, q_m and K_a, were listed in Table 4.20 for 0.45 μm filtration fraction of humic acid following adsorption onto S- doped TiO_2 Hombikat UV-100 ($R^2 \geq 0.82$).
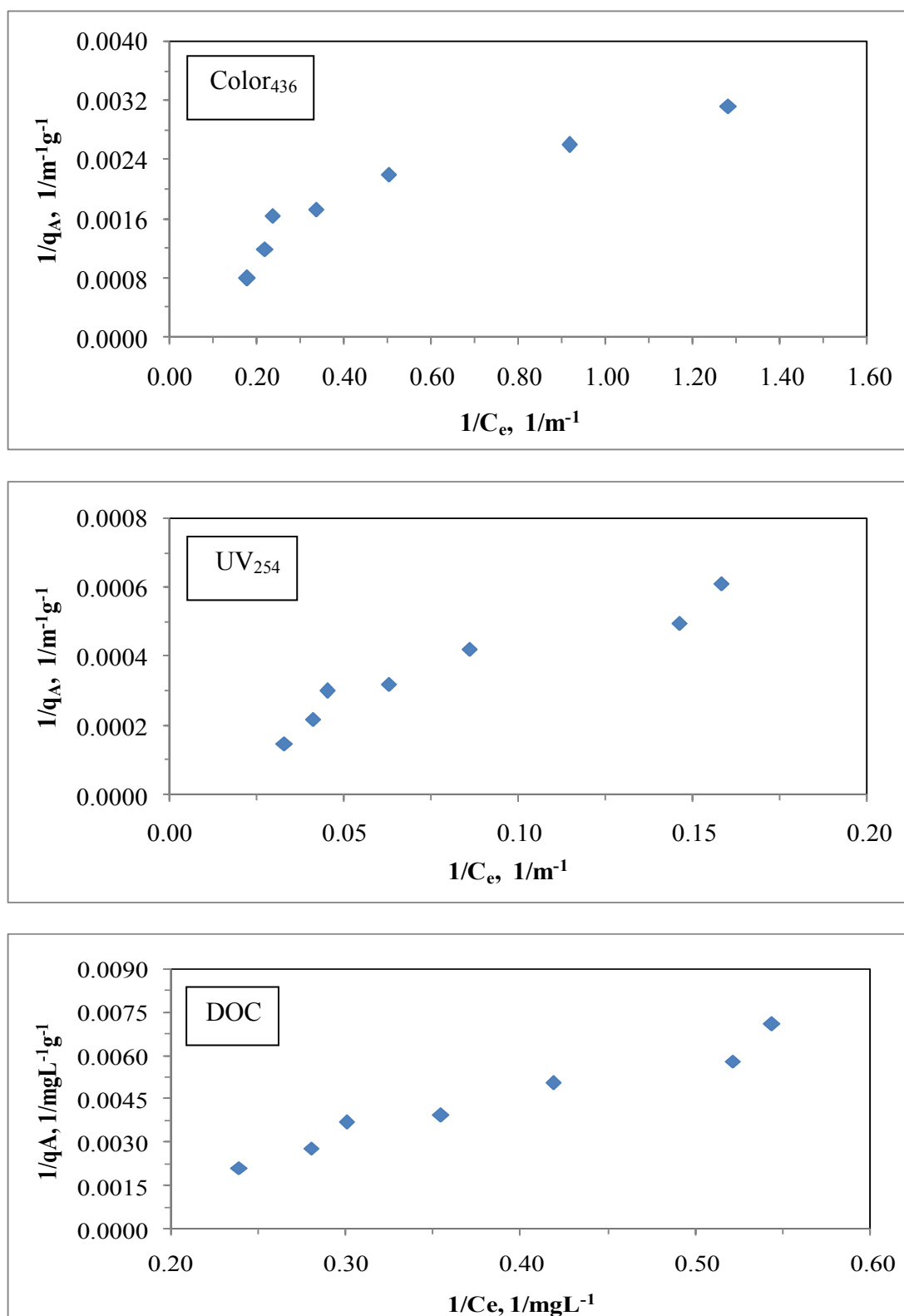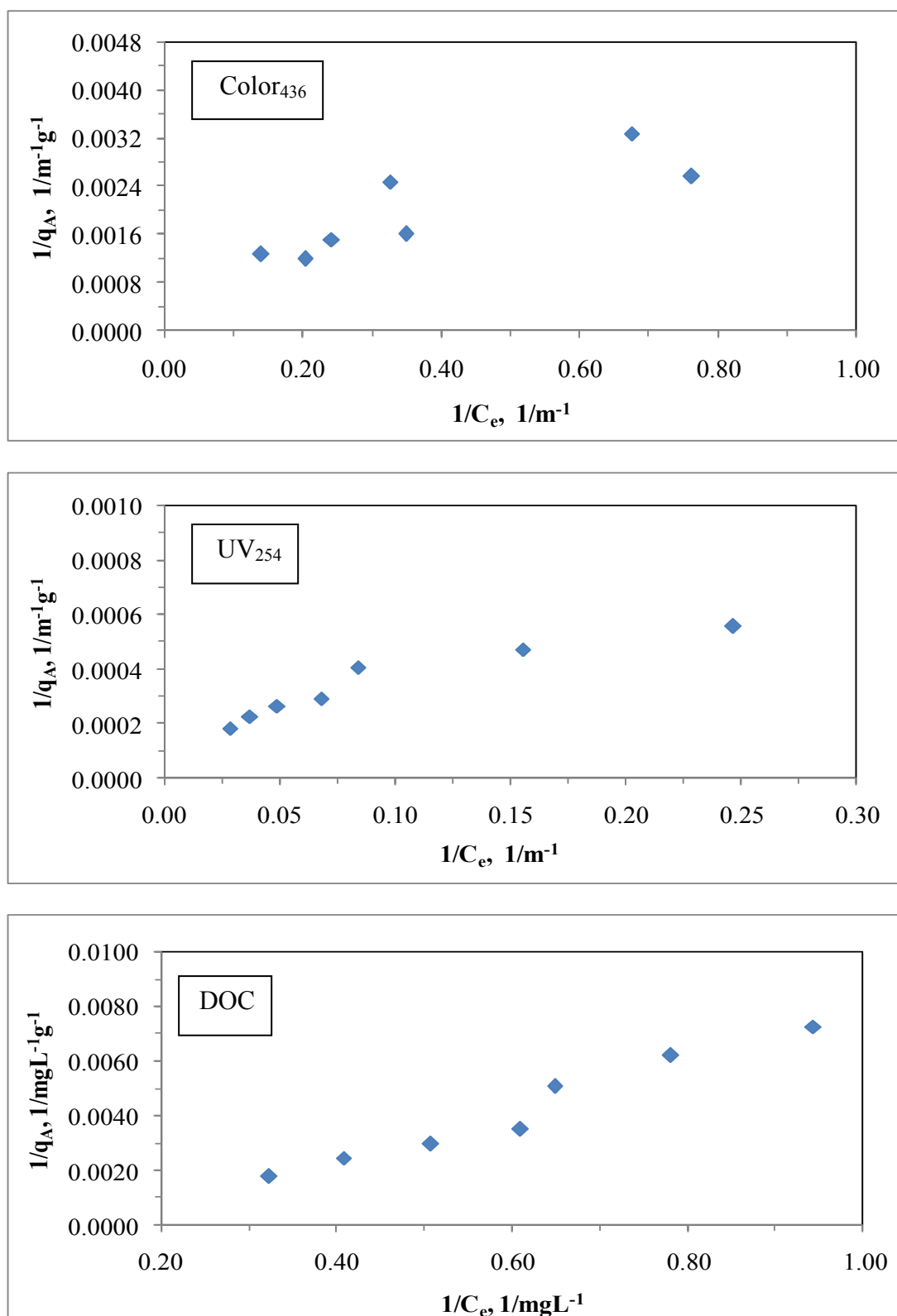
Figure 4.113. Langmuir adsorption isotherm of Color$_{436}$, UV$_{254}$ and DOC parameters of 0.45 μm filtration fraction of humic acid following adsorption onto S co-doped TiO$_2$ Hombikat UV-100.

Table 4.20. Langmuir isotherm model parameters for 0.45 μm filtration fraction of humic acid following adsorption onto S-doped TiO_2 Hombikat UV-100.

Humic acid, 0.45 μm filtration fraction		
UV-vis parameter	q_m m^{-1}g^{-1}	K_a
Color$_{436}$	1111	0.321
UV$_{365}$	2000	0.238
UV$_{280}$	5000	0.118
UV$_{254}$	5000	0.118
Dissolved Organic Carbon	q_m mg L^{-1}g^{-1}	K_a mg L^{-1}
DOC	1000	0.111

It could be easily seen from Table 4.20 that q_m values of UV$_{280}$ and UV$_{254}$ spectroscopic parameters were equal to each other and K_a values of the same UV-vis parameters were equal to each other, too. The order of all of the UV-vis spectroscopic parameters in terms of q_m value was UV$_{254}$ = UV$_{280}$ > UV$_{365}$ > Color$_{436}$ and this order was reverse for K_a value, namely, Color$_{436}$ > UV$_{365}$ > UV$_{280}$ = UV$_{254}$. The model parameters as q_m and K_a values for DOC were found to be 1000 mg L^{-1}g^{-1} and 0.111 mg L^{-1}, respectively.

It should be indicated that adsorption of 0.45 μm filtered fraction of humic acid onto S-doped TiO_2 Hombikat UV-100 could well be characterized both by Freundlich and Langmuir adsorption isotherm models.

Langmuir isotherm model parameters of 0.45 μm filtration fraction of humic acid recorded following adsorption onto four different TiO_2 specimens were compared (Table 4.14, Table 4.16 and Table 4.18 as well as Table 4.20). Langmuir isotherm model parameters calculated for UV-vis parameters displayed a different trend with respect to the both C-doped TiO_2 and S-doped TiO_2 Hombikat UV-100. This difference was more significant in terms of K_a with respect to q_m (Table 4.16and Table 4.20). Langmuir isotherm model parameters of DOC could be expressed in a decreasing order of; q_m: C-doped TiO_2 > S-doped TiO_2 > bare TiO_2 > N-doped TiO_2, K_a: N-doped TiO_2 > C-doped TiO_2 > S-doped TiO_2 > bare TiO_2 Hombikat UV-100.

4.6.2.5. Adsorption Isotherm Modeling of 0.45 μm Filtered Fraction of Humic Acid onto N-S co-doped TiO_2 Hombikat UV-100 Specimen. UV-vis spectroscopic parameters ($Color_{436}$, UV_{365}, UV_{280}, and UV_{254}) and DOC were fitted to Freundlich (2.7) and Langmuir (2.6) adsorption isotherm models.

Freundlich adsorption model. Freundlich adsorption isotherms were presented in Figure 4.114 for $Color_{436}$, UV_{254} and DOC parameters. Freundlich isotherms for UV_{365} and UV_{280} were presented in Appendix A.

C_e values altered between $0.02 - 5.51$ m^{-1} for $Color_{436}$ according to the loading of N-S co-doped TiO_2 Hombikat UV-100 in the solution. The values of q_A were found in the range of $364 - 1440$ $m^{-1}g^{-1}$ for the corresponding to the C_e values. ΔC_e and Δq_A values for 0.45 μm filtration fraction of humic acid were found as 5.49 m^{-1} and 1076 m^{-1} g^{-1} for $Color_{436}$. C_e values altered between $2.09 - 31.45$ m^{-1} for UV_{254}. The values of q_A were in the range of $1872 - 6976$ m^{-1} g^{-1} for the corresponding to the C_e values. ΔC_e and Δq_A values for UV_{254} were calculated as 29.36 m^{-1} and 5104 m^{-1} g^{-1}, respectively (Figure 4.114).

Adsorption isotherms relatively exhibited similar trend for both of the UV-vis parameters as expressed by $Color_{436}$ and UV_{254} parameters. The trends exhibited by the respective adsorption isotherms could be considered as S-curve type isotherm.

N-S co-doping of TiO_2 Hombikat UV-100 did not significantly alter the adsorption profiles of UV-vis spectral parameters in comparison to S-doping and N-doping of TiO_2Hombikat UV-100 (Figure 4.110, Figure 4.112 and Figure 4.114).

C_e values altered between $0.95 - 3.37$ mg L^{-1} for DOC. The values of q_A corresponding to the C_e values were in the range of $142 - 452$ mg L^{-1} g^{-1}. ΔC_e and Δq_A values for DOC were calculated as 2.42 mg L^{-1} and 310 mg L^{-1} g^{-1}, respectively (Figure 4.114).

Freundlich isotherm model coefficients; adsorption capacity, K_f, and adsorption intensity, $1/n$, for 0.45 μm filtration fraction of humic acid following adsorption onto N-S co-doped TiO_2 Hombikat UV-100 were listed in Table 4.21 ($R^2 \geq 0.94$).
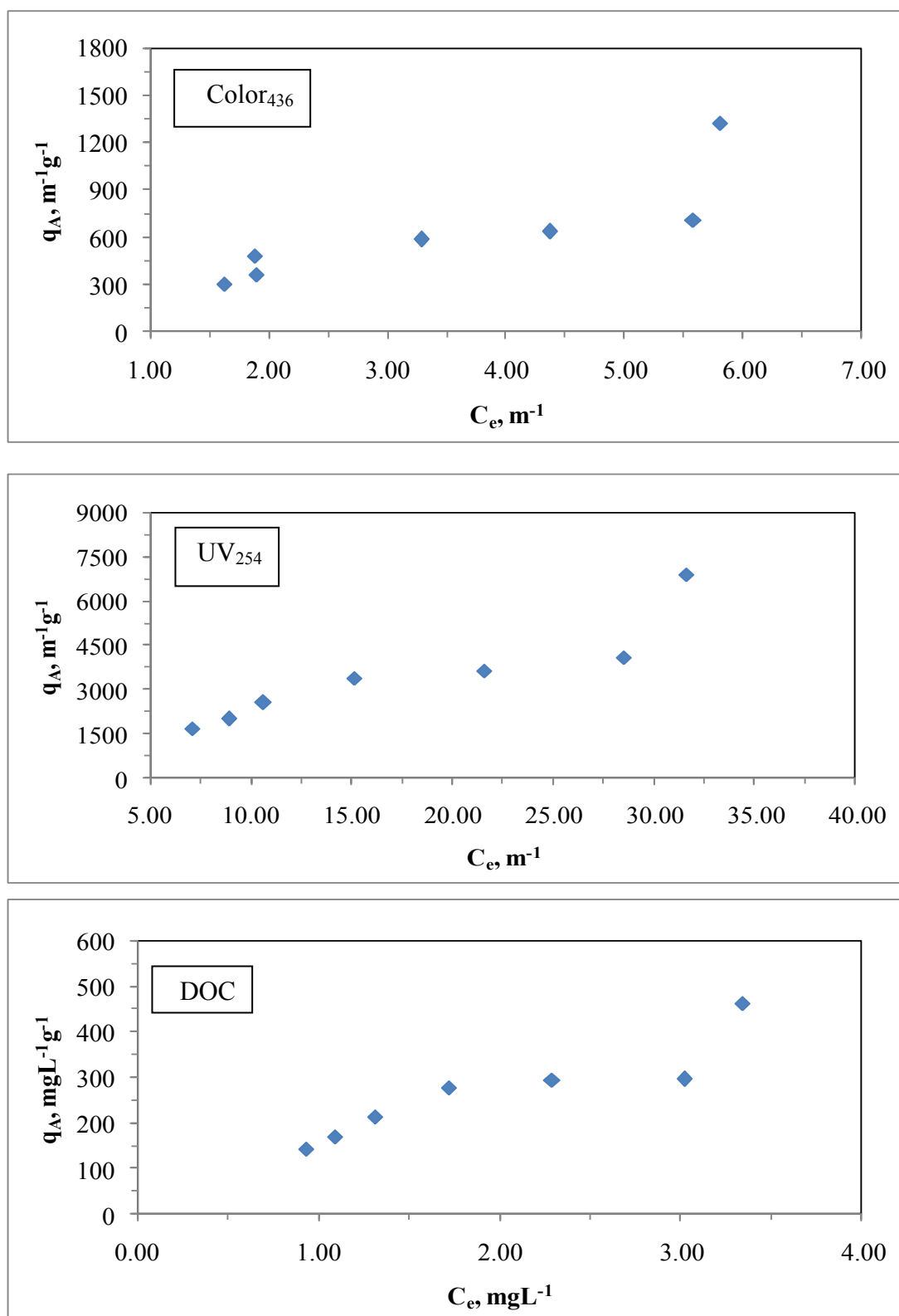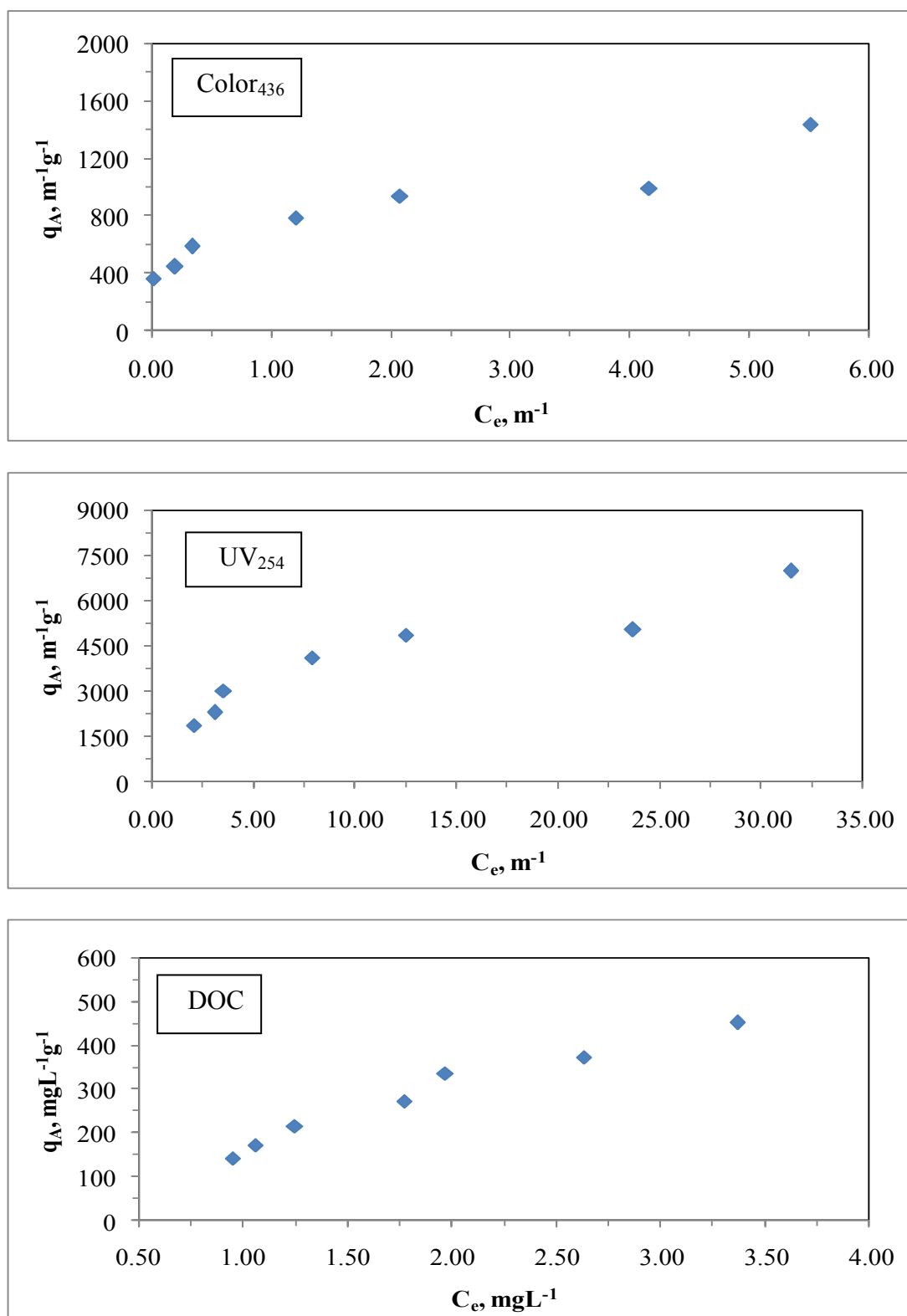
Figure 4.114. Freundlich adsorption isotherm of Color$_{436}$, UV$_{254}$ and DOC parameters of 0.45 μm filtration fraction of humic acid following adsorption onto N-S co-doped TiO$_2$ Hombikat UV-100.

Table 4.21. Freundlich isotherm model parameters for 0.45 µm filtration fraction of humic acid following adsorption onto N-S co-doped TiO_2 Hombikat UV-100.

Humic acid, 0.45 µm filtration fraction		
UV-vis parameter	K_f	$1/n$
$Color_{436}$	783	0.233
UV_{365}	1067	0.340
UV_{280}	1432	0.422
UV_{254}	1511	0.433
Dissolved Organic Carbon	K_f	$1/n$
DOC	164	0.882

Comparison of UV-vis parameters indicated that the adsorption capacity constant of $Color_{436}$ was the lowest value. An increasing order of adsorption capacity constant could be given as $Color_{436} < UV_{365} < UV_{280} < UV_{254}$. Furthermore, adsorption intensity values of $Color_{436}$ and UV_{365} had the lower values than adsorption intensity values of UV_{280} and UV_{254}. An increasing order of adsorption intensity could be given as $Color_{436} < UV_{365} < UV_{280} \leq UV_{254}$.

Freundlich isotherm model parameters of DOC for 0.45 µm filtration fraction of humic acid could be expressed by a decreasing order for K_f: N-S co-doped $TiO_2 \geq$ C-doped $TiO_2 >$ S-doped $TiO_2 >$ bare $TiO_2 >$ N-doped TiO_2 for $1/n$: N-doped $TiO_2 >$ S-doped TiO2 > bare $TiO_2 >$ N-S co-doped $TiO_2 >$ C-doped TiO_2 Hombikat UV-100.

Langmuir adsorption model. Langmuir adsorption isotherms for 0.45 µm filtration fraction of humic acid following adsorption onto N-S co-doped TiO_2 Hombikat UV-100 were presented in Figure 4.115 for $Color_{436}$, UV_{254} and DOC parameters. Langmuir isotherms for UV_{365} and UV_{280} were presented in Appendix B. Two parameters of Langmuir equation outlined in section 2.3, q_m and K_a, were listed in Table 4.22 for 0.45 µm filtration fraction of humic acid following adsorption onto N-S co- doped TiO_2 Hombikat UV-100 ($R^2 \geq 0.86$). It could be easily seen from Table 4.21 that the highest value of q_m was in UV_{254} spectroscopic parameter. The order of all of UV-vis spectroscopic parameters in terms of q_m value was $Color_{436} < UV_{365} < UV_{280} < UV_{254}$.
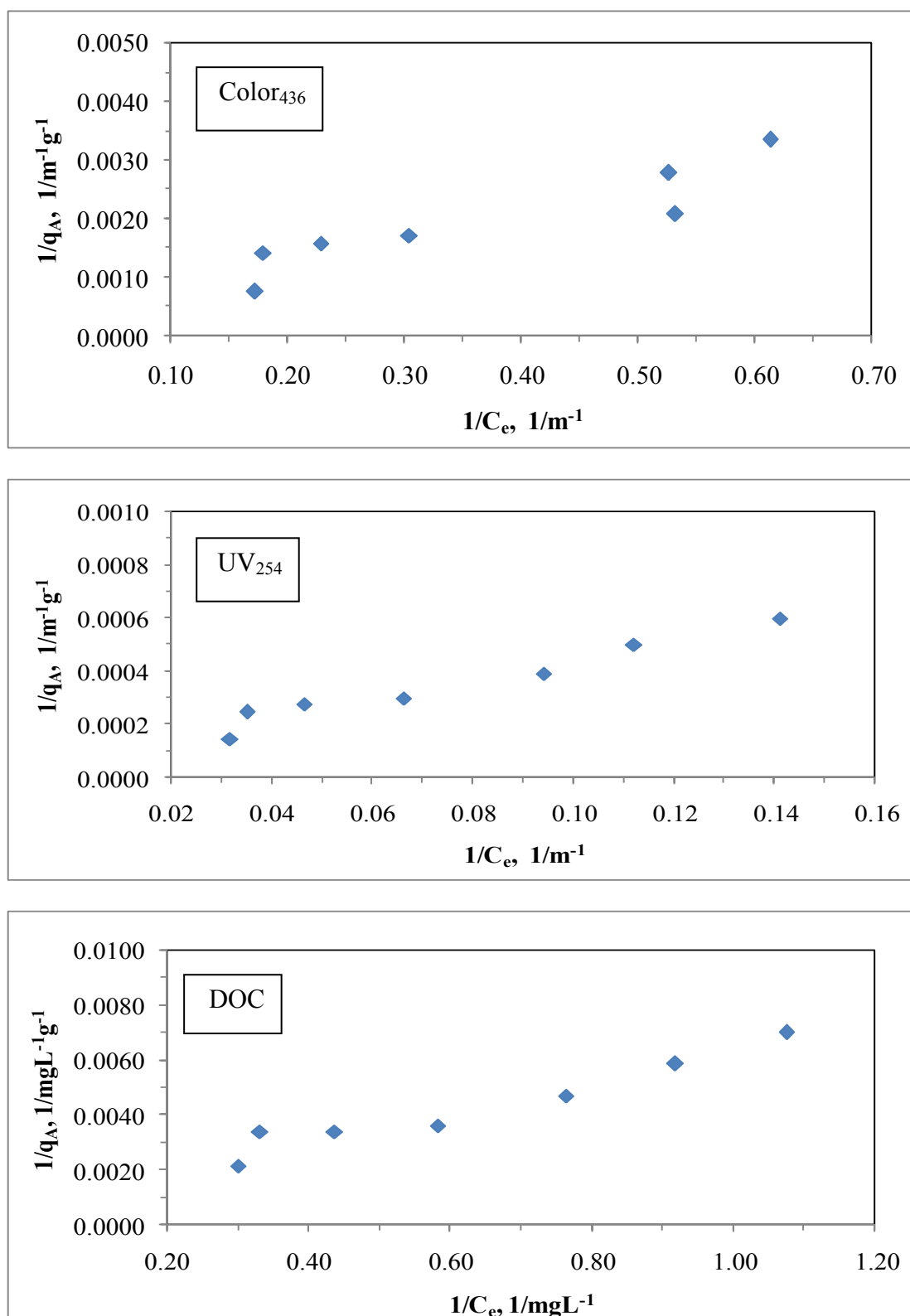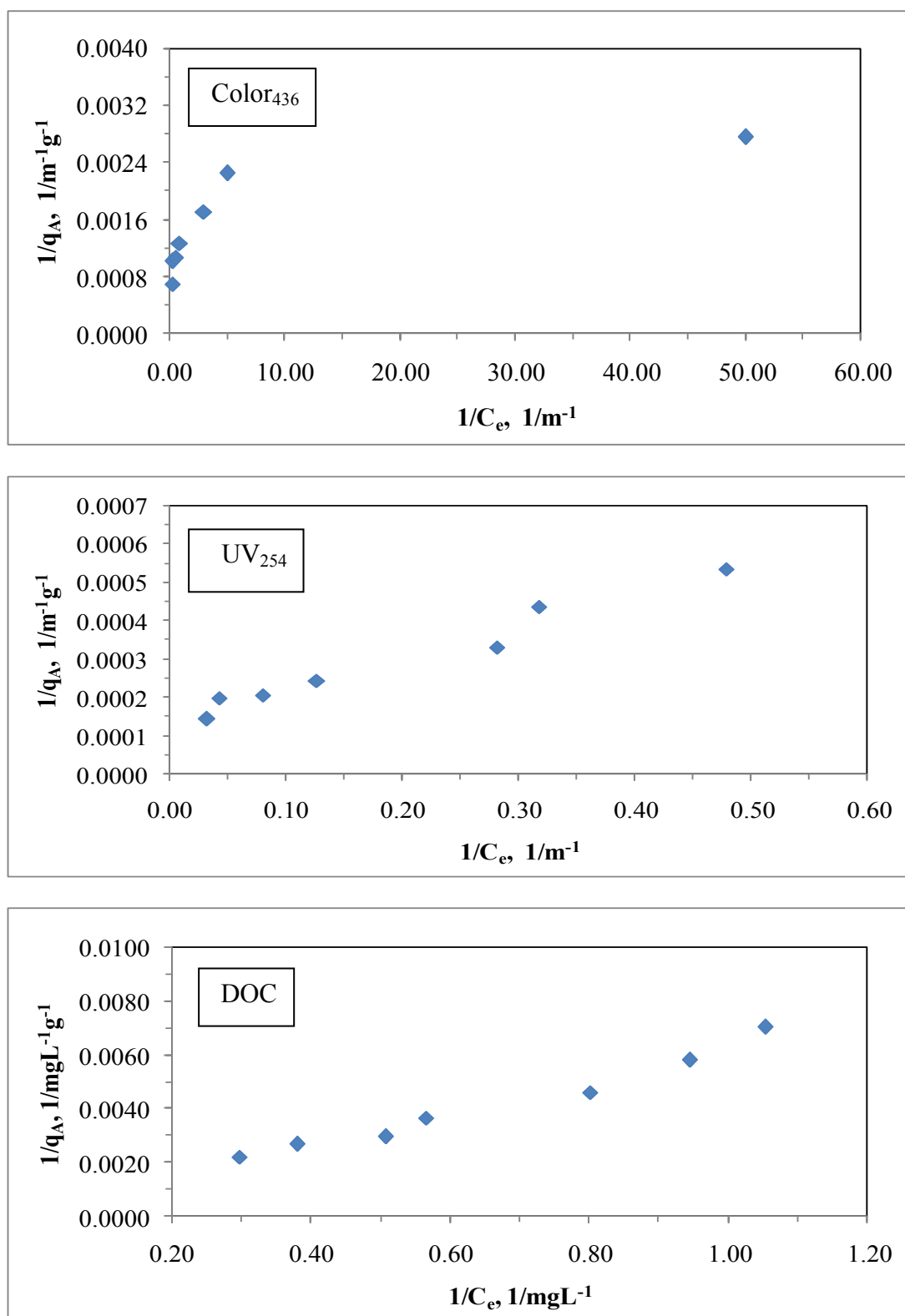
Figure 4.115. Langmuir adsorption isotherm of Color$_{436}$, UV$_{254}$ and DOC parameters of 0.45 μm filtration fraction of humic acid following adsorption onto N-S co-doped TiO$_2$ Hombikat UV-100.

Table 4.22. Langmuir isotherm model parameters for 0.45 μm filtration fraction of humic acid following adsorption onto N-S co-doped TiO_2 Hombikat UV-100.

Humic acid, 0.45 μm filtration fraction		
UV-vis parameter	q_m $m^{-1}g^{-1}$	K_a
Color$_{436}$	1000	33.33
UV$_{365}$	2000	1.67
UV$_{280}$	5000	0.250
UV$_{254}$	10000	0.120
Dissolved Organic Carbon	q_m mg $L^{-1}g^{-1}$	K_a mg L^{-1}
DOC	5000	0.0330

It could be easily seen from Table 4.22 that the order for K_a could be given as UV$_{254}$ < UV$_{280}$ < UV$_{365}$ < Color$_{436}$. Moreover, K_a value of Color$_{436}$ parameter had very high value from other spectroscopic parameters.

4.7. Adsorption Isotherm Modeling of 100 kDa Fraction of Humic Acid onto TiO$_2$ Specimens

The experimental adsorption data were fitted to both Freundlich and Langmuir isotherm models. The Freundlich isotherm model was explained with equation (2.7) outlined in theoretical background section and the Langmuir isotherm model was expressed with equation (2.6).

4.7.1. Adsorption Isotherm Modeling of 100 kDa Fraction of Humic Acid onto TiO$_2$ Degussa P-25 Specimens

The experimental data related to 100 kDa fraction of humic acid following adsorption onto TiO$_2$ Degussa P-25 specimens were fitted to both Freundlich and Langmuir isotherm models.

4.7.1.1. Adsorption Isotherm Modeling of 100 kDa Fraction of Humic Acid onto Bare TiO$_2$ Degussa P-25 Specimen. UV-vis spectroscopic parameters (Color$_{436}$, UV$_{365}$, UV$_{280}$, and UV$_{254}$) and DOC were fitted to Freundlich (2.7) and Langmuir (2.6) adsorption isotherm models.

Freundlich adsorption model. Freundlich adsorption isotherms were presented in Figure 4.116 for Color$_{436}$, UV$_{254}$ and DOC parameters. Freundlich isotherms for UV$_{365}$ and UV$_{280}$ were presented in Appendix A.

C$_e$ values altered between $0.73 - 4.37$ m^{-1} for Color$_{436}$ according to the loading of bare TiO$_2$ Degussa P-25 in the solution. The values of q$_A$ were in the range of $235 - 896$ m^{-1} g^{-1} for the corresponding to the C$_e$ values. ΔC$_e$ and Δq$_A$ values for 100 kDa fraction of humic acid were calculated as 3.64 m^{-1} and 661 m^{-1} g^{-1} for Color$_{436}$. C$_e$ values altered between $13.35 - 31.64$ m^{-1} for UV$_{254}$. The values of q$_A$ were in the range of $1262 - 5304$ m^{-1} g^{-1} for

the corresponding to the C_e values. ΔC_e and Δq_A values for UV_{254} were found as 18.29 m^{-1} and 4042 m^{-1} g^{-1}; respectively (Figure 4.116).

Adsorption isotherms relatively exhibited similar trend for both of the UV-vis parameters as expressed by $Color_{436}$ and UV_{254} parameters. The trends exhibited by the respective adsorption isotherms could be considered as C-curve type isotherm.

C_e values altered between 1.45 - 3.42 mg L^{-1} for DOC. The values of q_A corresponding to the C_e values were in the range of 139- 604 mg L^{-1} g^{-1}. ΔC_e and Δq_A values for DOC were calculated as 1.97 mg L^{-1} and 465 mg L^{-1} g^{-1}; respectively (Figure 4.116). DOC adsorption isotherm displayed an increasing trend with respect to the decreasing dose of TiO_2 Degussa P-25. Considering the initial DOC of 0.45 μm filtration fraction of humic acid (4.93 mg L^{-1}), 31 % DOC was removed for 0.1 mg mL^{-1} dose of bare TiO_2 Degussa P-25 and 71 % DOC was removed for 1.0 mg mL^{-1} dose of bare TiO_2 Degussa P-25 upon adsorption under equilibrium conditions.

Freundlich isotherm model coefficients; adsorption capacity, K_f, and adsorption intensity, $1/n$, for 100 kDa fraction of humic acid following adsorption onto bare TiO_2 Degussa P-25 were listed in Table 4.23 ($R^2 \geq 0.83$).

Figure 4.116. Freundlich adsorption isotherm of $Color_{436}$, UV_{254} and DOC parameters of 100 kDa fraction of humic acid following adsorption onto bare TiO_2 Degussa P-25.

Table 4.23. Freundlich isotherm model parameters for 100 kDa fraction of humic acid following adsorption onto bare TiO_2 Degussa P-25.

Humic acid, 100kDa fraction		
UV-vis parameter	K_f	$1/n$
$Color_{436}$	223.4	0.720
UV_{365}	116.6	0.840
UV_{280}	16.57	0.890
UV_{254}	12.46	0.860
Dissolved Organic Carbon	K_f	$1/n$
DOC	67.95	1.70

Comparison of UV-vis parameters indicated that the adsorption capacity constant of $Color_{436}$ was the highest value. Adsorption capacity constants were found to be in the order of $Color_{436}$ > UV_{365} > UV_{280} > UV_{254}. Also, adsorption intensity of $Color_{436}$ was the lowest value. Furthermore, adsorption intensity of UV_{280} and UV_{254} were very much close to each other. The order of adsorption intensity could be given as $UV_{280} \geq UV_{254} \geq UV_{365}$ > $Color_{436}$. Adsorption intensity of DOC was found to be >1 representing strong adsorption bond.

Comparative evaluation of Freundlich isotherm model parameters of 100 kDa fraction of humic acid with 0.45 µm filtration fraction of humic acid onto following adsorption bare TiO_2 Degussa P-25 revealed the most significant difference in both UV-vis parameters and DOC (Table 4.3 and Table 4.23).

Langmuir adsorption model. Langmuir adsorption isotherms for 100 kDa fraction of humic acid following adsorption onto bare TiO_2 Degussa P-25 were presented in Figure 4.117 for $Color_{436}$, UV_{254} and DOC parameters. Langmuir isotherms for UV_{365} and UV_{280} were presented in Appendix B.

Two parameters of Langmuir equation outlined in section 2.3, q_m and K_a, were listed in Table 4.24 for 100 kDa fraction of humic acid following adsorption onto bare TiO_2 Degussa P-25 ($R^2 \geq 0.92$).

Figure 4.117. Langmuir adsorption isotherm of Color$_{436}$, UV$_{254}$ and DOC parameters of 100 kDa fraction of humic acid following adsorption onto bare TiO$_2$ Degussa P-25.

Table 4.24. Langmuir adsorption isotherm model parameters for 100 kDa fraction of humic acid following adsorption onto bare TiO_2 Degussa P-25.

Humic acid, 100 kDa fraction		
UV-vis parameter	q_m m^{-1}g^{-1}	K_a m^{-1}
Color$_{436}$	1250	0.0930
UV$_{365}$	1429	0.0590
UV$_{280}$	2000	0.0270
UV$_{254}$	2500	0.0200
Dissolved Organic Carbon	q_m mg L^{-1}g^{-1}	K_a mg L^{-1}
DOC	500	0.143

It could be easily seen from Table 4.24 that the order of UV-vis spectroscopic parameters for q_m value was UV$_{254}$ > UV$_{280}$ > UV$_{365}$ > Color$_{436}$ and this order was reverse for K_a value. The model parameters as q_m and K_a values for DOC were calculated as 500 mg L^{-1}g^{-1} and 0.143 mg L^{-1}.

It should be indicated that adsorption of 100 kDa fraction of humic acid onto bare TiO_2 Degussa P-25 could well be characterized both by Freundlich and Langmuir adsorption isotherm models.

Comparative evaluation of Freundlich isotherm model parameters of 100 kDa fraction of humic acid with 0.45 μm filtration fraction of humic acid following adsorption onto bare TiO_2 Degussa P-25 revealed the most significant difference in both UV-vis parameters and DOC (Table 4.4 and Table 4.24). Langmuir isotherm model parameter, q_m was found to be significantly lower than the values calculated from the data attained for 100 kDa fraction of humic acid (Table 4.4and Table 4.24) for UV-vis parameters in comparison to DOC. Langmuir isotherm model parameter, K_a was found to be slightly different for diverse molecular size fractions of humic acid, namely K_a = 0.111 mg L^{-1} for 0.45 μm filtration fraction of humic acid following adsorption onto bare TiO_2 Degussa P-25 and K_a = 0.143 mg L^{-1} for 100 kDa fraction of humic acid following adsorption onto bare TiO_2 Degussa P-25 in terms of DOC.

4.7.1.2. Adsorption Isotherm Modeling of 100 kDa Fraction of Humic Acid onto C-doped TiO$_2$ Degussa P-25 Specimen. UV-vis spectroscopic parameters (Color$_{436}$, UV$_{365}$, UV$_{280}$, UV$_{254}$) and DOC were fitted to Freundlich (2.7) and Langmuir (2.6) adsorption isotherm models.

Freundlich adsorption model. Freundlich adsorption isotherms were presented in Figure 4.118 for Color$_{436}$, UV$_{254}$ and DOC parameters. Freundlich isotherms for UV$_{365}$ and UV$_{280}$ were presented in Appendix A.

C$_e$ values altered between 2.67 – 5.92 m^{-1} for Color$_{436}$ in concern with the loading of C-doped TiO$_2$ Degussa P-25 in the solution. The calculated values of q$_A$ were in the range of 158 - 524 m^{-1} g^{-1} for the corresponding to the C$_e$ values. ΔC$_e$ and Δq$_A$ values for 100 kDa fraction of humic acid were found as 3.25 m^{-1} and 366 m^{-1} g^{-1} for Color$_{436}$. C$_e$ values altered between 20.21 – 37.43 m^{-1} for UV$_{254}$. The values of q$_A$ were calculated as between 988 - 2988 m^{-1} g^{-1} for the corresponding to the C$_e$ values. ΔC$_e$ and Δq$_A$ values for UV$_{254}$ were calculated as 17.22 m^{-1} and 2000 m^{-1} g^{-1}, respectively (Figure 4.118).

Freundlich adsorption isotherms of 100 kDa fraction of humic acid following adsorption onto 0.6 mg mL^{-1} dose of C- doped TiO$_2$ Degussa P-25 demonstrated a notable difference for both of the UV-vis parameters as expressed by Color$_{436}$ and UV$_{254}$ specific parameters. The trends presented by adsorption isotherms could be considered as S-curve type isotherm. The role of C-doping could be visualized in adsorption isotherm profiles of UV-vis parameters (Figure 4.116 and Figure 4.118).

C$_e$ values altered between 2.41 – 4.12 mg L^{-1} for DOC. The values of q$_A$ corresponding to the C$_e$ values were in the range of 101 - 324 mg L^{-1} g^{-1}. ΔC$_e$ and Δq$_A$ values for DOC were calculated as 1.71 mg L^{-1} and 223 mg L^{-1} g^{-1}, respectively (Figure 4.118).

Freundlich isotherm model coefficients; adsorption capacity, K$_f$, and adsorption intensity, 1/n, for 100 kDa fraction of humic acid following adsorption onto C-doped TiO$_2$ Degussa P-25 were listed in Table 4.25 (R^2≥0.85).

Figure 4.118. Freundlich adsorption isotherm of Color$_{436}$, UV$_{254}$ and DOC parameters of 100 kDa fraction of humic acid following adsorption onto C-doped TiO$_2$ Degussa P-25.

Table 4.25. Freundlich isotherm model parameters for 100 kDa fraction of humic acid following adsorption onto C-doped TiO_2 Degussa P-25.

Humic acid, 100kDa fraction		
UV-vis parameter	K_f	1/n
$Color_{436}$	45	1.35
UV_{365}	23	1.48
UV_{280}	18	1.35
UV_{254}	16	1.36
Dissolved Organic Carbon	K_f	1/n
DOC	21	1.67

Comparison of UV-vis parameters indicated that adsorption capacity constant of $Color_{436}$ was the highest value. Moreover, adsorption capacity constants of UV_{280} and UV_{254} were nearly equal to each other and also they had the lowest values. A decreasing order of adsorption capacity constant could be given as $UV_{254} \leq UV_{280} < UV_{365} < Color_{436}$. Also, adsorption intensity of UV_{280} was the lowest value contrary to adsorption intensity of UV_{365}. Furthermore, adsorption intensity of UV_{280} and $Color_{436}$ were relatively close to each other. The order of adsorption intensity could be given as $UV_{280} = Color_{436} \leq UV_{254} < UV_{365}$. Adsorption intensity of DOC was found to be >1 representing strong adsorption bond. Freundlich isotherm model parameters of 100 kDa fraction of humic acid recorded following adsorption onto two different TiO_2 specimens were compared. Freundlich isotherm model parameters displayed significantly lower values for C-doping TiO_2 Degussa P-25 (Table 4.23 and Table 4.25).

Langmuir adsorption model. Langmuir adsorption isotherms for 100 kDa fraction of humic acid following adsorption onto C-doped TiO_2 Degussa P-25 were presented in Figure 4.119 for $Color_{436}$, UV_{254} and DOC parameters. Langmuir adsorption isotherm models for UV_{365} and UV_{280} were presented in Appendix B.

Two parameters of Langmuir equation outlined in section 2.3, q_m and K_a, were listed in Table 4.26 for 100 kDa fraction of humic acid following adsorption onto C- doped TiO_2 Degussa P-25 ($R^2 \geq 0.84$).

Figure 4.119. Langmuir adsorption isotherm of Color$_{436}$, UV$_{254}$ and DOC parameters of 100 kDa fraction of humic acid following adsorption onto C-doped TiO$_2$ Degussa P-25.

Table 4.26. Langmuir isotherm model parameters for 100 kDa fraction of humic acid following adsorption onto C-doped TiO_2 Degussa P-25.

Humic acid, 100 kDa fraction		
UV-vis parameter	q_m $m^{-1}g^{-1}$	K_a m^{-1}
$Color_{436}$	1000	0.0530
UV_{365}	1250	0.0360
UV_{280}	5000	0.00800
UV_{254}	5000	0.00800
Dissolved Organic Carbon	q_m mg $L^{-1}g^{-1}$	K_a mg L^{-1}
DOC	292	0.103

It could be easily seen from Table 4.26 that q_m values of UV_{280} and UV_{254} spectroscopic parameters were equal to each other and K_a values of the same UV-vis specific parameters were equal to each other, too. The order of all UV-vis spectroscopic parameters in terms of q_m value was $UV_{254} = UV_{280} > UV_{365} > Color_{436}$ and this order was reverse for K_a value, namely, $Color_{436} > UV_{365} > UV_{280} = UV_{254}$. The model parameters as q_m and K_a values for DOC were calculated as 292 mg $L^{-1}g^{-1}$ and 0.103 mg L^{-1}.

It should be indicated that adsorption 100 kDa fraction of humic acid onto C-doped TiO_2 Degussa P-25 could well be characterized both by Freundlich and Langmuir adsorption isotherm models. Comparative evaluation of Langmuir isotherm model parameters of 100 kDa fraction of humic acid with 0.45 μm filtration fraction of humic acid following adsorption onto C-doped TiO_2 Degussa P-25 revealed the most significant difference in both UV-vis parameters and DOC

Langmuir isotherm model parameters of 100 kDa fraction of humic acid recorded following adsorption onto three different TiO_2 specimens were compared (Table 4.4, Table 4.24 and Table 4.26). Although a consistent trend could be expressed within the UV-vis parameters and DOC, K_a values was significantly lower for 100 kDa fraction of humic acid C-doped TiO_2 Degussa P-25, namely $K_a = 0.00800$ mg L^{-1} for 100 kDa fraction of humic acid C-doped TiO_2 Degussa P-25 and $K_a = 0.0200$ mg L^{-1} for 100 kDa fraction of humic acid bare TiO_2 Degussa P-25 in terms of UV_{254} spectroscopic parameter.

4.7.1.3. Adsorption Isotherm Modeling of 100 kDa Fraction of Humic Acid onto N-doped TiO$_2$ Degussa P-25 Specimen. UV-vis spectroscopic parameters (Color$_{436}$, UV$_{365}$, UV$_{280}$, and UV$_{254}$) and DOC were fitted to Freundlich (2.7) and Langmuir (2.6) adsorption isotherm models.

Freundlich adsorption model. Freundlich adsorption isotherms were presented in Figure 4.120 for Color$_{436}$, UV$_{254}$ and DOC parameters. Freundlich isotherms for UV$_{365}$ and UV$_{280}$ were presented in Appendix A.

C$_e$ values altered between 4.52 – 6.14 m^{-1} for Color$_{436}$ according to the loading of N-doped TiO$_2$ Degussa P-25 in the solution. The values of q$_A$ were found in the range of 84 – 188 m^{-1} g^{-1} for the corresponding to the C$_e$ values. ΔC$_e$ and Δq$_A$ values for Color$_{436}$ were calculated as 1.62 m^{-1} and 104 m^{-1}g^{-1}; respectively. C$_e$ values altered between 30.10 – 41.84 m^{-1} for UV$_{254}$. The calculated values of q$_A$ were in the range of 592 - 1224 m^{-1} g^{-1} for the corresponding to the C$_e$ values. ΔC$_e$ and Δq$_A$ values for UV$_{254}$ were calculated as 11.74 m^{-1} and 632 m^{-1} g^{-1}; respectively (Figure 4.120).

Freundlich adsorption isotherms of 100 kDa fraction of humic acid following adsorption onto 0.8 mg mL^{-1} dose of N-doped TiO$_2$ Degussa P-25 demonstrated a remarkable diversity for both of the UV-vis parameters as expressed by Color$_{436}$ and UV$_{254}$ specific parameters. The trends presented by adsorption isotherms could be considered as C-curve type isotherm.

N-doping of TiO$_2$ Degussa P-25 significantly altered the adsorption isotherm trend of 100 kDa fraction of humic acid in comparison to both bare and C-doped TiO$_2$ Degussa P-25 (Figure 4.116, Figure 4.1188 and Figure 4.120).

C$_e$ values altered between 1.25 – 4.25 mg L^{-1} for DOC. The values of q$_A$ corresponding to the C$_e$ values were calculated as between 147 - 272 mg L^{-1} g^{-1}. ΔC$_e$ and Δq$_A$ values for DOC were calculated as 3.00 mg L^{-1} and 125 mg L^{-1} g^{-1}; respectively (Figure 4.120). Freundlich isotherm model coefficients; adsorption capacity, K$_f$, and adsorption intensity, 1/n, for 100 kDa fraction of humic acid following adsorption onto N-doped TiO$_2$ Degussa P-25 were listed in Table 4.27 (R^2≥0.86).

Figure 4.120. Freundlich adsorption isotherm of Color$_{436}$, UV$_{254}$ and DOC parameters of 100 kDa fraction of humic acid following adsorption onto N-doped TiO$_2$ Degussa P-25. Table 4.27. Freundlich isotherm model parameters for 100 kDa fraction of humic acid following adsorption onto N-doped TiO$_2$ Degussa P-25.

Humic acid, 100kDa fraction		
UV-vis parameter	K$_f$	1/n
Color$_{436}$	3.460	2.13
UV$_{365}$	3.949	1.75
UV$_{280}$	2.200	1.71
UV$_{254}$	2.650	1.62
Dissolved Organic Carbon	K$_f$	1/n
DOC	141.2	0.405

Comparison of UV-vis parameters indicated that the adsorption capacity constant of UV$_{365}$ was the highest value. Moreover, adsorption capacity constants of UV$_{280}$ had the lowest value. The order was UV$_{280}$ < UV$_{254}$ < Color$_{436}$ < UV$_{365}$ for adsorption capacity constant. Also, adsorption intensity of UV$_{254}$ was the lowest value. Furthermore, adsorption intensity of UV$_{280}$ and UV$_{365}$ were relatively close to each other. The order of adsorption intensity values could be given as Color$_{436}$ > UV$_{365}$ ≥ UV$_{280}$ > UV$_{254}$. Adsorption intensity, 1/n values were found to be > 1 representing strong adsorption bond.

Freundlich isotherm model parameters of 100 kDa of humic acid recorded following adsorption onto two different TiO$_2$ specimens were compared (Table 4.25 and Table 4.27). Freundlich isotherm model parameters displayed significantly lower values for N-doped TiO$_2$ Degussa P-25 than C-doped TiO$_2$ Degussa P-25 for UV-vis parameters in comparison to DOC.

Langmuir adsorption model. Langmuir adsorption isotherm models for 100 kDa fraction of humic acid following adsorption onto N-doped TiO$_2$ Degussa P-25 were presented in Figure 4.121 for Color$_{436}$, UV$_{254}$ and DOC parameters. Langmuir isotherms for UV$_{365}$ and UV$_{280}$ were presented in Appendix B. Two parameters of Langmuir equation outlined in

section 2.3, q_m and K_a, were listed in Table 4.28 for 100 kDa fraction of humic acid following adsorption onto N- doped TiO_2 Degussa P-25($R^2 \geq 0.83$).
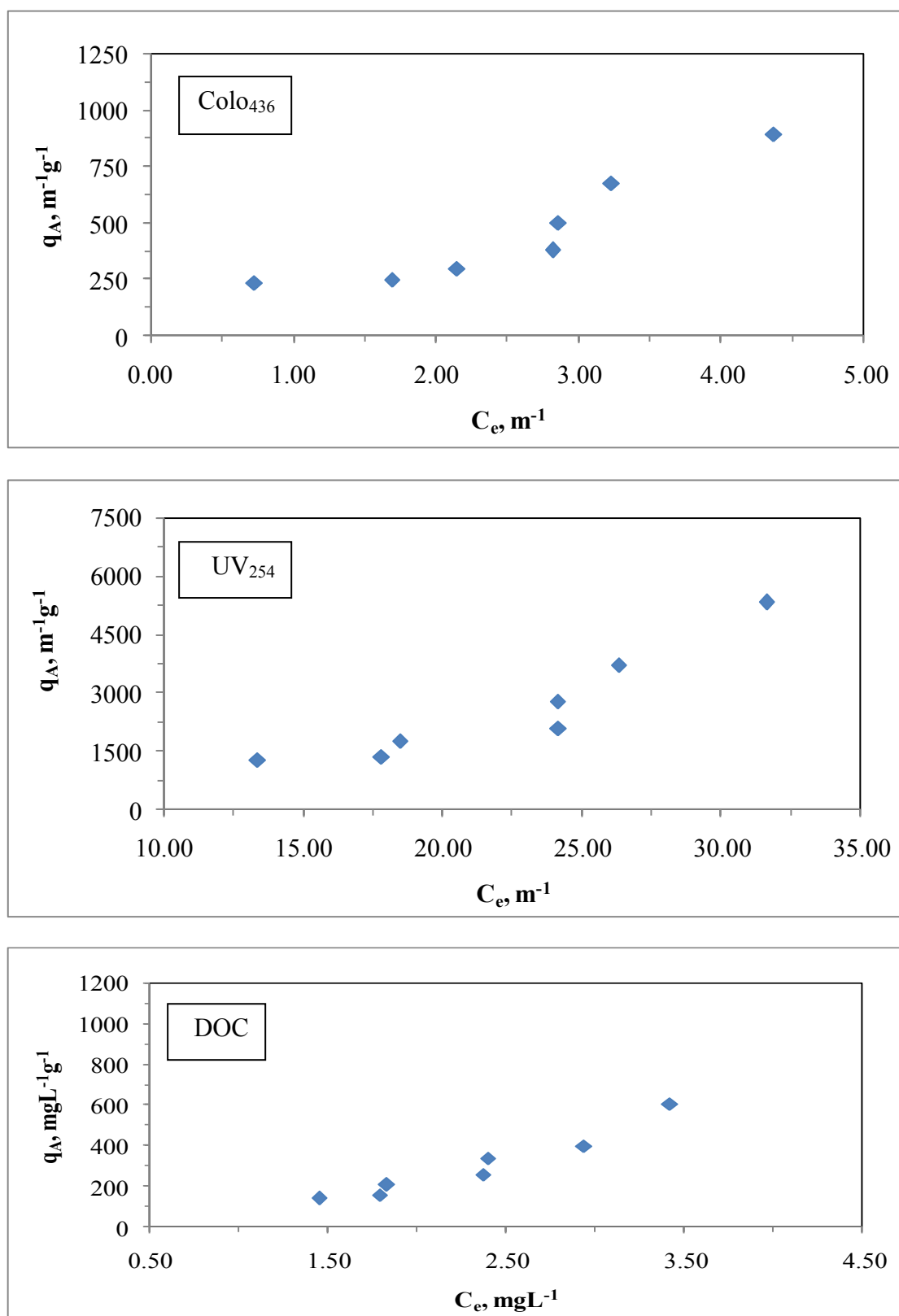
Figure 4.121. Langmuir adsorption isotherm of $Color_{436}$, UV_{254} and DOC parameters of 100 kDa fraction of humic acid following adsorption onto N-doped TiO_2 Degussa P-25.

Table 4.28. Langmuir isotherm model parameters for 100 kDa fraction of humic acid following adsorption onto N-doped TiO_2 Degussa P-25.

Humic acid, 100 kDa fraction		
UV-vis parameter	q_m $m^{-1}g^{-1}$	K_a m^{-1}
$Color_{436}$	111	0.100
UV_{365}	383	0.0370
UV_{280}	1010	0.0140
UV_{254}	1344	0.0110
Dissolved Organic Carbon	q_m mg $L^{-1}g^{-1}$	K_a mg L^{-1}
DOC	333	0.750

It could be easily seen from Table 4.28 the order of all of the UV-vis spectroscopic parameters in terms of q_m value was $UV_{254} > UV_{280} > UV_{365} > Color_{436}$ and this order was reverse for K_a value, namely, $Color_{436} > UV_{365} > UV_{280} > UV_{254}$. The model parameters as q_m and K_a values for DOC were calculated as 333 mg $L^{-1}g^{-1}$ and 0.750 mg L^{-1}.

It should be indicated that adsorption of 100 kDa fraction of humic acid onto N-doped TiO_2 Degussa P-25 could well be characterized both by Freundlich and Langmuir adsorption isotherm models.

Langmuir isotherm model parameters of 100 kDa fraction of humic acid recorded following adsorption onto three different TiO_2 specimens were compared (Table 4.24, Table 4.26 and Table 4.28). Although a consistent trend could be expressed within the UV-vis parameters and DOC, q_m was significantly lower for N-doped TiO_2 Degussa P-25 in comparison to slightly different K_a values as $K_a = 0.143$ mg L^{-1} for bare TiO_2 Degussa P-25 and $K_a = 0.103$ mg L^{-1} for C-doped TiO_2 Degussa P-25 as well as $K_a = 0.750$ mg L^{-1} for N-doped TiO_2 Degussa P-25 in terms of DOC. .

Comparative evaluation of Langmuir isotherm model parameters of 100 kDa fraction of humic acid with 0.45 μm filtration fraction of humic acid following adsorption onto N-

doped TiO$_2$ Degussa P-25 revealed the most significant difference in both UV-vis parameters and DOC.

4.7.1.4. Adsorption Isotherm Modeling of 100 kDa Fraction of Humic Acid onto S-doped TiO$_2$ Degussa P-25 Specimen. UV-vis spectroscopic parameters (Color$_{436}$, UV$_{365}$, UV$_{280}$, and UV$_{254}$) and DOC were fitted to Freundlich (2.7) and Langmuir (2.6) adsorption isotherm models.

Freundlich adsorption model. Freundlich adsorption isotherms were presented in Figure 4.122 for Color$_{436}$, UV$_{254}$ and DOC parameters. Freundlich isotherms for UV$_{365}$ and UV$_{280}$ were presented in Appendix A.

C$_e$ values altered between 2.10 – 5.45 m^{-1} for Color$_{436}$ according to the loading of S-doped TiO$_2$ Degussa P-25 in the solution. The values of q$_A$ were found in the range of 180 - 464 m^{-1} g^{-1} for the corresponding to the C$_e$ values. ΔC$_e$ and Δq$_A$ values for Color$_{436}$ were calculated as 3.35 m^{-1} and 284 m^{-1} g^{-1}; respectively. C$_e$ values altered between 16.20 – 39.27 m^{-1} for UV$_{254}$. The values of q$_A$ were calculated as between 1148 - 2252 m^{-1} g^{-1} for the corresponding to the C$_e$ values. ΔC$_e$ and Δq$_A$ values for UV$_{254}$ were calculated as 23.07 m^{-1} and 1104 m^{-1} g^{-1}, respectively (Figure 4.122).

Adsorption isotherms relatively exhibited similar trend for both of the UV-vis parameters as expressed by Color$_{436}$ and UV$_{254}$ parameters. The trends exhibited by the respective adsorption isotherms could be considered as C-curve type isotherm.

S-doping of TiO$_2$ Degussa P-25 significantly altered the adsorption isotherm trend of 100 kDa fraction of humic acid in comparison to both C-doped TiO$_2$ Degussa P-25 and N-doped TiO$_2$ Degussa P-25 (Figure 4.118, Figure 4.120 and Figure 4.122).

C$_e$ values altered between 1.70 – 4.02 mg L^{-1} for DOC. The values of q$_A$ corresponding to the C$_e$ values were calculated as between 129- 364 mg L^{-1} g^{-1}. ΔC$_e$ and Δq$_A$ values for DOC were calculated as 2.32 mg L^{-1} and 235 mg L^{-1} g^{-1}, respectively (Figure 4.122).

Freundlich isotherm model coefficients; adsorption capacity, K_f, and adsorption intensity, $1/n$, for 100 kDa fraction of humic acid following adsorption onto S-doped TiO_2 Degussa P-25 were listed in Table 4.29 ($R^2 \geq 0.73$).
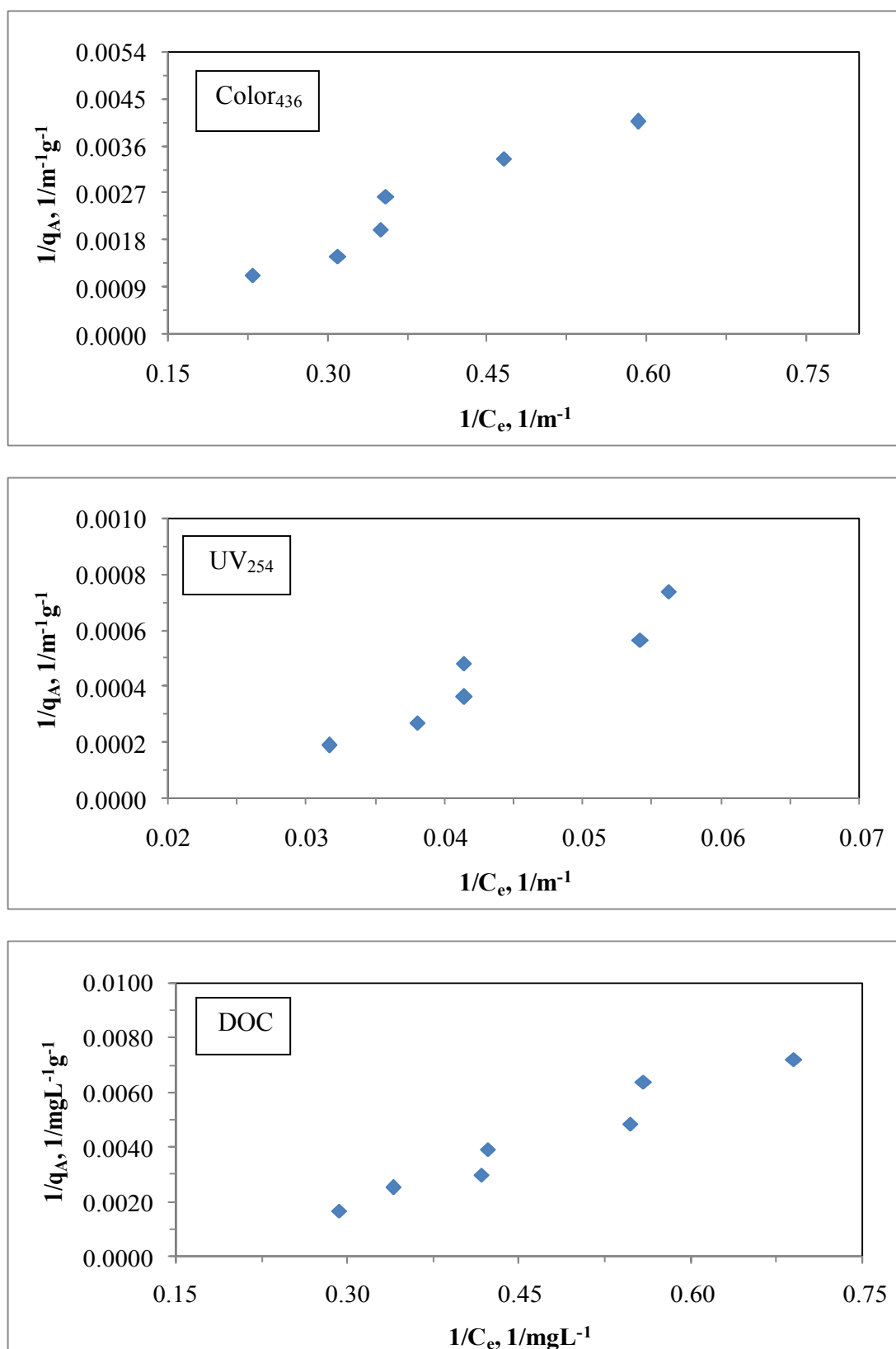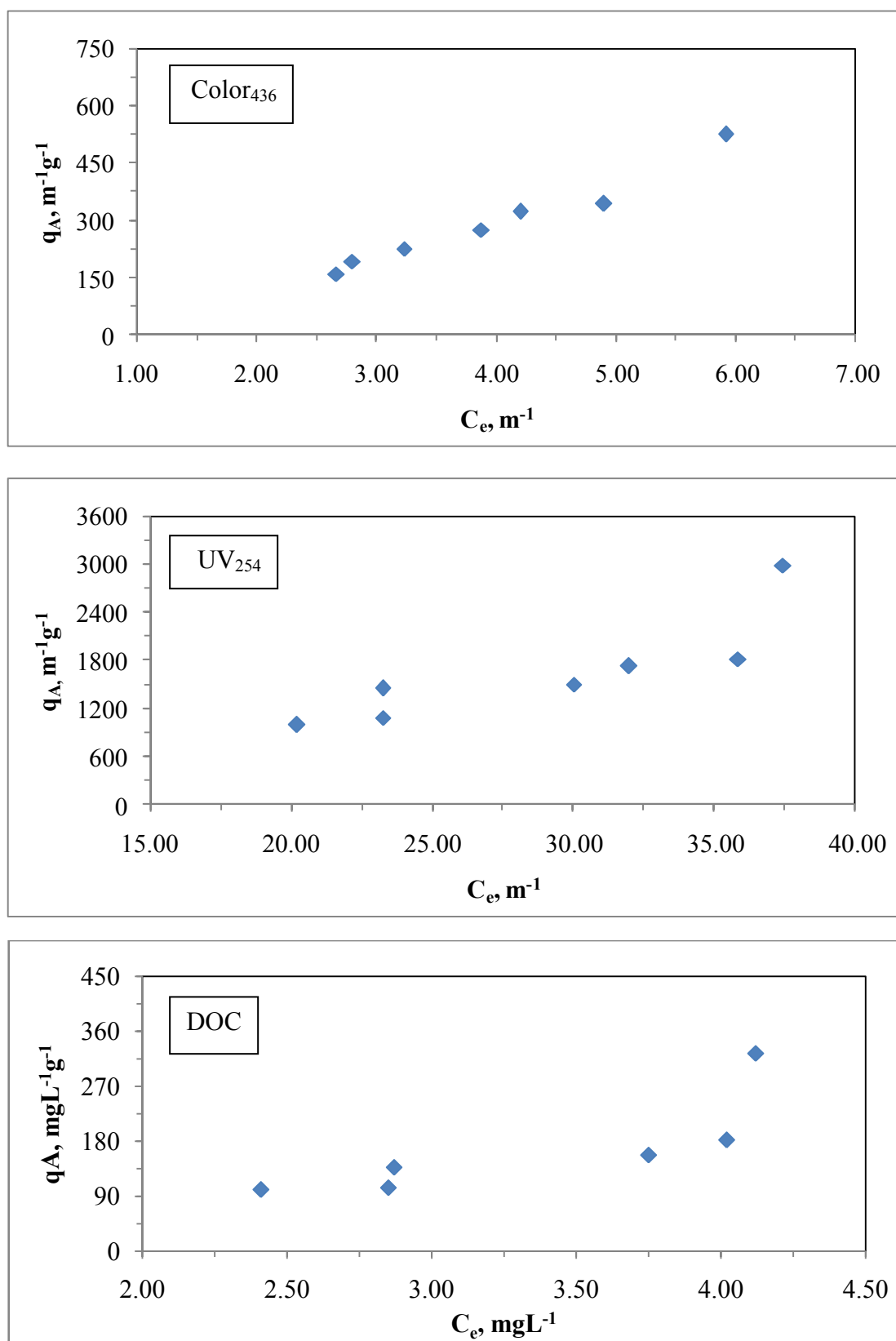
Figure 4.122. Freundlich adsorption isotherm of Color$_{436}$, UV$_{254}$ and DOC parameters of 100 kDa fraction of humic acid following adsorption onto S-doped TiO$_2$ Degussa P-25.

Table 4.29. Freundlich isotherm model parameters for 100 kDa fraction of humic acid following adsorption onto S-doped TiO$_2$ Degussa P-25.

Humic acid, 100kDa fraction		
UV-vis parameter	K_f	$1/n$
Color$_{436}$	78.76	0.848
UV$_{365}$	81.15	0.868
UV$_{280}$	171.9	0.620
UV$_{254}$	125.5	0.746
Dissolved Organic Carbon	K_f	$1/n$
DOC	55.58	1.24

Comparison of UV-vis parameters indicated that the adsorption capacity constant of Color$_{436}$ was the lowest value. The order was Color$_{436}$ < UV$_{365}$ < UV$_{254}$ < UV$_{280}$ for adsorption capacity constant. Also, adsorption intensity of UV$_{280}$ was the lowest value. The order was UV$_{280}$ < UV$_{254}$ < Color$_{436}$ ≤ UV$_{365}$ for adsorption intensity constant. Adsorption intensity of DOC was found to be >1 representing strong adsorption bond.

Freundlich isotherm model parameters, K_f values could be displayed as following an order of bare TiO$_2$ > S-doped TiO$_2$ > C-doped TiO$_2$ > N-doped TiO$_2$ Degussa P-25. The order of $1/n$ values could be given as N-doped TiO$_2$ > C-doped TiO$_2$ > S-doped TiO$_2$ > bare TiO$_2$ Degussa P-25.

Langmuir adsorption model. Langmuir adsorption isotherms for 100 kDa fraction of humic acid following adsorption onto S-doped TiO$_2$ Degussa P-25 were presented in Figure 4.123 for Color$_{436}$, UV$_{254}$ and DOC parameters. Langmuir isotherms for UV$_{365}$ and UV$_{280}$ were presented in Appendix B.

Two parameters of Langmuir equation outlined in section 2.3, q_m and K_a, were listed in Table 4.30 for 100 kDa fraction of humic acid following adsorption onto S- doped TiO_2 Degussa P-25 ($R^2 \geq 0.67$).
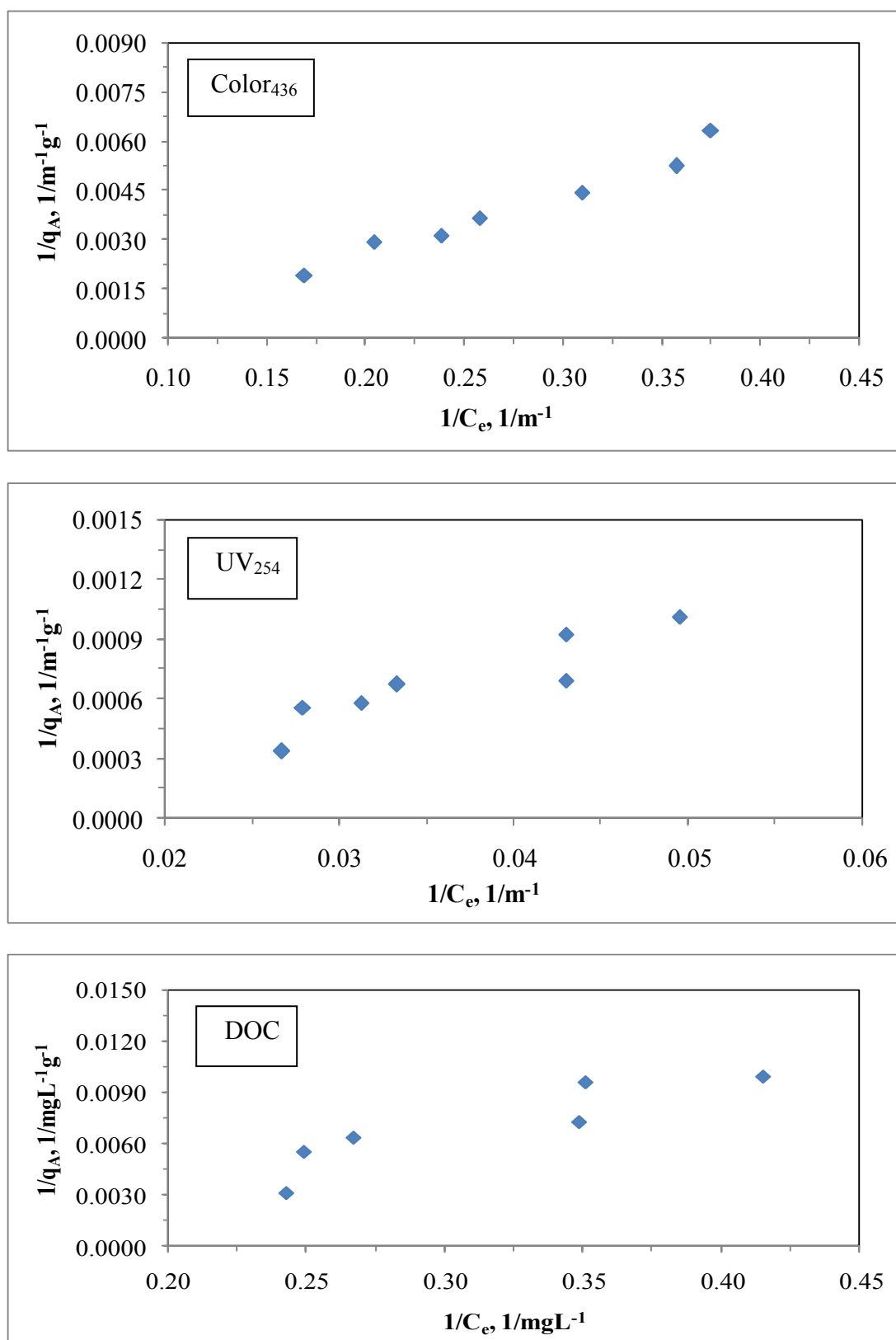
Figure 4.123. Langmuir adsorption isotherm of Color$_{436}$, UV$_{254}$ and DOC parameters of 100 kDa fraction of humic acid following adsorption onto S-doped TiO$_2$ Degussa P-25.

Table 4.30. Langmuir isotherm model parameters for 100 kDa fraction of humic acid following adsorption onto S-doped TiO$_2$ Degussa P-25.

Humic acid, 100 kDa fraction		
UV-vis parameter	q$_m$ m^{-1}g^{-1}	K$_a$ m^{-1}
Color$_{436}$	1000	0.111
UV$_{365}$	1429	0.0640
UV$_{280}$	2500	0.0410
UV$_{254}$	3333	0.0270
Dissolved Organic Carbon	q$_m$ mg L^{-1}g^{-1}	K$_a$ mg L^{-1}
DOC	3333	0.0200

It could be easily seen from Table 4.30 the order of all of the UV-vis spectroscopic parameters in terms of q$_m$ value was UV$_{254}$ > UV$_{280}$ > UV$_{365}$ > Color$_{436}$ and this order was reverse for K$_a$ value, namely, Color$_{436}$ > UV$_{365}$ > UV$_{254}$ > UV$_{280}$. The model parameters as q$_m$ and K$_a$ values for DOC were calculated as 3333 mg L^{-1}g^{-1} and 0.0200 mg L^{-1}.

It should be indicated that adsorption 100 kDa fraction of humic acid onto S-doped TiO$_2$ Degussa P-25 could well be characterized both by Freundlich and Langmuir adsorption isotherm models.

Langmuir isotherm model parameters of 100 kDa fraction of humic acid recorded following adsorption onto four different TiO$_2$ specimens were compared (Table 4.24, Table 4.26 and Table 4.28 as well as Table 4.30). Langmuir isotherm model parameters calculated for UV-vis parameters displayed a different trend with respect to the both N-doped TiO$_2$ and S-doped TiO$_2$. This difference was more significant in terms of K$_a$ with respect to q$_m$ (Table 4.28, Table 4.30). Langmuir isotherm model parameters of DOC could be expressed in a decreasing order of; q$_m$: S-doped TiO$_2$ > bare TiO$_2$ > N-doped TiO$_2$ > C-doped TiO$_2$ >, K$_a$: N-doped TiO$_2$ > bare TiO$_2$ > C-doped TiO$_2$ > S-doped TiO$_2$. Comparative evaluation of Langmuir isotherm model parameters of 100 kDa fraction of

humic acid with 0.45 μm filtration fraction of humic acid following adsorption onto S-doped TiO_2 Degussa P-25 revealed the most significant difference in both UV-vis parameters and DOC.

<u>4.7.1.5. Adsorption Isotherm Modeling of 100 kDa Fraction of Humic Acid onto N-S co-doped TiO_2 Degussa P-25 Specimen.</u> UV-vis spectroscopic parameters ($Color_{436}$, UV_{365}, UV_{280}, and UV_{254}) and DOC were fitted to Freundlich (2.7) and Langmuir (2.6) adsorption isotherm models.

Freundlich adsorption model. Freundlich adsorption isotherms were presented in Figure 4.124 for $Color_{436}$, UV_{254} and DOC parameters. Freundlich isotherms for UV_{365} and UV_{280} were presented in Appendix A.

C_e values altered between 2.04 – 5.61 m^{-1} for $Color_{436}$ according to the loading of N-S co-doped TiO_2 Degussa P-25 in the solution. The values of q_A were found in the range of 183 - 400 m^{-1} g^{-1} for the corresponding to the C_e values. ΔC_e and Δq_A values for 100 kDa fraction of humic acid following adsorption onto N-S co-doped TiO_2 Degussa P-25 were found as 3.57 m^{-1} and 217 m^{-1} g^{-1} for $Color_{436}$. C_e values altered between 13.42 – 38.98 m^{-1} for UV_{254}. The values of q_A were calculated as between 1259 - 2368 m^{-1} g^{-1} for the corresponding to the C_e values. ΔC_e and Δq_A values for UV_{254} were calculated as 25.56 m^{-1} and 1109 m^{-1} g^{-1}, respectively (Figure 4.124).

Adsorption isotherms relatively exhibited similar trend for both of the UV-vis parameters as expressed by $Color_{436}$ and UV_{254} parameters. The trends exhibited by the respective adsorption isotherms could be considered as L-curve type isotherm. N-S co-doping of TiO_2 Degussa P-25 did not significantly alter the adsorption profiles of UV-vis spectral parameters in comparison to S-doping of TiO_2 Degussa P-25.

C_e values altered between 1.83 - 3.83 mg L^{-1} for DOC. The calculated values of q_A corresponding to the C_e values were between 124 - 440 mg L^{-1} g^{-1}. ΔC_e and Δq_A values for DOC were calculated as 2.00 mg L^{-1} and 316 mg L^{-1} g^{-1}, respectively (Figure 4.124).

Freundlich isotherm model coefficients; adsorption capacity, K_f, and adsorption intensity, $1/n$, for 100 kDa fraction of humic acid following adsorption onto N-S co-doped TiO$_2$ Degussa P-25 were listed in Table 4.31 ($R^2 \geq 0.82$).
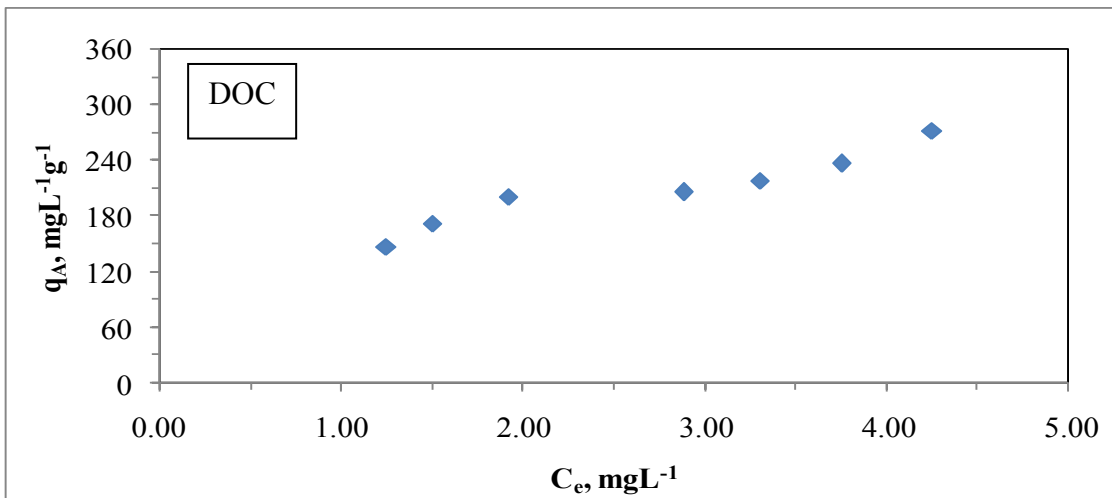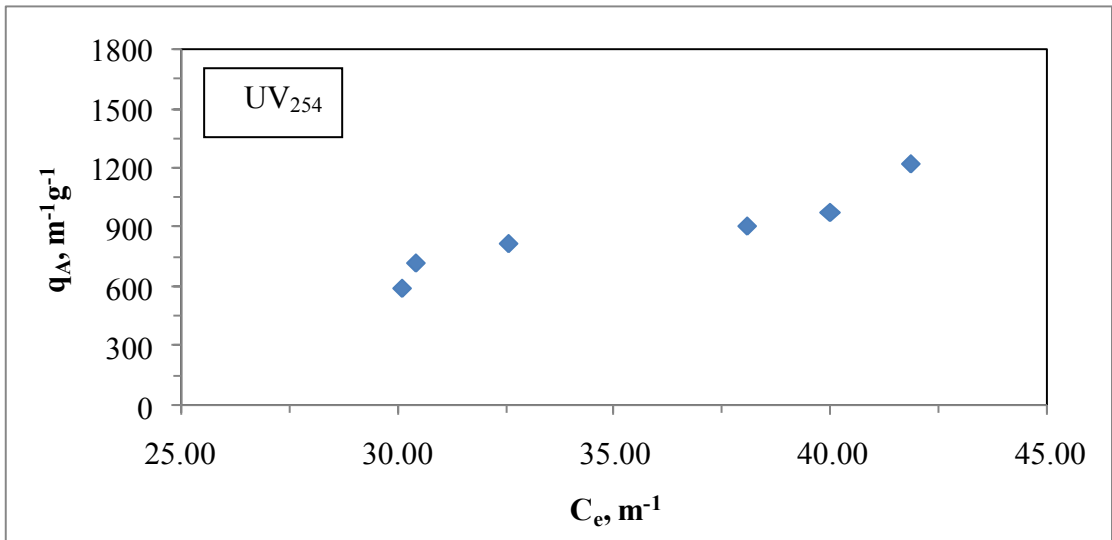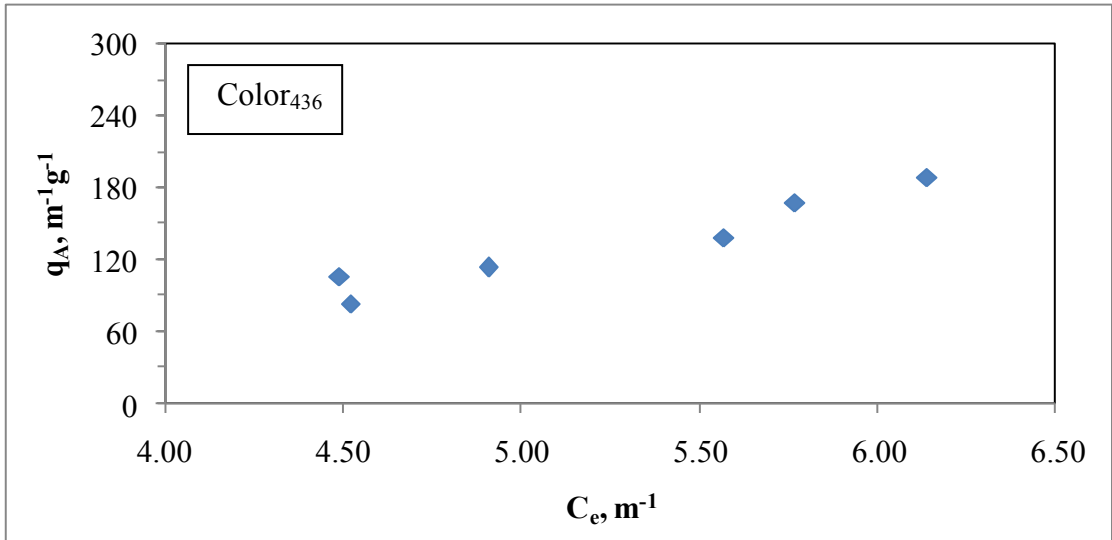
Figure 4.124. Freundlich adsorption isotherm of $Color_{436}$, UV_{254} and DOC parameters of 100 kDa fraction of humic acid following adsorption onto N-S co-doped TiO_2 Degussa P-25.

Table 4.31. Freundlich isotherm model parameters for 100 kDa fraction of humic acid following adsorption onto N-S co-doped TiO_2 Degussa P-25.

Humic acid, 100kDa fraction		
UV-vis parameter	K_f	$1/n$
$Color_{436}$	100.0	0.723
UV_{365}	133.9	0.686
UV_{280}	217.7	0.603
UV_{254}	241.8	0.595
Dissolved Organic Carbon	K_f	$1/n$
DOC	34.91	1.63

Comparison of UV-vis parameters indicated that the adsorption capacity constant of $Color_{436}$ was the lowest value. Moreover, adsorption capacity constants of UV_{280} and UV_{254} were almost equal to each other and also they had the highest values. The order was $Color_{436}$ < UV_{365} < UV_{280} ≤ UV_{254} for adsorption capacity constant. Also, adsorption intensity constant of UV_{254} had the lowest value. A decreasing order of adsorption intensity values could be given as $Color_{436}$ > UV_{365} > UV_{280} ≥ UV_{254}. Adsorption intensity of DOC was found to be >1 representing strong adsorption bond.

Comparative evaluation of Freundlich isotherm model parameter, K_f of 100 kDa fraction of humic acid with 0.45 μm filtration fraction of humic acid did not reveal the most significant difference in both UV-vis parameters and DOC.

Langmuir adsorption model. Langmuir adsorption isotherms for 100 kDa fraction of humic acid following adsorption onto N-S co-doped TiO_2 Degussa P-25 were presented in Figure 4.125 for $Color_{436}$, UV_{254} and DOC parameters. Langmuir isotherms for UV_{365} and UV_{280} were presented in Appendix B.

Two parameters of Langmuir equation outlined in section 2.3, q_m and K_a, were listed in Table 4.32 for 100 kDa fraction of humic acid following adsorption onto N-S co-doped TiO$_2$ Degussa P-25 ($R^2 \geq 0.74$).
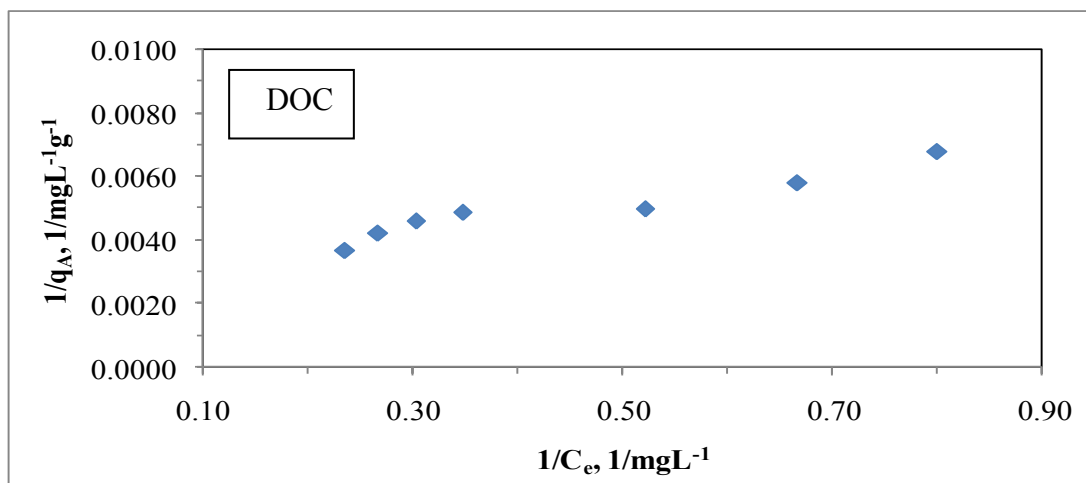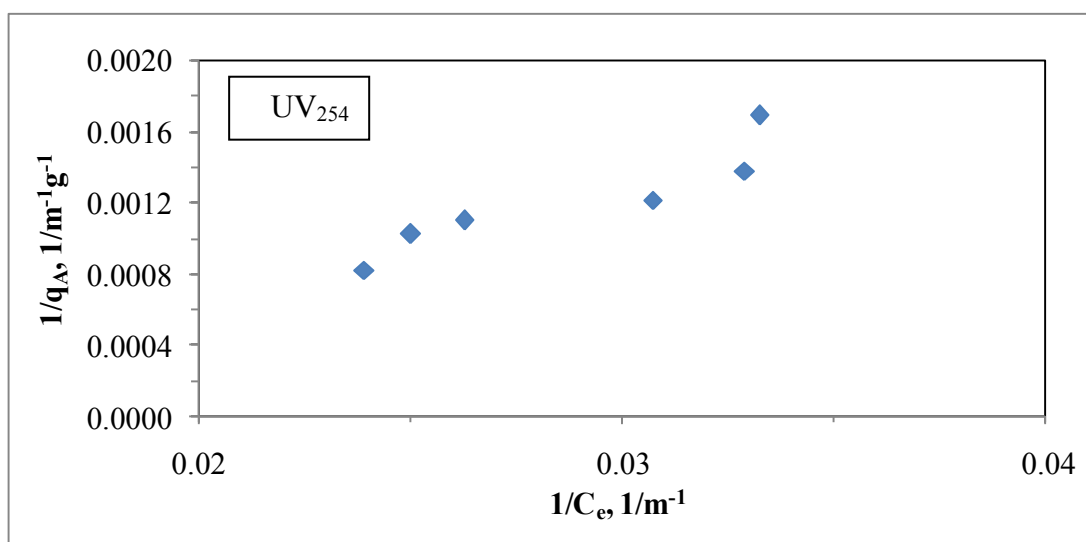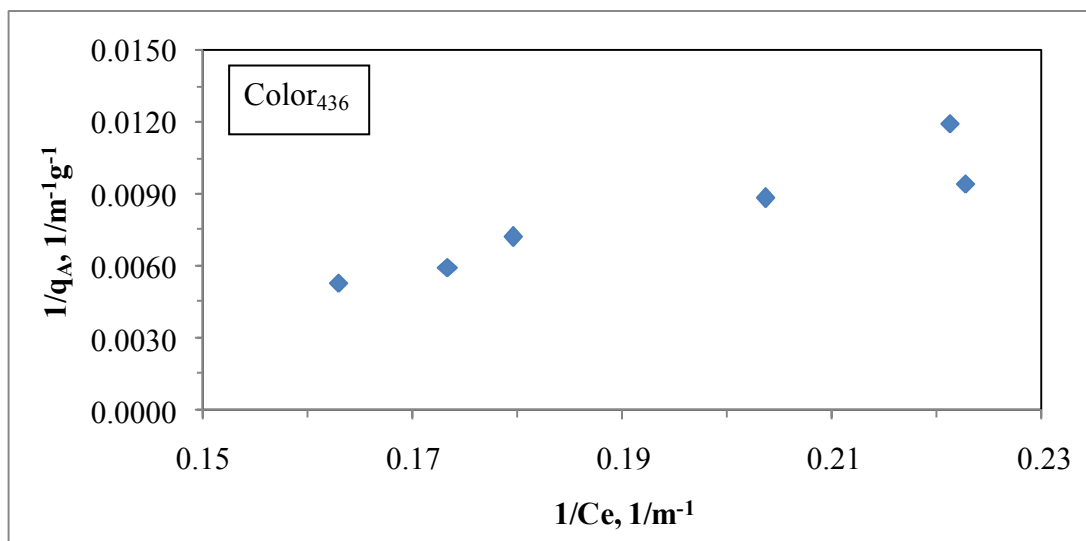
Figure 4.125. Langmuir adsorption isotherm of $Color_{436}$, UV_{254} and DOC parameters of 100 kDa fraction of humic acid following adsorption onto N-S co-doped TiO_2 Degussa P-25.

Table 4.32. Langmuir isotherm model parameters for 100 kDa fraction of humic acid following adsorption onto N-S co-doped TiO_2 Degussa P-25.

Humic acid, 100 kDa fraction		
UV-vis parameter	q_m m^{-1}g^{-1}	K_a m^{-1}
$Color_{436}$	1000	0.125
UV_{365}	1250	0.0990
UV_{280}	2500	0.0530
UV_{254}	3333	0.0410
Dissolved Organic Carbon	q_m mg L^{-1}g^{-1}	K_a mg L^{-1}
DOC	1000	0.0530

It could be easily seen from Table 4.32 the order of all of UV-vis spectroscopic parameters in terms of q_m value was $Color_{436} < UV_{365} < UV_{280} < UV_{254}$ and also a decreasing order of K_a value could be given as $Color_{436} > UV_{365} > UV_{280} > UV_{254}$. The model parameters as q_m and K_a values for DOC were calculated as 1000 mg L^{-1}g^{-1} and 0.0530 mg L^{-1}.

It should be indicated that adsorption of 100 kDa fraction of humic acid onto N-S co-doped TiO_2 Degussa P-25 could well be characterized both by Freundlich and Langmuir adsorption isotherm models.

Langmuir isotherm model parameter, K_f calculated for UV-vis parameters displayed a similar trend with respect to the both S-doped TiO_2 and N-S co-doped TiO_2 Degussa P-25 (Table 4.30 and Table 4.32). Langmuir isotherm model parameters of DOC could be expressed in a decreasing order of; q_m: S-doped TiO_2 > N-S co-doped TiO_2 > bare TiO_2 > N-doped TiO_2 > C-doped TiO_2, K_a: N-doped TiO_2 > bare TiO_2.> C-doped TiO_2 > N-S co-doped TiO_2 > S-doped TiO_2. Comparative evaluation of Langmuir isotherm model parameters of 100 kDa fraction of humic acid with 0.45 μm filtration fraction of humic

acid following adsorption onto N-S co-doped TiO_2 Degussa P-25 revealed the most significant difference in both UV-vis parameters and DOC.

4.7.2. Adsorption Isotherm Modeling of 100 kDa Fraction of Humic Acid onto TiO_2 Hombikat UV-100 Specimens

The experimental data related to 100 kDa fraction of humic acid following adsorption onto TiO_2 Hombikat UV-100 specimens were fitted to both Freundlich and Langmuir isotherm models.

<u>4.7.2.1. Adsorption Isotherm Modeling of 100 kDa Fraction of Humic Acid onto Bare TiO_2 Hombikat UV-100 Specimen.</u> UV-vis spectroscopic parameters ($Color_{436}$, UV_{365}, UV_{280} and UV_{254}) and DOC were fitted to Freundlich (2.7) and Langmuir (2.6) adsorption isotherm models.

Freundlich adsorption model. Freundlich adsorption isotherms were presented in Figure 4.126 for $Color_{436}$, UV_{254} and DOC parameters. Freundlich isotherms for UV_{365} and UV_{280} were presented in Appendix A.

C_e values changed between $1.27 - 3.92$ m^{-1} for $Color_{436}$ in concern with the loading of bare TiO_2 Hombikat UV-100 in the solution. The values of q_A were found in the range of $214 - 1076$ m^{-1} g^{-1} for the corresponding to the C_e values. ΔC_e and Δq_A values for 100 kDa fraction of humic acid were found as 2.65 m^{-1} and 862 m^{-1} g^{-1} for $Color_{436}$. C_e values altered between $9.85 - 27.13$ m^{-1} for UV_{254}. The values of q_A were calculated as between $1402 - 7108$ m^{-1} g^{-1} for the corresponding to the C_e values. ΔC_e and Δq_A values for UV_{254} were calculated as 17.28 m^{-1} and 5706 m^{-1} g^{-1}, respectively. C_e values altered between $1.11 - 2.89$ mg L^{-1} for DOC. The values of q_A corresponding to the C_e values were calculated as $153-816$ mg L^{-1} g^{-1}. ΔC_e and Δq_A values for DOC were calculated as 1.78 mg L^{-1} and 663 mg L^{-1} g^{-1}, respectively (Figure 4.126).

Adsorption isotherms relatively exhibited similar trend for both of the UV-vis parameters as expressed by $Color_{436}$ and UV_{254} parameters. The trends exhibited by the

respective adsorption isotherms could be considered as S-curve type isotherm. Freundlich isotherm model coefficients; adsorption capacity, K_f, and adsorption intensity, $1/n$, for 100 kDa fraction of humic acid following adsorption onto bare TiO_2 Hombikat UV-100 were listed in Table 4.33 ($R^2 \geq 0.76$).
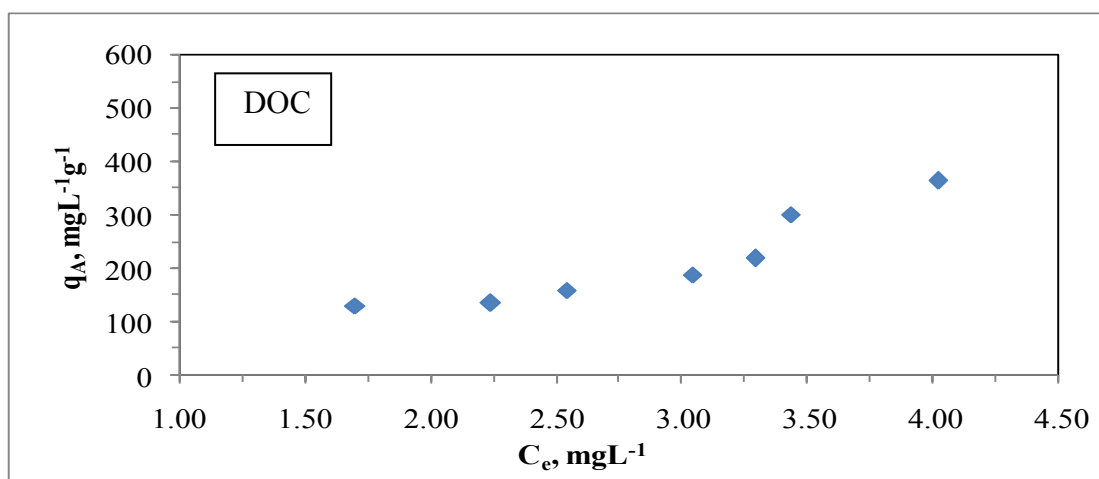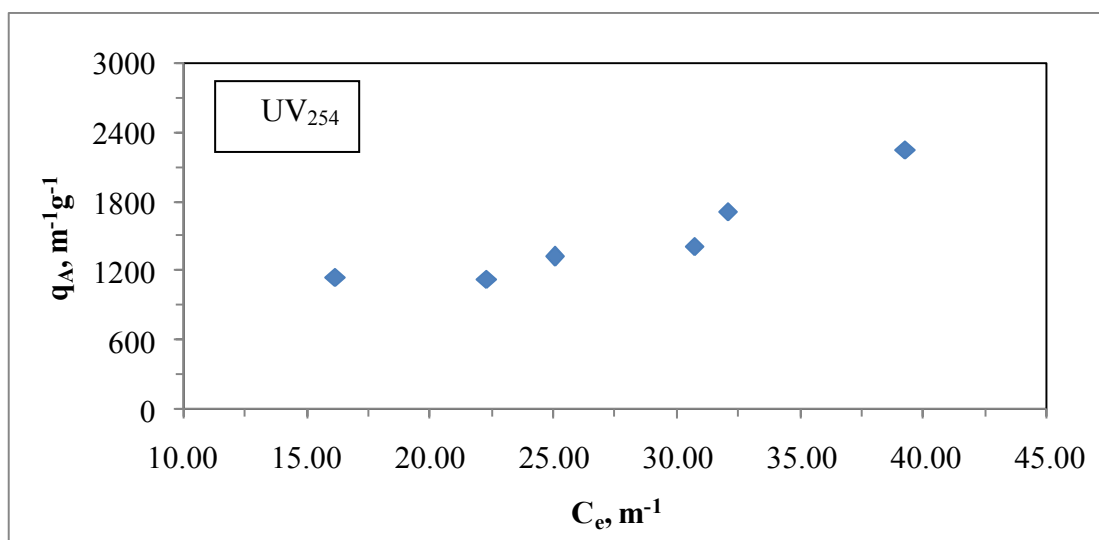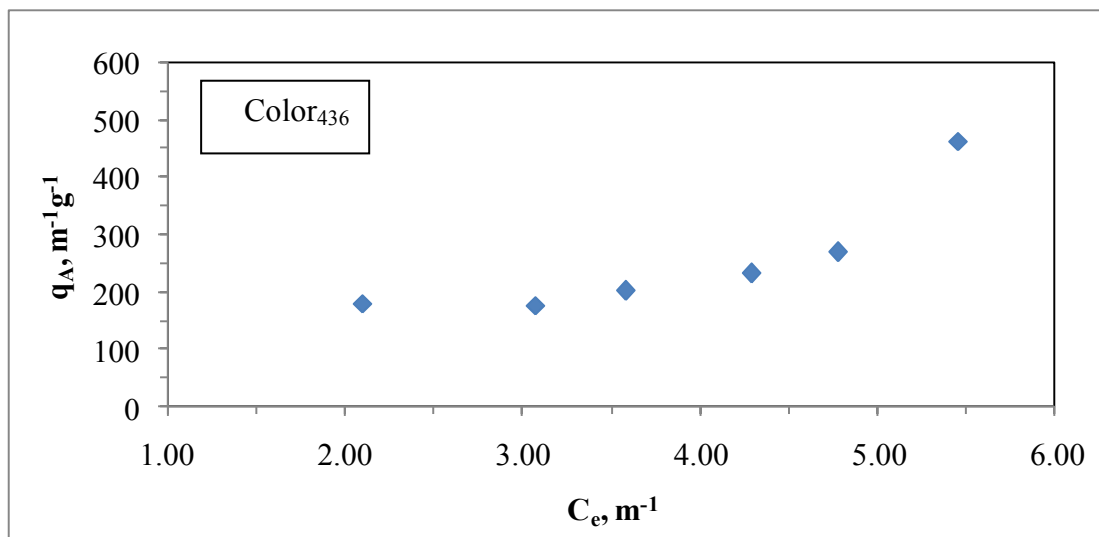
Figure 4.126. Freundlich adsorption isotherm of $Color_{436}$, UV_{254} and DOC parameters of 100 kDa fraction of humic acid following adsorption onto bare TiO_2 Hombikat UV-100.
Table 4.33. Freundlich isotherm model parameters for 100 kDa fraction of humic acid following adsorption onto bare TiO_2 Hombikat UV-100.

Humic acid, 100kDa fraction		
UV-vis parameter	K_f	$1/n$
$Color_{436}$	141.5	1.16
UV_{365}	110.3	1.21
UV_{280}	53.56	1.35
UV_{254}	42.64	1.41
Dissolved Organic Carbon	K_f	$1/n$
DOC	112.4	1.32

Comparison of UV-vis parameters indicated that the adsorption capacity constant of $Color_{436}$ was the highest value. Moreover, adsorption capacity constants of UV_{280} and UV_{254} were nearly equal to each other. The order was $Color_{436} > UV_{365} > UV_{280} > UV_{254}$ for adsorption capacity constant. An increasing order of adsorption intensity could be given as $UV_{254} > UV_{280} > UV_{365} > Color_{436}$. Adsorption intensity of DOC was found to be bigger than 1 representing strong adsorption bond.

Freundlich isotherm model parameters of 100 kDa fraction of humic acid recorded following adsorption onto two different bare TiO_2 specimens were compared (Table 4.23 and Table 4.33). Freundlich isotherm model parameters displayed significantly lower values for bare TiO_2Degussa P-25.

Langmuir adsorption model. Langmuir adsorption isotherms for 100 kDa fraction of humic acid were presented in Figure 4.127 for $Color_{436}$, UV_{254} and DOC parameters. Langmuir isotherms for UV_{365} and UV_{280} were presented in Appendix B.

Two parameters of Langmuir equation outlined in section 2.3, q_m and K_a, were listed in Table 4.34 for 100 kDa fraction of humic acid following adsorption onto bare TiO_2 Hombikat UV-100 ($R^2 \geq 0.68$).
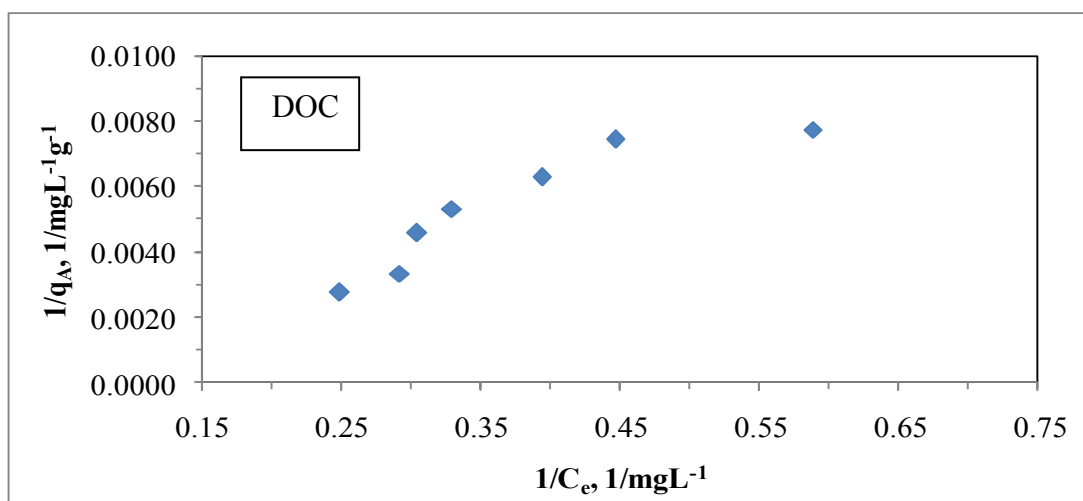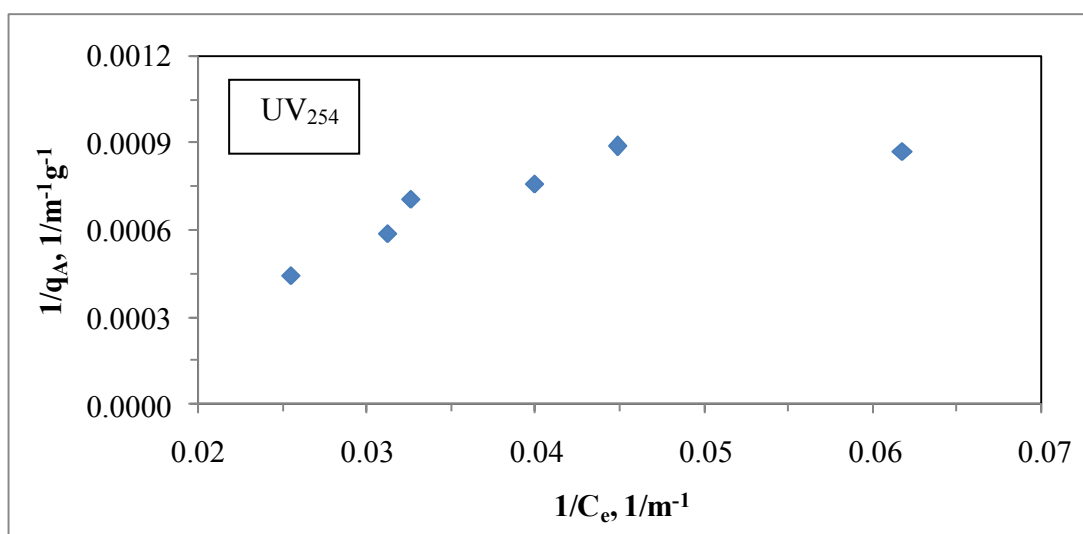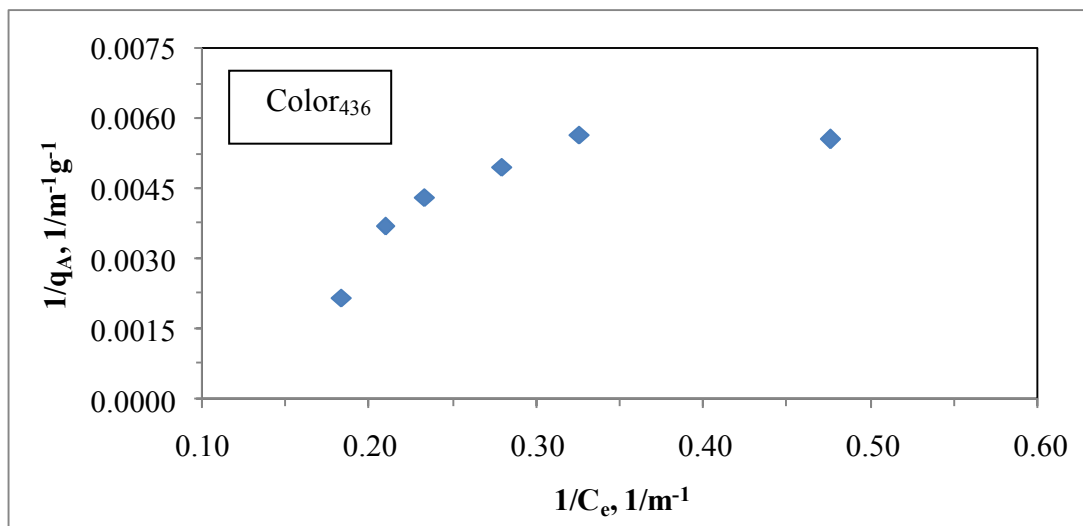
Figure 4.127. Langmuir adsorption isotherm of $Color_{436}$, UV_{254} and DOC parameters of 100 kDa fraction of humic acid following adsorption onto bare TiO_2 Hombikat UV-100.

Table 4.34. Langmuir isotherm model parameters for 100 kDa fraction of humic acid following adsorption onto bare TiO_2 Hombikat UV-100.

Humic acid, 100 kDa fraction		
UV-vis parameter	q_m $m^{-1}g^{-1}$	K_a m^{-1}
$Color_{436}$	20000	0.00800
UV_{365}	50000	0.00300
UV_{280}	25000	0.00600
UV_{254}	50000	0.00300
Dissolved Organic Carbon	q_m mg $L^{-1}g^{-1}$	K_a mg L^{-1}
DOC	2500	0.0490

It could be easily seen from Table 4.34 that q_m and K_a values equal to each other for UV_{365} and UV_{254} spectroscopic parameters. The order of all of UV-vis spectroscopic parameters in terms of q_m value was $UV_{254} = UV_{365} > UV_{280} > Color_{436}$ and this order was reverse for K_a value, namely, $Color_{436} > UV_{280} > UV_{365} = UV_{254}$. The model parameters as q_m and K_a values for DOC were calculated as 2500 mg $L^{-1}g^{-1}$ and 0.0490 mg L^{-1}.

It should be indicated that adsorption of 100 kDa fraction of humic acid onto bare TiO_2 Hombikat UV-100 could well be characterized both by Freundlich and Langmuir adsorption isotherm models.

Langmuir isotherm model parameters of 100 kDa fraction of humic acid recorded following adsorption onto two different TiO_2 (Degussa P-25 and Hombikat UV-100) specimens were compared (Table 4.24 and Table 4.34).

Although a consistent trend could be expressed within the UV-vis parameters and DOC, q_m was significantly higher for bare TiO_2 Hombikat UV-100. Langmuir isotherm model parameter, K_a value was also significantly higher for bare TiO_2 Hombikat UV-100,

namely K_a = 0.143 mg L^{-1} for bare TiO_2 Degussa P-25 and K_a = 0.0490 mg L^{-1} for bare TiO_2 Hombikat UV-100 in terms of DOC.

4.7.2.2. Adsorption Isotherm Modeling of 100 kDa Fraction of Humic Acid onto C-doped TiO_2 Hombikat UV-100 Specimen.

UV-vis spectroscopic parameters ($Color_{436}$, UV_{365}, UV_{280}, and UV_{254}) and DOC were fitted to Freundlich (2.7) and Langmuir (2.6) adsorption isotherm models.

Freundlich adsorption model. Freundlich adsorption isotherms were presented in Figure 4.128 for $Color_{436}$, UV_{254} and DOC parameters. Freundlich isotherms for UV_{365} and UV_{280} were presented in Appendix A.

C_e values altered between 1.06 – 5.28 m^{-1} for $Color_{436}$ according to the loading of C-doped TiO_2 Hombikat UV-100 in the solution. The values of q_A were found in the range of 222 - 532 $m^{-1}g^{-1}$ for the corresponding to the C_e values. ΔC_e and Δq_A values for $Color_{436}$ were calculated as 4.22 m^{-1} and 310 $m^{-1}g^{-1}$; respectively. C_e values altered between 14.26 – 32.27 m^{-1} for UV_{254}. The values of q_A were calculated as between 1532 - 5052 $m^{-1}g^{-1}$ for the corresponding to the C_e values. ΔC_e and Δq_A values for UV_{254} were calculated as 18.01 m^{-1} and 3520 $m^{-1}g^{-1}$, respectively (Figure 4.128).

Adsorption isotherms relatively exhibited similar trend for both of the UV-vis parameters as expressed by $Color_{436}$ and UV_{254} parameters. The trends exhibited by the respective adsorption isotherms could be considered as S-curve type isotherm.

C_e values altered between 1.68 – 3.19 mg L^{-1} for DOC. The values of q_A corresponding to the C_e values were calculated as 130 - 696 mg $L^{-1} g^{-1}$. ΔC_e and Δq_A values for DOC were calculated as 1.51 mg L^{-1} and 566 mg $L^{-1} g^{-1}$, respectively (Figure 4.128).

C-doping of TiO_2 Hombikat UV-100 did not significantly alter the adsorption isotherm trend of 100 kDa fraction of humic acid in comparison to bare TiO_2 Hombikat UV-100 (Figure 4.126 and Figure 4.128)

Freundlich isotherm model coefficients; adsorption capacity, K_f, and adsorption intensity, $1/n$, for 100 kDa fraction of humic acid following adsorption onto C-doped TiO_2 Hombikat UV-100 were listed in Table 4.35 ($R^2 \geq 0.69$).
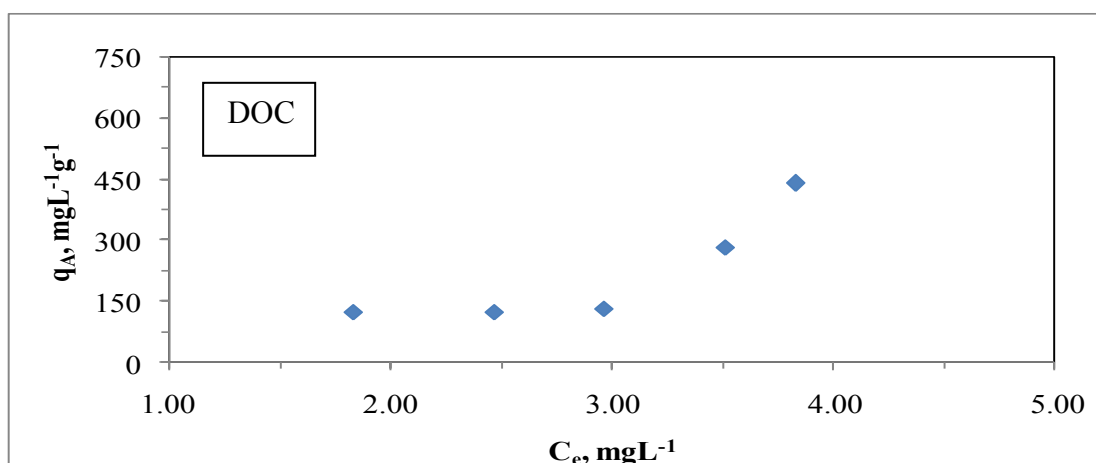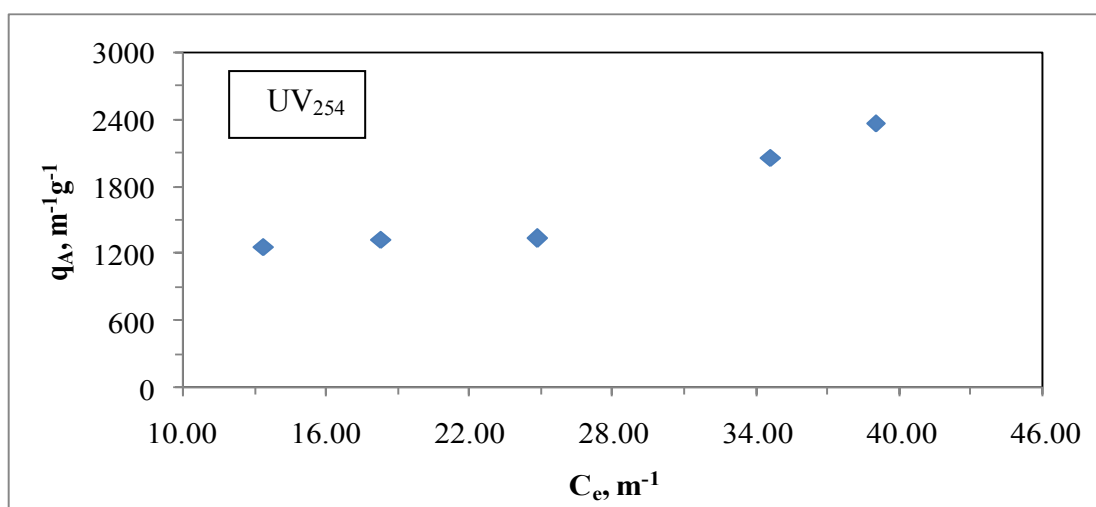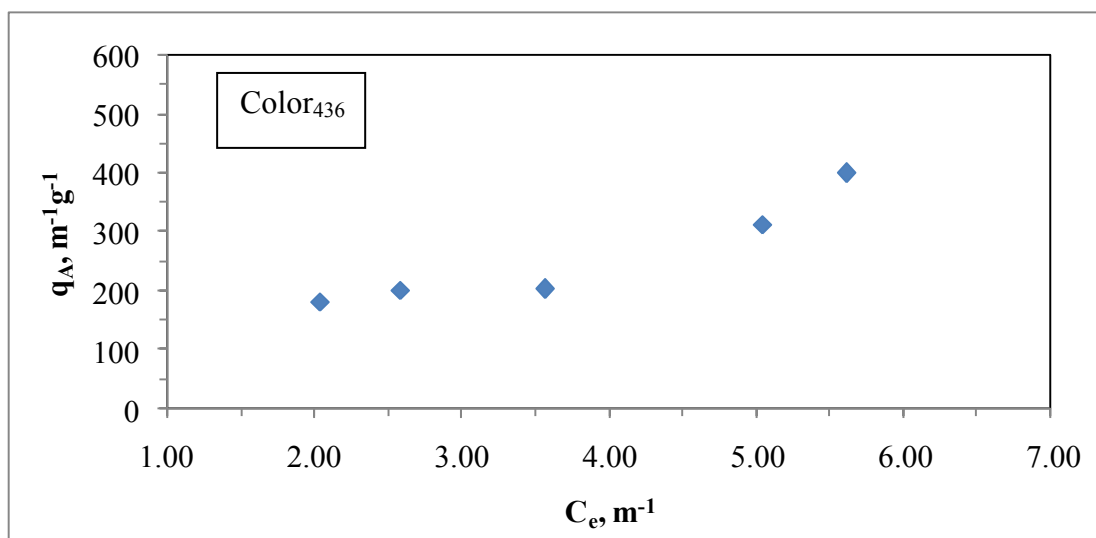
Figure 4.128. Freundlich adsorption isotherm of $Color_{436}$, UV_{254} and DOC parameters of 100 kDa fraction of humic acid following adsorption onto C-doped TiO_2 Hombikat UV-100.

Table 4.35. Freundlich isotherm model parameters for 100 kDa fraction of humic acid following adsorption onto C-doped TiO_2 Hombikat UV-100.

Humic acid, 100kDa fraction		
UV-vis parameter	K_f	1/n
$Color_{436}$	201.7	0.441
UV_{365}	336.3	0.470
UV_{280}	96.25	1.02
UV_{254}	84.12	1.06
Dissolved Organic Carbon	K_f	1/n
DOC	35.73	2.15

Comparison of UV-vis parameters indicated that the adsorption capacity constant of $Color_{436}$ was the lowest value. Moreover, adsorption capacity constants of UV_{280} and UV_{254} were nearly equal to each other. The order was $UV_{254} < UV_{280} < Color_{436} < UV_{365}$ for adsorption capacity constant. Also, adsorption intensity of $Color_{436}$ was the lowest value. Furthermore, adsorption intensity of UV_{280} and UV_{254} were relatively close to each other. The order of adsorption intensity could be given as $Color_{436} < UV_{365} < UV_{280} \leq UV_{254}$. Adsorption intensity of DOC was found to be >1 representing strong adsorption bond.

With reference to the differences observed in adsorption isotherm profiles of bare TiO_2 and C-doped TiO_2 Hombikat UV-100 specimens, the Freundlich isotherm model parameters were significantly different as expected (Table 4.33 and Table 4.35).

Langmuir adsorption model. Langmuir adsorption isotherms for 100 kDa fraction of humic acid following adsorption onto C-doped TiO_2 Hombikat UV-100 were presented in Figure 4.129 for $Color_{436}$, UV_{254} and DOC parameters. Langmuir isotherms for UV_{365} and UV_{280} were presented in Appendix B.

Two parameters of Langmuir equation outlined in section 2.3, q_m and K_a, were listed in Table 4.36 for 100 kDa fraction of humic acid following adsorption onto C- doped TiO_2 Hombikat UV-100 ($R^2 \geq 0.66$).
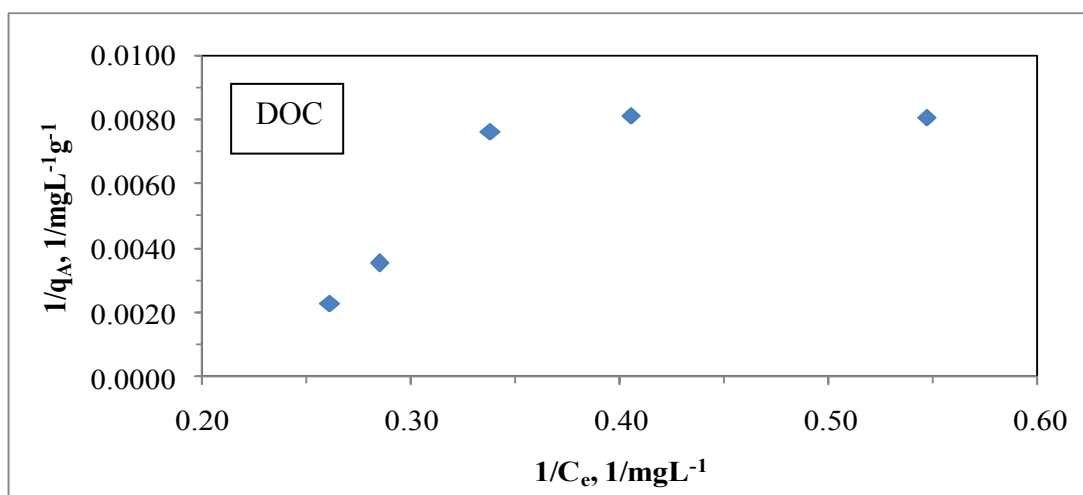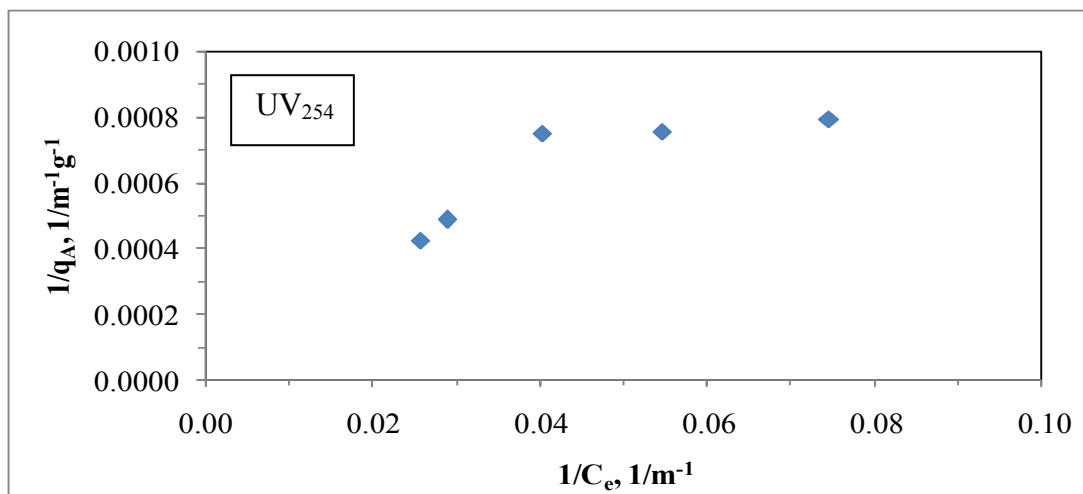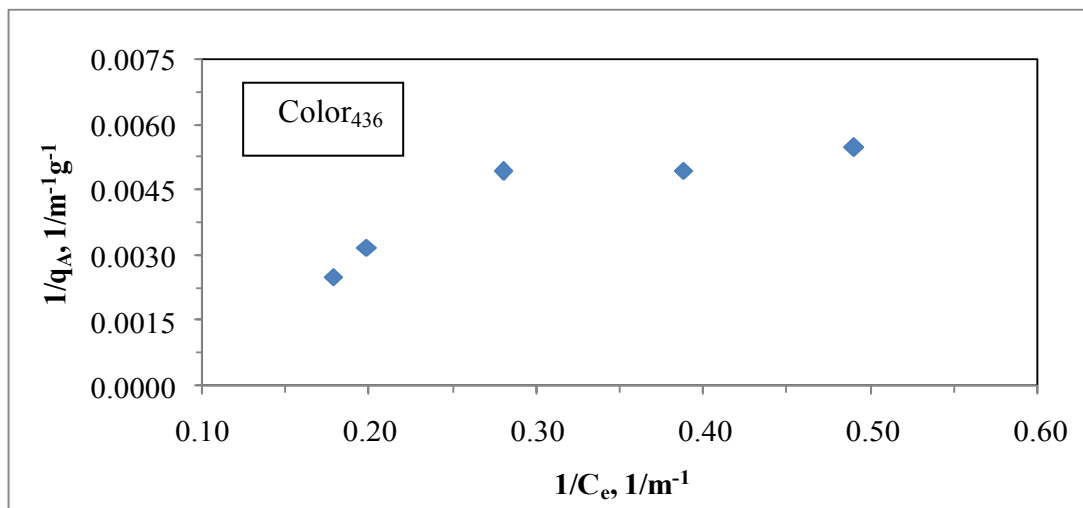
Figure 4.129. Langmuir adsorption isotherm of Color$_{436}$, UV$_{254}$ and DOC parameters of 100 kDa fraction of humic acid following adsorption onto C-doped TiO$_2$ Hombikat UV-100.

Table 4.36. Langmuir isotherm model parameters for 100 kDa fraction of humic acid following adsorption onto C-doped TiO$_2$ Hombikat UV-100.

Humic acid, 100 kDa fraction		
UV-vis parameter	q$_m$ m^{-1}g^{-1}	K$_a$ m^{-1}
Color$_{436}$	500	1.00
UV$_{365}$	1111	0.409
UV$_{280}$	2500	0.160
UV$_{254}$	3333	0.111
Dissolved Organic Carbon	q$_m$ mg L^{-1}g^{-1}	K$_a$ mg L^{-1}
DOC	333	0.150

It could be easily seen from Table 4.36 that q$_m$ value had the highest value in UV$_{254}$ spectroscopic parameter. The order of all of the UV-vis spectroscopic parameters in terms of q$_m$ value was UV$_{254}$ > UV$_{280}$ > UV$_{365}$ > Color$_{436}$ and this order was reverse for K$_a$ value, namely, Color$_{436}$ > UV$_{365}$ > UV$_{280}$ > UV$_{254}$. The model parameters as q$_m$ and K$_a$ values for DOC were calculated as 333 mg L^{-1}g^{-1} and 0.150 mg L^{-1}.

It should be indicated that adsorption of 100 kDa fraction of humic acid onto C-doped TiO$_2$ Hombikat UV-100 could well be characterized both by Freundlich and Langmuir adsorption isotherm models.

Langmuir isotherm model parameters of 100 kDa fraction of humic acid recorded following adsorption onto three different TiO$_2$ specimens were compared (Table 4.34 and Table 4.35).

Comparison of Table 4.34 and Table 4.35 could display the role of C-doping on adsorption of 100 kDa fraction of humic acid onto TiO$_2$ Hombikat UV-100. An inconsistent trend could be visualized for the UV-vis parameters. Langmuir isotherm

model parameters of DOC, q_m was significantly higher for bare TiO_2 Hombikat UV-100 and also K_a values were significantly lower in comparison to C-doped TiO_2 Hombikat UV-100. Moreover, $K_a = 0.0490$ mg L^{-1} for bare TiO_2 Hombikat UV-100 while $K_a = 0.150$ mg L^{-1}. for C-doped TiO_2 Hombikat UV-100.

4.7.2.3. Adsorption Isotherm Modeling of 100 kDa Fraction of Humic Acid onto N-doped TiO_2 Hombikat UV-100 Specimen. UV-vis spectroscopic parameters ($Color_{436}$, UV_{365}, UV_{280} and UV_{254}) and DOC were fitted to Freundlich (2.7) and Langmuir (2.6) adsorption isotherm models.

Freundlich adsorption model. Freundlich adsorption isotherms were presented in Figure 4.130 for $Color_{436}$, UV_{254} and DOC parameters. Freundlich isotherms for UV_{365} and UV_{280} were presented in Appendix A.

C_e values altered between $1.99 - 5.55$ m^{-1} for $Color_{436}$ according to the loading of N-doped TiO_2 Hombikat UV-100 in the solution. The values of q_A were found in the range of $185 - 424$ m^{-1} g^{-1} for the corresponding to the C_e values. ΔC_e and Δq_A values for $Color_{436}$ were calculated as 3.56 m^{-1} and 239 m^{-1} g^{-1}. C_e values altered between $14.98 - 34.70$ m^{-1} for UV_{254}. The values of q_A were calculated as between $1233 - 4268$ m^{-1} g^{-1} for the corresponding to the C_e values. ΔC_e and Δq_A values for UV_{254} were calculated as 19.72 m^{-1} and 2883 m^{-1} g^{-1}, respectively (Figure 4.130).

Adsorption isotherms relatively exhibited similar trend for both of the UV-vis parameters as expressed by $Color_{436}$ and UV_{254} parameters. The trends exhibited by the respective adsorption isotherms could be considered as S-curve type isotherm.

N-doping of TiO_2 Degussa P-25 significantly altered the adsorption isotherm trend of 100 kDa fraction of humic acid in comparison to both bare and C-doped TiO_2 Hombikat UV-100 (Figure 4.126, Figure 4.128 and Figure 4.130).

C_e values altered between $1.83 - 3.97$ mg L^{-1} for DOC. The values of q_A corresponding to the C_e values were calculated as between $124 - 384$ mg L^{-1} g^{-1}. ΔC_e and Δq_A values for DOC were calculated as 2.14 mg L^{-1} and 260 mg L^{-1} g^{-1}, respectively (Figure 4.130).

Freundlich isotherm model coefficients; adsorption capacity, K_f, and adsorption intensity, $1/n$, for 100 kDa fraction of humic acid following adsorption onto N-doped TiO_2 Hombikat UV-100 were listed in Table 4.37 ($R^2 \geq 0.82$).
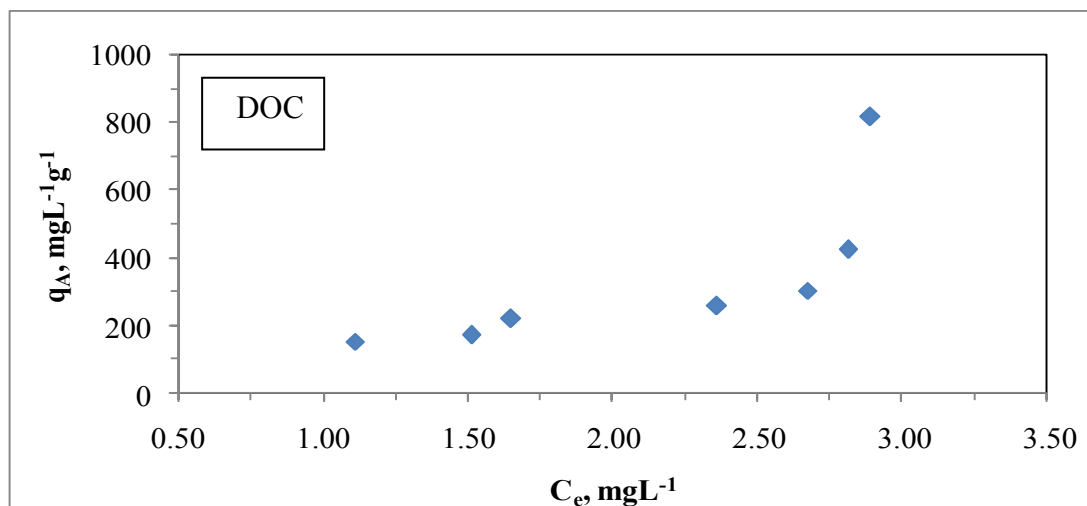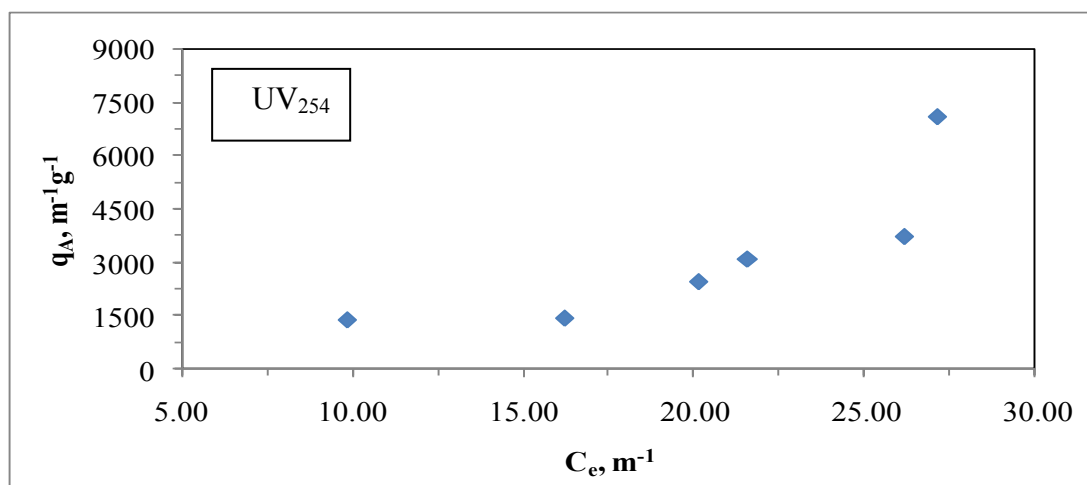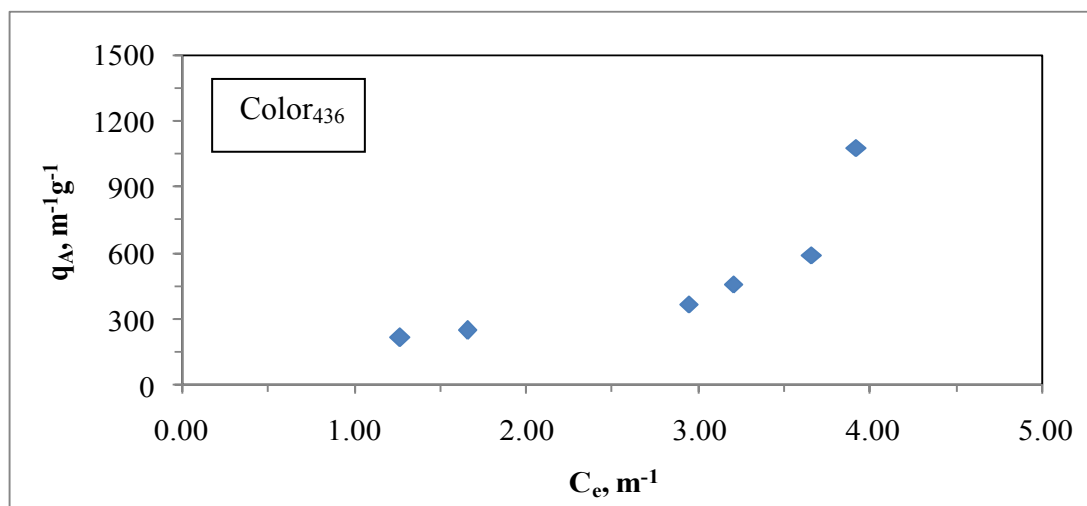
Figure 4.130. Freundlich adsorption isotherm of $Color_{436}$, UV_{254} and DOC parameters of 100 kDa fraction of humic acid following adsorption onto N- doped TiO_2 Hombikat UV-100.

Table 4.37. Freundlich isotherm model parameters for 100 kDa fraction of humic acid following adsorption onto N-doped TiO_2 Hombikat UV-100.

Humic acid, 100kDa fraction		
UV-vis parameter	K_f	$1/n$
$Color_{436}$	92.11	0.871
UV_{365}	75.63	1.05
UV_{280}	54.63	1.11
UV_{254}	46.89	1.16
Dissolved Organic Carbon	K_f	$1/n$
DOC	54.35	1.32

Comparison of UV-vis parameters indicated that the adsorption capacity constant of $Color_{436}$ was the highest value. The order was $Color_{436} > UV_{365} > UV_{280} > UV_{254}$ for adsorption capacity constant. Also, adsorption intensity of $Color_{436}$ was the lowest value. Furthermore, the order was $Color_{436} < UV_{365} < UV_{280} \leq UV_{254}$ for adsorption intensity. Adsorption intensity of DOC was found to be >1 representing strong adsorption bond.

Comparative evaluation of Freundlich isotherm model parameter, K_f of 100 kDa fraction of humic acid with 0.45 μm filtration fraction of humic acid did not reveal the most significant difference in both UV-vis parameters and DOC.

Langmuir adsorption model. Langmuir adsorption isotherms for 100 kDa fraction of humic acid following adsorption onto N-doped TiO_2 Hombikat UV-100 were presented in Figure 4.131 for $Color_{436}$, UV_{254} and DOC parameters. Langmuir isotherms for UV_{365} and UV_{280} were presented in Appendix B.

Two parameters of Langmuir equation outlined in section 2.3, q_m and K_a, were listed in Table 4.38 for 100 kDa fraction of humic acid following adsorption onto N- doped TiO_2 Hombikat UV-100 ($R^2 \geq 0.83$).
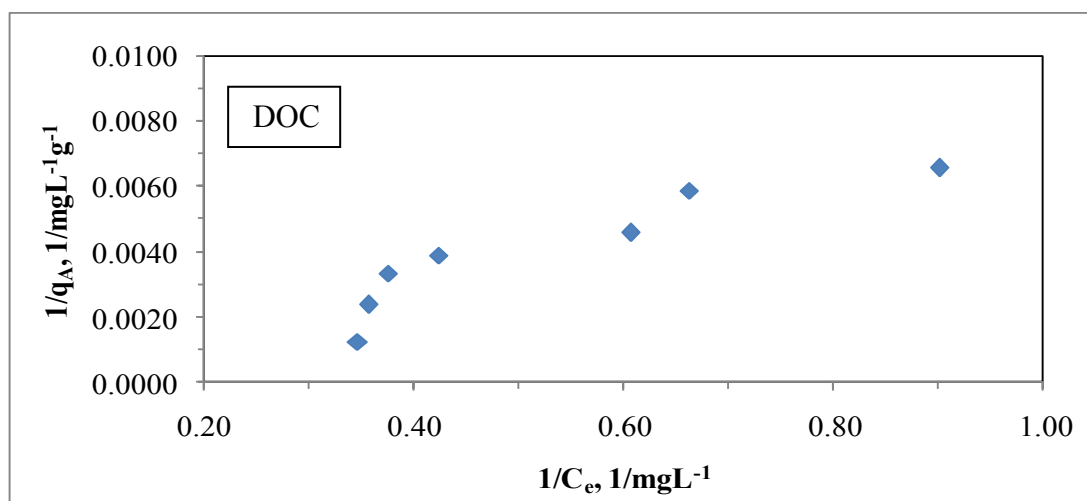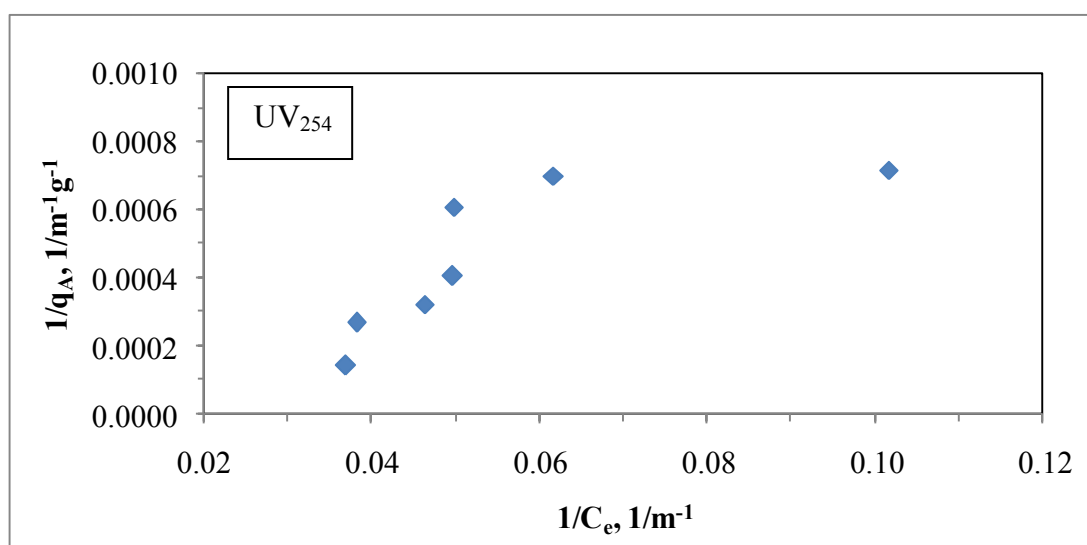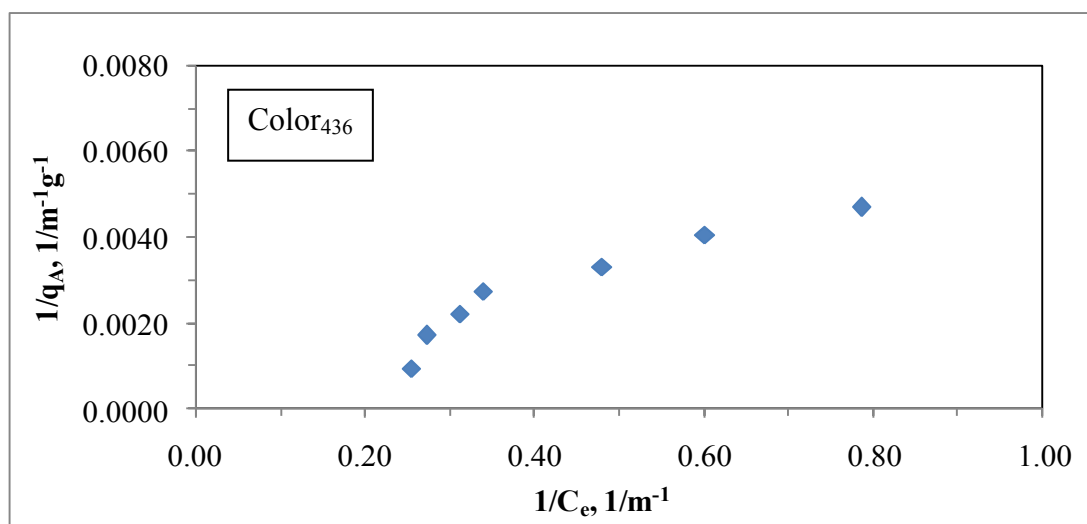
Figure 4.131. Langmuir adsorption isotherm of Color$_{436}$, UV$_{254}$ and DOC parameters of 100 kDa fraction of humic acid following adsorption onto N- doped TiO$_2$ Hombikat UV-100.

Table 4.38. Langmuir isotherm model parameters for 100 kDa fraction of humic acid following adsorption onto N-doped TiO_2 Hombikat UV-100.

Humic acid, 100 kDa fraction		
UV-vis parameter	q_m $m^{-1}g^{-1}$	K_a m^{-1}
$Color_{436}$	1250	0.0400
UV_{365}	10000	0.00900
UV_{280}	100000	0.00100
UV_{254}	50000	0.00200
Dissolved Organic Carbon	q_m mg $L^{-1}g^{-1}$	K_a mg L^{-1}
DOC	1000	0.0590

It could be easily seen from Table 4.38 that the highest value of q_m was in UV_{365} spectroscopic parameters. The order of all of the UV-vis spectroscopic parameters in terms of q_m value was $Color_{436} < UV_{365} < UV_{254} < UV_{280}$ and this order was $UV_{280} < UV_{254} < UV_{365} < Color_{436}$ for K_a. The model parameters as q_m and K_a values for DOC were calculated as 1000 mg $L^{-1}g^{-1}$ and 0.0590 mg L^{-1}.

It should be indicated that adsorption of 100 kDa fraction of humic acid onto N-doped TiO_2 Hombikat UV-100 could well be characterized both by Freundlich and Langmuir adsorption isotherm models.

Langmuir isotherm model parameters of 100 kDa fraction of humic acid recorded following adsorption onto three different TiO_2 specimens were compared (Table 4.34, Table 4.36 and Table 4.38). Langmuir isotherm model parameter, q_m was found to be significantly higher than the values calculated from the data attained in case of C-doped TiO_2 Hombikat UV-100 (Table 4.36 and Table 4.38) for both UV-vis parameters and DOC. Langmuir isotherm model parameter, K_a was found to be slightly different for diverse TiO_2 Hombikat UV-100 specimens, namely K_a = 0.0490 mg L^{-1} for bare TiO_2 Hombikat UV-100 and K_a = 0.150 mg L^{-1} for C-doped TiO_2 Hombikat UV-100 as well as K_a = 0.0590 mg L^{-1} for N-doped TiO_2 Hombikat UV-100 in terms of DOC (Table 4.34, Table 4.36 and Table 4.38). Comparison of N-doping with bare TiO_2 Hombikat UV-100 could be regarded as non-discriminating between the effects of dopants.

4.7.2.4. Adsorption Isotherm Modeling of 100 kDa Fraction of Humic Acid onto S-doped TiO$_2$ Hombikat UV-100 Specimen. UV-vis spectroscopic parameters (Color$_{436}$, UV$_{365}$, UV$_{280}$ and UV$_{254}$) and DOC were fitted to Freundlich (2.7) and Langmuir (2.6) adsorption isotherm models.

Freundlich adsorption model. Freundlich adsorption isotherms were presented in Figure 4.132 for Color$_{436}$, UV$_{254}$ and DOC parameters. Freundlich isotherms for UV$_{365}$ and UV$_{280}$ were presented in Appendix A.

C$_e$ values altered between 2.33 – 4.65 m^{-1} for Color$_{436}$ according to the loading of S-doped TiO$_2$ Hombikat UV-100 in the solution. The values of q$_A$ were found in the range of 171-784 m^{-1}g^{-1} for the corresponding to the C$_e$ values. ΔC$_e$ and Δq$_A$ values for Color$_{436}$ were calculated as 2.32m^{-1} and 613 m^{-1} g^{-1}, respectively. C$_e$ values altered between 13.62 – 32.21 m^{-1} for UV$_{254}$. The values of q$_A$ were calculated as between 1251 - 5076 m^{-1} g^{-1} for the corresponding to the C$_e$ values. ΔC$_e$ and Δq$_A$ values for UV$_{254}$ were calculated as 18.59 m^{-1} and 3825 m^{-1} g^{-1}, respectively (Figure 4.132).

Adsorption isotherms relatively exhibited similar trend for both of the UV-vis parameters as expressed by Color$_{436}$ and UV$_{254}$ parameters. The trends exhibited by the respective adsorption isotherms could be considered as C-curve type isotherm.

The role of S-doping could be visualized in adsorption isotherm profiles of UV-vis parameters. S-doping of TiO$_2$ Hombikat UV-100 affected the adsorption isotherm profiles of UV-vis spectral parameters as well as DOC in comparison to the bare TiO$_2$ Hombikat UV-100 (Figure 4.126 and Figure 4.132).

C$_e$ values altered between 1.49 - 3.87 mg L^{-1} for DOC. The values of q$_A$ corresponding to the C$_e$ values were calculated as between 138 - 424 mg L^{-1} g^{-1}. ΔC$_e$ and Δq$_A$ values for DOC were calculated as 2.38 mg L^{-1} and 286 mg L^{-1} g^{-1}, respectively (Figure 4.132). Freundlich isotherm model coefficients; adsorption capacity, K$_f$, and adsorption intensity, 1/n, for 100 kDa fraction of humic acid following adsorption onto S-doped TiO$_2$ Hombikat UV-100 were listed in Table 4.39 (R$^2 \geq$0.96).
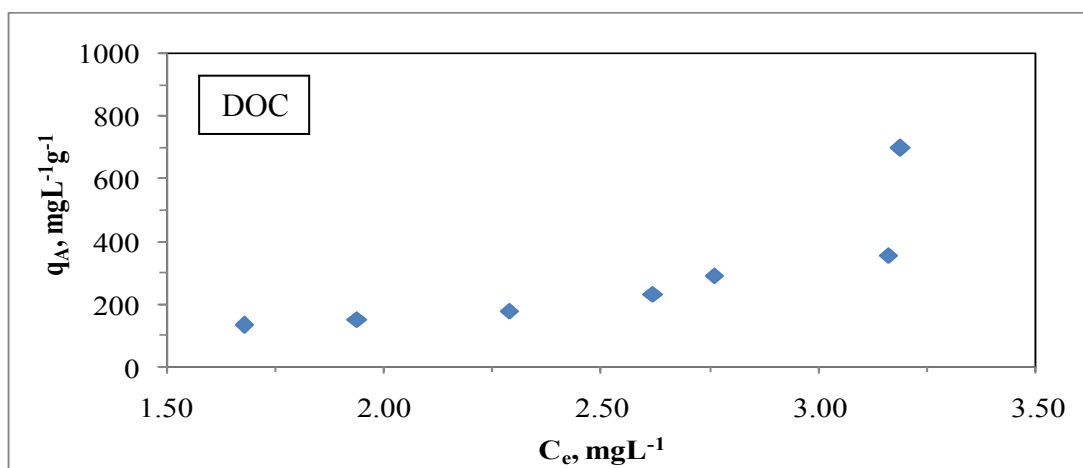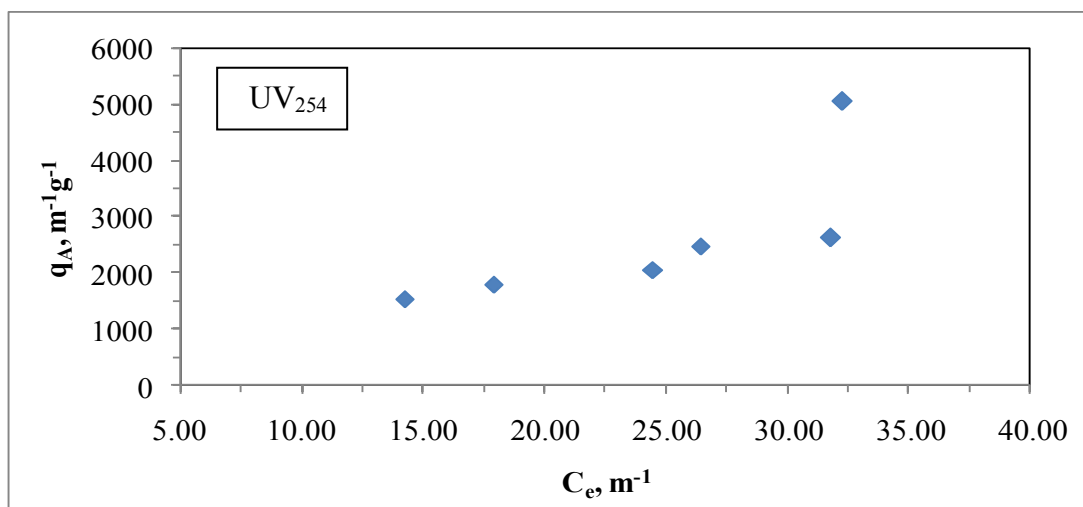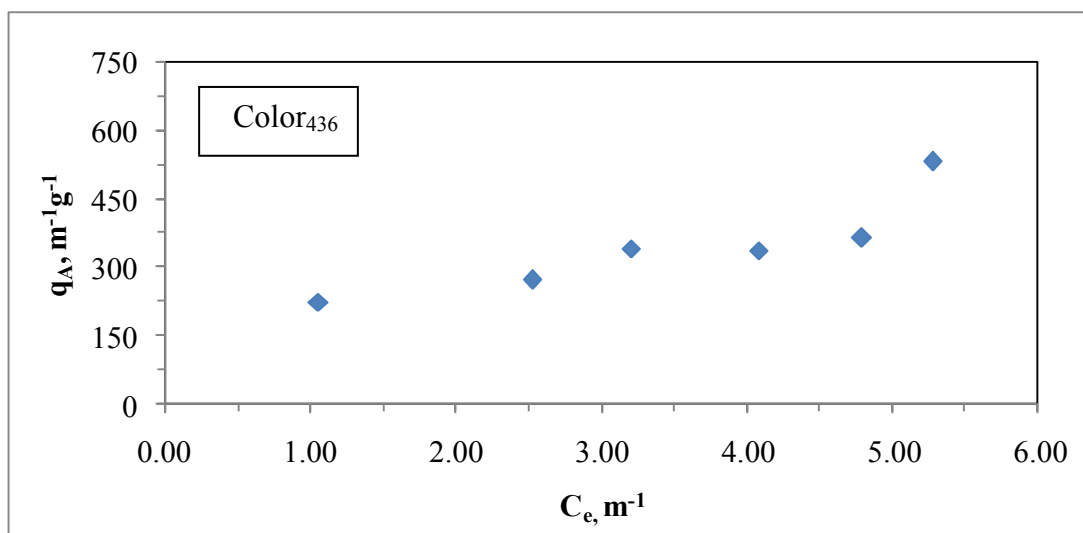
Figure 4.132. Freundlich adsorption isotherm of $Color_{436}$, UV_{254} and DOC parameters of 100 kDa fraction of humic acid following adsorption onto S-doped TiO_2 Hombikat UV-100.

Table 4.39. Freundlich isotherm model parameters for 100 kDa fraction of humic acid following adsorption onto S-doped TiO_2 Hombikat UV-100.

Humic acid, 100kDa fraction		
UV-vis parameter	K_f	$1/n$
$Color_{436}$	38.19	1.93
UV_{365}	40.05	1.61
UV_{280}	26.78	1.53
UV_{254}	24.04	1.54
Dissolved Organic Carbon	K_f	$1/n$
DOC	82.95	1.05

Comparison of UV-vis parameters indicated that the adsorption capacity constant of UV_{254} was the lowest value. Moreover, adsorption capacity constant of UV_{365} was the highest value. The order was $UV_{254} < UV_{280} < Color_{436} < UV_{365}$ for adsorption capacity constant. Also, adsorption intensity of UV_{280} was the lowest value. Furthermore, adsorption intensity of $Color_{436}$ had the highest value. A decreasing order of adsorption intensity could be given as $Color_{436} > UV_{365} > UV_{254} \geq UV_{280}$. Adsorption intensity of DOC was found to be >1 representing strong adsorption bond.

Freundlich isotherm model parameters of DOC for 100 kDa fraction of humic acid following adsorption onto TiO_2 Hombikat UV-100 could be expressed by a decreasing order for K_f : N-S co-doped TiO_2 > bare TiO_2 > S-doped TiO_2 > N-doped TiO_2 > C-doped TiO_2 for $1/n$: C-doped TiO_2 > N-doped TiO_2 = bare TiO_2 > S-doped TiO_2 >. N-S co-doped TiO_2.

Langmuir adsorption model. Langmuir adsorption isotherms for 100 kDa fraction of humic acid following adsorption onto S-doped TiO_2 Hombikat UV-100 were presented in Figure 4.133 for $Color_{436}$, UV_{254} and DOC parameters. Langmuir isotherms for UV_{365} and UV_{280} were presented in Appendix B. Two parameters of Langmuir equation outlined in section 2.3, q_m and K_a, were listed in Table 4.40 for 100 kDa fraction of humic acid following adsorption onto S- doped TiO_2 Hombikat UV-100 ($R^2 \geq 0.94$).
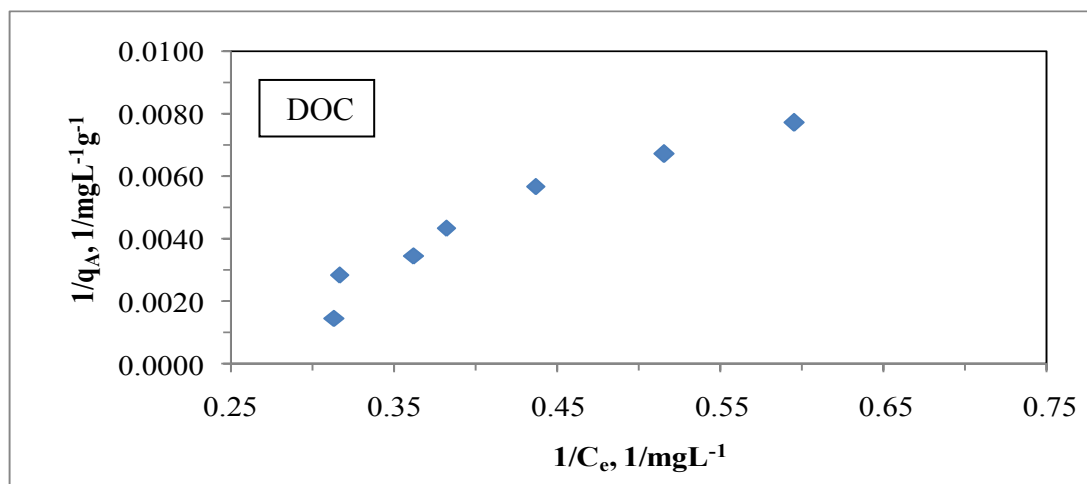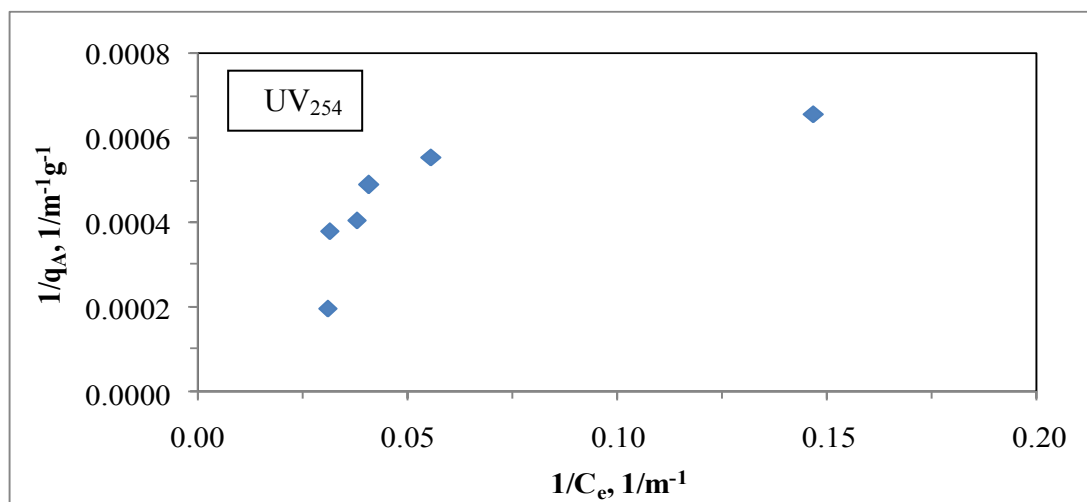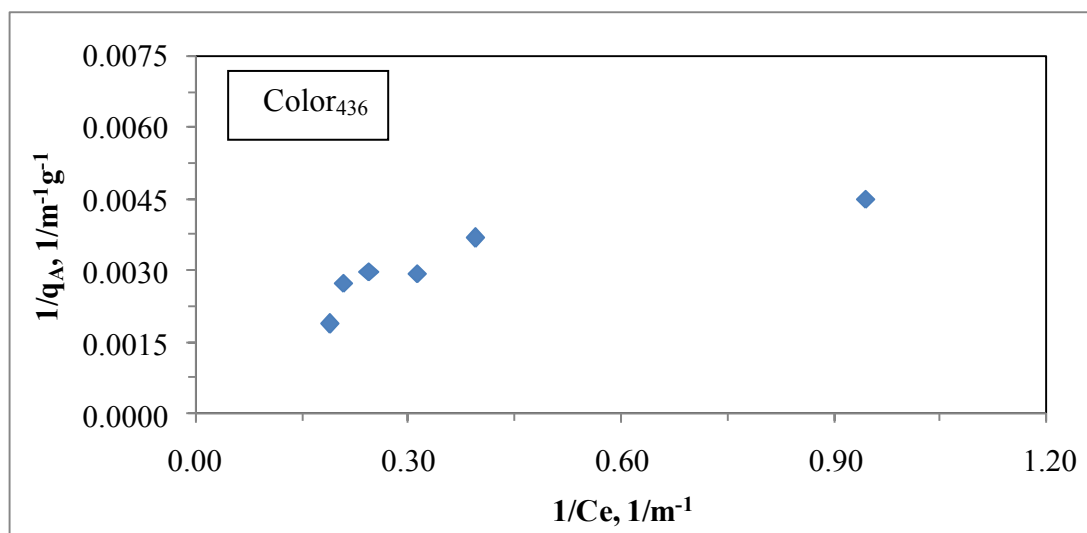
Figure 4.133. Langmuir adsorption isotherm of Color$_{436}$, UV$_{254}$ and DOC parameters of 100 kDa fraction of humic acid following adsorption onto S-doped TiO$_2$ Hombikat UV-100.

Table 4.40. Langmuir isotherm model parameters for 100 kDa fraction of humic acid following adsorption onto S-doped TiO_2 Hombikat UV-100.

Humic acid, 100 kDa fraction		
UV-vis parameter	q_m $m^{-1}g^{-1}$	K_a m^{-1}
Color$_{436}$	500	0.111
UV_{365}	1250	0.0500
UV_{280}	3333	0.0230
UV_{254}	5000	0.0150
Dissolved Organic Carbon	q_m mg $L^{-1}g^{-1}$	K_a mg L^{-1}
DOC	3333	0.0280

It could be easily seen from Table 4.40 that the order of all of the UV-vis spectroscopic parameters in terms of q_m value was $UV_{254} > UV_{280} > UV_{365} > Color_{436}$. It could be easily seen from Table 4.40 that a decreasing order of K_a value could be given as $Color_{436} > UV_{365} > UV_{280} > UV_{254}$. The model parameters as q_m and K_a values for DOC were calculated as 3333 mg $L^{-1}g^{-1}$ and 0.0280 mg L^{-1}.

It should be indicated that adsorption of 100 kDa fraction of humic acid onto S-doped TiO_2 Hombikat UV-100 could well be characterized both by Freundlich and Langmuir adsorption isotherm models.

Langmuir isotherm model parameters of 100 kDa fraction of humic acid recorded following adsorption onto four different TiO_2 specimens were compared (Table 4.34, Table 4.36, Table 4.38 and Table 4.40). A consistent trend could be visualized for the UV-vis parameters (Table 4.34, Table 4.36 and Table 4.38 as well as Table 4.40) upon comparison of the Langmuir isotherm model parameters, q_m and K_a. Langmuir isotherm model parameters of DOC could be presented in a decreasing order of; for q_m: S-doped TiO_2> bare TiO_2 > N-doped TiO_2 > C-doped TiO_2 for Ka: C-doped TiO_2 >N-doped TiO_2 > bare TiO_2 > S-doped TiO_2. Comparative evaluation of Langmuir isotherm model parameters of 100 kDa fraction of humic acid with 0.45 μm filtration fraction of humic acid following adsorption onto S-doped TiO_2 Hombikat UV-100 revealed the most significant difference in both UV-vis parameters and DOC especially for K_a values.

4.7.2.5. Adsorption Isotherm Modeling of 100 kDa Fraction of Humic Acid onto N-S co-doped TiO$_2$ Hombikat UV-100 Specimen. UV-vis spectroscopic parameters (Color$_{436}$, UV$_{365}$, UV$_{280}$, and UV$_{254}$) and DOC were fitted to Freundlich (2.7) and Langmuir (2.6) adsorption isotherm models.

Freundlich adsorption model. Freundlich adsorption isotherms were presented in Figure 4.134 for Color$_{436}$, UV$_{254}$ and DOC, respectively. Freundlich isotherms for UV$_{365}$ and UV$_{280}$ were presented in Appendix A.

C$_e$ values altered between 1.09 – 4.71 m^{-1} for Color$_{436}$ according to the loading of N-S co-doped TiO$_2$ Hombikat UV-100 in the solution. The values of q$_A$ were found in the range of 221 - 760 m^{-1} g^{-1} for the corresponding to C$_e$ values. ΔC$_e$ and Δq$_A$ values for Color$_{436}$ were calculated as 3.62 m^{-1} and 539 m^{-1} g^{-1}, respectively. C$_e$ values altered between 3.98 – 34.29 m^{-1} for UV$_{254}$. The calculated values of q$_A$ were in the range of 1637 - 4244 m^{-1} g^{-1} for the corresponding to the C$_e$ values. ΔC$_e$ and Δq$_A$ values for UV$_{254}$ were calculated as 30.31 m^{-1} and 2607 m^{-1} g^{-1}, respectively (Figure 4.134).

Adsorption isotherms relatively exhibited similar trend for both of the UV-vis parameters as expressed by Color$_{436}$ and UV$_{254}$ parameters. The trends exhibited by the respective adsorption isotherms could be considered as L-curve type isotherm.

The role of N-S co-doping could be visualized in adsorption isotherm profiles of UV-vis parameters. N-S co-doping of TiO$_2$ Hombikat UV-100 affected the adsorption isotherm profiles of UV-vis spectral parameters as well as DOC in comparison to the bare TiO$_2$ Hombikat UV-100 (Figure 4.126 and Figure 4.134).

C$_e$ values altered between 0.65 - 3.98 mg L^{-1} for DOC. The values of q$_A$ corresponding to the C$_e$ values were calculated as between 171 - 380 mg L^{-1} g^{-1}. ΔC$_e$ and Δq$_A$ values for DOC were calculated as 3.33 mg L^{-1} and 209 mg L^{-1} g^{-1}, respectively (Figure 4.134). Freundlich isotherm model coefficients; adsorption capacity, K$_f$, and adsorption intensity, 1/n, for 100 kDa fraction of humic acid following adsorption onto N-S co-doped TiO$_2$ Hombikat UV-100 were listed in Table 4.41 (R$^2 \geq 0.76$).
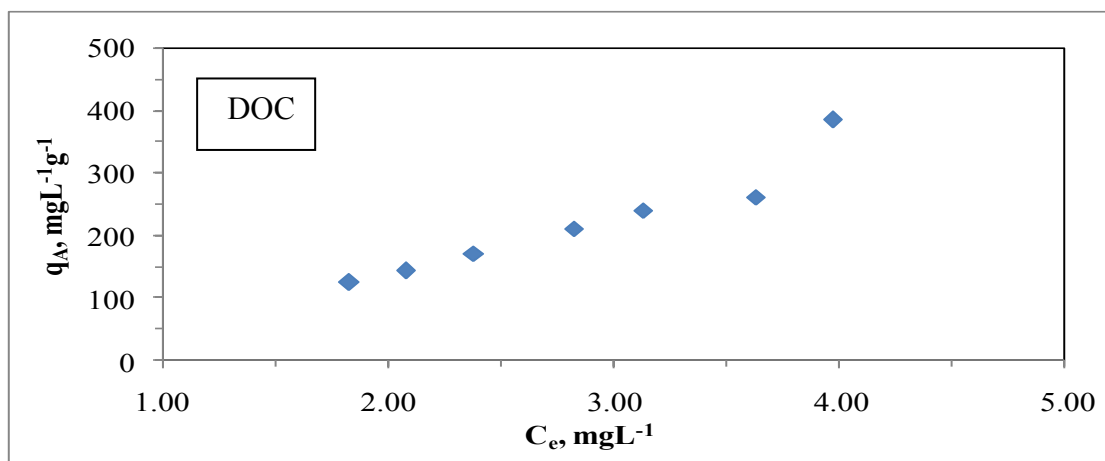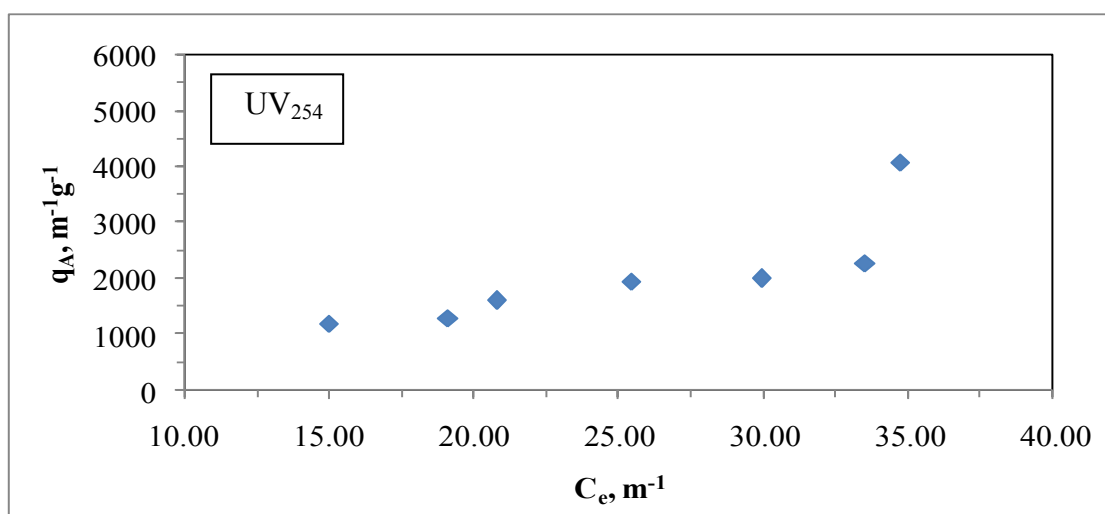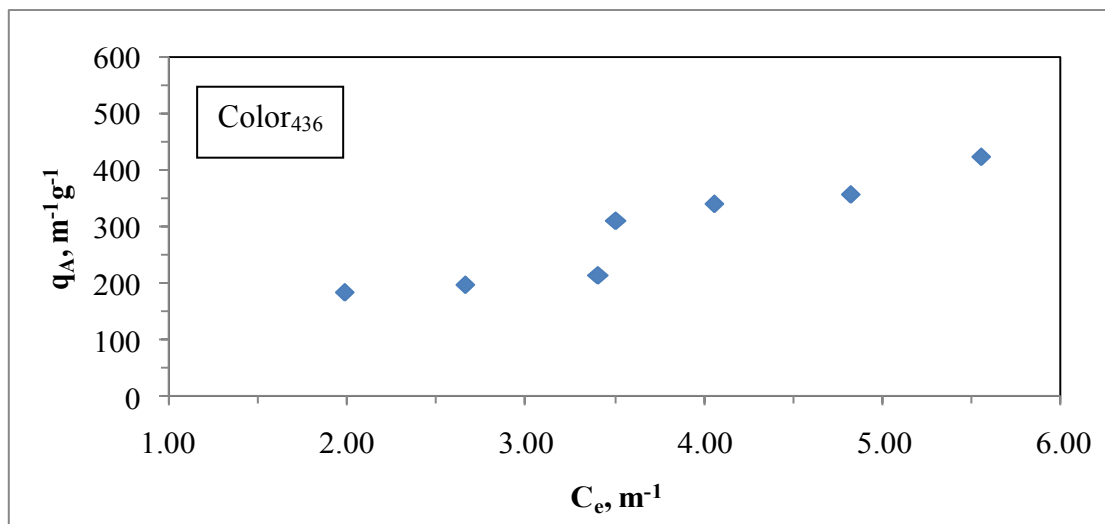
Figure 4.134. Freundlich adsorption isotherm of Color$_{436}$, UV$_{254}$ and DOC parameters of 100 kDa fraction of humic acid following adsorption onto N-S co-doped TiO$_2$ Hombikat UV-100.

Table 4.41. Freundlich isotherm model parameters for 100 kDa fraction of humic acid following adsorption onto N-S co-doped TiO_2 Hombikat UV-100.

Humic acid, 100kDa fraction		
UV-vis parameter	K_f	$1/n$
$Color_{436}$	201.5	0.643
UV_{365}	299.9	0.616
UV_{280}	740.0	0.391
UV_{254}	830.9	0.385
Dissolved Organic Carbon	K_f	$1/n$
DOC	182.3	0.322

According to Table 4.41, adsorption capacity constant of $Color_{436}$ was the lowest value. The order was $Color_{436} < UV_{365} < UV_{280} < UV_{254}$ for adsorption capacity constant. Furthermore, adsorption intensity values of $Color_{436}$ and UV_{365} were equal to each other and they had the highest values in contrast to adsorption intensity values of UV_{280} and UV_{254}. A decreasing order of adsorption intensity values could be given as $Color_{436} \geq UV_{365} > UV_{280} \geq UV_{254}$.

Freundlich isotherm model parameters of DOC for 100 kDa fraction of humic acid could be expressed by a decreasing order for K_f: N-S co-doped TiO_2 > bare TiO_2 > S-doped TiO_2 > N-doped TiO_2 > C-doped TiO_2 for $1/n$: C-doped TiO_2 > N-doped TiO_2 = bare TiO_2 > S-doped TiO_2 >.N-S co-doped TiO_2 Hombikat UV-100.

Langmuir adsorption model. Langmuir adsorption isotherms for 100 kDa fraction of humic acid following adsorption onto N-S co-doped TiO_2 Hombikat UV-100 were presented in Figure 4.135 for $Color_{436}$, UV_{254} and DOC parameters. Langmuir isotherms for UV_{365} and UV_{280} were presented in Appendix B.

Two parameters of Langmuir equation outlined in section 2.3, q_m and K_a, were listed in Table 4.42 for 100 kDa fraction of humic acid following adsorption onto N-S co- doped TiO_2 Hombikat UV-100 ($R^2 \geq 0.67$).
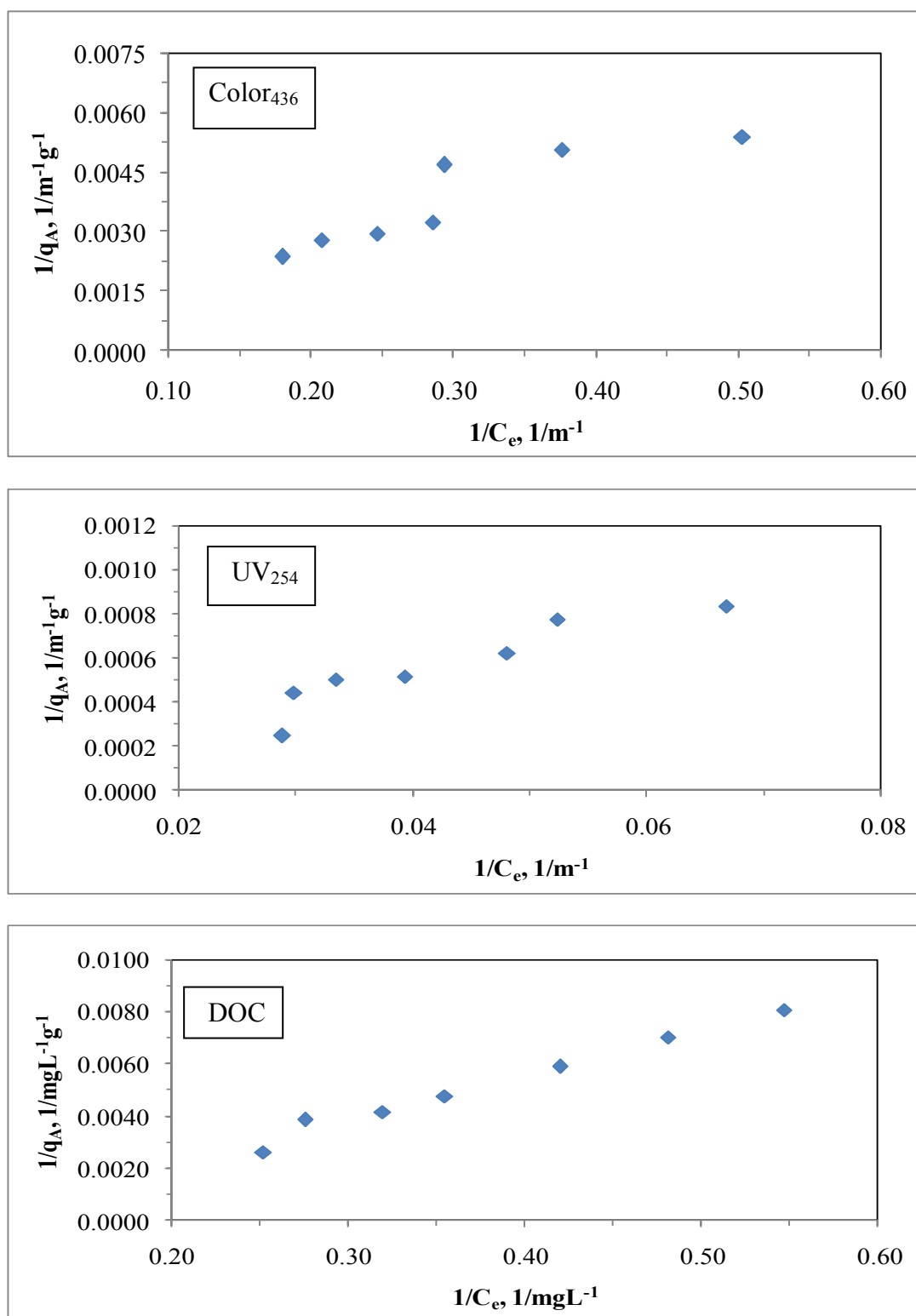
Figure 4.135. Langmuir adsorption isotherm of Color$_{436}$, UV$_{254}$ and DOC parameters of 100 kDa fraction of humic acid following adsorption onto N-S co-doped TiO$_2$ Hombikat UV-100.

Table 4.42. Langmuir isotherm model parameters for 100 kDa fraction of humic acid following adsorption onto N-S co-doped TiO_2 Hombikat UV-100.

Humic acid, 100 kDa fraction		
UV-vis parameter	q_m m^{-1}g^{-1}	K_a m^{-1}
Color$_{436}$	1000	0.333
UV$_{365}$	1429	0.292
UV$_{280}$	2500	0.286
UV$_{254}$	3333	0.231
Dissolved Organic Carbon	q_m mg L^{-1}g^{-1}	K_a mg L^{-1}
DOC	294	1.90

It could be easily seen from Table 4.42 that the highest value of q_m was in UV$_{254}$ spectroscopic parameter. The order of all of UV-vis spectroscopic parameters in terms of q_m value was Color$_{436}$ < UV$_{365}$ < UV$_{280}$ < UV$_{254}$ and a decreasing order of K_a values could be given as UV$_{254}$ < UV$_{280}$ < UV$_{365}$ < Color$_{436}$. The model parameters as q_m and K_a values for DOC were calculated as 294 mg L^{-1}g^{-1} and 1.90 mg L^{-1}.

It should be indicated that adsorption of 100 kDa fraction of humic acid onto N-S co-doped TiO_2 Hombikat UV-100 could well be characterized both by Freundlich and Langmuir adsorption isotherm models.

Langmuir isotherm model parameters of 100 kDa fraction of humic acid recorded following adsorption onto different TiO_2 specimens were compared (Table 4.34, Table 4.36, Table 4.38, Table 4.40 and Table 4.42). Langmuir isotherm model parameters of DOC could be expressed in a decreasing order of; q_m: S-doped TiO_2 > bare TiO_2 > N-doped TiO_2 > C-doped TiO_2 > N-S co-doped TiO_2 K_a: N-S co-doped TiO_2 > C-doped TiO_2 > N-doped TiO_2 > bare TiO_2 > S-doped TiO_2. Comparative evaluation of Langmuir isotherm model parameters of 100 kDa fraction of humic acid with 0.45 μm filtration fraction of humic acid following adsorption onto N-S co-doped TiO_2 Hombikat UV-100 revealed the most significant difference in both UV-vis parameters and DOC.

4.8. Adsorption Isotherm Modeling of 30 kDa Fraction of Humic Acid onto TiO$_2$ Specimens

The data obtained for the adsorption of 30 kDa fraction of humic acid onto TiO$_2$ specimens were fitted to both Freundlich and Langmuir isotherm models. Freundlich isotherm model was explained with equation (2.7) as outlined in the theoretical background section and Langmuir isotherm model was expressed with equation (2.6).

4.8.1. Adsorption Isotherm Modeling of 30 kDa Fraction of Humic Acid onto TiO$_2$ Degussa P-25 Specimens

The experimental data related to 30 kDa fraction of humic acid following adsorption onto TiO$_2$ Degussa P-25 specimens were fitted to both Freundlich and Langmuir isotherm models.

4.8.1.1. Adsorption Isotherm Modeling of 30 kDa Fraction of Humic Acid onto Bare TiO$_2$ Degussa P-25 Specimen. UV-vis spectroscopic parameters (Color$_{436}$, UV$_{365}$, UV$_{280}$, and UV$_{254}$) and DOC were fitted to Freundlich (2.7) and Langmuir (2.6) adsorption isotherm models.

Freundlich adsorption model. Freundlich adsorption isotherms were presented in Figure 4.136 for Color$_{436}$, UV$_{254}$ and DOC parameters. Freundlich isotherms for UV$_{365}$ and UV$_{280}$ were presented in Appendix A.

C$_e$ values altered between 0.57 – 2.23 m^{-1} for Color$_{436}$ according to the loading of bare TiO$_2$ Degussa P-25 in the solution. The calculated values of q$_A$ were in the range of 118 – 520 m^{-1} g^{-1} for the corresponding to the C$_e$ values. ΔC$_e$ and Δq$_A$ values for 30 kDa fraction of humic acid were calculated as 1.66 m^{-1} and 402 m^{-1} g^{-1} for Color$_{436}$. C$_e$ values altered between 6.20 – 18.94 m^{-1} for UV$_{254}$. The values of q$_A$ were calculated as between 752 – 2424 m^{-1} g^{-1} for the corresponding to the C$_e$ values. ΔC$_e$ and Δq$_A$ values for UV$_{254}$ were found as 12.74 m^{-1} and 1672 m^{-1} g^{-1}, respectively (Figure 4.136).
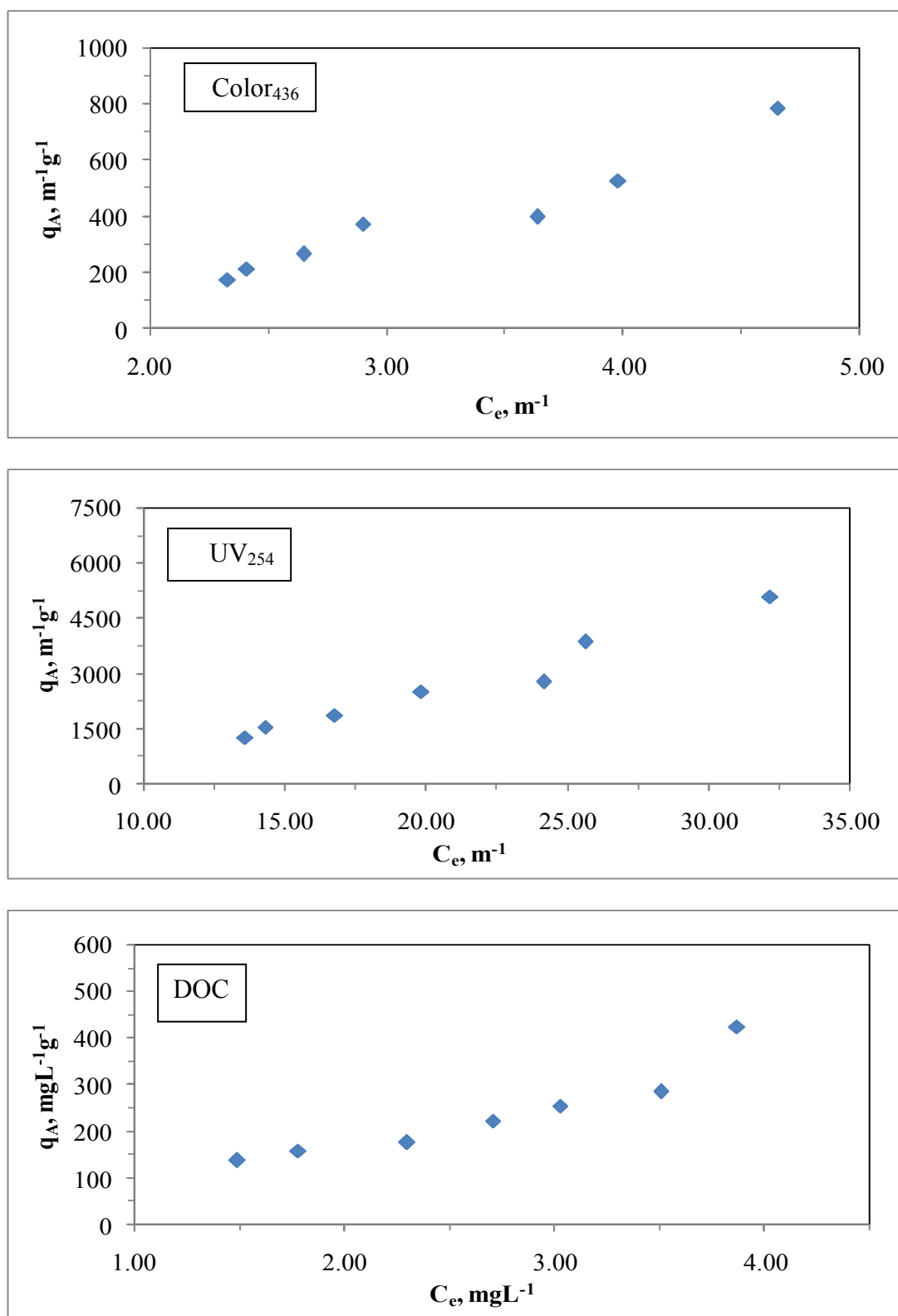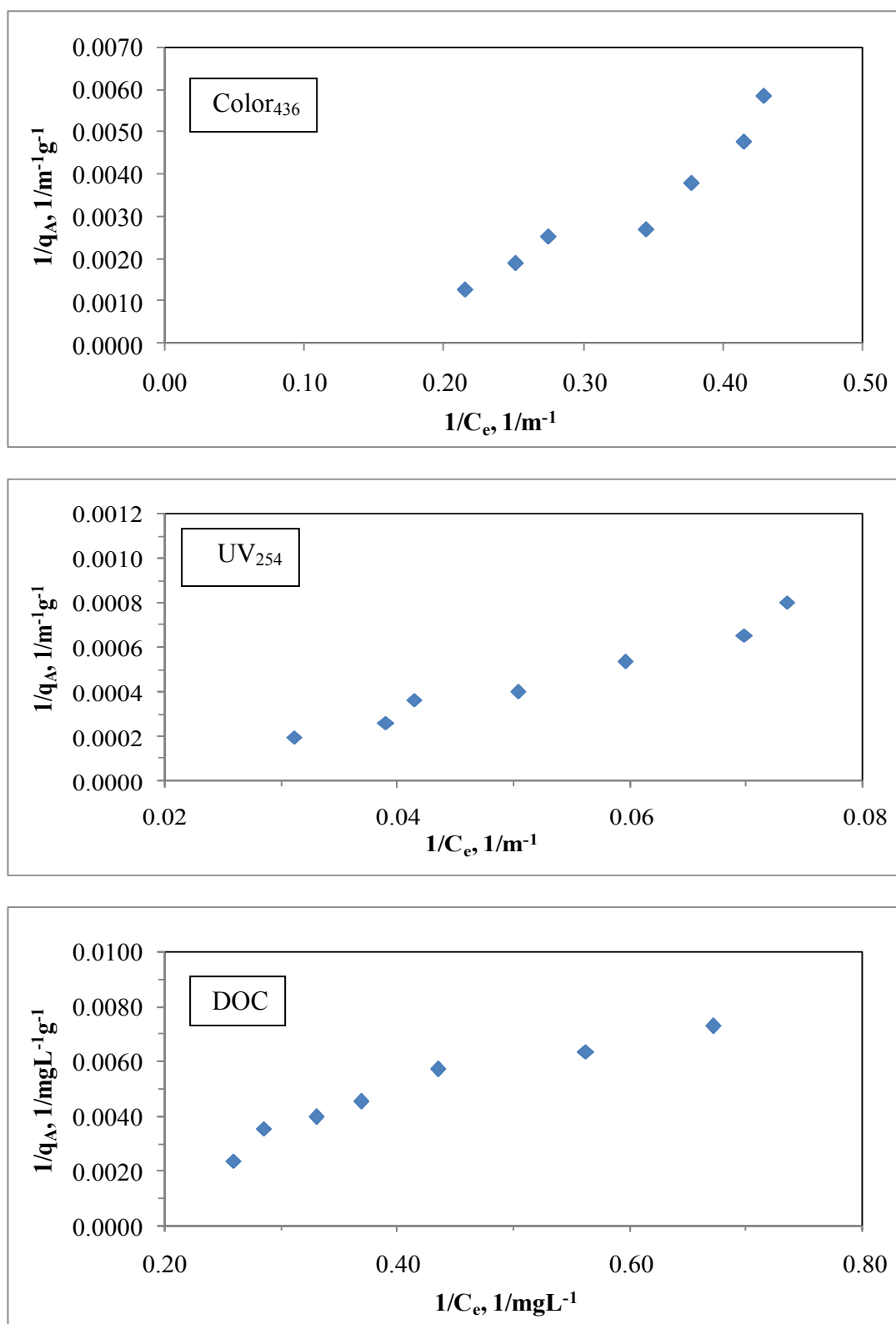
Figure 4.136. Freundlich adsorption isotherm of $Color_{436}$, UV_{254} and DOC parameters of 30 kDa fraction of humic acid following adsorption onto bare TiO_2 Degussa P-25.

Adsorption isotherms relatively exhibited similar trend for both of the UV-vis parameters as expressed by $Color_{436}$ and UV_{254} parameters. The trends exhibited by the respective adsorption isotherms could be considered as C-curve type isotherm.

C_e values altered between 1.45 – 2.52 mg L^{-1} for DOC. The values of q_A corresponding to the C_e values were calculated as between 52 - 88 mg L^{-1} g^{-1}. ΔC_e and Δq_A values for DOC were calculated as 1.07 mg L^{-1} and 36 mg L^{-1} g^{-1}, respectively (Figure 4.136).

UV-vis parameters of 30 kDa fraction of humic acid as expressed by $Color_{436}$ and UV_{254} displayed similar trends contrary to the DOC adsorption profile (Figure 4.136). DOC adsorption isotherm displayed an increasing trend with respect to the decreasing dose of TiO_2 Degussa P-25. Considering the initial DOC of 30 kDa fraction of humic acid (2.74 mg L^{-1}), 8.03 % DOC was removed for 0.1 mg mL^{-1} dose of bare TiO_2 Degussa P-25 and 47 % DOC was removed for 1.0 mg mL^{-1} dose of bare TiO_2 Degussa P-25 upon adsorption under equilibrium conditions.

Comparative evaluation of the initial DOC of 30 kDa fraction of humic acid with 0.45 μm filtration fraction of humic acid revealed that the ratio of the removal of DOC was significantly high in the latter for the same dose of bare TiO_2 Degussa P-25 (1.0 mg mL^{-1}). The reason could be attributed to the decreasing of the fluorophoric and chromophoric groups existing in the different molecular size fractions of humic acid.

When the initial concentration of 30 kDa fraction of humic acid was considered as 50 mg L^{-1}, the percentage of the removal of DOC was considerably high. In other words, considering the initial DOC of 30 kDa fraction of humic acid (3.21 mg L^{-1}), 19 % DOC was removed for 0.1 mg mL^{-1} dose of bare TiO_2 Degussa P-25 and 50 % DOC was removed for 1.0 mg mL^{-1} dose of bare TiO_2 Degussa P-25 upon adsorption under equilibrium conditions.

Freundlich isotherm model coefficients; adsorption capacity, K_f, and adsorption intensity, $1/n$, for 30 kDa fraction of humic acid following adsorption onto bare TiO_2 Degussa P-25 were listed in Table 4.43. ($R^2 \geq 0.93$).

Table 4.43. Freundlich isotherm model parameters for 30 kDa fraction of humic acid following adsorption onto bare TiO_2 Degussa P-25.

Humic acid, 30kDa fraction		
UV-vis parameter	K_f	$1/n$
$Color_{436}$	212.8	1.08
UV_{365}	169.2	1.05
UV_{280}	134.9	0.921
UV_{254}	125.7	0.961
Dissolved Organic Carbon	K_f	$1/n$
DOC	35.76	0.960

Comparison of UV-vis parameters indicated that the adsorption capacity constant of $Color_{436}$ was the highest value. Adsorption capacity constants were found to be in the order of $Color_{436} > UV_{365} > UV_{280} > UV_{254}$. Also, adsorption intensity of $Color_{436}$ was the highest value. Furthermore, adsorption intensity of UV_{280} and UV_{254} were close to each other. The order of adsorption intensity values could be given as $Color_{436} \geq UV_{365} > UV_{254} \geq UV_{365}$.

Comparative evaluation of Freundlich isotherm model parameter, K_f of 30 kDa fraction of humic acid with 100 kDa fraction of humic acid following adsorption onto bare TiO_2 Degussa P-25 did not reveal the most significant difference in both UV-vis parameters and DOC (Table 4.23 and Table 4.43).

Langmuir adsorption model. Langmuir adsorption isotherms for 30 kDa fraction of humic acid following adsorption onto bare TiO_2 Degussa P-25 were presented in Figure 4.137 for $Color_{436}$, UV_{254} and DOC parameters. Langmuir isotherms for UV_{365} and UV_{280} were presented in Appendix B.

Two parameters of Langmuir equation outlined in section 2.3, q_m and K_a, were listed in Table 4.44 for 30 kDa fraction of humic acid following adsorption onto bare TiO_2 Degussa P-25 ($R^2 \geq 0.92$).
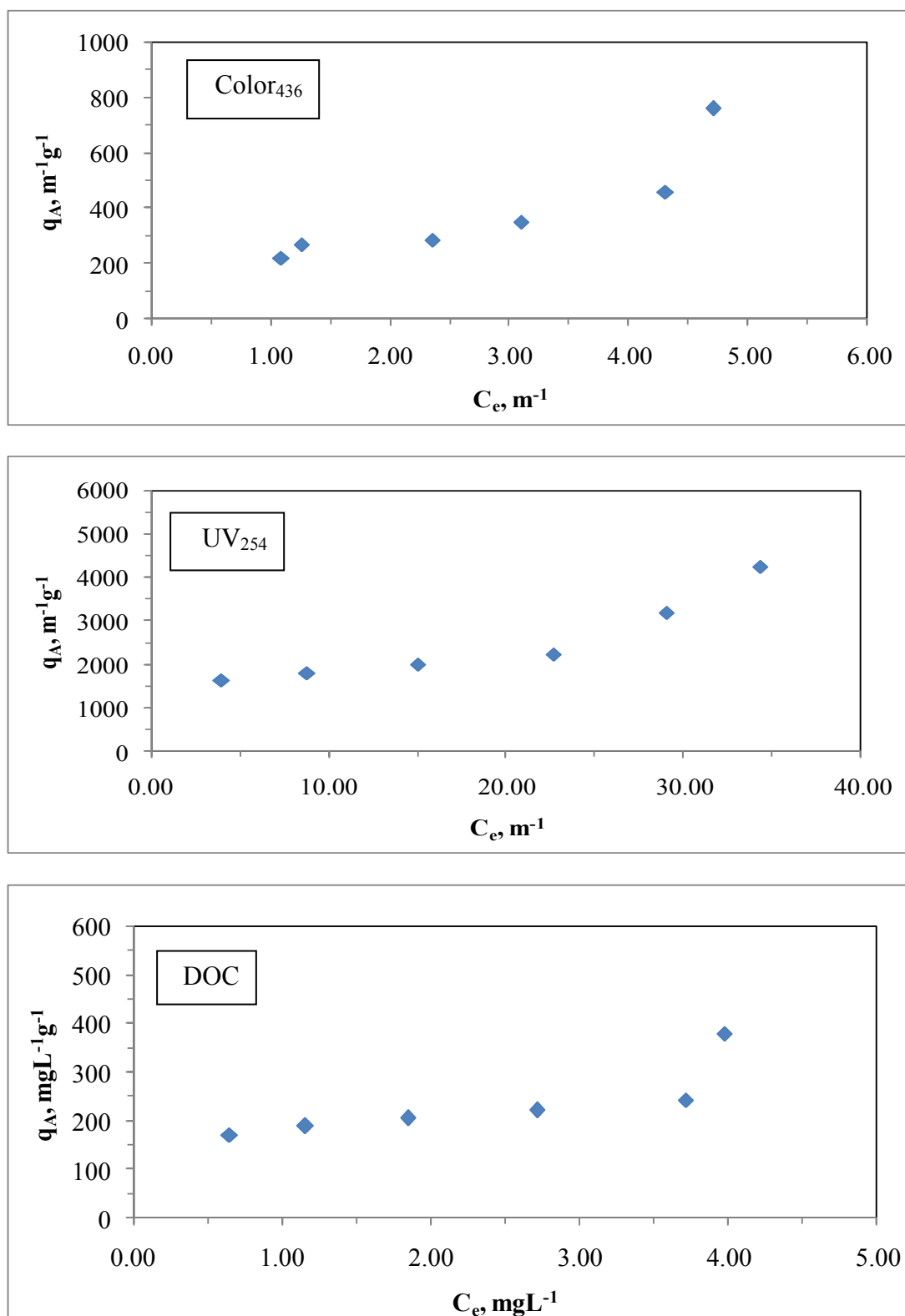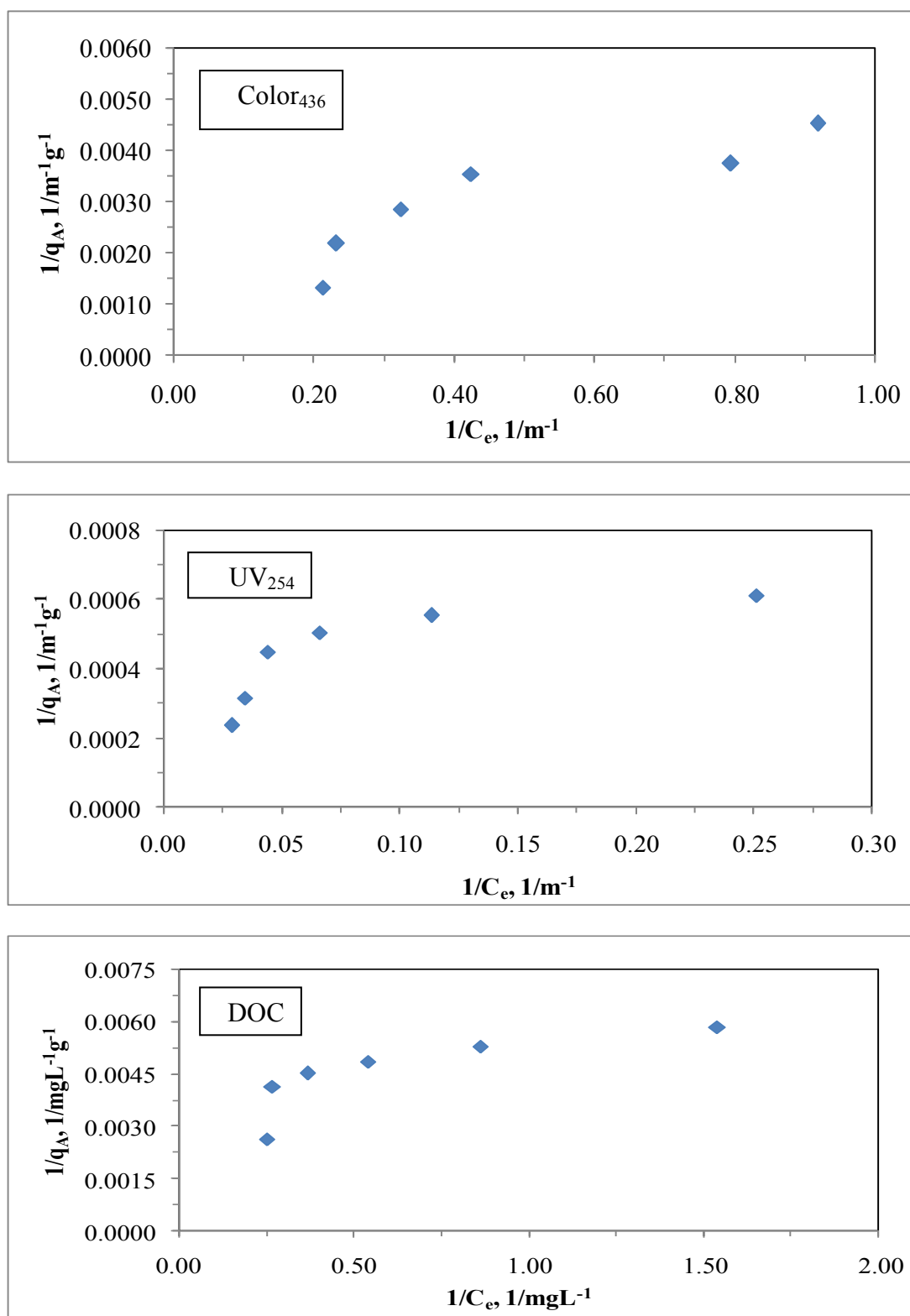
Figure 4.137. Langmuir adsorption isotherm of Color$_{436}$, UV$_{254}$ and DOC parameters of 30 kDa fraction of humic acid following adsorption onto bare TiO$_2$ Degussa P-25.

Table 4.44. Langmuir adsorption isotherm model parameters for 30 kDa fraction of humic following adsorption onto bare TiO_2 Degussa P-25.

Humic acid, 30 kDa fraction		
UV-vis parameter	q_m $m^{-1}g^{-1}$	K_a m^{-1}
Color$_{436}$	10000	0.0200
UV$_{365}$	14287	0.00100
UV$_{280}$	5000	0.0280
UV$_{254}$	10000	0.0140
Dissolved Organic Carbon	q_m mg $L^{-1}g^{-1}$	K_a mg L^{-1}
DOC	1000	0.0590

It could be easily seen from Table 4.44 that the order of UV-vis spectroscopic parameters for q_m value was Color$_{436}$ = UV$_{254}$ > UV$_{365}$ > UV$_{280}$ and this order was UV$_{280}$ > Color$_{436}$ > UV$_{254}$ > UV$_{365}$ for K_a value. The model parameters as q_m and K_a values for DOC were calculated as 1000 mg $L^{-1}g^{-1}$ and 0.0590 mg L^{-1}.

It should be indicated that adsorption of 30 kDa fraction of humic acid onto bare TiO_2 Degussa P-25 could well be characterized both by Freundlich and Langmuir adsorption isotherm models.

Langmuir isotherm model parameters of 30 kDa fraction of humic acid recorded following adsorption onto bare TiO_2 Degussa P-25 specimen with Langmuir isotherm model parameters of 100 kDa fraction of humic acid recorded following adsorption onto bare TiO_2 Degussa P-25 were compared (Table 4.24 and Table 4.44).

Langmuir isotherm model parameter, q_m was found to be significantly lower than the values calculated from the data attained for 100 kDa fraction of humic acid (Table 4.24, Table 4.44) for both UV-vis parameters and DOC. Comparative evaluation of Langmuir isotherm model parameters of 30 kDa fraction of humic acid with 0.45 μm filtration fraction of humic acid following adsorption onto bare TiO_2 Degussa P-25 revealed the most significant difference in both UV-vis parameters and DOC.

4.8.1.2. Adsorption Isotherm Modeling of 30 kDa Fraction of Humic Acid onto C-doped TiO$_2$ Degussa P-25 Specimen. UV-vis spectroscopic parameters (Color$_{436}$, UV$_{365}$, UV$_{280}$, and UV$_{254}$) and DOC were fitted to Freundlich (2.7) and Langmuir (2.6) adsorption isotherm models.

Freundlich adsorption model. Freundlich adsorption isotherms were presented in Figure 4.138 for Color$_{436}$, UV$_{254}$ and DOC parameters. Freundlich isotherms for UV$_{365}$ and UV$_{280}$ were presented in Appendix A.

C$_e$ values altered between 1.32 – 2.81 m^{-1} for Color$_{436}$ according to the loading of C-doped TiO$_2$ Degussa P-25 in the solution. The values of q$_A$ were found in the range of 88 - 288 m^{-1} g^{-1} for the corresponding to the C$_e$ values. ΔC$_e$ and Δq$_A$ values for Color$_{436}$ were found as 1.49 m^{-1} and 200 m^{-1} g^{-1}; respectively. C$_e$ values altered between 10.34 – 20.67 m^{-1} for UV$_{254}$. The values of q$_A$ were calculated as between 586 - 1732 m^{-1} g^{-1} for the corresponding to the C$_e$ values. ΔC$_e$ and Δq$_A$ values for UV$_{254}$ were calculated as 10.33 m^{-1} and 1146 m^{-1} g^{-1}, respectively (Figure 4.138).

Adsorption isotherms relatively exhibited similar trend for both of the UV-vis parameters as expressed by Color$_{436}$ and UV$_{254}$ parameters. The trends exhibited by the respective adsorption isotherms could be considered as S-curve type isotherm.

C-doping of TiO$_2$ Degussa P-25 considerably changed the adsorption isotherm trend of 30 kDa fraction of humic acid in comparison to bare TiO$_2$ Degussa P-25 (Figure 4.136, and Figure 4.138).

C$_e$ values altered between 1.36 – 2.48 mg L^{-1} for DOC. The values of q$_A$ corresponding to the C$_e$ values were calculated as between 55 - 104 mg L^{-1} g^{-1}. ΔC$_e$ and Δq$_A$ values for DOC were calculated as 1.12 mg L^{-1} and 49 mg L^{-1} g^{-1}, respectively (Figure 4.138).

Freundlich isotherm model coefficients; adsorption capacity, K$_f$, and adsorption intensity, 1/n, for 30 kDa fraction of humic acid adsorption onto C-doped TiO$_2$ Degussa P-25 were listed in Table 4.45 (R$^2 \geq$0.79).
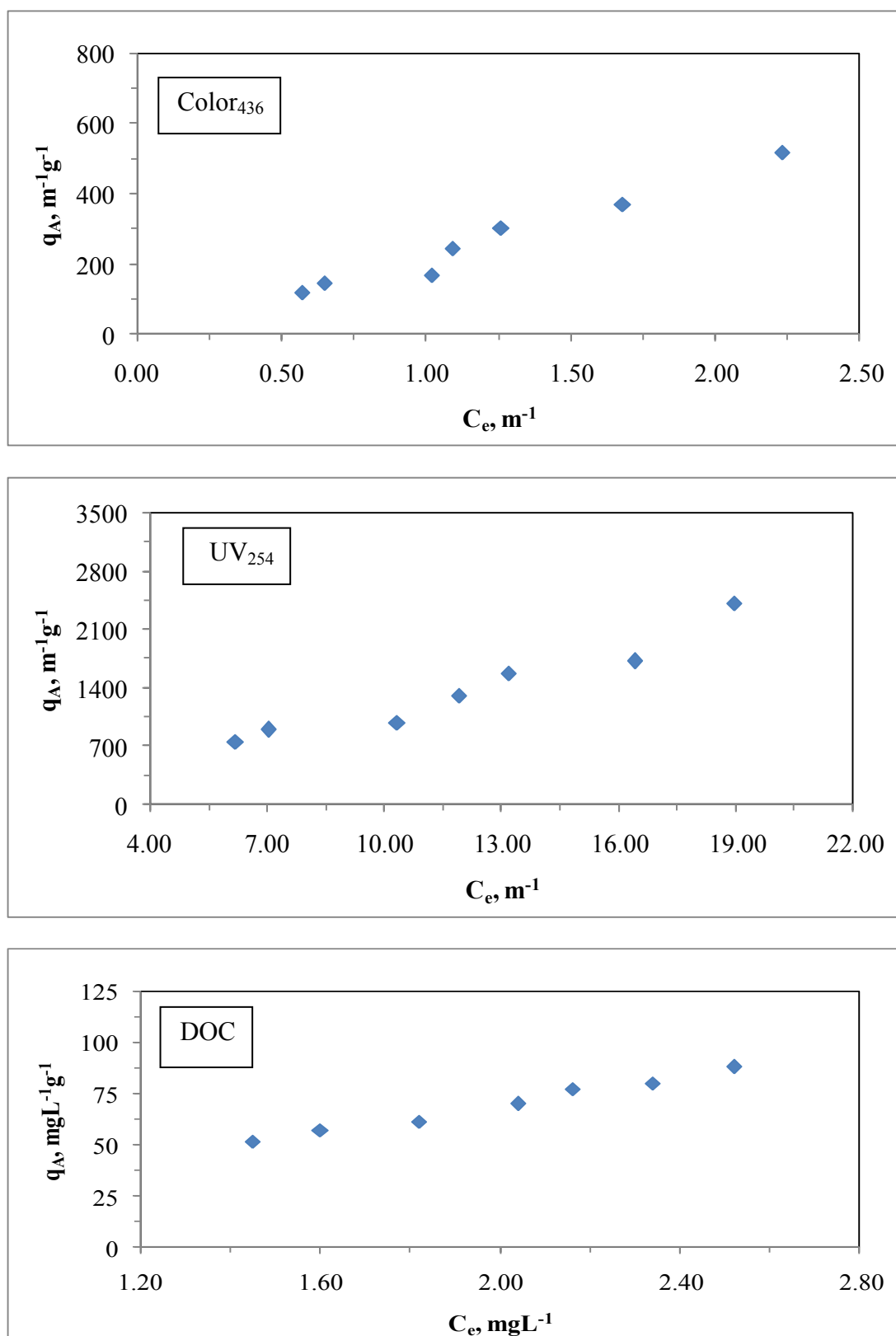
Figure 4.138. Freundlich adsorption isotherm of $Color_{436}$, UV_{254} and DOC parameters of 30 kDa fraction of humic acid following adsorption onto C-doped TiO_2 Degussa P-25.

234

Table 4.45. Freundlich isotherm model parameters for 30 kDa fraction of humic acid following adsorption onto C-doped TiO_2 Degussa P-25.

Humic acid, 30kDa fraction		
UV-vis parameter	K_f	$1/n$
$Color_{436}$	50.10	0.880
UV_{365}	39.75	0.820
UV_{280}	39.74	0.730
UV_{254}	32.17	0.740
Dissolved Organic Carbon	K_f	$1/n$
DOC	37.04	1.01

Comparison of UV-vis parameters indicated that the adsorption capacity constant of $Color_{436}$ was the highest value. Moreover, adsorption capacity constants of UV_{365} and UV_{280} were equal to each other. The order was $UV_{254} < UV_{280} \leq UV_{365} < Color_{436}$ for adsorption capacity constant. Also, adsorption intensity of UV_{280} was the lowest value contrary to adsorption intensity of $Color_{436}$. A decreasing order of adsorption intensity values could be given as $UV_{254} = UV_{280} < UV_{365} < Color_{436}$. Adsorption intensity of DOC was found to be >1 representing strong adsorption bond.

Freundlich isotherm model parameters of 30 kDa fraction of humic acid recorded following adsorption onto two different TiO_2 Degussa P-25 specimens were compared (Table 4.43 and Table 4.45). Freundlich isotherm model parameters displayed significantly lower values for C-doping TiO_2 Degussa P-25.

Langmuir adsorption model. Langmuir adsorption isotherms for 30 kDa fraction of humic acid adsorption onto C-doped TiO_2 Degussa P-25 were presented in Figure 4.139 for $Color_{436}$, UV_{254} and DOC parameters. Langmuir adsorption isotherm models for UV_{365} and UV_{280} were presented in Appendix B.

Two parameters of Langmuir equation outlined in section 2.3, q_m and K_a, were listed in Table 4.46 for 30 kDa fraction of humic acid adsorption onto C- doped TiO_2 Degussa P-25 ($R^2 \geq 0.76$).

Figure 4.139. Langmuir adsorption isotherm of Color$_{436}$, UV$_{254}$ and DOC parameters of 30 kDa fraction of humic acid following adsorption onto C-doped TiO$_2$ Degussa P-25.

Table 4.46.   Langmuir isotherm model parameters for 30 kDa fraction of humic acid following adsorption onto C-doped TiO_2 Degussa P-25.

Humic acid, 30 kDa fraction		
UV-vis parameter	q_m m^{-1}g^{-1}	K_a m^{-1}
Color$_{436}$	500	0.105
UV$_{365}$	10000	0.00600
UV$_{280}$	33333	0.00200
UV$_{254}$	12500	0.00400
Dissolved Organic Carbon	q_m mg L^{-1}g^{-1}	K_a mg L^{-1}
DOC	1000	0.0420

It could be easily seen from Table 4.46 that the order of all UV-vis spectroscopic parameters in terms of q_m value was UV$_{280}$ > UV$_{254}$ > UV$_{365}$ > Color$_{436}$ and this order was reverse for K_a value, namely, Color$_{436}$ > UV$_{365}$ > UV$_{254}$ > UV$_{280}$. The model parameters as q_m and K_a values for DOC were calculated as 1000 mg L^{-1}g^{-1} and 0.0420 mg L^{-1}.

It should be indicated that adsorption of 30 kDa fraction of humic acid onto C-doped TiO_2 Degussa P-25 could well be characterized both by Freundlich and Langmuir adsorption isotherm models.

Comparative evaluation of Langmuir isotherm model parameters of 30 kDa fraction of humic acid with 100 kDa fraction of humic acid following adsorption onto C-doped TiO_2 Degussa P-25 revealed the most significant difference in both UV-vis parameters and DOC.

Langmuir isotherm model parameters of 30 kDa fraction of humic acid recorded following adsorption onto two different TiO_2 specimens were compared (Table 4.44 and Table 4.46). Comparison of Table 4.44 and Table 4.46 could display the role of C-doping on adsorption of 30 kDa fraction of humic acid onto TiO_2 Degussa P-25. An inconsistent trend could be visualized for the UV-vis parameters upon comparison of the Langmuir isotherm model parameters, q_m and K_a.

4.8.1.3. Adsorption Isotherm Modeling of 30 kDa Fraction of Humic Acid onto N-doped TiO$_2$ Degussa P-25 Specimen. UV-vis spectroscopic parameters (Color$_{436}$, UV$_{365}$, UV$_{280}$, and UV$_{254}$) and DOC were fitted to Freundlich (2.7) and Langmuir (2.6) adsorption isotherm models.

Freundlich adsorption model. Freundlich adsorption isotherms were presented in Figure 4.140 for Color$_{436}$, UV$_{254}$ and DOC parameters. Freundlich isotherms for UV$_{365}$ and UV$_{280}$ were presented in Appendix A.

C$_e$ values altered between 1.90 – 2.84 m^{-1} for Color$_{436}$ according to the loading of N-doped TiO$_2$ Degussa P-25 in the solution. The values of q$_A$ were found in the range of 65 – 276 m^{-1} g^{-1} for the corresponding to the C$_e$ values. ΔC$_e$ and Δq$_A$ values for Color$_{436}$ were calculated as 0.94 m^{-1} and 211 m^{-1} g^{-1}; respectively. C$_e$ values altered between 13.16 – 19.57 m^{-1} for UV$_{254}$. The values of q$_A$ were calculated as between 474 - 2172 m^{-1}g^{-1} for the corresponding to the C$_e$ values. ΔC$_e$ and Δq$_A$ values for UV$_{254}$ were calculated as 6.41 m^{-1} and 1698 m^{-1} g^{-1}, respectively (Figure 4.140).

Freundlich adsorption isotherms relatively exhibited similar trend for both of the UV-vis parameters as expressed by Color$_{436}$ and UV$_{254}$ parameters. The trends exhibited by the respective adsorption isotherms could be considered as S-curve type isotherm.

N-doping of TiO$_2$ Degussa P-25 affected the adsorption isotherm profiles of UV-vis spectral parameters as well as DOC in comparison to the bare TiO$_2$ Degussa P-25 (Figure 4.136 and Figure 4.140).

C$_e$ values altered between 1.13 – 2.19 mg L^{-1} for DOC. The values of q$_A$ corresponding to the C$_e$ values were calculated as between 64 - 220 mg L^{-1} g^{-1}. ΔC$_e$ and Δq$_A$ values for DOC were calculated as 1.06 mg L^{-1} and 156 mg L^{-1} g^{-1}, respectively (Figure 4.140).

Freundlich isotherm model coefficients; adsorption capacity, K$_f$, and adsorption intensity, 1/n, for 30 kDa fraction of humic acid following adsorption onto N-doped TiO$_2$ Degussa P-25 were listed in Table 4.47 (R^2≥0.75).
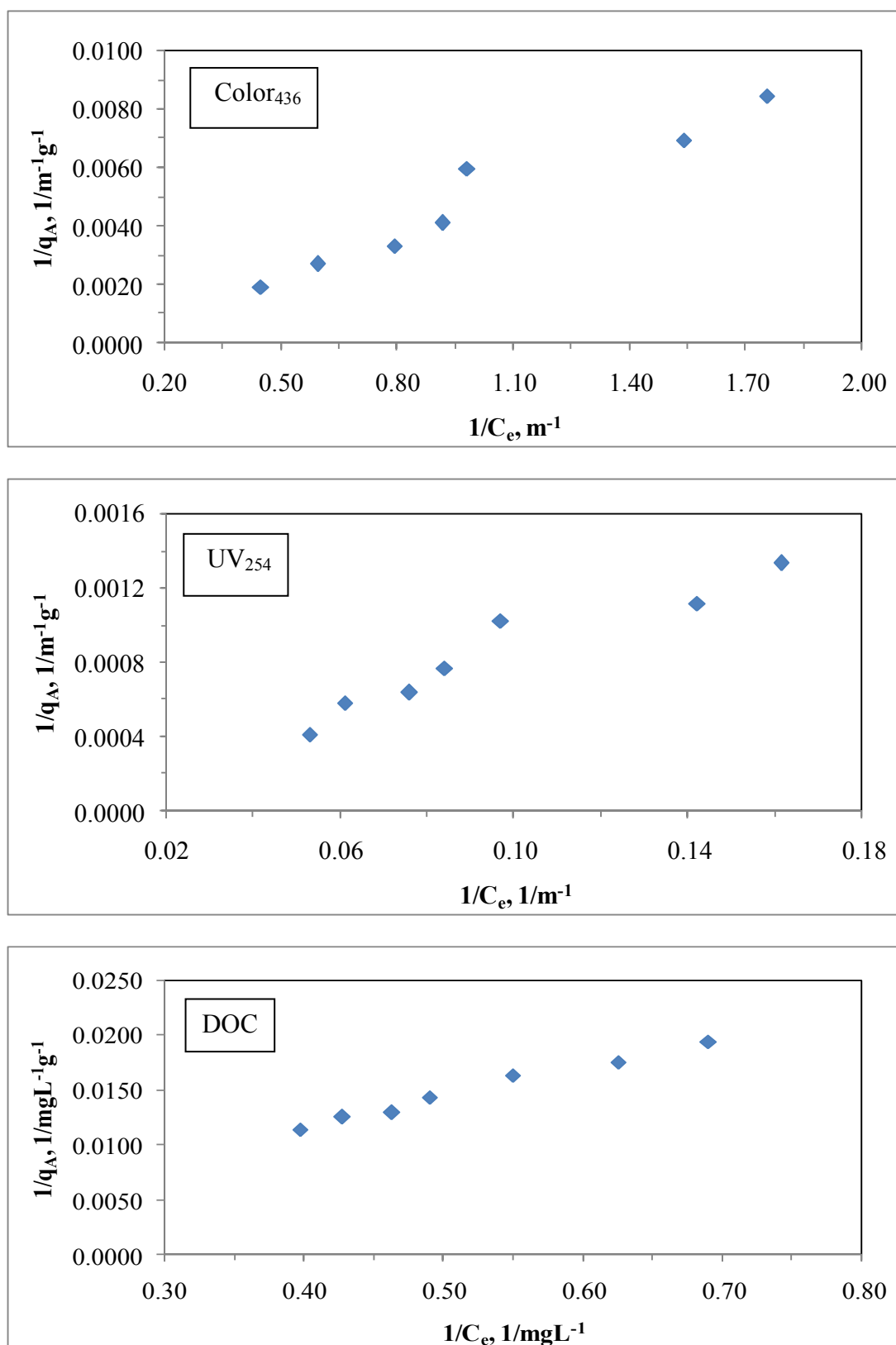
Figure 4.140. Freundlich adsorption isotherm of $Color_{436}$, UV_{254} and DOC parameters of 30 kDa fraction of humic acid following adsorption onto N-doped TiO_2 Degussa P-25.

Table 4.47. Freundlich isotherm model parameters for 30 kDa fraction of humic acid following adsorption onto N-doped TiO_2 Degussa P-25.

Humic acid, 30kDa fraction		
UV-vis parameter	K_f	$1/n$
Color$_{436}$	5.236	3.46
UV$_{365}$	1.007	3.24
UV$_{280}$	0.06738	3.46
UV$_{254}$	0.03295	3.61
Dissolved Organic Carbon	K_f	$1/n$
DOC	47.93	1.90

Comparison of UV-vis parameters indicated that the adsorption capacity constant of Color$_{436}$ was the highest value. Moreover, adsorption capacity constants of UV$_{254}$ had the lowest value. The order was UV$_{254}$ < UV$_{280}$ < UV$_{365}$ < Color$_{436}$ for adsorption capacity constant. Furthermore, adsorption intensity of UV$_{365}$ was the lowest value. Moreover, adsorption intensity of Color$_{436}$ and UV$_{280}$ were equal to each other. Adsorption intensity of DOC was found to be >1 representing strong adsorption bond. The order of adsorption intensity values could be given as UV$_{365}$ < UV$_{280}$ = Color$_{436}$ < UV$_{254}$.

With reference to the differences observed in adsorption isotherm profiles of bare TiO_2 and C-doped TiO_2 as well as N-doped TiO_2 Degussa P-25 specimens, the Freundlich isotherm model parameters were significantly different as expected (Table 4.43, Table 4.45 and Table 4.47).

Langmuir adsorption model. Langmuir adsorption isotherms for 30 kDa fraction of humic acid following adsorption onto N-doped TiO_2 Degussa P-25 were presented in Figure 4.141 for Color$_{436}$, UV$_{254}$ and DOC parameters. Langmuir isotherms for UV$_{365}$ and UV$_{280}$ were presented in Appendix B.

Two parameters of Langmuir equation outlined in section 2.3, q_m and K_a, were listed in Table 4.48 for 30 kDa fraction of humic acid following adsorption onto N- doped TiO_2 Degussa P-25 ($R^2 \geq 0.82$).
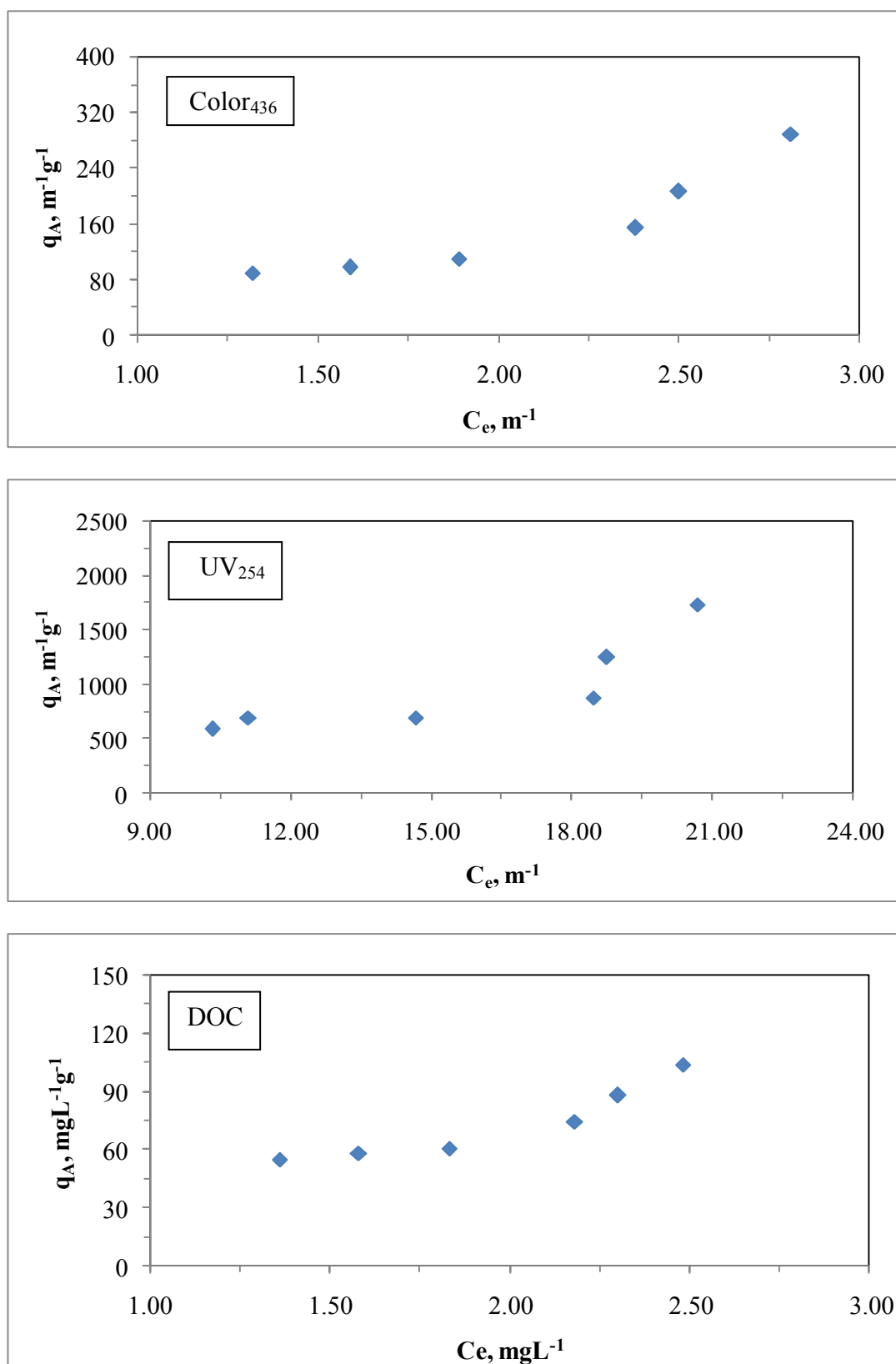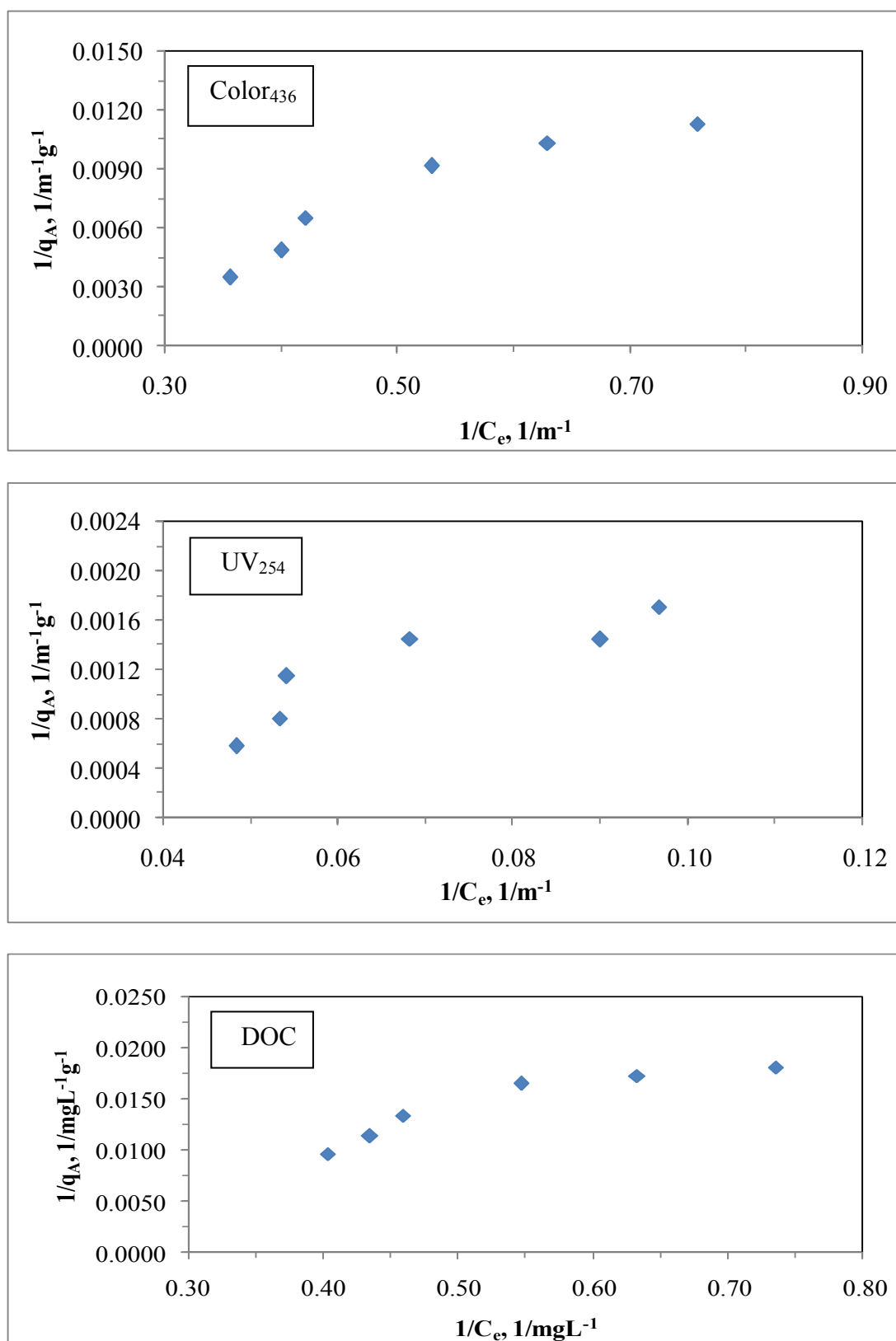
Figure 4.141. Langmuir adsorption isotherm of $Color_{436}$, UV_{254} and DOC parameters of 30 kDa fraction of humic acid following adsorption onto N-doped TiO_2 Degussa P-25.

Table 4.48. Langmuir isotherm model parameters for 30 kDa fraction of humic acid following adsorption onto N-doped TiO_2 Degussa P-25.

Humic acid, 30 kDa fraction		
UV-vis parameter	q_m $m^{-1}g^{-1}$	K_a m^{-1}
Color$_{436}$	53	0.273
UV$_{365}$	143	0.104
UV$_{280}$	313	0.0470
UV$_{254}$	366	0.0410
Dissolved Organic Carbon	q_m mg $L^{-1}g^{-1}$	K_a mg L^{-1}
DOC	134	0.284

It could be easily seen from Table 4.48 the order of all of the UV-vis spectroscopic parameters in terms of q_m value was UV$_{254}$ > UV$_{280}$ > UV$_{365}$ > Color$_{436}$ and this order was reverse for K_a value, namely, Color$_{436}$ > UV$_{365}$ > UV$_{280}$ > UV$_{254}$. The model parameters as q_m and K_a values for DOC were calculated as 134 mg $L^{-1}g^{-1}$ and 0.284 mg L^{-1}.

It should be indicated that adsorption of 30 kDa fraction of humic acid onto N-doped TiO_2 Degussa P-25 could well be characterized both by Freundlich and Langmuir adsorption isotherm models.

Comparative evaluation of Langmuir isotherm model parameters of 30 kDa fraction of humic acid with 100 kDa fraction of humic acid following adsorption onto N-doped TiO_2 Degussa P-25 revealed significant differences in both UV-vis parameters and DOC. Langmuir isotherm model parameter, q_m was found to be significantly lower than the values calculated from the data attained in case of bare TiO_2 and C-doped TiO_2 Degussa P-25 (Table 4.44, Table 4.46 and Table 4.48) for both UV-vis parameters and DOC. Langmuir isotherm model parameter, K_a was found to be significantly different for diverse TiO_2 Degussa P-25 specimens, namely K_a = 0.0590 mg L^{-1} for bare TiO_2 Degussa P-25 and K_a = 0.0420 mg L^{-1} for C-doped TiO_2 Degussa P-25 as well as K_a = 0.284 mg L^{-1} for N-doped TiO_2 Degussa P-25 in terms of DOC. Comparison of C-doping and N-doping with bare TiO_2 Degussa P-25 could be regarded as discriminating between the effects of dopants.

4.8.1.4. Adsorption Isotherm Modeling of 30 kDa Fraction of Humic Acid onto S-doped TiO$_2$ Degussa P-25 Specimen. UV-vis spectroscopic parameters (Color$_{436}$, UV$_{365}$, UV$_{280}$and UV$_{254}$) and DOC were fitted to Freundlich (2.7) and Langmuir (2.6) adsorption isotherm models.

Freundlich adsorption model. Freundlich adsorption isotherms were presented in Figure 4.142 for Color$_{436}$, UV$_{254}$ and DOC parameters. Freundlich isotherms for UV$_{365}$ and UV$_{280}$ were presented in Appendix A.

C$_e$ values altered between 1.80 – 2.81 m^{-1} for Color$_{436}$ according to the loading of S-doped TiO$_2$ Degussa P-25 in the solution. The values of q$_A$ were found in the range of 69 - 288 m^{-1} g^{-1} for the corresponding to the C$_e$ values. ΔC$_e$ and Δq$_A$ values for 30 kDa fraction of humic acid were found as 1.01 m^{-1} and 219 m^{-1} g^{-1} for Color$_{436}$. C$_e$ values altered between 13.97 – 21.42 m^{-1} for UV$_{254}$. The values of q$_A$ were calculated as between 441 - 1432 m^{-1}g^{-1} for the corresponding to the C$_e$ values. ΔC$_e$ and Δq$_A$ values for UV$_{254}$ were calculated as 7.45 m^{-1} and 991 m^{-1} g^{-1}, respectively (Figure 4.142).

Freundlich adsorption isotherms relatively exhibited similar trend for both Color$_{436}$ and UV$_{254}$ parameters. The trends exhibited by respective adsorption isotherms could be considered as S-curve type isotherm.

C$_e$ values altered between 0.82 – 2.27 mg L^{-1} for DOC. The values of q$_A$ corresponding to the C$_e$ values were calculated as between 77 - 188 mg L^{-1} g^{-1}. ΔC$_e$ and Δq$_A$ values for DOC were calculated as 1.45 mg L^{-1} and 111 mg L^{-1} g^{-1}, respectively (Figure 4.142).

S-doping of TiO$_2$ Degussa P-25 affected the adsorption isotherm profiles of UV-vis spectral parameters as well as DOC in comparison to the bare TiO$_2$ Degussa P-25 (Figure 4.136 and Figure 4.142).

Freundlich isotherm model coefficients; adsorption capacity, K$_f$, and adsorption intensity, 1/n, for 30 kDa fraction of humic acid following adsorption onto S-doped TiO$_2$ Degussa P-25 were listed in Table 4.49 (R^2$\geq$0.76).
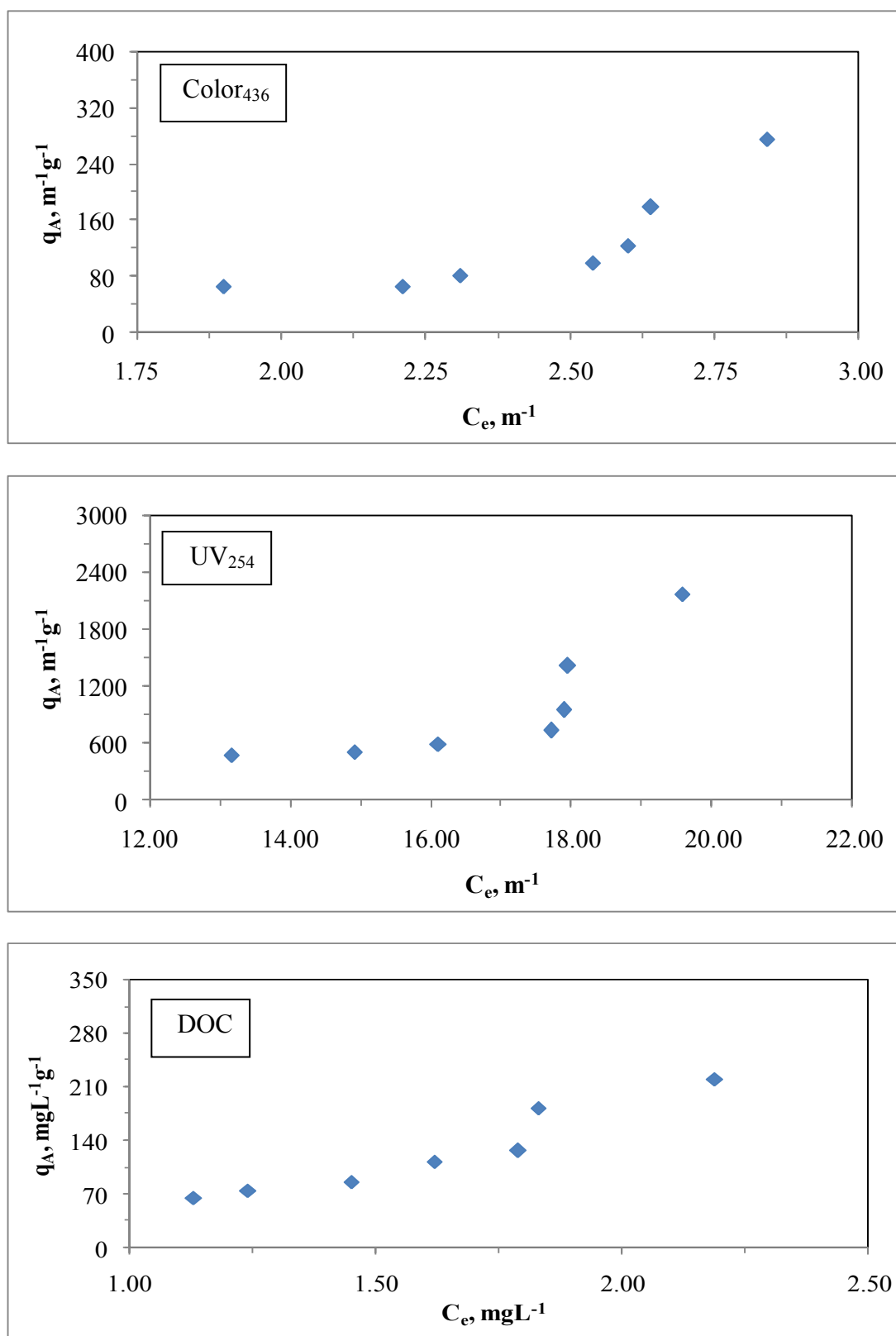
Figure 4.142. Freundlich adsorption isotherm of $Color_{436}$, UV_{254} and DOC parameters of 30 kDa fraction of humic acid following adsorption onto S-doped TiO_2 Degussa P-25.

244

Table 4.49. Freundlich isotherm model parameters for 30 kDa fraction of humic acid following adsorption onto S-doped TiO_2 Degussa P-25.

Humic acid, 30kDa fraction		
UV-vis parameter	K_f	$1/n$
$Color_{436}$	12.10	2.91
UV_{365}	4.990	2.30
UV_{280}	4.860	1.75
UV_{254}	2.970	1.87
Dissolved Organic Carbon	K_f	$1/n$
DOC	83.67	0.611

Comparison of UV-vis parameters indicated that the adsorption capacity constant of $Color_{436}$ was the highest value. A decreasing order of adsorption capacity values could be given as $Color_{436} > UV_{365} \geq UV_{280} > UV_{254}$. Moreover, it was clear from Table 4.49, adsorption intensity of UV_{280} was the lowest value. The order of adsorption intensity values could be given as $UV_{280} < UV_{254} < UV_{365} < Color_{436}$. According to Table 4.49, adsorption intensity values for UV-vis parameters were found to be >1 representing strong adsorption bond. The binding mechanism of humic acid could be affected by mixed crystalline nature TiO_2, in such a way that adsorption constants increased as mentioned before. Freundlich isotherm model parameters of 30 kDa fraction of humic acid recorded following adsorption onto different TiO_2 specimens were compared (Table 4.43, Table 4.45, Table 4.47 and Table 4.49). Freundlich isotherm model parameters of DOC for 30 kDa fraction of humic acid could be expressed by a decreasing order for K_f: S-doped TiO_2 > N-doped TiO_2 > C-doped TiO_2 > bare TiO_2 for $1/n$: N-doped TiO_2 > C-doped TiO_2 > bare TiO_2. > S-doped TiO_2.

Langmuir adsorption model. Langmuir adsorption isotherms for 30 kDa fraction of humic acid following adsorption onto S-doped TiO_2 Degussa P-25 were presented in Figure 4.143 for $Color_{436}$, UV_{254} and DOC parameters. Langmuir isotherms for UV_{365} and UV_{280} were presented in Appendix B. Two parameters of Langmuir equation outlined in section 2.3, q_m and K_a, were listed in Table 4.50 for 30 kDa fraction of humic acid following adsorption onto S- doped TiO_2 Degussa P-25 ($R^2 \geq 0.79$).
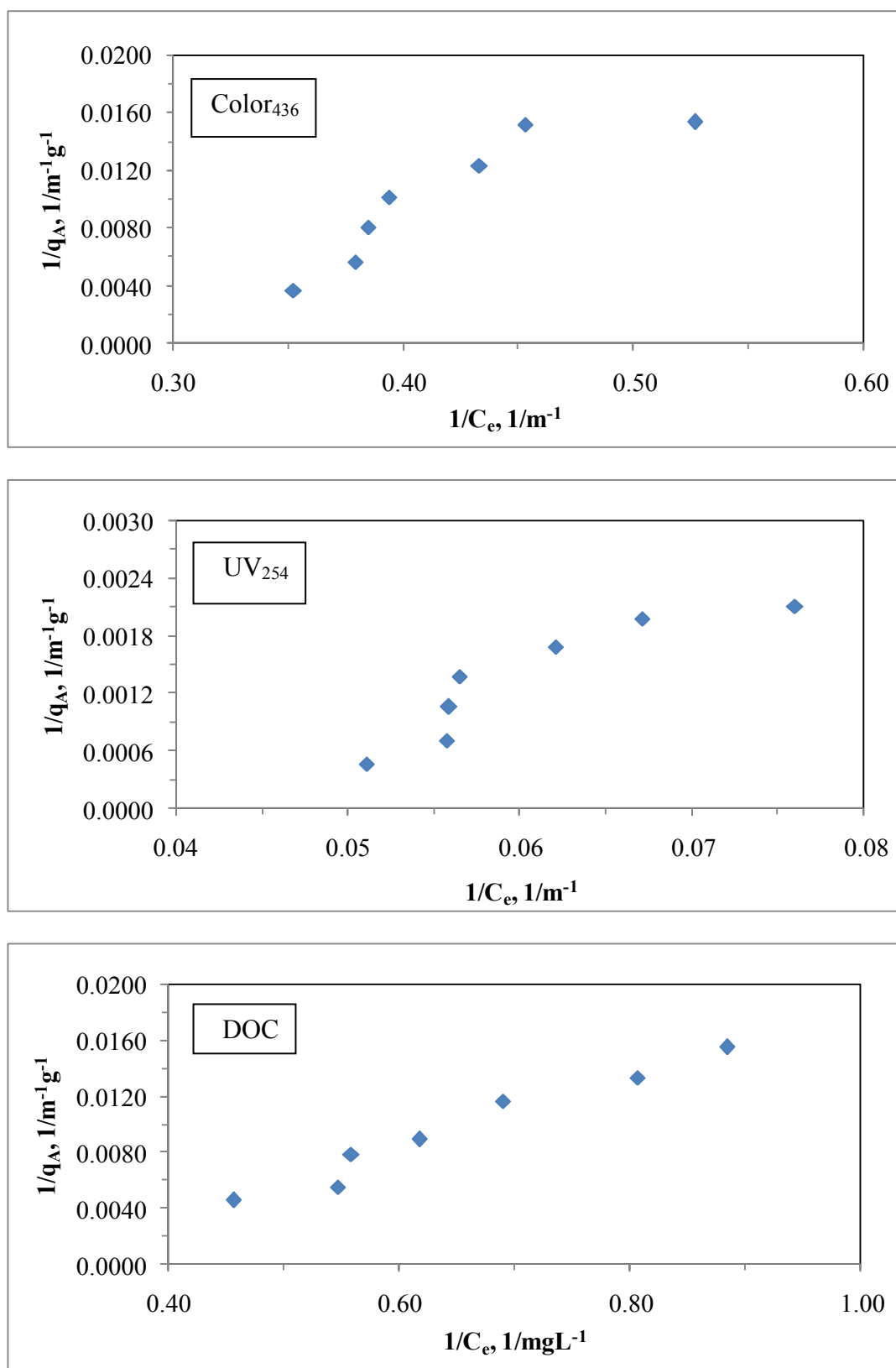
Figure 4.143. Langmuir adsorption isotherm of $Color_{436}$, UV_{254} and DOC parameters of 30 kDa fraction of humic acid following adsorption onto S-doped TiO_2 Degussa P-25.

Table 4.50. Langmuir isotherm model parameters for 30 kDa fraction of humic acid following adsorption onto S-doped TiO$_2$ Degussa P-25.

Humic acid, 30 kDa fraction		
UV-vis parameter	q$_m$ m^{-1}g^{-1}	K$_a$ m^{-1}
Color$_{436}$	71.0	0.282
UV$_{365}$	250	0.0820
UV$_{280}$	1000	0.0230
UV$_{254}$	1000	0.0210
Dissolved Organic Carbon	q$_m$ mg L^{-1}g^{-1}	K$_a$ mg L^{-1}
DOC	250	0.571

It could be easily seen from Table 4.50 the order of all of the UV-vis spectroscopic parameters in terms of q$_m$ value was UV$_{254}$ = UV$_{280}$ > UV$_{365}$ > Color$_{436}$. The order of K$_a$ values could be given as Color$_{436}$ > UV$_{365}$ > UV$_{280}$ ≥ UV$_{254}$. The model parameters as q$_m$ and K$_a$ values for DOC were calculated as 250 mg L^{-1}g^{-1} and 0.571 mg L^{-1}.

It should be indicated that adsorption of 30 kDa fraction of humic acid onto S-doped TiO$_2$ Degussa P-25 could well be characterized both by Freundlich and Langmuir adsorption isotherm models.

Langmuir isotherm model parameters of 30 kDa fraction of humic acid recorded following adsorption onto different TiO$_2$ specimens were compared (Table 4.44, Table 4.46 and Table 4.48 as well as Table 4.50). Langmuir isotherm model parameters of DOC could be expressed in a decreasing order of; q$_m$: bare TiO$_2$ = C-doped TiO$_2$ > S-doped TiO$_2$ > N-doped TiO$_2$, K$_a$: S-doped TiO$_2$ > N-doped TiO$_2$ > bare TiO$_2$ > C-doped TiO$_2$. Langmuir isotherm model parameter, K$_a$ was found to be slightly different for diverse TiO$_2$ Degussa P-25 specimens, namely K$_a$ = 0.0590 mg L^{-1} for bare TiO$_2$ Degussa P-25, K$_a$ = 0.0420 mg L^{-1} for C-doped TiO$_2$ Degussa P-25 and K$_a$ = 0.284 mg L^{-1} for N-doped TiO$_2$ Degussa P-25 as well as K$_a$ = 0.571 mg L^{-1} for S-doped TiO$_2$ Degussa P-25 in terms of DOC.

4.8.1.5. Adsorption Isotherm Modeling of 30 kDa Fraction of Humic Acid onto N-S co-doped TiO_2 Degussa P-25 Specimen. UV-vis spectroscopic parameters ($Color_{436}$, UV_{365}, UV_{280}, and UV_{254}) and DOC were fitted to Freundlich (2.7) and Langmuir (2.6) adsorption isotherm models.

Freundlich adsorption model. Freundlich adsorption isotherms were presented in Figure 4.144 for $Color_{436}$, UV_{254} and DOC parameters. Freundlich isotherms for UV_{365} and UV_{280} were presented in Appendix A.

C_e values altered between $0.91 – 2.63$ m^{-1} for $Color_{436}$ according to the loading of N-S co-doped TiO_2 Degussa P-25 in the solution. The values of q_A were found in the range of $131 - 360$ m^{-1} g^{-1} for the corresponding to the C_e values. ΔC_e and Δq_A values for $Color_{436}$ were calculated as 1.72 m^{-1} and 229 m^{-1} g^{-1}, respectively. C_e values altered between $7.53 – 18.06$ m^{-1} for UV_{254}. The values of q_A were calculated as between $874 - 2776$ $m^{-1}g^{-1}$ for the corresponding to the C_e values. ΔC_e and Δq_A values for UV_{254} were calculated as 10.53 m^{-1} and 1902 m^{-1} g^{-1}, respectively (Figure 4.144).

Freundlich adsorption isotherms of 30 kDa fraction of humic acid adsorption onto 0.4 mg mL^{-1} dose of N-S co-doped TiO_2 Degussa P-25 demonstrated a remarkable diversity for both $Color_{436}$ and UV_{254} specific parameters. The trends presented by respective adsorption isotherms could be considered as S-curve type isotherm.

N-S co-doping of TiO_2 Degussa P-25 significantly altered the adsorption profiles of UV-vis spectral parameters in comparison to S-doping of TiO_2 Degussa P-25.

C_e values altered between $1.10 – 2.09$ mg L^{-1} for DOC. The values of q_A corresponding to the C_e values were calculated as between $66 - 260$ mg L^{-1} g^{-1}. ΔC_e and Δq_A values for DOC were calculated as 0.99 mg L^{-1} and 194 mg L^{-1} g^{-1}, respectively (Figure 4.144).

Freundlich isotherm model coefficients; adsorption capacity, K_f, and adsorption intensity, $1/n$, for 30 kDa fraction of humic acid following adsorption onto N-S co-doped TiO_2 Degussa P-25 were listed in Table 4.51 ($R^2 \geq 0.81$).
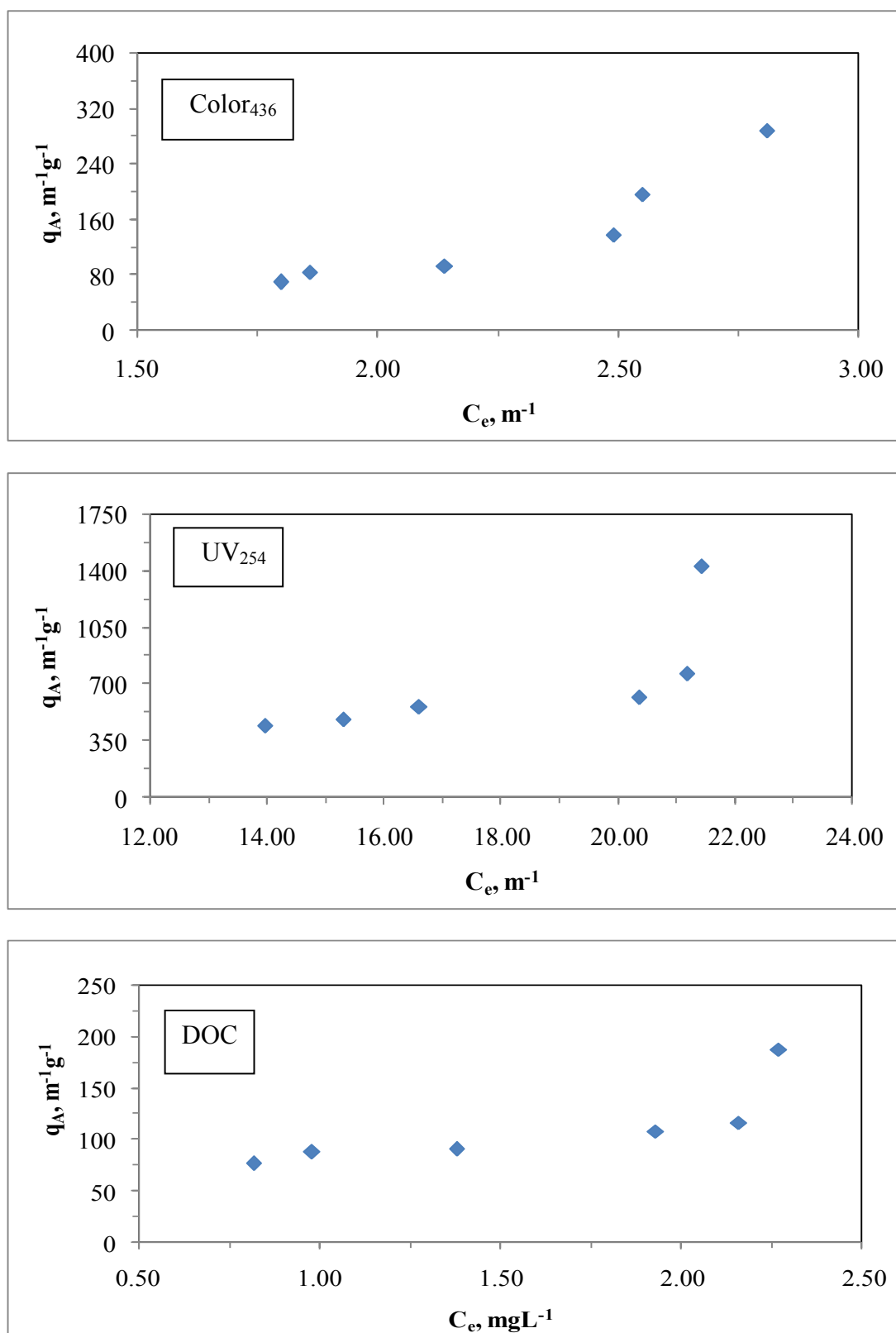
Figure 4.144. Freundlich adsorption isotherm of $Color_{436}$, UV_{254} and DOC parameters of 30 kDa fraction of humic acid following adsorption onto N-S co-doped TiO_2 Degussa P-25.

Table 4.51. Freundlich isotherm model parameters for 30 kDa fraction of humic acid following adsorption onto N-S co-doped TiO$_2$ Degussa P-25.

Humic acid, 30kDa fraction		
UV-vis parameter	K$_f$	1/n
Color$_{436}$	164.8	0.866
UV$_{365}$	69.93	1.39
UV$_{280}$	70.79	1.16
UV$_{254}$	79.97	1.11
Dissolved Organic Carbon	K$_f$	1/n
DOC	46.01	1.79

Comparison of UV-vis parameters indicated that the adsorption capacity constant of Color$_{436}$ was the highest value. Moreover, adsorption capacity constants of UV$_{280}$ and UV$_{365}$ were almost equal to each other and also they had the lowest values. The order was Color$_{436}$ > UV$_{254}$ > UV$_{280}$ $\geq$ UV$_{254}$ for adsorption capacity constant. The order of adsorption intensity could be given as Color$_{436}$ < UV$_{254}$ $\leq$ UV$_{280}$ < UV$_{365}$.

Freundlich isotherm model parameters of DOC for 30 kDa fraction of humic acid could be expressed by a decreasing order for K$_f$: S-doped TiO$_2$ > N-doped TiO$_2$ > N-S co-doped TiO$_2$ > C-doped TiO$_2$ > bare TiO$_2$ for 1/n: N-doped TiO$_2$ > N-S co-doped TiO$_2$ > C-doped TiO$_2$ > bare TiO$_2$ > S-doped TiO$_2$.

Langmuir adsorption model. Langmuir adsorption isotherms for 30 kDa fraction of humic acid following adsorption onto N-S co-doped TiO$_2$ Degussa P-25 were presented in Figure 4.145 for Color$_{436}$, UV$_{254}$ and DOC parameters. Langmuir isotherms for UV$_{365}$ and UV$_{280}$ were presented in Appendix B.

Two parameters of Langmuir equation outlined in section 2.3, q$_m$ and K$_a$, were listed in Table 4.52 for 30 kDa fraction of humic acid following adsorption onto N-S co-doped TiO$_2$ Degussa P-25 (R^2$\geq$0.81).
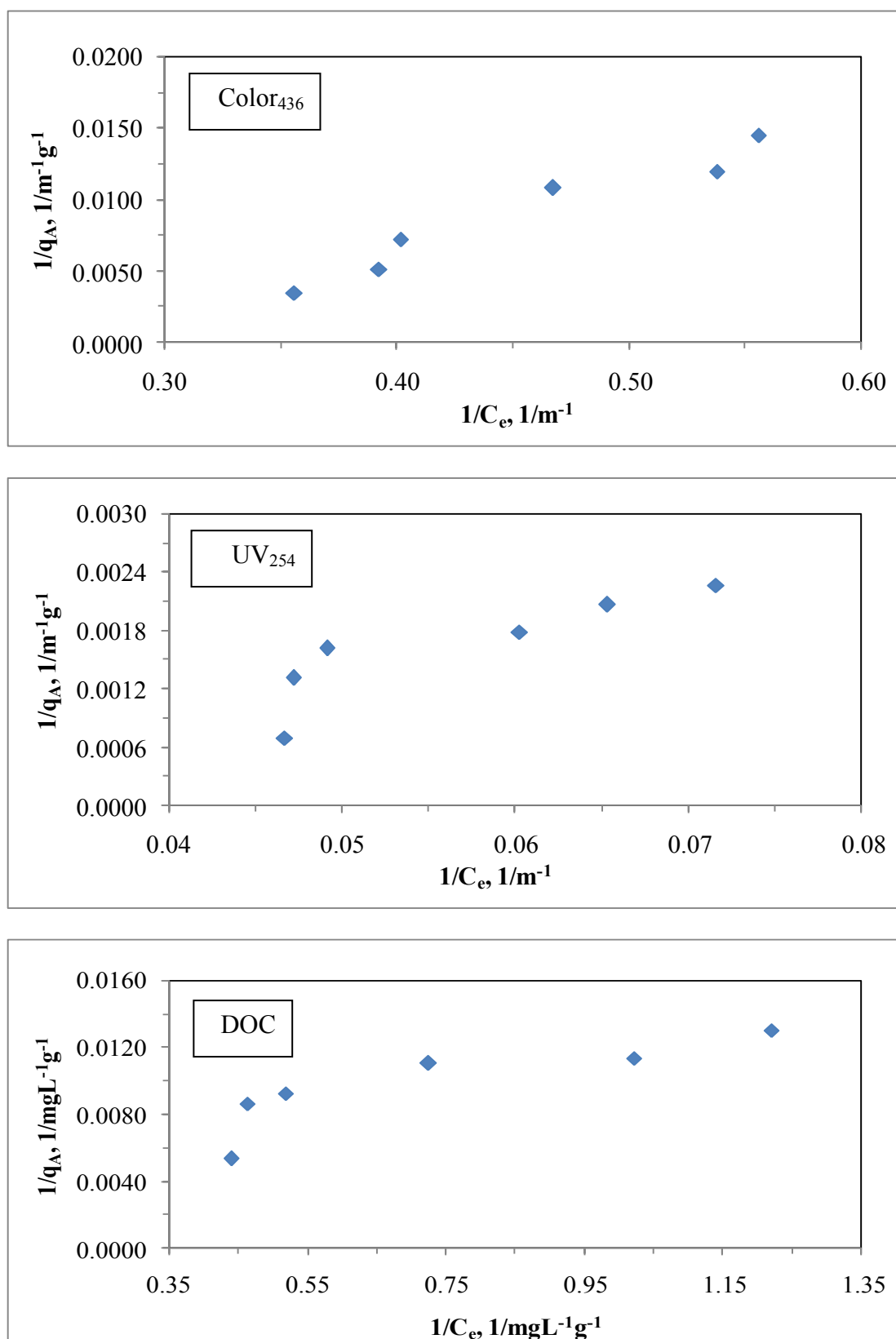
Figure 4.145. Langmuir adsorption isotherm of Color$_{436}$, UV$_{254}$ and DOC parameters of 30 kDa fraction of humic acid following adsorption onto N-S co-doped TiO$_2$ Degussa P-25.

Table 4.52. Langmuir isotherm model parameters for 30 kDa fraction of humic acid following adsorption onto N-S co-doped TiO_2 Degussa P-25.

Humic acid, 30 kDa fraction		
UV-vis parameter	q_m $m^{-1}g^{-1}$	K_a m^{-1}
Color$_{436}$	62500	0.00300
UV$_{365}$	1318	0.0650
UV$_{280}$	17857	0.00600
UV$_{254}$	12987	0.00900
Dissolved Organic Carbon	q_m mg $L^{-1}g^{-1}$	K_a mg L^{-1}
DOC	192	0.216

It could be easily seen from Table 4.52 the order of all of UV-vis spectroscopic parameters in terms of q_m value was Color$_{436}$ > UV$_{280}$ > UV$_{254}$ > UV$_{254}$ and also this order was Color$_{436}$ < UV$_{280}$ < UV$_{254}$ < UV$_{365}$ for K_a value. The model parameters as q_m and K_a values for DOC were calculated as 192 mg $L^{-1}g^{-1}$ and 0.216 mg L^{-1}.

It should be indicated that adsorption of 30 kDa fraction of humic acid onto N-S co-doped TiO_2 Degussa P-25 could well be characterized both by Freundlich and Langmuir adsorption isotherm models.

Langmuir isotherm model parameter, q_m was found to be significantly higher than the values calculated from the data attained in case of C-doped TiO_2, N-doped TiO_2, S-doped TiO_2 and N-S co-doped TiO_2 Degussa P-25 (Table 4.45, Table 4.47 and Table 4.49 as well as Table 51) for both UV-vis parameters and DOC. An inconsistent trend could be visualized for the UV-vis parameters (Table 4.43, Table 4.45, Table 4.47 and Table 4.49 as well as Table 4.51) upon comparison of the Langmuir isotherm model parameters, q_m and K_a. Langmuir isotherm model parameters of DOC could be presented in a decreasing order of; for q_m: S-doped TiO_2 > N-doped TiO_2 > N-S co-doped TiO_2 > C-doped TiO_2 > bare TiO_2 for Ka: N-doped TiO_2 > N-S co-doped TiO_2 > C-doped TiO_2 > bare TiO_2 > S-doped TiO_2.

4.8.2. Adsorption Isotherm Modeling of 30 kDa Fraction of Humic Acid onto TiO$_2$ Hombikat UV-100 Specimens

The experimental data related to 30 kDa fraction of humic acid following adsorption onto TiO$_2$ Hombikat UV-100 specimens were fitted to both Freundlich and Langmuir isotherm models.

4.8.2.1. Adsorption Isotherm Modeling of 30 kDa Fraction of Humic Acid onto Bare TiO$_2$ Hombikat UV-100 Specimen. UV-vis spectroscopic parameters (Color$_{436}$, UV$_{365}$, UV$_{280}$, and UV$_{254}$) and DOC were fitted to Freundlich (2.7) and Langmuir (2.6) adsorption isotherm models.

Freundlich adsorption model. Freundlich adsorption isotherms were presented in Figure 4.146 for Color$_{436}$, UV$_{254}$ and DOC parameters. Freundlich isotherms for UV$_{365}$ and UV$_{280}$ were presented in Appendix A. C$_e$ values changed between 0.15 – 2.68 m^{-1} for Color$_{436}$ in concern with the loading of bare TiO$_2$ Hombikat UV-100 in the solution. The values of q$_A$ were found in the range of 135 - 340 m^{-1} g^{-1} for the corresponding to the C$_e$ values. ΔC$_e$ and Δq$_A$ values for 30 kDa fraction of humic acid were calculated as 2.53 m^{-1} and 205 m^{-1} g^{-1} for Color$_{436}$. C$_e$ values altered between 1.74 – 14.30 m^{-1} for UV$_{254}$. The values of q$_A$ were calculated as between 930 - 4280 m^{-1} g^{-1} for the corresponding to the C$_e$ values. ΔC$_e$ and Δq$_A$ values for UV$_{254}$ were calculated as 12.56 m^{-1} and 3350 m^{-1} g^{-1}, respectively. C$_e$ values altered between 1.77 – 2.52 mg L^{-1} for DOC. The values of q$_A$ corresponding to the C$_e$ values were calculated as between 39 - 76 mg L^{-1} g^{-1}. ΔC$_e$ and Δq$_A$ values for DOC were calculated as 0.75 mg L^{-1} and 37 mg L^{-1} g^{-1}, respectively (Figure 4.146).

Freundlich adsorption isotherms relatively exhibited similar trend for both Color$_{436}$ and UV$_{254}$ parameters. The trends exhibited by respective adsorption isotherms could be considered as L-curve type isotherm.

Freundlich isotherm model coefficients; adsorption capacity, K$_f$, and adsorption intensity, 1/n, for 30 kDa fraction of humic acid following adsorption onto bare TiO$_2$ Hombikat UV-100 were listed in Table 4.53 (R^2≥0.82).
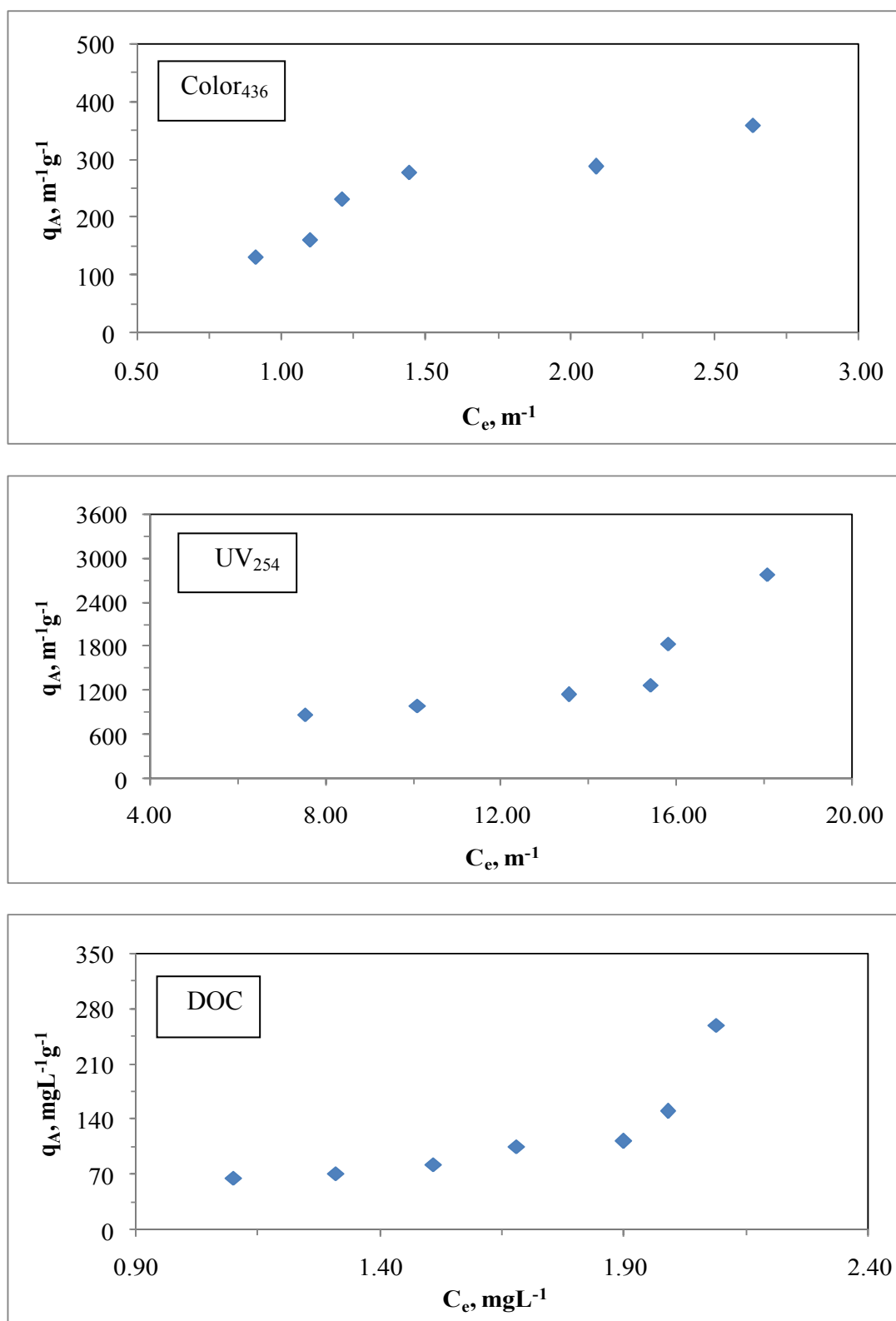
Figure 4.146. Freundlich adsorption isotherm of $Color_{436}$, UV_{254} and DOC parameters of 30 kDa fraction of humic acid following adsorption onto bare TiO_2 Hombikat UV-100.

Table 4.53. Freundlich isotherm model parameters for 30 kDa fraction of humic acid following adsorption onto bare TiO_2 Hombikat UV-100.

Humic acid, 30kDa fraction		
UV-vis parameter	K_f	1/n
$Color_{436}$	197	0.266
UV_{365}	409	0.535
UV_{280}	434	0.782
UV_{254}	486	0.790
Dissolved Organic Carbon	K_f	1/n
DOC	12.5	2.01

Comparison of UV-vis parameters indicated that the adsorption capacity constant of $Color_{436}$ was the lowest value. Moreover, the order was $Color_{436} < UV_{365} < UV_{280} < UV_{254}$ for adsorption capacity constant. An increasing order of adsorption intensity values could be given as $Color_{436} < UV_{365} < UV_{280} \leq UV_{254}$. Adsorption intensity of DOC was found to be >1 representing strong adsorption bond.

Freundlich isotherm model parameters of 30 kDa fraction of humic acid recorded following adsorption onto two different bare TiO_2 specimens were compared (Table 4.43 and Table 4.53). Freundlich isotherm model parameter, K_f displayed significantly lower values for bare TiO_2 Hombikat UV-100 in comparison to adsorption intensity values (1/n). Comparative evaluation of Freundlich isotherm model parameter, K_f of 30 kDa fraction of humic acid with 100 kDa fraction of humic acid notably revealed significant differences in both UV-vis parameters and DOC (Table 4.33 and Table 4.53).

Langmuir adsorption model. Langmuir adsorption isotherm models for 30 kDa fraction of humic acid were presented in Figure 4.147 for $Color_{436}$, UV_{254} and DOC parameters. Langmuir isotherms for UV_{365} and UV_{280} were presented in Appendix B.

Two parameters of Langmuir equation outlined in section 2.3, q_m and K_a, were listed in Table 4.54 for 30 kDa fraction of humic acid following adsorption onto bare TiO_2 Hombikat UV-100 ($R^2 \geq 0.69$).
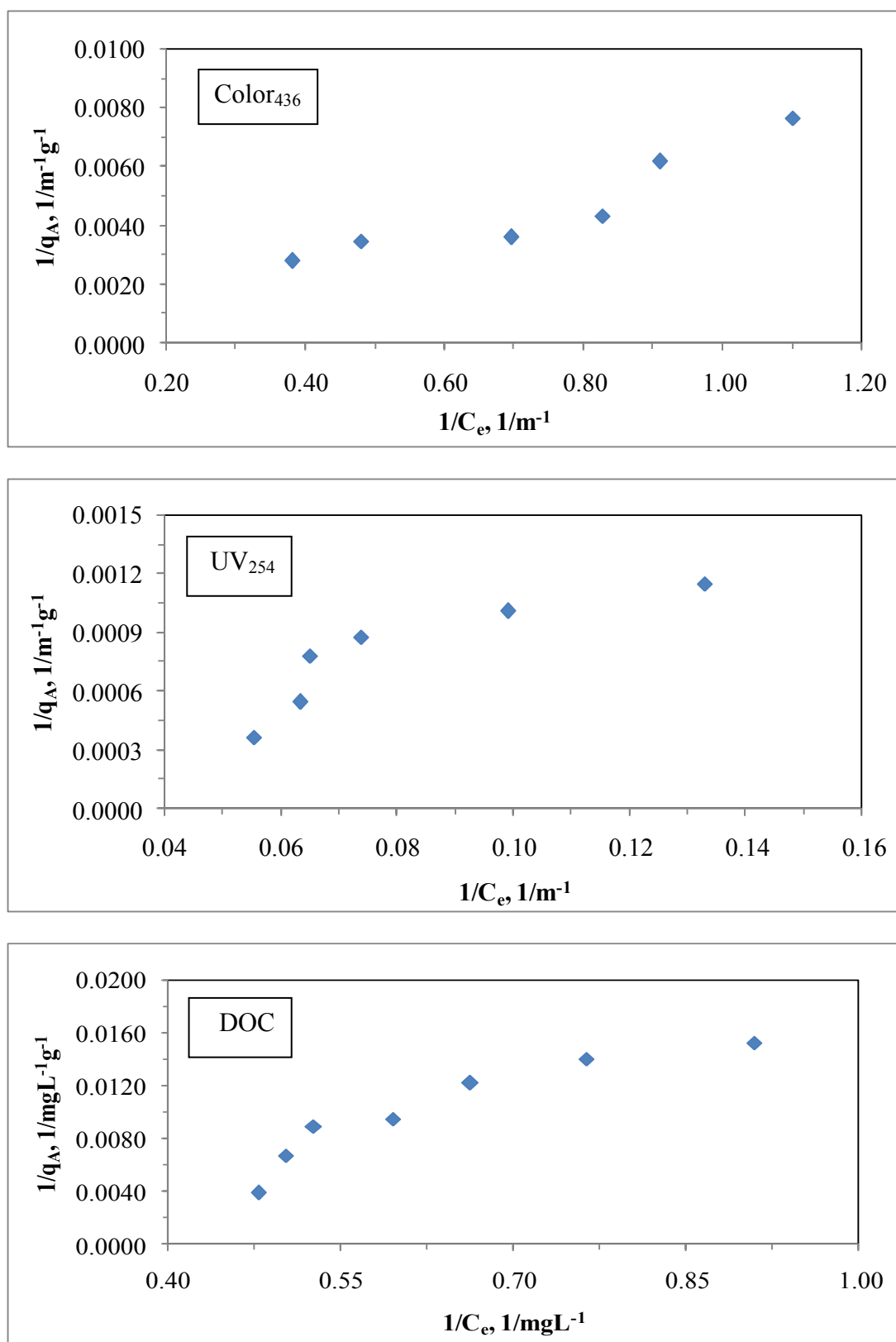
Figure 4.147. Langmuir adsorption isotherm of Color$_{436}$, UV$_{254}$ and DOC parameters of 30 kDa fraction of humic acid following adsorption onto bare TiO$_2$ Hombikat UV-100.

Table 4.54. Langmuir isotherm model parameters for 30 kDa fraction of humic acid following adsorption onto bare TiO_2 Hombikat UV-100.

Humic acid, 30 kDa fraction		
UV-vis parameter	q_m m^{-1}g^{-1}	K_a m^{-1}
Color$_{436}$	2270	8.81
UV$_{365}$	7690	1.63
UV$_{280}$	3333	0.158
UV$_{254}$	5000	0.118
Dissolved Organic Carbon	q_m mg L^{-1}g^{-1}	K_a mg L^{-1}
DOC	53.0	0.244

It could be easily seen from Table 4.54 that the order of UV-vis spectroscopic parameters for q_m value was Color$_{436}$ < UV$_{280}$ < UV$_{254}$< UV$_{365}$ and this order for K_a value was Color$_{436}$ > UV$_{365}$ > UV$_{280}$ > UV$_{254}$. The model parameters as q_m and K_a values for DOC were calculated as 53.0 mg L^{-1}g^{-1} and 0.244 mg L^{-1}.

It should be indicated that adsorption of 30 kDa fraction of humic acid onto bare TiO_2 Hombikat UV-100 could well be characterized both by Freundlich and Langmuir adsorption isotherm models.

Langmuir isotherm model parameters of 30 kDa fraction of humic acid recorded following adsorption onto different bare TiO_2 specimens (Degussa P-25 and Hombikat UV-100) were compared (Table 4.44and Table 4.54). Langmuir isotherm model parameter, q_m was found to be significantly lower than the values calculated from the data attained in case of bare TiO_2 Degussa P-25 for both UV-vis parameters and DOC in contrast to K_a. Langmuir isotherm model parameter, K_a was found to be significantly different for diverse TiO_2 specimens, namely K_a = 0.244 mg L^{-1} for bare TiO_2 Degussa P-25 and K_a = 0.0590 mg L^{-1} for bare TiO_2 Hombikat UV-100. Comparison of bare TiO_2 Degussa P-25 with bare TiO_2 Hombikat UV-100 could be regarded as discriminating between the effects of dopants.

4.8.2.2. Adsorption Isotherm Modeling of 30 kDa Fraction of Humic Acid onto C-doped TiO$_2$ Hombikat UV-100 Specimen. UV-vis spectroscopic parameters (Color$_{436}$, UV$_{365}$, UV$_{280}$, and UV$_{254}$) and DOC were fitted to Freundlich (2.7) and Langmuir (2.6) adsorption isotherm models.

Freundlich adsorption model. Freundlich adsorption isotherms were presented in Figure 4.148 for Color$_{436}$, UV$_{254}$ and DOC parameters. Freundlich isotherms for UV$_{365}$ and UV$_{280}$ were presented in Appendix A.

C_e values altered between 0.59 – 2.36 m^{-1} for Color$_{436}$ according to the loading of C-doped TiO$_2$ Hombikat UV-100 in the solution. The values of q_A were found in the range of 118 - 468 m^{-1} g^{-1} for the corresponding to the C_e values. ΔC_e and Δq_A values for Color$_{436}$ were found as 1.77 m^{-1} and 350 m^{-1} g^{-1}; respectively. C_e values altered between 4.18 – 16.89 m^{-1} for UV$_{254}$. The values of q_A were calculated as between 833 - 3244 m^{-1}g^{-1} for the corresponding to the C_e values. ΔC_e and Δq_A values for UV$_{254}$ were calculated as 12.71 m^{-1} and 2411 m^{-1} g^{-1}, respectively (Figure 4.148).

Freundlich adsorption isotherms relatively exhibited similar trend for both Color$_{436}$ and UV$_{254}$ parameters. The trends exhibited by respective adsorption isotherms could be considered as C-curve type isotherm.

C_e values altered between 1.37 – 2.37 mg L^{-1} for DOC. The values of q_A corresponding to the C_e values were calculated as between 55 - 148 mg L^{-1} g^{-1}. ΔC_e and Δq_A values for DOC were calculated as 1.00 mg L^{-1} and 93 mg L^{-1} g^{-1}, respectively (Figure 4.148).

The effect of C-doping did not significantly alter the DOC adsorption isotherm trend of 30 kDa fraction of humic acid onto TiO$_2$ Hombikat UV-100.

Freundlich isotherm model coefficients; adsorption capacity, K_f, and adsorption intensity, 1/n, for 30 kDa fraction of humic acid adsorption onto C-doped TiO$_2$ Hombikat UV-100 were listed in Table 4.55 (R^2≥0.96).
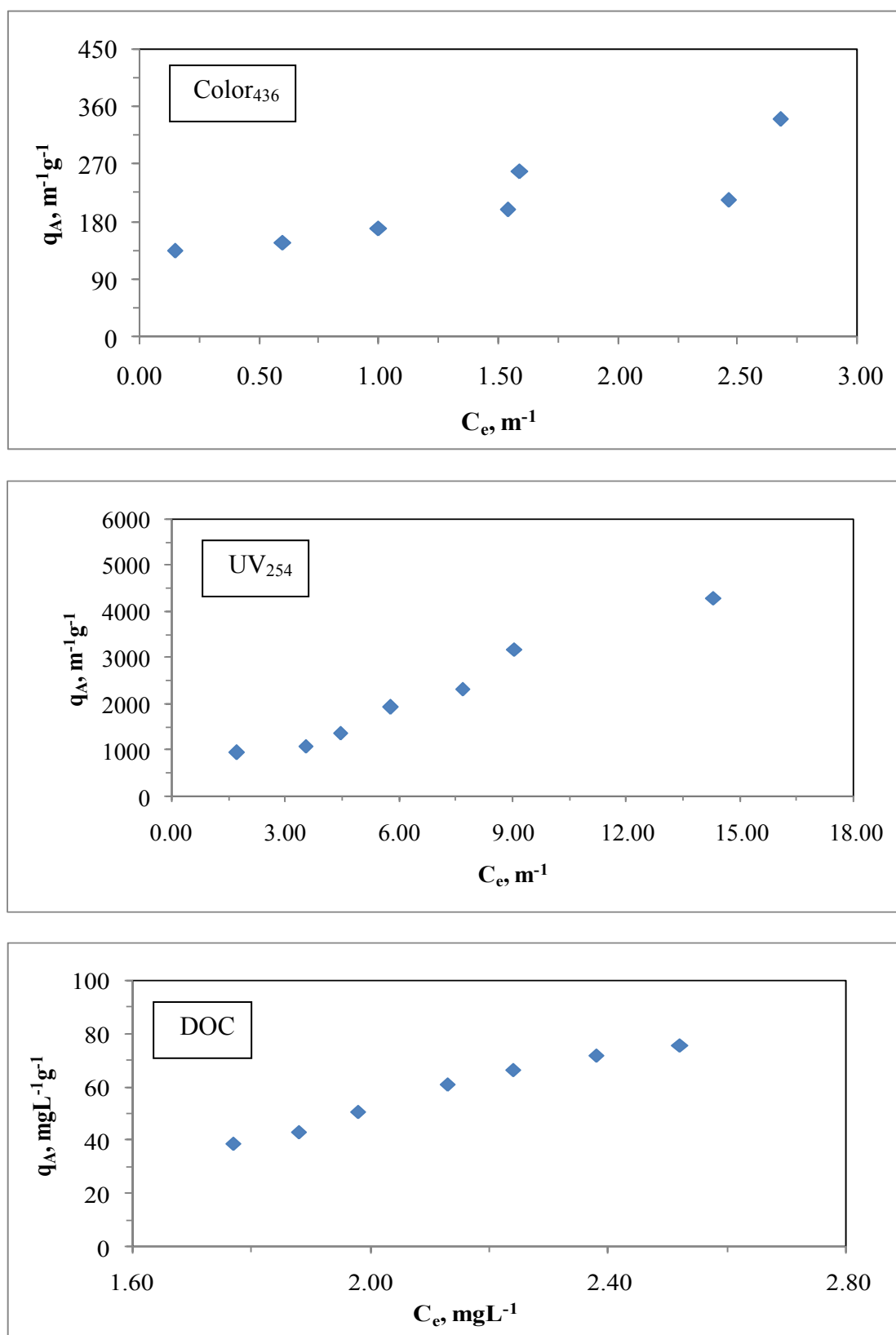
Figure 4.148. Freundlich adsorption isotherm of Color$_{436}$, UV$_{254}$ and DOC parameters of 30 kDa fraction of humic acid following adsorption onto C-doped TiO$_2$ Hombikat UV-100.

Table 4.55. Freundlich isotherm model parameters for 30 kDa fraction of humic acid following adsorption onto C-doped TiO_2 Hombikat UV-100.

Humic acid, 30kDa fraction		
UV-vis parameter	K_f	$1/n$
$Color_{436}$	191	0.951
UV_{365}	238	0.865
UV_{280}	178	0.980
UV_{254}	201	0.957
Dissolved Organic Carbon	K_f	$1/n$
DOC	26.9	1.80

Comparison of UV-vis parameters indicated that the adsorption capacity constant of UV_{280} was the lowest value. The order was UV_{280} < $Color_{436}$ < UV_{254} < UV_{365} for adsorption capacity constant. Also, adsorption intensity of UV_{365} was the lowest value. The order of adsorption intensity values could be given as UV_{365} < $Color_{436}$ ≤ UV_{254} < UV_{280}. Adsorption intensity of DOC was found to be >1 representing strong adsorption bond.

Freundlich isotherm model parameters of 30 kDa fraction of humic acid recorded following adsorption onto two different TiO_2 specimens were compared (Table 4.53 and Table 4.55). Freundlich isotherm model parameter, K_f displayed slightly lower values for C-doped TiO_2 Hombikat UV-100 in comparison to $1/n$.

Langmuir adsorption model. Langmuir adsorption isotherms for 30 kDa fraction of humic acid following adsorption onto C-doped TiO_2 Hombikat UV-100 were presented in Figure 4.149 for $Color_{436}$, UV_{254} and DOC parameters. Langmuir isotherms for UV_{365} and UV_{280} were presented in Appendix B.

Two parameters of Langmuir equation outlined in section 2.3, q_m and K_a, were listed in Table 4.56 for 30 kDa fraction of humic acid following adsorption onto C- doped TiO_2 Hombikat UV-100 ($R^2 \geq 0.96$).
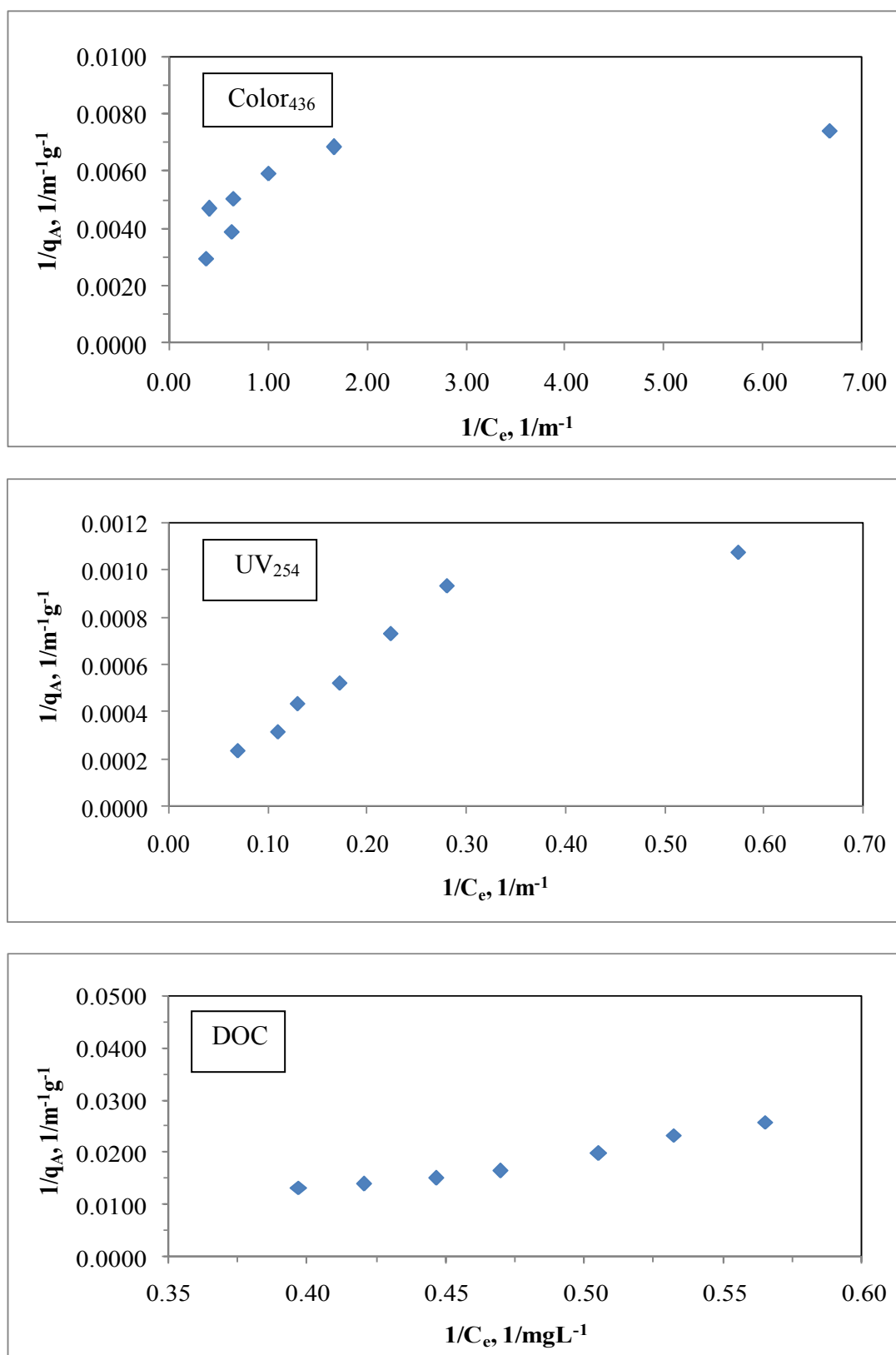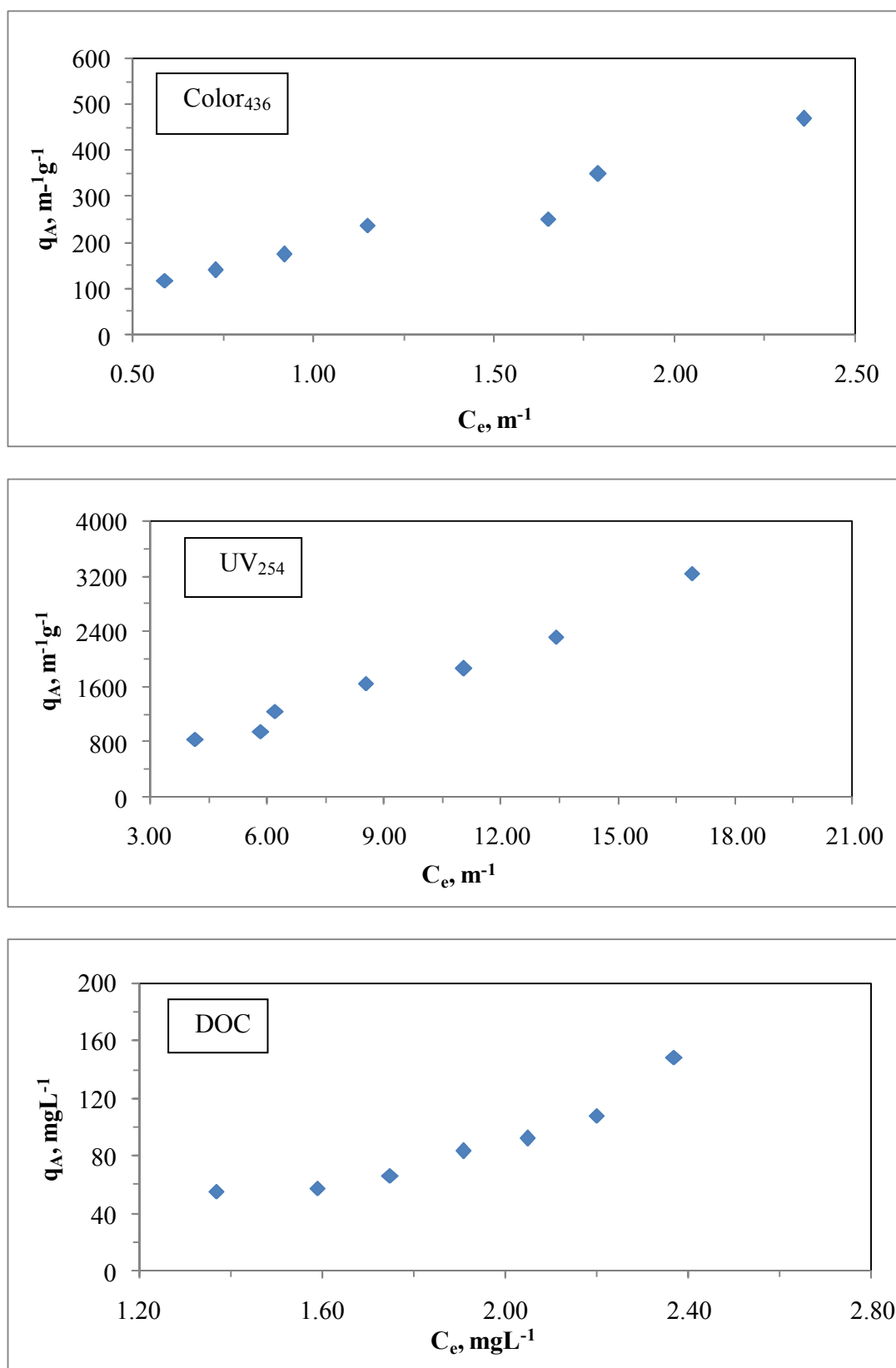
Figure 4.149. Langmuir adsorption isotherm of Color$_{436}$, UV$_{254}$ and DOC parameters of 30 kDa fraction of humic acid following adsorption onto C-doped TiO$_2$ Hombikat UV-100.

Table 4.56. Langmuir isotherm model parameters for 30 kDa fraction of humic acid following adsorption onto C-doped TiO_2 Hombikat UV-100.

Humic acid, 30 kDa fraction		
UV-vis parameter	q_m $m^{-1}g^{-1}$	K_a m^{-1}
$Color_{436}$	3333	0.0610
UV_{365}	3333	0.0750
UV_{280}	14286	0.0140
UV_{254}	20000	0.0100
Dissolved Organic Carbon	q_m mg $L^{-1}g^{-1}$	K_a mg L^{-1}
DOC	125	0.211

It could be easily seen from Table 4.56 that q_m value had the highest value in UV_{254} spectroscopic parameter. The order of all of the UV-vis spectroscopic parameters in terms of q_m value was $UV_{254} > UV_{280} > UV_{365} = Color_{436}$. The order of all of the UV-vis spectroscopic parameters in terms of K_a value was $UV_{365} > Color_{436} > UV_{280} > UV_{254}$. The model parameters as q_m and K_a values for DOC were calculated as 125 mg $L^{-1}g^{-1}$ and 0.211 mg L^{-1}.

It should be indicated that adsorption of 30 kDa fraction of humic acid onto bare TiO_2 Degussa P-25 could well be characterized both by Freundlich and Langmuir adsorption isotherm models.

Comparison of Table 4.54 and Table 4.56 could display the role of C-doping on adsorption of 30 kDa fraction of humic acid onto TiO_2 Hombikat UV-100. Although a consistent trend could be expressed within the UV-vis parameters and DOC, q_m was significantly higher for C-doped TiO_2 Hombikat UV-100 in comparison to slightly different K_a values as $K_a = 0.244$ mg L^{-1} for bare TiO_2 Hombikat UV-100 and $K_a = 0.211$ mg L^{-1} for C-doped TiO_2 Hombikat UV-100. Comparative evaluation of Langmuir isotherm model parameters of 30 kDa fraction of humic acid with 100 kDa fraction of humic acid following adsorption onto C-doped TiO_2 Hombikat UV-100 revealed the most significant difference in both UV-vis parameters and DOC.

4.8.2.3. Adsorption Isotherm Modeling of 30 kDa Fraction of Humic Acid onto N-doped TiO$_2$ Hombikat UV-100 Specimen. UV-vis spectroscopic parameters (Color$_{436}$, UV$_{365}$, UV$_{280}$, and UV$_{254}$) and DOC were fitted to Freundlich (2.7) and Langmuir (2.6) adsorption isotherm models.

Freundlich adsorption model. Freundlich adsorption isotherms were presented in Figure 4.150 for Color$_{436}$, UV$_{254}$ and DOC parameters. Freundlich isotherms for UV$_{365}$ and UV$_{280}$ were presented in Appendix A.

C$_e$ values altered between 0.74 – 2.47 m^{-1} for Color$_{436}$ according to the loading of N-doped TiO$_2$ Hombikat UV-100 in the solution. The values of q$_A$ were found in the range of 112 - 424 m^{-1}g^{-1} for the corresponding to the C$_e$ values. ΔC$_e$ and Δq$_A$ values for 30 kDa fraction of humic acid were found as 1.73 m^{-1} and 312 m^{-1} g^{-1} for Color$_{436}$. Ce values altered between 6.34 – 17.34 m^{-1} for UV$_{254}$. The values of q$_A$ were calculated as between 746 - 3064 m^{-1}g^{-1} for the corresponding to the C$_e$ values. ΔC$_e$ and Δq$_A$ values for UV$_{254}$ were calculated as 11 m^{-1} and 2318 m^{-1}g^{-1}, respectively (Figure 4.150).

Freundlich adsorption isotherms relatively exhibited similar trend for both of the UV-vis parameters as expressed by Color$_{436}$ and UV$_{254}$ parameters. The trends exhibited by the respective adsorption isotherms could be considered as C-curve type isotherm.

C$_e$ values altered between 1.25 – 2.14 mg L^{-1} for DOC. The values of q$_A$ corresponding to the C$_e$ values were calculated as between 60 - 240 mg L^{-1} g^{-1}. ΔC$_e$ and Δq$_A$ values for DOC were calculated as 0.89 mg L^{-1} and 180 mg L^{-1} g^{-1}, respectively (Figure 4.150).

N-doping of TiO$_2$ Hombikat UV-100 did not significantly alter the adsorption profiles of both UV-vis spectral parameters and DOC in comparison to C-doping of TiO$_2$ Hombikat UV-100.

Freundlich isotherm model coefficients; adsorption capacity, K$_f$, and adsorption intensity, 1/n, for 30 kDa fraction of humic acid following adsorption onto N-doped TiO$_2$ Hombikat UV-100 were listed in Table 4.57. (R^2≥0.95).
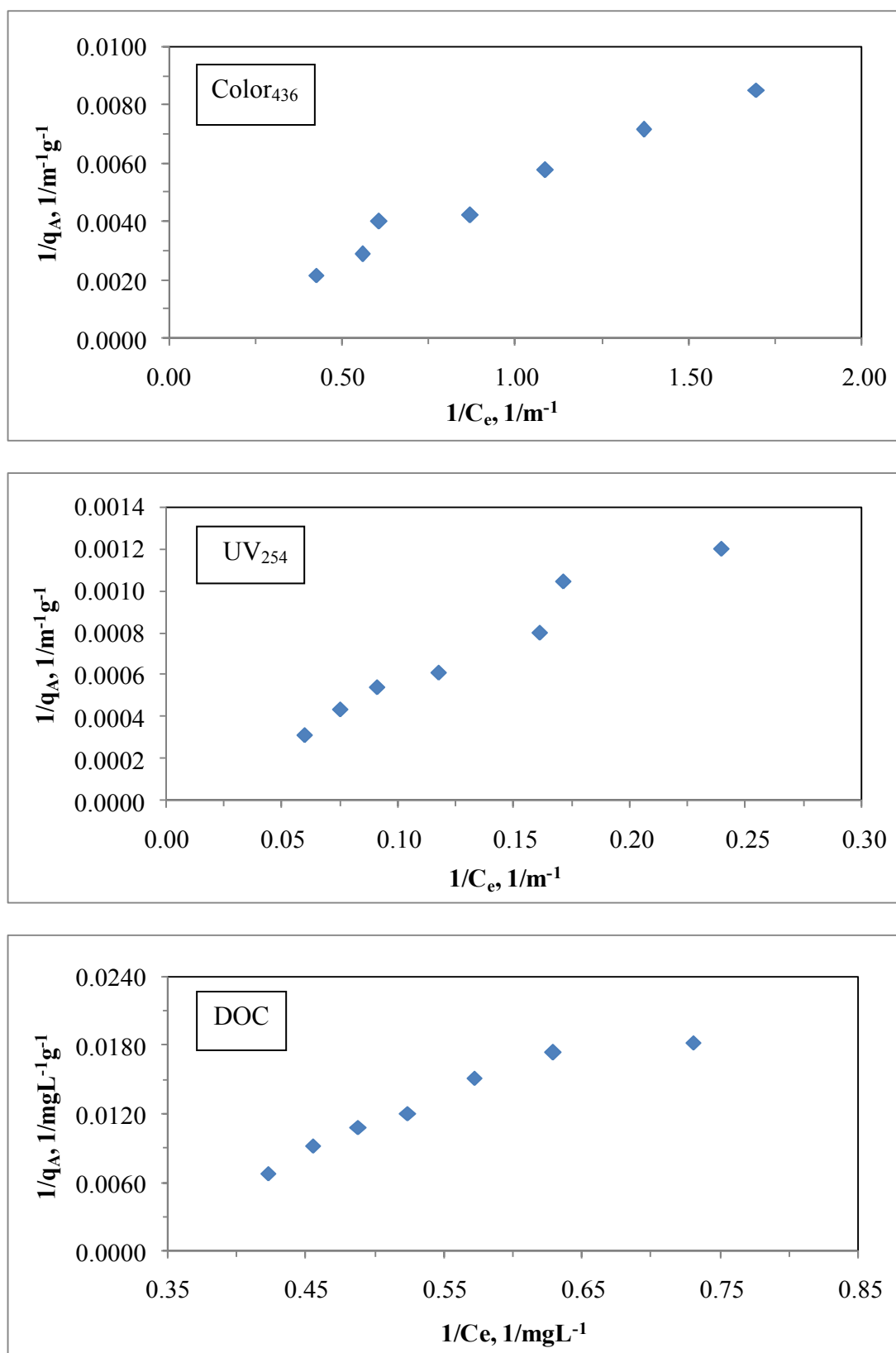
Figure 4.150. Freundlich adsorption isotherm of $Color_{436}$, UV_{254} and DOC parameters of 30 kDa fraction of humic acid following adsorption onto N-doped TiO_2 Hombikat UV-100.

Table 4.57. Freundlich isotherm model parameters for 30 kDa fraction of humic acid following adsorption onto N-doped TiO_2 Hombikat UV-100.

Humic acid, 30kDa fraction		
UV-vis parameter	K_f	1/n
$Color_{436}$	139.0	1.11
UV_{365}	124.2	1.17
UV_{280}	53.92	1.36
UV_{254}	49.97	1.40
Dissolved Organic Carbon	K_f	1/n
DOC	65.75	1.31

Comparison of UV-vis parameters indicated that the adsorption capacity constant of $Color_{436}$ was the highest value. The order was $Color_{436} > UV_{365} > UV_{280} > UV_{254}$ for adsorption capacity constant. Also, adsorption intensity of $Color_{436}$ was the lowest value. Furthermore, the order was $Color_{436} \leq UV_{365} < UV_{280} \leq UV_{254}$ for adsorption intensity. Adsorption intensity of DOC was found to be >1 representing strong adsorption bond. The binding mechanism of humic acid could be affected by mixed crystalline nature of TiO_2, in such a way that adsorption constants increased as mentioned before.

Freundlich isotherm model parameters, K_f values could be displayed as following an order of N-doped TiO_2 > C-doped TiO_2 > bare TiO_2 Hombikat UV-100. The order of 1/n values could be given as bare TiO_2 > C-doped TiO_2 > N-doped TiO_2 Hombikat UV-100 in terms of DOC (Table 4.53, Table 4.55 and Table 4.57).

Langmuir adsorption model. Langmuir adsorption isotherm models for 30 kDa fraction of humic acid following adsorption onto N-doped TiO_2 Hombikat UV-100 were presented in Figure 4.151 for $Color_{436}$, UV_{254} and DOC parameters. Langmuir isotherms for UV_{365} and UV_{280} were presented in Appendix B.

Two parameters of Langmuir equation outlined in section 2.3, q_m and K_a, were listed in Table 4.58 for 30 kDa fraction of humic acid following adsorption onto N- doped TiO_2 Hombikat UV-100 ($R^2 \geq 0.96$).
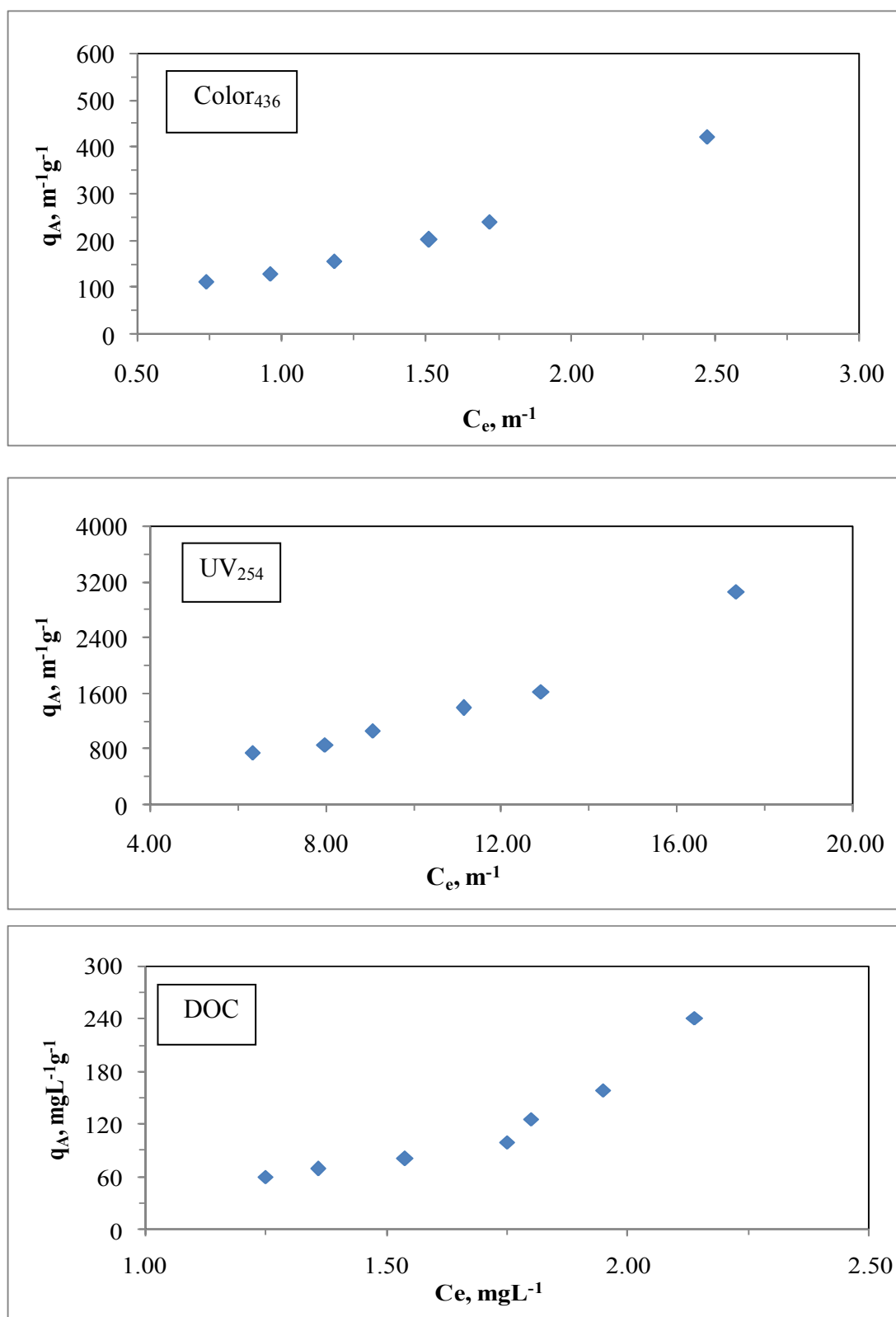
Figure 4.151. Langmuir adsorption isotherm of Color$_{436}$, UV$_{254}$ and DOC parameters of 30 kDa fraction of humic acid following adsorption onto N-doped TiO$_2$ Hombikat UV-100.

Table 4.58. Langmuir isotherm model parameters for 30 kDa fraction of humic acid following adsorption onto N-doped TiO_2 Hombikat UV-100.

Humic acid, 30 kDa fraction		
UV-vis parameter	q_m m^{-1}g^{-1}	K_a m^{-1}
Color$_{436}$	12500	0.0110
UV$_{365}$	16667	0.0860
UV$_{280}$	5000	0.0190
UV$_{254}$	5000	0.0190
Dissolved Organic Carbon	q_m mg L^{-1}g^{-1}	K_a mg L^{-1}
DOC	83.0	0.324

It could be easily seen from Table 4.58 that the order of all of the UV-vis spectroscopic parameters in terms of q_m value was $UV_{254} = UV_{280} < Color_{436} < UV_{365}$. The order of K_a value could be given as $Color_{436} < UV_{254} = UV_{280} < UV_{365}$. The model parameters as q_m and K_a values for DOC were calculated as 83.0 mg L^{-1}g^{-1} and 0.324 mg L^{-1}.

It should be indicated that adsorption of 30 kDa fraction of humic acid onto N-doped TiO_2 Hombikat UV-100 could well be characterized both by Freundlich and Langmuir adsorption isotherm models.

Langmuir isotherm model parameter, q_m was found to be significantly lower than the values calculated from the data attained in case of C-doped TiO_2 Hombikat UV-100 (Table 4.56 and Table 4.58) for UV-vis parameters in comparison to DOC. Langmuir isotherm model parameter, K_a was found to be slightly different for diverse TiO_2 Hombikat UV-100 specimens, namely K_a = 0.244 mg L^{-1} for bare TiO_2 Hombikat UV-100 and K_a = 0.211 mg L^{-1} for C-doped TiO_2 Hombikat UV-100 as well as K_a = 0.324 mg L^{-1} for N-doped TiO_2 Hombikat UV-100 in terms of DOC. Comparison of C-doping and N-doping with bare TiO_2 Hombikat UV-100 could be regarded as non-discriminating between the effects of dopants (Table 4.54, Table 4.56 and Table 4.58).

4.8.2.4. Adsorption Isotherm Modeling of 30 kDa Fraction of Humic Acid onto S-doped TiO$_2$ Hombikat UV-100 Specimen. UV-vis spectroscopic parameters (Color$_{436}$, UV$_{365}$, UV$_{280}$, and UV$_{254}$) and DOC were fitted to Freundlich (2.7) and Langmuir (2.6) adsorption isotherm models.

Freundlich adsorption model. Freundlich adsorption isotherms were presented in Figure 4.152 for Color$_{436}$, UV$_{254}$ and DOC parameters. Freundlich isotherms for UV$_{365}$ and UV$_{280}$ were presented in Appendix A.

C$_e$ values altered between 0.21 – 1.90 m^{-1} for Color$_{436}$ according to the loading of S-doped TiO$_2$ Hombikat UV-100 in the solution. The values of q$_A$ were found in the range of 133-652 m^{-1} g^{-1} for the corresponding to the C$_e$ values. ΔC$_e$ and Δq$_A$ values for 30 kDa fraction of humic acid were found as 1.69 m^{-1} and 519 m^{-1} g^{-1} for Color$_{436}$. C$_e$ values altered between 2.40 – 14.90 m^{-1} for UV$_{254}$. The values of q$_A$ were calculated as between 904 - 4040 m^{-1}g^{-1} for the corresponding to the C$_e$ values. ΔC$_e$ and Δq$_A$ values for UV$_{254}$ were calculated as 12.5 m^{-1} and 3136 m^{-1}g^{-1}, respectively (Figure 4.152).

Freundlich adsorption isotherms relatively exhibited similar trend for both of the UV-vis parameters as expressed by Color$_{436}$ and UV$_{254}$ parameters. The trends exhibited by the respective adsorption isotherms could be considered as S-curve type isotherm.

C$_e$ values altered between 1.15 – 2.22 mg L^{-1} for DOC. The values of q$_A$ corresponding to the C$_e$ values were in the range of 64 - 208 mg L^{-1} g^{-1}. ΔC$_e$ and Δq$_A$ values for DOC were calculated as 1.07 mg L^{-1} and 144 mg L^{-1} g^{-1}, respectively (Figure 4.152).

The adsorption isotherm trends of 30 kDa fraction of humic acid following adsorption onto S-doping of TiO$_2$ Hombikat UV-100 with N-doping of TiO$_2$ Hombikat UV-100 displayed similarities in terms of UV-vis spectral parameters as well as DOC.

Freundlich isotherm model coefficients; adsorption capacity, K$_f$, and adsorption intensity, 1/n, for 30 kDa fraction of humic acid following adsorption onto S-doped TiO$_2$ Hombikat UV-100 were listed in Table 4.59 (R^2≥0.83).
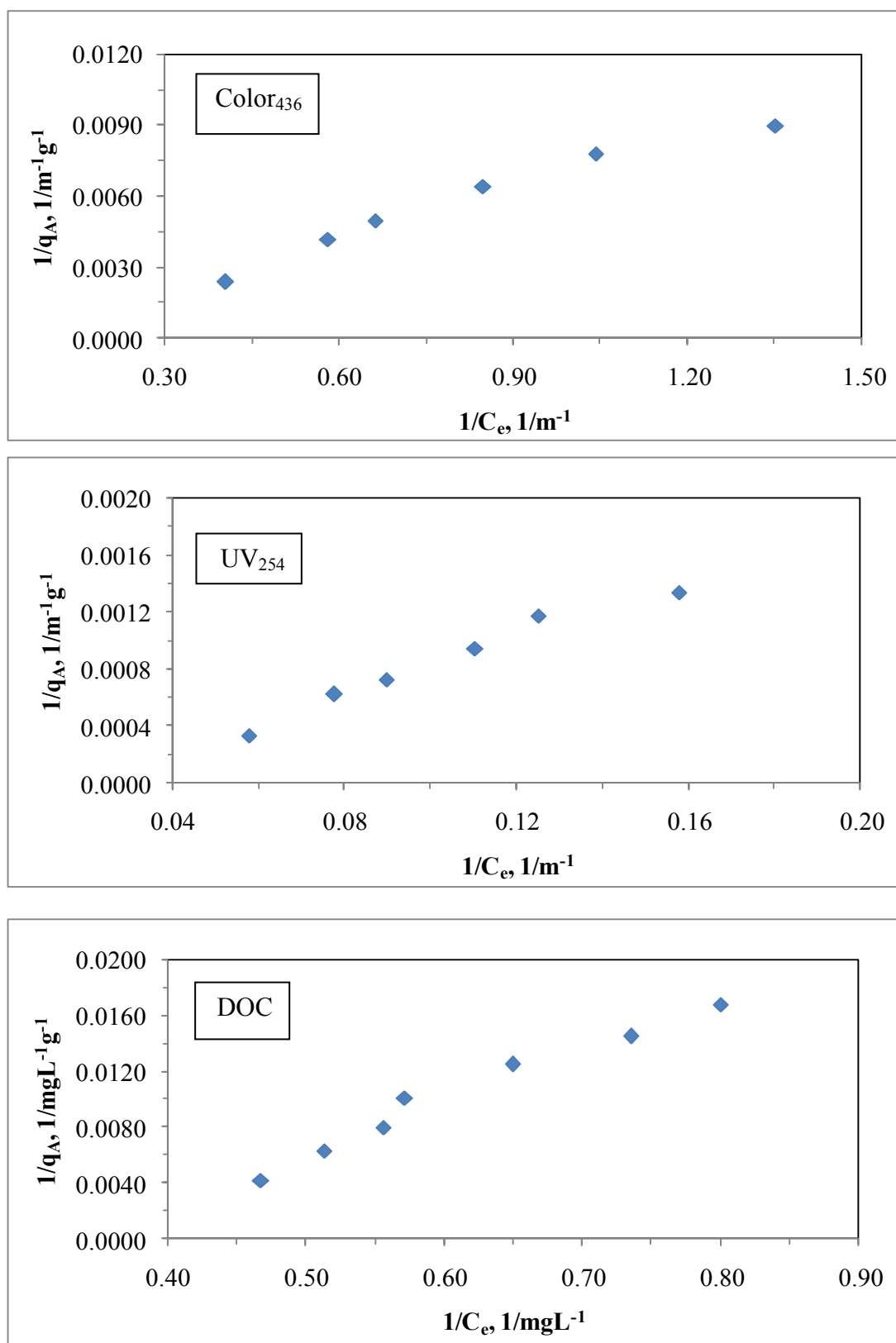
Figure 4.152. Freundlich adsorption isotherm of Color$_{436}$, UV$_{254}$ and DOC parameters of 30 kDa fraction of humic acid following adsorption onto S-doped TiO$_2$ Hombikat UV-100.

Table 4.59. Freundlich isotherm model parameters for 30 kDa fraction of humic acid following adsorption onto S-doped TiO_2 Hombikat UV-100.

Humic acid, 30kDa fraction		
UV-vis parameter	K_f	1/n
$Color_{436}$	281	0.656
UV_{365}	356	0.705
UV_{280}	354	0.806
UV_{254}	338	0.839
Dissolved Organic Carbon	K_f	1/n
DOC	44.9	1.86

Comparison of UV-vis parameters indicated that the adsorption capacity constant of $Color_{436}$ was the lowest value. Moreover, adsorption capacity constant of UV_{365} was the highest value. The order was $Color_{436} < UV_{254} < UV_{280} \leq UV_{365}$ for adsorption capacity constant. Also, adsorption intensity of $Color_{436}$ was the lowest value. Furthermore, adsorption intensity of UV_{254} had the highest value. An increasing order of adsorption intensity values could be given as $Color_{436} < UV_{365} < UV_{280} < UV_{254}$. Adsorption intensity of DOC was found to be >1 representing strong adsorption bond.

Freundlich isotherm model parameters, K_f values could be displayed as following an order of N-doped TiO_2 > S-doped TiO_2 > C-doped TiO_2 > bare TiO_2 Hombikat UV-100. The order of 1/n values could be given as bare TiO_2 > S-doped TiO_2 > C-doped TiO_2 > N-doped TiO_2 Hombikat UV-100 in terms of DOC.

Langmuir adsorption model. Langmuir adsorption isotherms for 30 kDa fraction of humic acid following adsorption onto S-doped TiO_2 Hombikat UV-100 were presented in Figure 4.153 for $Color_{436}$, UV_{254} and DOC parameters. Langmuir isotherms for UV_{365} and UV_{280} were presented in Appendix B.

Two parameters of Langmuir equation outlined in section 2.3, q_m and K_a, were listed in Table 4.60 for 30 kDa fraction of humic acid following adsorption onto S- doped TiO_2 Hombikat UV-100 ($R^2 \geq 0.75$).
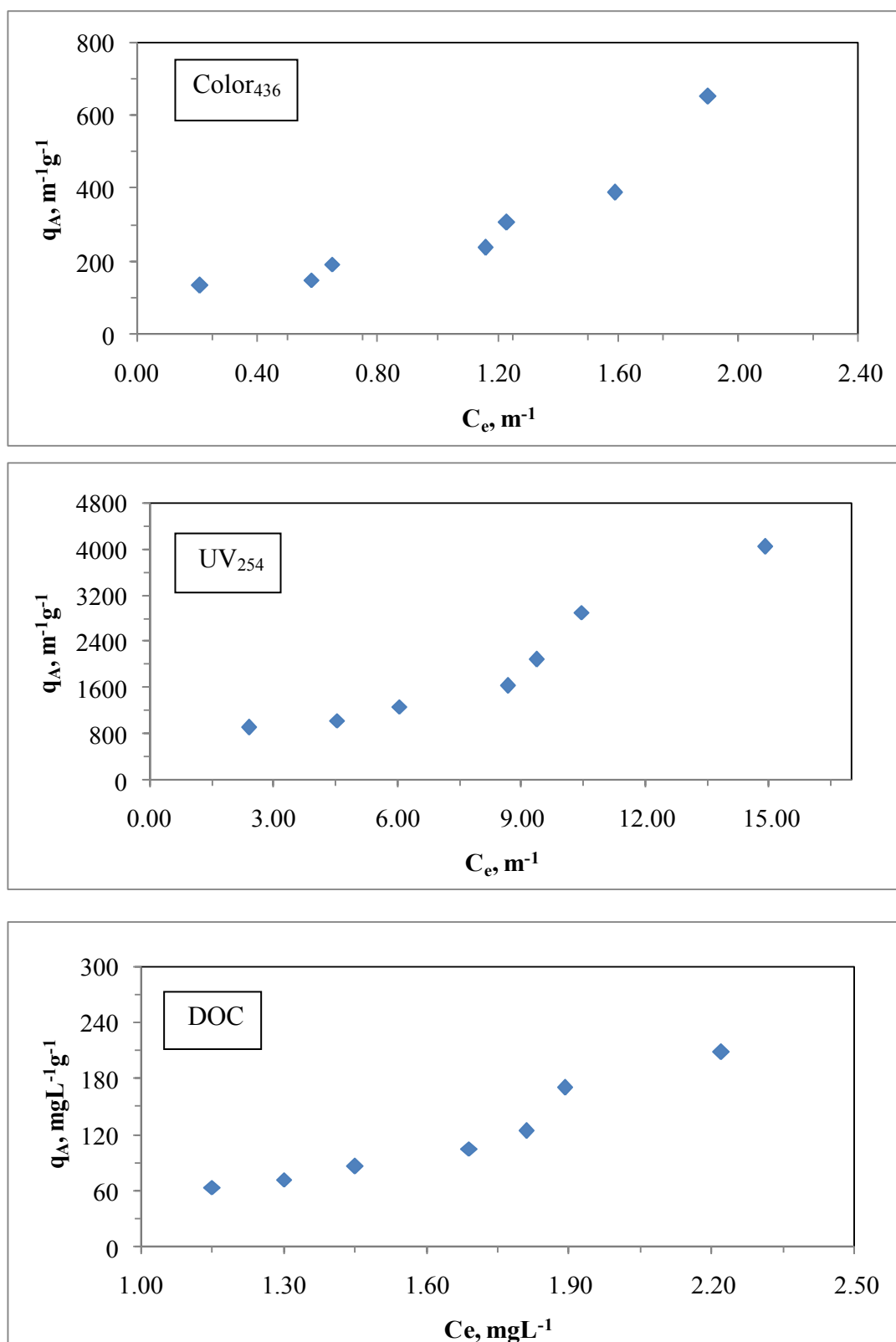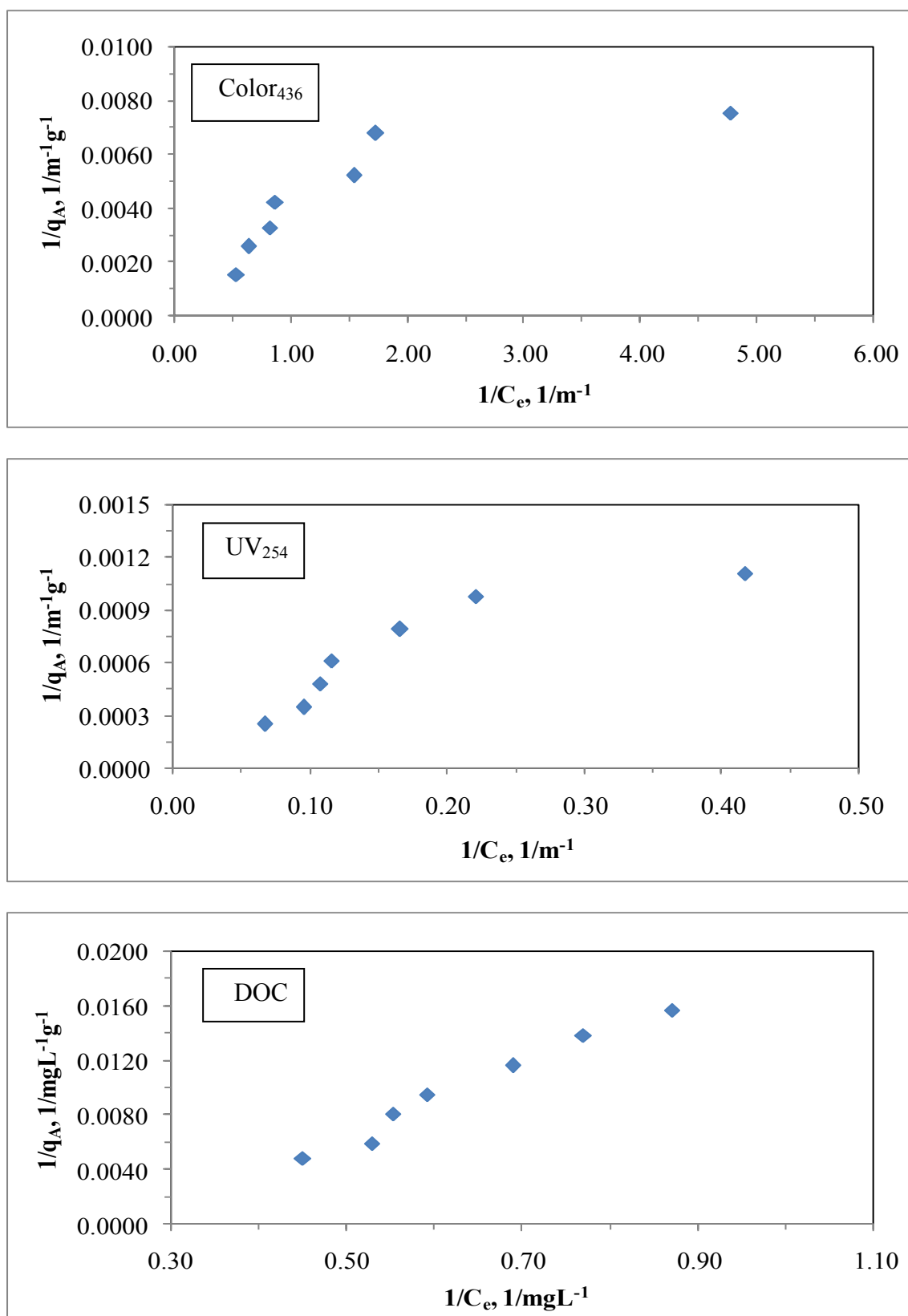
Figure 4.153. Langmuir adsorption isotherm of $Color_{436}$, UV_{254} and DOC parameters of 30 kDa fraction of humic acid following adsorption onto S-doped TiO_2 Hombikat UV-100.

Table 4.60. Langmuir isotherm model parameters for 30 kDa fraction of humic acid following adsorption onto S-doped TiO_2 Hombikat UV-100.

Humic acid, 30 kDa fraction		
UV-vis parameter	q_m $m^{-1}g^{-1}$	K_a m^{-1}
$Color_{436}$	500	2.00
UV_{365}	1000	1.00
UV_{280}	3333	0.130
UV_{254}	5000	0.0830
Dissolved Organic Carbon	q_m mg $L^{-1}g^{-1}$	K_a mg L^{-1}
DOC	143	0.259

It could be easily seen from Table 4.60 that the order of all of the UV-vis spectroscopic parameters in terms of q_m value was $UV_{254} > UV_{280} > UV_{365} > Color_{436}$ and this order was reverse for K_a value, namely, $Color_{436} > UV_{365} > UV_{280} > UV_{254}$. The model parameters as q_m and K_a values for DOC were found as 143 mg $L^{-1}g^{-1}$ and 0.259 mg L^{-1}.

It should be indicated that adsorption of 30 kDa fraction of humic acid onto S-doped TiO_2 Hombikat UV-100 could well be characterized both by Freundlich and Langmuir adsorption isotherm models.

Langmuir isotherm model parameters calculated for UV-vis parameters and DOC displayed a different trend with respect to the both N-doped TiO_2 and S-doped TiO_2 Hombikat UV-100. An inconsistent trend could be visualized for the UV-vis parameters (Table 4.54, Table 4.56 and Table 4.58 as well as Table 4.60) upon comparison of the Langmuir isotherm model parameters, q_m and K_a. Langmuir isotherm model parameters of DOC could be presented in a decreasing order of; for q_m: S-doped TiO_2 > C-doped TiO_2 > N-doped TiO_2 > bare TiO_2 for Ka: N-doped TiO_2 > S-doped TiO_2 > bare TiO_2 > C-doped TiO_2 Hombikat UV-100. Comparative evaluation of Langmuir isotherm model parameters of 30 kDa fraction of humic acid with 100 kDa fraction of humic acid following adsorption onto S-doped TiO_2 Hombikat UV-100 did not reveal the most significant difference in both UV-vis parameters in contrast to DOC (Table 4.40 and Table 4.60).

4.8.2.5. Adsorption Isotherm Modeling of 30 kDa Fraction of Humic Acid onto N-S co-doped TiO$_2$ Hombikat UV-100 Specimen. UV-vis spectroscopic parameters (Color$_{436}$, UV$_{365}$, UV$_{280}$, and UV$_{254}$) and DOC were fitted to Freundlich (2.7) and Langmuir (2.6) adsorption isotherm models.

Freundlich adsorption model. Freundlich adsorption isotherms were presented in Figure 4.154 for Color$_{436}$, UV$_{254}$ and DOC parameters. Freundlich isotherms for UV$_{365}$ and UV$_{280}$ were presented in Appendix A.

C$_e$ values altered between 0.61 – 2.24 m^{-1} for Color$_{436}$ according to the loading of N-S co-doped TiO$_2$ Hombikat UV-100 in the solution. The values of q$_A$ were found in the range of 117 - 516 m^{-1} g^{-1} for the corresponding to the C$_e$ values. ΔC$_e$ and Δq$_A$ values for Color$_{436}$ were found as 1.63 m^{-1} and 399 m^{-1} g^{-1}, respectively. C$_e$ values altered between 1.54 – 17.39 m^{-1} for UV$_{254}$. The calculated values of q$_A$ were in the range of 938 - 3044 m^{-1}g^{-1} for the corresponding to the C$_e$ values. ΔC$_e$ and Δq$_A$ values for UV$_{254}$ were calculated as 15.85 m^{-1} and 2106 m^{-1} g^{-1}, respectively (Figure 4.154).

Freundlich adsorption isotherms relatively exhibited similar trend for both of the UV-vis parameters as expressed by Color$_{436}$ and UV$_{254}$ parameters. The trends exhibited by the respective adsorption isotherms could be considered as L-curve type isotherm.

C$_e$ values altered between 0.92 – 2.18 mg L^{-1} for DOC. The values of q$_A$ corresponding to the C$_e$ values were in the range of 73 - 224 mg L^{-1} g^{-1}. ΔC$_e$ and Δq$_A$ values for DOC were calculated as 1.26 mg L^{-1} and 151 mg L^{-1} g^{-1}, respectively (Figure 4.154).

N-S co-doping of TiO$_2$ Hombikat UV-100 along with N-doped TiO$_2$ and S-doped TiO$_2$ Hombikat UV-100 significantly did not change the adsorption isotherm trend of 30 kDa fraction of humic acid (Figure 4.150, Figure 4.152 and Figure 4.154).

Freundlich isotherm model coefficients; adsorption capacity, K$_f$, and adsorption intensity, 1/n, for 30 kDa fraction of humic acid following adsorption onto N-S co-doped TiO$_2$ Hombikat UV-100 were listed in Table 4.61 (R$^2 \geq 0.82$).

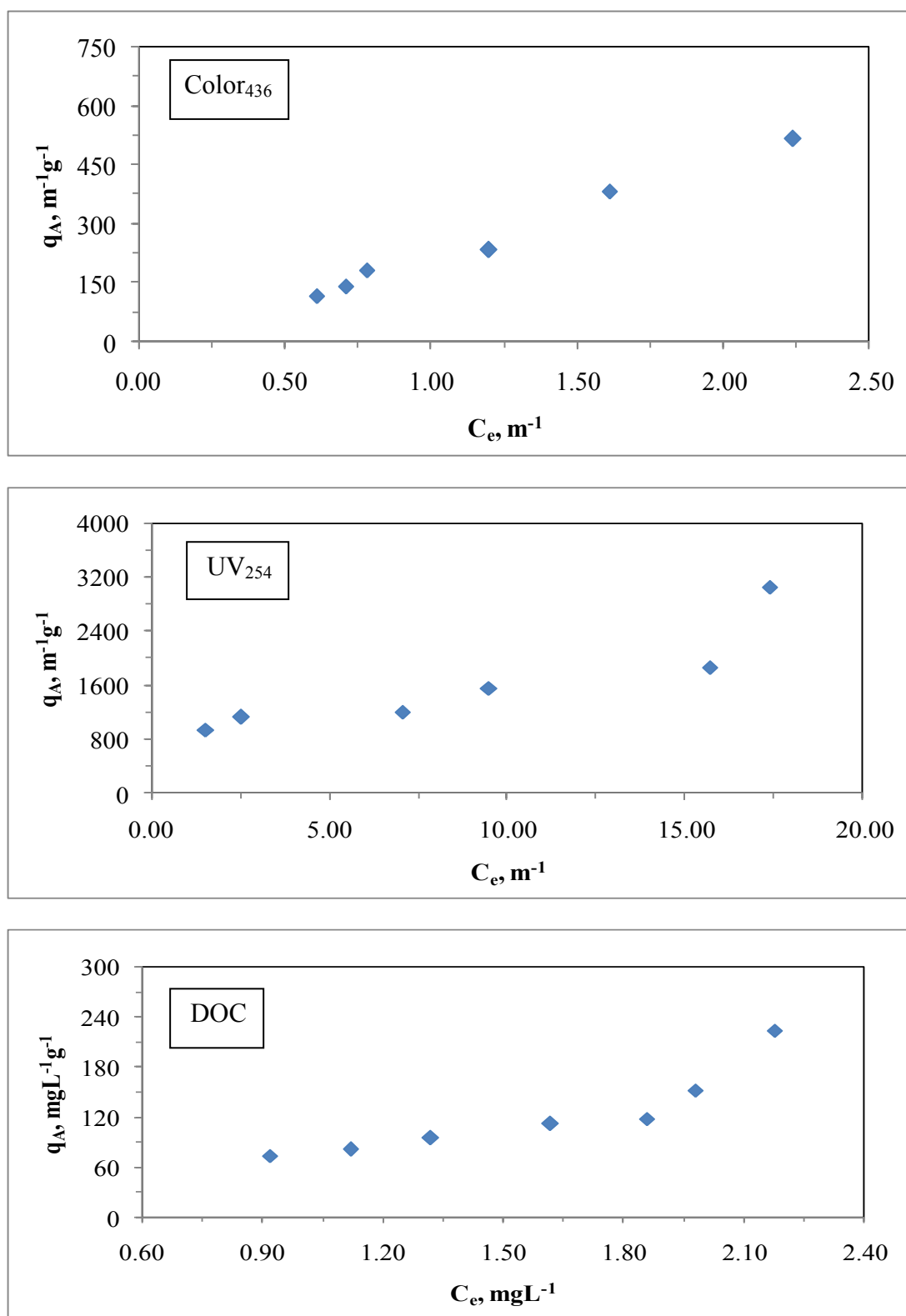Figure 4.154. Freundlich adsorption isotherm of $Color_{436}$, UV_{254} and DOC parameters of 30 kDa fraction of humic acid following adsorption onto N-S co-doped TiO_2 Hombikat UV-100.

Table 4.61. Freundlich isotherm model parameters for 30 kDa fraction of humic acid following adsorption onto N-S co-doped TiO_2 Hombikat UV-100.

Humic acid, 30kDa fraction		
UV-vis parameter	K_f	$1/n$
$Color_{436}$	212	1.12
UV_{365}	314	0.572
UV_{280}	686	0.359
UV_{254}	740	0.376
Dissolved Organic Carbon	K_f	$1/n$
DOC	72.1	1.12

Comparison of UV-vis parameters indicated that the adsorption capacity constant of $Color_{436}$ was the lowest value. The order was $Color_{436} < UV_{365} < UV_{280} < UV_{254}$ for adsorption capacity constant. Furthermore, adsorption intensity values of $Color_{436}$ had the highest value in contrast to adsorption intensity value of UV_{280}. Adsorption intensity of DOC was found to be >1 representing strong adsorption bond. A decreasing order of adsorption intensity values could be given as $Color_{436} > UV_{365} > UV_{254} > UV_{280}$.

Freundlich isotherm model parameters of DOC for 30 kDa fraction of humic acid could be expressed by a decreasing order for K_f: N-S co-doped TiO_2 > N-doped TiO_2 > S-doped TiO_2 > C-doped TiO_2 > bare TiO_2 for $1/n$: bare TiO_2 > S-doped TiO_2 > C-doped TiO_2 > N-doped TiO_2 > N-S co-doped TiO_2 Hombikat UV-100. Comparative evaluation of Freundlich isotherm model parameter, K_f of 30 kDa fraction of humic acid with 100 kDa fraction of humic acid following adsorption onto N-S co-doped TiO_2 Hombikat UV-100 did not reveal the most significant difference in both UV-vis parameters and DOC.

Langmuir adsorption model. Langmuir adsorption isotherms for 30 kDa fraction of humic acid following adsorption onto N-S co-doped TiO_2 Hombikat UV-100 were presented in Figure 4.155 for $Color_{436}$, UV_{254} and DOC parameters. Langmuir isotherms for UV_{365} and UV_{280} were presented in Appendix B. Two parameters of Langmuir equation outlined in section 2.3, q_m and K_a, were listed in Table 4.62 for 30 kDa fraction of humic acid following adsorption onto N-S co- doped TiO_2 Hombikat UV-100.
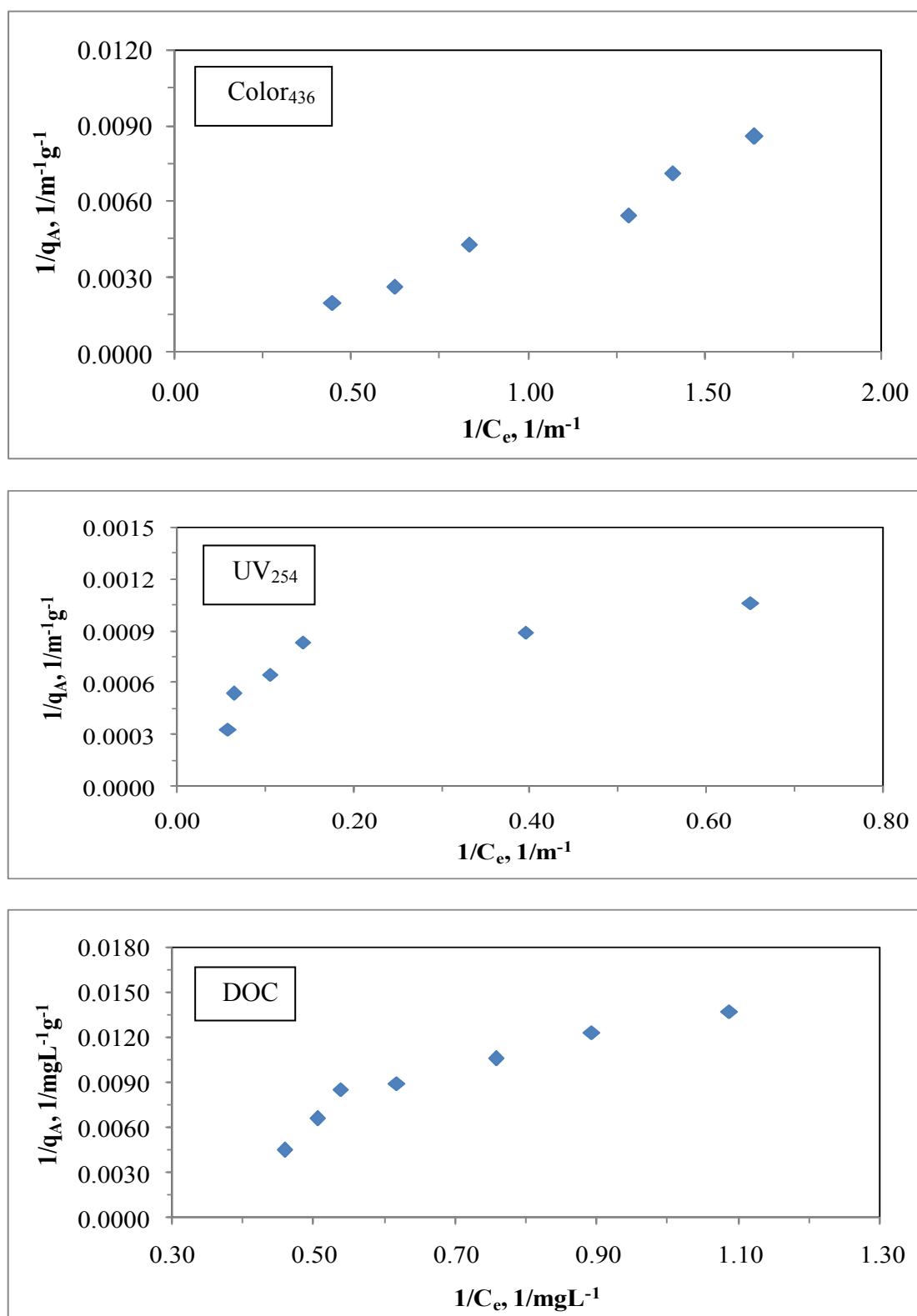
Figure 4.155. Langmuir adsorption isotherm of Color$_{436}$, UV$_{254}$ and DOC parameters of 30 kDa fraction of humic acid following adsorption onto N-S co-doped TiO$_2$ Hombikat UV-100.

Table 4.62. Langmuir isotherm model parameters for 30 kDa fraction of humic acid following adsorption onto N-S co-doped TiO_2 Hombikat UV-100.

Humic acid, 30 kDa fraction		
UV-vis parameter	q_m $m^{-1}g^{-1}$	K_a m^{-1}
Color$_{436}$	1862	0.101
UV$_{365}$	1000	1.000
UV$_{280}$	1667	0.667
UV$_{254}$	2000	0.500
Dissolved Organic Carbon	q_m mg $L^{-1}g^{-1}$	K_a mg L^{-1}
DOC	8620	0.00900

It could be easily seen from Table 4.62 that the highest value of q_m was in UV$_{254}$. The order of all of UV-vis spectroscopic parameters in terms of q_m value was UV$_{254}$ > Color$_{436}$ > UV$_{280}$ > UV$_{365}$ and this order was Color$_{436}$ < UV$_{254}$ < UV$_{280}$ < UV$_{365}$ for K_a. The model parameters as q_m and K_a values for DOC were calculated as 8620 mg $L^{-1}g^{-1}$ and 0.00900 mg L^{-1}.

It should be indicated that adsorption of 30 kDa fraction of humic acid onto N-S co-doped TiO_2 Hombikat UV-100 could well be characterized both by Freundlich and Langmuir adsorption isotherm models.

Langmuir isotherm model parameters calculated for UV-vis parameters displayed a different trend with respect to the both N-doped TiO_2 and S-doped TiO_2 (Table 4.58, Table 4.60 and Table 4.62). Langmuir isotherm model parameters of DOC could be expressed in a decreasing order of; q_m: N-S co-doped TiO_2 > S-doped TiO_2 > C-doped TiO_2 > N-doped TiO_2 > bare TiO_2 K_a: N-doped TiO_2 > S-doped TiO_2 > bare TiO_2 > C-doped TiO_2 > N-S co-doped TiO_2. Comparative evaluation of Langmuir isotherm model parameters of 30 kDa fraction of humic acid with 100 kDa fraction of humic acid following adsorption onto N-S co-doped TiO_2 Hombikat UV-100 revealed the significant differences in both UV-vis parameters and DOC.

5. CONCLUSIONS

In this study, surface interactions between different molecular size fractionations of humic acid (0.45 μm filtered fraction, 100 kDa fraction and 30 kDa fraction) and TiO_2 specimens, namely bare TiO_2 and anion doped TiO_2 (N-doped TiO_2, S-doped TiO_2, C-doped TiO_2 and N-S co-doped TiO_2) were investigated. Adsorption properties of humic acid and its molecular size fractions onto bare TiO_2 and anion doped TiO_2 specimens were evaluated and compared in terms of *i*. UV-vis spectroscopic parameters *i.e.* color forming moieties (Color$_{436}$) and UV absorbing centers (UV$_{365}$, UV$_{280}$ and UV$_{254}$) *ii*. fluorescence spectroscopy acquired in emission and synchronous scan modes and *iii*. dissolved organic carbon. Adsorption isotherms were evaluated in terms of the adsorption isotherm types (Types C, L and S). Adsorption isotherms were modeled to Freundlich and Langmuir adsorption isotherm models.

Comparative evaluation of UV-vis spectral features of 0.45 μm filtration fraction of humic acid with 100 kDa fraction of humic acid and 30 kDa fraction of humic acid recorded following adsorption onto bare TiO_2 specimens Degussa P-25 indicated that the lower molecular size fraction of humic acid (30 kDa) exhibited similar UV-vis spectral features as expected. Similar trends could also be visualized in synchronous scan fluorescence spectral features. Comparative evaluation of the spectroscopic features of 100 kDa fraction of humic acid with 0.45 μm filtration fraction of humic acid recorded following adsorption onto bare TiO_2 specimens Degussa P-25 revealed the most significant difference in emission scan fluorescence spectral features. The reason could be attributed to the role of the fluorophoric groups present on the different molecular size fractions of humic acid. It should also be signified that decreasing molecular size given rise to decreasing amounts of chromophores and fluorophores in accordance with decreasing DOC.

Comparative evaluation of UV-vis spectral features of 0.45 μm filtration fraction of humic acid with 100 kDa fraction of humic acid and 30 kDa fraction of humic acid recorded following adsorption onto bare TiO_2 specimens Hombikat UV-100 revealed the significant differences in UV spectral features and emission scan fluorescence spectral

features as well as synchronous scan fluorescence spectral features. However, no significant difference could be visualized in the visible region.

Comparison of UV-vis spectral features of 0.45 μm filtration fraction of humic acid with lower molecular size fractions of humic acid recorded following adsorption onto two bare TiO_2 specimens (Degussa P-25 and Hombikat UV-100) indicated that the influence of pure anatase form (Hombikat UV-100) was more pronounced with respect to the presence of mixed crystal phases (Degussa P-25) in the UV region. On the other hand, no remarkable differences could be visualized in the visible region.

Chromophoric as well as fluorophoric groups of humic acid could be stated by the UV-vis and fluorescence spectral features. The observed close similarities in the UV-vis spectroscopic features indicated the possible use of specified UV-vis parameters *i.e.* color forming moieties ($Color_{436}$) and UV absorbing centers (UV_{365}, UV_{280} and UV_{254}) in presentation of the adsorption isotherms and adsorption isotherm modeling.

Fluorescence spectral features attained either upon emission scan mode or synchronous scan mode displayed an inconsistent trend both with respect to the molecular size of humic acid. These results indicated that fluorescence intensities should be regarded as specific for characterization of humic acid but non-specific in terms of quantification of humic acid. It should also be indicated that UV-vis parameters could well serve as indicative parameters of humic chromophores that played significant effects in adsorptive interactions.

Adsorption isotherms were presented with different molecular size fractions such as 0.45 μm filtered fraction, 100 kDa fraction and 30 kDa fraction of Aldrich humic acid solution with bare TiO_2 and anion doped TiO_2 (N-doped TiO_2, S-doped TiO_2, C-doped TiO_2 and N-S co-doped TiO_2). Adsorption isotherms were modeled to Freundlich and Langmuir adsorption isotherm models by evaluating the results of specified UV-vis parameters as well as DOC.

Comparative presentation of the attained results using Freundlich adsorption isotherm model in terms of DOC could be summarized as follows:

1. TiO$_2$ Degussa P-25 specimens:

1.1. Freundlich isotherm model parameters of DOC of 0.45 µm filtration fraction of humic acid could be expressed by a decreasing order for K$_f$: bare TiO$_2$ > N-S co-doped TiO$_2$ > C-doped TiO$_2$ > S-doped TiO$_2$ > N-doped TiO$_2$ for 1/n: N-doped TiO$_2$ > C-doped TiO$_2$ > N-S co-doped TiO$_2$ > S-doped TiO$_2$ > bare TiO$_2$ Degussa P-25.

1.2. Freundlich isotherm model parameters of DOC of 100 kDa fraction of humic acid could be expressed by a decreasing order for K$_f$: N-doped TiO$_2$ > bare TiO$_2$ > S-doped TiO$_2$ > N-S co-doped TiO$_2$ > C-doped TiO$_2$ for 1/n: bare TiO$_2$ > C-doped TiO$_2$ > N-S co-doped TiO$_2$ > S-doped TiO$_2$ > N-doped TiO$_2$ Degussa P-25.

1.3. Freundlich isotherm model parameters of DOC of 30 kDa fraction of humic acid could be expressed by a decreasing order for K$_f$: S-doped TiO$_2$ > N-doped TiO$_2$ > N-S co-doped TiO$_2$ > C-doped TiO$_2$ > bare TiO$_2$ for 1/n: N-doped TiO$_2$ > N-S co-doped TiO$_2$ > C-doped TiO$_2$ > bare TiO$_2$ > S-doped TiO$_2$ Degussa P-25.

2. TiO$_2$ Hombikat UV-100 specimens:

2.1. Freundlich isotherm model parameters of DOC of 0.45 µm filtration fraction of humic acid could be expressed by a decreasing order for K$_f$: N-S co-doped TiO$_2$ ≥ C-doped TiO$_2$ > S-doped TiO$_2$ > bare TiO$_2$ > N-doped TiO$_2$ for 1/n: N-doped TiO$_2$ > S-doped TiO2 > bare TiO2 > N-S co-doped TiO$_2$ > C-doped TiO$_2$ Hombikat UV-100.

2.2. Freundlich isotherm model parameters of DOC of 100 kDa fraction of humic acid could be expressed by a decreasing order for K$_f$: N-S co-doped TiO$_2$ > bare TiO$_2$ > S-doped TiO$_2$ > N-doped TiO$_2$ > C-doped TiO$_2$ for 1/n: C-doped TiO$_2$ > N-doped TiO$_2$ = bare TiO$_2$ > S-doped TiO$_2$ >.N-S co-doped TiO$_2$ Hombikat UV-100.

2.3. Freundlich isotherm model parameters of DOC of 30 kDa fraction of humic acid could be expressed by a decreasing order for K_f: N-S co-doped TiO_2 > N-doped TiO_2 > S-doped TiO_2 > C-doped TiO_2 > bare TiO_2 for 1/n: bare TiO_2 > S-doped TiO_2 > C-doped TiO_2 > N-doped TiO_2 > N-S co-doped TiO_2 Hombikat UV-100.

Comparative presentation of the attained results using Langmuir adsorption isotherm model in terms of DOC could be summarized as follows:

1. TiO₂ Degussa P-25 specimens:

1.1. Langmuir isotherm model parameters of DOC of 0.45 µm filtration fraction of humic acid could be expressed in a decreasing order of; q_m: bare TiO_2 > N-S co-doped TiO_2 > C-doped TiO_2 > S-doped TiO_2 > N-doped TiO_2, K_a: C-doped TiO_2 > N-S co-doped TiO_2 > S-doped TiO_2 > N-doped TiO_2 > bare TiO_2 Degussa P-25.

1.2. Langmuir isotherm model parameters of DOC of 100 kDa fraction of humic acid could be expressed in a decreasing order of; q_m: S-doped TiO_2 > N-S co-doped TiO_2 > bare TiO_2 > N-doped TiO_2 > C-doped TiO_2, K_a: N-doped TiO_2 > bare TiO_2.> C-doped TiO_2 > N-S co-doped TiO_2 > S-doped TiO_2 Degussa P-25.

1.3. Langmuir isotherm model parameters of DOC of 30 kDa fraction of humic acid could be presented in a decreasing order of; for q_m: S-doped TiO_2> N-doped TiO_2 > N-S co-doped TiO_2> C-doped TiO_2 > bare TiO_2 for Ka: N-doped TiO_2 > N-S co-doped TiO_2> C-doped TiO_2 > bare TiO_2 > S-doped TiO_2 Degussa P-25.

2. TiO₂ Hombikat UV-100 specimens:

2.1. Langmuir isotherm model parameters of DOC of 0.45 µm filtration fraction of humic acid could be expressed in a decreasing order of; q_m: N-S co-doped TiO_2 > C-doped TiO_2 > S-doped TiO_2 > bare TiO_2 > N-doped TiO_2, K_a: > N-doped TiO_2 > C-doped TiO_2 > S-doped TiO_2 > bare TiO_2 > N-S co-doped TiO_2 Hombikat UV-100.

2.2. Langmuir isotherm model parameters of DOC of 100 kDa fraction of humic acid could be expressed in a decreasing order of; q_m: S-doped TiO_2 > bare TiO_2 > N-doped TiO_2 > C-doped TiO_2 > N-S co-doped TiO_2 K_a: N-S co-doped TiO_2 > C-doped TiO_2 > N-doped TiO_2 > bare TiO_2 > S-doped TiO_2 Hombikat UV-100.

2.3. Langmuir isotherm model parameters of DOC of 30 kDa fraction of humic acid could be expressed in a decreasing order of; q_m: N-S co-doped TiO_2 > S-doped TiO_2 > C-doped TiO_2 > N-doped TiO_2 > bare TiO_2 K_a: N-doped TiO_2 > S-doped TiO_2 > bare TiO_2 > C-doped TiO_2 > N-S co-doped TiO_2 Hombikat UV-100.

As summarized above, Freundlich and Langmuir isotherm model parameters of DOC for 0.45 μm filtration fraction of humic acid, 100 kDa fraction of humic acid and 30 kDa fraction of humic acid following adsorption onto bare TiO_2 and anion doped TiO_2 Degussa P-25 and Hombikat UV-100 displayed significantly differences. The reason could be attributed to the role of the functional groups (fluorophoric and chromophoric groups) present on the different molecular size fractions of humic acid.

Evaluation of the results based on varying molecular size fractions of humic acid indicated remarkable differences both with respect to the type of the dopant as well as to the morphological character of TiO_2 specimens. N-S co-doped TiO_2 Hombikat UV-100 displayed higher adsorption capacity for higher molecular size fractions of humic. In the presence of lower molecular size fraction, Freundlich model displayed that S-doped TiO_2 Degussa P-25 was more superior to the mono phase counterpart. However, Langmuir adsorption model expressed highest maximum adsorption for N-S co-doped TiO_2 Hombikat UV-100. The reason could be attributed to the compositional properties of humic acid sub-fractions rather than the alterations in the TiO_2 specimens due to doping.

Referring to the main purpose of the study indicated that the studied loading range of TiO_2 was selected with respect to the photocatalytically active concentration range, the attained results should be carefully interpreted. In this context, the adsorption properties of N-doped TiO_2 specimens should be examined prior to the application of any photocatalytic treatment of strongly adsorbing high molecular weight organic matrix.

REFERENCES

Adams, W. A., Impellitteri, C. A., 2009. The photocatalysis of N,N-diethyl-m-toluamide (DEET) using dispersions of Degussa P-25 TiO_2 particles. Journal of Photobiology A: Chemistry, 202, 28-32.

Al-Rasheed, R., Cardin, D. J., 2003. Photocatalytic degradation of humic acid in saline waters. Part 1. Artificial seawater: influence of TiO_2, temperature, pH, and air-flow. Chemosphere, 51, 925-933.

Anandan, S., Kumar, P. S., Pugazhenthiran, N., Madhavan, J., Maruthamuthu, P., 2008. Effect of loaded silver nanoparticles on TiO_2 for photocatalytic degradation of Acid Red 88. Solar Energy Materials and Solar Cells, 92, 929-937.

Anirudhan, T. S., Suchitra, P. S., Rijith, S., 2008. Amine-modified polyacrylamide-bentonite composite for the adsorption of humic acid in aqueous solutions. Colloids and Surfaces A: Physicochemical and Engineering Aspects, 326, 147-156.

Antelo, J., Arce, F., Avena, M., Fiol, S., López, R., Macías, F., 2007. Adsorption of a soil humic acid at the surface of goethite and its competitive interaction with phosphate. Geoderma, 138, 12-19.

Asahi, R., Morikawa, T., Ohwaki, T., Aoki, K., Taga, Y., 2001. Visible-light photocatalysis in nitrogen-doped titanium oxides. Science, 293, 269-271.

Avena, M. J., Koopal, L. K., 1999. Kinetics of humic acid adsorption at solid-water interfaces. Environmental Science and Technology, 33, 2739-2744.

Awala, H. A., El Jamal, M. M., 2011. Equilibrium and kinetics study of adsorption of some dyes onto feldspar. Journal of the University of Chemical Technology and Metallurgy, 46(1), 45-52.

Aykac, H., 2011. Semiconductor Assisted Photodegradation of Humic Acid Using Fe Doped TiO$_2$, M.S. Thesis, Boğaziçi University.

Balzani, V., and Scandola, F., 1991. Supramolecular Photochemistry, Horwood, Chichester, England.

Bangkedphol, S., Keenan, H. E., Davidson, C. M., Sakultantimetha, A., Sirisaksoontorn, W., Songsasen, A., 2010. Enhancement of tributyltin degradation under natural light by N-doped TiO$_2$ photocatalyst. Journal of Hazardous Materials, 184, 533-537.

Bas, T., 2001. Humic Acid and Oxide Surface Interactions: Adsorption, Desorption and Surface Charge Effects, M.S. Thesis, Boğaziçi University.

Bekbolet, M., Cecen, F., and Ozkosemen, G., 1996. Photocatalytic oxidation and subsequent adsorption characteristic of humic acids. Water Science and Technology, 34, 65-72.

Bekbolet, M., Suphandag, A. S., Uyguner, C. S., 2002. An investigation of the photocatalytic efficiencies of TiO$_2$ powders on the decolourisation of humic acids. Journal of Photochemistry and Photobiology A: Chemistry, 148, 121-128.

Boehm, H. P., 1971. Discussion, Faraday Society, 52, 264-271 reference in, Pelizetti, E., and Minero, C., 1993. Mechanism of the Photo-oxidative Degradation of Organic Pollutants over TiO$_2$ Particles. Electrochimica Acta, 38, (1), 47-55.

Buffle, J., 1988. Complexation Reactions in Aquatic Systems - An Analytical Approach. Ellis Harwood Series in Analytical Chemistry, 692, Chichester, UK.

Burba, P., Aster, B., Nifant'eva, T., Shkinev, V., Spivakov, B. Ya., 1998. Membrane filtration studies of aquatic humic substances and their metal species: a concise overview Part 1. Analytical fractionation by means of sequential-stage ultrafiltration. Talanta, 45, 977-988.

Chen, Q., Yin, D., Zhu, S., Hu, X., 2012. Adsorption of cadmium (II) on humic acid coated titanium dioxide. Journal of Colloid and Interface Science, 367, 241-248.

Clemente, Z., Castro, V. L., Jonsson, C. M., Fraceto, L. F., 2012. Ecotoxicology of nano-TiO_2 – An evaluation of its toxicity to organisms of aquatic ecosystems. International Journal of Environmental Research, 6(1), 33-50.

Cong, Y., Zhang, J., Chen, F., Anpo, M., He, D., 2007a. Preparation, photocatalytic activity and mechanism of nano-TiO_2 co-doped with nitrogen and iron (III). The Journal of Physical Chemistry C, 111, 10618-10623.

Cong, Y., Zhang, J., Chen, F., Anpo, M., 2007b. Synthesis and characterization of nitrogen-doped TiO_2 nanophotocatalyst with high visible light activity. The Journal of Physical Chemistry C, 111, 6976-6982.

Degirmenci Ilhan, E., 2010., Assessment of Molecular Size Distribution Effects on the Nonselective Oxidation of Trace Metal Humic Acid Binary System, M.S. Thesis, Boğaziçi University.

Deng, S., Bai, R. B., 2003. Aminated polyacrylonitrile fibers for humic acid adsorption: behaviors and mechanisms. Environmental Science and Technology, 37, 5799-5805.

Di Paola, A., García-Lópeza E., Marcía, G., and Palmisano, L., 2012. A survey of photocatalytic materials for environmental remediation. Journal of Hazardous Materials, 211-212, 3-29.

Dong, F., Zhao, W., Wu, Z., Guo, S., 2009. Band structure and visible light photocatalytic activity of multi-type nitrogen doped TiO_2 nanoparticles prepared by thermal decomposition. Journal of Hazardous Materials, 162, 763-770.

Duan, J., Gregory, J., 2003. Coagulation by hydrolysing metal salts. Advances in Colloid and Interface Science, 100–102, 475-502.

Edzwald, J. K., 1993. Coagulation in drinking water treatment: particles, organics and coagulants. Water Science and Technology, 27(11), 21-35.

Edzwald, J. K., Becker, W. C., Wattier, K. L., 1985. Surrogate parameters for monitoring organic matter and THM precursors. Journal – American Water Works Association, 77, 122-132.

Gaffney, J. S., Marley, N. A., Clark, S. B., 1996. Humic and fulvic acids: isolation, structure and environmental role, ACS Symposium Series 651, American Chemical Society, U.S.A.

Giasuddin, A. B. M., Kanel, S. R., Choi, H., 2007. Adsorption of humic acid onto nanoscale zerovalent iron and its effect on arsenic removal. Environmental Science and Technology, 41, 2022-2027.

Giles, C. H., MacEwan, T. H., Nakhwa, S. N., Smith, D., 1960. A system of classification of solution adsorption isotherms, and its use in diagnosis of adsorption mechanisms and in measurement of specific surface areas of solids. Journal of Chemical Society, 33, 3973-3993.

Giles, C. H., D'Silva, A. P., Easton, I. A., 1974a. A general treatment and classification of the solute adsorption isotherm, Part II: Experimental interpretation. Journal of Colloid and Interface Science, 47, 3, 766-778.

Giles, C. H., Smith, D., Huitson, A., 1974b. A general treatment and classification of the solute adsorption isotherm. Journal of Colloid and Interface Science, 47, 755-765.

Gu, B., Schmitt, J., Chen, Z., Liang, L., McCarthy, J. F., 1994. Adsorption and desorption of natural organic matter on iron oxide: Mechanisms and models. Environmental Science and Technology, 28, 38-46.

Gurkan, Y. Y., Turkten, N., Hatipoglu, A., Cinar, Z., 2012. Photocatalytic degradation of cefazolin over N-doped TiO_2 under UV and sunlight irradiation: prediction of the reaction paths via conceptual DFT. Chemical Engineering Journal, 184, 113-124.

Han, C., Pelaez, M., Likodimos, V., Kontos, A. G., Falaras, P., O'Shea, K., Dionysiou, D. D., 2011. Innovative visible light-activated sulfur doped TiO_2 films for water treatment. Applied Catalysis B: Environmental, 107, 77-87.

Hanaor, D. A. H., Assadi, M. H. N., Li, S., Yu, A., Sorrell, C. C., 2012. Ab initio study of phase stability in doped TiO_2. Computational Mechanics, 50, 185-194.

Hatipoglu, A., Vione, D., Yalcin, Y., Minero, C., Cinar, Z., 2010. Photo-oxidative degradation of toluene in aqueous media by hydroxyl radicals. Journal of Photochemistry and Photobiology A: Chemistry, 215, 59-68.

Hendricks, D., 2006. Water Treatment Unit Processes, Physical and Chemical, Taylor and Francis Group, New York.

Hizal, J., Apak, R., 2006. Modeling of cadmium (II) adsorption on kaolinite-based clays in the absence and presence of humic acid. Applied Clay Science, 32, 232-244.

Hoffmann, M. R., Martin, S. T., Choi, W., Bahnemann, D. W., 1995. Environmental applications of semiconductor photocatalysis. Chemical Reviews, 95, 69-96.

Hoshimoto, K., Irie, H., Watanabe, Y., 2003. Nitrogen-concentration dependence on photocatalytic activity of $TiO_{2-x}N_x$. The Journal of Physical Chemistry B., 107(23), 5483-5486.

Hussain, S. T., Khan, K., Hussain, R., 2009. Size control synthesis of sulfur doped titanium dioxide (anatase) nano particles, its optical property and its photo catalytic reactivity for $CO_2 + H_2O$ conversion and phenol degradation. Journal of Natural Gas Chemistry, 18, 383-391.

Illés, E., Tombácz, E., 2006. The effect of humic acid adsorption on pH-dependent surface charging and aggregation of magnetite nanoparticles. Journal of Colloid and Interface Science, 295, 115-123.

Irie, H., Watanabe, Y., Hashimoto, K., 2003. Nitrogen-concentration dependence on photocatalytic activity of $TiO_2 - {}_xN_x$ powders. The Journal of Physical Chemistry B, 107, 5483-5486.

Jagadale, T. C., Takale, S. P., Sonawane, R. S., Joshi, H. M., Patil, S. I., Kale, B. B., Ogale, S. B., 2008. N-doped TiO_2 nanoparticle based visible light photocatalyst by modified peroxide sol-gel method. The Journal of Physical Chemistry C, 112, 14595-14602.

Joung, S. K., Amemiya, T., Murabayashi, M., Itoh, K., 2006. Relation between photocatalytic activity and preparation conditions for nitrogen-doped visible light-driven TiO_2 photocatalysts. Applied Catalysis A: General, 312, 20-26.

Kasapbasi, E., Cinar, Z., 2011. A density functional theory study on the nitrogen/sulfur codoping effect of TiO_2. The 16th International Conference on TiO_2 Photocatalytic Fundamentals and Applications, November 7-10, San Diego, California, USA.

Khan, S. U. M., Al-Shahry, M., Ingler, W. B. Jr., 2002. Efficient photochemical water splitting by a chemically modified n-TiO_2. Science, 297, 2243-2245.

Kim, E. K., Walker, H. W., 2001. Effect of cationic polymer additives on the adsorption of humic acid onto iron oxide particles. Colloids and Surfaces A: Physicochemical and Engineering Aspects, 194, 123-131.

Knapik, H. G., Fernandes, C. V. S., Rodrigues de Azevedo, J. C., 2011. Characterization of organic matter using fluorescence and absorbance spectroscopy: the case study of a Brazilian polluted river, IWA Specialty Conference on Natural Organic Matter, Costa Mesa, CA, USA, 27-29 July 2011.

Kobayakawa, K., Murakami, Y., Sato, Y., 2005. Visible-light active N-doped TiO_2 prepared by heating of titanium hydroxide and urea. Journal of Photochemistry and Photobiology A: Chemistry, 170, 177-179.

Koh, K., Wong-Foy, A. G., Matzger, A. J., 2009. A porous coordination copolymer with over 5000 m^2/g BET surface area. Journal of the American Chemical Society, 131, 4184-4185.

Komai, Y., Okitsu, K., Nishimura, R., Ohtsu, N., Miyamoto, G., Furuhara, T., Semboshi, S., Mizukoshi, Y., Masahashi, N., 2011. Visible light response of nitrogen and sulfur co-doped TiO_2 photocatalysts fabricated by anodic oxidation. Catalysis Today, 164, 399-403.

Ksibi, M., Rossignol, S., Tatibouët, J. M., Trapalis, C., 2008. Synthesis and solid characterization of nitrogen and sulfur-doped TiO_2 photocatalysts active under near visible light. Materials Letters, 62, 4204-4206.

Kumpulainen, S., Kammer, F. V. D., Hofmann, T., 2008. Humic acid adsorption and surface charge effects on schwertmannite and goethite in acid sulphate waters. Water Research, 42, 2051-2060.

Kuznetsov, V. N., Serpone, N., 2006. Visible light absorption by various titanium dioxide specimens. The Journal of Physical Chemistry B, 110, 25203-25209.

Lapworth, D. J., Gooddy, D. C., Butcher, A. S., Morris, B. L., 2008. Tracing groundwater flow and sources of organic carbon in sandstone aquifers using fluorescence properties of dissolved organic matter. Applied Geochemistry, 23, 3384-3390.

Leenheer, J. A., 1981. Comprehensive approach to preparative isolation and fractionation of dissolved organic carbon from natural waters and wastewaters. Environmental Science and Technology, 15(5), 578-587.

Leenher, J. A., Rostad, C. E., Gates, P. M., Furlong, E. T., Ferrer, I., 2001. Molecular resolution and fragmentation of fulvic acid by electroscopy ionization /multistage tandem mass spectroscopy. Analytical Chemistry, 73, 1461-1471.

Li, D., Ohashi, N., Hishita, S., Kolodiazhnyi, T., Haneda, H., 2005. Origin of visible-light-driven photocatalysis: A comparative study on N/F-doped and N-F-codoped TiO_2 powders by means of experimental characterizations and theoretical calculations. Journal of Solid State Chemistry, 178, 3293-3302.

Li, F. T., Zhaoa, Y., Haoa, Y. J., Wanga, X. J., Liua, R. H., Zhaoa, D. S., Chen, D. M., 2012. N-doped P25 TiO_2–amorphous Al_2O_3 composites: One-step solution combustion preparation and enhanced visible-light photocatalytic activity. Journal of Hazardous Materials, 239-240, 118-127.

Liao, C. H., Lu, M. C., Su, S. H., 2001. Role of cupric ions in the H_2O_2/UV oxidation of humic acids. Chemosphere, 44, 913-919.

Lin, J., Zhan, Y., 2012. Adsorption of humic acid from aqueous solution onto unmodified and surfactant-modified chitosan/zeolite composites. Chemical Engineering Journal, 200-202, 202-213.

Lin, S. H., Juang, R. S., 2009. Adsorption of phenol and its derivatives from water using synthetic resins and low-cost natural adsorbents: A review. 90, 1336-1349.

Linsebigler, A. L., Lu, G., Yates, J. T., 1995. Photocatalysis on TiO_2 surfaces: Principles, mechanisms, and selected results. Chemical Reviews, 95, 735-758.

Liu, Y., Chen, X., Li, J., Burda, C., 2005. Photocatalytic degradation of azo dyes by nitrogen-doped TiO_2 nanocatalysts. Chemosphere, 61, 11-18.

Liu, S., Lim, M., Fabris, R., Chow, C., Chaing, K., Drikas, M., Amal, R., 2008. Removal of humic acid using TiO_2 photocatalytic process − Fractionation and molecular weight characterization studies. Chemosphere, 72, 263-271.

MacCarthy, P., 2001. The Principles Of Humic Substances: An Introduction To The First Principle. Proceedings of the fifth Humic Substances Seminar, Northeastern University, Boston, Massachusetts, 221.

Mansoori, G. A., Rohani.Bastami, T., Ahmadpour, A., Eshaghi Z., 2008. Environmental application of nanotechnology. Annual Review of Nano Research, 2, Chapter 2.

Marshall, S. J., House, W. A., Russell, N. J., White, G. F., 1998. Comparative adsorption of natural and commercially available humic acids to river sediments. Colloids and Surfaces A: Physicochemical and Engineering Aspects, 144, 127-137.

Matilainen, A., Sillanpää, M., 2010. Removal of natural organic matter from drinking water by advanced oxidation processes. Chemosphere, 80, 351-365.

Matilainen, A., Vepsäläinen, M., Sillanpää, M., 2010. Natural organic matter removal by coagulation during drinking water treatment: A review. Advances in Colloid and Interface Science, 159, 189-197.

Michalow, K. A., Logvinovich, D., Weidenkaff, A., Amberg, M., Fortunato, G., Heel, A., Graule, T., Rekas, M., 2009. Synthesis, characterization and electronic structure of nitrogen-doped TiO_2 nanopowder. Catalysis Today, 144, 7-12.

Moura, M. N., Martín, M. J., Burguillo, F. J., 2007. A comparative study of the adsorption of humic acid, fulvic acid and phenol onto Bacillus subtilis and activated sludge. Journal of Hazardous Materials, 149, 42-48.

Moussavi, G., Talebi, S., Farrokhi, M., Sabouti, R. M., 2011. The investigation of mechanism, kinetic and isotherm of ammonia and humic acid co-adsorption onto natural zeolite. Chemical Engineering Journal, 171, 1159-1169.

Murray, C. A., Parsons, S. A., 2004. Removal of NOM from drinking water: Fenton's and photo-Fenton's processes. Chemosphere, 54, 1017-1023.

Nakamura, R., Tanaka T., Nakato, Y., 2004. Mechanism for visible light responses in anodic photocurrents at N-doped TiO_2 film electrodes. The Journal of Physical Chemistry B, 108, 10617-10620.

Nifant'eva, T. I., Shkinev, V. M., Spivakov, B. Y., Burba, P., 1999. Membrane filtration studies of aquatic humic substances and their metal species: a concise overview Part 2. Evaluation of conditional stability constants by using ultrafiltration. Talanta, 48, 257-267.

Nosaka, Y., Matsushita, M., Nishino, J., Nosaka, A. Y., 2005. Nitrogen-doped titanium dioxide photocatalysts for visible response prepared by using organic compounds. Science and Technology of Advanced Materials, 6, 143-148.

Ohno, T., Akiyoshi, M., Umebayashi, T., Asai, K., Mitsui, T., Matsumura, M., 2004a. Preparation of S-doped TiO_2 photocatalysts and their photocatalytic activities under visible light. Applied Catalysis A: General, 265, 115-121.

Ohno, T., Tsubota, T., Toyofuku, M., Inaba, R., 2004b. Photocatalytic activity of a TiO_2 photocatalysts doped with C^{4+} and S^{4+} ions having a rutile phase under visible light. Catalysis Letters, 98(4), 255-258.

Pap, Z., Baia, L., Mogyorósi, K., Dombi, A., Oszkó, A., Danciu, V., 2012. Correlating the visible light photoactivity of N-doped TiO_2 with brookite particle size and bridged-nitro surface species. Catalysis Communications, 17, 1-7.

Parilti, N. B., Uyguner Demirel, C. S., Bekbolet, M., 2011. Response surface methodological approach for the assessment of the photocatalytic degradation of NOM. Journal of Photochemistry and Photobiology A: Chemistry, 225, 26-35.

Park, Y., Kim, W., Park, H., Tachikawa, T., Majima, T., Choi, W., 2009. Carbon-doped TiO_2 photocatalyst synthesized without using an external carbon precursor and the visible light activity. Applied Catalysis B: Environmental, 91, 355-361.

Peña-Méndez, E. M., Havel, J., Potočka, J., 2005. Humic substances – compounds of still unknown structure: applications in agriculture, industry, environment, and biomedicine. Journal of Applied Biomedicine, 3, 13-24.

Peuravuori, J., Pihlija, K., 1997. Molecular size distribution and spectroscopic properties of aquatic humic substances. Analytica Chimica Acta, 337, 133-149.

Portjanskaja, E., Preis, S., Kallas, J., 2006. Aqueous photocatalytic oxidation of lignin and humic acids with supported TiO_2. International Journal of Photoenergy, 85927, 1-7.

Rafatullah, M., Sulaiman, O., Hashim, R., Ahmad, A., 2010. Adsorption of methylene blue on low-cost adsorbents: A review. Journal of Hazardous Materials, 177, 70-80.

Rajeswari, R. and Kanmani, S., 2009. A study on degradation of pesticide wastewater by TiO_2 photocatalysis. Journal of Scientific and Industrial Research, 68, 1063-1067.

Rashed, M. N., El-Amin, A. A., 2007. Photocatalytic degradation of methyl orange in aqueous TiO_2 under different solar irradiation sources. International Journal of Physical Sciences, 2(3), 073-081.

Rengifo-Herrera, J. A., Kiwi, J., Pulgarin, C., 2009. N, S co-doped and N-doped Degussa P-25 powders with visible light response prepared by mechanical mixing of thiourea and urea. Reactivity towards E. coli inactivation and phenol oxidation. Journal of Photochemistry and Photobiology A: Chemistry, 205, 109-115.

Rockafellow, E. M., Stewart, L. K., Jenks, W. S., 2009. Is sulfur-doped TiO_2 an effective visible light photocatalyst for remediation? Applied Catalysis B: Environmental, 91, 554-562.

Sakthivel, S., Janczarek, M., Kisch, H., 2004. Visible light activity and photoelectrochemical properties of nitrogen-doped TiO_2. The Journal of Physical Chemistry B, 108, 19384-19387.

Sakthivel, S., Kisch, H., 2003a. Daylight photocatalysis by carbon-modified titanium dioxide. Angewandte Chemie International Edition, 42, 4908-4911.

Sakthivel, S., Kisch, H., 2003b. Photocatalytic and photoelectrochemical properties of nitrogen-doped titanium dioxide. ChemPhysChem, 4, 487-490.

Sakthivel, S., Shankar, M. V., Palanichamy, M., Arabindoo, B., Bahnemann, D.W., Murugesan, V., 2004. Enhancement of photocatalytic activity by metal deposition: characterization and photonic efficiency of Pt, Au and Pd deposited on TiO_2 catalyst. Water Research, 38, 3001-3008.

Sathish, M., Viswanathan, B., Viswanath, R. P., Gopinath, C. S., 2005. Synthesis, characterization, electronic structure and photocatalytic activity of nitrogen-doped TiO_2 nanocatalysts. Chemistry of Materials, 17, 6349-6353.

Sato, S., 1986. Photocatalytic activity of NO_x-doped TiO_2 in the visible light region. Chemical Physics Letters, 123, 126-128.

Sato, S., Nakamura, R., Abe, S., 2005. Visible-light sensitization of TiO_2 photocatalysts by wet-method N doping. Applied Catalysis A: General, 284, 131-137.

Sayle, D. C., Catlow, C. R. A., Perrin, M. A., Nortier, P., 1995. Computer simulation study of the defect chemistry of rutile TiO_2. Journal of Physics and Chemistry of Solids, 56(6), 799-805.

Sen Kavurmaci, S., 2013. Photocatalytic Oxidation of Humic Acid in Heterogeneous Aqueous Systems: A Comparative Investigation between Montmorillonite and Kaolinite, Ph.D. Thesis, Boğaziçi University.

Senesi, N., Miano, T. M., Provenzano, M. R., Brunetti, G., 1989. Spectroscopy and compositional comparative characterization of I.H.S.S reference and standard fulvic and humic acids of various origins. The Science of The Total Environment, 81/82, 143-156.

Serpone, N., 2006. Is the band gap of pristine TiO_2 narrowed by anion-and cation-doping of titanium dioxide in second-generation photocatalysts? The Journal Physical Chemistry B, 110, 24287-24293.

Sever, S. Y., Yalcın Gurkan, Y., Cinar, Z., 2010. N-S-co-doped TiO_2: Preparation, characterization and photocatalytic activity. The 9th Chemical Physics Congress, October 14-16, İzmir Institute of Technology, Çeşme, Turkey.

Snoeyink, V. L., Summers, R. S., 1999. Adsorption of organic compounds, Chapter 13, in Letterman, R.D., (Ed.), water quality and treatment, Fifth Ed., McGraw Hill, Inc., USA, 13.1-13.83.

Šojić, D., Despotović, V., Abramović, B., Todorova, N., Giannakopoulou, T., Trapalis, C., 2010. Photocatalytic degradation of mecoprop and clopyralid in aqueous suspensions of nanostructured N-doped TiO_2. Molecules, 15, 2994-3009.

Sontheimer, H., Crittenden, J. C., Summers, R. S., 1988. Activated Carbon for Water Treatment, Second Ed., DVG W-Forschungstelle am Engler-Bunte-Institut der Universitat Karlsruhe, Karlsruhe, Germany.

Soto, M. L., Moure, A., Domínguez, H., Parajó, J. C., 2011. Recovery, concentration and purification of phenolic compounds by adsorption: A review. Journal of Food Engineering, 105, 1-27.

Sposito, G., 1989. The Chemistry of Soils, Oxford University Press, New York.

Stevenson, F. J., 1982. Humus Chemistry: Genesis, Composition, Reactions, Wiley and Sons, New York.

Suffet, I. H., MacCarthy, P., 1989. Aquatic Humic Substances: Influence on Fate and Treatment of Pollutants, American Chemical Society, Washington, DC, USA.

Sun, H., Bai, Y., Cheng, Y., Jin, W., Xu, N., 2006. Preparation and characterization of visible-light-driven carbon-sulfur-codoped TiO_2 photocatalysts. Industrial and Engineering Chemistry Research, 45, 4971-4976.

Suphandag, S. A, 1998. Adsorption Capacity of Natural Organic Matter on Semiconductor Powders, M.S. Thesis, Boğaziçi University.

Suphandag, S. A., 2006. Evaluation of Natural Organic Matter - Metal Oxide Adsorption System under Influential Structural Concepts, Ph.D. Thesis, Boğaziçi University.

Suphandag, S. A., Bekbölet, M., 2000. Constituting an adsorption profile of humic acid on semiconductor powders, Chemical Speciation and Reactivity in Water Chemistry and Water Technology: A Symposium in Honor of James J. Morgan, Washington, DC, 20-24 August, 40 (2), 580-581.

Tan, X., Wang, X., Chen, C., Sun, A., 2007. Effect of soil and fulvic acids, pH and ionic strength on Th (IV) sorption to TiO_2 nanoparticles. Applied Radiation and Isotopes, 65, 375-381.

Tang, Y., Liang, S., Yu, S., Gao, N., Zhang, J., Guo, H., Wang, Y., 2012. Enhanced adsorption of humic acid on amine functionalized magnetic mesoporous composite microspheres. Colloids and Surfaces A: Physicochemical and Engineering Aspects, 406, 61-67.

Tchobanoglous, G., Burton, F. L., Stensel, H. D., 2003. Wastewater Engineering Treatment and Reuse, Fourth Ed., McGraw-Hill Companies, Inc., New York.

Thurman, E. M., Malcolm, R. L., 1981. Preparative isolation of aquatic humic substances. American Chemical Society, 15(4), 463-466.

Tryba, B., Piszcz, M., Morawski, A. W., 2009. Photocatalytic activity of TiO_2-WO_3 composites. International Journal of Photoenergy, 2009, 297319, 1-7.

Tseng, D. H., Juang, L. C., Huang, H. H., 2012. Effect of oxygen and hydrogen peroxide on the photocatalytic degradation of monochlorobenzene in TiO_2 aqueous suspension. International Journal of Photoenergy, 2012, 1-9.

Ulker, Y., 2008. Effect of Fractionation on the Sorption Properties of NOM onto Modified TiO_2 Surfaces, M.S. Thesis, Boğaziçi University.

Umebayashi, T., Yamaki, T., Itoh, H., Asai, K., 2002. Band gap narrowing of titanium dioxide by sulfur doping. Applied Physics Letters, 81(3), 454-456.

Umebayashi, T., Yamaki, T., Tanaka, S., Asai, K., 2003. Visible light induced degradation of methylene blue on S-doped TiO_2. Chemistry Letters, 32, 4, 330.

Uyguner, C. S., Bekbolet, M., 2004. Evaluation of humic acid, chromium (VI) and TiO_2 ternary system in relation to adsorptive interactions. Applied Catalysis B: Environmental, 49, 267-275.

Uyguner, C. S., Bekbolet, M., 2005a. A comparative study on the photocatalytic degradation of humic substances of various origins. Desalination, 176, 167-176.

Uyguner, C. S., Bekbolet, M., 2005b. Implementation of spectroscopic parameters for practical monitoring of natural organic matter. Desalination, 176, 47-55.

Uyguner-Demirel, C. S., Bekbolet, M., 2011. Significance of analytical parameters for the understanding of natural organic matter in relation to photocatalytic oxidation. Chemosphere, 84, 1009-1031.

Uyguner, C. S., Suphandag, S. A., Kerc, A., Bekbolet, M., 2007. Evaluation of adsorption and coagulation characteristics of humic acids preceded by alternative advanced oxidation techniques. Desalination, 210, 183-193.

Ulker, Y., 2008. Effect of Fractionation on the Sorption Properties of NOM onto Modified TiO_2 Surfaces, M.S. Thesis Boğaziçi University.

vanLoon, G. W., Duffy, S. J., 2010. Environmental Chemistry A Global Perspective. Third Ed., Oxford University Press, United Kingdom, 254-272.

van Veen, J. A. R., 1989. Zeitschrift fur Physikalische Chemie, 162, 215-221, reference in, Pelizetti, E., and Minero, C., 1993. Mechanism of the photo-oxidative degradation of organic pollutants over TiO_2 particles. Electrochimica Acta, 388(1), 47-55.

Vermeer, A. W. P., van Riemsdijk, W. H., Koopal, L. K., 1998. Adsorption of humic acid to mineral particles. 1. Specific and electrostatic interactions. Langmuir, 14, 2810-2819.

Vreysen, S., Maes, A., 2008. Adsorption mechanism of humic and fulvic acid onto Mg/Al layered double hydroxides. Applied Clay Science, 38, 237-249.

Wan Ngah, W. S., Hanafiah, M. A. K. M., Yong, S. S., 2008. Adsorption of humic acid from aqueous solutions on crosslinked chitosan-epicchlorohydrin beads: Kinetics and isotherm studies. Colloids and Surfaces B: Biointerfaces, 65, 18-24.

Wang, G. S., Hsieh, S. T., Hong, C. S., 2000. Destruction of humic acid in water by UV light-catalyzed oxidation with hydrogen peroxide. Water Research, 34(15), 3882-3887.

Wang, G. S., Liao, C. H., Wu, F. J., 2001. Photodegradation of humic acids in the presence of hydrogen peroxide. Chemosphere, 42, 379-387.

Wang, H., Lewis, J. P., 2006. Second-generation photocatalytic materials: anion-doped TiO_2. Journal of Physics: Condensed Matter, 18, 421-434.

Wang, J., Tafen, D. N., Lewis, J. P., Hong, Z., Manivannan, A., Zhi, M., Li, M., Wu, N., 2009. Origin of photocatalytic activity of nitrogen-doped TiO_2 Nanobelts. Journal of American Chemical Society, 131, 12290-12297.

Wang M., Liao, L., Zhang, X., Li, Z., 2012. Adsorption of low concentration humic acid from water by palygorskite. Applied Clay Science, 67-68, 164-168.

Wang, Q., Wei, S., Huang, Y., Zhang, J., 2008. Characteristics of isothermal adsorption and desorption of aluminum ion to/from humic acids. Journal of Environmental Sciences, 20, 579-584.

Wang, Z., Cai, W., Hong, X., Zhao, X., Xu, F., Cai, C., 2005. Photocatalytic degradation of phenol in aqueous nitrogen-doped TiO_2 suspensions with various light sources. Applied Catalysis B: Environmental, 57, 223-231.

Weber, W.J., 1972. Physicochemical Processes: For Water Quality Control, First Ed., Wiley- Interscience, New York.

Weishaar, J. L., Aiken, G. R., Bergamaschi, B. A., Fram, M. S., Fujij, R., Mopper, K., 2003. Evaluation of specific ultraviolet absorbance as an indicator of the chemical composition and reactivity of dissolved organic carbon. Environmental Science and Technology, 37, 4702-4708.

Xekoukoulokatis, N. P., Mantzavinos, D., Dillert, R., Bahnemann, D., 2010. Synthesis and photocatalytic activity of boron-doped TiO_2 in aqueous suspensions under UV-A irradiation. Water Science and Technology, 61(10), 2501-2506.

Xiao, Q., Ouyang, L., 2009. Photocatalytic activity and hydroxyl radical formation of carbon-doped TiO_2 nanocrystalline: Effect of calcinations temperature. Chemical Engineering Journal, 148, 248-253.

Xiao, Q., Ouyang, L., Gao, L., Yao, C., 2011. Preparation and visible light photocatalytic activity of mesoporous N, S-codoped TiO_2 (B) nanobelts. Applied Surface Science, 257, 3652-3656.

Xiao, Q., Zhang, J., Xiao, C., Si, Z., Tan, X., 2008. Solar photocatalytic degradation of methylene blue in carbon-doped TiO_2 nanoparticles suspension. Solar Energy, 82, 706-713.

Xu, J. Z., Fan, Q. H., Niu, Z. W., Li, Y., Li, P., Wu, W. S., 2012. Studies of Eu(III) sorption on TiO$_2$: Effects of pH, humic acid and poly(acrylic acid). Chemical Engineering Journal, 179, 186-192.

Yalcin, Y., Kılıç, M., Cinar, Z., 2008a. N-doped TiO$_2$: Characterization and DFT modeling. Chemical Physics Conference VIII, Istanbul Technical University, Istanbul, 24-25 April, 106.

Yalcin, Y., Kılıç, M., Cinar, Z., 2008b. Carbon-doped TiO$_2$: Characterization and DFT modeling of the surface. 25 Years in TiO$_2$ Photocatalysis: Retrospective and Perspective Views TiO$_2$-13, 22-25 September, San Diago, California, ABD.

Yalcin, Y., Kılıç, M., Cinar, Z., 2009a. The role of non-metal doping in TiO$_2$ photocatalysis. The 14th International Conference on TiO$_2$ Photocatalysis: Fundamentals and Applications TiO$_2$-14, 5-8 October, Niagara Falls, USA.

Yalcin, Y., Kılıç, M., Cinar, Z., 2009b. Visible-light active TiO$_2$ photocatalysts by nitrogen doping. First International Workshop on Application of Redox Technologies in the Environment ARTE'2009, 129-131, 14-15 September, Istanbul, Turkey.

Yalcin, Y., Kılıç, M., Cinar, Z., 2009c. The structure and photocatalytic activity of C-doped TiO$_2$ and DFT modeling. First International Workshop on Application of Redox Technologies in the Environment ARTE'2009, 195-198, 14-15 September, Istanbul, Turkey.

Yalcin, Y., Kılıç, M., Cinar, Z., 2010. The role of non-metal doping in TiO$_2$ photocatalysis. Journal of Advanced Oxidation Technologies, 113, 3, 281-296.

Yalcin Gurkan, Y., Cinar, Z., 2010a. An experimental and computational approach to the visible light activity of C-doped TiO$_2$. The 9th Chemical Physics Congress, October 14-16, İzmir Institute of Technology, Çeşme, Turkey.

Yalcin Gurkan, Y., Cinar, Z., 2010b. Origin of visible-light activity N-doped TiO_2 photocatalysts. The 9th Chemical Physics Congress, October 14-16, İzmir Institute of Technology, Çeşme, Turkey.

Yalcin, Y., Kılıç, M., Cinar, Z., 2010. Fe^{3+}-doped TiO_2: A combined experimental and computational approach to the evaluation of visible light activity. Applied Catalysis B: Environmental, 99, 3-4, 469-477.

Yan, W. L., Bai, R., 2005. Adsorption of lead and humic acid on chitosan hydrogel beads. Water Research, 39, 688-698.

Yang, K., Dai, Y., Huang, B., 2007. Understanding photocatalytic activity of S- and P-doped TiO_2 under visible light from first-principles. The Journal of Physical Chemistry C, 111, 18985-18994.

Yates, D. E., Healy, T. W., 1980. Journal of Chemical Society Faraday, 76, 9-14, reference in, Pelizetti, E., and Minero, C, 1993. Mechanism of the photo- oxidative degradation of organic pollutants over TiO_2 Particles. Electrochimica Acta, 388(1), 47-55.

Yu, J. C., Ho, W., Yu, J., Yip, H., Wong, P. K., Zhao, J., 2005. Efficient visible-light induced photocatalytic disinfection on sulfur-doped nanocrystalline titania. Environmental Science and Technology, 39, 1175-1179.

Yu, J., Zhou, M., Cheng, B., Zhao, X., 2006. Preparation, characterization and photocatalytic activity of in situ N,S-codoped TiO_2 powders. Journal of Molecular Catalysis A: Chemical 246, 176-184.

Zaleska, A., 2008a. Characteristics of doped-TiO_2 photocatalysts. Physicochemical Problems of Mineral Processing, 42, 211-222.

Zaleska, A., 2008b. Doped-TiO_2: A Review. Recent Patents On Engineering, 2, 157-164.

Zhang, F. J., Chen, M. L., Oh, W. C., 2009. Characterization of CNT/TiO$_2$ electrode prepared through impregnation with TNB and their photoelectrocatalytic properties. Environmental Engineering Research, 14(1), 32-40.

Zhang, H., Tan, K., Zheng, H., Gu, Y., Zhang, W. F., 2011. Preparation, characterization and photocatalytic activity of TiO$_2$ codoped with yttrium and nitrogen. Materials Chemistry and Physics, 125, 156-160.

Zhang, S., Song, L., Zhang, S., Sun, D., Chen, B., 2009a. Facile preparation of visible-light-sensetive sulfur-nitrogen-codoped titanium dioxide. Reaction Kinetic and Catalysis Letters, 97, 199-205.

Zhang, W., Zou, L., Wang, L., 2009b. Photocatalytic TiO$_2$/adsorbent nanocomposites prepared via wet chemical impregnation for wastewater treatment: A review. Applied Catalysis A: General, 371, 1-9.

Zhao, L., Luo, F., Wasikiewicz, J. M., Mitomo, H., Nagasawa, N., Yagi, T., Tamada, M., Yoshii, F., 2008. Adsorption of humic acid from aqueous solution onto irradiation-crosslinked carboxymethylchitosan. Bioresource Technology, 99, 1911-1917.

APPENDIX A

Freundlich Adsorption Isotherms of Different Molecular Size Fractions of Humic Acid for UV_{365} and UV_{280}
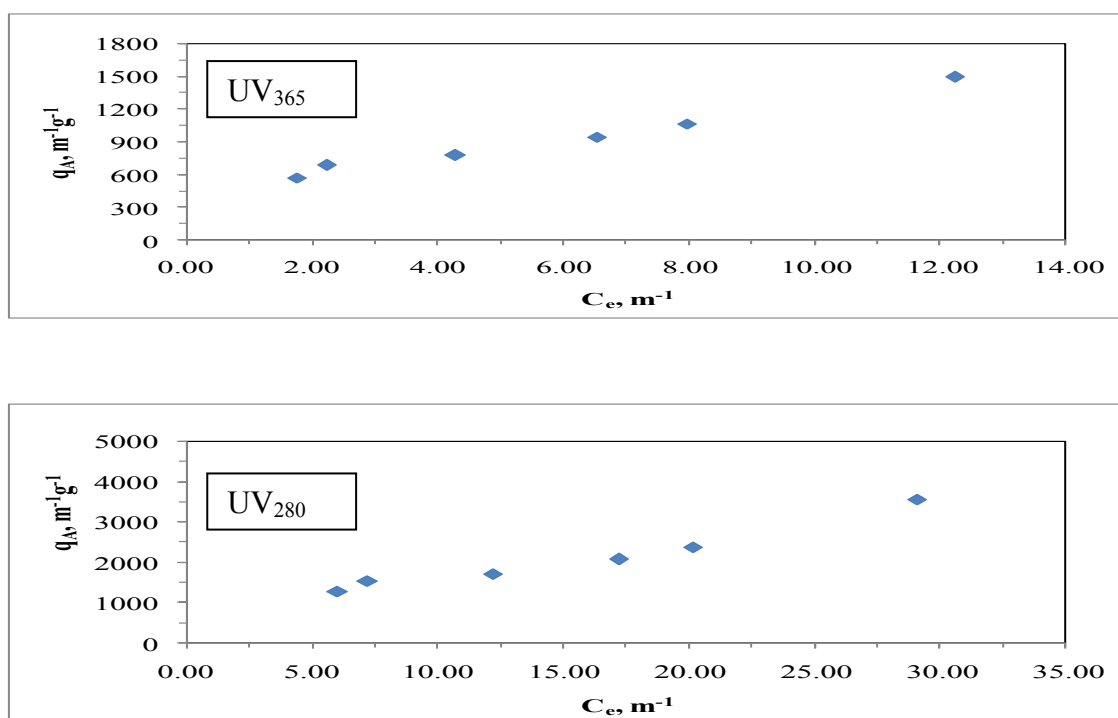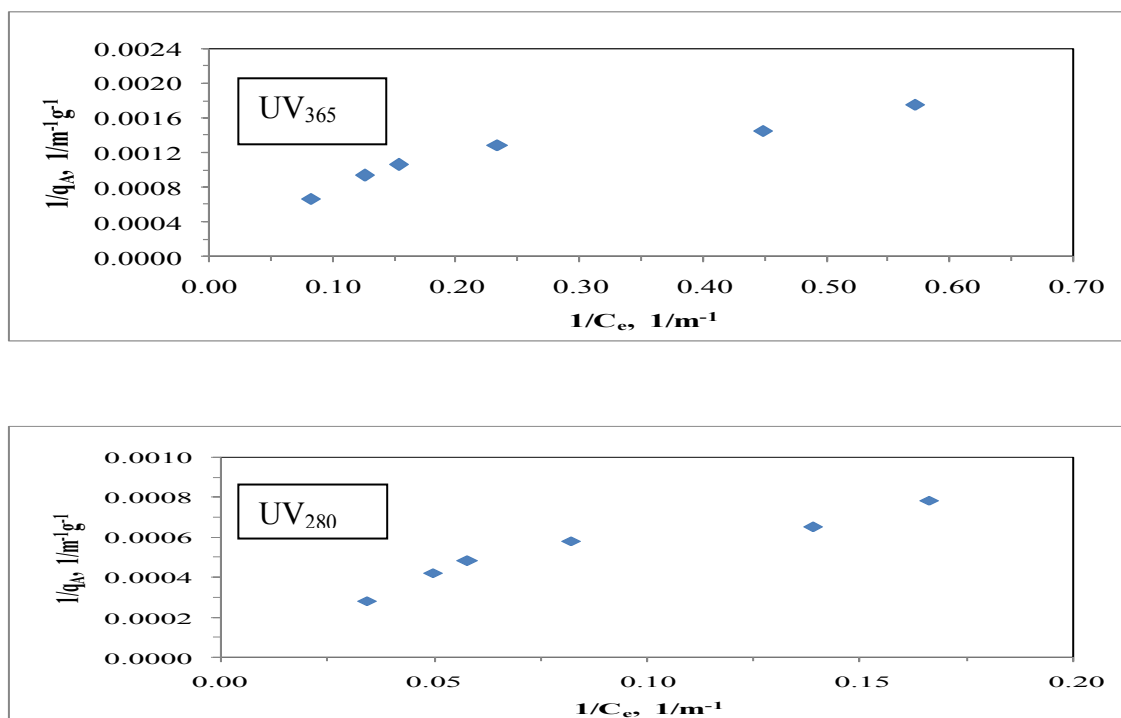
Figure A.1.   Freundlich adsorption isotherm of UV_{365} and UV_{280} parameters of 0.45 μm filtration fraction of humic acid following adsorption onto bare TiO_2 Degussa P-25.
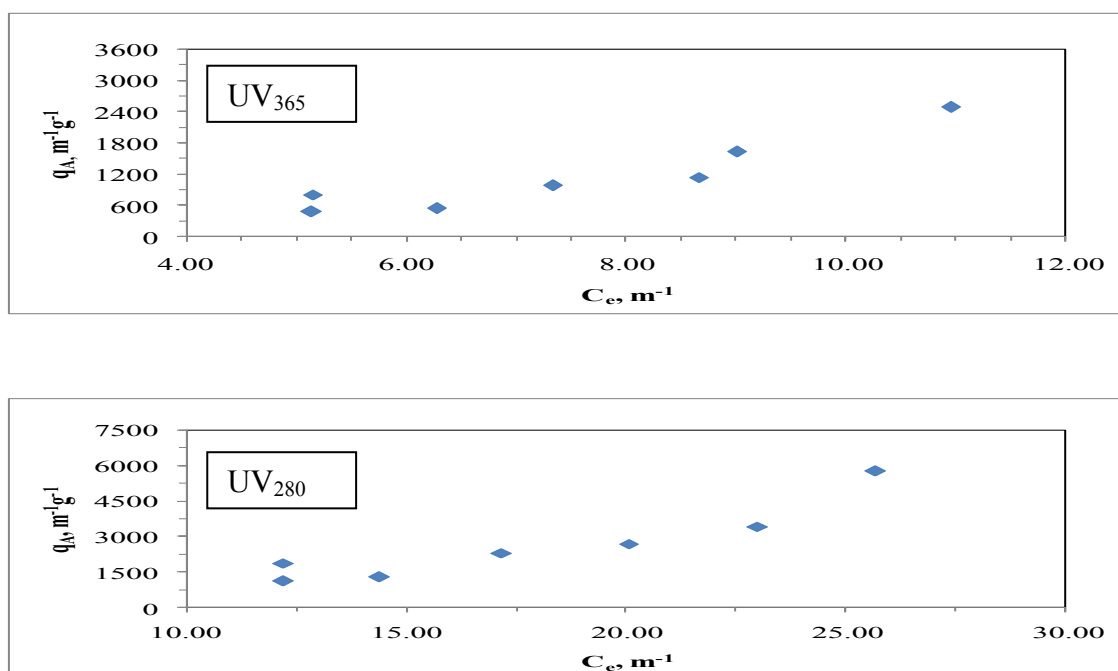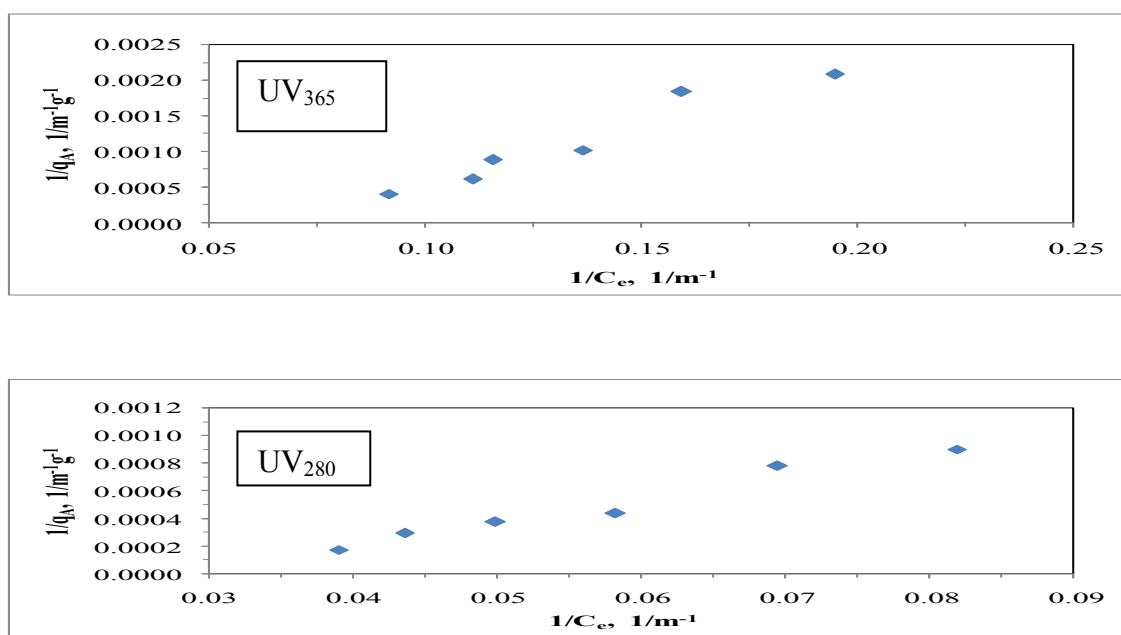

Figure A.2.   Freundlich adsorption isotherm of UV_{365} and UV_{280} parameters of 0.45 μm filtration fraction of humic acid following adsorption onto C-doped TiO_2 Degussa P-25.
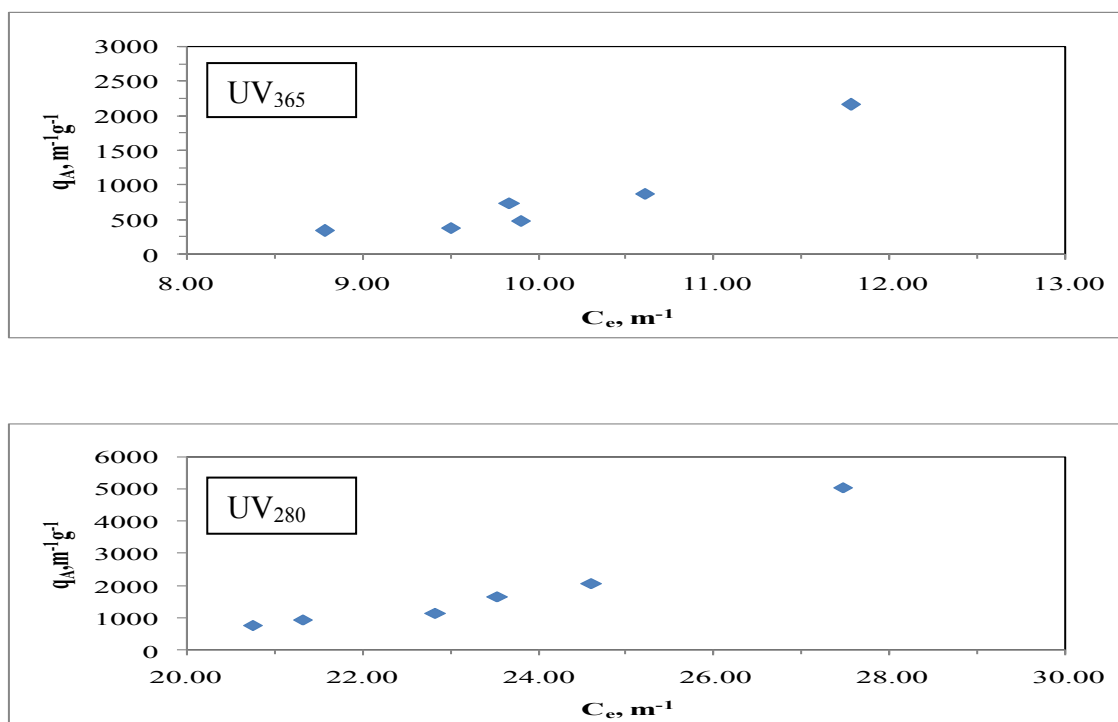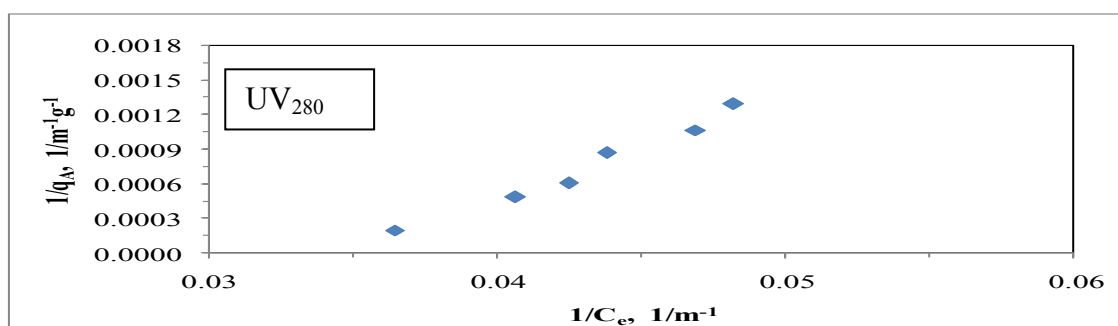
Figure A.3. Freundlich adsorption isotherm of UV_{365} and UV_{280} parameters of 0.45 μm filtration fraction of humic acid following adsorption onto N-doped TiO_2 Degussa P-25.
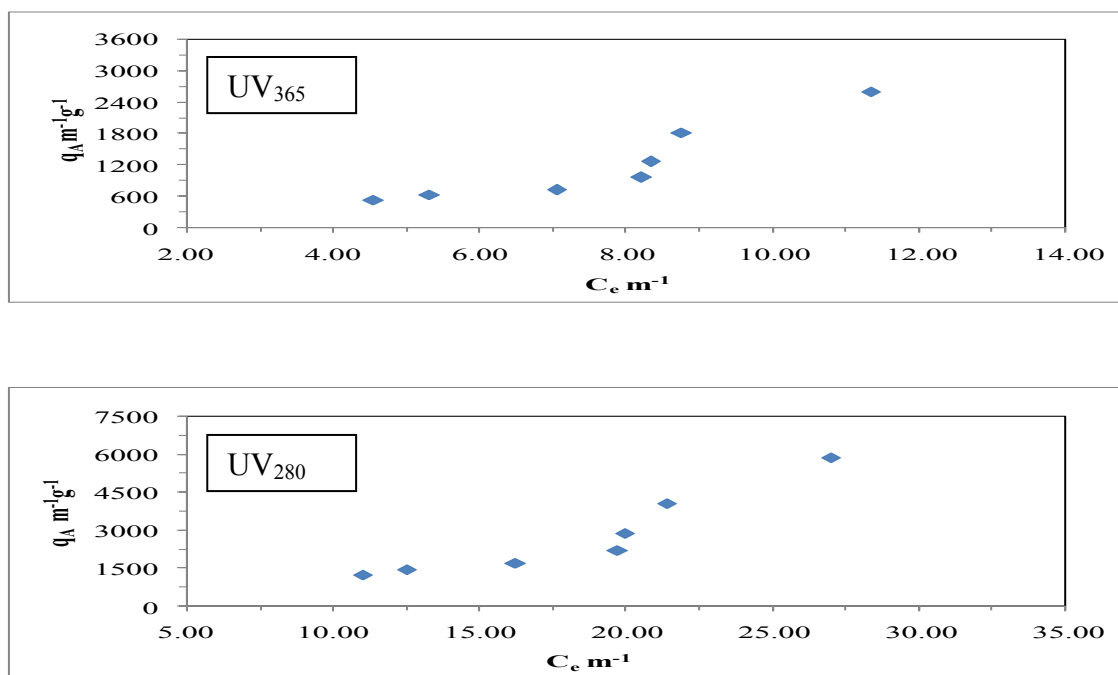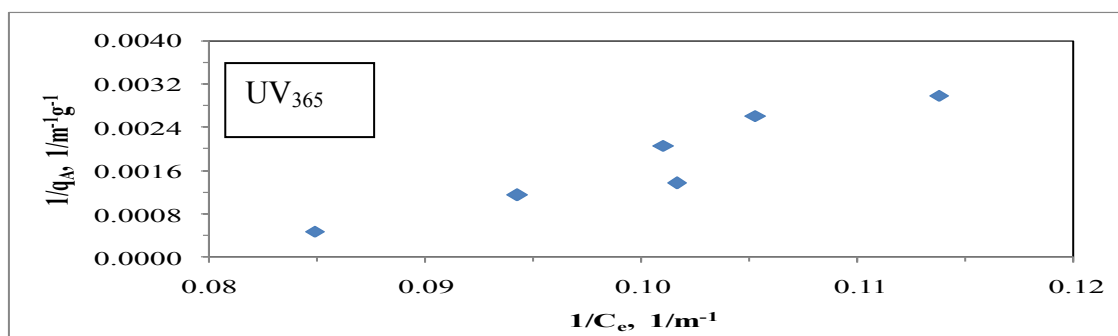

Figure A.4. Freundlich adsorption isotherm of UV_{365} and UV_{280} parameters of 0.45 μm filtration fraction of humic acid following adsorption onto S-doped TiO_2 Degussa P-25.
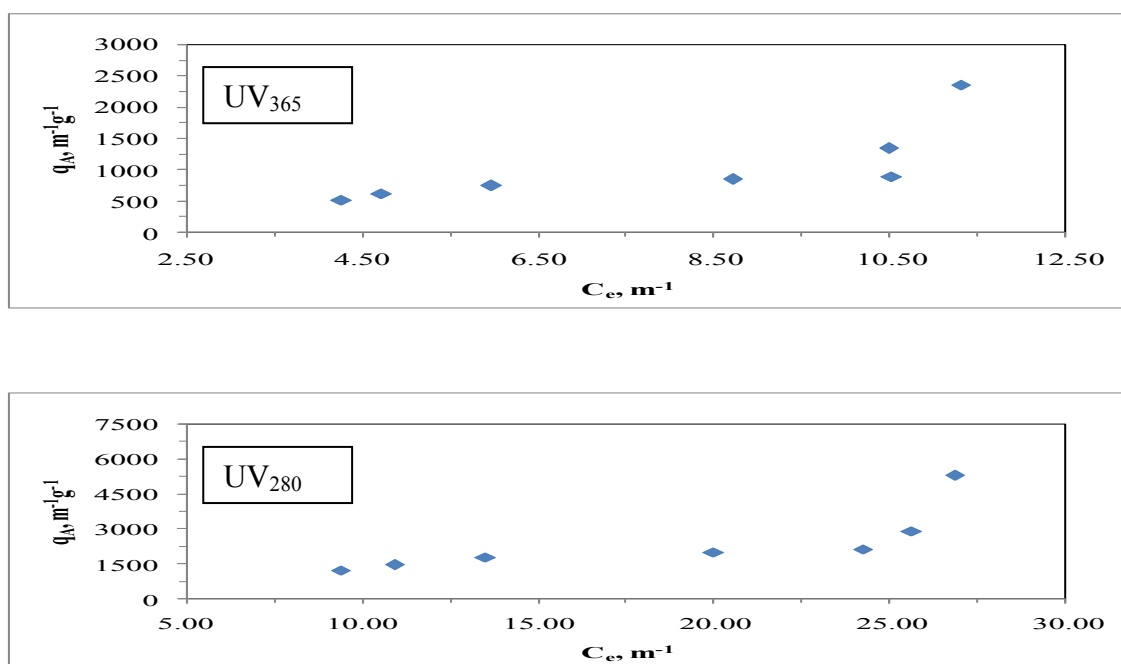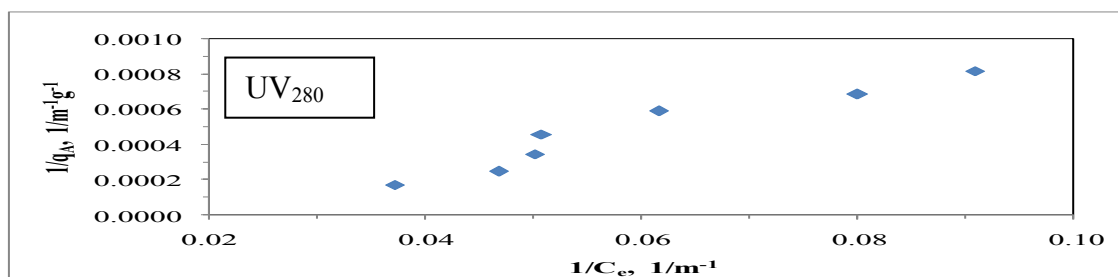
Figure A.5. Freundlich adsorption isotherm of UV_{365} and UV_{280} parameters of 0.45 μm filtration fraction of humic acid following adsorption onto N-S co-doped TiO_2 Degussa P-25.
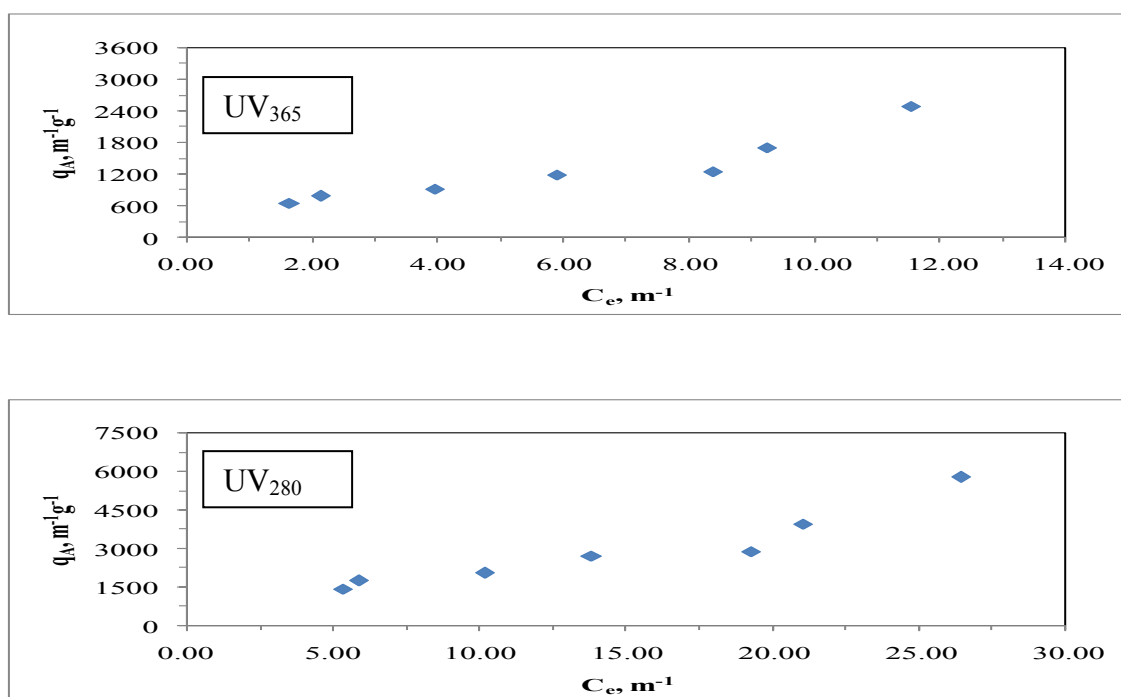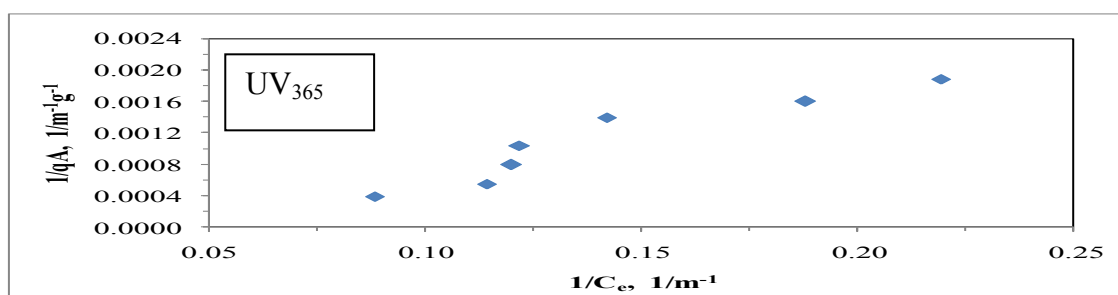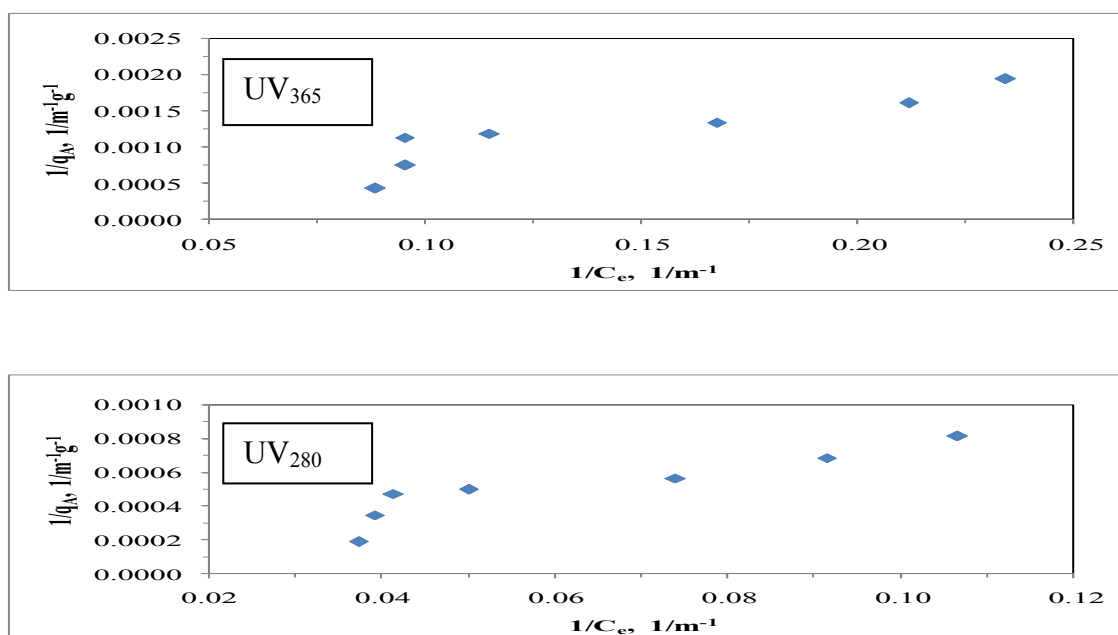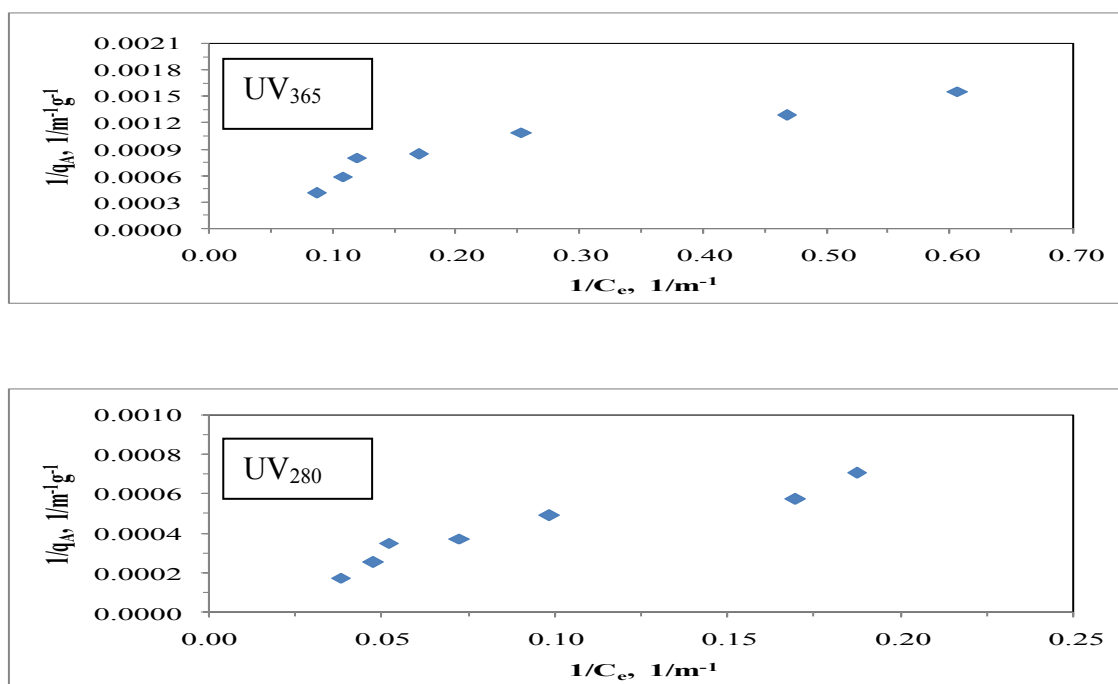

Figure A.6. Freundlich adsorption isotherm of UV_{365} and UV_{280} parameters of 0.45 μm filtration fraction of humic acid following adsorption onto bare TiO_2 Hombikat UV-100.
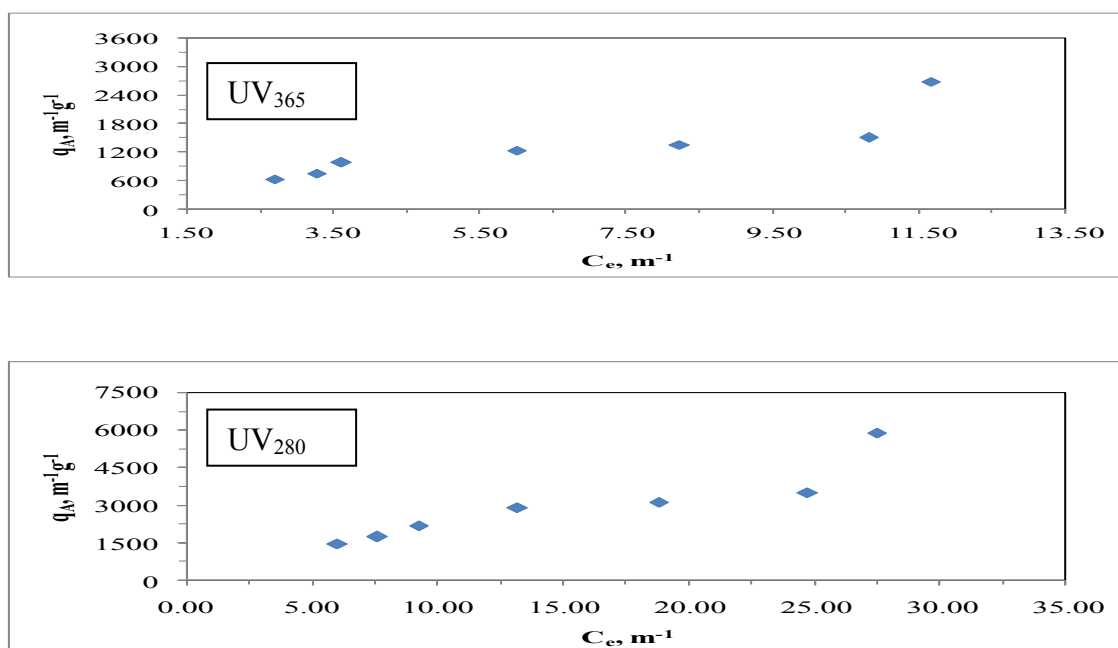
Figure A.7. Freundlich adsorption isotherm of UV_{365} and UV_{280} parameters of 0.45 µm filtration fraction of humic acid following adsorption onto C-doped TiO_2 Hombikat UV-100.
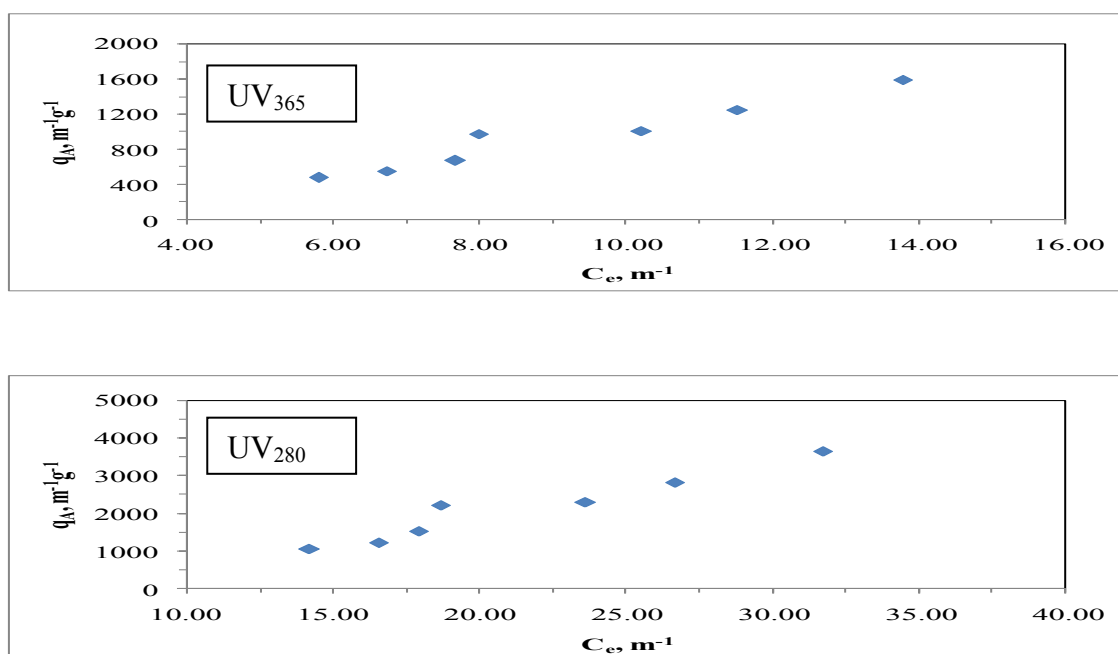
Figure A.8. Freundlich adsorption isotherm of UV_{365} and UV_{280} parameters of 0.45 µm filtration fraction of humic acid following adsorption onto N-doped TiO_2 Hombikat UV-100.
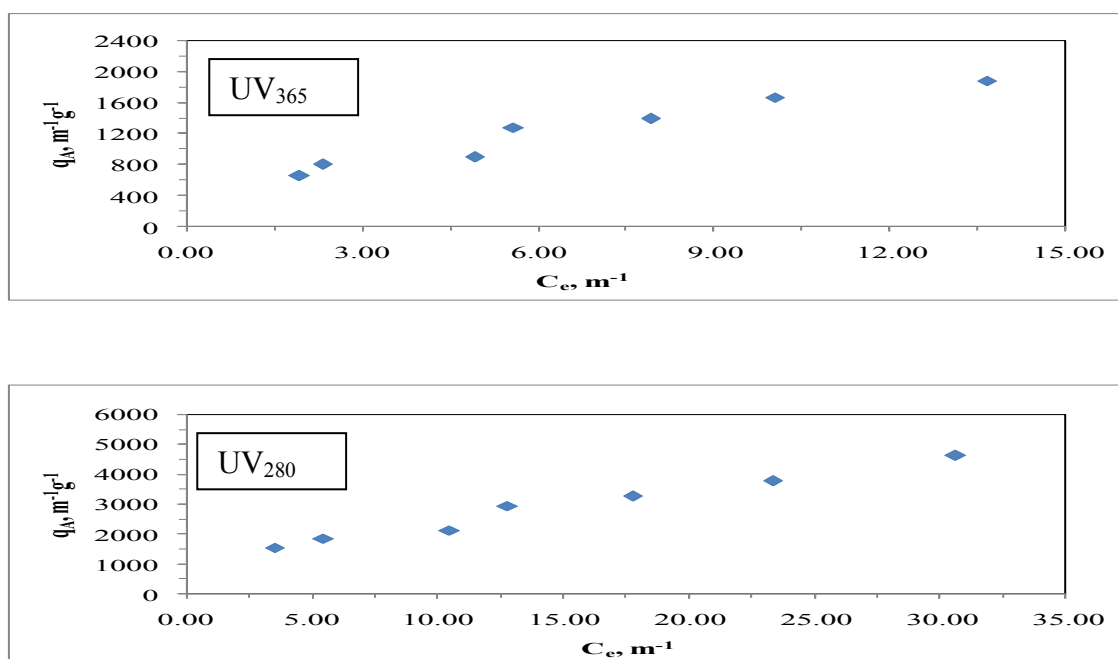
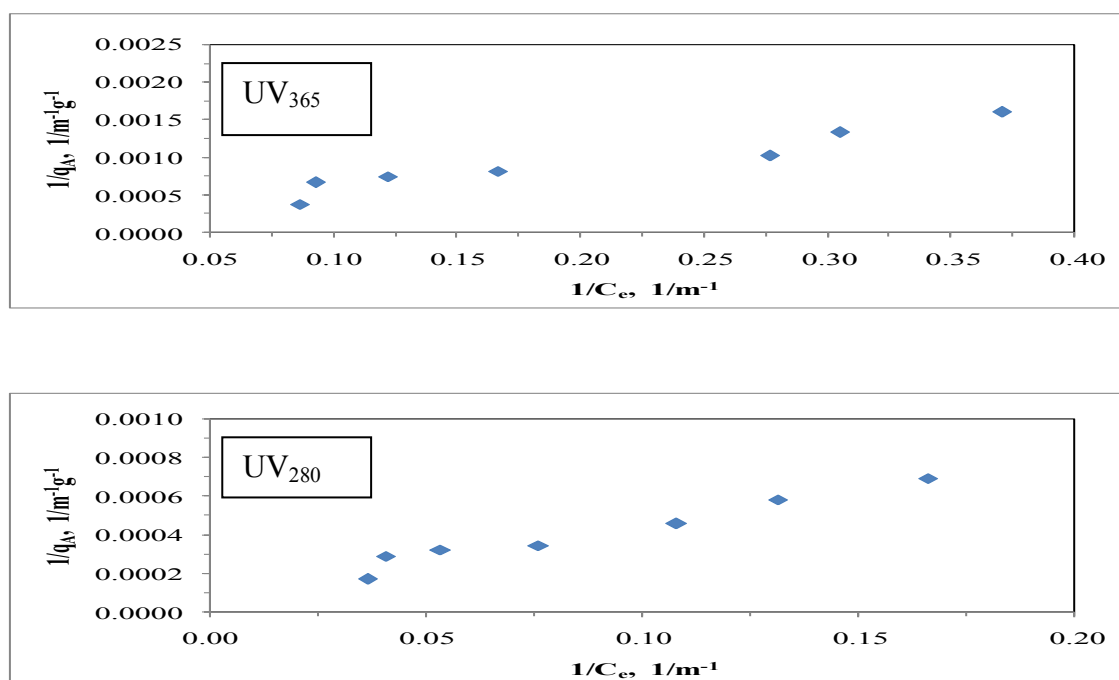Figure A.9. Freundlich adsorption isotherm of UV_{365} and UV_{280} parameters of 0.45 μm filtration fraction of humic acid following adsorption onto S-doped TiO_2 Hombikat UV-100.
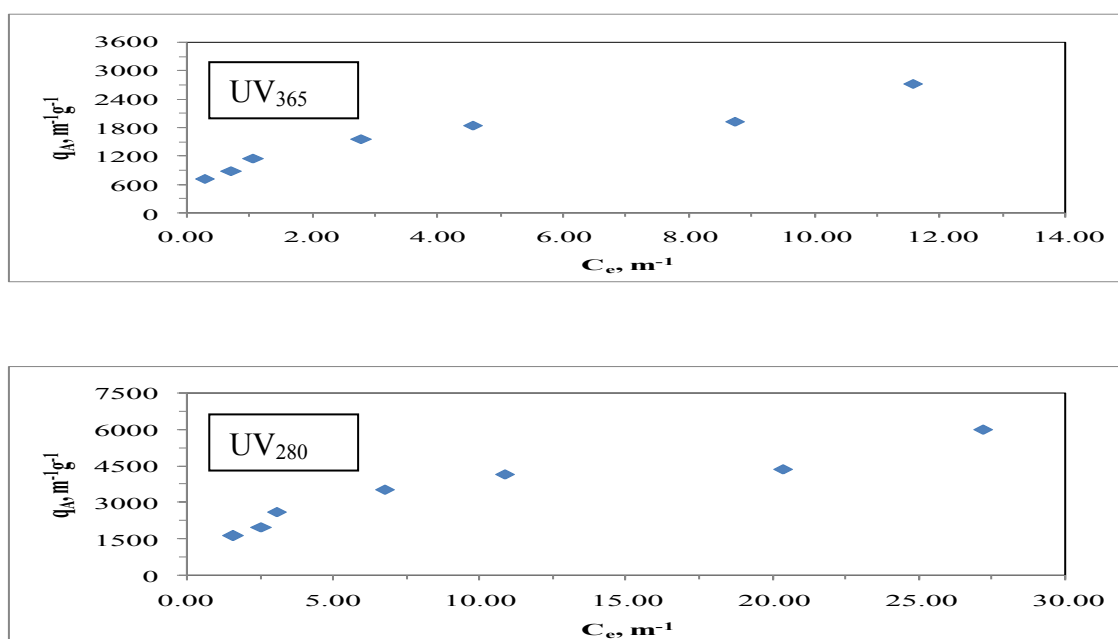
Figure A.10. Freundlich adsorption isotherm of UV_{365} and UV_{280} parameters of 0.45 μm filtration fraction of humic acid following adsorption onto N-S co-doped TiO_2 Hombikat UV-100.
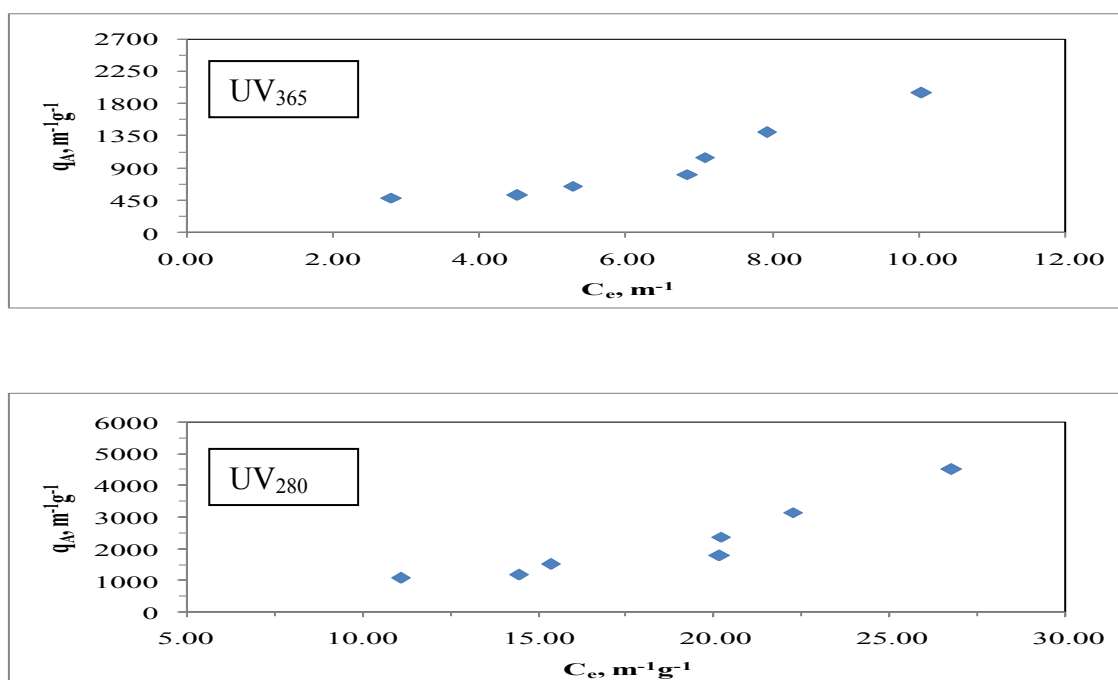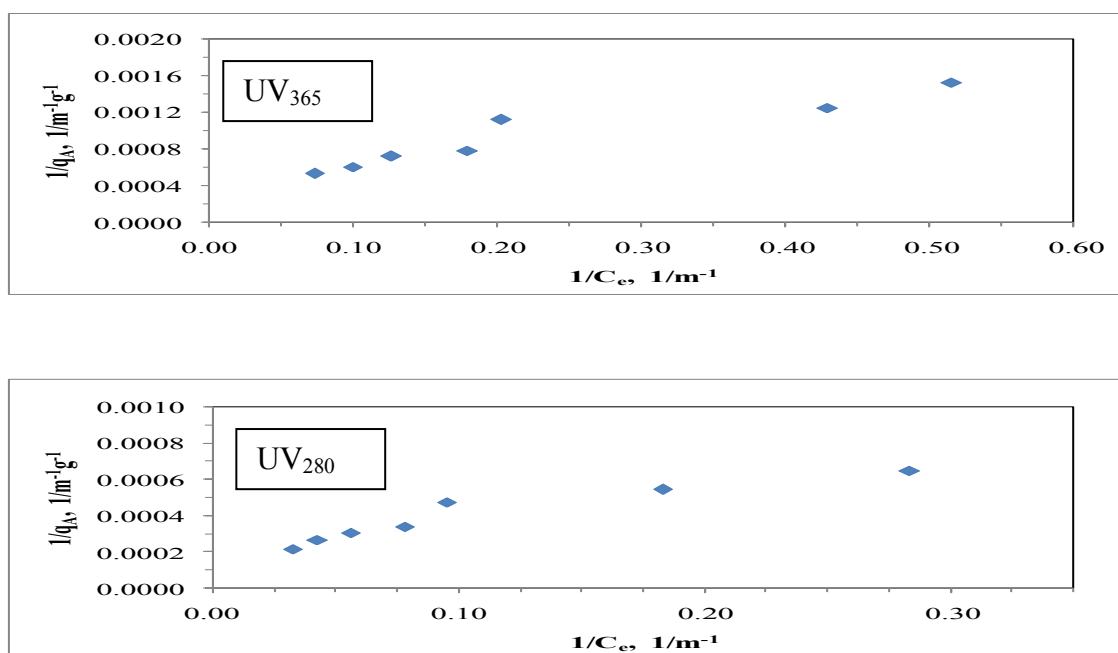
Figure A.11. Freundlich adsorption isotherm of UV_{365} and UV_{280} parameters of 100 kDa fraction of humic acid following adsorption onto bare TiO_2 Degussa P-25.
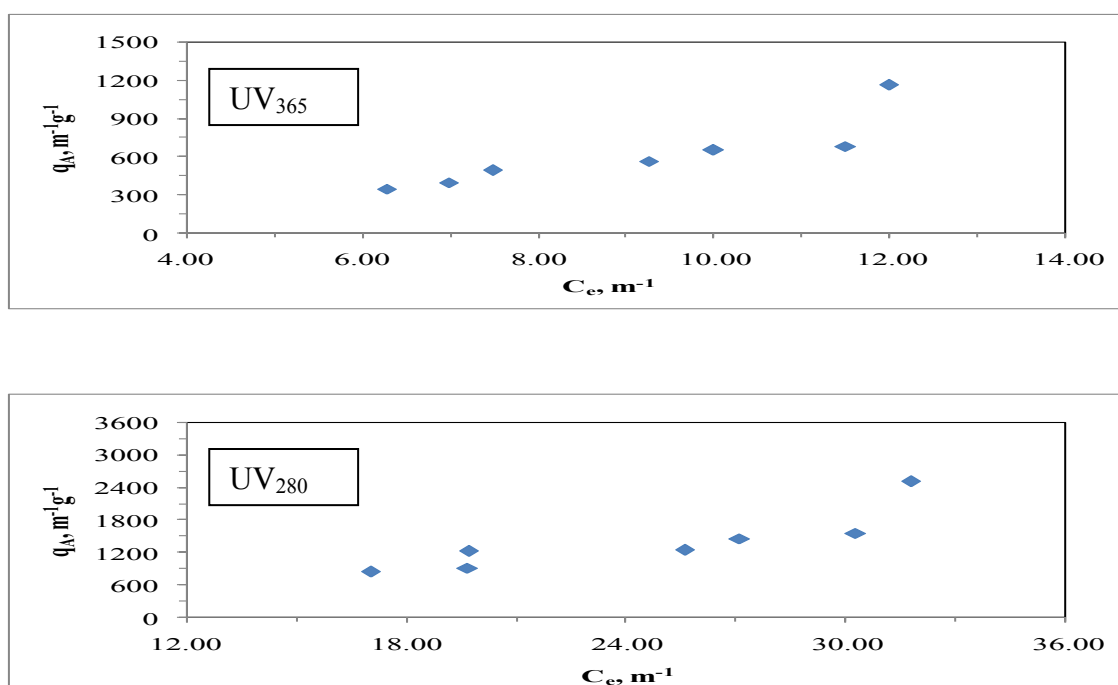
Figure A.12. Freundlich adsorption isotherm of UV_{365} and UV_{280} parameters of 100 kDa fraction of humic acid following adsorption onto C-doped TiO_2 Degussa P-25.
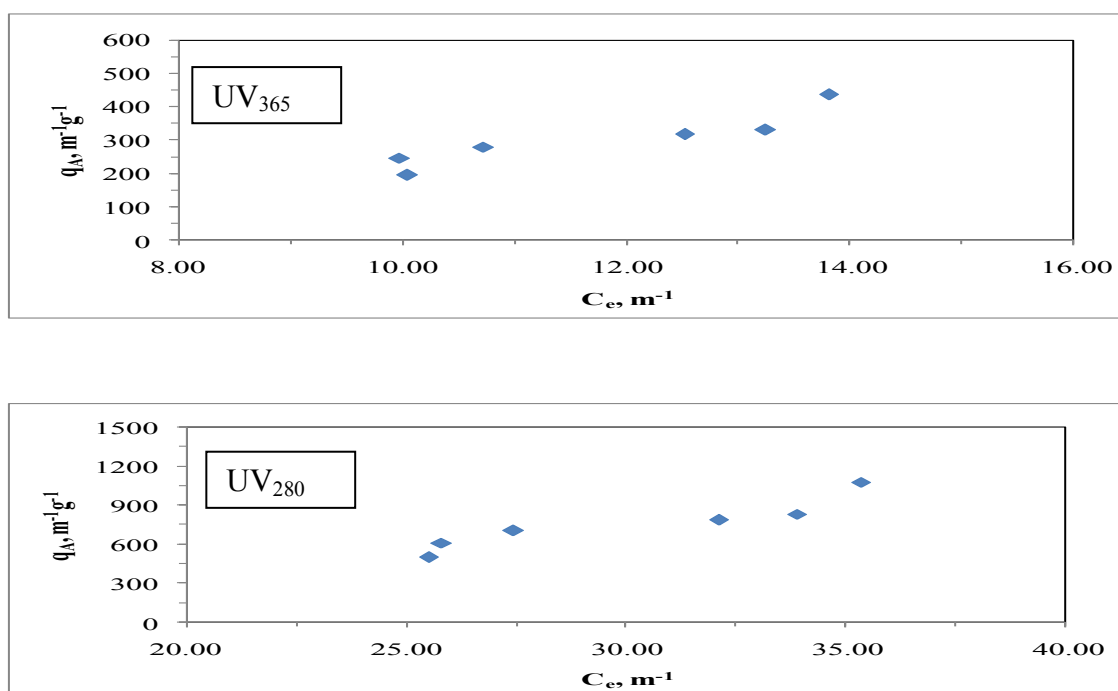
Figure A.13. Freundlich adsorption isotherm of UV_{365} and UV_{280} parameters of 100 kDa fraction of humic acid following adsorption onto N-doped TiO_2 Degussa P-25.
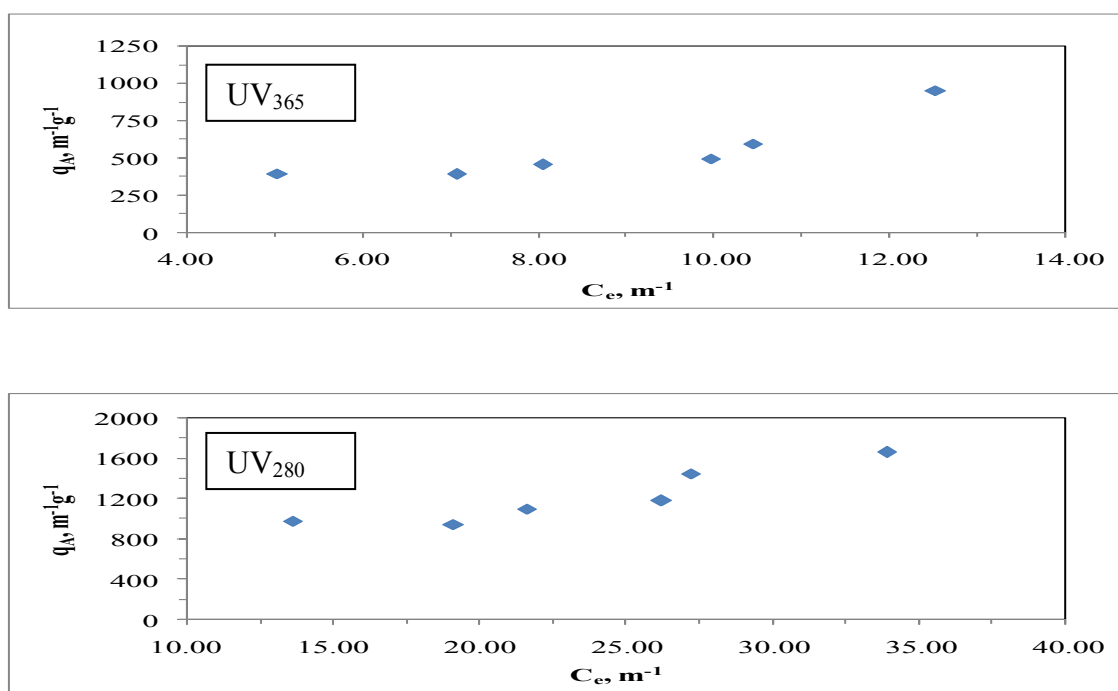
Figure A.14. Freundlich adsorption isotherm of UV_{365} and UV_{280} parameters of 100 kDa fraction of humic acid following adsorption onto S-doped TiO_2 Degussa P-25.
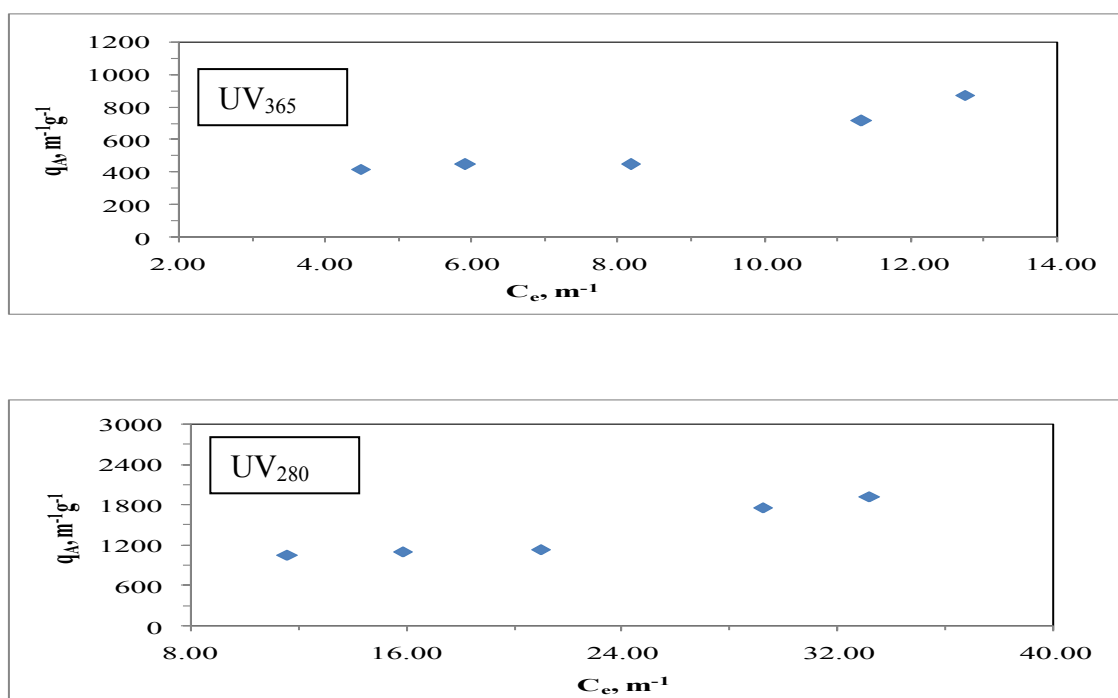
Figure A.15. Freundlich adsorption isotherm of UV$_{365}$ and UV$_{280}$ parameters of 100 kDa fraction of humic acid following adsorption onto N-S co-doped TiO$_2$ Degussa P-25.
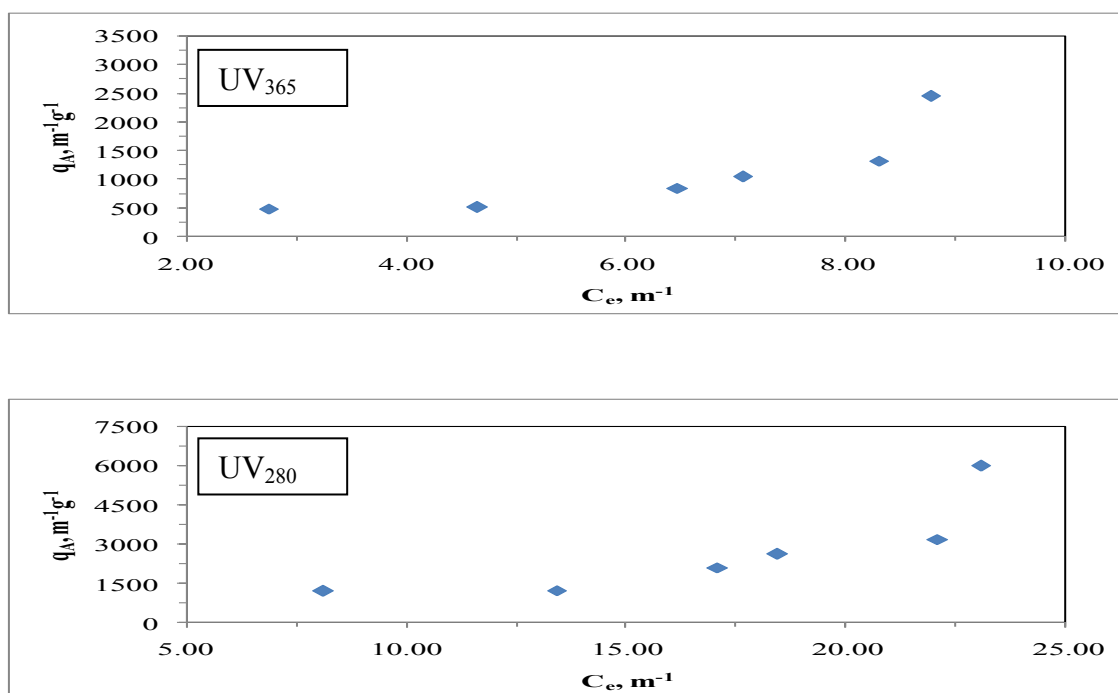
Figure A.16. Freundlich adsorption isotherm of UV$_{365}$ and UV$_{280}$ parameters of 100 kDa fraction of humic acid following adsorption onto bare TiO$_2$ Hombikat UV-100.
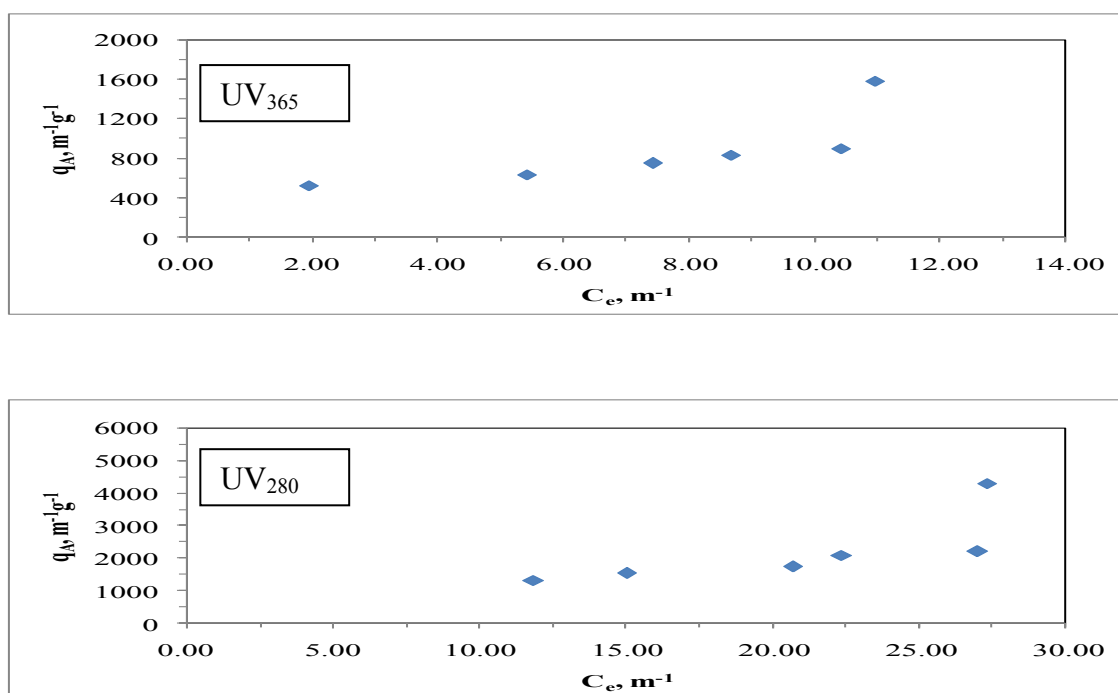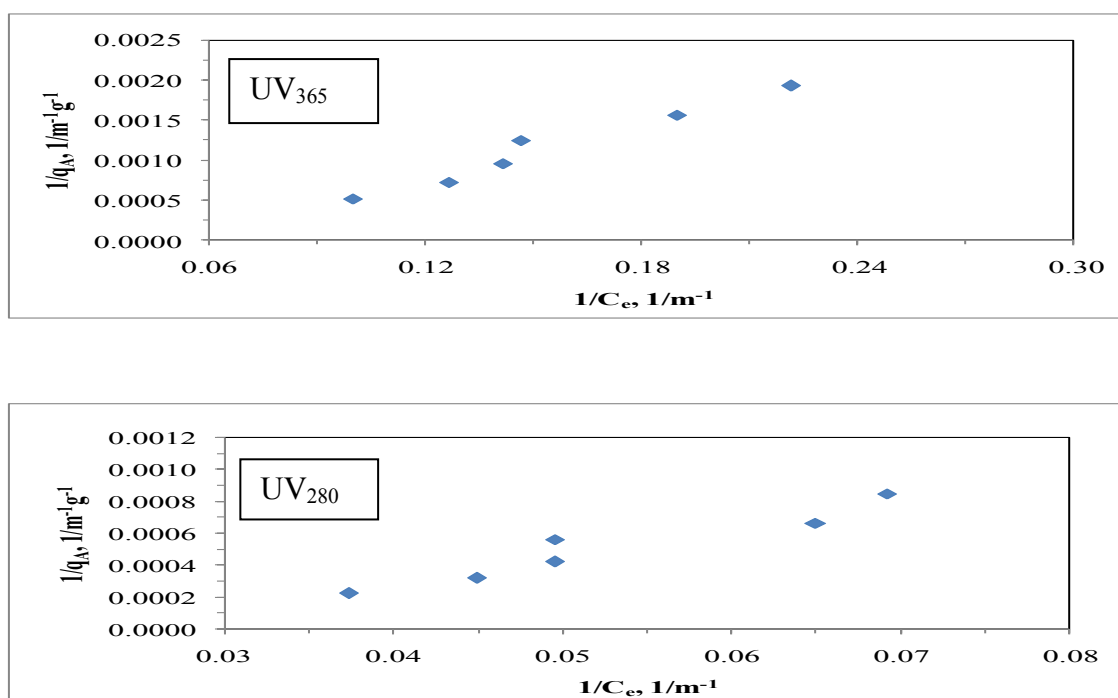
Figure A.17. Freundlich adsorption isotherm of UV_{365} and UV_{280} parameters of 100 kDa fraction of humic acid following adsorption onto C-doped TiO_2 Hombikat UV-100.
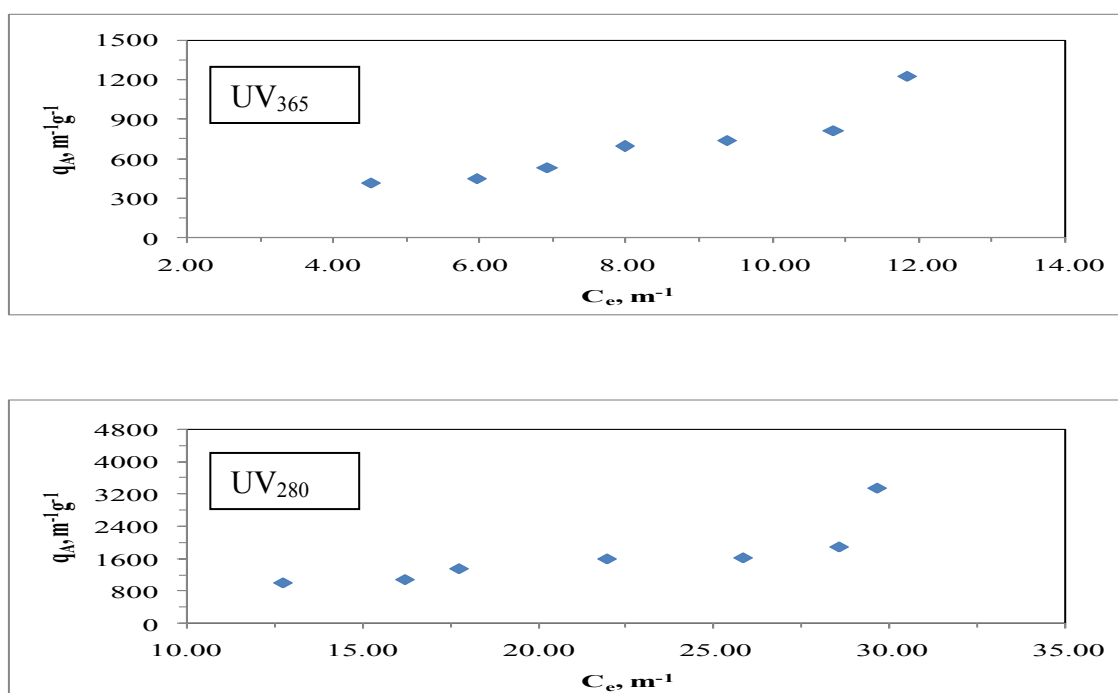
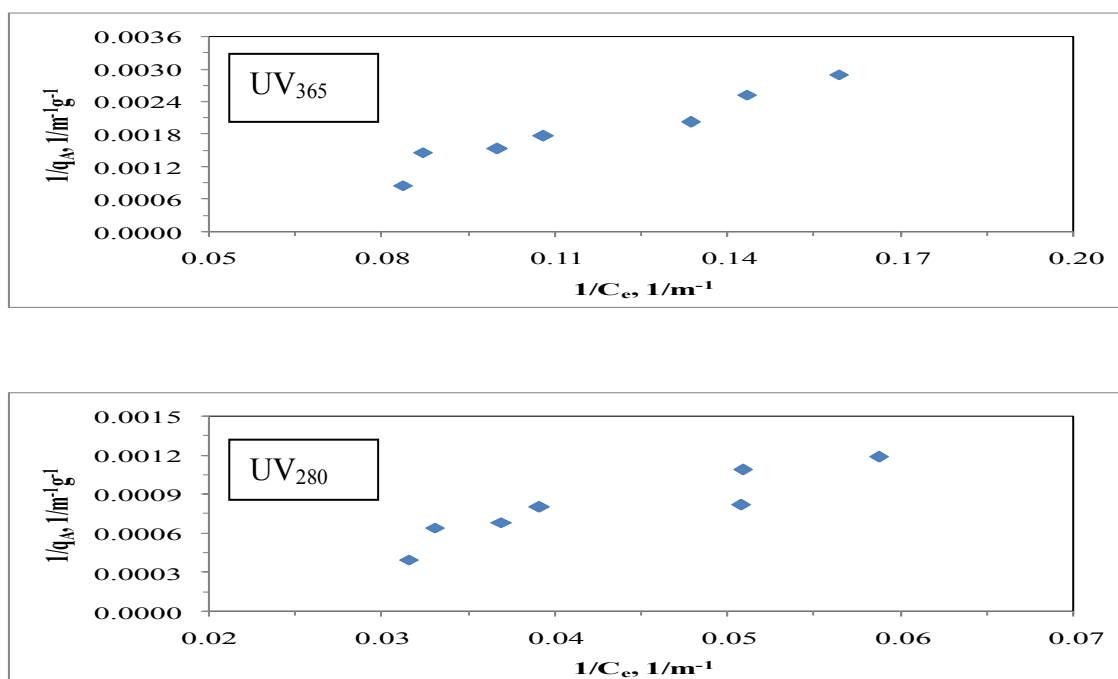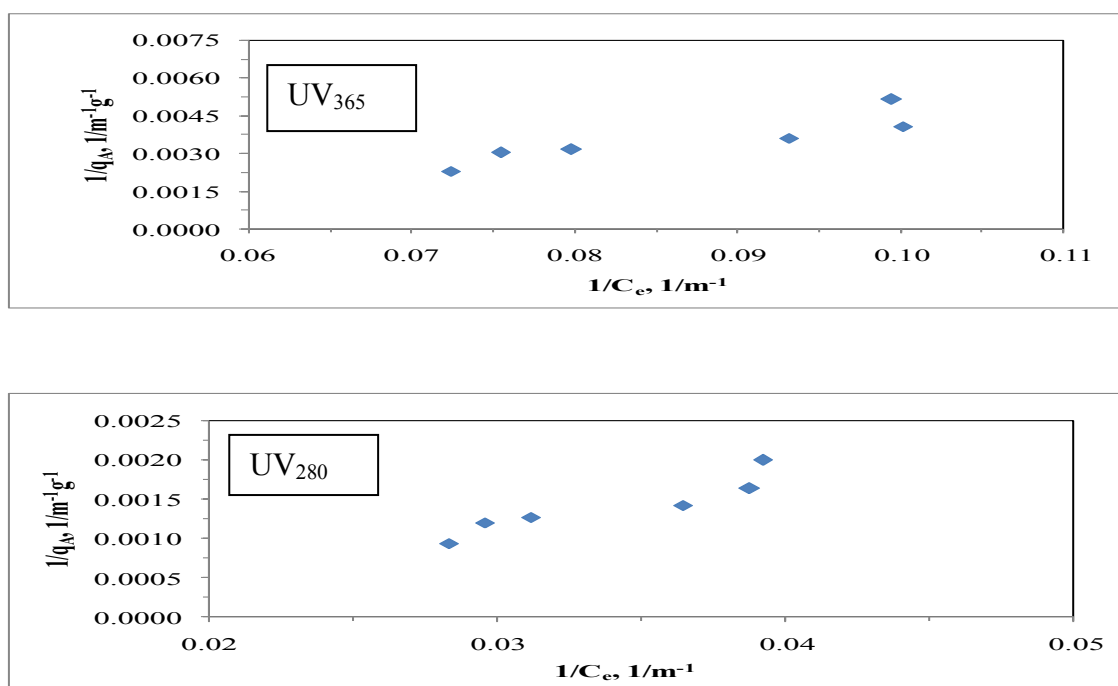Figure A.18. Freundlich adsorption isotherm of UV_{365} and UV_{280} parameters of 100 kDa fraction of humic acid following adsorption onto N-doped TiO_2 Hombikat UV-100.
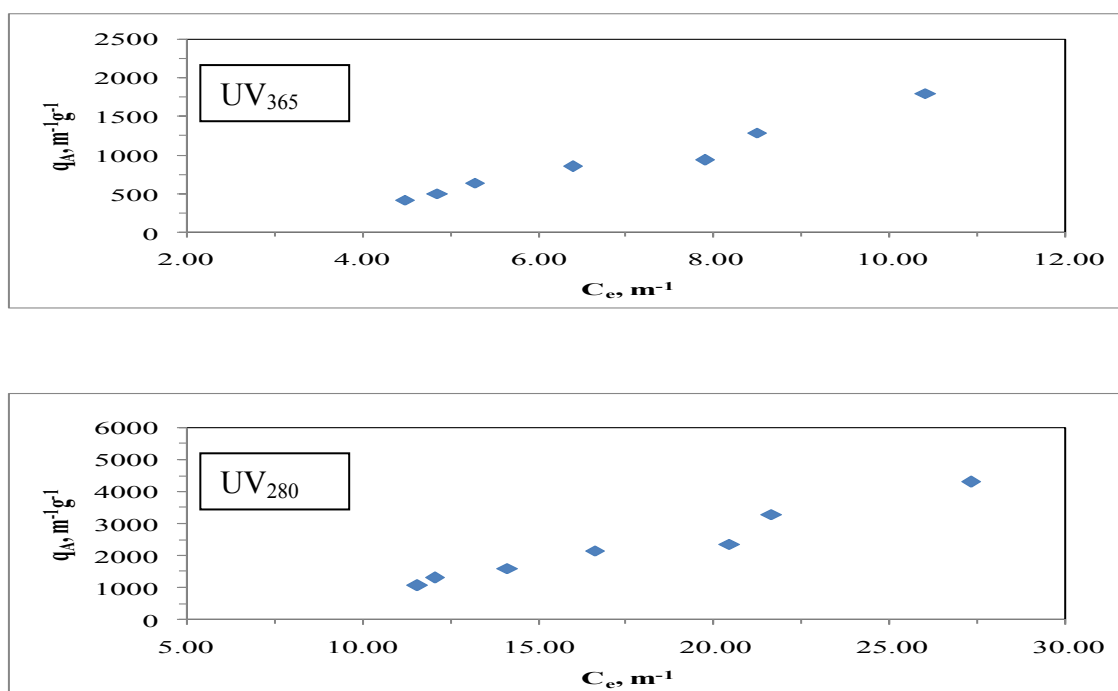
Figure A.19. Freundlich adsorption isotherm of UV_{365} and UV_{280} parameters of 100 kDa fraction of humic acid following adsorption onto S-doped TiO_2 Hombikat UV-100.
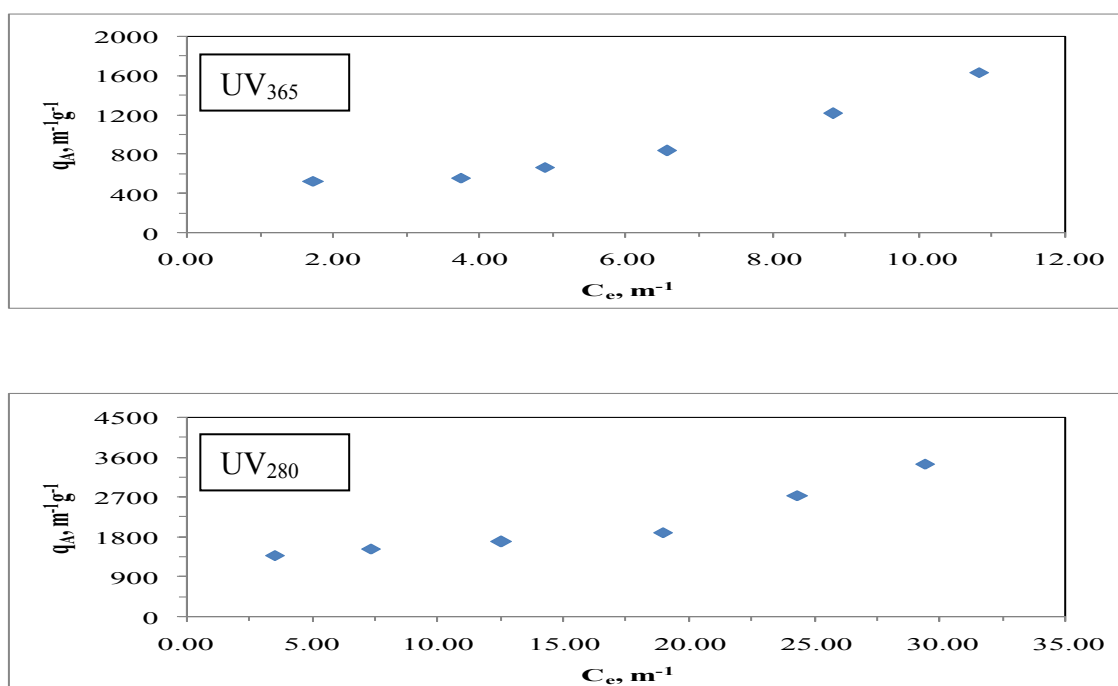
Figure A.20. Freundlich adsorption isotherm of UV_{365} and UV_{280} parameters of 100 kDa fraction of humic acid following adsorption onto N-S co-doped TiO_2 Hombikat UV-100.
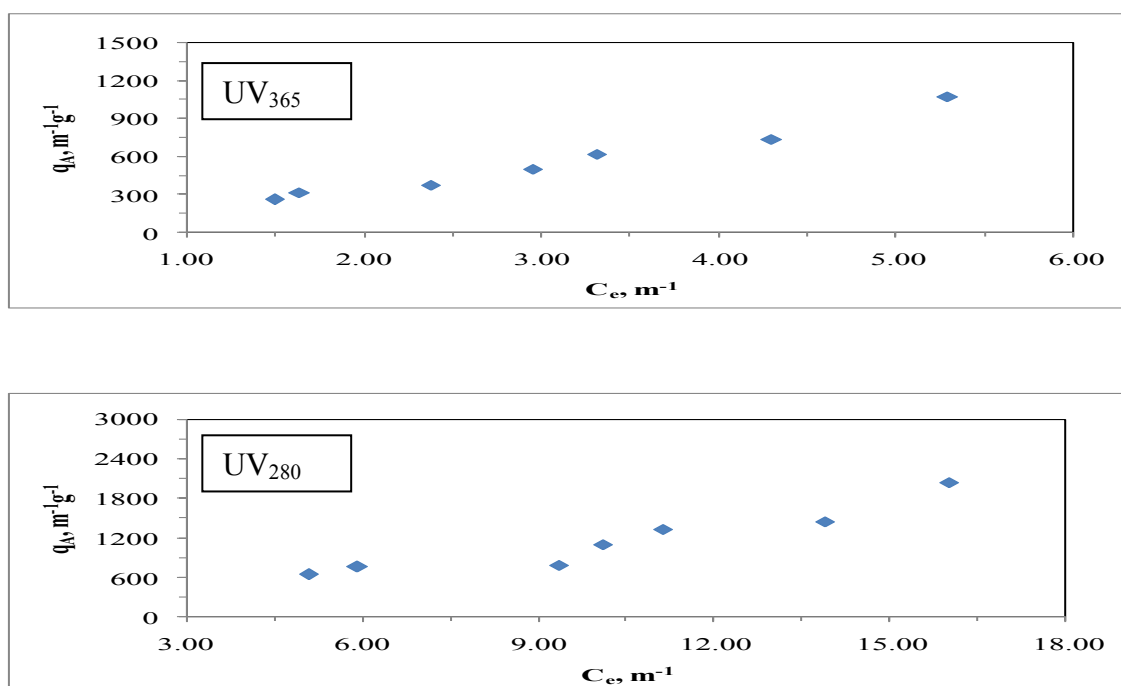
Figure A.21. Freundlich adsorption isotherm of UV_{365} and UV_{280} parameters of 30 kDa fraction of humic acid following adsorption onto bare TiO_2 Degussa P-25.
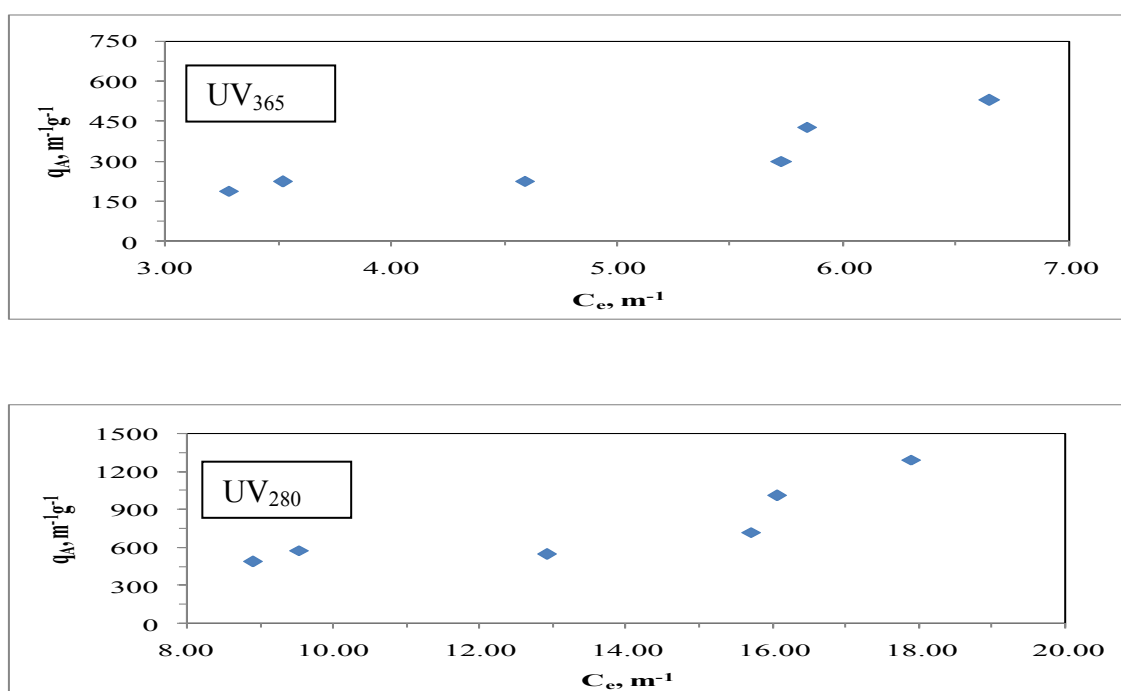
Figure A.22. Freundlich adsorption isotherm of UV_{365} and UV_{280} parameters of 30 kDa fraction of humic acid following adsorption onto C-doped TiO_2 Degussa P-25.
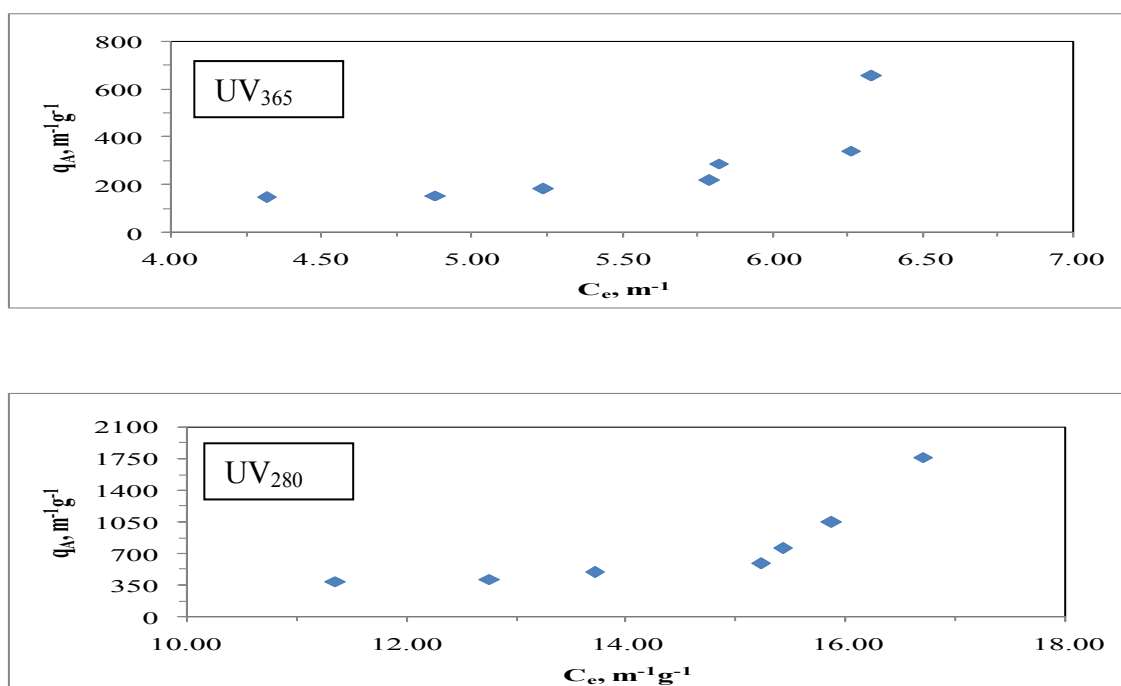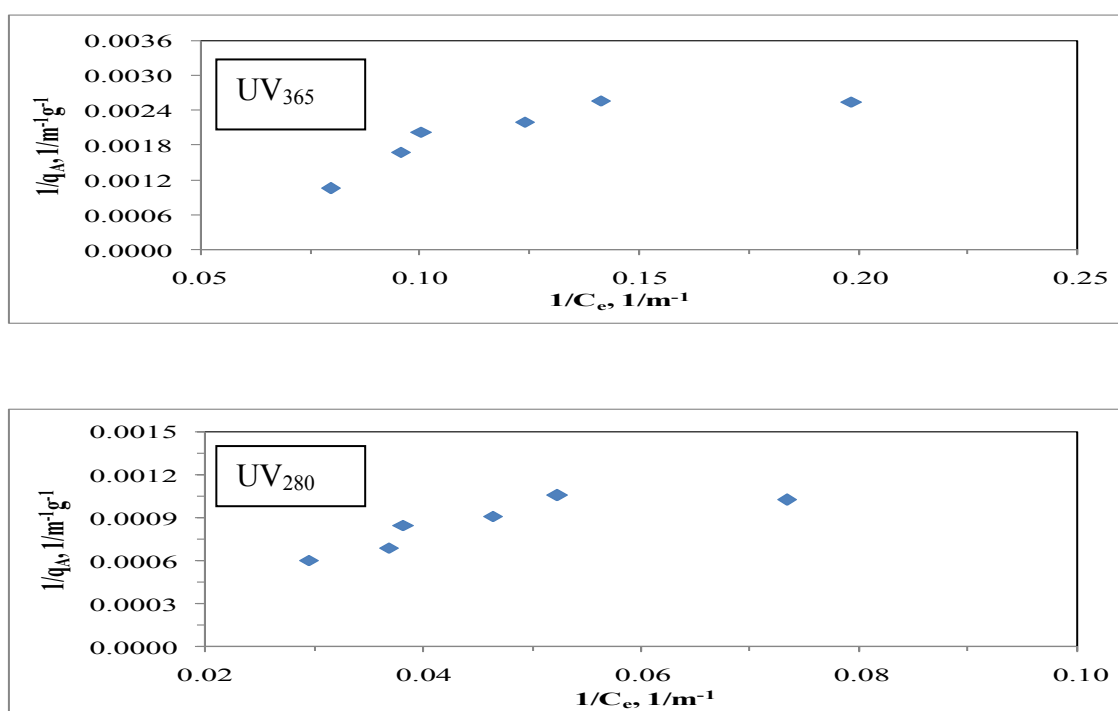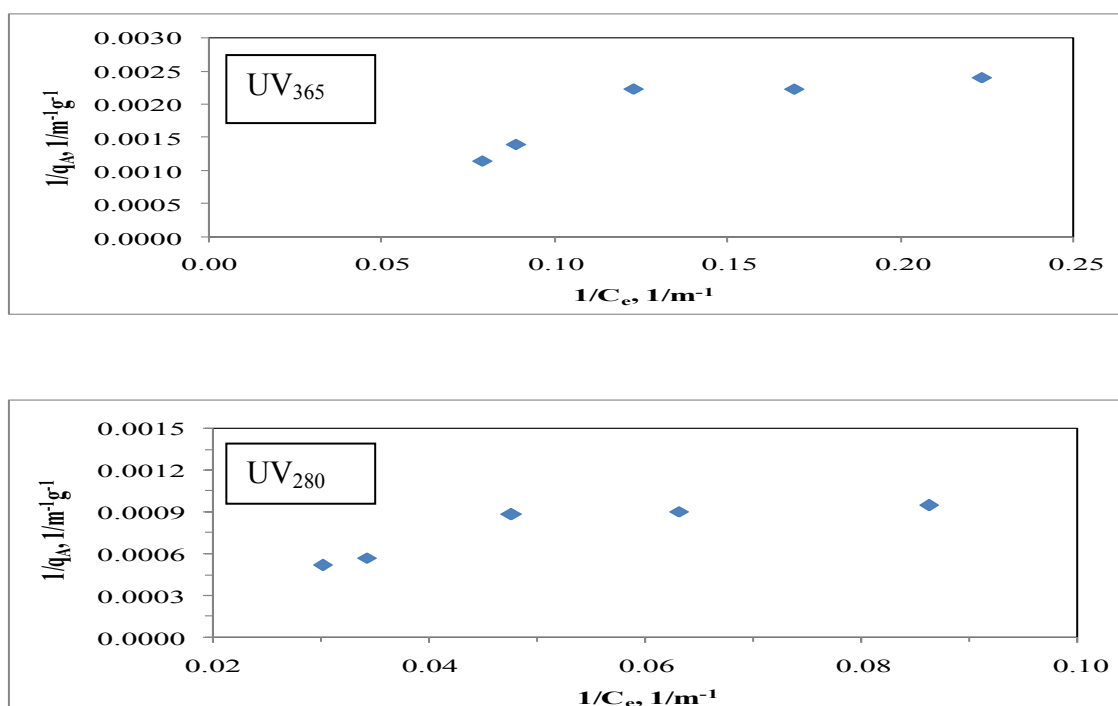
Figure A.23. Freundlich adsorption isotherm of UV_{365} and UV_{280} parameters of 30 kDa fraction of humic acid following adsorption onto N-doped TiO_2 Degussa P-25.
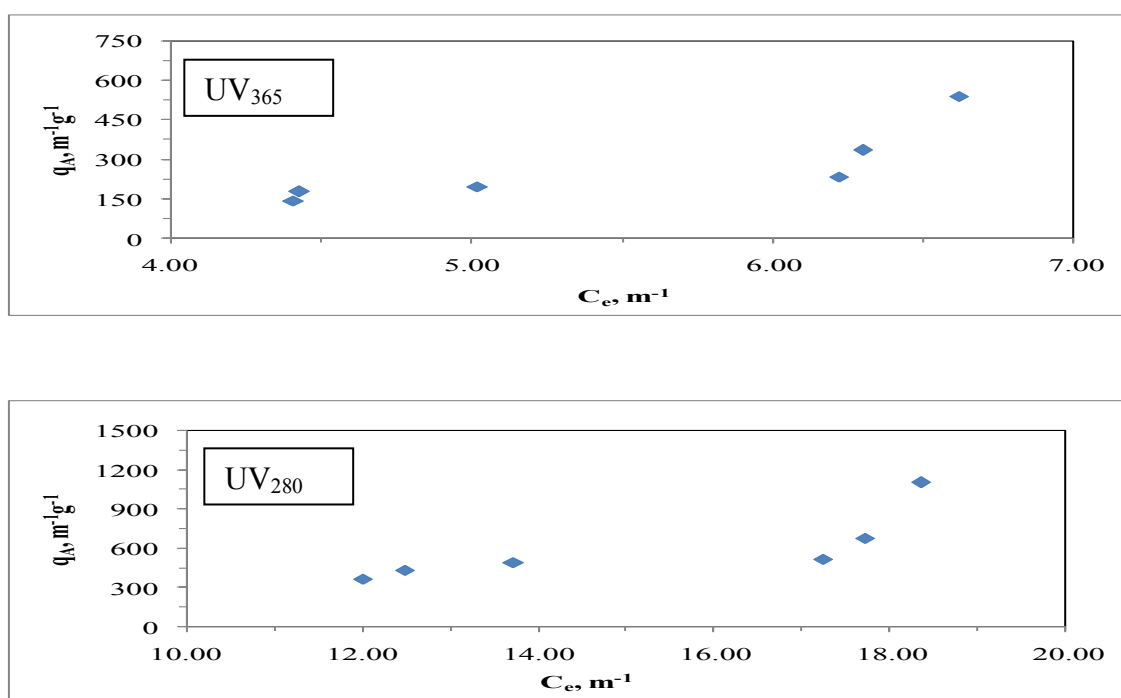
Figure A.24. Freundlich adsorption isotherm of UV_{365} and UV_{280} parameters of 30 kDa fraction of humic acid following adsorption onto S-doped TiO_2 Degussa P-25.
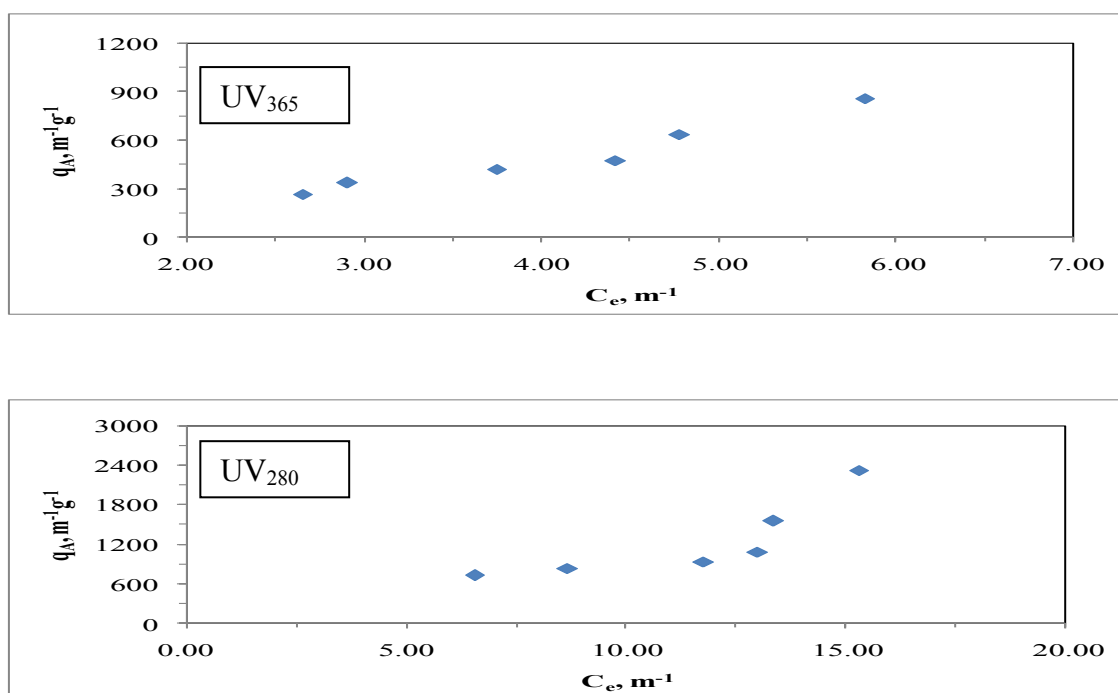
Figure A.25. Freundlich adsorption isotherm of UV_{365} and UV_{280} parameters of 30 kDa fraction of humic acid following adsorption onto N-S co-doped TiO_2 Degussa P-25.
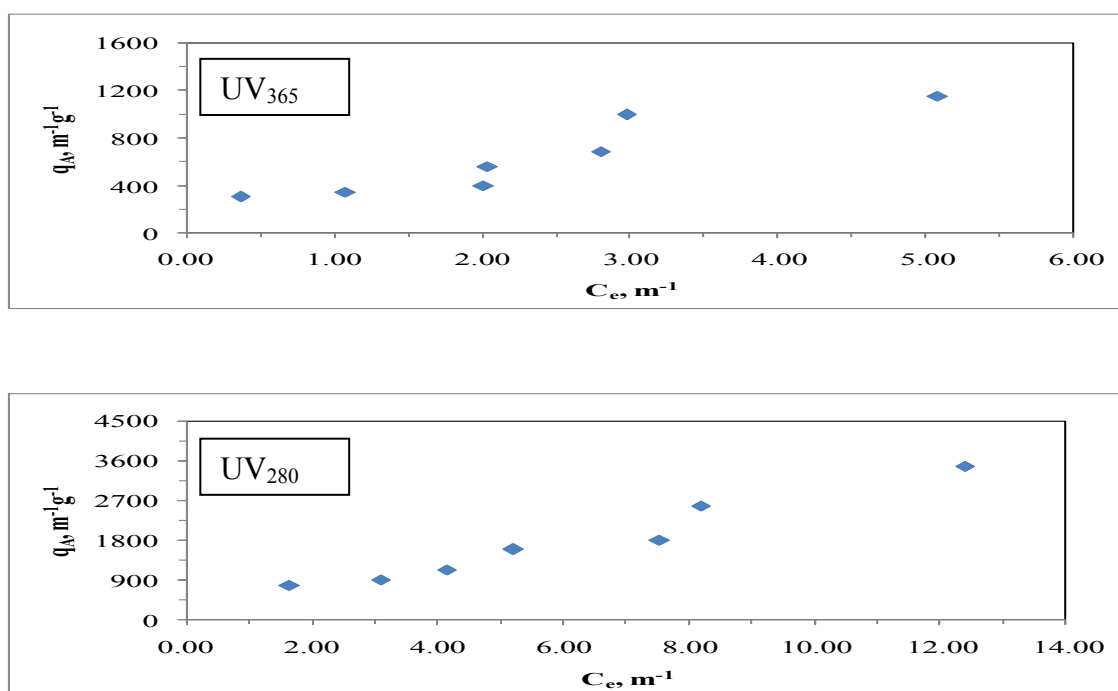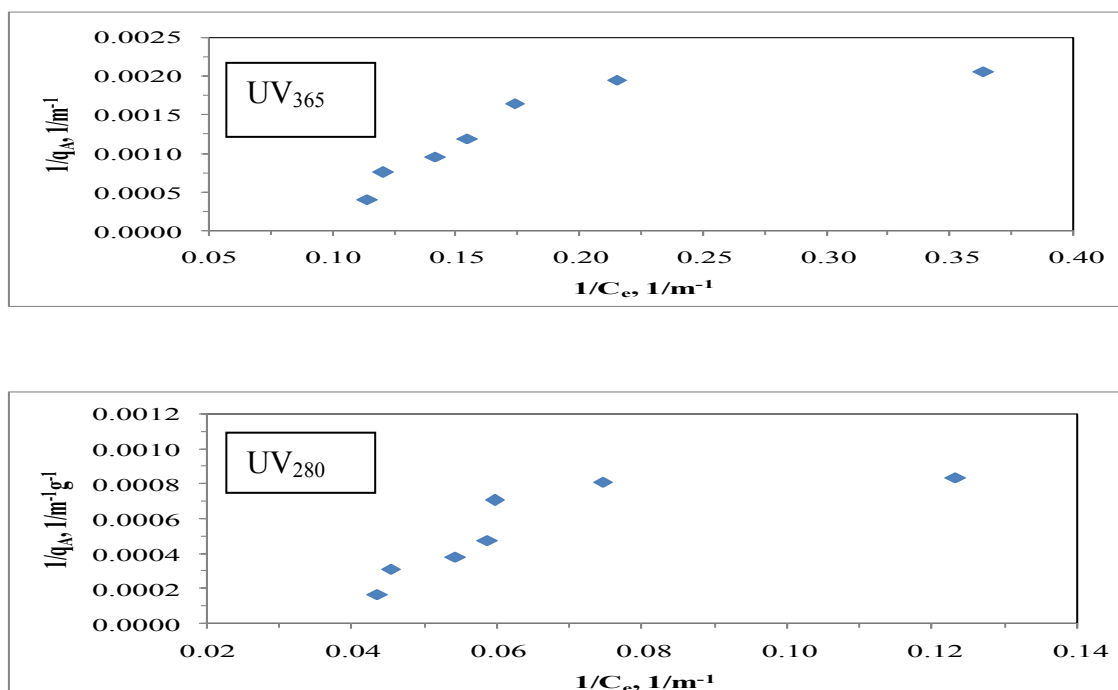

Figure A.26. Freundlich adsorption isotherm of UV_{365} and UV_{280} parameters of 30 kDa fraction of humic acid following adsorption onto bare TiO_2 Hombikat UV-100.
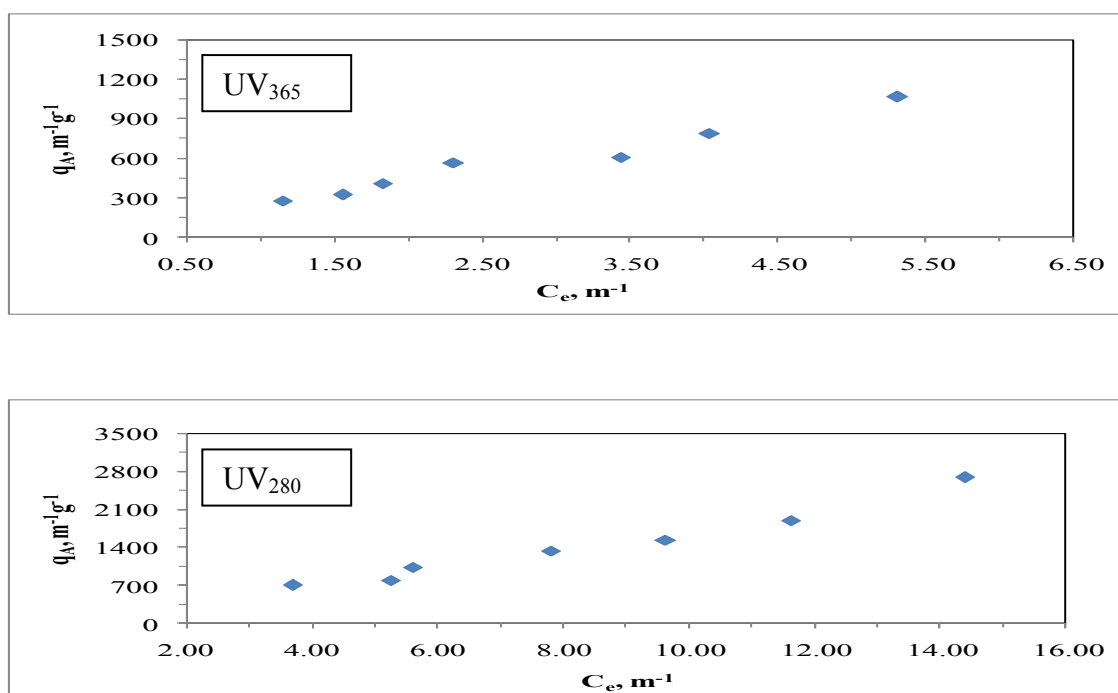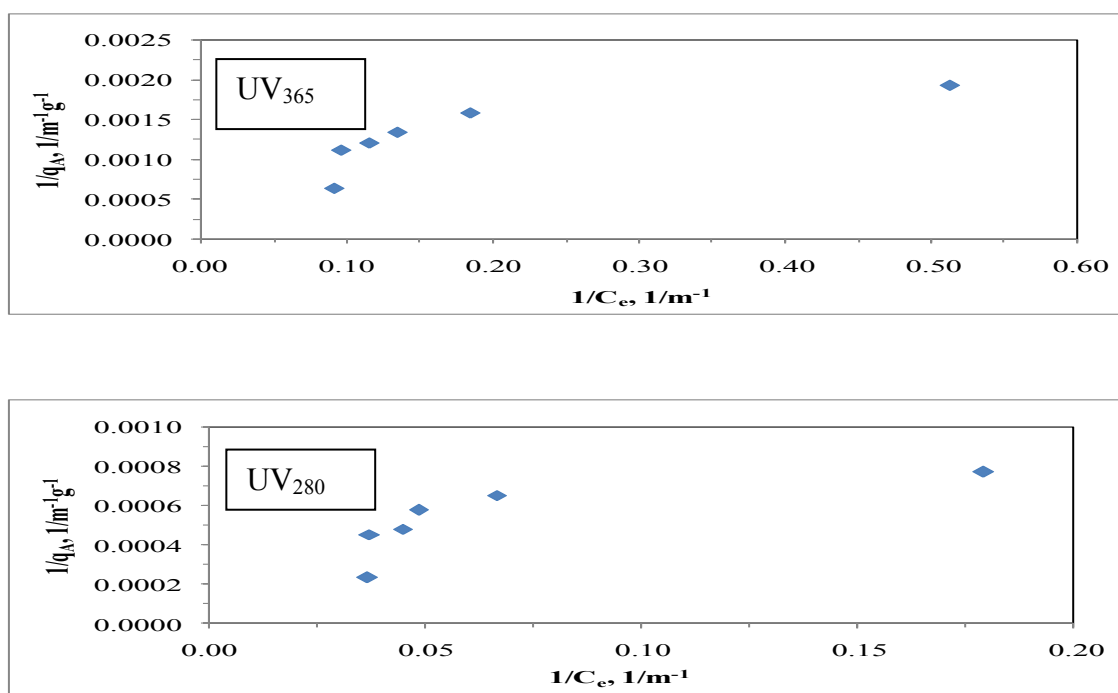
Figure A.27. Freundlich adsorption isotherm of UV_{365} and UV_{280} parameters of 30 kDa fraction of humic acid following adsorption onto C-doped TiO_2 Hombikat UV-100.
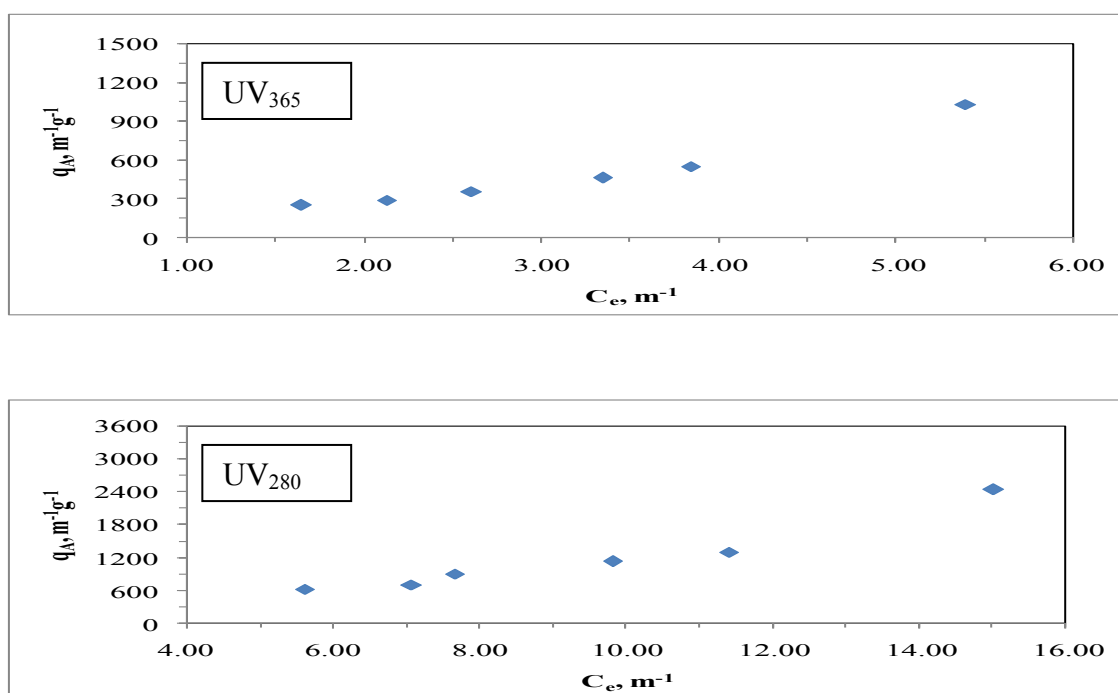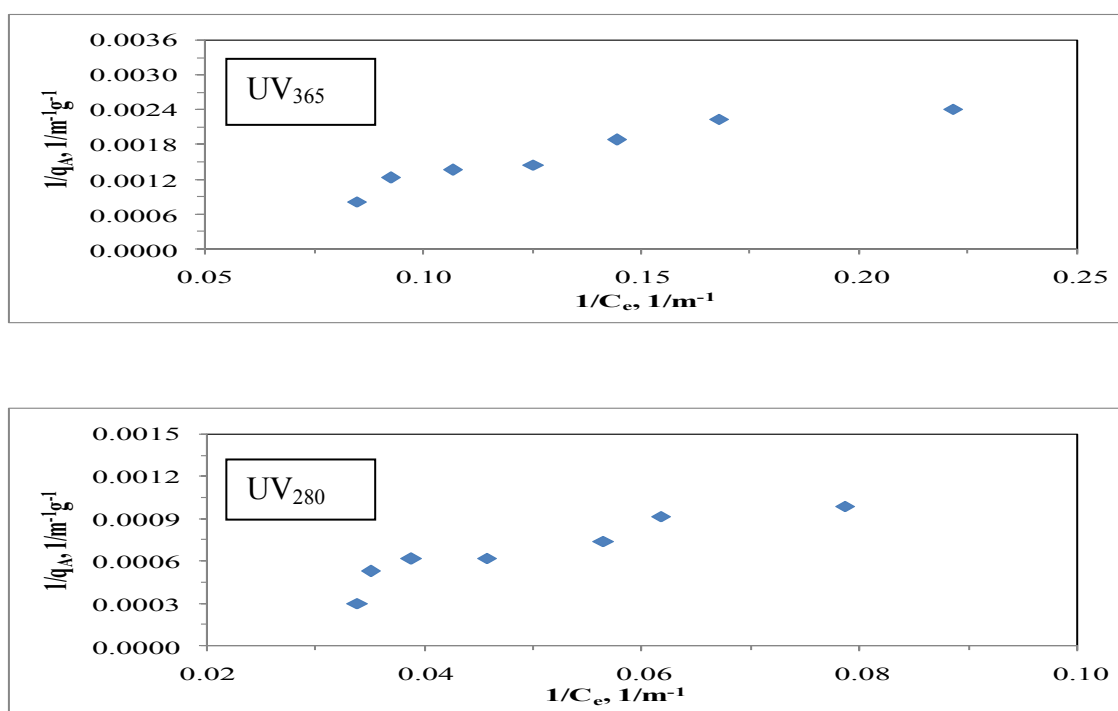

Figure A.28. Freundlich adsorption isotherm of UV_{365} and UV_{280} parameters of 30 kDa fraction of humic acid following adsorption onto N-doped TiO_2 Hombikat UV-100.
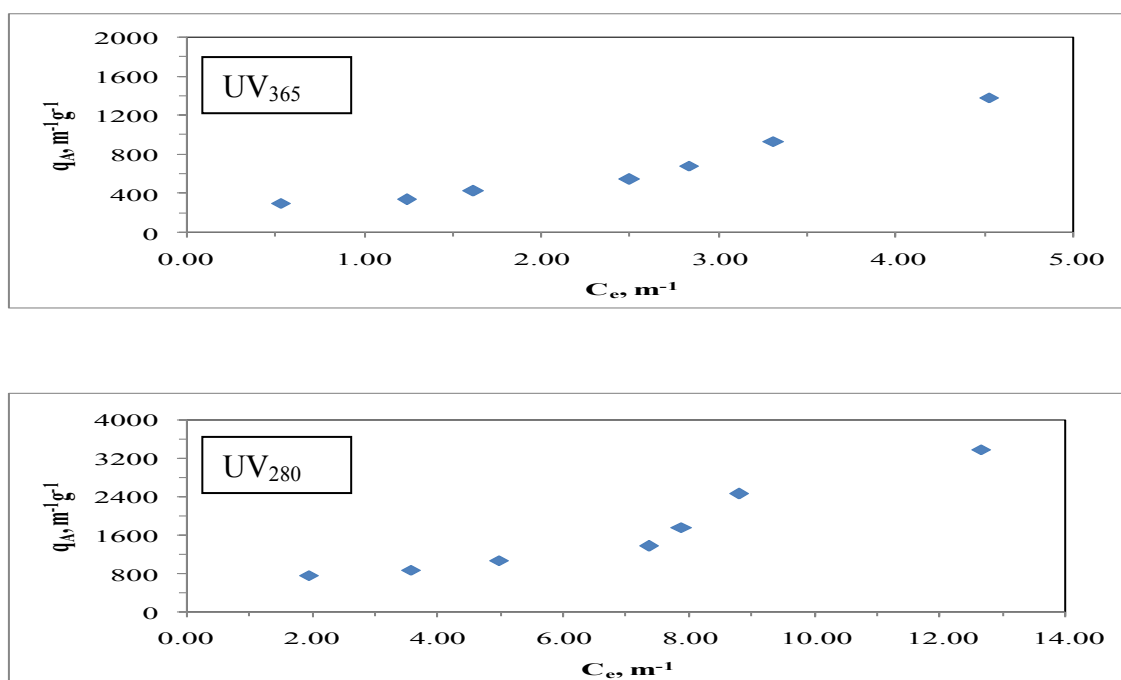
Figure A.29.   Freundlich adsorption isotherm of UV_{365} and UV_{280} parameters of 30 kDa fraction of humic acid following adsorption onto S-doped TiO_2 Hombikat UV-100.
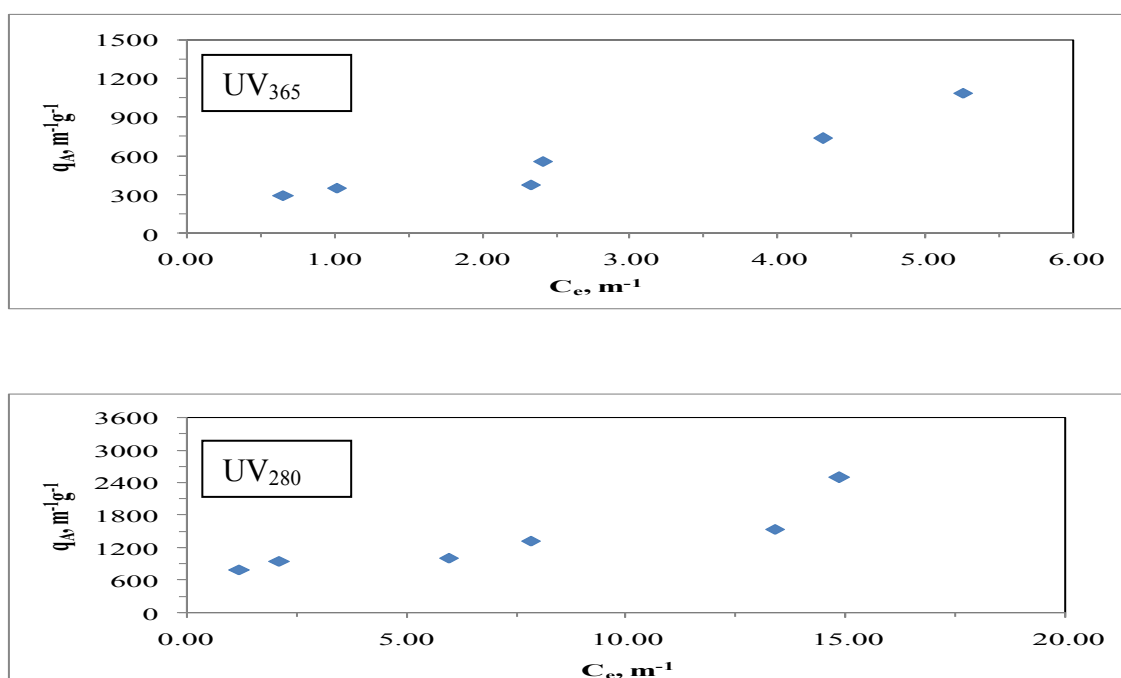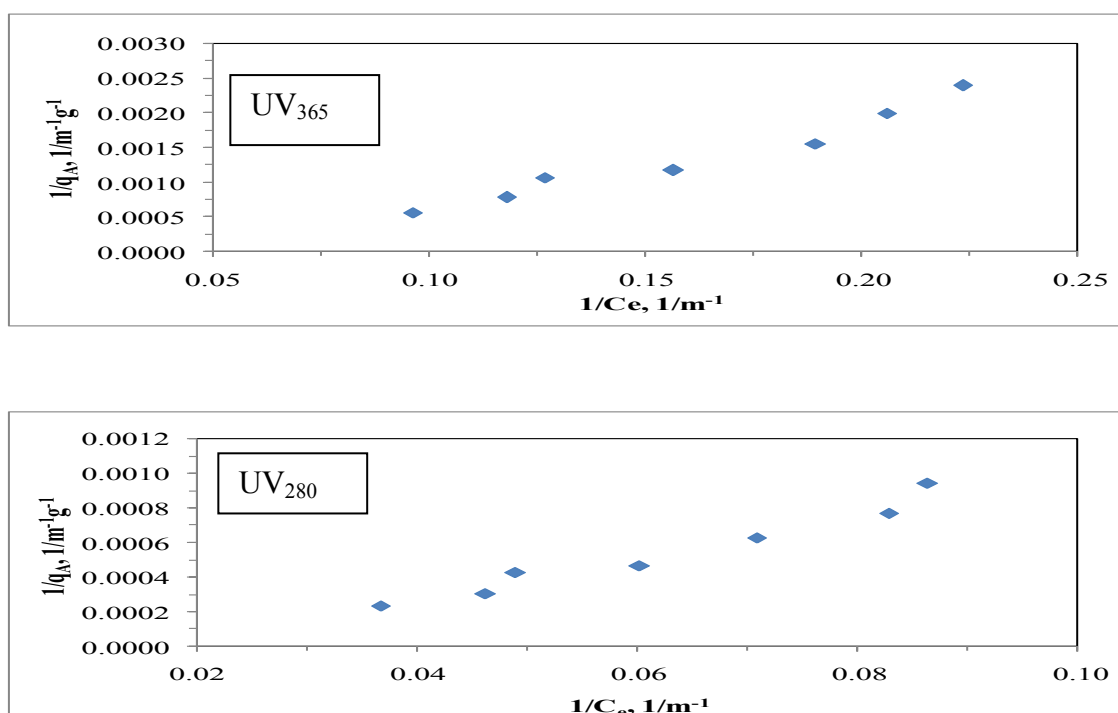

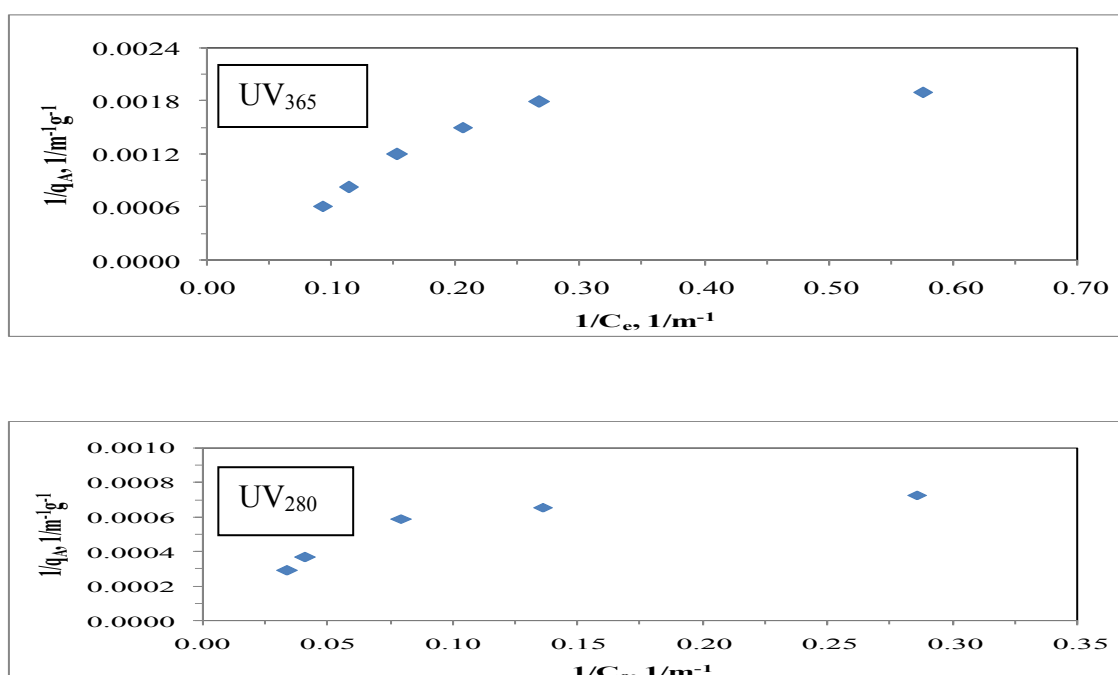Figure A.30.   Freundlich adsorption isotherm of UV_{365} and UV_{280} parameters of 30 kDa fraction of humic acid following adsorption onto N-S co-doped TiO_2 Hombikat UV-100.
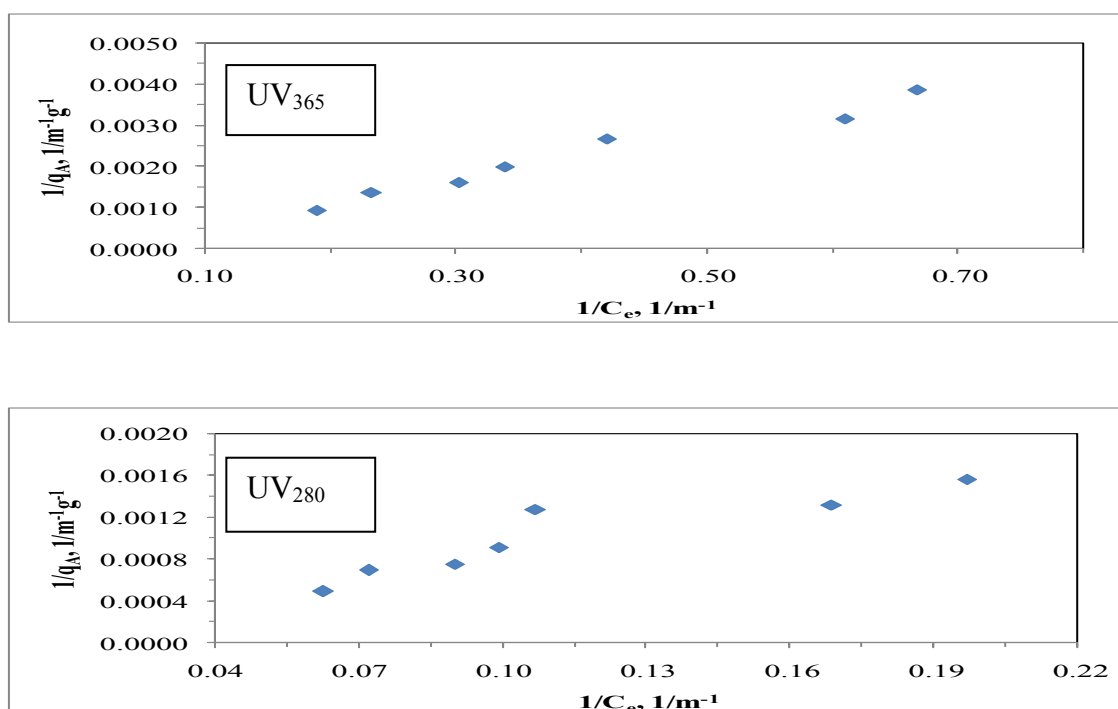
APPENDIX B

Langmuir Adsorption Isotherms of Different Molecular Size Fractions of Humic Acid for UV_{365} and UV_{280}

Figure B.1. Langmuir adsorption isotherm of UV_{365} and UV_{280} parameters of 0.45 μm filtration fraction of humic acid following adsorption onto bare TiO_2 Degussa P-25.

Figure B.2. Langmuir adsorption isotherm of UV_{365} and UV_{280} parameters of 0.45 μm filtration fraction of humic acid following adsorption onto C-doped TiO_2 Degussa P-25.

Figure B.3. Langmuir adsorption isotherm of UV_{365} and UV_{280} parameters of 0.45 μm filtration fraction of humic acid following adsorption onto N-doped TiO_2 Degussa P-25.

Figure B.4. Langmuir adsorption isotherm of UV_{365} and UV_{280} parameters of 0.45 μm filtration fraction of humic acid following adsorption onto S-doped TiO_2 Degussa P-25.

Figure B.5. Langmuir adsorption isotherm of UV_{365} and UV_{280} parameters of 0.45 μm filtration fraction of humic acid following adsorption onto N-S co-doped TiO_2 Degussa P-25.

Figure B.6. Langmuir adsorption isotherm of UV_{365} and UV_{280} parameters of 0.45 μm filtration fraction of humic acid following adsorption onto bare TiO_2 Hombikat UV-100.

Figure B.7. Langmuir adsorption isotherm of UV_{365} and UV_{280} parameters of 0.45 μm filtration fraction of humic acid following adsorption onto C-doped TiO_2 Hombikat UV-100.
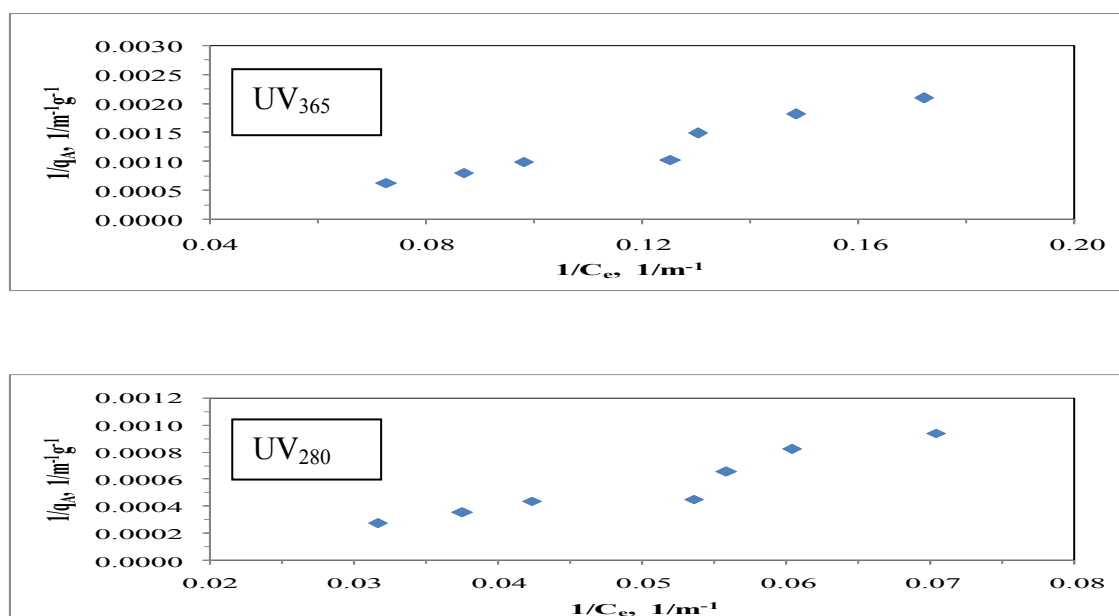
Figure B.8. Langmuir adsorption isotherm of UV_{365} and UV_{280} parameters of 0.45 μm filtration fraction of humic acid following adsorption onto N-doped TiO_2 Hombikat UV-100.

Figure B.9. Langmuir adsorption isotherm of UV_{365} and UV_{280} parameters of 0.45 μm filtration fraction of humic acid following adsorption onto S-doped TiO_2 Hombikat UV-100.
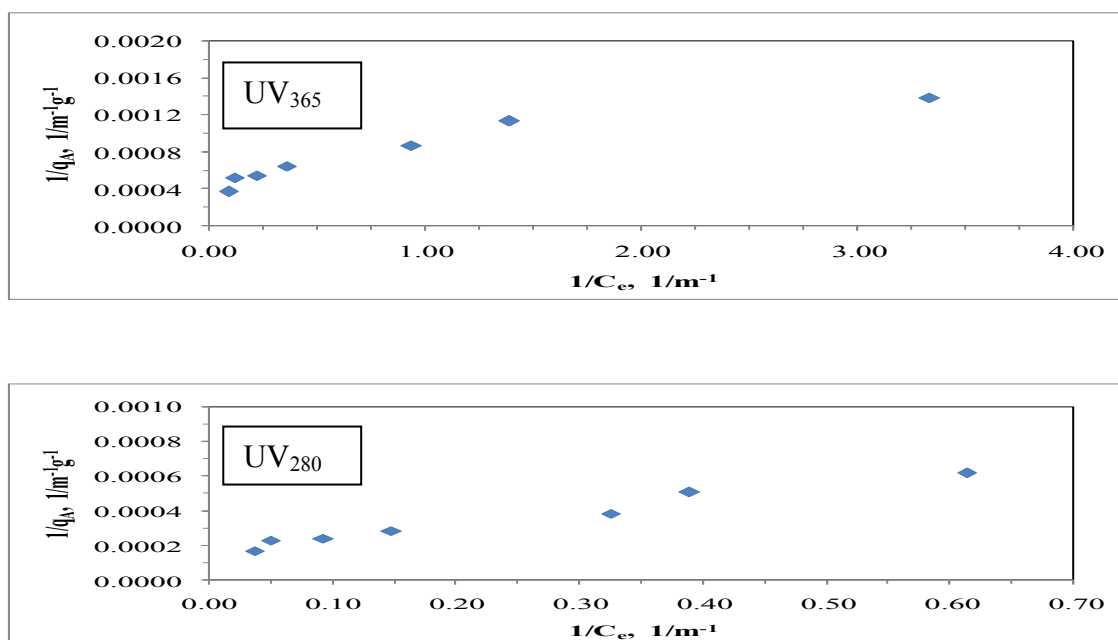
Figure B.10. Langmuir adsorption isotherm of UV_{365} and UV_{280} parameters of 0.45 μm filtration fraction of humic acid following adsorption onto N-S co-doped TiO_2 Hombikat UV-100.

Figure B.11. Langmuir adsorption isotherm of UV_{365} and UV_{280} parameters of 100 kDa fraction of humic acid following adsorption onto bare TiO_2 Degussa P-25.
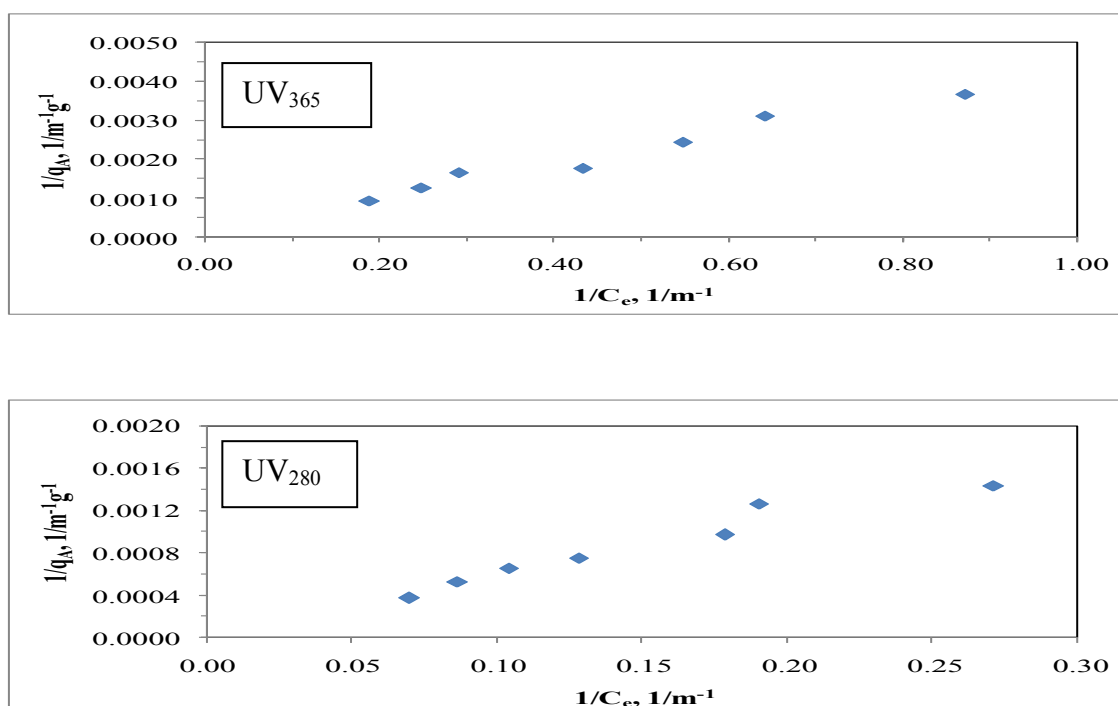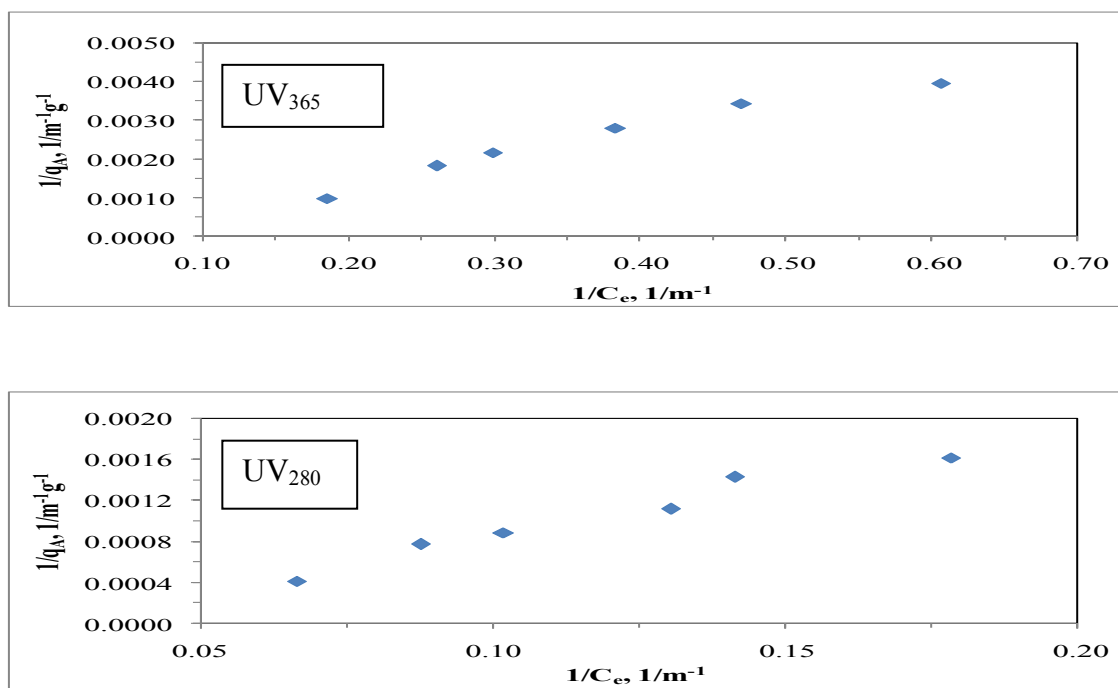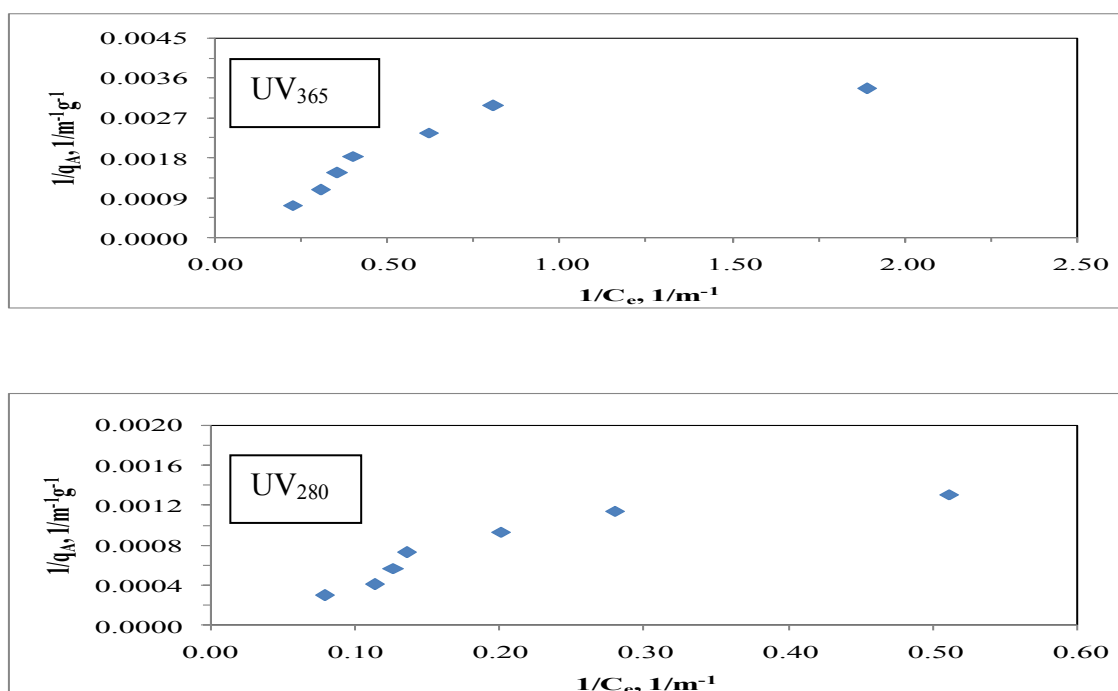

Figure B.12. Langmuir adsorption isotherm of UV_{365} and UV_{280} parameters of 100 kDa fraction of humic acid following adsorption onto C-doped TiO_2 Degussa P-25.

Figure B.13. Langmuir adsorption isotherm of UV_{365} and UV_{280} parameters of 100 kDa fraction of humic acid following adsorption onto N-doped TiO_2 Degussa P-25.
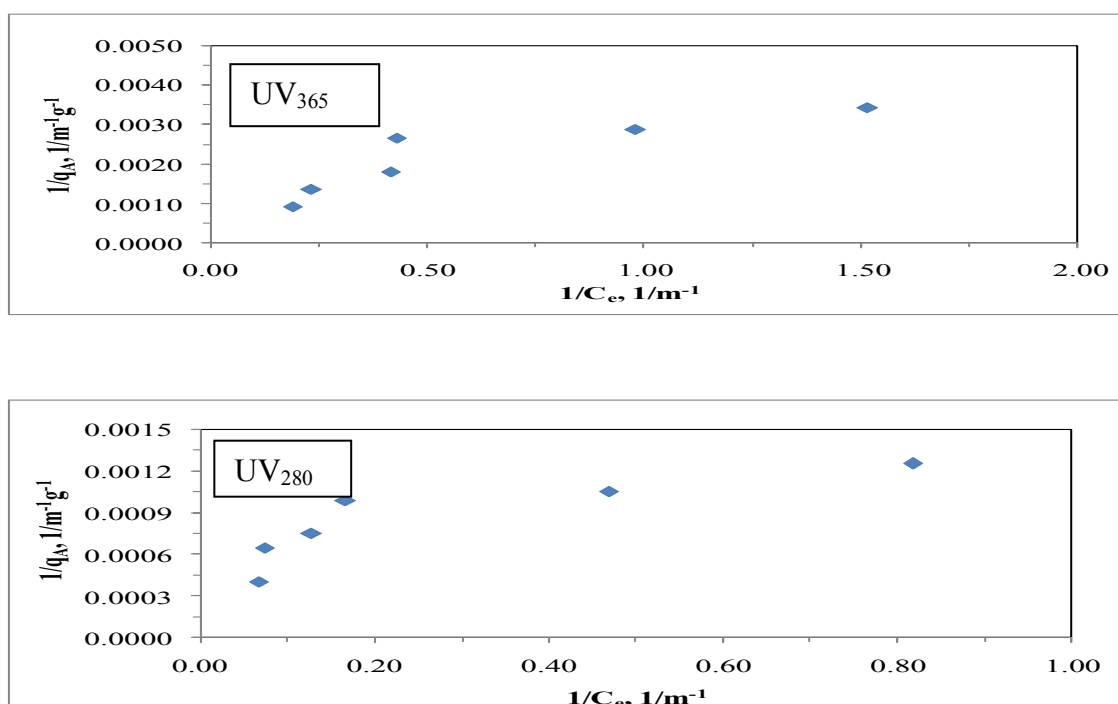

Figure B.14. Langmuir adsorption isotherm of UV_{365} and UV_{280} parameters of 100 kDa fraction of humic acid following adsorption onto S-doped TiO_2 Degussa P-25.

Figure B.15. Langmuir adsorption isotherm of UV_{365} and UV_{280} parameters of 100 kDa fraction of humic acid following adsorption onto N-S co-doped TiO_2 Degussa P-25.

Figure B.16. Langmuir adsorption isotherm of UV_{365} and UV_{280} parameters of 100 kDa fraction of humic acid following adsorption onto bare TiO_2 Hombikat UV-100.

Figure B.17. Langmuir adsorption isotherm of UV_{365} and UV_{280} parameters of 100 kDa fraction of humic acid following adsorption onto C-doped TiO_2 Hombikat UV-100.

Figure B.18. Langmuir adsorption isotherm of UV_{365} and UV_{280} parameters of 100 kDa fraction of humic acid following adsorption onto N-doped TiO_2 Hombikat UV-100.

Figure B.19. Langmuir adsorption isotherm of UV_{365} and UV_{280} parameters of 100 kDa fraction of humic acid following adsorption onto S-doped TiO_2 Hombikat UV-100.

Figure B.20. Langmuir adsorption isotherm of UV_{365} and UV_{280} parameters of 100 kDa fraction of humic acid following adsorption onto N-S co-doped TiO_2 Hombikat UV-100.

329

Figure B.21. Langmuir adsorption isotherm of UV_{365} and UV_{280} parameters of 30 kDa fraction of humic acid following adsorption onto bare TiO_2 Degussa P-25.
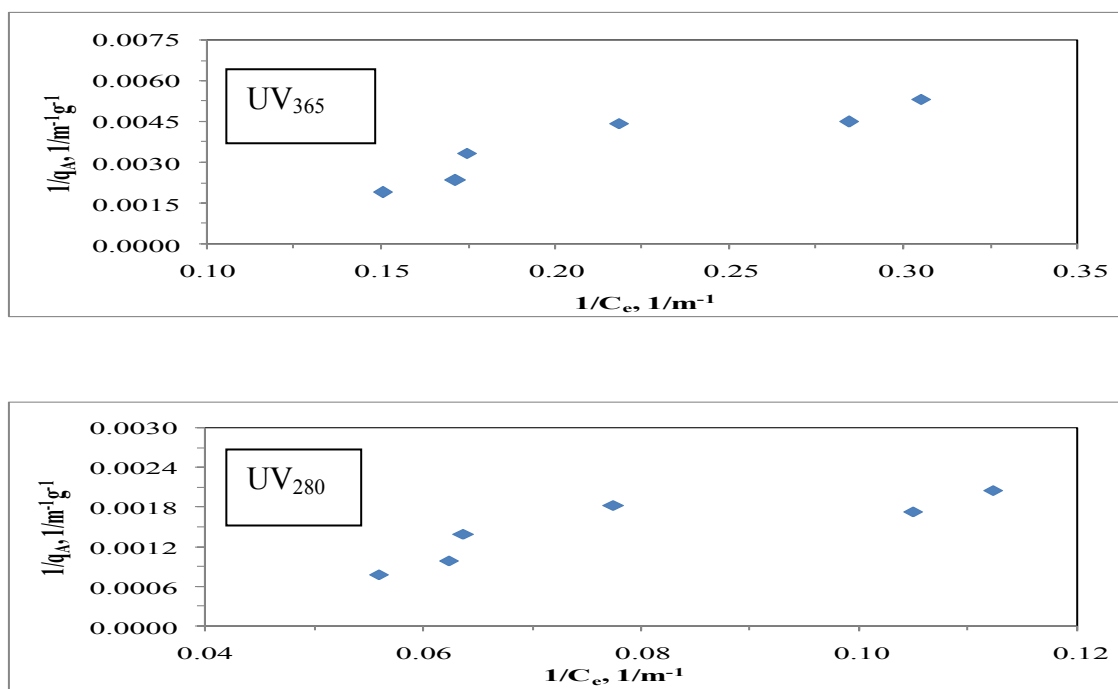
Figure B.22. Langmuir adsorption isotherm of UV_{365} and UV_{280} parameters of 30 kDa fraction of humic acid following adsorption onto C-doped TiO_2 Degussa P-25.
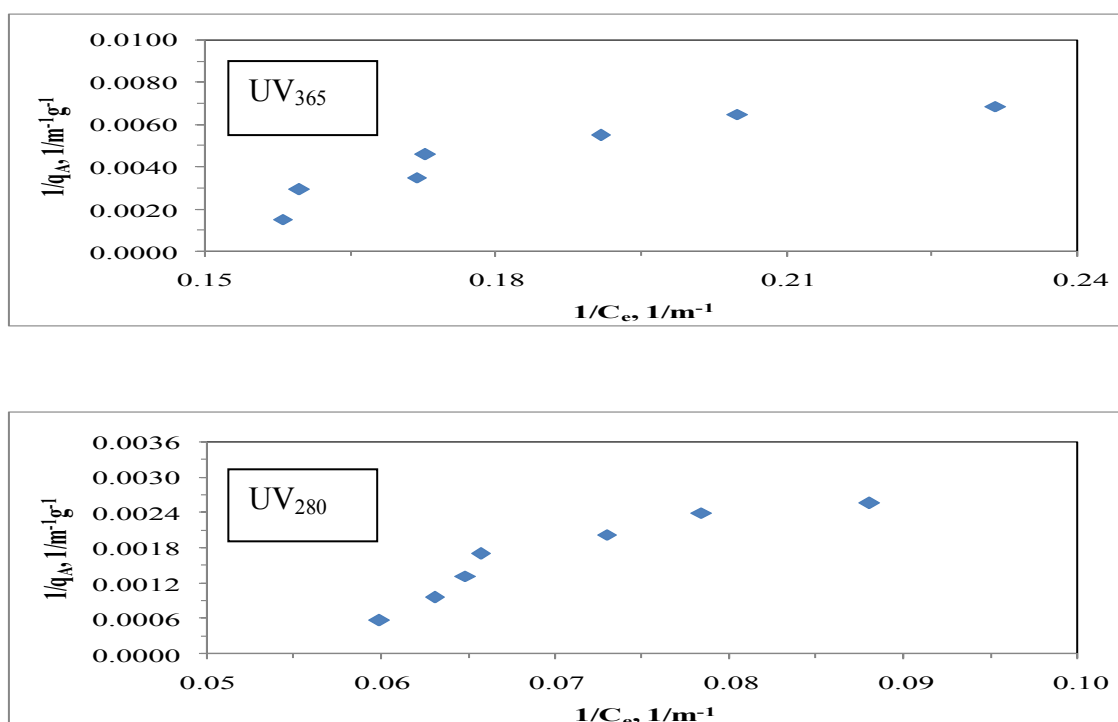
Figure B.23. Langmuir adsorption isotherm of UV$_{365}$ and UV$_{280}$ parameters of 30 kDa fraction of humic acid following adsorption onto N-doped TiO$_2$ Degussa P-25.
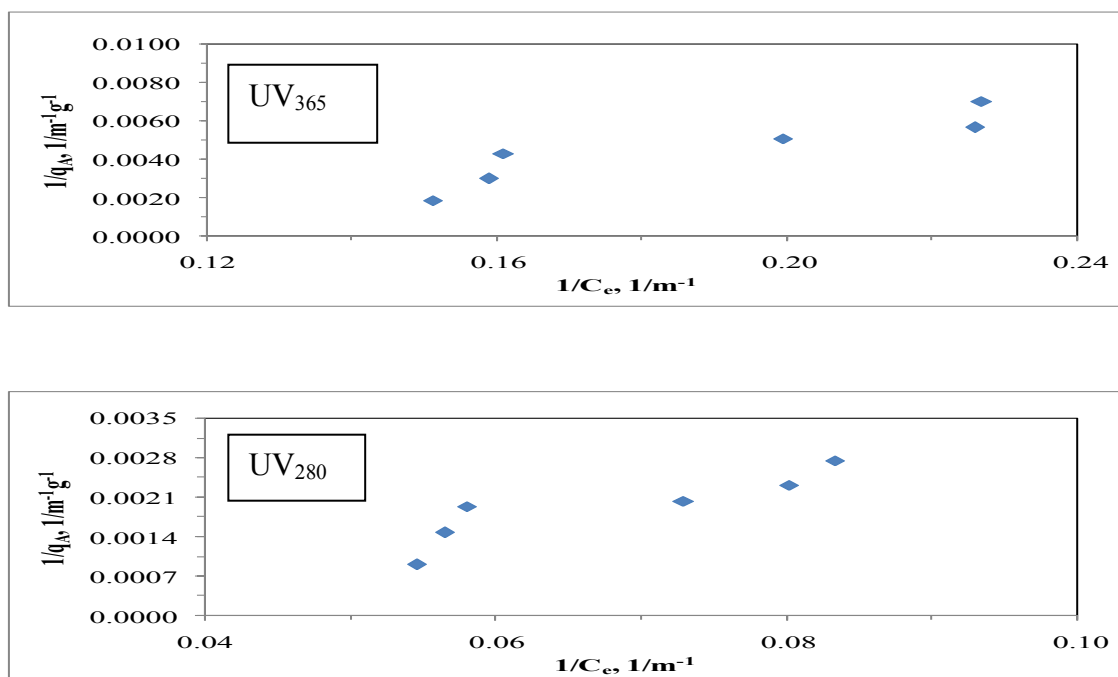
Figure B.24. Langmuir adsorption isotherm of UV$_{365}$ and UV$_{280}$ parameters of 30 kDa fraction of humic acid following adsorption onto S-doped TiO$_2$ Degussa P-25.
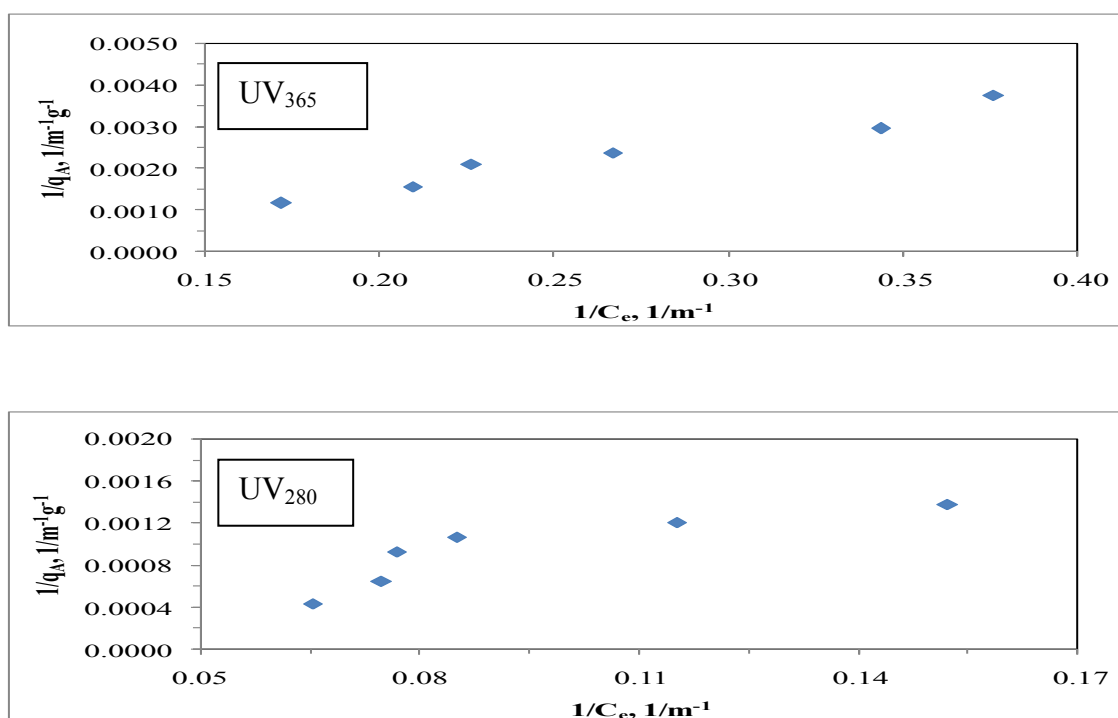
Figure B.25. Langmuir adsorption isotherm of UV_{365} and UV_{280} parameters of 30 kDa fraction of humic acid following adsorption onto N-S co-doped TiO_2 Degussa P-25.
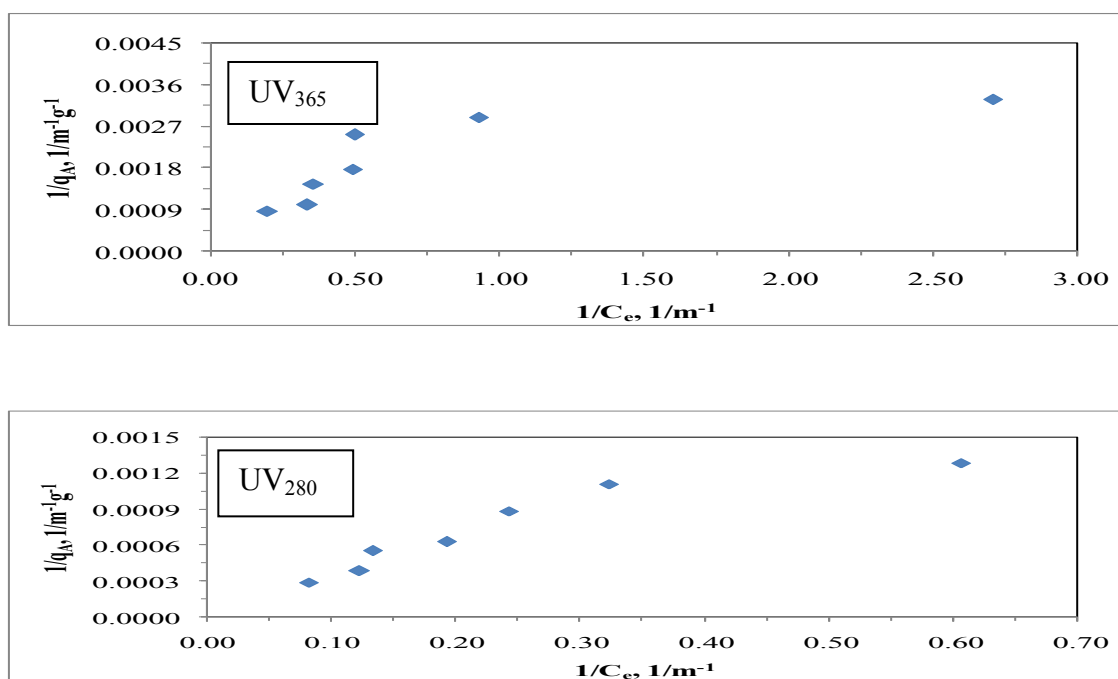
Figure B.26. Langmuir adsorption isotherm of UV_{365} and UV_{280} parameters of 30 kDa fraction of humic acid following adsorption onto bare TiO_2 Hombikat UV-100.

Figure B.27. Langmuir adsorption isotherm of UV_{365} and UV_{280} parameters of 30 kDa fraction of humic acid following adsorption onto C-doped TiO_2 Hombikat UV-100.

Figure B.28. Langmuir adsorption isotherm of UV_{365} and UV_{280} parameters of 30 kDa fraction of humic acid following adsorption onto N-doped TiO_2 Hombikat UV-100.

Figure B.29. Langmuir adsorption isotherm of UV_{365} and UV_{280} parameters of 30 kDa fraction of humic acid following adsorption onto S-doped TiO_2 Hombikat UV-100.

Figure B.30. Langmuir adsorption isotherm of UV_{365} and UV_{280} parameters of 30 kDa fraction of humic acid following adsorption onto N-S co-doped TiO_2 Hombikat UV-100.

APPENDIX C

Emission Scan Fluorescence Spectra of Different Molecular Size Fractions of Humic Acid at 370 nm Excitation Wavelength
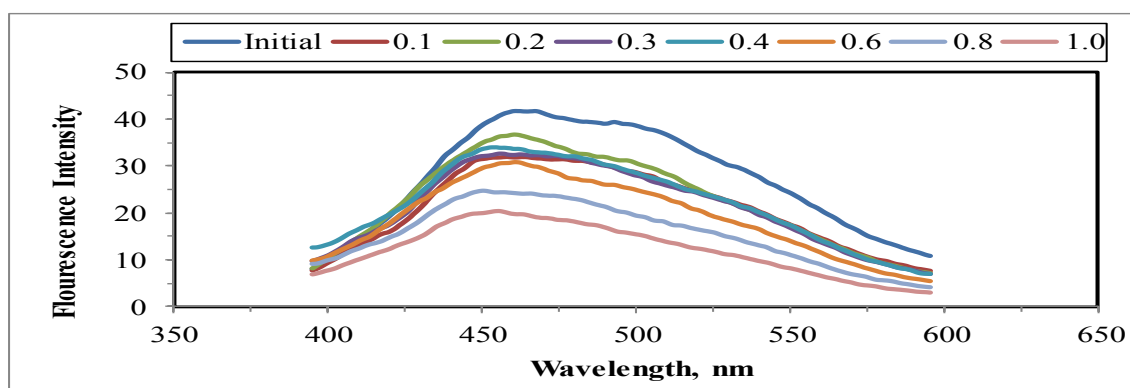
Figure C.1. Emission scan fluorescence spectra of 0.45 µm filtered fraction of humic acid following adsorption onto bare TiO$_2$ Degussa P-25 at 370 nm excitation wavelength.
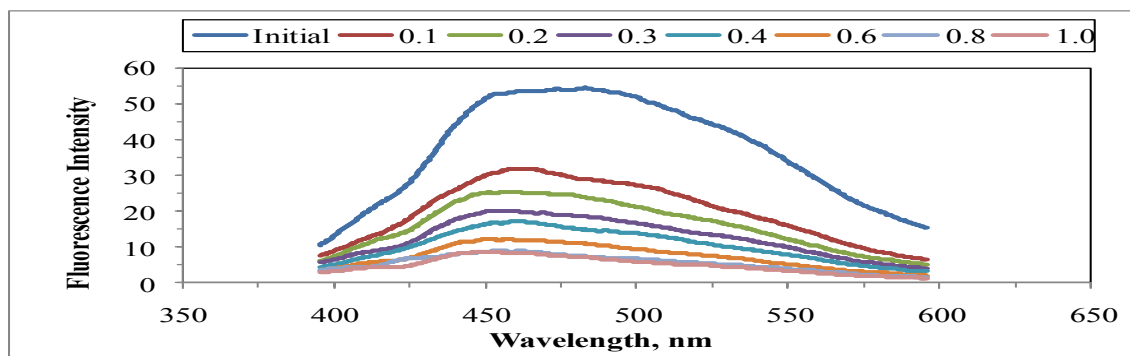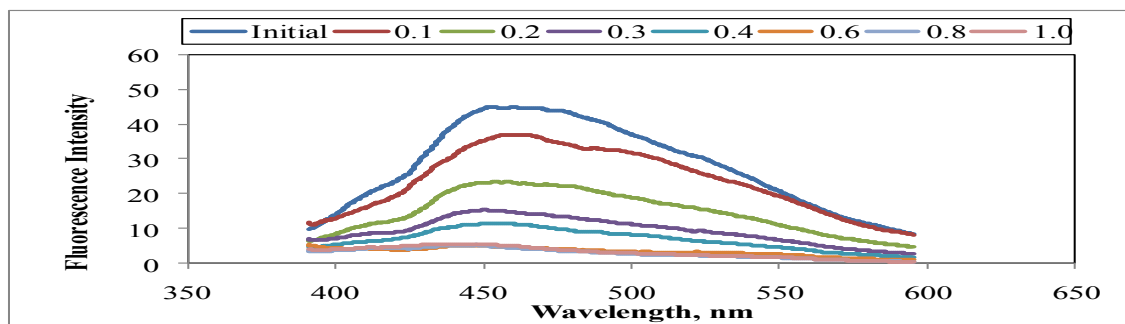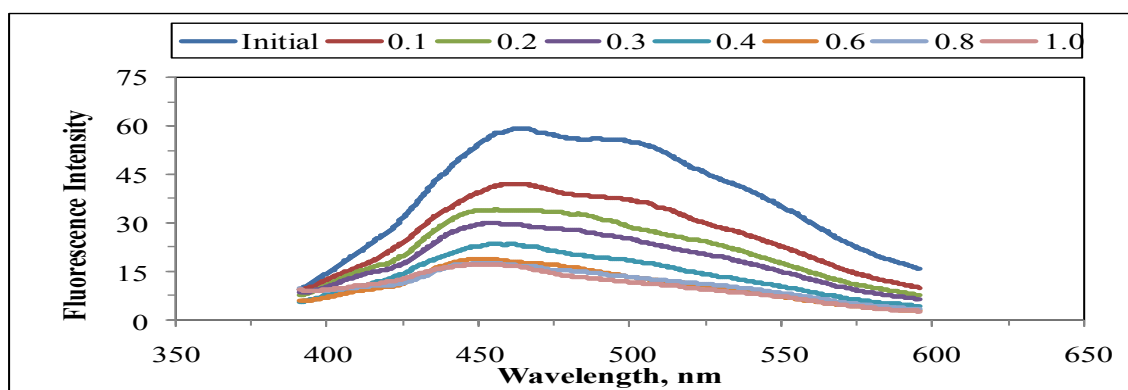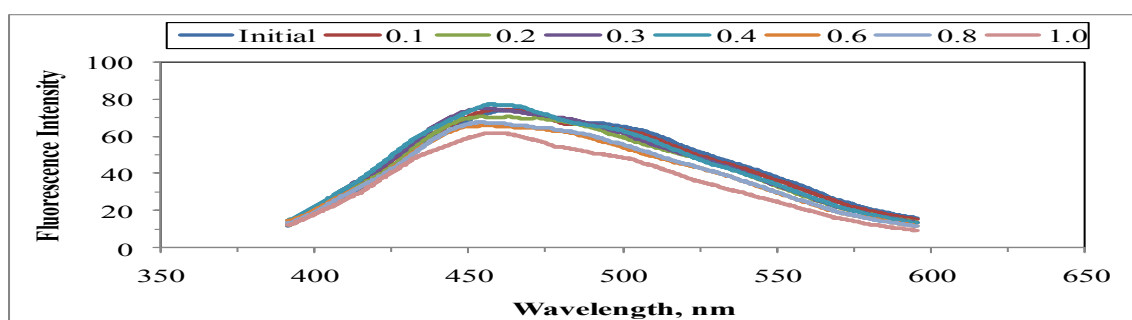

Figure C.2. Emission scan fluorescence spectra of 0.45 µm filtered fraction of humic acid following adsorption onto C-doped TiO$_2$ Degussa P-25 at 370 nm excitation wavelength.
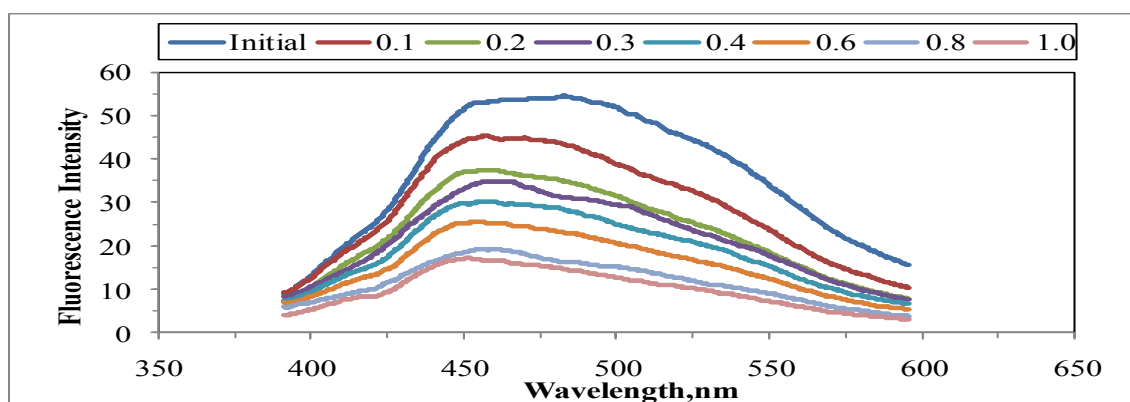
Figure C.3. Emission scan fluorescence spectra of 0.45 µm filtered fraction of humic acid following adsorption onto N-doped TiO$_2$ Degussa P-25 at 370 nm excitation wavelength.
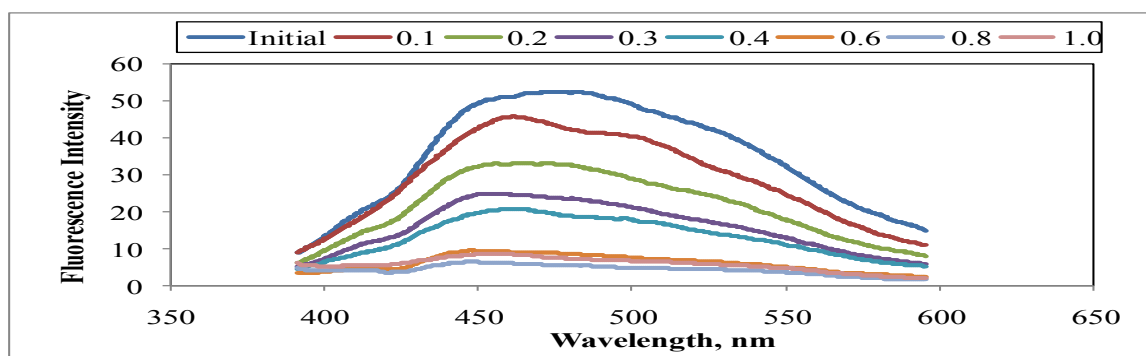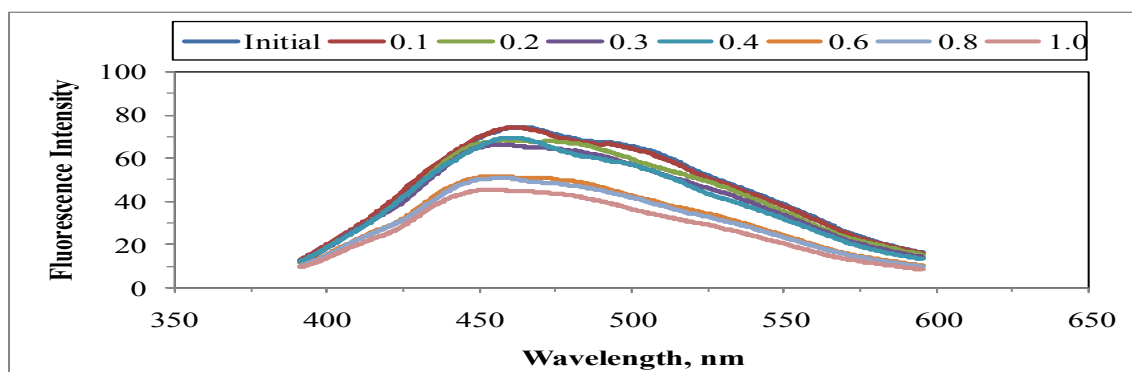
Figure C.4. Emission scan fluorescence spectra of 0.45 µm filtered fraction of humic acid following adsorption onto S-doped TiO_2 Degussa P-25 at 370 nm excitation wavelength.
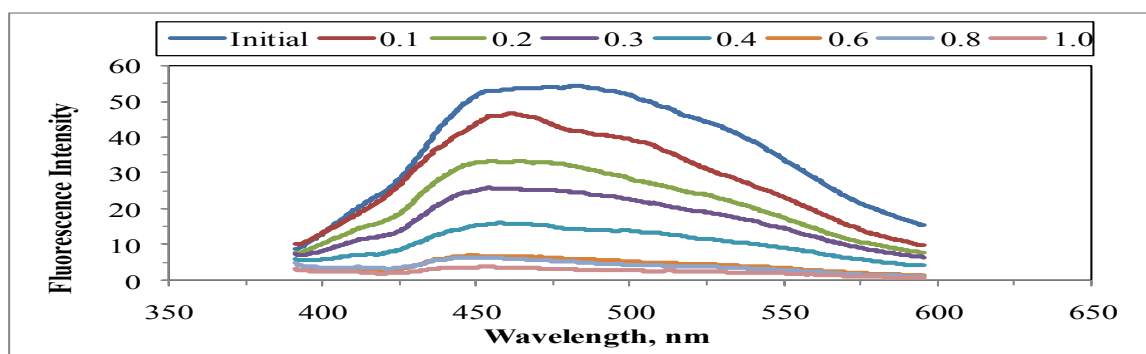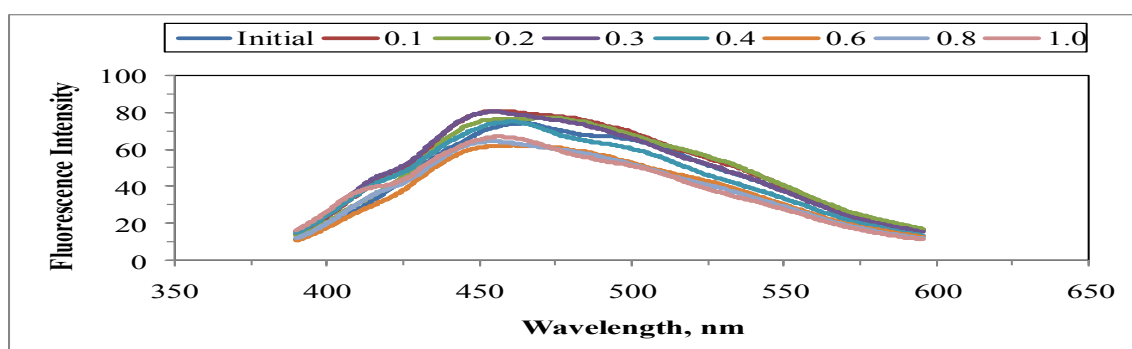

Figure C.5. Emission scan fluorescence spectra of 0.45 µm filtered fraction of humic acid following adsorption onto N-S co-doped TiO_2 Degussa P-25 at 370 nm excitation wavelength.
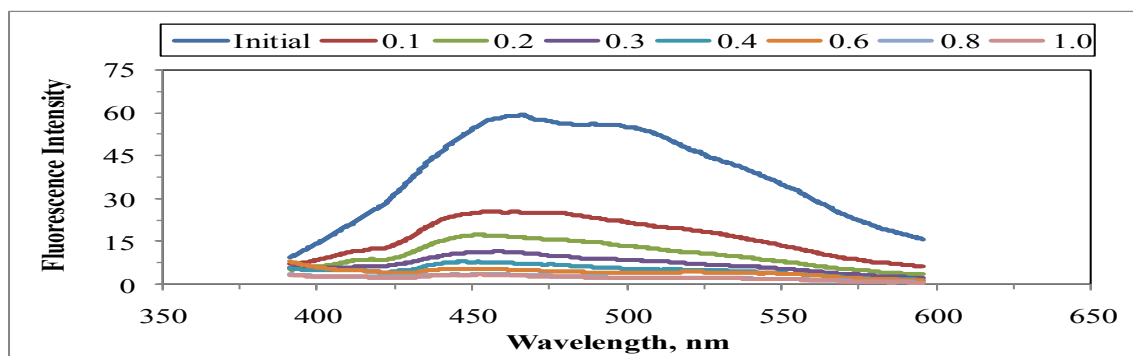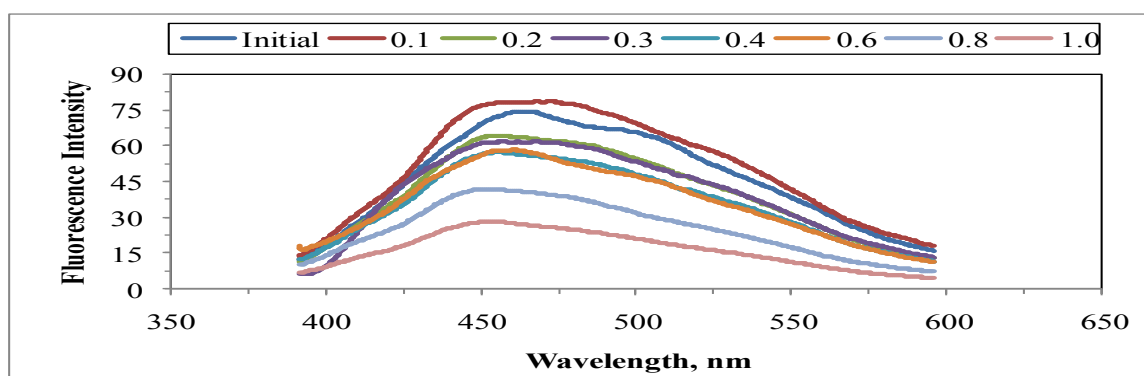

Figure C.6. Emission scan fluorescence spectra of 0.45 µm filtered fraction of humic acid following adsorption onto bare TiO_2 Hombikat UV-100 at 370 nm excitation wavelength.
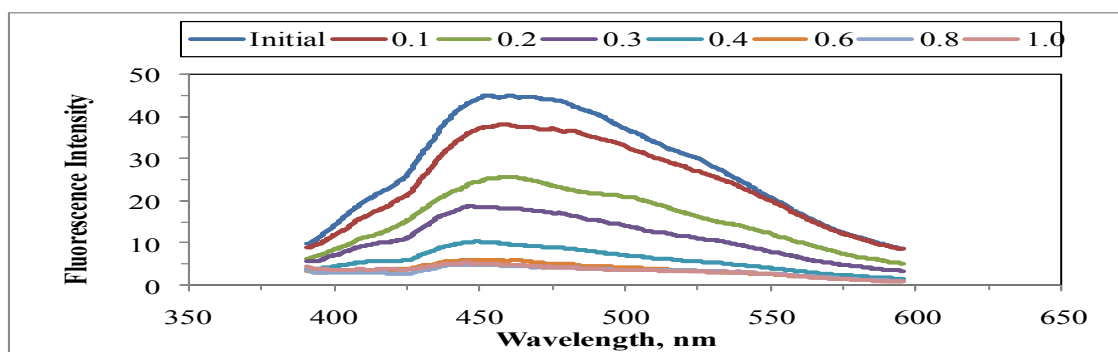
Figure C.7. Emission scan fluorescence spectra of 0.45 μm filtered fraction of humic acid following adsorption onto C-doped TiO_2 Hombikat UV-100 at 370 nm excitation wavelength.
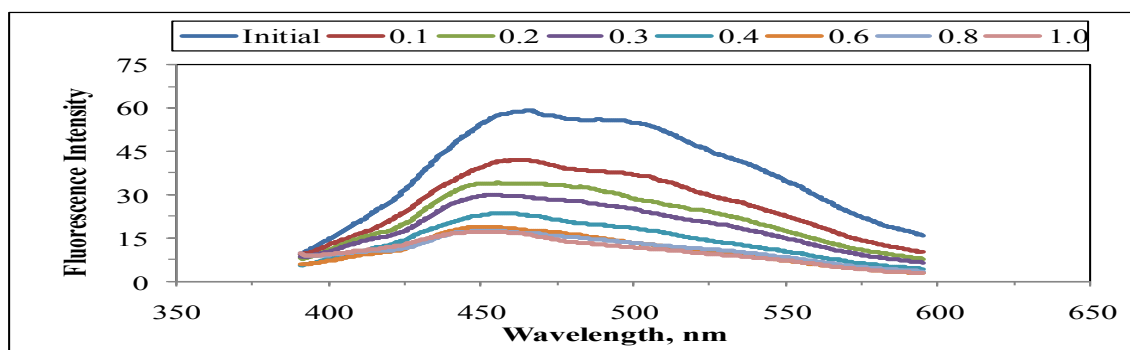
Figure C.8. Emission scan fluorescence spectra of 0.45 μm filtered fraction of humic acid following adsorption onto N-doped TiO_2 Hombikat UV-100 at 370 nm excitation wavelength.

Figure C.9. Emission scan fluorescence spectra of 0.45 μm filtered fraction of humic acid following adsorption onto S-doped TiO_2 Hombikat UV-100 at 370 nm excitation wavelength.

Figure C.10. Emission scan fluorescence spectra of 0.45 μm filtered fraction of humic acid following adsorption onto N-S co-doped TiO_2 Hombikat UV-100 at 370 nm excitation wavelength.

Figure C.11. Emission scan fluorescence spectra of 100 kDa fraction of humic acid following adsorption onto bare TiO_2 Degussa P-25 at 370 nm excitation wavelength.
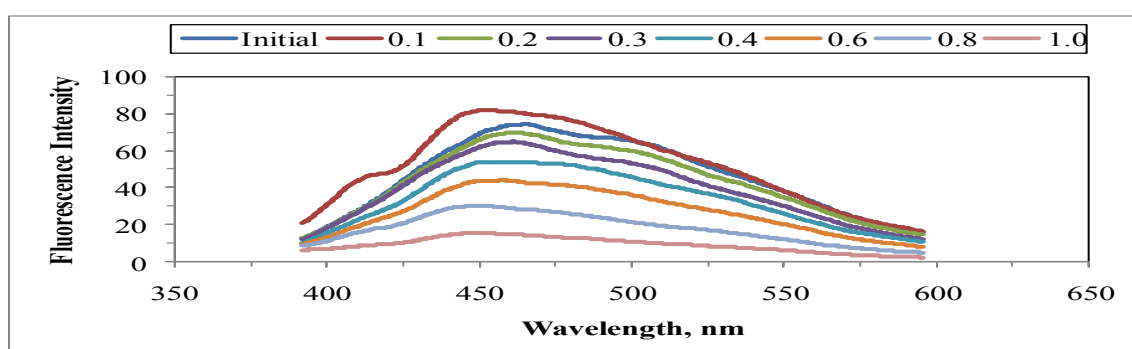

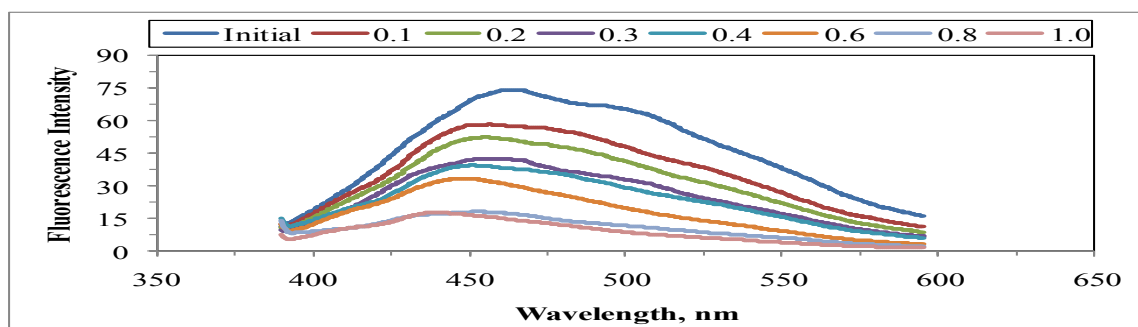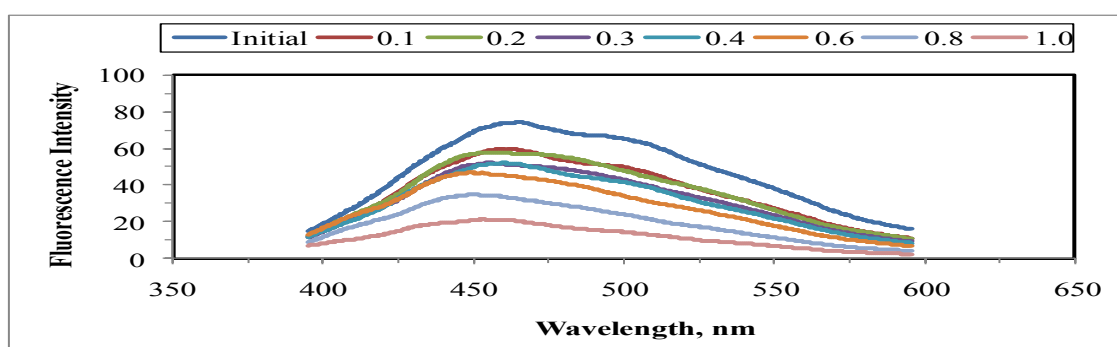Figure C.12. Emission scan fluorescence spectra of 100 kDa fraction of humic acid following adsorption onto C-doped TiO_2 Degussa P-25 at 370 nm excitation wavelength.
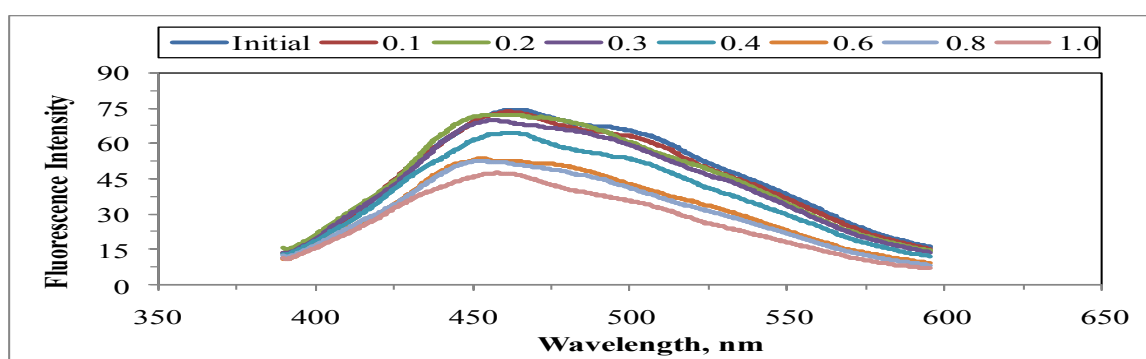
Figure C.13. Emission scan fluorescence spectra of 100 kDa fraction of humic acid following adsorption onto N-doped TiO_2 Degussa P-25 at 370 nm excitation wavelength.
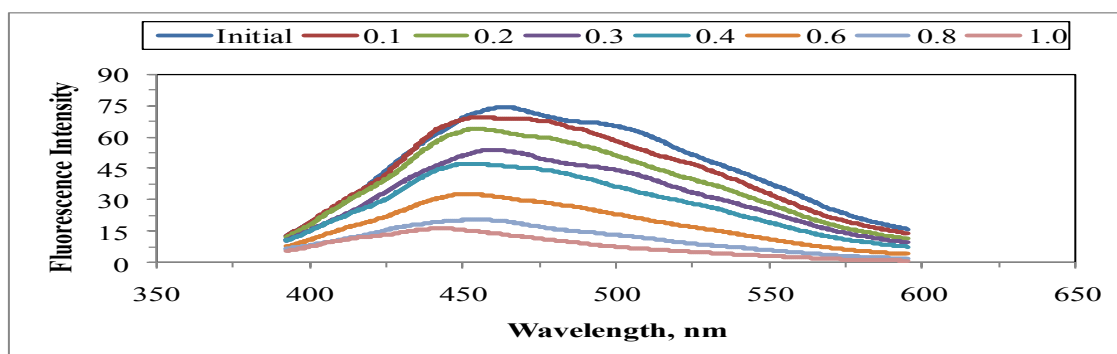

Figure C.14. Emission scan fluorescence spectra of 100 kDa fraction of humic acid following adsorption onto S-doped TiO_2 Degussa P-25 at excitation 370 nm wavelength.

Figure C.15. Emission scan fluorescence spectra of 100 kDa fraction of humic acid following adsorption onto N-S co-doped TiO_2 Degussa P-25 at 370 nm excitation wavelength.

Figure C.16.   Emission scan fluorescence spectra of 100 kDa fraction of humic acid following adsorption onto bare TiO$_2$ Hombikat UV-100 at 370 nm excitation wavelength.

Figure C.17.   Emission scan fluorescence spectra of 100 kDa fraction of humic acid following adsorption onto C-doped TiO$_2$ Hombikat UV-100 at 370 nm excitation wavelength.
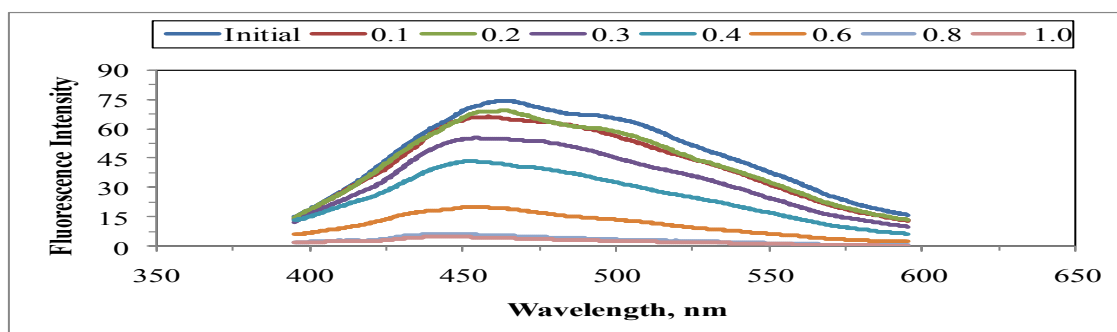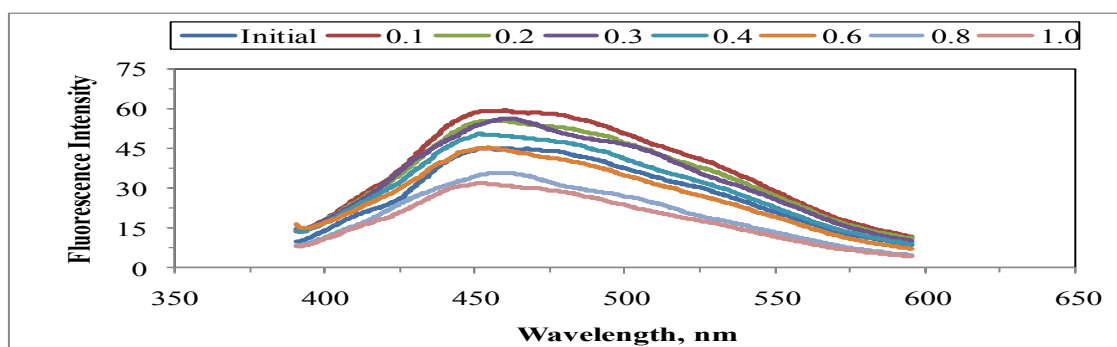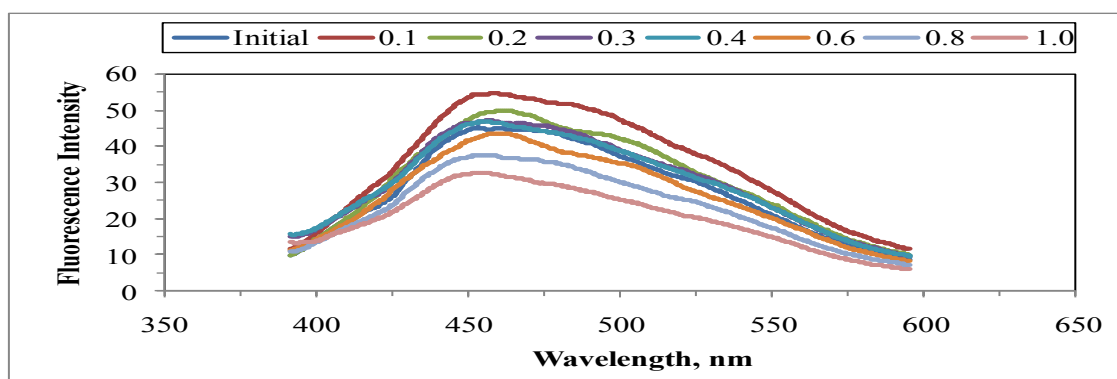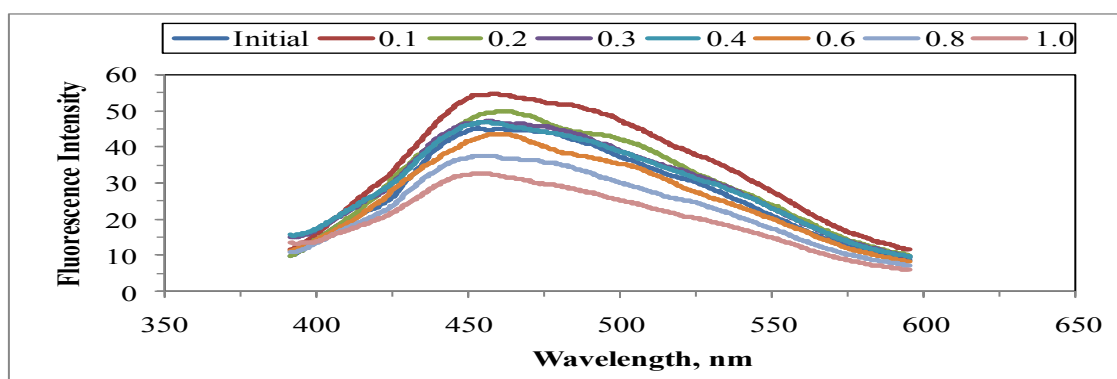

Figure C.18.   Emission scan fluorescence spectra of 100 kDa fraction of humic acid following adsorption onto N-doped TiO$_2$ Hombikat UV-100 at 370 nm excitation wavelength.

Figure C.19.   Emission scan fluorescence spectra of 100 kDa fraction of humic acid following adsorption onto S-doped TiO$_2$ Hombikat UV-100 at 370 nm excitation wavelength.

Figure C.20.   Emission scan fluorescence spectra of 100 kDa fraction of humic acid following adsorption onto N-S co-doped TiO$_2$ Hombikat UV-100 at 370 nm excitation wavelength.

Figure C.21.   Emission scan fluorescence spectra of 30 kDa fraction of humic acid following adsorption onto bare TiO$_2$ Degussa P-25 at 370 nm excitation wavelength.

Figure C.22.   Emission scan fluorescence spectra of 30 kDa fraction of humic acid following adsorption onto C-doped TiO_2 Degussa P-25 at 370 nm excitation wavelength.

Figure C.23.   Emission scan fluorescence spectra of 30 kDa fraction of humic acid following adsorption onto N-doped TiO_2 Degussa P-25 at 370 nm excitation wavelength.
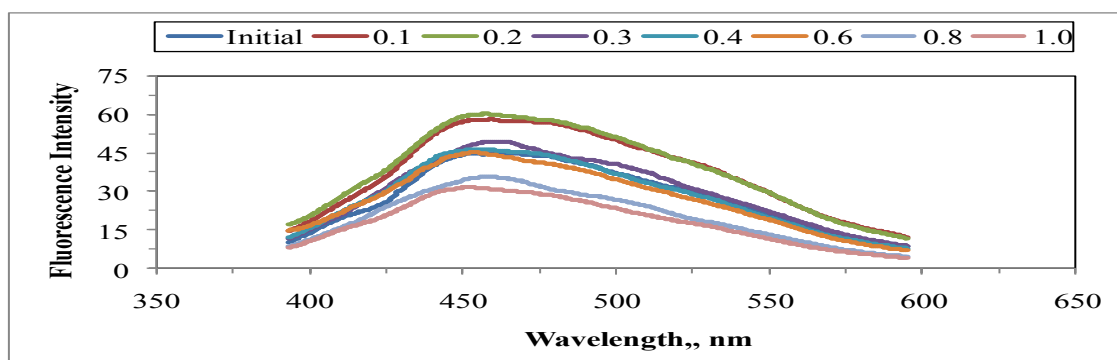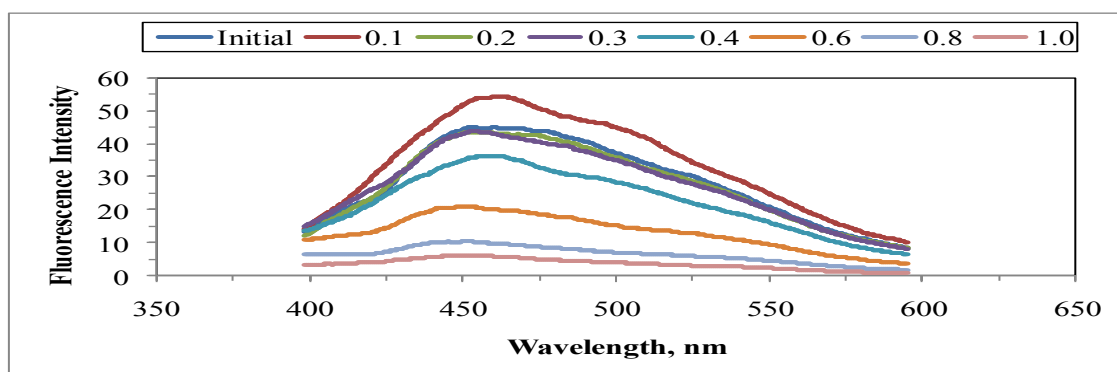

Figure C.24.   Emission scan fluorescence spectra of 30 kDa fraction of humic acid following adsorption onto S-doped TiO_2 Degussa P-25 at excitation 370 nm wavelength.

Figure C.25. Emission scan fluorescence spectra of 30 kDa fraction of humic acid following adsorption onto N-S co-doped TiO$_2$ Degussa P-25 at 370 nm excitation wavelength.
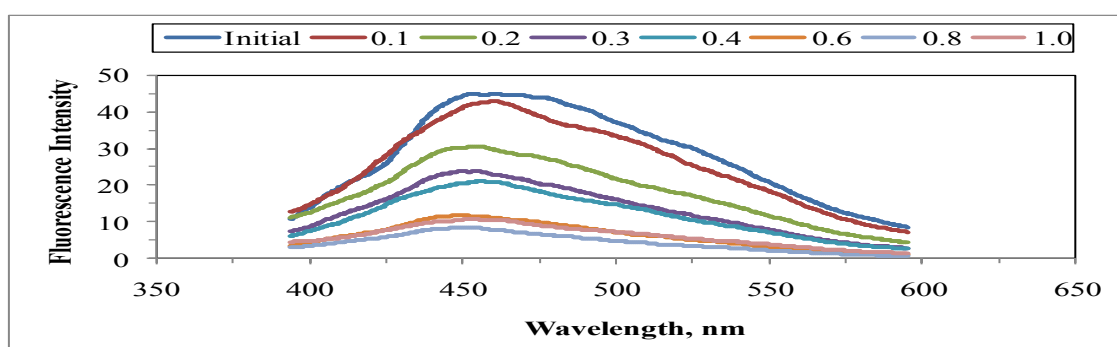

Figure C.26. Emission scan fluorescence spectra of 30 kDa fraction of humic acid following adsorption onto bare TiO$_2$ Hombikat UV-100 at 370 nm excitation wavelength.
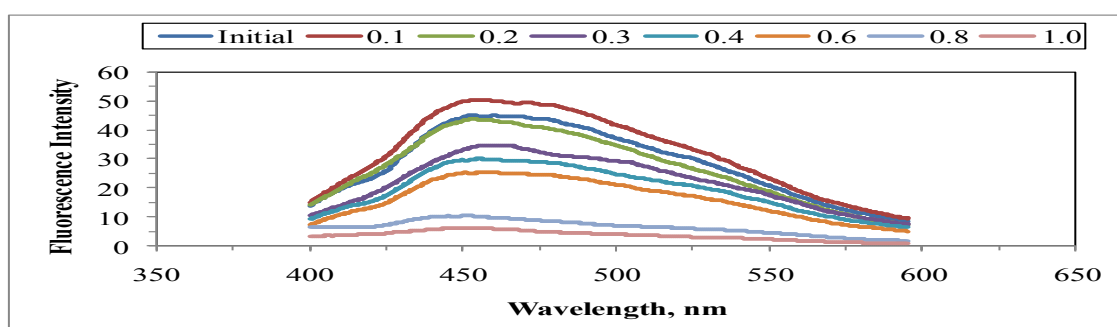

Figure C.27. Emission scan fluorescence spectra of 30 kDa fraction of humic acid following adsorption onto C-doped TiO$_2$ Hombikat UV-100 at 370 nm excitation wavelength.
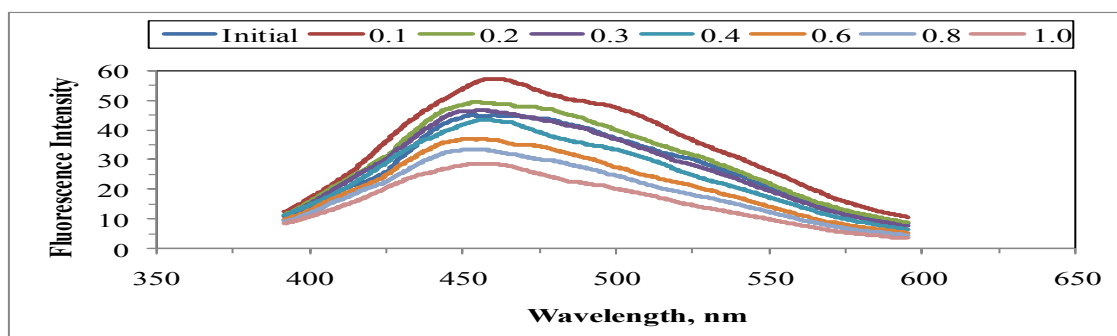
Figure C.28.   Emission scan fluorescence spectra of 30 kDa fraction of humic acid following adsorption onto N-doped TiO_2 Hombikat UV-100 at 370 nm excitation wavelength.
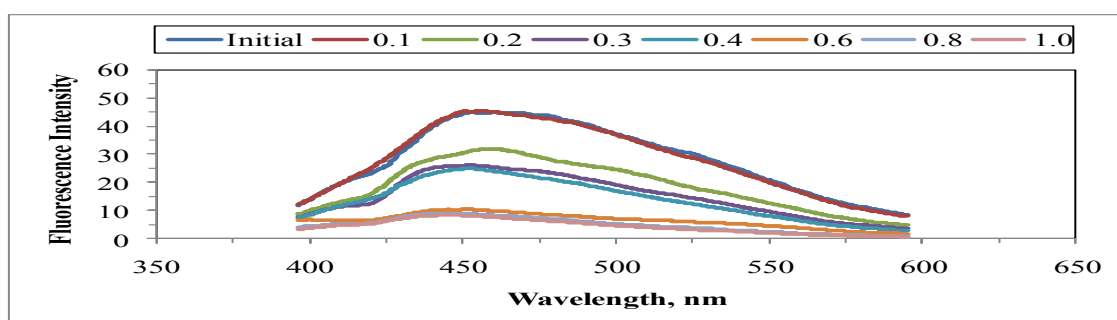

Figure C.29.   Emission scan fluorescence spectra of 30 kDa fraction of humic acid following adsorption onto S-doped TiO_2 Hombikat UV-100 at 370 nm excitation wavelength.
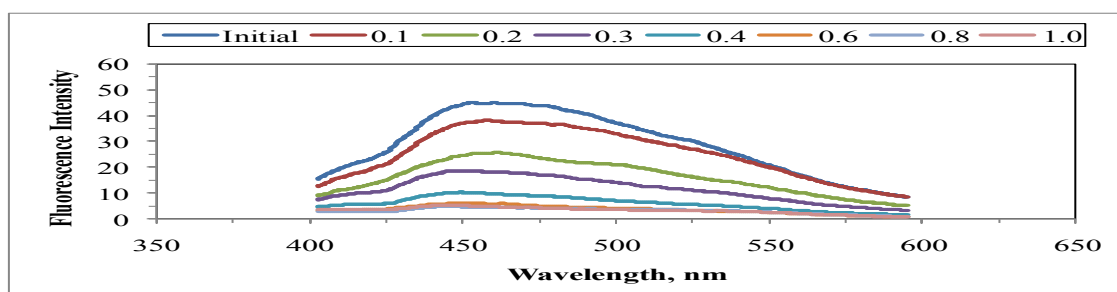

Figure C.30.   Emission scan fluorescence spectra of 30 kDa fraction of humic acid following adsorption onto N-S co-doped TiO_2 Hombikat UV-100 at 370 nm excitation wavelength.